Electronic Thesis and Dissertation Repository

12-11-2012 12:00 AM

Passive and Semi-Active Structure-Multiple Tuned Liquid Damper Systems

Islam Soliman
The University of Western Ontario

Supervisor
Dr. Ashraf El Damatty
The University of Western Ontario Joint Supervisor
Dr. Michael Tait
The University of Western Ontario

Graduate Program in Civil and Environmental Engineering
A thesis submitted in partial fulfillment of the requirements for the degree in Doctor of Philosophy
© Islam Soliman 2012

Recommended Citation

Passive and Semi-Active Structure-Multiple Tuned Liquid Damper Systems

(Spine title: Passive and Semi-Active Structure-MTLD Systems)

(Thesis format: Integrated-Article)

By

Islam M. Soliman

Faculty of Engineering
Department of Civil and Environmental Engineering

A thesis submitted in partial fulfilment
of the requirements for the degree of
Doctor of Philosophy

The School of Graduate and Postdoctoral Studies
The University of Western Ontario
London, Ontario, Canada

THE UNIVERSITY OF WESTERN ONTARIO
School of Graduate and Postdoctoral Studies

CERTIFICATE OF EXAMINATION

Supervisors   Examiners

_____   _____
Dr. Ashraf El Damatty   Dr. Girma Bitsuamlak

_____   _____
Dr. Michael Tait   Dr. Hesham El Naggar

Supervisory Committee
                                                              _____
                                                              Dr. Samuel Asokanthan
_____
Dr.
                                                              _____
                                                              Dr. Sriram Narasimhan
_____
Dr.

The thesis by

Islam Mohamed Soliman

entitled:

Passive and Semi-Active Structure-Multiple Tuned Liquid Damper Systems

is accepted in partial fulfillment of the
requirements for the degree of
Doctor of Philosophy

_____   _____
            Date   Chair of the Thesis Examination Board

Abstract

The resonant vibration motion of tall buildings due to dynamic loading, such as wind storms and earthquakes, can be reduced by adding passive dynamic vibration absorbers (DVAs). A single sway mode of vibration is usually considered, however, for certain structures, multiple modes may need to be suppressed. Furthermore, the location of the TLD on the floor plate is important for certain modes, such as the torsional mode. As a result, a three dimensional finite element structure-TLD system model capable of dynamically analyzing a 3D structure is developed and validated. Two different nonlinear TLD models are considered. A full dynamic analysis of a 3D single-story structure-TLD system is carried out utilizing the two TLD models and results under harmonic and random excitation are compared with experimental values. The three dimensional finite element structure-tuned liquid damper system model (3D-Structure-TLD) is expanded to include multiple tuned liquid dampers (3D-Structure-MTLD) and employed to estimate the response of a full-scale model of a 38-story multi-modal high-rise building subjected to wind tunnel loads recorded at different locations along the building's width and height.

To further improve TLD effectiveness, the nonlinear TLD fluid model is modified in order to simulate the influence of inclined damping screens. The updated passive TLD model is used to investigate the performance of both a single-story structure-TLD system and a 38-story structure-MTLD system with inclined damping screens over a range of structural response amplitudes utilizing random excitation and wind tunnel loads, respectively. Thus, the methodology to optimize the effective damping provided by the TLD over a range of structural responses is addressed.

Finally, a control strategy based on gain scheduling scheme is developed, by actively controlling the damping screen inclination angle. The updated nonlinear fluid model of a TLD equipped with inclined damping screens is used to determine the resulting TLD base shear force and free surface response of a novel semi-active (SA) TLD. The semi-active TLD control technique is also expanded to include semi-active multiple TLDs (3D-Structure-SA-MTLD) and employed to analyze a 38-story building over a range of wind angles and return periods. The improved performance of a semi-active TLD system over a passive TLD system is addressed.

Co-Authorship

This thesis has been prepared in accordance with the regulations for an Integrated-Article format thesis stipulated by the School of Graduate and Postdoctoral Studies at the University of Western Ontario and has been co-authored as:

Chapter 2: Development and Validation of Finite Element Structure-Tuned Liquid Damper System Models

The numerical studies were conducted by I.M. Soliman under the supervision of Dr. A.A. El Damatty and Dr. M.J. Tait, and modifications were done under the close supervision of Dr. M.J. Tait and Dr. A.A. El Damatty. Drafts of Chapter 2 were written by I.M. Soliman, and modifications were done under the close supervision of Dr. M.J. Tait and Dr. A.A. El Damatty. Portions of this Chapter have been accepted to be presented at the 3rd International Structural Specialty Conference in Edmonton, Alberta, Canada (June 2012), which is a part of 125th Anniversary Conference of the Canadian Society for Civil Engineers. Portions of this chapter have been presented at the 3rd International Structural Speciality Conference in Edmonton, Alberta, Canada, June 2012.

Chapter 3: Three Dimensional Analysis of a High-Rise Building Equipped with Multiple Tuned Liquid Dampers Using Wind Tunnel Loads

The numerical studies were conducted by I.M. Soliman under the supervision of Dr. A.A. El Damatty and Dr. M.J. Tait, and modifications were done under the close supervision of Dr. M.J. Tait and Dr. A.A. El Damatty. Drafts of Chapter 3 were written by I.M. Soliman, and modifications were done under the close supervision of Dr. M.J. Tait and Dr. A.A. El Damatty.

Chapter 4: Finite Element Modelling of Structure-MTLD Systems with Inclined Damping Screens

The numerical studies were conducted by I.M. Soliman under the supervision of Dr. A.A. El Damatty and Dr. M.J. Tait, and modifications were done under the close supervision of Dr. M.J. Tait and Dr. A.A. El Damatty. Drafts of Chapter 4 were written by I.M. Soliman, and modifications were done under the close supervision of Dr. M.J. Tait and Dr. A.A. El Damatty.

Chapter 5: Development and Validation of a Finite Element Structure Semi-Active Tuned Liquid Damper System Model

The numerical studies were conducted by I.M. Soliman under the supervision of Dr. A.A. El Damatty and Dr. M.J. Tait, and modifications were done under the close supervision of Dr. M.J. Tait and Dr. A.A. El Damatty. Drafts of Chapter 5 were written by I.M. Soliman, and modifications were done under the close supervision of Dr. M.J. Tait and Dr. A.A. El Damatty.

Chapter 6: Applications of Multiple Semi-Active TLDs for Structural Control of Three Dimensional High-Rise Buildings Using Wind Tunnel Loads

The numerical studies were conducted by I. M. Soliman under the supervision of Dr. A.A. El Damatty and Dr. M.J. Tait, and modifications were done under the close supervision of Dr. M.J. Tait and Dr. A.A. El Damatty. Drafts of Chapter 6 were written by I.M. Soliman, and modifications were done under the close supervision of Dr. M.J. Tait and Dr. A.A. El Damatty.

To my parents

Acknowledgment

I would like to express my appreciation and sincere gratitude to my research supervisors, Dr. Ashraf El Damatty and Dr. Michael Tait. Their guidance and patience were essential to the development of this thesis.

I want to express my deep appreciation to my supervisor, Dr. Michael Tait, for his endless support, understanding, discussions and continuous encouragement.

I would like to thank Dr. Eric Ho from the Boundary Layer Wind Tunnel Laboratory for providing me the wind tunnel data and for his helpful discussions.

I would also like to extend my sincere thanks to all my colleagues and friends, who I have worked beside and have had many interesting conversation with.

Special thanks are given to my parents, brothers, sister and parents-in-law who I owe a lot for accepting my small family's absence during my study period here in Canada. They have been a constant source of patience and encouragements.

I wish to dedicate this thesis to my wife, Yara, for her love and patience over the time that I have spent on this thesis. Her care and support have made it possible for me to accomplish this work.

Last but not least, I would like to thank my son, Ahmed, for making my life happier and relieving my research stress times with his innocent smiles and laughs.

Table of Contents

Chapter 1: Introduction

Chapter 2: Development and Validation of Finite Element Structure-Tuned Liquid Damper System Models

Chapter 3: Three Dimensional Analysis of a High-Rise Building Equipped with Multiple Tuned Liquid Dampers Using Wind Tunnel Loads

Chapter 5: Development and Validation of a Finite Element Structure Semi-Active Tuned Liquid Damper System Model

Chapter 7: Conclusions and Recommendations

Appendices

List of Tables

List of Figures

Nomenclature

List of Symbols

A	Excitation amplitude
A	Cross sectional area
I_x	Moments of inertia in the x-direction
I_y	Moments of inertia in the y-direction
I_z	Moments of inertia in the z-direction
$x(t)$	Displacement component in the x-direction - 3D beam element
$y(t)$	Displacement component in the y-direction - 3D beam element
$z(t)$	Displacement component in the z-direction - 3D beam element
$\dot{x}(t)$	Velocity component in the x-direction - 3D beam element
$\dot{y}(t)$	Velocity component in the y-direction - 3D beam element
$\dot{z}(t)$	Velocity component in the z-direction - 3D beam element
$\ddot{x}(t)$	Acceleration component in the x-direction - 3D beam element
$\ddot{y}(t)$	Acceleration component in the y-direction - 3D beam element
$\ddot{z}(t)$	Acceleration component in the z-direction - 3D beam element
$\theta_x(t)$	Rotational component in the x-direction - 3D beam element
$\theta_y(t)$	Rotational component in the y-direction - 3D beam element
$\theta_z(t)$	Rotational component in the z-direction - 3D beam element
$\dot{\theta}_x(t)$	Torsional velocity component in the x-direction - 3D beam element
$\dot{\theta}_y(t)$	Torsional velocity component in the y-direction - 3D beam element
$\dot{\theta}_z(t)$	Torsional velocity component in the z-direction - 3D beam element
$\ddot{\theta}_x(t)$	Torsional acceleration component in the x-direction - 3D beam element
$\ddot{\theta}_y(t)$	Torsional acceleration component in the y-direction - 3D beam element
$\ddot{\theta}_z(t)$	Torsional acceleration component in the z-direction - 3D beam element

Δt	Time Step
T	Time period
t	Time
$P_\circ$	Sinusoidal force amplitude
f_s	Natural frequency of the primary structure
f_{ex}	Excitation frequency
f_{TLD}	Nonlinear natural frequency of the damper
g	Gravitational acceleration
h	Water depth
k_{TLD}	Damper Stiffness
L	Tank Length
b	Tank width
L_x	2D Tank length in x-direction
L_y	2D Tank length in y-direction
i	Integer value associated with different sloshing modes
j	Integer value associated with different sloshing modes
m_{TLD}	Nonlinear TLD mass
M	Mass of the primary structure
$m_\circ$	Non-participating (rigid) portion of fluid mass
n	Integer value associated with different modes/harmonics
f_w	Fundamental sloshing frequency
Ω	Tuning ratio
M^*	Generalized mass
K^*	Generalized stiffness
C^*	Generalized damping
μ	Mass ratio (TLD)

v_w	Kinematic viscosity of water
ζ_{TLD}	Damping ratio of TLD (% critical)
ζ_{eff}	Effective Damping (% critical)
ζ_s	Equivalent viscous damping of the structure (% critical)
Δp	Pressure drop across damping screens
PF	Peak factor
C_l	Pressure loss coefficient of vertical damping screen
C_θ	Pressure loss coefficient of inclined damping screen
A_s	Solid Area of damping screens submerged in water
c_{TLD}	Nonlinear damping of the damper
$\ddot{X}$	Horizontal base excitation acceleration of the tank
ζ_w	Viscous damping coefficient
U_{DS}	Average horizontal water velocity at damping screens
u	Average horizontal water particle velocity
η	Free surface elevation or wave height
C_d	Drag coefficient
E_d	Energy dissipation by equivalent damper
$\left|H_{z/x}(f)\right|$	Frequency response function
$\theta_{z/x}$	Phase angle between output z to input x
$[M_s]$	Mass Matrix of 3D-Structure
$[K_s]$	Stiffness Matrix of 3D-Structure
$[C_s]$	Damping Matrix of 3D-Structure
$\{F_a\}$	Vector of the applied external dynamic loads acting on the 3D-Structure
F_{TLD}	TLD base shear force
x_s	Maximum structural displacement amplitude experienced at the TLD location and in its placement direction

$\ddot{x}_s$	Instantaneous structural acceleration at the TLD location and in its placement direction
A_{cycle}	Complete structural response cycle at the TLD location and in its placement direction
P_1	Peak displacement value during the 1st half structural response cycle at the TLD location and in its placement direction
P_2	Peak displacement value during the 2nd half structural response cycle at the TLD location and in its placement direction
F_{max}	Maximum amplitude excitation
CM	Centre of mass of the actual 38-story high-rise building
CT	Centre of twist of the actual 38-story high-rise building
θ_w	Wind loading angle (degree)
$\ddot{x}$	Average peak hourly acceleration response in x-direction
$\ddot{y}$	Average peak hourly acceleration response in y-direction
$\sigma_{\ddot{x}}$	RMS of structural acceleration response in x-direction
$\sigma_{\ddot{y}}$	RMS of structural acceleration response in y-direction
$R_{peak-hr}$	Average peak hourly of structural resultant acceleration response
PF_x	Peak factor in x-direction
PF_y	Peak factor in y-direction
ϕ	Normalized modal deflection value of the structure at the TLD location
S	Screen solidity ratio
A_s	Solid Area of damping screen submerged in water
$\sigma_{\ddot{x}-target}$	Target RMS structural acceleration response in x-direction
$\sigma_{\ddot{y}-target}$	Target RMS structural acceleration response in y-direction
$\ddot{x}_{initial}$	Initial average peak hourly structural acceleration response in x-direction
$\ddot{y}_{initial}$	Initial average peak hourly structural acceleration response in y-direction
$\ddot{x}_{target}$	Target average peak hourly structural acceleration response in x-direction
$\ddot{y}_{target}$	Target average peak hourly structural acceleration response in y-direction

$\zeta_{eff-opt}$	Optimal effective damping (% critical)
$\sigma_{\ddot{x}-target-m}$	Target modal RMS structural acceleration response component in x-direction
$\sigma_{\ddot{y}-target-m}$	Target modal RMS structural acceleration response component in y-direction
$\sigma_{\ddot{x}-initial-m}$	Initial modal RMS structural acceleration response component in x-direction
$\sigma_{\ddot{y}-initial-m}$	Initial modal RMS structural acceleration response component in y-direction
θ	Inclination angle of the damping screens
ζ_{opt}	Optimal TLD Damping ratio (% critical)
MF	Modal Factor
T_{s-x}	Structural time period in x-direction
T_{s-y}	Structural time period in y-direction
f_{s-x}	Structural cyclic frequency in x-direction
f_{s-y}	Structural cyclic frequency in y-direction
ω_{s-x}	Structural natural frequency in x-direction
ω_{s-y}	Structural natural frequency in y-direction
$\zeta_{TLD-eff-opt_x}$	Optimal effective damping provided by TLD in x-direction
$\zeta_{TLD-eff-opt_y}$	Optimal effective damping provided by TLD in y-direction
$\zeta_{TLD-opt_x}$	Optimal TLD damping ratio in x-direction
$\zeta_{TLD-opt_y}$	Optimal TLD damping ratio in y-direction
Ω_{opt_x}	Optimal tuning ratio in x-direction
Ω_{opt_y}	Optimal tuning ratio in y-direction
$f_{TLD-opt_x}$	Optimal TLD cyclic frequency in x-direction
$f_{TLD-opt_y}$	Optimal TLD cyclic frequency in y-direction
R_{opt_x}	Optimal TLD response ratio in x-direction
R_{opt_y}	Optimal TLD response ratio in y-direction
ζ_{tot-x}	Total damping of structure in x-direction

ζ_{tot-y}	Total damping of structure in y-direction
$\sigma_{x-target-m}$	Target modal RMS structural displacement response component in x-direction
$\sigma_{y-target-m}$	Target modal RMS structural displacement response component in y-direction
σ_{r-x}	TLD response in x-direction
σ_{r-y}	TLD response in y-direction
C_D	Drag coefficient
C_c	Contraction Coefficient
F_D	Drag force
ρ	Density of water
Ψ	Flow deflection angle
$U_\circ$	Average fluid velocity throughout the depth
γ_θ	Reduction in losses as a fraction of the losses for a vertical screen
E'_w	TLD non-dimensional energy dissipation
η'	Non-dimensional free-surface amplitude
η	Free-surface response amplitude
Λ	Non-dimensional excitation amplitude
A	Applied excitation amplitude
β	Excitation frequency ratio
$f_n = \omega_n/2\pi$	Natural sloshing frequency
$F'_w(t)$	Non-dimensional base shear force
$F_w(t)$	Base shear force produced by the nonlinear TLD fluid model
E'_w	Non-dimensional energy dissipation per cycle
T	Applied excitation period
ψ	Efficiency of a TLD
$\ddot{x}_{peak-hr}$	Peak hourly structural acceleration response in x-direction
$\ddot{y}_{peak-hr}$	Peak hourly structural acceleration response in y-direction

R	Percentage response reduction values of the average peak hourly resultant accelerations
T_d	Duration time in seconds used to calculate the peak factor
SF	Scale factor
$\ddot{x}_{target-min}$	Minimum target peak hourly structural acceleration response in x-direction
$\ddot{x}_{target-max}$	Maximum target peak hourly structural acceleration response in x-direction
AT	Averaging time used in the gain schedule scheme
UT	Updating time used in the gain schedule scheme
IT	Initial time used in the gain schedule scheme
$\sigma_{\ddot{x}-target-max}$	Maximum target RMS structural acceleration response in x-direction
$\sigma_{\ddot{y}-target-max}$	Maximum target RMS structural acceleration response in y-direction
$\sigma_{\ddot{x}-target-min}$	Minimum target RMS structural acceleration response in x-direction
$\sigma_{\ddot{y}-target-min}$	Minimum target RMS structural acceleration response in y-direction
C_{l-max}	Maximum damping screen loss coefficient value
C_{l-min}	Minimum damping screen loss coefficient value
θ_{max}	Maximum inclination angle of the damping screen
PV	Peak hourly acceleration response values for the 1/10 scale model
$C1$	Corner 1 of the high-rise building ($z = 154.6$ m)
$C2$	Corner 2 of the high-rise building ($z = 154.6$ m)
$C3$	Corner 3 of the high-rise building ($z = 154.6$ m)
$C4$	Corner 4 of the high-rise building ($z = 154.6$ m)
$\sigma_{\ddot{x}-target-t}$	Total target RMS acceleration response value in x-direction
$\sigma_{\ddot{y}-target-t}$	Total target RMS acceleration response value in y-direction
$C_{\theta x_1}$	Damping screen loss coefficient value for mode 1 tanks in x-direction
C_{lx-max_1}	Maximum damping screen loss coefficient value for mode 1 tanks in x-direction
C_{lx-min_1}	Minimum damping screen loss coefficient value for mode 1 tanks in x-direction

$C_{ly-passive_3}$ Passive damping screen loss coefficient value for mode 3 tanks in y-direction

$C_{\theta x_{1-average}}$ Average damping screens loss coefficient value for mode 1 tanks in x-direction

$C_{\theta y_{2-average}}$ Average damping screens loss coefficient value for mode 2 tanks in y-direction

$C_{\theta x_{3-average}}$ Average damping screens loss coefficient value for mode 3 tanks in x-direction

$C_{\theta y_{3-average}}$ Average damping screens loss coefficient value for mode 3 tanks in y-direction

Superscripts

A Excitation amplitude

E_d' Theoretical expression to match both the maximum value of the energy dissipated and the total energy dissipated over the range of frequency tested

M^* Generalized properties of M

$\dot{x}$ First time derivative of x

$\ddot{x}$ Second time derivative of x

Subscripts

A Excitation amplitude

TLD   Tuned Liquid Damper

TMD   Tuned Mass Damper

opt Optimal

w Water

x x-axis

y y-axis

z z-axis

eff Effective

r r-axis (Local coordinate system)

s s-axis (Local coordinate system)

t t-axis (Local coordinate system)

Abbreviations

DVA	Dynamic Vibration Absorber
EADTMD	Equivalent Amplitude Dependent Tuned Mass Damper
SDOF	Single Degree of Freedom
TMD	Tuned Mass Damper
TLD	Tuned Liquid Damper
SA-TLD	Semi-Active Tuned Liquid Damper
SA-MTLD	Semi-Active Multiple Tuned Liquid Dampers
MTLD	Multiple Tuned Liquid Dampers
3D-Structure	Three Dimensional Structure
DOF	Degree of freedom
SHARCNET ™	Shared Hierarchical Academic Research Computing Network
NBC	National Building Code of Canada
BLWTL	Boundary layer wind tunnel laboratory
ASCE	American Society of Civil Engineers
RMS	Root-mean-square
MR-TLCD	Semi-active TLCD using magneto-rheological fluid
1D TLD	Uni-directional TLD
2D TLD	Bi-directional TLD

Chapter 1: Introduction

1.1.   General Overview

Implementation of supplemental damping systems (i.e. the dynamic vibration absorbers, DVAs) to mitigate excessive building vibrations induced by external dynamic loads (i.e. wind storms and earthquakes) has increased over the last several decades. A DVA increases the effective damping of a structure by dissipating a portion of the energy when it is subjected to movement, thus a portion of the energy transmitted to the primary structure by the external forces is dissipated. Considerations when designing high-rise structures are the utilization of space, prevention of urban sprawl and an efficient use of resources, especially when buildings are often built to accommodate the urban economic core. Therefore, as new structures become taller, lighter, more flexible and lightly damped, which magnifies their sensitivity to dynamic excitation, this leads to additional design considerations in order to satisfy both strength and serviceability requirements.

1.2.   Categorization of Structural Response Mitigation Systems

Soong and Dargush 1997 divided structural response mitigation systems into three main categories; isolation, passive and semi-active/active systems. Table 1.1 shows examples of systems that belong to each of these categories. Isolation systems isolate the structure from input excitation (i.e. earthquake) and are typically located at the foundation level. The first four systems listed in the middle column of Table 1.1 represent direct passive energy dissipation systems. Direct energy dissipation mechanisms include the flow of a highly viscous fluid through an orifice and the shearing action of a polymeric/rubber-like material in viscoelastic dampers (Kareem et al. 1999). Indirect energy dissipation mechanisms consist of a secondary auxiliary system that provides effective damping by modifying the frequency response characteristics of the structure (Kareem 1983). Semi-active and active control systems offer improved performance over traditional passive systems.

Housner et al. (1997) described different energy dissipation systems utilized for structural control including active, semi-active, passive and hybrid systems. Kareem et al. (1999) described different control systems installed in various buildings around the globe. Soong and Spencer (2002) summarized the state of the art of different energy dissipation systems and their structural applications. The main reason to implement a control system in a building is to improve its serviceability and/or its safety against natural hazards, which are mainly

wind and earthquakes. Schematic diagrams of various energy dissipation systems are shown in Figure 1.1 and discussed briefly in the following sections.

1.2.1   Active Control Systems

An active control system is one that uses an external power source to drive actuator(s) that apply forces to the structure in a prescribed manner. These forces can be used to both add and dissipate energy (Housner et al. 1997). In an active feedback control system, the signals sent to the control actuators, which are measured with physical sensors (optical, mechanical, electrical, chemical, etc.), are a function of the response of the structure. The effectiveness of an active control system could be compromised due to a loss of power during the loading event. As shown in Figure 1.1a, based on the measured excitation, the controller introduces a control force to the secondary mass through the actuator to counteract the structure's motion. Although, active control systems have been implemented in the fields of mechanical and electrical engineering for a considerable period of time, applications in civil engineering are much more recent. Soong (1988) and Housner et al. (1996) describe the development of various active control systems and their uses in civil engineering.

1.2.2   Passive Control Systems

A passive control system does not require an external power source, which is the main advantage of this system type relative to an active control system (see Figure 1.1b). Passive control systems impart forces that develop in response to the motion of the structure. The main function of a passive control system is to alter the characteristics of the structure such as its damping and/or stiffness. Tuned mass dampers (TMD), tuned liquid column dampers (TLCD) and tuned liquid dampers (TLD) represent common dynamic vibration absorber passive control systems. Due to their simplicity and efficiency in reducing structural response, these passive control systems are commonly used in civil engineering applications. TMD, TLCD and TLD involve adding an auxiliary system to the primary system. Their basic function is to dissipate a portion of the input energy from the external excitation source (i.e. wind or earthquake), thereby, reducing the energy dissipation demand on the primary structure (Soong and Dargush 1997).

1.2.3 Hybrid Control Systems

The hybrid control system typically implies the combined use of active and passive control systems. For example, a structure equipped with distributed viscoelastic damping supplemented with an active mass damper on or near the top of the structure, or a base isolated structure with actively controlled actuators to enhance performance (Housner et al. 1997). As shown in Figure 1.1c, a tertiary mass is connected to the auxiliary secondary mass using a spring, damper and actuator. The motion of the secondary mass system is set and magnified by the active tertiary mass, making it more efficient. In this system, the active control is used only during large amplitude structural excitation. In the event of power failure, or extreme excitation, the system automatically switches to a passive control system, thus eliminating the risk of total system failure. Most of the applications of hybrid control systems have been in Japan (see Section 1.8 for full-scale application examples). A reduction of about 50% of uncontrolled structural response due to the addition of the hybrid control systems was reported in Kareem et al. (1999).

1.2.4 Semi-Active Control Systems

Semi-active control systems are a class of control systems for which the external energy requirements are typically orders of magnitude smaller than that of active control systems. Semi-active control systems do not add significant amounts of mechanical energy to the structural system (including the structure and the control actuators), therefore bounded-input bounded-output stability is guaranteed (Housner et al. 1997). Semi-active control systems are often viewed as controllable passive systems. Researchers have developed this control system by combining the best features of active and passive control systems. For a semi-active control system, the properties of the auxiliary system are altered and optimized during the time history to achieve improved efficiency of the semi-active system leading to maximum structural response reduction. Examples of such semi-active systems include variable-orifice fluid dampers, variable-stiffness systems, controllable friction systems, controllable fluid dampers and controllable impact dampers (see Section 1.8 for full-scale application examples).

Spencer and Soong (1999) describe structures with various control schemes as shown in Figure 1.2. When only the structural response variables are measured, the control configuration is referred to as feedback control since the structural response is continually

monitored and this information is used to make continual corrections to the applied control forces. A feedforward control results when the control forces are regulated only by the measured excitation, which can be achieved, for example, for earthquake inputs by measuring structural base accelerations. In cases where both the response quantities and excitation are utilized for control, the term feedback-feedforward control is used (Suhardjo et al. 1990). For example, an active structural control system has the basic configuration as shown schematically in Figure 1.2c. It consists of (a) sensors located about the structure to measure either external excitations, or structural response variables, or both; (b) devices to process the measured information and to compute the necessary control force needed based on a given control algorithm; and (c) actuators, usually powered by external sources, to produce the required forces.

1.3.   Passive/Active/Semi-Active TMD

Mitigation of the induced vibration caused by external dynamic excitation, such as wind and earthquake, by employing supplemental damping systems has been widely investigated. Among passive control systems, tuned mass dampers (TMDs) have been widely used in engineering practice for wind and earthquake induced vibration mitigation of high-rise buildings (McNamara 1977; Kwok 1984; Kowk and Samali 1995; Kitagawa and Midorikawa 1998; Breukelman and Haskett 2001; Soong 2002). By installing a TMD system in the primary structure, a secondary mass system is utilized to reduce accelerations. A TMD consists of a mass (m_a), a spring (stiffness, k_a), and a dashpot (damping, c_a) as shown in Figure 1.3. The structure is represented similarly utilizing the generalized parameters of the target mode of vibration to be suppressed, where M^*, K^* and C^* are the generalized mass, stiffness and viscous damping, respectively. The simple mechanism of reducing building vibration is the inertial force from the TMD being exerted back onto the primary structure and applied anti-phase to the excitation force.

In a TMD system, the secondary mass is attached to the main structure through a spring and a dashpot, where the dynamic characteristics of the secondary mass are related to those of the primary structure. The objective is to optimize the transfer of the vibration energy from the building to the damper by considering the resonant frequency of the damper. Therefore, three important characteristics should be considered. These characteristics are, the mass ratio of the secondary mass to the mass of the main system (μ), the frequency ratio of the two

systems (tuning ratio, Ω) and the damping ratio of the secondary system (ζ_{TMD}). The TMD parameters are tuned to the selected mode of vibration to be suppressed. By selecting the appropriate values of these ratios, the dynamic response of the main system can be significantly reduced.

The drawbacks of the above approach is that a TMD system provides protection against external dynamic loads with a frequency only near the natural frequency of the structure, which the TMD is tuned to. However, for certain types of excitation, wind for example, a range of frequencies or bandwidth usually exist. In other words, the TMD system reduces the resonant response values of the structure, in contrast with the mean or background response values. In fact, the fluctuations in the wind can be thought of as resulting from a composite of sinusoidally varying winds superimposed on the mean steady wind, which varies along the building's height (see Figure 1.4). These sinusoidal variations have a variety of frequencies, amplitudes and phases that change with the wind speed (van der Tempel 2006; Manwell et al. 2010). In addition, the optimal values of the TMD parameters depend on the type of external excitation (i.e. sinusoidal or random) and the dynamic properties of the structure (i.e. the natural frequency and the damping ratio), which can be response-amplitude-dependent (Tamura and Suganuma 1996).

To improve the robustness of a TMD system, active and semi-active TMD systems have been investigated by several researchers, where values of the TMD system parameters are changed based on the frequency and the amplitude of excitation in real time (Hrovat et al.1983; Kim and Adeli 2005a; Kim and Adeli 2005b). In an actively or semi-actively controlled TMD system, the efficiency of the TMD system is improved by retuning its frequency (Varadarajan and Nagarajaiah 2004; Hazra et al. 2010; Roffel et al. 2011) or by adjusting the TMD damping ratio (Abé and Igusa 1996; Roffel et al. 2011). On the other hand, multiple TMD systems, where more than one TMD system is designed and distributed within the structure to cover a range of dominant frequencies, have been proposed to further enhance robustness (Kareem and Kline 1995).

The semi-active concept has been successfully applied to a broad class of vehicle vibration isolation problems, ranging from tractors and other farm vehicles to high speed ground transportation vehicles (Margolis et al. 1975; Hrovat and Margolis 1981). The extension of the semi-active concept from the vehicle vibration isolation field to a structural

control of buildings was proposed in Hrovat et al. 1983. They indicated that employing the semi-active concept in buildings appears to be quite natural and extremely promising in view of the relatively low bandwidth requirements (less than ≈ 5 Hz), which compares favourably with bandwidth requirements for vehicle suspension (up to ≈ 50 Hz).

The semi-active control is promising as an effective method of mitigating structural damage from large environmental loads, with two main benefits over active and passive control solutions. First, for semi-active control systems, a large power supply is not required to have a significant impact on the response. Therefore, a broad feedback adaptive range of control can be provided. Second, semi-active control systems are also strictly dissipative and do not add energy into the system, ensuring stability. Thus, semi-active control over time should be better able to respond to changes in structural behaviour, particularly due to nonlinearities, damage or degradation of both systems (i.e. the semi-active and active) (Chey et al. 2010).

1.4.   Passive TLCD/TLD

The tuned liquid damper (TLD) has been utilized in the shipping industry since the beginning of the 20th century to prevent the rolling motion of large ships (Den Hartog 1985). Figure 1.5b shows the Frahm anti-rolling tank used in large ships. It consists of two tanks half filled with water, communicating through a water pipe below and through an air pipe above (Den Hartog 1985). Thus, the anti-rolling tanks were possibly the first use of tuned liquid column dampers (TLCD) as shown in Figure 1.5a. Sakai et al. (1989) proposed the TLCD to be used as a new type of DVA in structural applications (cable-stayed bridge towers). Similar to TLCD, TLDs were applied as vibration absorbers to reduce the oscillations of space satellites (Carrier and Mills 1960) and were called nutation dampers. Figure 1.5c shows the nutation damper, which consists of a ring of liquid around the satellite to reduce its rotation about the cylindrical principle axis.

Tuned liquid dampers (TLD) and tuned liquid column dampers (TLCD) have been investigated by several researchers as another type of secondary mass system for structural application (Sakai et al. 1989; Wakahara et al. 1992; Kareem 1994; Won et al. 1996; Kareem et al. 1999; Tamura et al. 1996; Soong and Dargush 1997; Kareem et al. 1999; Yalla et al. 2001; Tait et al. 2004a; Tait et al. 2005a). A TLD is a special type of TMD that consists of a rigid tank which is partially filled with a liquid, usually water. The sloshing liquid inside the

tank provides inertia forces that counteract the forces acting on the structure, thus reducing the building motion. A TLCD is a special type of TLD that relies on the motion of liquid column in a U-tube container to counteract the action of external forces acting on the structure, with inherent damping typically being introduced in the oscillating liquid column through an orifice.

1.5.   TLD Modelling Techniques

1.5.1   Equivalent Mechanical Models

As the same basic principles are applied in implementing a TLD to reduce the vibration motions of structures as a TMD, a TLD is often modelled as an equivalent mechanical system, allowing well established TMD theory to be implemented (see Figure 1.6). However, the primary difference from a TMD is the amplitude dependent (nonlinear) nature of the fluid response. Figure 1.7 shows a number of different proposed TLD equivalent mechanical models. The properties of the linear lumped mass system shown in Figure 1.7a can be derived using potential flow theory (Graham and Rodriguez 1952). This particular equivalent linear mechanical model allows a TLD to be modelled as an equivalent linear TMD (Kareem and Sun 1987). Sun et al. (1995) experimentally estimated amplitude dependent TMD parameters by matching the virtual mass and damping values of a TLD to that of a TMD at different excitation amplitudes (see Figure 1.7b). An extensive experimental program conducted by Yu et al. (1999) resulted in the development of an equivalent nonlinear TMD model (see Figure 1.7c). The model assumes the entire water mass participates in the response along with the non-linear stiffness hardening parameter and the non-linear damping based on the excitation amplitude. The model utilizes experimentally calibrated energy equivalent amplitude dependent stiffness and damping parameters. Tait (2004) expanded on Yu et al. (1999) by considering only the participating portion of the fluid (m_a) in a TLD contributes to the inertial force, while the non-participating portion of the fluid ($m_\circ$) is added to the primary mass of the structure (see Figure 1.6c). The dynamic characteristics of the equivalent TMD model, in terms of mass, stiffness and damping parameters were determined by energy equivalence from a series of shake table tests (Tait et al. 2004a) and the validity of the nonlinear TLD model was examined (Tait et al. 2004b). A sloshing-slamming model has been introduced by Yalla (2001), which accounts for the impact forces that develop from the sloshing water slamming on the container walls at higher response levels (see Figure 1.7d).

1.5.2   Fluid Models and Energy Dissipating Devices

The main source of damping for a TLD without additional damping devices arises from viscous dissipation in the boundary layers at the walls and bottom of the tank and from free surface contamination (Miles 1967). The inherent damping (ζ_{TLD}) for a TLD without additional energy dissipating devices is usually significantly less than optimal, resulting in a less effective vibration absorber. Additionally, the response of an under-damped TLD is more nonlinear and less controllable, reducing its reliability. Often, poles, screens, and other objects are submerged in the water to provide additional energy dissipating mechanisms as the damping provided by the water alone is often insufficient. Usually, the TLD is used as a water storage tank preventing the use of a higher-viscosity liquid. Several approaches have been implemented to increase the energy dissipated by the sloshing fluid, including roughness elements (Fujino et al. 1988), surface contaminants (Tamura et al. 1995), wave breaking in shallow water TLDs (Sun et al. 1995), and nets or screens (Welt 1983; Noji et al. 1998; Warnitchai and Pinkaew 1998; Kaneko and Ishikawa 1999). Warnitchai and Pinkaew (1998) developed a mathematical model based on potential flow theory and determined the damping characteristics of poles and wire-mesh screens. In this section, several fluid numerical models of TLDs without/with screens are briefly introduced.

1.5.2.1   TLD Modelling with No Screens

A nonlinear TLD numerical model, based on shallow water wave theory, was developed by Lepelletier and Raichlen (1988). Sun et al. (1992) developed a nonlinear model for a rectangular TLD, which utilized the shallow water wave theory with consideration of wave breaking. Faltinsen et al. (2000) developed a method, which included the coupling of sloshing modes through the nonlinear free surface boundary conditions. Bulian et al. (2010) studied the roll motion response of a single degree of freedom (SDOF) structural system connected to a rigid rectangular partially filled liquid tank. The TLD wave breaking effects on the response curves were characterised by performing tests on liquids of different viscosity and the capabilities of smoothed-particle hydrodynamics (SPH) to treat this coupling problem were assessed. Marsh et al. (2010) demonstrated the stability of the SPH method to numerically model the sloshing dynamics in an egg-shaped shell.

1.5.2.2   TLD Modelling with Screens

The addition of damping screens, installed inside the tank to increase the amount of energy dissipated by the sloshing water motion, was studied (Noji et al. 1998; Fediw et al. 1995; Tait et al. 2005b). A linear fluid model (Fediw et al. 1995) and a nonlinear fluid model (Kaneko and Ishikawa 1999) that simulate the sloshing fluid of a TLD equipped with damping screens are examined by Tait et al. (2005b). In both models, it is assumed that the liquid is inviscid, irrotational and incompressible; the pressure is constant on the free surface; the quiescent water depth is constant; and the tank walls are rigid. In addition, it is assumed that the water depth to tank length ratio (h/L) for a TLD equipped with damping screens, satisfies the shallow water wave theory limitations. The effect of the screens is simulated in both models through a loss coefficient (C_l). Findings from Tait et al. (2005b) indicate that a linear fluid model is capable of providing a first estimate of the energy dissipation characteristics of a TLD. However, a linear model does not provide realistic estimates of the free surface response amplitude. A nonlinear fluid model can accurately describe the free surface motion, the resulting base shear forces and the energy dissipated over a range of excitation amplitudes.

Fediw (1992) and Tait (2004) tested and modelled screens in a TLD showing that their drag characteristics can often be considered independent of the sloshing fluid inside a TLD with wire-mesh and thin-sharp-edged-horizontal-slat screens, respectively. Both studies utilized a linearized velocity loss coefficient. Cassolato (2007) experimentally studied thin sharp-edged-horizontal slat screens held at various fixed angles in a tuned liquid damper. Also, Cassolato (2007) employed two existing formulations of the pressure loss coefficient for inclined screens (C_θ) and developed a new one, using results from the study, to theoretically investigate the effect of fixed inclined damping screens using two linear numerical models. The two linear flow models were based on shallow water wave theory and potential flow theory. The linear model calculations were found to deviate from the experimental test results at high screen inclination values (i.e. $\theta > 45.0°$), as the linear models could not capture the actual response of the nonlinear free-surface elevation (Fediw 1992; Tait 2004; Tait et al. 2004a; Tait et al. 2004b). Love and Tait (2011) developed a nonlinear multimodal model, which describes the sloshing behaviour of a fluid in a flat-bottom tank of arbitrary geometry. In that model, the mode shapes of the sloshing fluid were found by solving the Helmholtz equation over the tank domain using the finite element method,

while the Bateman-Luke variational principle was used to develop a system of ordinary differential equations which account for the coupling of the sloshing modes through the non-linear free surface boundary conditions. Also, damping was incorporated into the model by considering the drag produced on a set of damping screens inserted in the fluid.

1.6. Advantages and Disadvantages of TLCD/TLD

Similar to a TMD system, TLD and TLCD systems can reduce the response of the main system by modifying its frequency response function. In both systems (i.e. TLD and TLCD), the secondary mass is liquid and the damping forces are established through the motion of liquid through viscosity, wave breaking and/or damping screens in the TLD (Kaneko and Ishikawa 1999; Tait et al. 2004a; Tait et al. 2004b; Tait et al. 2005a; Tait et al. 2005b), while the motion of liquid in a U-shape tube container through an orifice in the TLCD (Kareem et al. 1999; Yalla et al. 2001). It has been reported from an investigation on vibration control of a 76-story benchmark building that the performance of a passive TLCD is similar to that of a passive TMD system for (Samali et al. 1998).

Several advantages of using TLCD/TLD have been found over the more popular TMD system. These advantages include low construction costs, installation and maintenance costs, ease of tuning to the desired frequency and ability to apply as a simple retrofitting tool to existing structures, such as in Yokohama marine tower (Tamura et al. 1995). In addition, TLD/TLCD systems can provide dual-function capability to be used as emergency fire water storage. Using a liquid in the TLCD/TLD systems can be effectively mobilized at all levels of structural motion, thereby eliminating the activation required in conventional TMD systems, where a certain level of threshold excitation is required to activate the TMD system.

Bi-directional TLDs, which act as two independent TLDs, can be used to control two vibration modes of the structure in two orthogonal directions, simultaneously (Tait 2004; Tait et al. 2005a; Tait et al. 2008). Circular tanks have been used to mitigate resonant motions in axis-symmetric structures (Tamura et al. 1995). A bi-directional tuned liquid column damper with period adjustment (LCD-PA) was experimentally investigated and installed in a structure (Shimizu and Teramura 1994). Soong and Dargush (1997) indicated that rectangular tanks may be used to mitigate the motions of a structure with different fundamental frequencies in two major directions.

Utilizing TLD devices to suppress bi-directional (2D) resonant structural motions, such as two fundamental sway modes of a structure simultaneously was studied by Tait et al. (2007). The study experimentally examined 2D structure-TLD behavior over a range of excitation amplitude values covering the practical range of serviceability accelerations for buildings subjected to wind loads. Experimental results were used to verify the applicability of a uni-directional structure-TLD numerical model to 2D structure-TLD analysis. Findings indicated that the structure-TLD model was capable of describing the structure-TLD response within the range of system response amplitudes experimentally tested. Also, the study indicated that by choosing the appropriate aspect ratio for the TLD it can be used to reduce structural responses in two modes of vibration simultaneously with no penalty on its performance.

The full scale installation of a bi-directional passive tuned liquid column damper (TLCD) on a 67 m steel communications tower has been reported by Hitchcock et al. (1999). The device did not include an orifice to dissipate energy, as such; it was not possible to control the damping ratio of the TLCD. It was acknowledged that due to the absence of an orifice, the damping ratio of the TLCD was not expected to be the optimum. It was also observed that TLCD did not perform optimally at various wind speeds.

Furthermore, the ability dictate the shape of the TLD tank provides an additional space flexibility feature. In other words, simple TLD tank geometries may not always be feasible due to space limitations. While the non-linear modelling of sloshing fluid was limited to tanks of simple geometries, Love and Tait (2011) developed a non-linear multimodal model, which describes the sloshing behaviour of a fluid in a flat-bottom tank of arbitrary geometry. In addition, TLCD/TLD system parameters can be easily tuned, when there are changes in the dynamic characteristics of the primary structure after construction. Meanwhile, TLCD/TLD systems have some disadvantages due to their nonlinear amplitude dependent response behaviour, and only a portion of the water mass participates, thus a relatively larger space (particularly height) is required to achieve the desired mass ratio compared to a TMD.

The performance of a TLD for a given mass ratio (μ) is a function of the tuning ratio (Ω) and the inherent TLD damping ratio (ζ_{TLD}) (Tait et al. 2004b). The damping ratio of a TLD equipped with fixed vertical damping screens is related to the screen pressure loss coefficient (C_l) and the square of the fluid velocity at the screen location (Tait 2004). Therefore, the

inherent damping ratio that develops due to the screen is amplitude dependent. As a result, a TLD equipped with damping screens may only operate at maximum efficiency at a single excitation amplitude, unless the screen angle is adjusted (Cassolato 2007).

1.7.   Adjustable Inherent Absorber Damping Ratio

The required level of damping can be rapidly achieved and controlled through the damping screen inclination in a TLD system (Cassolato and Tait 2005), or through an orifice in a TLCD system (Yalla et al. 2001) making both systems suitable for semi-active control applications. As a result, a number of studies focused on overcoming limitations of conventional passive TLCD systems have been carried out. Haroun et al. (1994 and 1995) introduced the concept of a hybrid liquid column damper by actively controlling the orifice opening ratio. Yalla et al. (2001) introduced a semi-active TLCD that achieves variable damping by using a controllable valve to adjust the orifice opening. They also studied the effectiveness of different control algorithms for a TLCD for structural control applications. Yalla and Kareem (2003) examined the performance of a prototype semi-active TLCD. In addition, they verified a control strategy, based on gain scheduling, with experimental results. Kim and Adeli (2005) proposed wind-induced motion control of 76-story benchmark building using a hybrid damper-TLCD system. Wang et al. (2005) introduced a semi-active TLCD using magneto-rheological fluid (MR-TLCD) for wind-induced vibration mitigation of tall building structures.

A new type of actively tuned liquid damper to reduce vibrations in large civil structures, which may be induced by earthquake or high winds, was suggested by Lou (1996). The effective length of the liquid damper tank determines the natural frequency of the liquid, and thus the effectiveness of the damper at particular excitation frequencies. The liquid damper was tuned by rotating baffles to regulate the effective length of the damper tank. In addition, a TLD equipped with rotatable baffles (see Figure 1.8) was studied experimentally by Zahrai et al. (2012). The main idea behind the baffles was to compensate the effects of probable mistuning of the TLD. By observing the performance of TLD with baffles, the study investigated the influence of a number of parameters, which included the following: baffle angle, frequency ratio, mass ratio and the effect of probable mistuning by varying the depth of water and orientation of the baffles. Results from the study indicated that the displacement

and acceleration responses of a five story benchmark problem under scaled down earthquakes decreased up to 24.1% and 27.2%, respectively.

Few studies have focused on structural control of tall buildings using semi-active single/multiple TLDs. Thus, it is important to further investigate TLDs with variable damping that can be adjusted through various mechanisms to achieve optimal control performance for a wide range of loading conditions and structural uncertainties in a semi-active mode of control. The ability to passively control the inherent damping ratio of a TLD (ζ_{TLD}) over a range of excitation amplitudes was first introduced theoretically in Cassolato and Tait (2005). The modification of ζ_{TLD} by adjusting the screen angle, which alters the screen loss coefficient (C_θ), has been experimentally investigated (Cassolato 2007; Cassolato et al. 2011). Results indicated that rotating the damping screens inside the TLD to adjust the screen loss coefficient (C_θ) is a plausible method to maintain a constant level of ζ_{TLD} over a range of excitation amplitudes.

Thus, the semi-active TLD operating principle can be achieved through the ability to vary the inclination angle (θ) of adjustable damping screens. A semi-active TLD is a consequence of the fact that the control of the damping screen inclination angle requires a small amount of input energy, as opposed to a fully conventional passive TLD. However, the required amount of energy to change the inclination angle is expected to be small in comparison with the total energy dissipated by the damping screens. In this study, the semi-active TLD is essentially a time-varying damper in which the damper parameter (ζ_{TLD}) is varied with time and requires only a small amount of energy to modulate the damping. In contrast with the fully active TMD control system, it is expected that the semi-active TLD actuator will require very low input power, basic control hardware/software and low construction costs.

1.8.   Full-Scale Damper Applications

1.8.1   Example TMD Applications

The following provides examples of TMD applications. Two TMDs were installed in the 244 m tall Hancock Tower in Boston, NA, USA at opposite ends of the 58th floor to counteract wind-induced torsional motions (Kareem et al. 1999). Each TMD is essentially a steel box filled with lead weighing 300 tons that is activated at 3 milli-g of motion. Another TMD system, consisting of a 410 ton concrete block with two-spring damping mechanisms, was installed in the 278 m high Citicorp Building in New York, NY, USA. One spring-

damping mechanisms was installed for the north-south motion and the other for east-west motion on the 63rd floor (Kareem et al. 1999). The block motion is arrested by 2 pneumatic springs tuned to the natural period of the building. A series of 12 hydraulic pressure-balanced bearings have been used to balance the concrete block. A 40% reduction of the wind-induced response in both directions simultaneously has been achieved (Wiesner 1979). In Canada, the 554 m high CN tower in Toronto, ON (see Figure 1.9) has 20 ton donut-shaped lead pendulum TMDs installed during the construction in 1975 (Kareem et al. 1999). A pendulum-type TMD is utilized in Taipei 101 in Taipei, Taiwan. It consists of a 680 ton steel ball suspended from cables at the 92nd floor and visible from observation decks and a restaurant (see Figure 1.10). It represents the largest anti-sway system in the world (Hadenius 2004). The pendulum-type TMD, which works on the same principle as a typical translational TMD, uses swinging motion to exert its inertial restoring force onto the structure (Gerges and Vickery 2003).

1.8.2   Example HMD/AMD Applications

The hybrid mass damper (HMD) is a common control device employed in full-scale civil engineering applications (Spencer and Nagarajaiah 1999). An HMD is a combination of a passive tuned mass damper (TMD) and an active control actuator. The ability of this device to reduce structural response relies primarily on the natural motion of the TMD. The forces from the control actuator are employed to increase the efficiency of the HMD and to increase its robustness to changes in the dynamic characteristics of the structure. The energy and forces required to operate a typical HMD are far less than those associated with a fully active mass damper system of comparable performance.

An example of such an application is the HMD system installed in the Sendagaya INTES building in Tokyo in 1991 (see Figures 1.11a and 1.11b). The HMD was installed at the 11th floor and consists of two masses to control transverse and torsional motions of the structure, while hydraulic actuators provide the active control capabilities. The top view of the control system is shown in Figure 1.11c, where ice thermal storage tanks are used as mass blocks so that no extra mass was introduced. The masses are supported by multi-stage rubber bearings intended for reducing the control energy consumed in the HMD and for ensuring smooth mass movements (Higashino and Aizawa 1993; Soong et al. 1994).

Variations of such an HMD configuration include multi-step pendulum HMDs (see Figure 1.12b), which have been installed in, for example, the Yokohama Landmark Tower in Yokohama, Japan (see Figure 1.12a) (Yamazaki et al. 1992) and in the TC Tower in Kaohsiung, Taiwan. Additionally, the DUOX HMD system, which consists of a TMD actively controlled by an auxiliary mass, has been installed in the Ando Nishikicho Building in Tokyo (see Figure 1.12c). Design constraints, such as severe space limitations, can prevent the use of an HMD system. Thus, the active mass damper (AMD) system was designed and installed in the Kyobashi Seiwa building in Tokyo and the Nanjing Communication Tower in Nanjing, China (Spencer and Nagarajaiah 2003). The Kyobashi Seiwa building, the first full-scale implementation of active control technology, is an 11-story building with a total floor area of 423 m^2 (see Figure 1.13a). The control system consists of two AMDs where the primary AMD is used for transverse motion and has a weight of 4 tons, while the secondary AMD has a weight of 1 ton and is employed to reduce torsional motion (see Figure 1.13b). The role of the active system is to reduce building vibration under strong winds and moderate earthquake excitations and consequently to increase occupant comfort.

In the case of the Nanjing Communication Tower (See Figure 1.14a), numerous physical constraints had to be accounted for the system design of the mass damper (Spencer and Nagarajaiah 1999). The physical size of the damper was constrained to a ring-shaped floor area with inner and outer radii of 3 m and 6.1 m, respectively. In addition, the damper was by necessity elevated off the floor on steel supports with Teflon bearings to allow free access to the floor area. The final ring design allowed the damper to move ± 750 mm from its rest position. Simulations indicate that this stroke is sufficient to control the tower; however, a greater stroke would allow substantially more improvement in the response. The strength of the observation deck limited the weight of the damper to 60 tons. Lack of sufficient lateral space made the use of mechanical springs impractical for restoring forces. Thus the active control actuators provide restoring force as well as the damping control forces. The final design of the active mass damper is shown in Figure 1.14b, which uses three servo-controlled hydraulic actuators, each with a total stroke of ±1.50 m and a peak control force of 50 kN. These actuators are arranged 120° apart around the circumference of the ring. The actuators control three degrees of freedom: two orthogonal lateral directions of motion and torsional rotation, which is held to zero. Since the frictional force between the Teflon bearings and mass can have a critical influence on the response of the system, a detailed analysis was

performed to verify the system performance in the presence of this friction (Reinhorn et al. 1998).

1.8.3   Example TLCD/TLD Applications

The use of TLCD/TLDs has gradually increased as alternative systems to mitigate structural response since their initial applications in civil engineering in the late 1980s. TLDs were first installed in Japan, where most of the initial research and development initiated (Tamura et al. 1995; Kaneko and Ishikawa1999). Full-scale experiments on the effectiveness of TLDs in buildings under wind excitations have been conducted on four buildings that are frequently referenced as outlined in Tamura et al. 1995. Multi cylindrical TLDs were installed in all four structures: the Nagasaki Airport Tower, the Yokohama Marine Tower, the Shin-Yokohama Prince Hotel (SYPH) and the Tokyo International Airport Tower. A TLD system consists of a multi-layer stack of 9 circular containers each 2 m in diameter and 22 cm high, yielding to a total height of 2 m was installed in the SYPH (see Figure 1.15). As a result, the root-mean-square (RMS) accelerations in each direction were reduced in the range between 50% and 70% at wind speeds over 20 m/s. Extra reduction was achieved at higher wind speeds when TLDs achieving their optimal damping (Tamura et al. 1995).

Two more recent applications of TLD and TLCD that have been installed in Canada are One King West in Toronto, ON and One Wall Centre in Vancouver, BC (see Figure 1.16). One King West in Toronto has a height of 176 m and a slenderness ratio of 1:11 (SkyscraperPage.com). Two insulated rectangular concrete TLDs equipped with damping screens were installed on the fifty first floor on each side of the building. The 12x9x2 size tanks were divided into 5 chambers by cross-walls causing predominate water flow in the East-West direction, which is the critical direction for the One King West (Discovery 2005). One Wall Centre is the tallest building in Vancouver with a 150 m high, a 21.3 m wide elliptical footprint and 7:1 slenderness ratio. Two TLCDs were installed that consist of a 4-story high, 189000 Liter U-shaped water tank oriented across the narrow aspect of the building. An estimated $2M in construction costs were saved compared to alternative conventional damping systems. Additional overall cost savings were achieved by using water in TLCD tanks to meet fire suppression water storage requirements (Motioneering 2004). This solution was the first of its kind and size in the world.

1.9.   Impetus of Study

i. The resonant vibration motion of tall buildings due to dynamic loadings, such as wind and earthquake, can be reduced by adding passive dynamic vibration absorbers (DVAs). The inertia forces, which develop from the DVA motion, modify the frequency response of the primary structure's mode to which the DVA is tuned. A single sway mode of vibration is usually considered, however, for certain structures, multiple modes may need to be suppressed. In addition, the location of the TLD on the floor plate is important for certain modes, such as the torsional mode. Adding TLDs to suppress modes of interest may lead to the excitation of higher structural modes. These are important issues to be investigated using the proposed three dimensional finite element model, which considers exact locations of TLDs, multiple building modes of vibration and distribution of load over the entire building width and height.

ii. Full-scale implementation of active control systems have been realized in several structures, mainly in Japan; however, cost effectiveness and reliability considerations have limited their wide spread acceptance (Spencer and Nagarajaiah 2003). Thus, there is a growing need for innovative and effective techniques to reduce the vibration responses of increasingly taller, lighter, and more flexible buildings. Because of their mechanical simplicity, low power requirements, and large controllable force capacity, semi-active control systems provide an attractive alternative to active and hybrid control systems for structural vibration reduction. The implementation of passive TLDs in real buildings has shown the benefits and effectiveness of using this cost effective control system. Therefore, developing a novel semi-active TLD control system is of significant interest. In addition, implementing the novel semi-active TLD control technique in the proposed three dimensional finite element model will provide an important tool to build better performing and more economical high-rise buildings.

1.10.   Research Objectives

The main objectives of this research are:

i. Develop and validate a three dimensional finite element structure-tuned liquid damper system model (3D-Structure-TLD) employing two nonlinear TLD models. The first, a

nonlinear TLD fluid model; and the second, an equivalent amplitude dependent TMD model.

ii. Expand the 3D-Structure-TLD system model to a multiple TLD system model (3D-Structure-MTLD) and employ it to evaluate the dynamic response of an actual multi-modal high-rise building utilizing wind tunnel loading data with TLDs to suppress the first two and the first three modes of vibration, respectively.

iii. Update and validate the nonlinear TLD fluid model to simulate TLDs equipped with inclined damping screens.

iv. Investigate the performance of an actual multi-modal high-rise building with TLDs equipped with inclined damping screens over a wide range of return period wind speeds from 1 month to 50 years.

v. Develop and validate a novel semi-active TLD control technique based on a gain scheduling scheme and implement the novel control technique in a three dimensional finite element model (3D-Structure-SA-TLD).

vi. Expand the novel control technique to semi-active multiple TLD system model (3D-Structure-SA-MTLD) for multi-modal high-rise building applications.

vii. Investigate the applicability of utilizing the semi-active multiple TLD control technique to enhance structural responses of an actual multi-modal high-rise building subjected to wind tunnel loading data at:

  a. Different loading directions from 0° to 360°.
  b. Different loading return period wind speeds from 1 month to 50 years.

1.11. Organization of Thesis

This thesis uses the Integrated-Article format. As a result, each chapter includes its own bibliography. As the chapters are discrete but related, overlaps occur in the introduction of each of the chapters, allowing the chapters to become stand-alone documents.

Chapter 2 presents a three dimensional finite element model capable of simulating the behaviour of a 3D structure, using 3D beam elements under a source of dynamic loading (i.e. wind or earthquake). The finite element model is used to estimate the response of a structure outfitted with TLDs (3D-Structure-TLD). The base shear force resulting from the TLD is estimated using two nonlinear TLD models; a nonlinear TLD fluid model that simulates the TLD sloshing force and an equivalent amplitude dependent TMD model. Numerical

simulations from the finite element model utilizing both nonlinear TLD models are compared to shake table experimental results found in the literature.

Chapter 3 presents a full dynamic analysis of an actual 38-story high-rise building (Indianapolis building) equipped with TLDs to suppress the first two and the first three modes of vibration, respectively, employing the 3D finite element structure-multiple tuned liquid damper system model (3D-Structure-MTLD). A total of 36 numerical simulations utilizing different wind tunnel loading directions in the range between 0° and 360° are conducted.

Chapter 4 describes the steps employed to update the nonlinear TLD fluid model to simulate TLDs fitted with inclined damping screens and compares the numerical simulation of the updated model with experimental results found in the literature. The updated nonlinear TLD fluid model is implemented in the 3D finite element model, developed in Chapter 2, and employed to examine the enhanced efficiency of a TLD fitted with inclined damping screens utilizing a 3D single-story structure. Full dynamic analysis is conducted utilizing the updated numerical simulation to investigate the behaviour of an actual 38-story high-rise building equipped with TLDs fitted with inclined damping screens to suppress the first three modes of vibration over a wide range of return period wind speeds between 1 month and 50 years.

Chapter 5 presents the steps followed to develop and validate a novel semi-active TLD control system based on a gain scheduling scheme (3D-Structure-SA-TLD). The goal of this semi-active system is to achieve optimal passive performance over a range of excitation amplitudes and wind angles. The semi-active TLD control technique is implemented in the 3D finite element model, developed in Chapter 2, and employed to conduct a performance comparison between the conventional passive and semi-active TLD control systems utilizing a 3D single-story structure.

Chapter 6 describes the steps followed to expand the novel semi-active TLD control system (3D-Structure-SA-TLD) to a semi-active multiple TLD control system (3D-Structure-SA-MTLD). The expanded control system is subsequently implemented in a three dimensional finite element model developed in Chapter 2. A full dynamic analysis is conducted to investigate the applicability of utilizing the expanded semi-active multiple TLD control technique to enhance structural responses of an actual 38-story multi-modal high-rise building subjected to wind tunnel loading data at different directions in the range between 0°

and 360° and at different return period wind speeds in the range between 1 month and 50 years.

Chapter 7 reviews and discusses some of the important research contributions and conclusions drawn from the presented research and highlights areas of future work.

1.12.   References

Abé, M. and Igusa, T. (1996). "Semi-Active Dynamic Vibration Absorbers for Controlling Transient Response", *Journal of Sound and Vibration*, 198(5), 547-569.

Breukelman, B. and Haskett, T. (2001). "Good Vibrations", *Civil Engineering: the Magazine of the American Society of Civil Engineers*, 71(12), 54-59.

Bulian, G., Souto-Iglesias, A., Delorme, L. and Botia-Vera, E. (2010). "SPH Simulation of a Tuned Liquid Damper with Angular Motion", *Journal of Hydraulic Research*, 48, 28-39.

Carrier, G.F., and Miles, J.W. (1960). "On the Annular Damper for a Freely Processing Gyroscope", *Journal of Applied Mechanics*, 27, 237-240.

Cassolato, M. and Tait, M. (2005). "A Preliminary Study of a Tuned Liquid Damper with Smart Screens", *Proceeding of the 1st Canadian Conference on Effective Design of Structures*, McMaster University, Hamilton, ON, Canada, 960-971.

Cassolato, M. R. (2007). "*The Performance of a Tuned Liquid Damper Equipped with Inclined and Oscillating Damping Screens*", M.E.Sc. Thesis, McMaster University, Hamilton, Canada.

Cassolato, M. R., Love, J. S. and Tait, M. J. (2011). "Modelling of a Tuned Liquid Damper with Inclined Damping Screens", *Structural Control and Health Monitoring*, 18(6), 674-681.

Chey, M. H., Chase, G., Mander, J. and Carr, A. (2010). "Semi-Active Tuned Mass Damper Building Systems: Design", *Earthquake Engineering and Structural Dynamics*, 39, 119-139.

Den Hartog, J. P. (1985). "*Mechanical Vibrations*". Dover Publications, Inc.: New York, NY, USA, (republication of 4th edition, 1956).

Discovery Channel Canada (2005), "Skinny Skyscraper".

<http://www.exn.calnews/video/exn2005/11129/exn20051129-

skyscraper.asx> (online - streaming video).

Fujino, Y., Pacheco, B. M., Chaiseri, P., and Sun, L. M. (1988). "Parametric Studies on Tuned Liquid Damper (TLD) Using Circular Containers by Free-Oscillation

Experiments", *Journal of Structural Engineering and Earthquake Engineering*, 5(2), 381–391.

Gerges, R. R. and Vickery, B. J. (2003). "Wind Tunnel Study of the Across-Wind Response of a Slender Tower with a Nonlinear Tuned Mass Damper", *Journal of Wind Engineering and Industrial Aerodynamics*, 91, 1069-1092.

Graham, E. W. and Rodriguez, A. M. (1952), "The Characteristics of Fuel Motion Which Affect Airplane Dynamics", *Journal of Applied Mechanics*, 19(3), 381-388.

Hadenius, P. (2004). "The World's Tallest Buildings", Technology Review Magazine, July/August Edition, 51-54.

Haroun, M. A., Pires, J. A. and Won, A. (l994). "Active Orifice Control in Hybrid Liquid Column Dampers", *Proceeding of the First World Conference on Structural Control*, Los Angeles, CA, USA, FA1, 69-78.

Haroun, M. A., Pires J. A. and Won, A. Y. J. (1995). "Effectiveness of Hybrid Liquid Column Dampers for Suppressing Structural Vibrations", *Proceedings of the 13th International Modal Analysis Conference*, Nashville, Tennessee, 1, 525–531.

Hazra, B., Sadhu, A., Lourenco, R. and Narasimhan, S. (2010). "Re-tuning Tuned Mass Dampers using Ambient Vibration Measurements" *Smart Materials and Structures*, 19(11), 115002.

Higashino, M. and Aizawa, S. (1993). "*Application of Active Mass Damper System in Actual Buildings*", Housner, G. W. and Masri, S. F. (eds), *Proceeding of the International Workshop on Structural Control*, Los Angeles, CA, USA, 194-205.

Hitchcock, P. A, Glanville, M. J, Kwok, K. C. S, Watkins, R. D. and Samali, B. (1999). "Damping Properties and Wind-Induced Response of a Steel Frame Tower Fitted with Liquid Column Vibration Absorbers", *Journal of Wind Engineering and Industrial Aerodynamics*, 83(1-3), 183-196.

Housner, G. W., Soong, T. T. and Masri, S. F. (1996). "Second Generation of Active Structural Control in Civil Engineering", *Microcomputers in Civil Engineering*, 11, 289-296.

Housner, G. W., Bergman, L. A., Caughey, T. K., Chassiakos, A. G., Claus, R. O., Masri, S. F., Skelton, R. E., Soong, T. T., Spencer, B. F. and Yao, J. T. P. (1997) "Structural Control: Past, Present, and Future", *Journal of Engineering Mechanics*, 123 (9), 897-971.

Hrovat, D. and Margolis, D. L. (1981). "An experimental Comparison between Semi-Active and Passive Suspension for Air Cushion Vehicles", *International Journal of Vehicle Design*, 2(3), 308-321.

Hrovat, D., Barak, P. and Rabins, M. (1983). "Semi-Active Versus Passive or Active Tuned Mass Dampers for Structural Control", *Journal of Engineering Mechanics*, 109(3), 691-705.

Kaneko, S., and Ishikawa, M. (1999). "Modeling of Tuned Liquid Damper with Submerged Nets", *Journal of Pressure Vessel Technology*, 121(3), 334–343.

Kareem, A. (1983), "Mitigation of Wind Induced Motion of Tall Buildings", *Journal of Wind Engineering and Industrial Aerodynamics*, 11(1-3), 273-284.

Kareem, A. and Sun, W. J. (1987). "Stochastic Response of Structures with Fluid Containing Appendages", *Journal of Sound and Vibration*, 119(3), 389–408.

Kareem, A. (1994). "The Next Generation of Tuned Liquid Dampers", *Proceeding of the 1st World Conference on Structural Control*, Los Angeles, FP5-19-FP5-28.

Kareem, A. and Kline, S. (1995). "Performance of Multiple Mass Dampers under Random Loading", *Journal of Structural Engineering*, 121(2), 348-361.

Kareem, A., Kijewski, T. and Tamura, Y. (1999). "Mitigation of Motions of Tall Buildings with Specific Examples of Recent Application", *Wind and Structures*, 2(3), 201-251.

Kim, H. and Adeli, H. (2005a). "Hybrid Conrol of Smart Strucutres using a Novel Wavelet-Based Algorithm", *Computer Aided Civil and Infrastrucutre Engineering*, 20(1), 7-22.

Kim, H. and Adeli, H. (2005b). "Wind-Induced Motion Control of 76-Story Benchmark Building Using the Hybrid Damper-TLCD System", *Journal of Structural Engineering*, 131(12), 1794-1802.

Kitagawa, Y. and Midorikawa, M. (1998). "Seismic Isolation and Passive Response-Control Building in Japan", *Smart Materials and Structures*, 7, 581-587.

Kwok, K. C. S. (1984). "Damping Increase in Building with Tuned Mass Damper", *Journal of Engineering Mechanics*, 110, 1645-1709.

Kwok, K. C. S. and Samali B. (1995). "Performance of Tuned Mass Dampers under Wind Loads", *Engineering Structures*, 17(9), 655-667.

Lou, J. Y. K. (1996). "*Actively Tuned Liquid Damper*", United States Patent, Patent Number: 5,560,161- Patent Date: Oct. 1, 1996.

Love, J. S., Tait, M. J. and Toopchi-Nezhad, H. (2011). "A Hybrid Structural Control System Using a Tuned Liquid Damper to Reduce the Wind Induced Motion of a Base Isolated Structure", *Engineering Structures*, 33, 738-746.

Love, J. S., Tait, M. J. (2011). "Non-linear Multimodal Model for Tuned Liquid Dampers of Arbitrary Tank Geometry", *International Journal of Non-Linear Mechanics*, 46, 1065-1075.

Lepelletier, T. G. and Raichlen, F. (1988). "Nonlinear Oscillations in Rectangular Tanks", *Journal of Engineering Mechanics*, 114(1), 1–23.

Manwell, J.F., McGowan, J.G. and Rogers, A.L. (2010). "*Wind Energy Explained: Theory, Design and Application*", Wiley, Chichester, England.

Margolis, D., Tylee, J. L. and Hrovat, D. (1975). "Heave Mode Dynamics of a Tracked Air Cushion Vehicle with Semi-Active Airbag Secondary Suspension", *Journal of Dynamic Systems, Measurement and Control*, 79(4), 339-407.

Marsh, A.P., Parkash, M., Semercigil, S.E. and Turan, Ö.F. (2010). "Energy Dissipation Through Sloshing in An Egg-Shaped Shell", *Proceeding of the 17th Australian Fluid Mechanics Conference*, Auckland, New Zealand.

McNamara, R. J. (1977). "Tuned Mass Dampers for building", *Journal of Structural Division*, 103, 1785-1798.

Motioneering (2004). <http://www.motioneering.calUser/Doc/pp_wall_centre.pdf> (online) Project Brochure.

Miles, J.W. (1967). "Surface Wave Damping in Closed Basins", *Proceedings of the Royal Society of London. Series A, Mathematical and Physical Sciences*, 297(1451): 459-475.

Noji, T., Yoshida, H., Tatsumi, E., Kosaka, H., and Hagiuda, H. (1998). "Study on Vibration Control Damper Utilizing Sloshing of Water", *Wind Engineering*, 37, 557–566.

Faltinsen, O.M., Rognebakke, O.F, Lukovsky, .I.A., and A.N. Timokha. (2000). "Multidimensional Modal Analysis of Nonlinear Sloshing in a Rectangular Tank with Finite Water Depth", *Journal of Fluid Mechanics*, 407, 201–234.

Reinhorn, A. M., Soong, T. T., Helgeson, R. J., Riley, M. A. and Cao, H. (1998). "Analysis, Design and Implementation of an Active Mass Damper for a Communication Tower", *Proceeding of the 2nd World Conference on Structural Control*, Kyoto, Japan, 3, 1727-1736.

Roffel, A., Lourenco, R., Narasimhan, S. and Yarusevych, S. (2011). "Adaptive Compensation for Detuning in Pendulum Tuned Mass Dampers" *ASCE Journal of Structural Engineering*, 137(2), 242-251.

Sakai, F., Takaeda, S. and Tamaki, T. (1989). "Tuned Liquid Column Damper-New Type Device for Suppression of Building Vibrations", *Proceeding of the International Conference on High-Rise Buildings*, Nanjing, China, 926-931.

Samail, B., Kwok, K. and Gao, H. (1998). "Wind Induced Motion Control of a 76 Storey Building By Liquid Dampers", *Proceeding of the 2nd World Conference on Structural Control*, Volume 2, Wiley, New York, 1473-1480.

Shimizu, K., and Teramura, A. (1994). "Development of Vibration Control System Using U-Shaped Water Tank" *Proceeding of the 1st International Workshop and Seminar on Behavior of Steel Structures in Seismic Areas*, Timisoara, Romania, 25–34.

Soong, T. T. (1988). "State-of-the-Art Review: Active Control in Civil Engineering", *Engineering Structures*, 10, 74-84.

Soong, T. T., Reinhorn, A. M., Aizawa, S. and Higashino, M. (1994). "Recent Structural Applications of Active Control Technology", *Journal of Structural Control*, 1(2), 5-21.

Soong, T. T., and Dargush, G. F. (1997). "*Passive Energy Dissipation Systems in Structural Engineering*", John Wiley and Sons, New York, NY, USA.

Soong, T. T. and Spencer, B. F. Jr. (2002). "Supplemental Energy Dissipation: State-of-the-Art and State-of-the-Practice", *Engineering Structures*, 24, 243-259.

Spencer, B. F. Jr. and Soong, T. T. (1999). "New Applications and Development of Active, Semi-Active and Hybrid Control Techniques for Seismic and Non-Seismic Vibration in the USA", *Proceeding of International Post-SMiRT Conference Seminar on Seismic Isolation, Passive Energy Dissipation and Active Control Vibration of Structures*, Cheju, Korea.

Spencer, B. F. Jr. and Nagarajaiah, S. (2003). "State of the Art Structural Control", *Journal of Structural Engineering*, 129(7), 845-856.

Suhardjo, J., Spencer, B. F. Jr. and Sain, M. K. (1990). "Feedback-Feedforward Control of Structures under Seismic Excitation", *Structural Safety*, 8(1-4), 69-89.

Sun, L. M., Fujino, Y. and Koga, K. (1995). "A Model of Tuned Liquid Damper for Suppressing Pitching Motion of Structures", *Earthquake of Engineering and Structure Dynamics*, 24, 625-636.

Tait, M. J. (2004). "*The Performance of 1-D and 2-D Tuned Liquid Dampers*", Ph.D. Thesis, The University of Western Ontario, London, Canada.

Tait, M. J., E1 Damatty, A. A. and Isyumov, N. (2004a). "Testing of Tuned Liquid Damper with Screens and Development of Equivalent TMD Model", *Wind and Structures*, 7(4), 215–234.

Tait, M. J., Isyumov, N., and E1 Damatty, A. A. (2004b). "The Efficiency and Robustness of a Unidirectional Tuned Liquid Damper and Modelling with an Equivalent TMD", *Wind and Structures*, 7(4), 235–250.

Tait, M. J., El Damatty, A. A., and Isyumov, N. (2005a). "An Investigation of Tuned Liquid Dampers Equipped with Damping Screens Subjected to 2D Excitation", *Earthquake Engineering and Structural Dynamics*, 34(7), 719–735.

Tait, M. J., El Damatty, A. A., Isyumov, N. And Siddique, M. R. (2005b). "Numerical Fow Models to Simulate Tuned Liquid Dampers (TLD) with Slat Screens", *Journal of Fluid and Structures*, 20, 1007–1023.

Tait, M.J., Isyumov, N. and E1 Damatty, A.A. (2007). "Effectiveness of a 2D TLD and Its Numerical Modeling", *Journal of Structural Engineering*, 133(2): 251–263.

Tamura, Y., Fujii K., Ohtsuki, T., Wakahara, T. and Kohaska, R. (1995). "Effectivness of Tuned Liquid Dampers under Wind Excitation", Engineering Structures. 17, 609-621.

Tamura, Y and Suganuma, S. (1996). "Evaluation of Amplitude-Dependent Damping and Natural Frequency of Buildings during Strong Winds", *Journal of Wind Engineering and Industrial Aerodynamics*, 59(2-3), 115-130.

Tamura, Y., Kohsaka, R., Nakamura, O., Miyashita, K.-i. and Modi, V. J. (1996). "Wind Induced Responses of an airport Tower-Efficeincy of Tuned Liquid Damper", *Journal of Wind Engineering and Industrial Aerodynamics*, 65(1), 121-131.

van der Tempel, J. 2006. "*Design of Support Structures for Offshore Wind Turbines*", Ph.D. Thesis, Delft University of Technology, Delft, Netherland.

Varadarajan, N. and Nagarajaiah, S. (2004). "Wind Response Control of Building with Variable Stiffness Tuned Mass Damper using Empirical Mode Decomposition/Hilbert Transform", *Journal of Engineering Mechanics*, 130(4), 451-458.

Wakahara, T and Ohyama, T. and Fujii, K. (1992). "Suppression of Wind-Induced Vibration of a Tall Building Using Tuned Liquid Damper", *Journal of Wind Engineering and Industrial Aerodynamics*, 43 (1-3), 1895-1906.

Wang, J. Y., Ni, Y. Q., Ko, J. M. and Spencer, B. F. Jr. (2005). "Magneto-Rheological Tuned Liquid Column Dampers (MR-TLCDs) for Vibration Mitigation of Tall Buildings: Modelling and Analysis of Open-Loop Control", *Computer and Structures*, 83, 2023-2034.

Warnitchai, P. and Pinkaew, T. (1998). "Modeling of Liquid Sloshing in Rectangular Tanks with Flow-Dampening Devices", *Engineering Structures*, 20(7): 593–600.

Welt, F. (1983). "*A Parametric Study of Nutation Dampers*" M.A.Sc. Thesis, University of British Columbia, British Columbia, Canada.

Wiesner, K. B. (1979). "Tuned Mass Dampers to Reduce Building Wind Motion", *Proceedings of the ASCE Convention and Exposition*, Boston, MA, USA, 1-21.

Won, A. Y. J., Pires, J. A. and Haroun, M. A. (1996). "Stochastic Seismic Performance Evaluation of Tuned Liquid Column Dampers", *Earthquake Engineering and Structural Dynamics*, 25(11), 1259-1274.

Yalla, S. K. (2001). "*Liquid Dampers for Mitigation of Structural Response: Theoretical Development and Experimental Validation*", Ph.D. Thesis, University of Notre Dame, Indiana, USA.

Yalla, S. K., Kareem, A. and Kantor, J. C. (2001). "Semi-Active Tuned Liquid Column Dampers for Vibration Control of Structures", *Engineering Structures*, 23, 1496-1479.

Yalla, S. and Kareem, A. (2003). "Semiactive Tuned Liquid Column Dampers: Experimental Study", *Journal of Structural Engineering*, 129(7), 960-971.

Yamazaki, S., Nagata, N., and Abiru, H. (1992). "Tuned Active Dampers Installed in the Minato Mirai (MM) 21 Landmark Tower in Yokohama", *Journal of Wind Engineering and Industrial Aerodynamics*, 43, 1937-1948.

Yu, J. K, Wakahara, T. and Reed, D. A. (1999). "A Non-Linear Numerical Model of the Tuned Liquid Damper", *Earthquake Engineering and Structural Dynamics*, 28, 671-686.

Zahari, S. M., Abbasi, S., Samali, B. and Vrcelj, Z. (2012). "Experimental Investigation of Utilizing TLD with Baffles in a Scaled Down5-Story Benchmark Building", *Journal of Fluid and Structures*, 28: 194–210.

Table 1.1. Structural Response Mitigation Systems (from Soong and Dargush 1997)

Seismic Isolation	Passive Energy Dissipation	Semi-Active and Active Control
Elastomeric Bearings	Metallic Dampers	Active Bracing Systems
	Friction Dampers	Active Mass Dampers
Lead Rubber Bearings	Viscoelastic Dampers	
	Viscous Fluid Dampers	Variable Stiffness or Damping Systems
Sliding Friction Pendulum	Tuned Mass Dampers	
	Tuned Liquid Dampers	Smart Materials
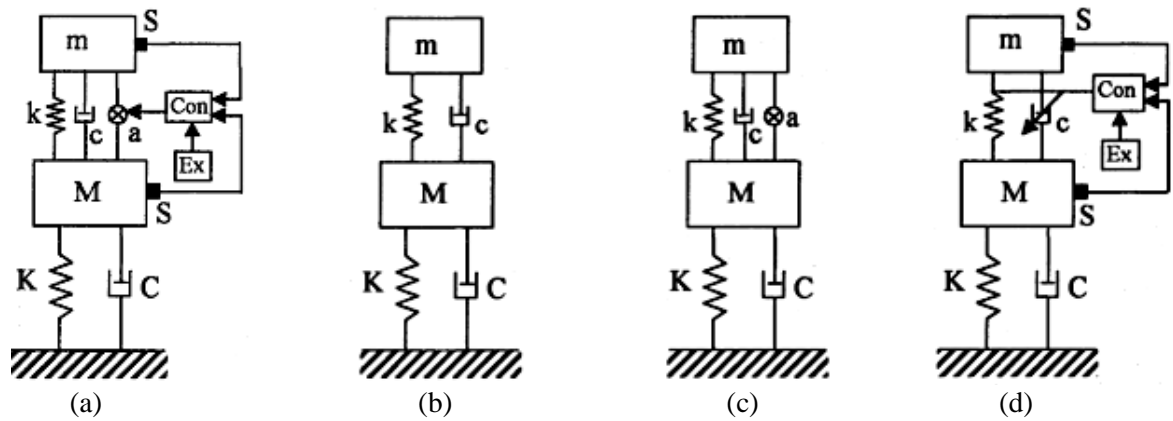
Fig. 1.1. Schematic of Various Control Systems (a: actuator, Con: control, Ex: excitation, S: sensor) (from Kareem et al. 1999)
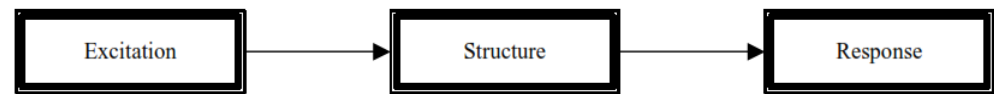
(a) Conventional Structure
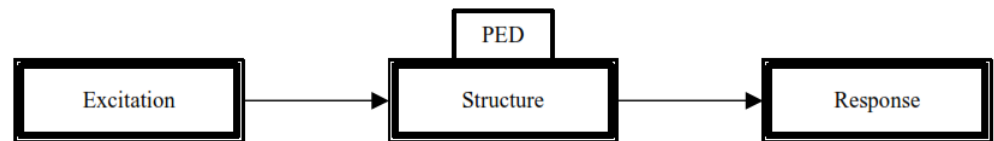
(b) Structure with Passive Energy Dissipation
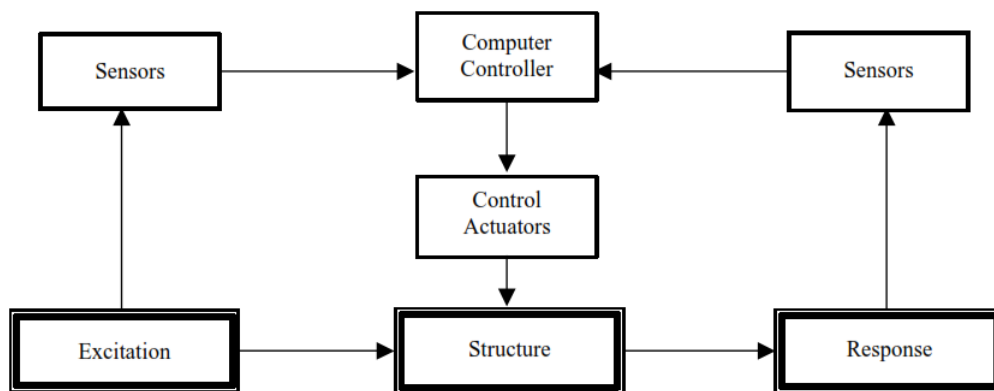
(c) Structure with Active Control

Fig. 1.2. Structures with Various Control Schemes (from Spencer and Soong 1999)

(d) Structure with Hybrid Control

(e) Structures with Semi-Active Control
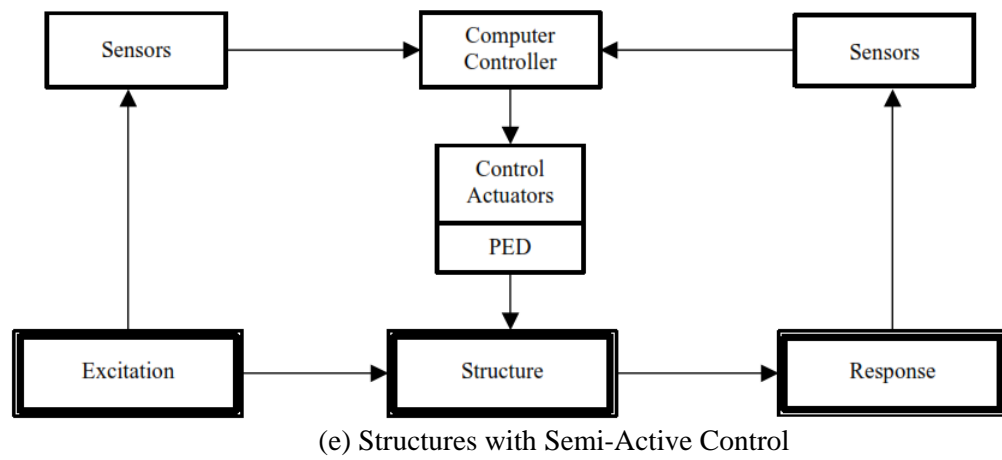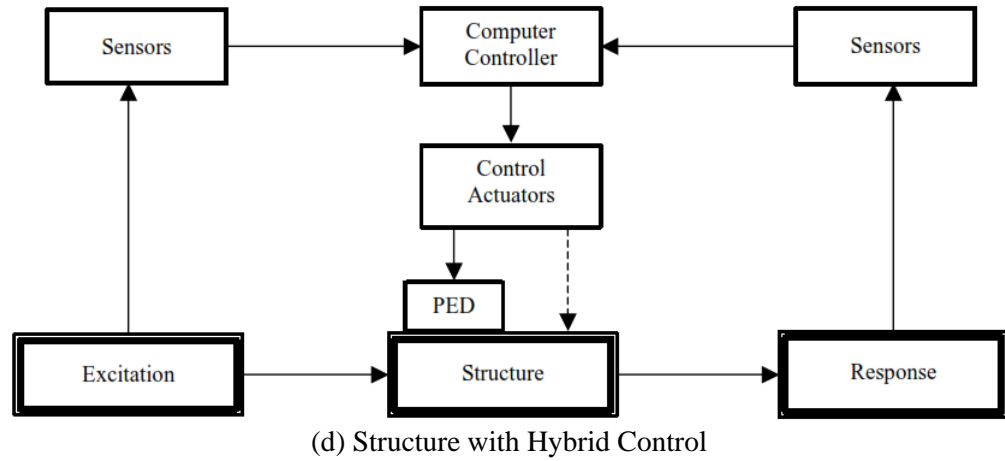
Fig. 1.2.   (cont.)
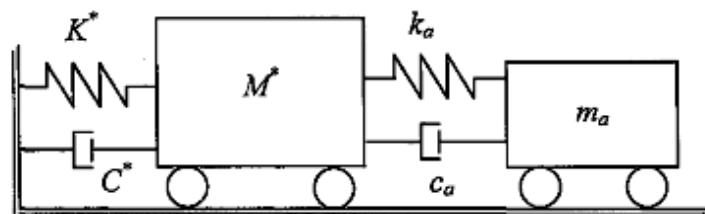
Fig. 1.3.   Theoretical Representation of a Structure-DVA System (form Cassolato 2007)
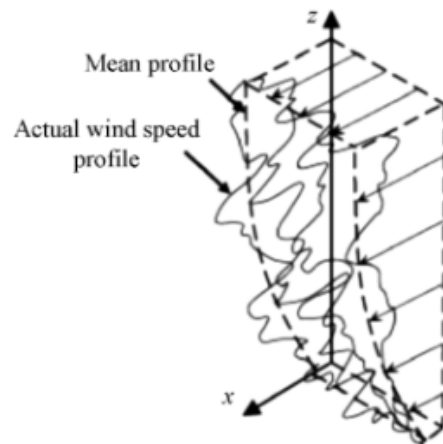
Fig. 1.4. Experimental Speed Profile (from van der Tempel 2006)

(a)   (b)   (c)
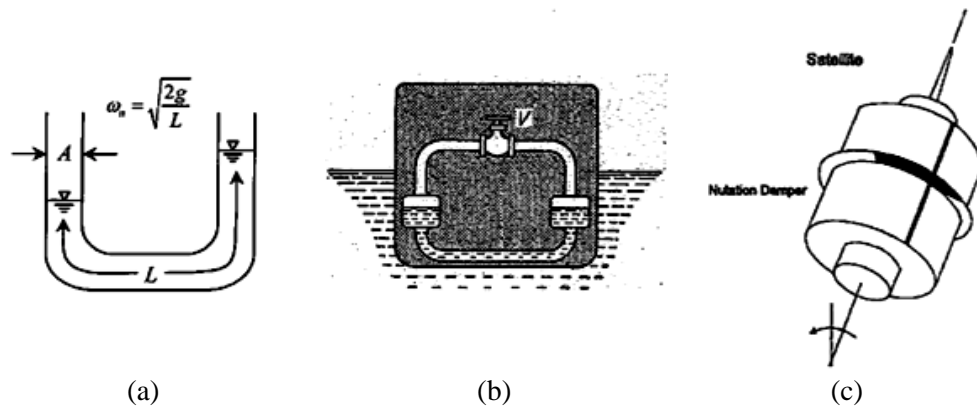
Fig. 1.5. (a) TLCD; (b) Frahm's Anti-Rolling Tank; and (c) Nutation Damper in Satellite (form Cassolato 2007)

(a)   (b)   (c)
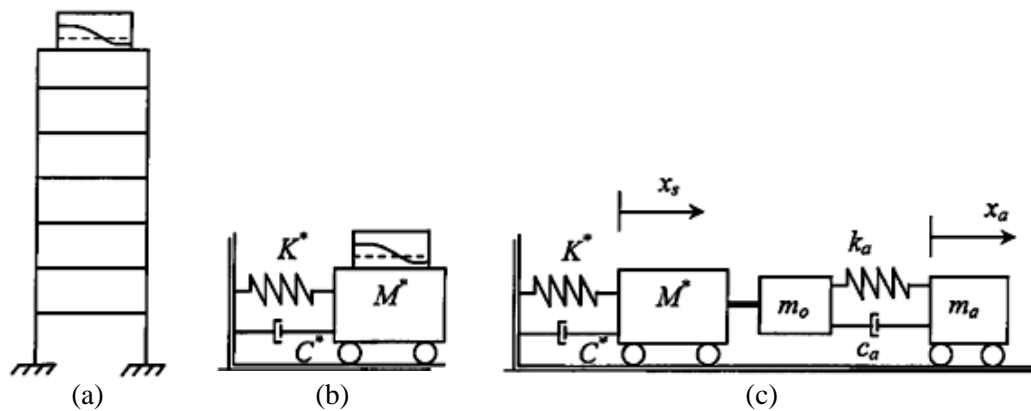
Fig. 1.6. (a) Structure-TLD System; (b) Theoretical Representation; and (c) TMD Analogy (form Cassolato 2007)

(a) Equivalent Linear Model
(Kareem and Sun 1986)

(b) Virtual Mass and Damping
(Sun et al. 1995)

(c) Nonlinear Equivalent TMD
(Yu et al. 1999)

(d) Sloshing-Slamming Model
(Yalla 2001)
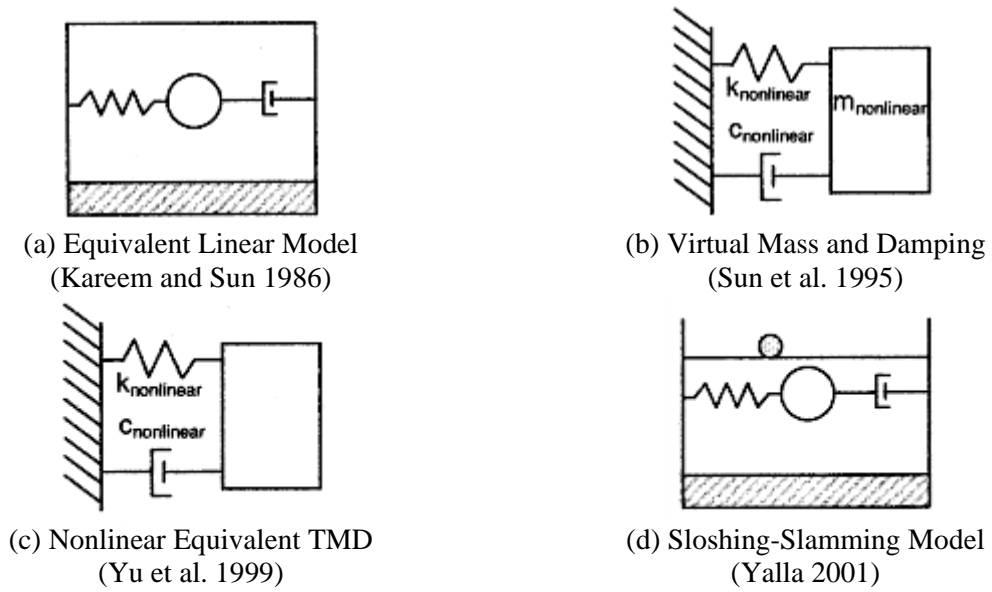
Fig. 1.7. Various Proposed Mechanical Models for Tuned Liquid Damper

(a)

(b)

(c)
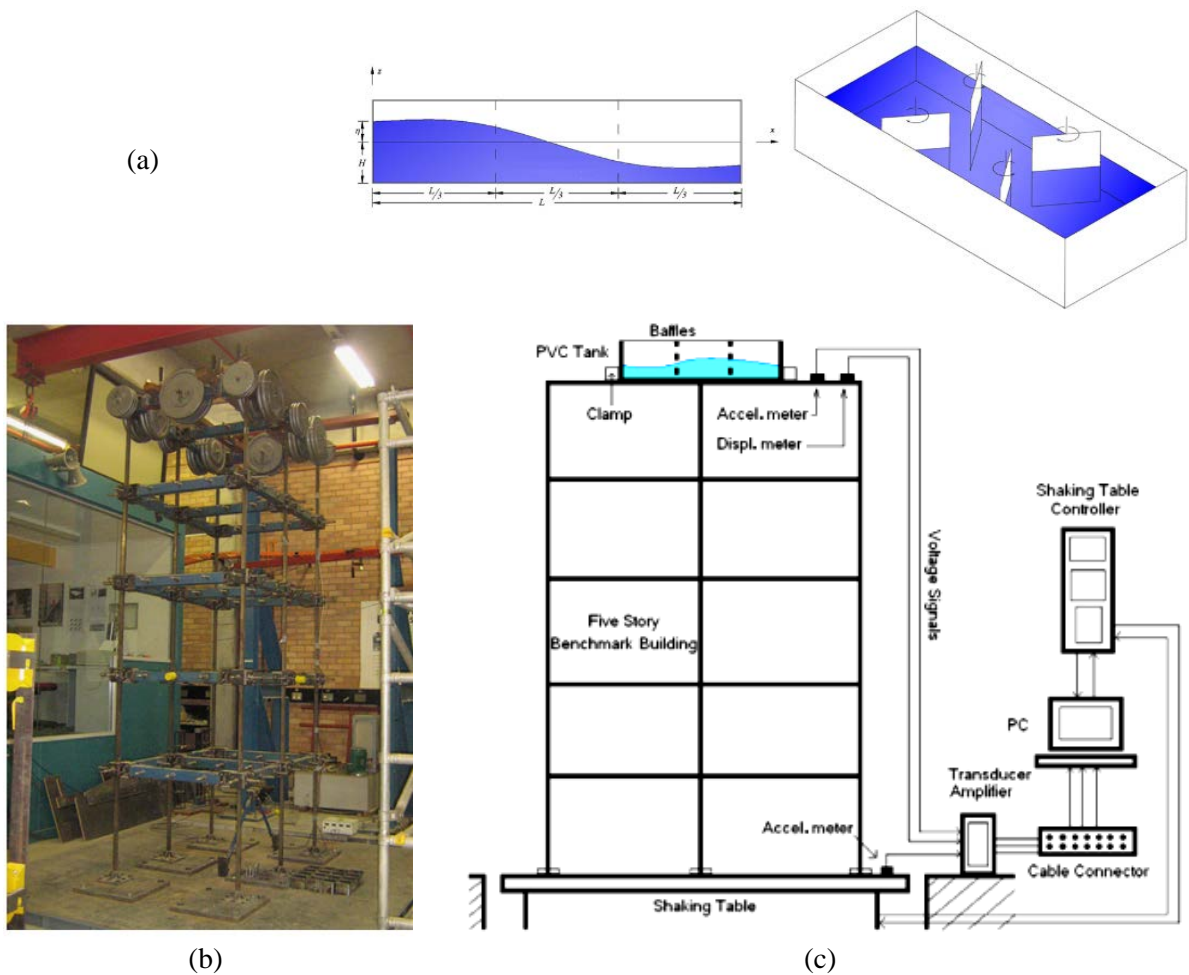
Fig. 1.8. (a) TLD with Standing Rotatable Baffles; (b) Five-Story Building Model Equipped with TLD with Baffles on the Top and Located on the UTS Shaking Table; and (c) Schematic of Experimental Set-up and Instrumentation (from Zahari et al. 2012)
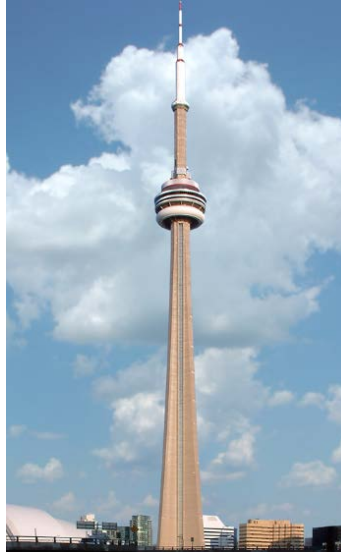
Fig. 1.9. CN Tower, Toronto, Canada

(from http://en.wikipedia.org/wiki/File:Toronto's_CN_Tower)

91st Floor [390.60 m]
(Outdoor Observation Deck)

89th Floor [382.20 m]
(Indoor Observation Deck)

98th Floor

87th Floor
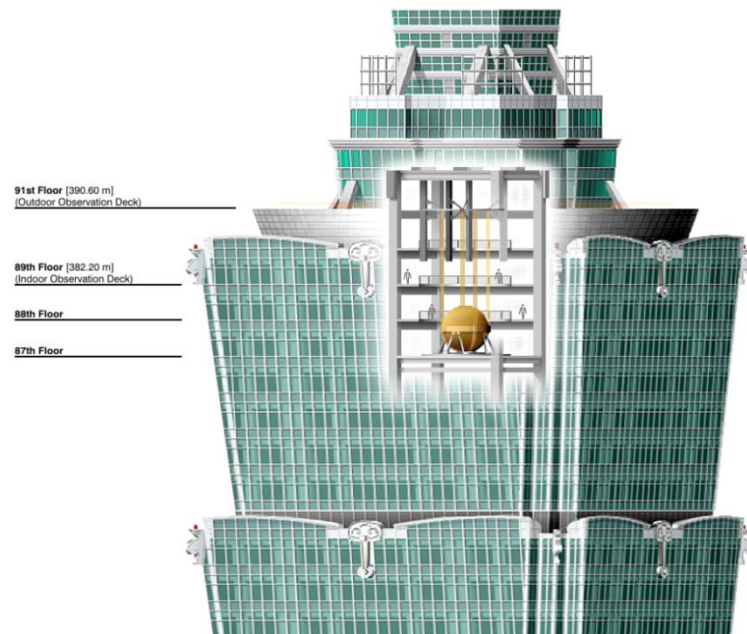
Fig. 1.10. Pendulum-Type TMD Utilized in Taipei 101 in Taipei, Taiwan

(from http://en.wikipedia.org/wiki/File:Taipei_101_Tuned_Mass_Damper)

(a)   (b)

(c)
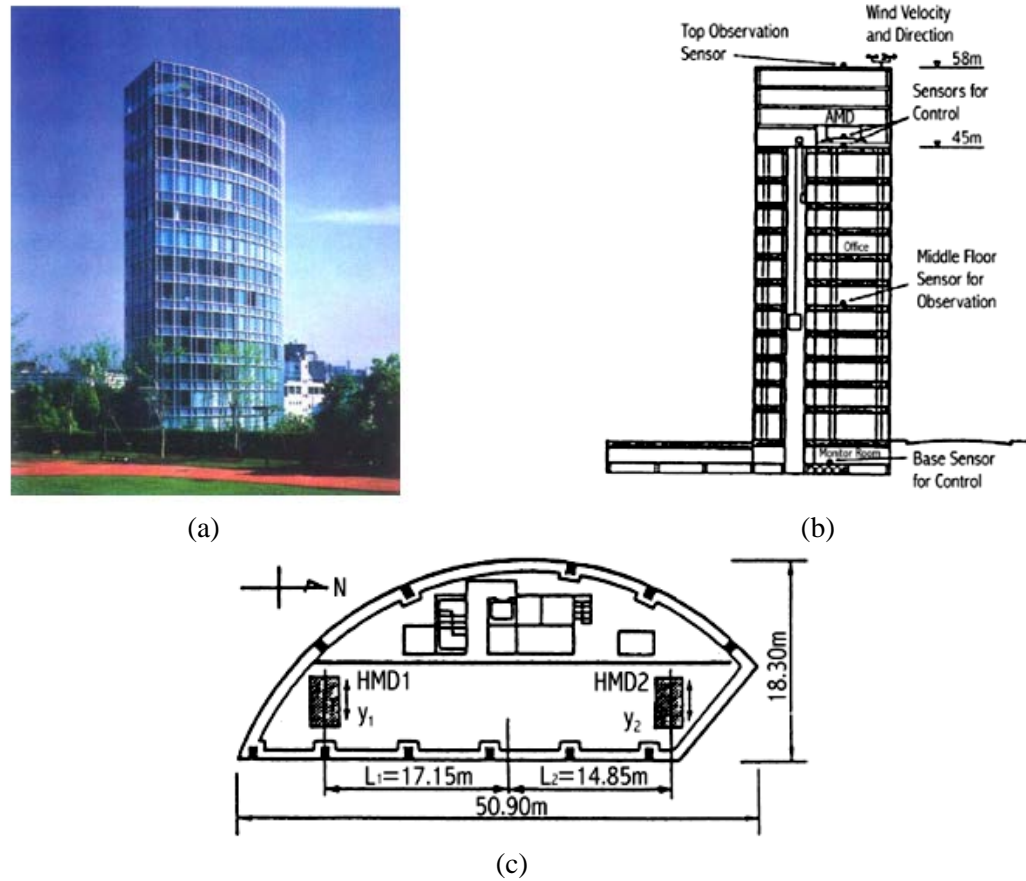
Fig. 1.11. (a) Sendagaya INTES Building; (b) Elevation View; and (c) Top View of the HMD Control System (from Spencer and Nagarajaiah 1999)

(a)   (b)
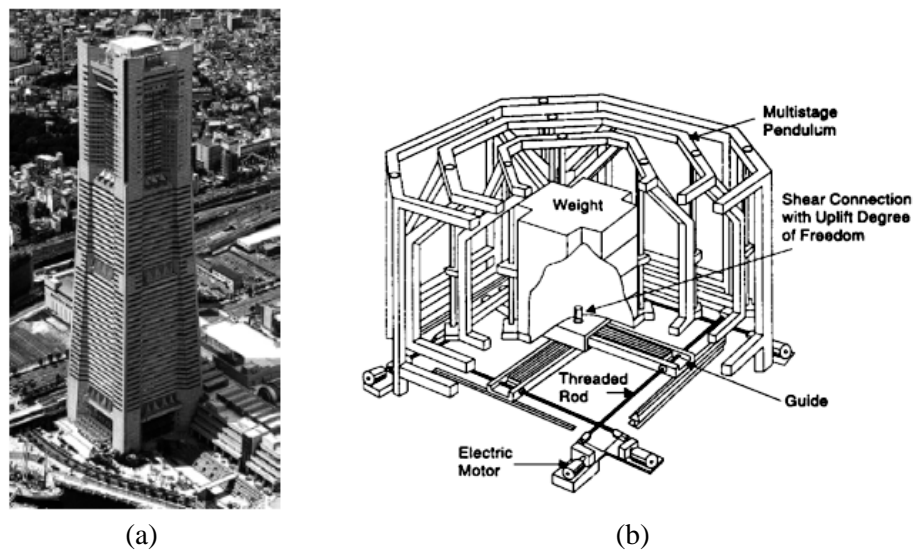
Fig. 1.12. (a) Yokohama Landmark Tower; (b) Schematic View of HMD; and (c) Principle of DUOX System (from Yamazaki et al. 1992)
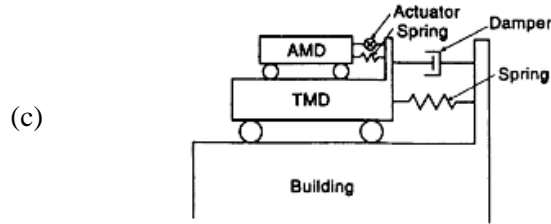
Fig. 1.12. (Cont.)
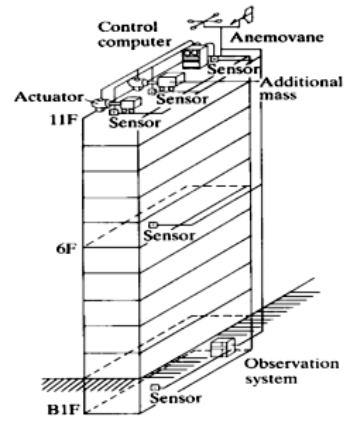
(a)   (b)

Fig. 1.13. (a) Kyobashi Seiwa Building; and (b) Schematic View of AMD Control System (from Spencer and Nagarajaiah 1999)
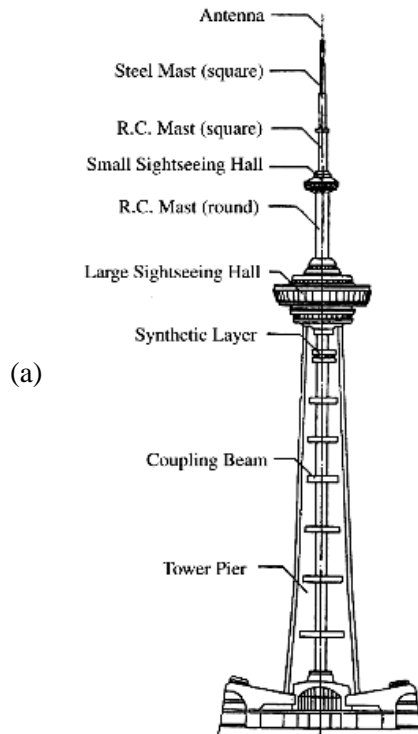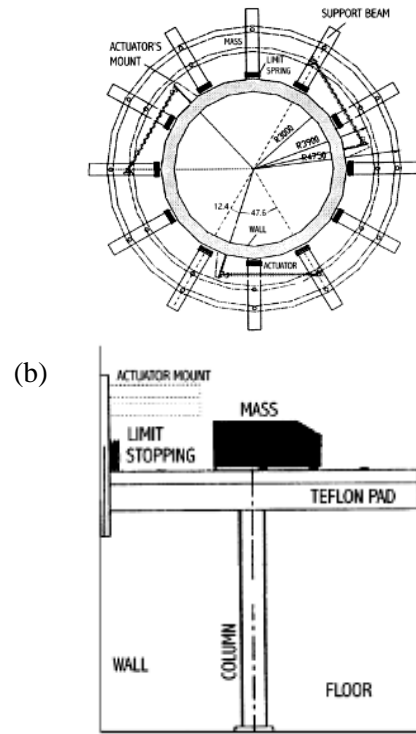
(a)   (b)

Fig. 1.14. Nanjing Communication Tower (a) Elevation View; and (b) AMD Design (from Spencer and Nagarajaiah 1999)

Fig. 1.15. Stacks of Cylindrical-TLD MMDs Installed in SYPH (from Tamura et al. 1995)

(a)   (b)

Fig. 1.16. (a) 1 King West, Toronto, Canada; and (b) 1 Wall Centre, Vancouver, Canada

[(a) from http://www.onekingwest.com/hotel/history/; and (b) from

http://www.affordableapartmentaccommodationsinvancouver.com/WallCentre-1.jpg]

Chapter 2: Development and Validation of Finite Element Structure-Tuned Liquid Damper System Models

2.1. Introduction

Resonant vibration motions in tall buildings due to dynamic loads, including wind and seismic, can be reduced by adding passive dynamic vibration absorbers (DVAs). The inertial forces, which develop from the DVA motion, modify the frequency response of the structure's mode of vibration to which the DVA is tuned to (Kareem et al. 1999). A tuned liquid damper (TLD) is a special type of DVA that consists of a rigid tank that is partially filled with a liquid, usually water. The TLDs are attached to the building at selected locations. The resulting inertia forces, developed from the sloshing liquid inside the tank, improve the dynamic response characteristics of the building. These forces are approximately anti-phase, when tuned properly, to the dynamic forces exciting the structure, thus reducing building motion.

Despite the simplicity of a TLD, its nonlinear dynamic characteristics are challenging to model. In an effort to validate various numerical models and to confirm the applicability of a TLD as DVA, experimental studies have been conducted on TLDs and Structure-TLD systems (Sun et al. 1989; Modi et al. 1990; Sun et al. 1992; Koh et al. 1994; Soong and Dargush 1997; Tait 2004; Tait et al. 2008). In addition to comprising of simple components, the TLD has a number of other advantages over the more traditional tuned mass damper (TMD). These include operation under small and large amplitude vibrations, ease of tuning, low probability of failure and relatively low manufacturing, installation and maintenance costs.

Typically a single sway mode of vibration is usually considered, however, multiple modes may need to be suppressed in a structure. In addition, a mode could be three dimensional in nature, such as a coupled sway-torsional mode, thus the location of a TLD on the floor plate is important parameter. Tait et al. (2005a) presented an example case where the dynamic response of a structure corresponding to two fundamental perpendicular sway modes is to be suppressed (see Figure 2.1a). Figure 2.1b shows where the dynamic response of the structure's torsional mode is to be suppressed. Finally, the case where the tanks are designed and arranged to suppress both a sway mode and a torsional mode is shown in Figure 2.1(c).

Finite element (FE) modelling can be efficiently employed to investigate structures where structural irregularities exist, torsionally sensitive structures (eccentric structures), or when the applied excitation results in torsional loading on the structure. Adding TLDs to suppress certain targeted modes may lead to the unexpected excitation of higher structural modes resulting in greater than anticipated structural dynamic response values. This has been observed to occur for the case of structures subjected to base excitation. The above cases can be investigated using the proposed finite element model, which considers distribution of load over the building's width and height. Furthermore, TLD placement and detailed modelling of the structural system and resulting induced force effects can be carried out.

In addition to reducing the response to an acceptable serviceability level using a TLD system, Ross (2009) demonstrated that the reduction in wind induced force effects experienced by a building led to a 16.9% reduction in the cost of steel reinforcement in the concrete shear walls. The structure-TLD system was modelled using generalized properties permitting the structure-TLD system to be represented by a two degree of freedom model (see Figure 2.2). Consequently, an accurate prediction of the straining actions in the vertical elements of the structure (normal force, shear force and bending moment), particularly the lateral load resisting system was not determined. However, these force effects, which must be evaluated for design purposes, can be determined using the finite element model outlined in this chapter.

In the proposed finite element model, the tanks can be placed at any location on the structure allowing the most effective positions in reducing the structure's dynamic response to be determined. This is particularly useful for situations where limited floor space is available for the tanks. The finite element model can be used to predict the response of a three dimensional structure (high-rise building, bridge, tower, etc.) fitted with multiple TLDs under a predetermined source of dynamic excitation (wind or earthquake) by considering the combined response from multiple modes. This type of three dimensional numerical analysis is recommended for torsionally sensitive structures (eccentric/irregular structures). In addition, three dimensional analysis of a structure fitted with TLD(s) and subjected to wind loads from different angles permits the response at any wind angle to be evaluated. To the best of the author's knowledge, no previous study has considered the simulation of a 3D-

Structure-TLD system model taking into account the response of higher modes using wind tunnel loading data.

The focus of this study is to investigate the response behaviour of three dimensional structures fitted with TLDs. The TLD base shear force is evaluated using two different numerical models. The first is a nonlinear fluid model of a TLD equipped with damping screens developed by Kaneko and Ishikawa (1999) and assessed by Tait et al. (2005b); and the second is an equivalent amplitude dependent tuned mass damper (EADTMD) model (Tait et al. 2004a; Tait et al. 2004b).

In this chapter, the development and validation of a finite element model, consisting of three dimensional beam elements (frame elements), capable of simulating the response of a three dimensional structure both with TLDs and without TLDs under dynamic excitation is presented. Two different nonlinear numerical models are used to evaluate the TLD base shear force and both are implemented into the finite element model. A full dynamic analysis of the coupled 3D-Structure-TLD system is carried out utilizing the two proposed TLD models. Results of the finite element model, under harmonic and random excitation, are compared with experimentally obtained values in order to evaluate both models.

2.2.   Description of the Finite Element Model

This section presents the steps followed to develop a finite element model that can be employed to conduct a dynamic analysis of a three dimensional structure and the subsequent validation of results using the commercial finite element package, SAP2000 (CSI 2004). Implementing two nonlinear TLD models (presented in Section 2.4.2) in open-source software (in-house software) is of interest compared to utilizing commercial software, particularly at an early-phase of the research study. In-house developed software permits the use of user defined error tracking features during the implementation and validation process of the nonlinear TLD numerical model, flexibility of modelling and updating the structure-TLD interaction process (presented in Section 2.5), and reduced computational effort. A user-defined TLD module can be implemented, at a later date, in commercial finite element software for analysis and design purposes.

2.2.1   Three Dimensional Beam Element

The general three dimensional elastic beam element (frame element) used in the finite element model is a straight line element formulated, which is based on continuum mechanics theory. A detailed derivation can be found in Bathe and Bolourchi (1979) and Bathe (2003). The element has two nodes, a start node and an end node, with 6 degrees of freedom (DOF) per node and can transmit axial force, shear forces, bending moments and torque (see Figure 2.3). The element is assumed to be straight and of constant cross section. It is assumed that plane sections of the beam element remain plane during deformation, but not necessarily perpendicular to the neutral axis, i.e. a constant shear is allowed. The principal moment of inertia axes of the beam element, which define the local co-ordinate system r, s, t, are shown in Figure 2.3. The two end nodes of the element, 1 and 2, plus a third secondary node, 3, can be used to define these axes. In the developed finite element model, nodes 1 and 2 are used to define the longitudinal local axis, while the moments of inertias about the other two axes are set in accordance with the right-hand role; hence it is not necessary to define the third node.

Nodes 1 and 2 have three translational and three rotational degrees of freedom, in the local and global coordinate systems. Either nodal forces or displacements can be applied to the element. This type of element is commonly used to model space frame members. By setting different frame element properties, the frame element can then be used to represent vertical structural components, i.e. columns and shear walls, and the horizontal structural components such as beams and slabs. These properties include: the two perpendicular moments of inertias (I_x and I_y, I_x and I_z or I_y and I_z); the cross sectional area (A_{cs}); the torsional rigidity (J); the modulus of elasticity (E); and the element connectivity. Details of the frame element's shape functions, stiffness matrix, mass matrix, and damping matrix can be found elsewhere (Bathe 2003).

In this study, the element capabilities are extended to include the dynamic analysis of three dimensional structures, both with and without TLDs installed, using Newmark's method (Chopra 2001; Bathe 2003). A total of 18 response components have been obtained from this analysis at each 3D frame element node; i.e. 3 translational components [$x(t)$, $y(t)$, $z(t)$], 3 velocity components [$\dot{x}(t)$, $\dot{y}(t)$, $\dot{z}(t)$], 3 acceleration components [$\ddot{x}(t)$, $\ddot{y}(t)$, $\ddot{z}(t)$], 3 rotational components [$\theta_x(t)$, $\theta_y(t)$, $\theta_z(t)$], 3 torsional velocity components [$\dot{\theta}_x(t)$,

$\dot{\theta}_y(t)$, $\dot{\theta}_z(t)$] and 3 torsional acceleration components [$\ddot{\theta}_x(t)$, $\ddot{\theta}_y(t)$, $\ddot{\theta}_z(t)$] in addition to the element straining actions, i.e. axial force, shear force, bending moment and torque.

2.2.2   Direct Integration Methods: Background

For the dynamic analysis to be performed, a direct integration method is used (Chopra 2001; Bathe 2003). In this method, the equations of motion of the system are integrated numerically through a step-by-step procedure providing a solution at discrete time intervals Δt. Initial values of displacements, velocities and accelerations must be specified. Numerous step-by-step direct integration methods exist. These methods vary in terms of the accuracy of the results and the stability of the analysis process itself. A direct integration method is said to be conditionally stable if the solution is stable. This can be achieved only when the value of $\Delta t/T$ is selected to remain less than a specific value, denoted the stability limit, where T is the smallest of the natural period of the highest mode of interest or the period of loading. If the value of $\Delta t/T$ exceeds this stability limit, the solution will not converge. A time step of 0.01 second, which satisfies the stability condition, is selected to perform the numerical analysis of the structure carried out in this chapter.

2.2.3   Explicit and Implicit Methods

Explicit methods, such as the central difference method, do not involve the solution of a set of linear equations at each step. These methods use the differential equation at time t to predict a solution at time $t + \Delta t$. For most real structures, which contain stiff elements, a very small time step is required in order to obtain a stable solution. Therefore, all explicit methods are conditionally stable with respect to the size of the time step. For this reason it is not recommended to use such type of methods for multi-degree of freedom systems (MDOF) (Chopra 2001).

Implicit methods, such as the Wilson-θ and Newmark method, attempt to satisfy the differential equation at time t when the solution at time $t - \Delta t$ is found (Bathe 2003). These methods require the solution of a set of linear equations at each time step; however, larger time steps may be used. Implicit methods can be conditionally or unconditionally stable depending on the parameters set in each of these methods.

In this study, the constant-average-acceleration method developed by Newmark (Chopra 2001; Bathe 2003) has been used to perform the dynamic analysis. This method was selected as it was found to provide good accuracy and stability.

2.3.   Validation of the Finite Element Model

To validate the finite element model, a 3D single-story structure, consisting of four columns and a slab 3.0 m × 3.0 m with a depth of 0.18 m (see Figure 2.4) is modelled using a general purpose finite element package (SAP2000). The generalized properties of this building are given in Table 2.1 along with the vertical element (columns) properties. In order to simulate the 3D structure using the finite element model shown in Figure 2.5, the vertical elements are modelled using frame elements with the same number of elements, properties and boundary conditions (i.e. fixed at the base and free at the roof) as their counterpart modelled in SAP2000. The horizontal slab is modelled using horizontal fame elements that are sufficiently rigid in plane (x-y plane) and flexible out of plane. This is accomplished by specifying a frame element width ≥ 0.25 span length and a depth equal to that of the real slab. A rigid diaphragm for all nodes at the same floor level is then achieved.

To check the selected dimensions of the horizontal and vertical elements, a second model, shown in Figure 2.6, is developed using SAP2000 with all specified dimensions in the finite model. The mass of the slab and the columns were lumped at the structural joints (nodes) located in the horizontal plane using the tributary area method. A mass of 1010 kg was lumped at the four corners, to be considered in the modal analysis. A damping ratio (ζ) of 0.1% is assumed. A modal analysis is then performed for the two models and their periods compared. The second SAP2000 frame model, shown in Figure 2.6, is found to simulate the behaviour of the real slab shown in Figure 2.4. Both SAP2000 models predicted similar structural periods and mode shapes with a percentage difference of less than 0.5% found to occur between the two SAP2000 models and the finite element model.

A time history analysis is subsequently conducted using the 3 models described above namely; SAP2000 with a real slab, SAP2000 with horizontal elements representing the slab and the 3D finite element model, which are denoted as Model 1, Model 2 and Model 3, respectively. Figure 2.7 shows the displacement, velocity and acceleration of the three models at the centre of the slab. For the results shown here, all models are excited by a sinusoidal force, having an amplitude (P_o) of 23 N; a frequency (f_{ex}) equals 0.50 Hz ($f_{ex} \approx$

0.9 f_s) and a point of application coinciding with the slab centre. Excellent agreement is found between all model responses with a maximum variation in the response values of less than 2%.

2.4. 3D-Structure-TLD System Model

In this section, the finite element model, validated in the previous section, is used to estimate the response of a three dimensional structure outfitted with TLDs (3D-Structure-TLD). The sloshing TLD force resulting from the interaction of the combined system is estimated using two numerical models found in the literature; a nonlinear TLD fluid model (Kaneko and Ishikawa 1999; Tait et al. 2005b) and an equivalent amplitude dependent tuned mass damper (EADTMD) model (Tait et al. 2004a; Tait et al. 2004b). Both TLD models are implemented in the finite element model in this section and subsequently validated in the following section.

2.4.1 TLD/TMD Background

Figure 2.8 shows the dimensions of the tank used by Tait (2004), which is modelled and subsequently used in the validation part of the 3D-Structure-TLD system model subjected to harmonic excitation. Results of this numerical model are compared to experimental test results from BM4-A building as reported on by Tait (2004). The dimensions L, b and h represent the tank length (in the direction of excitation), the tank width (perpendicular to the excitation) and the still water depth, respectively. The fundamental sloshing frequency (f_w) for the water inside this tank using the linear wave theory (Lamb 1932) can be estimated as

$$f_w = \frac{1}{2\pi} \sqrt{\frac{\pi g}{L} \tanh\left(\frac{\pi h}{L}\right)} \tag{2.1}$$

where g is the gravitational acceleration. Substituting L and h from Figure 2.8 into the above equation, leads to a value of $f_w \approx 0.546$ Hz. The TLD represents a 1:10 scale model of one of the prototype multiple tanks designed to be used in a full-scale high-rise building with a fundamental frequency of approximately 0.172 Hz.

The tuning ratio, which influences the performance of the TLD, is defined by

$$\Omega = \frac{f_{TLD}}{f_s} \tag{2.2}$$

where f_{TLD} is the natural frequency of the TLD; and f_s is the natural frequency of the generalized structure having generalized mass, stiffness and damping values of M^*, K^* and C^*, respectively. An estimate of the natural frequency of the TLD (f_{TLD}) for a small sloshing fluid response amplitude is approximately equal to f_w (Warnitchai and Pinkaew 1998; Ju et al. 2004; Tait et al. 2004a). Table 2.1 shows the generalized properties of the building used in the experimental test as well as the equivalent properties of the 3D single-story building used in the validation of the developed finite element model with and without a TLD installed.

Another factor affecting the response of the structure-TLD system is the mass ratio (μ), which is given by

$$\mu = \frac{\phi^2 m_{TLD}}{M^*} \tag{2.3}$$

where M^* is the generalized mass of the primary structure corresponding to the vibration mode being suppressed; and ϕ is the normalized modal deflection value of the structure at the TLD location. The absorber mass (m_{TLD}), for a TLD with damping screens can be approximated using potential flow theory (i.e. $m_{TLD} \approx m_1$). The value m_1 is calculated using the following equation (Graham and Rodriguez 1952)

$$m_1 = \frac{8 \tanh\left(\frac{\pi h}{L}\right)}{\left(\frac{\pi^3 h}{L}\right)} m_w \tag{2.4}$$

where m_w is the total mass of the contained water, h is the quiescent water depth; and L is the tank length in the direction of the fundamental sloshing mode of interest. A value of $m_1 = 0.77 m_w$ is obtained using the dimensions of the TLD considered in this study. A target value of μ equal to 2.5% is used to validate the numerical model, which matches that used in the experimental work of a structure-TLD system subjected to harmonic and random excitations (Tait 2004). Table 2.2 shows the properties of the TLD used in the model validation.

One more important parameter affecting the response of a structure-TLD system is the inherent damping ratio (ζ_{TLD}) of the sloshing fluid inside the tank. The inherent damping for the TLD used in the model validation is 5.7%. This is significantly greater than the damping related to the sloshing liquid inside the tank without the presence of additional energy dissipating devices, which is estimated to be 0.45% from the following equation (Sun 1991)

$$\zeta_{TLD} = \frac{1}{2\pi}\sqrt{\frac{v_w}{\pi f_w}}\left(1 + \frac{h}{b}\right) \tag{2.5}$$

where v_w is the kinematic viscosity of water.

The optimum inherent damping value for a linear tuned mass damper (TMD) as a function of the mass ratio (μ) can be obtained (Warburton 1982). Due to the analogy between the TMD and TLD devices, Warburton's formula is used to calculate the target value of $\zeta_{TLD} = 5.7\%$. Two screens formed by horizontal slats were used by Tait (2004a and 2004b) to increase ζ_{TLD} as shown in Figure 2.9. A solidity ratio (S) equal to 0.42 was used to achieve the targeted optimum inherent damping ratio of 5.7% at a particular response amplitude. In the numerical model, a loss coefficient parameter (C_l) equal to 2.16 is used to model the damping screens inside the tank. The loss coefficient (C_l), which is a function of the screen solidity ratio, is introduced and presented in detail elsewhere (Tait et al. 2005b). In order to achieve different values of ζ_{TLD}, the damping screens can be altered by adjusting the space between the slats shown in Figure 2.10.

2.4.2   Tuned Liquid Damper Models

A number of equivalent mechanical models capable of simulating the forces that develop in a TLD with screens resulting from the sloshing fluid exist (Noji et al. 1988; Warnitchai and Pinkaew; Tait et al. 2004a). Both a linear model (Fediw et al. 1995) and a nonlinear fluid model (Kaneko and Ishikawa 1999) that simulate the sloshing fluid of a TLD equipped with damping screens are examined by Tait et al. (2005b). In both models it is assumed that the liquid is inviscid, irrotational and incompressible, the pressure is constant on the free surface, the quiescent water depth is constant and the tank walls are rigid. In addition, it is assumed that the water depth to tank length ratio (h/L) for a TLD equipped with damping screens, satisfies shallow water wave theory limitations. Dean and Dalrymple (1984) suggest $h/L < 0.1$, but recognize that this limitation can be relaxed for particular applications. This has been verified by test results from Tait et al. (2007). The effect of the screens is simulated in both models through a loss coefficient (C_l). Findings from Tait et al. (2005b) indicate that the linear model is capable of providing a first estimate of the energy dissipation characteristics of a TLD. However, the linear model does not provide realistic estimates of the free surface response amplitude. The nonlinear model can accurately describe the free surface motion, the

resulting base shear forces and the energy dissipated over a range of excitation amplitudes. Therefore, a nonlinear numerical model based on shallow water wave theory (Lepelletier and Raichlen 1988) with damping screens (Kaneko and Ishikawa 1999; Tait et al. 2005b) is selected for this study and results from previous experimental studies are compared to verify the results of the 3D-Structure-TLD system model under both harmonic and random excitation (Tait 2004).

2.4.2.1   Nonlinear Shallow Water Fluid Model (TLD Model 1)

The nonlinear numerical model is briefly described below. Additional details can be found elsewhere (Kaneko and Ishikawa 1999; Tait et al. 2005b). Considering the tank, shown in Figure 2.11, is excited in a unidirectional motion, the nonlinear sloshing response can be expressed using shallow water theory as (Lepelletier and Raichlen 1988)

$$\frac{\partial \eta}{\partial t} + \frac{\partial}{\partial x}[(h + \eta)u] = 0 \tag{2.6}$$

$$\frac{\partial u}{\partial t} + u\frac{\partial u}{\partial x} + g\frac{\partial \eta}{\partial x} - \frac{1}{3}(h + \eta)^2 \frac{\partial^3 u}{\partial t \partial x^2} + \zeta_w u + \ddot{X} = 0 \tag{2.7}$$

where $\eta(x, t)$ is the free surface elevation, $u(x, t)$ is the horizontal velocity averaged through the liquid depth, L is the tank length, h is still liquid depth, g is the gravitational acceleration, $\ddot{X}$ is the horizontal base excitation acceleration of the tank, which is equal to that of the nodal acceleration at the TLD location and in the direction of the tank placement ($\ddot{x}_s$), and ζ_w is a damping coefficient, introduced by Miles (1967) to account for the viscous dissipation.

The above set of nonlinear shallow water equations can be solved numerically once the initial state of the liquid is prescribed, i.e. the values of η and h are given at time $t = 0$. A one-dimensional finite difference discretization scheme is applied for both η and h as shown in Figure 2.12. The grid for u is staggered in a nonoverlapping fashion downstream to the η grid. The boundary conditions on the end walls of the tank are given as $u(-L/2, t) = u(L/2, t) = 0$. For a certain excitation amplitude, Equations 2.6 and 2.7 are integrated numerically using the Runge-Kutta-Fehlberg method after assigning the initial conditions for $\eta(x, 0) = 0$ and $u(x, 0) = 0$.

Using the method outlined by Kaneko and Ishikawa (1999) at locations where a damping screen is inserted as shown in Figure 2.13, the velocity at a particular screen (U_{DSi}) can be expressed as

$$U_{Dsi} = \frac{u_i + u_{i+1}}{2}$$ (2.8)

The pressure drop (Δp) caused by the screen can be expressed as

$$\Delta p = C_l \frac{\rho U_{DSi}^2}{2}$$ (2.9)

where C_l is defined as the pressure loss coefficient. A significant reduction in the dynamic response of a high-rise building can be achieved if the TLD has sufficient inherent damping. A preliminary design procedure outlined by Tait (2008) can be used to estimate the initial damping screen requirements; therefore an optimum inherent damping for the TLD can be achieved.

The relationship between the pressure loss coefficient and the free surface height difference across the screen is given by

$$|\eta_L - \eta_R| = \Delta\eta = C_l \frac{U_{DSi}^2}{2g}$$ (2.10)

Upon integrating the discretized continuity and momentum equations with respect to time, the values of free surface on the left (η_L) and right (η_R) sides of the screen can be determined by

$$\eta_L = \eta_i + \text{sign}[U_{DSi}]\frac{\Delta\eta}{2}$$ (2.11)

$$\eta_R = \eta_i - \text{sign}[U_{DSi}]\frac{\Delta\eta}{2}$$ (2.12)

Subsequently, the velocity and the wave height can be determined with the influence of the damping screen taken into consideration.

The base shear force that develops when the TLD is forced to move can be separated into the following three components: first, the inertial force due to the container (f_1); second, the inertial force due to the dead weight of the contained liquid (f_2); and third, fluid force generated by sloshing (f_3). Therefore, the TLD base shear force caused by the liquid motion is denoted by $F_{TLD_x-Model\ 1} = f_2 + f_3$. Applying momentum theory to calculate the TLD base shear force, the mass of the ith element is given by the following equation (Kaneko and Ishikawa 1999)

$$m_i = \rho \times \frac{L}{n_e} \times b \times \left(\frac{\eta_{i-1} + \eta_i}{2} + h \right) \tag{2.13}$$

where n_e is the total number of elements, L is the tank length, b is the tank width and ρ is the liquid unit weight.

Consequently, the momentum of the ith element can be described as follows

$$P = \sum_{i=1}^{n_e} m_i u_i = \frac{\rho L b}{n_e} \sum_{i=1}^{n_e} \left(\frac{\eta_{i-1} + \eta_i}{2} + h \right) u_i \tag{2.14}$$

The TLD base shear force ($F_{TLD_x - model\,1}$) can be determined by the following equation

$$F_{TLD_x - Model\,1} = \frac{1}{\Delta t} (P(t) - P(t + \Delta t)) \tag{2.15}$$

2.4.2.2 Equivalent Amplitude Dependent Tuned Mass Damper (EADTMD) Model (TLD Model 2)

In order to perform a dynamic analysis on a high-rise building equipped with TLDs employing the 3D-Structure-TLD system model, the equations of motion for the building must be solved according to the time step dictated by the fluid model. This time step is often considerably less than that required to perform a dynamic analysis on the building without TLDs. The computational time needed for the sloshing fluid model is approximately 18 times greater than the time needed for the equivalent amplitude dependent tuned mass damper (EADTMD) model. The time step (Δt_1) used by the fluid model is about $1/180$ of the structure's time period as recommended by Kaneko and Ishikawa (1999) in order to solve for the one-dimensional finite difference scheme, while the time step (Δt_2) needed for the EADTMD model is about $1/10$ of the structure's time period to achieve good accuracy from the numerical integration process as recommended by Chopra (2001). Therefore, significantly greater computational effort is required to conduct dynamic analysis using the nonlinear fluid model. SHARCNET ™ (Shared Hierarchical Academic Research Computing Network, www.sharcnet.ca) can be used to perform such analysis. Alternatively, a more rapid analysis can be conducted utilizing the EADTMD model.

Yu et al. (1999) experimentally evaluated equivalent TMD stiffness and damping properties to represent a TLD using the concept of equivalent energy dissipation. The model assumed full participation of the fluid mass, which is valid for large excitation amplitudes.

However, the calculated properties did not account for the presence of any additional energy dissipating mechanisms. As previously mentioned, the inherent damping of the sloshing fluid is usually significantly lower than the value required for the TLD to perform efficiently. An increase in the inherent damping can be achieved by installing a number of screens or baffles inside the tank (Noji et al. 1988; Fediw 1992; Warnitchai and Pinkaew 1998; Kaneko and Ishikawa 1999; Tait et al. 2005a; Tait et al. 2005b). As a result, a technique that utilizes the nonlinear fluid model to evaluate the properties of an EADTMD, which considers the presence of damping screens inside the tanks and treats the percentage of fluid mass that participates in the sloshing motion as a variable parameter, is demonstrated in this section. The steps followed to evaluate the properties of an EADTMD model are discussed in Section 2.4.2.2.2 and a validation example is provided in Section 2.4.2.2.3.

2.4.2.2.1. Equivalent TMD Analogy

An equivalent amplitude dependent tuned mass damper (EADTMD) representing a partially fluid tank containing screens (TLD) can be determined based on experimental shake table results. The dynamic characteristics of the equivalent TMD model, in terms of mass, stiffness and damping parameters can be determined by energy equivalence from a series of shake table tests (Tait et al. 2004a). The validity of this nonlinear TLD model has been examined (Tait et al. 2004b). The energy dissipated by the equivalent TMD (E_d) shown in Figure 2.14 can be expressed in terms of the excitation amplitude, as

$$E_d = m_{TLD}(2\pi f)^2 A^2 \pi |H_{z/x}(f)| \left(\frac{f}{f_{TLD}}\right)^2 \sin(\theta_{z/x}) \tag{2.16}$$

Normalizing this expression by $1/2\, m_w (A2\pi f)^2$, results in

$$E'_d = \frac{m_{TLD}}{m_w} |H_{z/x}(f)| \left(\frac{f}{f_{TLD}}\right) 2\pi \sin(\theta_{z/x}) \tag{2.17}$$

where $|H_{z/x}(f)|$ is the frequency response function, referred to the modulus of the mechanical admittance function, between the TMD relative response motion and the shake table input motion

$$|H_{z/x}(f)| = \frac{1}{\sqrt{\left(1 - \left(\frac{f}{f_{TLD}}\right)^2\right)^2 + \left(2\zeta_{TLD}\left(\frac{f}{f_{TLD}}\right)\right)^2}} \tag{2.18}$$

and ($\theta_{z/x}$) is the corresponding phase angle given by

$$\theta_{z/x} = tan^{-1}\left(\frac{2\zeta_{TLD}\left(\frac{f}{f_{TLD}}\right)}{1 - \left(\frac{f}{f_{TLD}}\right)^2}\right) \tag{2.19}$$

A curve fitting procedure with constraints forcing the theoretical expression E_d' to match both the maximum value of the energy dissipated and the total energy dissipated over the range of frequencies tested is applied. This procedure is used to estimate the EADTMD parameters m_{TLD}, f_{TLD} and ζ_{TLD} for all amplitudes of excitation (Tait et al. 2004a; Tait et al. 2004b).

The equation of motion of the equivalent TMD system, for a given excitation amplitude, can be written as

$$M_{TLD}.\ddot{x}_{TLD} + C_{TLD}.\dot{x}_{TLD} + K_{TLD}.x_{TLD} = -M_{TLD}.\ddot{x}_s \tag{2.20}$$

Hence, the TLD force $F_{TLD_x-Model\ 2}$ can be estimated as

$$F_{TLD_x-Model\ 2} = -M_{TLD}(\ddot{x}_s + \ddot{x}_{TLD}) \tag{2.21}$$

where x_s and x_{TLD} are the structure displacement and the relative displacement between the TLD and the structure, respectively (see Figure 2.2).

2.4.2.2.2. Construction of TLD Energy Dissipation Frequency Response Curves

The nonlinear TLD fluid model, described in Section 2.4.2.1, is employed to generate the required energy dissipation frequency response curves. Energy dissipation curves can be generated using the nonlinear TLD fluid model under both small and large excitation amplitudes making them suitable for small motions associated with wind loads and large motions more representative of earthquake excitation. Thus, the nonlinear fluid model can be used to produce the required dissipation energy curves required to evaluate the equivalent TMD parameters (m_{TLD}; f_{TLD}; ζ_{TLD}) without the need to conduct shake table tests.

2.4.2.2.3. Model Validation

In this section, the nonlinear shallow water fluid model is used to construct the energy dissipation frequency response curves at different excitation amplitude ratios listed in Table 2.3 for the TLD shown in Figure 2.8. The structural displacement response results are then compared to that produced by a series of shake table tests conducted and reported on by Tait et al. (2004a).

Figure 2.15 compares the numerically obtained energy dissipation curves with the fitted equivalent TMD curves determined by regression analysis. Excellent agreement is found between the two curves for $A/L = 0.0026$. This indicates that under low sloshing response amplitudes, the energy dissipation characteristics of the TLD can be matched with an equivalent SDOF system (i.e. wind excitation). As a result of the nonlinear response characteristics, which increase with larger sloshing response amplitudes, the equivalent TMD fit for $A/L = 0.0129$ energy dissipation curve shows greater deviation with experimentally generated curve (see Figure 2.15b).

The influence of the excitation amplitude on the estimated equivalent mass, damping and frequency are shown in Figures 2.16a to 2.16c, respectively. Trend lines are fit to each of the parameters in order to estimate the parameter values between the data points and to obtain the equations used by the finite element model in the simulation process. Excellent agreement is found between the experimentally obtained EADTMD parameters shown in Figure 2.16 and those reported by Tait et al. (2004a).

2.5.   Structure-TLD Interaction (Numerical Simulation)

This section presents the implementation approach of both nonlinear TLD models, described in this chapter, in the finite element model. Both models are capable of simulating the TLD behaviour under any source of dynamic loading (i.e. wind and earthquake) by accurately predicting its resulting base shear force.

The assumption that the fundamental sloshing water response remains uncoupled in the two principal directions of motion under both 1D and 2D excitation was confirmed by Tait et al. (2005a). In addition, two other important findings from the shake table experiments are briefly mentioned here. First, although the free surface response profile were affected by 2D excitations applied to the tank, the base shear force that develop in the principal tank axes as a result of the sloshing water motion were not. Second, no degradation in the amount of energy dissipated by the sloshing water was found to occur under 2D excitation.

Subsequently, this indicates that by selecting the appropriate aspect ratio for the TLD it can be used to reduce structural response motion in two modes of vibration simultaneously with no penalty on its performance. Thus, the effectiveness of the sloshing water is increased when it is used in both directions, simultaneously, by providing additional effective damping to the structure at no additional cost. Therefore, the developed 3D-Structure-TLD system

model uses the same concept for bi-directional tanks by representing them as two different unidirectional tanks predicting their resulting shear forces by the nonlinear TLD models (Model 1 or Model 2) at each time step independently. Consequently, the two orthogonal structural acceleration components resulting at the TLD location are used by the nonlinear TLD models as input excitations for the bi-directional tank.

The equation of motion of the combined system can be written as

$$[M]\{\ddot{x}\} + [C]\{\dot{x}\} + [K]\{x\} = \{F_{ext}(t)\} + [H]\{F_{TLD}(t)\} \tag{2.22}$$

where $[M]$, $[C]$ and $[K]$ are the mass, damping and stiffness matrices of the building (i.e. primary structure), $\{x\}$, $\{\dot{x}\}$ and $\{\ddot{x}\}$ represent the structural displacement, velocity and acceleration vectors, $\{F_{ext}(t)\}$ is the external load acting on the structure, $\{F_{TLD}(t)\}$ is control force vector of the TLD (i.e. base shear forces), and $[H]$ is the position matrix of the TLD in which its ith column vector $\{H\}_i = [0 \dots 0\ 1\ 0 \dots 0]_{1 \times n}^T$ (1 is in the jth column) is the ith group of TLDs that are installed on the jth story.

In the sloshing direction, the non-participating portion of the liquid is considered in the TLD base shear force values ($F_{TLD_x - Model\ 1}$) using the fluid model. As a result, $m_{x-non\ p.}$ has not been added to the primary structure mass (i.e. $m_{x-slosh.}^{TLD-Model\ 1} = 0$), while $m_{x-non\ p.}$ has been added to the primary structure mass using the EADTMD model (i.e. $m_{x-slosh.}^{TLD-Model\ 2} = m_{x-non\ p.}$) (see Equations 2.23 and 2.24).

In the orthogonal direction to the tank placement (i.e. out of plane), the non-participating portion of the liquid is assumed to be equal to the total mass of the contained water and is added to the attached TLD node in both TLD models for uni-directional tanks ($m_{y-orth.}^{TLD-Model\ 1} = m_{y-orth.}^{TLD-Model\ 2} = m_w$). For a bi-directional tank, the non-participating portion of the liquid is not considered in the TLD base shear force in the orthogonal direction ($F_{TLD_y - Model\ 1}$) using the fluid model (i.e. $m_{y-orth.}^{TLD-Model\ 1} = 0$), while it is added to the attached TLD node using the EADTMD model (i.e. $m_{y-orth.}^{TLD-Model\ 2} = m_{y-non\ p.}$).

In the vertical direction, the non-participating portion of the liquid is assumed to be equal to the total mass of the contained water and is added to the attached TLD node in both TLD models for uni- and bi-directional tanks (i.e. $m_z^{TLD-Model\ 1} = m_z^{TLD-Model\ 2} = m_w$).

Therefore, the mass matrix of the combined system, $[M]$, using the fluid model is given by

$$[M] = [M_S] + [H]\left[M_{fluid}^{TLD-Model\ 1}\right] = \begin{bmatrix} m_{1x} & & & & & \\ & m_{1y} & & \cdots & & 0 \\ & & m_{1z} & & & \\ & \vdots & & \ddots & & \vdots \\ & & & & m_{nx} & \\ & 0 & & \cdots & & m_{ny} \\ & & & & & & m_{nz} \end{bmatrix} +$$

$$[H]\begin{bmatrix} m_{1x-slosh.}^{TLD-Model\ 1} & & & & & \\ & m_{1y-orth.}^{TLD-Model\ 1} & & \cdots & & 0 \\ & & m_{1z}^{TLD-Model\ 1} & & & \\ & \vdots & & \ddots & & \vdots \\ & & & & m_{nx-slosh.}^{TLD-Model\ 1} & \\ & 0 & & \cdots & & m_{ny-orth.}^{TLD-Model\ 1} \\ & & & & & & m_{nz}^{TLD-Model\ 1} \end{bmatrix}$$

(2.23)

where $[M_S]$ is the stiffness matrix of the primary system and $\left[M_{fluid}^{TLD-Model\ 1}\right]$ is the added mass to the primary structure at the TLD locations in the x, y and z directions considering the fluid model (TLD Model 1).

The following equation represents the mass matrix of the combined systems using the EADTMD model

$$[M] = [M_S] + [H]\left[M_{fluid}^{TLD-Model\ 2}\right] = \begin{bmatrix} m_{1x} & & & & & \\ & m_{1y} & & \cdots & & 0 \\ & & m_{1z} & & & \\ & \vdots & & \ddots & & \vdots \\ & & & & m_{nx} & \\ & 0 & & \cdots & & m_{ny} \\ & & & & & & m_{nz} \end{bmatrix} +$$

$$[H]\begin{bmatrix} m_{1x-slosh.}^{TLD-Model\ 2} & & & & & \\ & m_{1y-orth.}^{TLD-Model\ 2} & & \cdots & & 0 \\ & & m_{1z}^{TLD-Model\ 2} & & & \\ & \vdots & & \ddots & & \vdots \\ & & & & m_{nx-slosh.}^{TLD-Model\ 2} & \\ & 0 & & \cdots & & m_{1n-orth.}^{TLD-Model\ 2} \\ & & & & & & m_{nz}^{TLD-Model\ 2} \end{bmatrix}$$

(2.24)

where $\left[M_{fluid}^{TLD-Model\ 2}\right]$ is the added mass to the primary structure at the TLD locations in the x, y and z directions considering the amplitude dependent TMD model (TLD Model 2).

From the analysis, the influence of adding the out-of-plane mass to the primary structure mass is found to have a negligible effect due to the small percentage ratio of the secondary system to the primary system.

2.5.1   Numerical Simulation Utilizing the Fluid Model (TLD Model 1)

The interaction between the TLD and the structure is captured by applying the resulting TLD base shear force ($F_{TLD-Model\ 1}$) on the structure at every time step at the TLD location and in its placement direction. The TLD base shear force is calculated utilizing the nonlinear TLD fluid model, which simulates the sloshing behaviour of a TLD subjected to a unidirectional excitation. The resulting structural acceleration at the TLD location is then used as the input excitation for the TLD in the following time step. This is accomplished employing Newmark's method for solving the equations of motion of the 3D structure (see Equation 2.22), while the TLD is modelled as a one-dimensional finite difference problem and solved employing Runge-Kutta-Fehlberg method at each time step (Δt_1) (see Equations 2.6-2.15). The developed 3D-Structure-TLD system model allows any number of TLDs to be placed at any location in the building. As a result, an accurate prediction of the response of the combined system (i.e. structural responses and TLD base shear forces) and applicability of using different dimensions of TLDs designed to suppress different modes of vibrations is achieved.

2.5.2   Numerical Simulation Utilizing the EADTMD Model (TLD Model 2)

Figure 2.5 shows the three dimensional finite element structure, which is investigated in this section. The TLD is simulated as a nonlinear tuned mass damper (TMD). The parameters m_{TLD}, k_{TLD} and ζ_{TLD} represent the mass, stiffness and damping of the equivalent TMD system, respectively (See Figure 2.14). These parameters are amplitude dependent; thus they vary with the excitation level experienced by the TLD (see Figure 2.16). It is assumed that x_s, $\dot{x}_s$ and $\ddot{x}_s$ are the instantaneous values of the displacement, velocity and acceleration at the TLD node at a certain time ($t = i$) resulting from the dynamic analysis of the structure. The base of the TLD, which is rigidly attached to the structure, experiences a displacement, velocity and acceleration equal to that of the TLD location. These structural

response components are used to calculate the instantaneous force exerted by the TLD on the structure at the TLD location ($F_{TLD-Model\,2}$) using Equation 2.21. This force is equal in magnitude and opposite in direction to the shear force acting at the base of the TLD. Treating the structure as multi-degree-of-freedom (MDOF), the equation of motion of the 3D-Structure-TLD system model (i.e. Equation 2.22) can be used.

The equations of motion are integrated numerically employing the constant-average-acceleration method developed by Newmark (Chopra 2001; Bathe 2003) to solve the equations of motion at every time step (Δt_2), while taking into consideration the added instantaneous value of the TLD force ($F_{TLD-Model\,2}$). This force depends on two important components; the maximum structural displacement amplitude (A_{cycle}) experienced during its response cycle and the instantaneous structural acceleration response ($\ddot{x}_s$), both at the TLD location and in its placement direction. The maximum displacement amplitude is used to estimate the EADTMD properties (m_{TLD}; k_{TLD}; ζ_{TLD}), which remain constant during the calculations of the TLD force in the current cycle. The instantaneous acceleration at the TLD location is required to solve the equivalent TMD system as an independent single-degree-of-freedom (SDOF) to instantaneously evaluate the TLD force ($F_{TLD-Model\,2}$) at each time step. The steps calculations are described, in detail, in the following section.

An EADTMD model has been implemented in a two dimensional finite element model to predict the response of a structure-TLD system under large amplitude transient type excitation (Mizan 2007). A displacement dependent method of adding the TLD force, as outlined by Mizan (2007), was not applicable for the case of wind excitation as the structure oscillates around a mean value. This shift in the displacement response of the structure must be considered to capture the maximum amplitude value for different structural response cycles. As a result, a velocity dependent method is introduced in the next section as an alternative method.

2.5.2.1 Velocity Dependent Method for EADTMD Model

In the velocity dependent method, the velocity in the direction of the TLD placement at the TLD location is used as a sensor to capture the time step where a peak displacement occurs every half cycle of the response during the entire response history. By checking the sign of the structural velocity response at the TLD location and in its placement direction every time step (Δt_2), the peak displacement response value achieved in the first half of the

response cycle is captured when the velocity sign changes (i.e. from positive to negative or vice versa), which is recorded as P_1. The iteration proceeds throughout the second half of the response cycle until the velocity sign again changes. Therefore, the peak displacement response is recorded as P_2. The maximum structural response amplitude throughout a complete response cycle (A_{cycle}) can be estimated as $|P_1 - P_2|/2$. The velocity dependent method provides the ability to capture the peak response value despite the mean value of the response. Consequently, predictions of the maximum response amplitudes, used to update the EADTMD model properties throughout different response cycles, can be estimated.

The following steps are carried out to obtain the response time history of the 3D-Structure-TLD system model subjected to an external dynamic loading:

1. At time $t = 0$, Equation 2.22 is first solved without considering the force resulting from the TLD (i.e. $F_{TLD-Model\ 2} = 0$) using Newmark's method as the numerical integration technique (Chopra 2001; Bathe 2003). The values of the displacements, velocities and accelerations are obtained at the TLD locations from the solution output. The assumption of zero force added by the TLDs is applied during all time steps until the structural response at each TLD location undergoes a complete cycle of vibration by checking its velocity sign at every increment. It should be noted that the structure may undergo different cycles in each of the two perpendicular axes at a particular TLD location. Therefore, the maximum displacement amplitude (A_{cycle}) experienced at each TLD location during the first cycle of vibration is determined.

2. At every remaining time step, the TLD force ($F_{TLD-Model\ 2}$) is calculated and included in the analysis using the instantaneous acceleration of TLD location ($\ddot{x}_s$) as the input excitation of the equivalent TMD system. The maximum amplitude from the previous cycle is used for each TLD to update the amplitude dependent parameters (m_{TLD}; k_{TLD}; ζ_{TLD}) using amplitude dependent equations obtained from charts prepared following the procedure outlined in Section 2.4.2.2 (see Figure 2.16). Charts need to be prepared and a best fit of the data should be used to implement the three equations required to estimate the equivalent TMD properties at each cycle for each TLD.

    To achieve this, the equation of motion of the equivalent TMD system at each TLD location i, and during every time step (Δt_2) throughout the different response cycles can be written as

$$(M_{TLD})_i \cdot (\ddot{x}_{TLD}(t))_i + (C_{TLD})_i \cdot (\dot{x}_{TLD}(t))_i + (K_{TLD})_i \cdot (x_{TLD}(t))_i$$
$$= -(M_{TLD})_i \cdot (\ddot{x}_s(t))_i \tag{2.25}$$

hence, the TLD force at each TLD location i, $(F_{TLD_x-Model\ 2})_i$ can be estimated as

$$(F_{TLD_x-Model\ 2})_i = -(M_{TLD})_i \left((\ddot{x}_s(t))_i + (\ddot{x}_{TLD}(t))_i \right) \tag{2.26}$$

3. Equations 2.22, 2.25 and 2.26 are solved simultaneously, while employing Newmark's numerical integration method to obtain different structural response component values (i.e. displacements $\{x_s(t)\}$, velocities $\{\dot{x}_s(t)\}$ and accelerations $\{\ddot{x}_s(t)\}$).

4. Step 2 is repeated during the third cycle and the subsequent cycles of vibration of the structure. During any given cycle, the properties of the equivalent TMD parameters are being updated based on the maximum amplitude experienced at the TLD location during the previous cycle.

2.6.   Validation of 3D FE-Structure-TLD System Model

In this section, the effect of a TLD on the response of a three dimensional single-story structure is investigated using the two algorithms described above under harmonic and random excitation. The natural frequency of the TLD used in the experimental test is equal to that of the TLD investigated in Section 2.4.2.2. Therefore, the charts and fitted equations, which are previously constructed (see Figure 2.16), are employed in the 3D-Structure-TLD system model to update the EADTMD model.

2.6.1   Validation Under Sinusoidal Excitation

A TLD is attached to the centre of the floor slab of a single-story building previously described in Section 2.3. The 3D-Structure-TLD system model is excited by steady-state sinusoidal excitation over a wide range of frequencies. The generalized characteristics of this system are listed in Tables 2.1 and 2.2. These values match those in the experimental study carried out by Tait (2004) using an amplitude force (P_o) of 23 N, mass ratio (μ) of 2.5% and tuning ratio (Ω) of 0.98. As observed from the frequency response curves plotted in Figure 2.17, the RMS structural displacement values predicted by both TLD models are found in close agreement with a variation of only 2%. Excellent agreement of the results obtained by the two nonlinear TLD models is achieved compared to experimental test results from BM4-A building as reported on by Tait (2004).

2.6.2   Validation Under Random Excitation

A time history analysis using the two nonlinear TLD models to simulate the resulted base shear force is carried out and compared to experimental test results reported on by Tait (2004). In that study, a two degree of freedom tests apparatus was designed to model the behaviour of a structure-TLD system excited by a four-hour duration random force time history, where the value of the amplitude excitation is F_{max} equal to 150 N. Thirty-cycles (i.e. $30T \approx 54$ seconds) duration portion of the random excitation, selected at the 31st minute of the 4-hour time history, are shown in Figure 2.18a. Numerical simulations of the developed 3D-Structure-TLD system model are carried out using the two proposed TLD models (TLD Model 1 and TLD Model 2). The natural frequency of the TLD used in the experimental test subjected to random excitation force is equal to that used in the experimental program subjected to harmonic excitation force. Therefore, the same charts and their fitted data equations, previously used, are employed to update the EADTMD model. The RMS structural displacement values of the 3D-Structure-TLD system model utilizing the EADTMD model (TLD Model 2) is found to be within 2% of the experimentally recorded RMS values (see Figure 2.18b). The nonlinear fluid model (TLD Model 1) gives an accurate prediction of the structural RMS response with less than 0.5% discrepancy with experimental results.

The root-mean-square (RMS) provides insight into the degree of fluctuation of the response. The RMS and peak values of a 3D-Structure-TLD system model are calculated for both nonlinear TLD models during the entire 4-hour time history and compared to the experimental results reported on by Tait (2004). RMS structural displacement response values of 3.40 mm, 3.45 mm and 3.38 mm are obtained for the nonlinear fluid model (TLD Model 1), the EADTMD model (TLD Model 2) and the experimental results, respectively. In contrast, an RMS structural displacement response value of 24.7 mm is obtained for the structure under random excitation without TLD attached. Figures 2.18c shows the displacement response time history of the structure with and without TLD demonstrating the ability of the TLD to control structural responses.

As noted above, the structural response is well predicted. The maximum error between the numerical and experimental values is found to be sufficiently accurate for the presented nonlinear TLD models, which are implemented in the finite element model.

2.7.   Conclusions

A finite element model capable of simulating the behaviour of a 3D structure, using 3D beam elements, is developed and validated under dynamic excitation. The validated finite element model is employed to estimate the response of a 3D structure outfitted with a TLD (3D-Structure-TLD). The interaction base shear force resulting from the TLD has been estimated using two nonlinear TLD models; the nonlinear fluid model that simulates the TLD sloshing force (TLD Model 1) and the EADTMD model (TLD Model 2). The numerical simulations of both nonlinear TLD models and their implementation in the developed finite element model are described through time history analysis.

A significant reduction in the computational effort to conduct dynamic analysis of a finite element 3D-Structure-TLD system model is achieved employing the EADTMD model as the computational time needed for the sloshing fluid model is approximately 20 times greater than the time needed for the EADTMD model. Therefore, two important steps are introduced to achieve this goal. First, an extension of the work done by the nonlinear TLD fluid model to produce the required energy dissipation curves to evaluate the EADTMD parameters (m_{TLD}; f_{TLD}; ζ_{TLD}) for the TLD without shake table testing is demonstrated. Consequently, the nonlinear TLD fluid model is used to generate the required energy dissipation frequency response curves in the range of excitation amplitude ratios that are suitable for small motions associated with wind loads and large motions more representative of earthquake excitation. Thus, designing different tank geometries to be implemented in the developed finite element model is achieved. Second, a modified implementation method of the EADTMD model in the finite element model utilizing the velocity tracking technique, which is applicable for various type of loading, is presented.

Finally, the developed finite element model has been validated under harmonic and random excitation with the experimental results using the two nonlinear TLD models simulating the resulting TLD base shear force. Good agreement is found using both TLD models and the experimental values. As a result, both validated numerical models can be employed to estimate the response of a full-scale multi-modal high-rise building subjected to wind tunnel data recorded at different locations on a building. Therefore, the wind-induced serviceability levels of accelerations can be estimated using the results obtained from the developed models.

2.8. References

Bathe, K.J. (2003). "*Finite Element Procedures in Engineering Analysis*", 7th Ed., Prentice-Hall.

Bathe, K.J. and Bolourchi, S. (1979). "Large Displacement Analysis of Three-Dimensional Beam Structures", *International Journal for Mechanical Methods of Engineering*, 14: 961-986.

Chopra, A.K. (2001). "*Dynamics of Structures: Theory and Applications to Earthquake Engineering*", 2nd Ed., Prentice-Hall, Toronto, ON, Canada.

CSI (Computers and Structures Inc.), (2004). "*SAP2000 version 10 Integrated Finite Element Analysis and Design of Structures*", CSI, Berkeley, CA, USA.

Dean, R.G. and Dalrymple, A.D. (1984). "*Water Wave Mechanics for Engineers and Scientists*" (first edition), Prentice-Hall Inc., Englewood Cliffs, NJ, USA.

Fediw, A.A. (1992). "*Performance of a One Dimensional Tuned Sloshing Water Damper*", M.E.Sc. Thesis. The University of Western Ontario, London, ON, Canada.

Fediw, A.A., Isyumov, N. and Vickery, B.J. (1995). "Performance of a Tuned Sloshing Water Damper", *Journal of Wind Engineering and Industerial Aerodynamics*, 56: 237-247.

Graham, E.W. and Rodriguez, A.M. (1952). "The Characteristics of Fuel Motion Which Affect Airplane Dynamics", *Journal of Applied Mechanics*, 19(3): 381-388.

Ju, Y.K., Yoon, S.W., and Kim, S.D. (2004). "Experimental Evaluation of a Tuned Liquid Damper System", *Proceeding of Institution of Civil Engineering-Structures and Building*, 157(4): 251–262.

Kaneko, S. and Ishikawa, M. (1999). "Modeling of Tuned Liquid Damper with Submerged Nets", *Journal of Pressure and Vessel Technology*, 121(3): 334–343.

Kareem, A. and Sun, W.J. (1987). "Stochastic Response of Structures with Fluid Containing Appendages", *Journal of Sound and Vibrations*, 119(3): 389–408.

Kareem, A., Kijewski, T. and Tamura, Y. (1999). "Mitigation of Motions of Tall Buildings with Specific Examples of Recent Application", *Wind and Structures*, 2(3): 201-251.

Koh, C.G., Mahatma, S. and Wang, C.M. (1994). "Theoretical and Experimental Studies on Rectangular Liquid Dampers under Arbitrary Excitations", *Journal of Earthquake Engineering and Structural Dynamics*, 23(1): 17–31.

Lamb, H. (1932). "*Hydrodynamics*", the University Press, Cambridge, England.

Lepelletier, T.G., and Raichlen, F. (1988). "Nonlinear Oscillations in Rectangular Tanks", *Journal of Engineering Mechanics*, 114(1): 1–23.

Miles, J.W. (1967). "Surface Wave Damping in Closed Basins", *Proceedings of the Royal Society of London. Series A, Mathematical and Physical Sciences*, 297(1451): 459-475.

Mizanur, R. (2007). "*The Use of Tuned Liquid Dampers to Enhance the Seismic Performance of Concrete Rigid Frame Buildings*", Ph.D. Thesis, The University of Western Ontario, London, ON, Canada.

Modi, V.J., Welt, F. and Irani, M.B. (1990). "On the Suppression of Vibrations Using Nutation Dampers", *Journal of Wind Engineering and Industerial Aerodynamics*, 33(1–2): 273–282.

Noji, T., Yoshida, H., Tatsumi, E., Kosaka, H. and Hagiuda, H. (1998). "Study on Vibration Control Damper Utilizing Sloshing of Water", *Wind Engineering*, 37: 557–566.

Roffel, A., Lourenco, R., Narasimhan, S. and Yarusevych, S. (2011). "Adaptive Compensation for Detuning in Pendulum Tuned Mass Dampers" *ASCE Journal of Structural Engineering*, 137(2): 242-251.

Ross, A.S. (2009). "*Application of Tuned Liquid Dampers to Mitigate Wind-Induced Torsional Motion*", M.E.Sc. Thesis, The University of Western Ontario, London, ON, Canada.

SHARCNET: is one of seven HPC consortia in Canada that operates under the umbrella of Compute/Calcul Canada, (https://www.sharcnet.ca).

Soong, T.T. and Dargush, G.F. (1997). "*Passive Energy Dissipation Systems in Structural Engineering*, Wiley", New York, NY, USA.

Sun, L.M., Fujino, Y., Pacheco, B.M. and Isobe, M. (1989). "Nonlinear Waves and Dynamic Pressures in Rectangular Tuned Liquid Dampers: Simulation and Experimental Verification", *Structural Engineering/Earthquake Engineering*, 6(2): 251-262.

Sun, L.M. (1991). "*Semi-Analytical Modelling of Tuned Liquid Damper (TLD) with Emphasis on Damping of Liquid Sloshing*", Ph.D. Thesis, University of Tokyo, Tokyo, Japan.

Sun, L.M., Fujino, Y. and Chaiseri, P. (1992). "Modeling of Tuned Liquid Damper (TLD)", *Journal of Wind Engineering and Industrial Aerodynamics*, 43(1–3): 1883–1894.

Tait, M.J. (2004). "*The Performance of 1D and 2D Tuned Liquid Dampers*" Ph.D. Thesis, The University of Western Ontario, London, ON, Canada.

Tait, M.J., E1 Damatty, A.A. and Isyumov, N. (2004a). "Testing of Tuned Liquid Damper with Screens and Development of Equivalent TMD Model", *Wind and Structures*, 7(4): 215–234.

Tait, M. J., Isyumov, N. and E1 Damatty, A. A. (2004b). "The Efficiency and Robustness of a Unidirectional Tuned Liquid Damper and Modelling with an Equivalent TMD", *Wind and Structures*, 7(4): 235–250.

Tait, M.J., El Damatty, A.A. and Isyumov, N. (2005a). "An Investigation of Tuned Liquid Dampers Equipped with Damping Screens Subjected to 2D Excitation", *Earthquake Engineering and Structural Dynamics*, 34(7): 719–735.

Tait, M.J., El Damatty, A.A., Isyumov, N. and Siddique, M.R. (2005b). "Numerical Flow Models to Simulate Tuned Liquid Dampers (TLD) with Slat Screens", *Journal of Fluid and Structures*, 20: 1007–1023.

Tait, M.J., Isyumov, N. and E1 Damatty, A.A. (2007). "Effectiveness of a 2D TLD and Its Numerical Modeling", *Journal of Structural Engineering*, 133(2): 251–263.

Tait, M.J. (2008). "Modelling and Preliminary Design of a Structure–TLD System", *Engineering Structures*, 30: 2644–2655.

Warburton, G.B. (1982). "Optimum Absorber Parameters for Various Combinations of Response and Excitation Parameters", *Earthquake Engineering and Structural Dynamics*, 10(3): 381–401.

Warnitchai, P. and Pinkaew, T. (1998). "Modeling of Liquid Sloshing in Rectangular Tanks with Flow-Dampening Devices", *Engineering Structures*, 20(7): 593–600.

Yu, J.K. (1997). "*Nonlinear Characteristics of Tuned Liquid Dampers*", Ph.D. Thesis, University of Washington, WA, USA.

Yu, J.K., Wakahara, T. and Reed, D. A. (1999). "A Non-Linear Numerical Model of the Tuned Liquid Damper", *Earthquake Engineering and Structural Dynamics*, 28: 671-686.

Table 2.1. Building Properties

Excitation Type	Excitation Amplitude (N)	f_s (Hz)	Ω	μ (%)	Generalized Model			Frame Element Model		
					M^* (kg)	K^* (N/m)	C^* (kg/sec)	ζ_s (%)	L_c (m)	EI_c (N.m^2)
Harmonic	23	0.558	0.98	2.50	4040	49,656	28.33	0.10	3.0	446,904
Random	150									

Table 2.2. TLD Properties

Excitation Type	f_{TLD} (Hz)	h (m)	L (m)	b (m)	m_w (kg)	m_{TLD} (kg)	S
Harmonic / Random	0.546	0.119	0.966	0.874	100.5	77.6	0.42

Table 2.3. Fluid Model Excitation Amplitudes

Excitation Amplitude	
A (mm)	A/L
2.5	0.0026
5.0	0.0052
7.5	0.0078
10.0	0.0100
12.5	0.0129
15.0	0.0155
20.0	0.0207
30.0	0.0311
40.0	0.0414
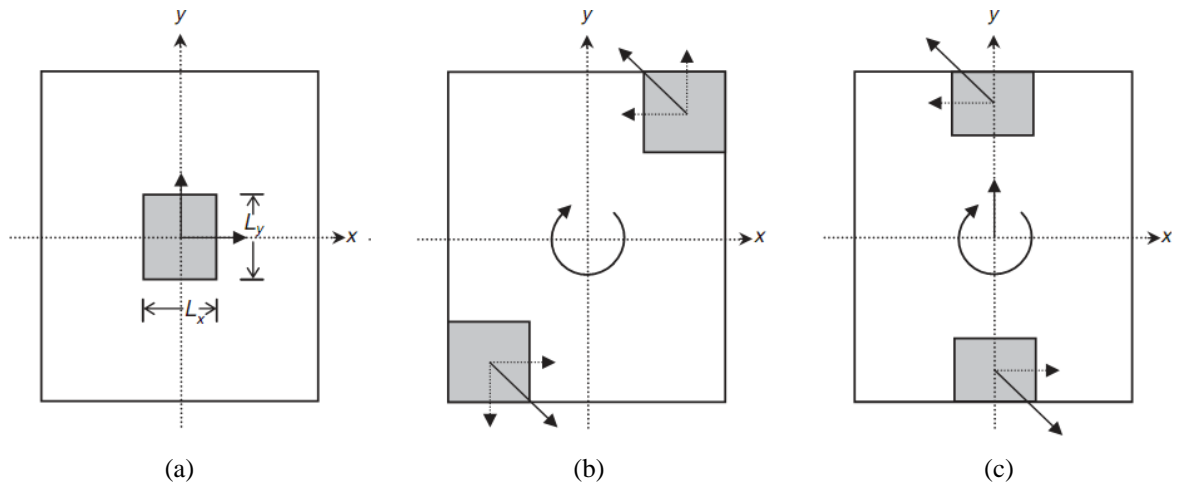
Fig. 2.1. Example of Bi-Directional TLD Configurations to Suppress: (a) Perpendicular Sway Modes, (b) a Pure Torsion Mode, and (c) Combined Sway and Torsion (from Tait et al. 2005)
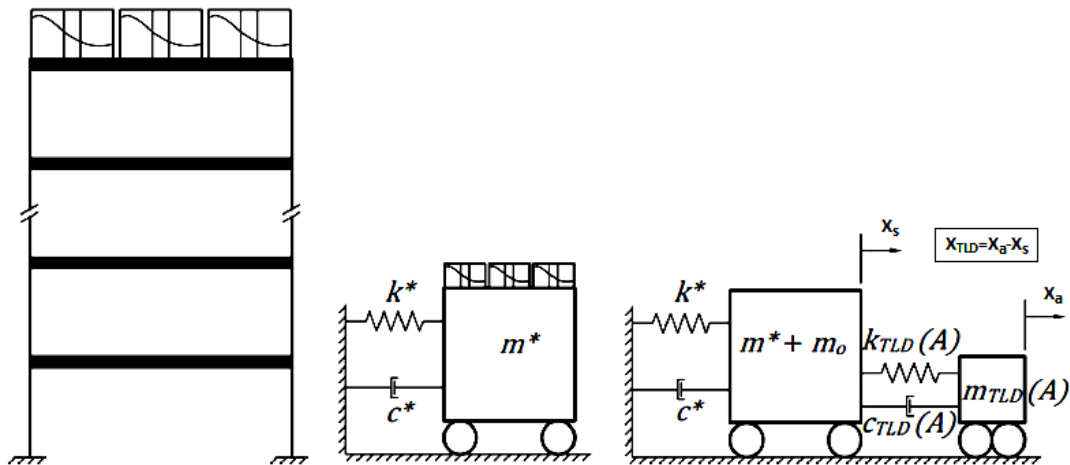
Fig. 2.2. The Evolution of (a) a Structure-TLD System into (b) a Generalized Structural System with TLDs then into (c) a System with Equivalent TMD Representation (after Ross 2009)
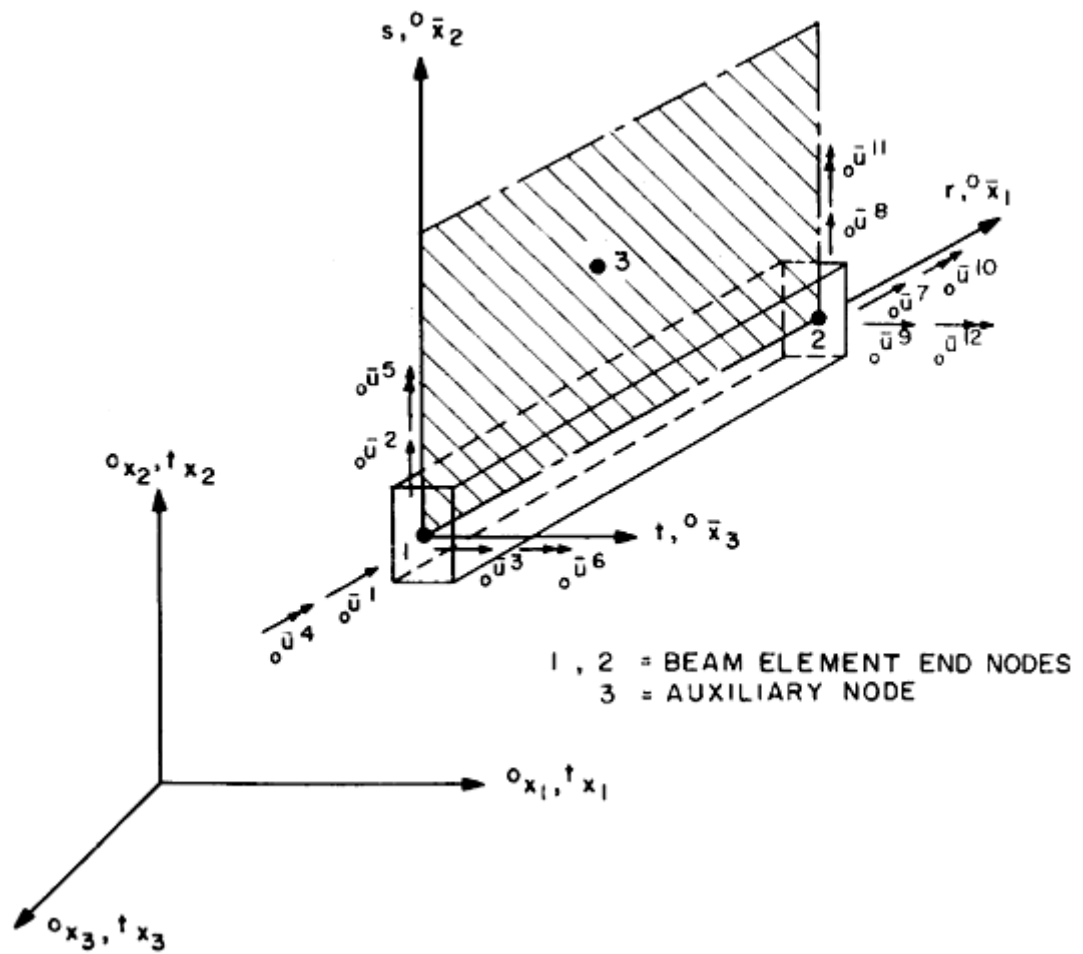
Fig. 2.3. Schematic View of the Three Dimensional Beam Element and Local Co-ordinate Axes (from Bathe and Bolourchi 1979)
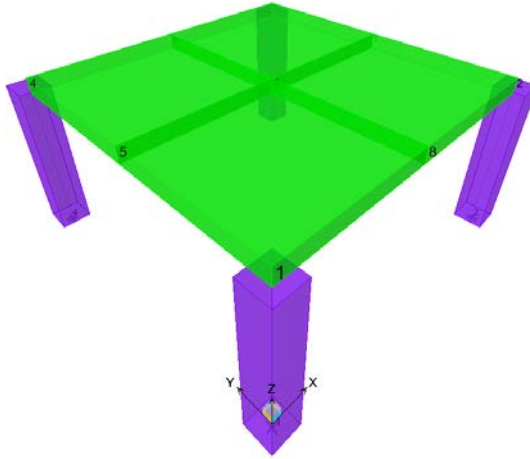
Fig. 2.4. 3D View of a Single-Story Structure Modelled with a Slab (SAP2000-Model 1)
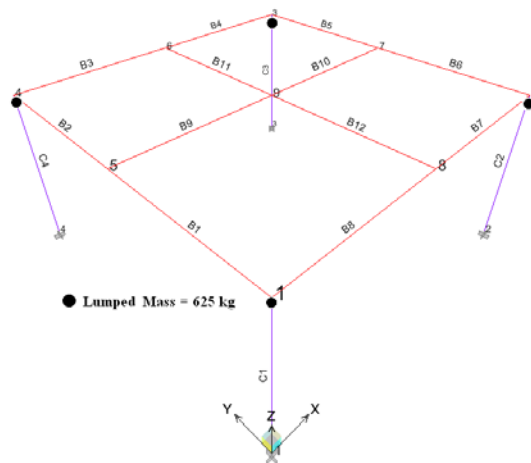
Fig. 2.5. A Schematic Diagram for the Frame Element Model Indicating Numbering and Lumped Mass Locations.
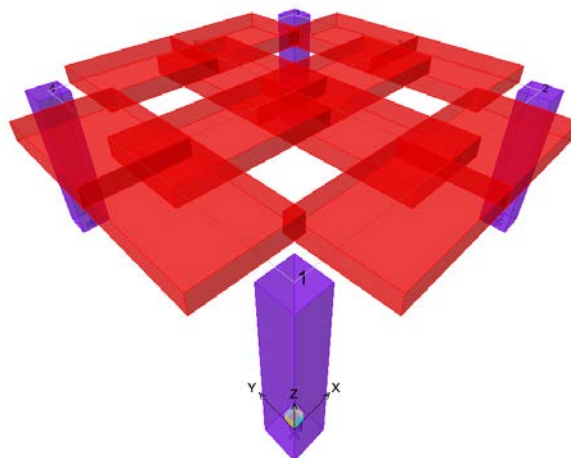
Fig. 2.6. A 3D Single-Story Structure Modelled with Horizontal Frame Elements to Simulate the Slab (SAP2000-Model 2)
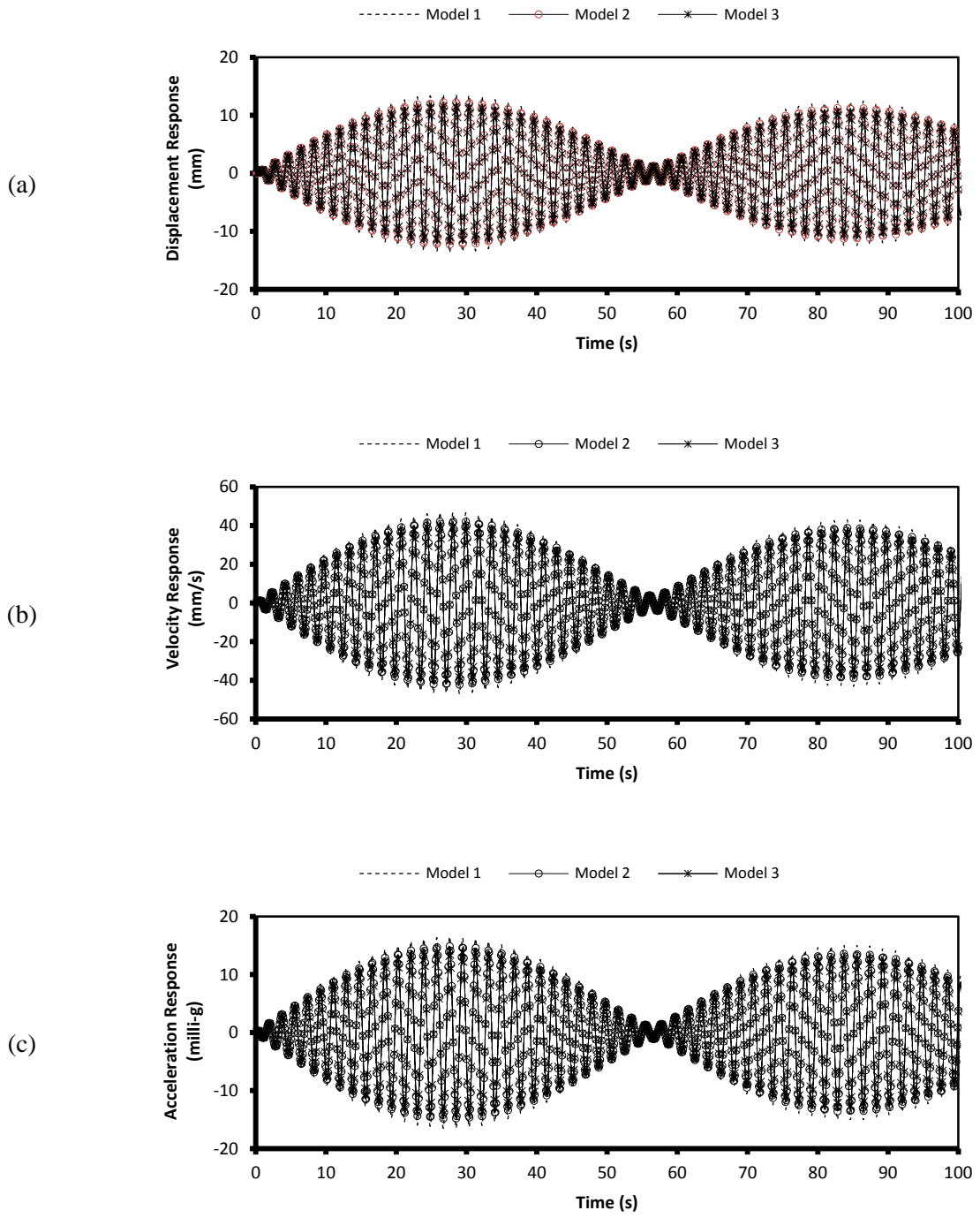
Fig. 2.7. 3D-Structure Responses for Harmonic Excitation (a) Displacement, (b) Velocity, and (c) Acceleration
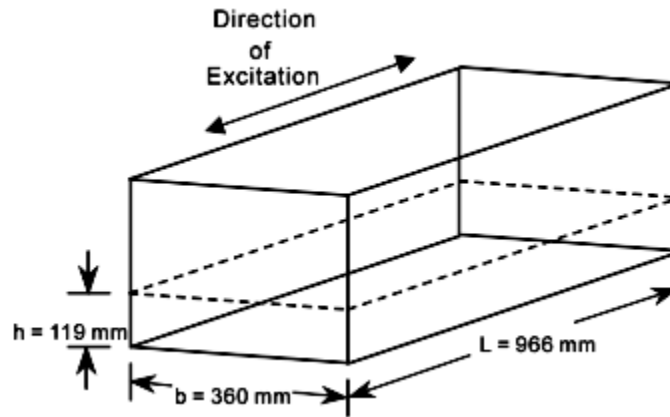
Fig. 2.8. Schematic of a TLD and its Dimensions (from Tait et al. 2004a)

Fig. 2.9. Photograph of a TLD Equipped with Internal Damping Screens (from Tait et al. 2004a)
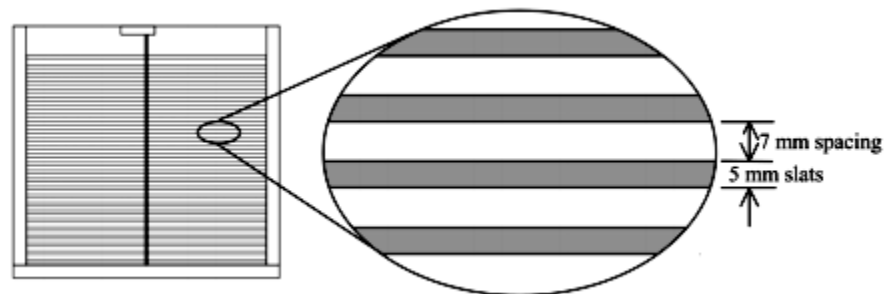
Fig. 2.10. View of the Tank Set-up End View and Enlarged View of the Screen (from Tait et al. 2004a)
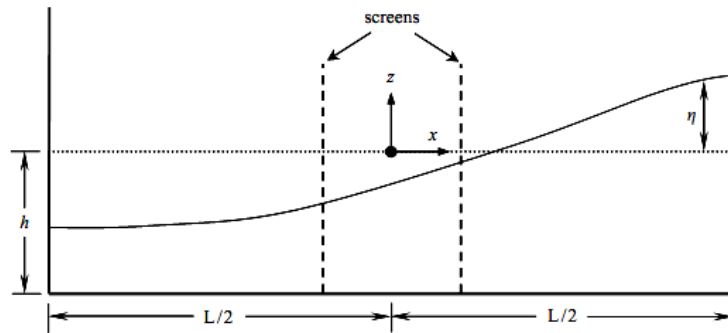
Fig. 2.11. Coordinate System for Nonlinear Shallow Water System (from Tait et al. 2005b)
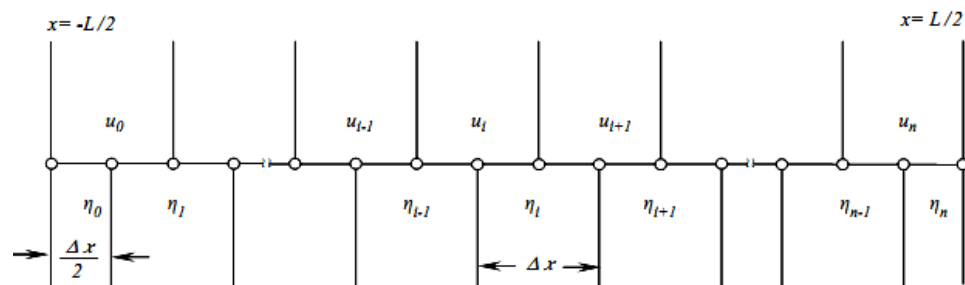
Fig. 2.12. Discretization of the Tank Length with Respect to x (from Tait et al. 2005b)
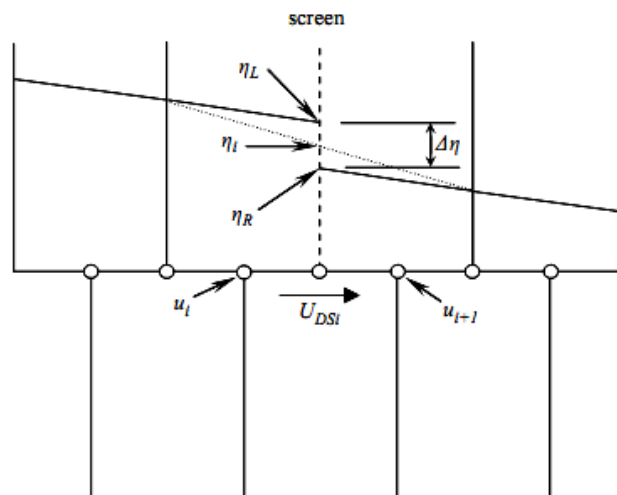
Fig. 2.13. Discretization and Modelling of the Screen (from Tait et al. 2005b)
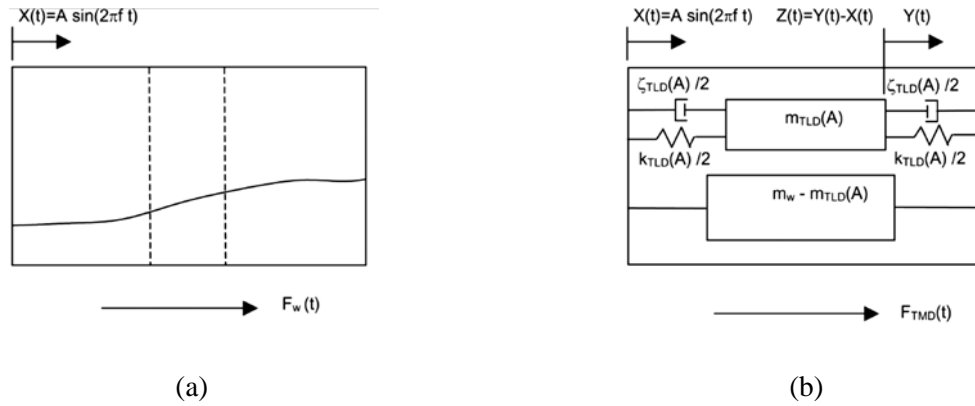
Fig. 2.14. TLD and EADTMD Model (a) TLD Equipped with Damping Screens, and (b) EADTMD Model (from Tait et al. 2004a)
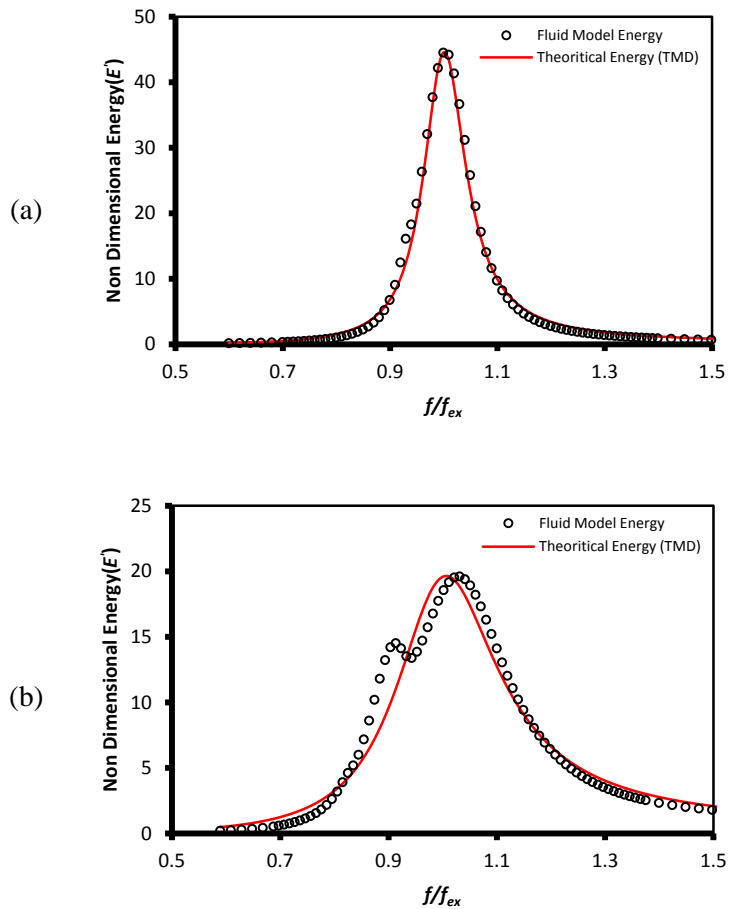
Fig. 2.15. Normalized Energy Dissipation Frequency Response Curves from the Nonlinear TLD Fluid Model and the EADTMD Model for (a) A/L=0.0026, and (b) A/L=0.0129
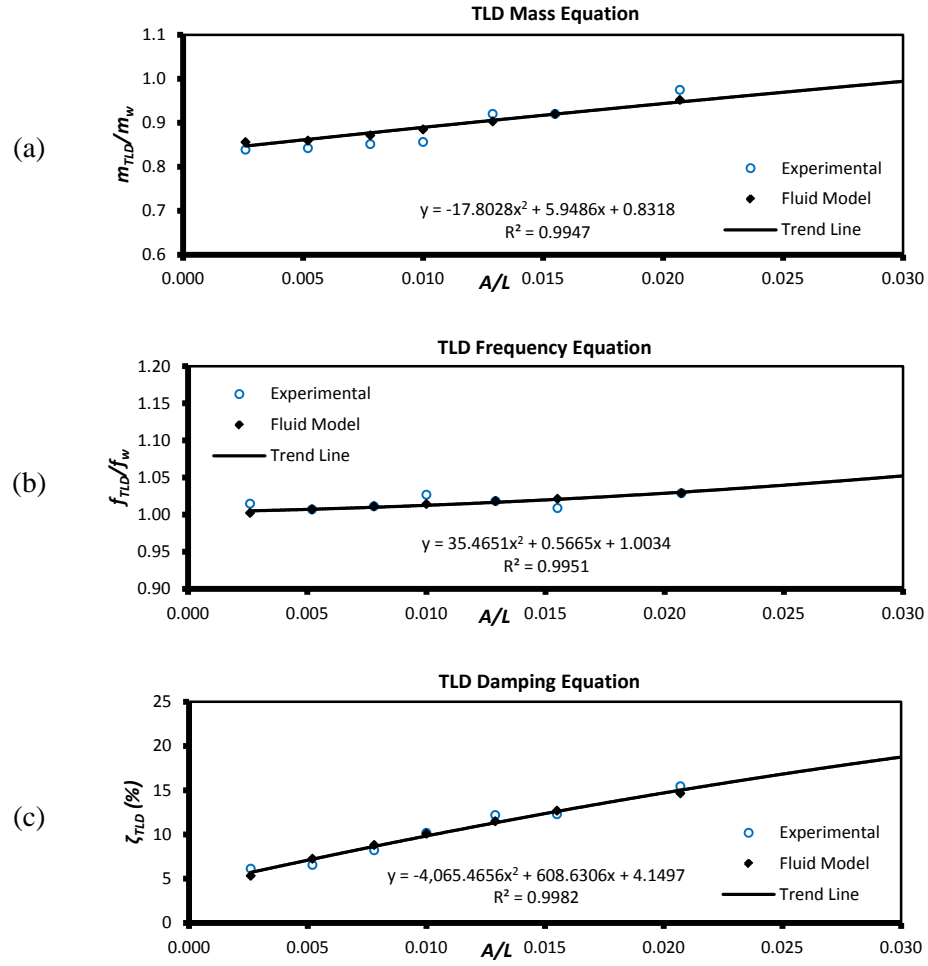
Fig. 2.16. Equivalent Amplitude Dependent Tuned Mass Damper (EADTMD) Properties
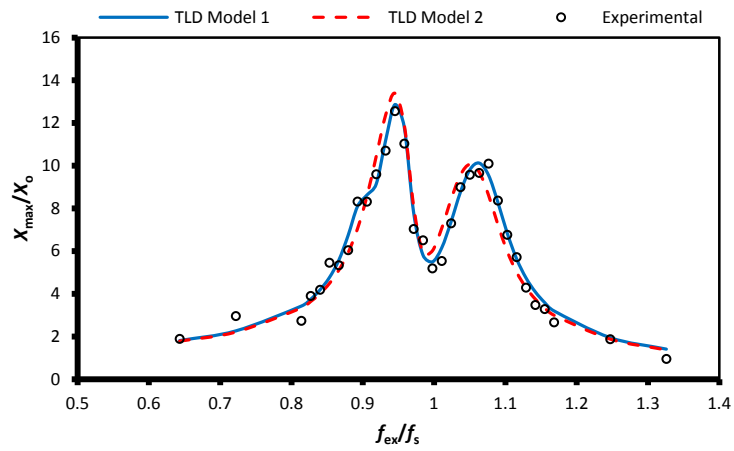
Fig. 2.17. Frequency Response Curves For the 3D-Structure-TLD System Model
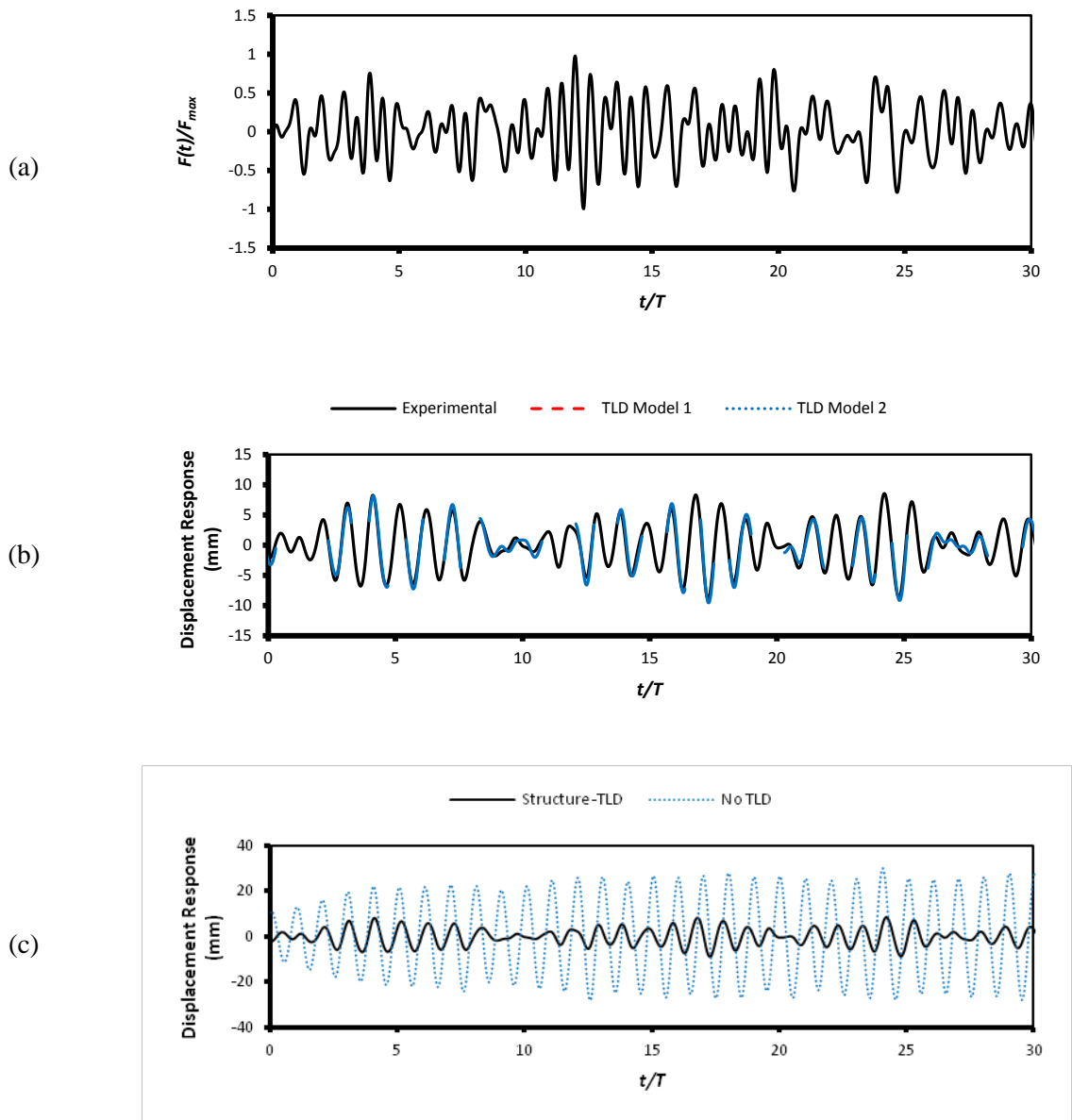
Fig. 2.18. For Minute 31 (a) Time History of the Random Excitation Force with F_{max}=150 N, (b) Displacement Response Comparison of 3D-Structure-TLD System Model Employing Two Nonlinear TLD Models, and (c) Structural Displacement Response with/without TLD Attached

Chapter 3: Three Dimensional Analysis of a High-Rise Building Equipped with Multiple Tuned Liquid Dampers Using Wind Tunnel Loads

3.1.   Introduction

A dynamic vibration absorber (DVA) can be used to reduce excessive resonant vibrations to acceptable levels by adding effective damping to a structure (Sun et al. 1989; Modi et al. 1990; Sun et al. 1992; Koh et al. 1994; Soong and Dargush 1997; Tait 2004). A tuned liquid damper (TLD) is a special type of passive DVA that consists of a rigid tank, which is partially filled with a liquid (usually water). The TLD is attached to the building at selected locations. The resulting inertia forces, which develop from the sloshing liquid motion inside the tank, modify the dynamic response of the building. These forces are approximately anti-phase to the excitation forces acting on the structure, resulting in a reduction in resonant motions (Kareem et al. 1999; Tait et al. 2004a; Tait et al. 2005a). The TLD has a number of potential advantages over the more commonly employed tuned mass damper (TMD). These advantages include: operation under small and large amplitude vibrations, ease of tuning, a low probability of failure and relatively low manufacturing, installation and maintenance costs.

Adding TLDs to suppress a particular mode of vibration, for example a sway mode, could result in increased excitation of other modes of vibration, such as a torsional mode. Accordingly, torsional response motions may result not only from the geometry of the structure itself and wind loading on the building at certain angles, but may also be amplified by the addition of TLDs. As a result, it is prudent to conduct a full three dimensional (3D) dynamic analysis of the building equipped with tuned liquid dampers, which captures the interaction of different modes of the building and the nonlinear behaviour of the TLD(s). Consequently, the 3D-Structure-TLD system model, developed and validated in Chapter 2, is expanded to a multiple 3D-Structure-TLD system model (3D-Structure-MTLD). This model is employed to estimate the response of a multi-modal full-scale high-rise building subjected to wind tunnel time history loads recorded at different locations on the building's width and height (i.e. surface).

Criteria for acceptable wind-induced motions are related to human perception thresholds, which are calculated using a probabilistic approach and experimental evaluation. Based on this concept, the BLWTL has recommended the following criteria for acceptable

accelerations for a 10-year return period, 10 to 15 milli-g for residential buildings, 15 to 20 milli-g for hotels and 20 to 25 milli-g for office buildings (Isyumov 1994). The serviceability criteria in the National Building Code of Canada (NBC) only addresses inter-story drift; therefore, serviceability criteria dictated by the BLWTL are taken as the acceptable limits.

A 38-story reinforced concrete building (Indianapolis building, Indianapolis, Indiana, USA) with a height of 154.6 m and plan dimensions of 32 m by 54 m is considered in this study, and is an actual structure tested previously in the Boundary Layer Wind Tunnel Laboratory (BLWTL) at the University of Western Ontario, London, Ontario, Canada. The lateral load resisting elements of the building are shear walls. The stiffness disparity and non-coinciding centre of mass (CM) and centre of twist (CT) (i.e. centre of rigidity), lead to a coupled lateral and torsional response. In addition, the applied wind loads from different directions causes a high torsional action at some specific wind loading angles (θ_w). Recorded wind loading information and structural response characteristics were considered when this particular building was selected.

In this chapter, the building described above is analyzed using recorded wind tunnel data, with and without TLDs placed at specified locations on the top of the building. The 3D-Structure-MTLD system model is used to conduct this analysis. TLDs to suppress the first two modes of vibration of the building are designed and placed at the centre of mass (CM) of the uppermost floor ($z = 154.6$ m). Subsequently, an additional set of TLDs is placed at selected corners of the building to achieve the target structural response values at both the centre and the four corners of the building.

3.2. Details of the Wind Climate Used in the Study (BLWT-SS3-2007)

3.2.1 Meteorological Data

The wind climate model has been developed using the meteorological data from the Indianapolis International Airport (Station 724380, period of record: Jan. 1973- Oct. 2006), obtained from the Boundary Layer Wind Tunnel Laboratory (BLWTL) at the University of Western Ontario. The methodology used for its development is detailed in BLWTL (1999). From this model, predicted wind speeds, regardless of wind direction, for various return periods can be derived. The record of annual extremes was used to predict wind speeds at various return periods. Based on the analysis of the hourly records, the predicted hourly-mean wind speed at 10 m, corrected for a standard open exposure definition, is 20.0 m/s

(45.0 mph) for a return period of 50 years, equivalent to a 3 seconds gust speed of 30.7 m/s (69.0 mph). Analysis of the annual extremes gives a 50-year return period hourly mean speed of approximately 24.0 m/s (54.0 mph).

3.2.2   Statistical Wind Climate Model

The predicted wind speeds have been determined using the up-crossing method as described in BLWTL (1999). A design probability distribution of upper level (at 500 m height) wind speed and direction representing the extra-tropical wind climate of Indianapolis was developed for the area on the basis of full-scale meteorological records. The directional characteristics of the wind events are indicated by the probability distributions discussed in detail elsewhere (BLWT-SS3-2007). Results from the wind tunnel study show that for strong winds, the southwest angle directions of the Indianapolis building are the most important, which is found to be in agreement with the results obtained in this study (see Section 3.4.2).

ASCE 7-05 recommended design wind speed in the Indianapolis area is specified as 40 m/s (90 mph, 3-seconds gust) at 10 m in open terrain for a return period of 50 years. This is equivalent to an hourly mean wind speed of 26.2 m/s (59 mph) at 10 m height. This is higher than the predicted wind speed from the annual extreme wind records of 24.0 m/s (54 mph). As such, for strength-related issues such as cladding pressures and loads, the wind climate model is scaled to match the wind speed requirement in ASCE 7-05. Therefore, the 3D-Structure-MTLD system model can be used to estimate different straining actions (i.e. normal force, shear force, bending moment and torque) for the lateral structural resisting elements (i.e. shear walls) utilizing the extreme mean hourly wind speed.

The wind speed at 10 m is converted to a mean hourly wind speed at a reference height of 500 m using a standard open exposure wind profile. Predictions of extreme and mean hourly wind speeds for various return periods are shown in Figure 3.1. The 10-year return period mean hourly wind speed at 500 m is 44 m/s (99 mph) for the code-matched model (i.e. strength-related issues) and 34 m/s (76.5 mph) for the unscaled wind climate model, which is used in this study for serviceability considerations.

3.3.   The Modelling of the Site and the Wind

3.3.1   Overall Approach

The basic tool used in BLWT-SS3-2007 is the boundary layer wind tunnel laboratory. The tunnel is designed with a long test section that allows extended models of upstream terrain to be placed in front of the model of the building under test. The modelling is done in more detail close to the site. The wind flow then develops characteristics, which are similar to the wind over the terrain approaching the actual site. This methodology is highly developed (Davenport and Isyumov 1968; Surry and Isyumov 1975; BLWT-SS3-2007) and is described below

3.3.2   Model Design

Close-up views of the 1:400 scale pressure model are shown in Figure 3.2. The main components of the model are:

1. The pressure model built in detail from ABS plastic and equipped with pressure measurement instrumentation (see Figure 3.2).
2. A detailed proximity model of the surrounding city built in block outline from Styrofoam for a radius of approximately 487.7 m (1600 ft) (see Figure 3.3).
3. Generic models of upstream terrain are detailed below (see Figure 3.3).

The building model and the proximity model are rotated to simulate different wind directions (θ_w) between $0°$ and $360°$ with the upstream terrain being appropriately changed. The upstream terrain was modelled using generic roughness blocks to produce wind characteristics representative of those at the project site. Three different exposures were used. They are shown in Figure 3.3 and the azimuth ranges, over which they were employed, are shown in Figure 3.4.

3.3.3   Characteristics of the Modelled Wind

The vertical profiles of the mean speed and the intensity of the longitudinal component of turbulence, measured just upstream of the centre of the turntable each upstream terrain exposure, are good representations of the expected full-scale wind speed variation with height but deviate somewhat from that expected in full-scale. To account for this, the reference wind speed measured in the wind tunnel has been adjusted to ensure that the roof height wind speed match the expected full-scale values (BLWT-SS3-2007).

3.4. Response of the Indianapolis Building with No-TLDs

3.4.1 Validation of a 3D Finite Element Model

The 38-story Indianapolis building is modelled using the commercial software package SAP2000 to compare its dynamic characteristics with that obtained from the 3D finite element model described in Chapter 2. Two techniques are employed to model the structure using the commercial software. The first technique models the slabs "as real slabs" including actual thickness and the mass distribution. The second technique uses beams that are rigid in plane, and sufficiently flexible out-of plane to represent the real action of the slabs in the building. These two techniques have been discussed and verified in Chapter 2.

A modal analysis is conducted on the building to investigate its fundamental vibration characteristics and to determine its mode shapes. Figure 3.5 displays the first three mode shapes, which correspond to natural periods of 7.31, 6.18 and 3.01 seconds. The torsional component of the mode shapes are multiplied by the overall radius of gyration (18.8 m) of the building to maintain dimensional consistency prior to being normalized. This technique allows for relative comparison of the mode shapes to be made in the three principles directions. It can be observed from Figure 3.5 that the structure has a dominate translational mode in the x-direction, a dominate translational mode in the y-direction and dominate torsional mode in the θ-direction with minor coupling action between x- and y-directions.

Figure 3.6 shows a typical floor plan of the building, modelled using the two different techniques discussed previously (i.e. Model 1: real slabs and shear walls using SAP2000; Model 2: slab beams and lumped mass using SAP2000). A modal analysis is carried out using both models and good agreement for the first three building periods and mode shapes are obtained with a maximum difference of less than 3% found. The shear walls are represented in the second model using frame elements with a box section having the same wall thickness and other dimensions. The shear walls that are connected together to make an L-shape or composed of two boxes adjacent to each other are joined by a rigid arm at the floor levels passing between their centres in order to behave as one unit. Each shear wall centre is then connected to nearby columns using beam elements, which are also used to connect the columns and act as the slabs. The second model is used to generate an input data file for the 3D finite element model (Model 3) to ensure the static and dynamic characteristics are matched.

Figures 3.7a and 3.7b show a 300-second time history of the structural displacement responses in the x- and y-directions, respectively, of the centre of mass (CM) at the uppermost floor ($z = 154.6$ m) corresponding to the critical wind loading angle (θ_w) of $210°$ (Section 3.4.2 further shows the critical wind loading angle). A 300-second time history of the structural velocity and acceleration responses in the x- and y-directions of CM at $z = 154.6$ m and $\theta_w = 210°$ are presented in Figures A1 and A2 (Appendix-A), respectively. The wind forces are applied to the structure as three different components, i.e. force in the x-direction, force in the y-direction and a moment that is transformed to an equivalent torque caused by two opposing forces separated by a distance. The forces are applied to the structure at 14 different elevations along its height as recorded by the pressure taps in the wind tunnel test model (BLWT-SS3-2007). Good agreement is found in the x- and y-directions between the different response histories for the three types of models, i.e. real slabs and shear walls using SAP2000, slab beams and lumped mass using SAP2000 and the 3D finite element model. The models are denoted as Model 1, Model 2 and Model 3 in Figures 3.7a and 3.7b, respectively.

3.4.2   Response of a 3D-FE Model Utilizing Excitation from Wind Tunnel Data

In this section, a dynamic analysis of a full-scale multi-modal 38-story high-rise building (Indianapolis building) is carried out using recorded wind tunnel loads as the applied excitation. A total of 36 tests are solved to represent different wind loading angles (θ_w) ranging between $0°$ and $360°$. The wind data includes the response-specific factors. These factors describe the relative importance of each wind loading angle tested (θ_w) and are calculated from the site-specific wind climate model obtained from the BLWTL (BLWT-SS3-2007). The response-specific factors are included in the wind tunnel loading data used in the dynamic analysis conducted in this study. The result is an average peak hourly acceleration response ($\ddot{x}$; $\ddot{y}$) and root-mean-square (RMS) acceleration response ($\sigma_{\ddot{x}}$; $\sigma_{\ddot{y}}$) of the centre of mass (CM) and the four corners ($C1$; $C2$; $C3$; $C4$) of the structure, in both x- and y-directions, at the uppermost floor ($z = 156.4$ m) to evaluate the building's serviceability conditions. The acceleration response values are expressed in terms of gravitational acceleration (milli-g). A response history analysis utilizing a 4-hour recorded wind loading event is carried out for each wind loading angle.

Figures 3.8 and 3.9 show the RMS acceleration responses of the structure in the x- and y-directions, respectively, for all wind loading angles. In the x-direction, the responses of the four corners and the structure's centre have similar values with the same trend. A peak RMS value ($\sigma_{\ddot{x}}$) of 6.3 milli-g occurs at wind loading angle (θ_w) of 210°. In contrast with the x-direction, the building responses at the centre of mass and the four corners display the same trend but have different values in the y-direction. A peak RMS value ($\sigma_{\ddot{y}}$) of 5.1 milli-g occurs at wind loading angle (θ_w) of 260° at $C1$ and $C4$, 4.3 milli-g at $C2$ and $C3$, and 4.6 milli-g at the CM. These results are in agreement with the BLWTL report (BLWT-SS3-2007), which stated that for strong winds, the southwest directions are the most important ($180° \leq \theta_w \leq 270°$), where θ_w equals 0° facing the north direction and increases in the clock-wise direction.

A maximum average peak hourly resultant acceleration response value ($R_{peak-hr}$) of 28.2 milli-g is calculated at $\theta_w = 210°$ as shown in Figure 3.10. This acceleration response value exceeds acceptable acceleration limits from wind-induced motion for residential buildings, hotels and office buildings. As described before, recommended limits for a 10-year return period were found to be 10 to 15 milli-g for residential buildings, 15 to 20 milli-g for hotels and 20 to 25 milli-g for office buildings (Isyumov 1994). Thus, the use of TLDs to reduce the Indianapolis building response accelerations to an acceptable perception level by adding effective damping to the system will be investigated.

3.5. TLD/TMD Background Information

Figure 3.11a shows a schematic of the TLD tank, which was used in the validation part of the 3D finite element model employed in this study and described in detail elsewhere (Chapter 2). Results of the 3D-Structure-TLD system model were compared to experimental work reported by Tait et al. (2004a and 2004b) and found to be in excellent agreement. The dimensions L, b and h represent the tank length (in the direction of excitation), the tank width (perpendicular to the excitation) and the still water depth, respectively. The fundamental sloshing frequency (f_w) for the water inside this tank using linear wave theory (Lamb 1932) can be estimated as

$$f_w = \frac{1}{2\pi} \sqrt{\frac{\pi g}{L} \tanh\left(\frac{\pi h}{L}\right)} \tag{3.1}$$

where g is the gravitational acceleration. An estimate of the natural frequency of the TLD (f_{TLD}) for small sloshing fluid response amplitudes, is approximately equal to f_w (Warnitchai and Pinkaew 1998; Ju et al. 2004; Tait et al. 2004a).

The tuning ratio, which influences the performance of the TLD, is defined as

$$\Omega = \frac{f_{TLD}}{f_s} \tag{3.2}$$

where f_{TLD} is the natural frequency of the TLD; and f_s is the natural frequency of the generalized structure having generalized mass, stiffness and damping values of M^*, K^* and C^*, respectively.

An important factor affecting the response of the system with TLD attached is the mass ratio (μ) which is given by

$$\mu = \frac{\phi^2 m_{TLD}}{M^*} \tag{3.3}$$

where M^* is the generalized mass of the primary structure corresponding to the vibration mode being suppressed and ϕ is the normalized modal deflection value of the structure at the TLD location. The absorber mass (m_{TLD}), for a TLD with damping screens can be approximated using potential flow theory (i.e. $m_{TLD} \approx m_1$), where m_1 is calculated using the following equation (Graham and Rodriguez 1952)

$$m_1 = \frac{8 \tanh\left(\frac{\pi h}{L}\right)}{\frac{\pi^3 h}{L}} m_w \tag{3.4}$$

where m_w is the total mass of the contained water.

Another parameter affecting the response of a structure-TLD system is the inherent damping ratio (ζ_{TLD}) of the sloshing fluid inside the tank. The inherent damping for sloshing liquid inside a rectangular TLD tank, without any additional devices inside, can be estimated by Sun (1992) using the following equation

$$\zeta_{TLD} = \frac{1}{2\pi} \sqrt{\frac{v_w}{\pi f_w}} \left(1 + \frac{h}{b}\right) \tag{3.5}$$

where v_w is the kinematic viscosity of water. An optimum inherent damping value for a linear tuned mass damper (TMD) as a function of the mass ratio (μ) can be obtained (Warburton 1982). Due to the analogy between the TMD and TLD devices, this formula can

be used to determine the target value of ζ_{TLD}. Screens formed by horizontal slats can be used as in the experimental work reported by Fediw (1992), Fediw et al. (1995) and Tait (2004) to increase ζ_{TLD} as shown in Figure 3.11b.

3.6. TLD Design Procedure to Suppress the First Two Modes of the Indianapolis Building

This section describes, in detail, the steps followed for the TLD design procedure to suppress the first mode of vibration of the building in one direction (x-direction) that can be repeated to suppress the second mode of vibration in the other direction (y-direction).

3.6.1 TLD Design Procedure

A TLD must be properly tuned and damped in order to perform effectively. While it is a straight forward procedure to optimally tune and damp a linear TMD to a linear structure, the process for a nonlinear TLD is more involved and requires knowledge of the target structural response amplitude to damp a TLD (Tait 2008) or to damp and tune a TLD (Love et al. 2011). The response of a TLD is amplitude dependent; therefore, it is necessary to establish the target RMS structural acceleration response value ($\sigma_{\ddot{x}-target}$). A reduction in the initial average peak hourly acceleration response value ($\ddot{x}_{initial}$) to a target average peak hourly value ($\ddot{x}_{target}$) utilizing a TLD has been achieved for a 2 DOF structure-TLD system model (i.e. generalized properties) by calculating the required mass ratio (μ) and the optimal TLD properties that satisfy the required level of effective damping ($\zeta_{eff-opt}$) (Tait 2008). In this study, a mass ratio value (μ) is selected, hence, the target average peak hourly acceleration response value utilizing a TLD is estimated ($\ddot{x}_{target}$) from the initial average peak hourly acceleration response ($\ddot{x}_{initial}$) occurring at the critical wind loading direction.

3.6.2 Modal Contribution Response Components (Modal Factors, *MF*)

To expand the applicability of using the preliminary TLD design procedure to a multi-modal high-rise building, which is the general case of the actual existing buildings; TLDs to suppress the first two modes of vibration of the Indianapolis building are designed utilizing the modal contribution response components following the preliminary TLD design procedure (Tait 2008). As a result, a spectral analysis is employed, using MATLAB®, to the uncontrolled response time history series of the centre and the four corners located at the uppermost floor ($z = 154.6$ m) obtained from the dynamic analysis in Section 3.5.

Consequently, the TLDs are designed according to the target modal RMS acceleration response component values ($\sigma_{\ddot{x}-target-m1}$; $\sigma_{\ddot{y}-target-m2}$) determined from the initial modal RMS values ($\sigma_{\ddot{x}-initial-m1}$; $\sigma_{\ddot{y}-initial-m2}$) at the TLD location and in its placement direction. Therefore, the modal contribution factors (MF) corresponding to each structural mode of vibration to be suppressed utilizing the TLDs must be determined.

Tables 3.1 and 3.2 show the initial RMS acceleration response values ($\sigma_{\ddot{x}-initial}$; $\sigma_{\ddot{y}-initial}$) of the Indianapolis building and their corresponding modal response component values ($\sigma_{\ddot{x}-initial-m1}$; $\sigma_{\ddot{y}-initial-m2}$). The TLDs, which are placed at the centre of mass of the uppermost floor (CM), are designed to suppress the first two modes (i.e. $m1$ and $m2$) that are mainly translational in the x- and y-directions. Spectral analysis results show that the CM response values in the x- and y-directions are mainly produced by the first two modes of the building where $MF > 94\%$. Therefore, the centre of mass (CM) is considered to be a suitable location for the TLDs. It should be noted that optimization of the TLD placement has not been considered in this study.

3.6.3   TLD Parameter Calculations

The assumed mass ratio for mode 1 in the x-direction (μ_x) enables the optimal structure-DVA tuning ratio (Ω_{opt_x}), the optimal DVA damping ratio (ζ_{opt_x}) and the optimal structure-DVA response ratio (R_{opt_x}) to be calculated for an undamped structure (Warburton 1982; Tait 2008; Love et al. 2011)

$$\Omega_{opt_x} = \frac{\sqrt{1+\frac{1}{2}\mu_x}}{1+\mu_x} \tag{3.6}$$

$$\zeta_{opt_x} = \sqrt{\frac{\mu_x+\frac{3}{4}\mu_x^2}{4+6\mu_x+2\mu_x^2}} \tag{3.7}$$

$$R_{opt_x} = \frac{\sigma_{r-x}}{\sigma_x} = \frac{1+\mu_x}{\sqrt{2\mu_x+\frac{3}{2}\mu_x^2}} \tag{3.8}$$

The effective damping provided by an optimally designed DVA ($\zeta_{eff-opt_x}$) is estimated using (Vickery and Davenport 1970; McNamara 1977; Gerges and Vickery 2003; Tait 2008; Love et al. 2011)

$$\zeta_{eff-opt_x} = \frac{1}{4}\sqrt{\frac{\mu_x+\mu_x^2}{1+\frac{3}{4}\mu_x}} \tag{3.9}$$

The total damping (ζ_{tot-x}) of a structure-DVA system consists of structural damping (ζ_s) and effective damping ($\zeta_{eff-opt_x}$) added by the optimally designed DVA can be obtained by (Luft 1979; Love et al. 2011)

$$\zeta_{tot-x} = 0.8\zeta_s + \zeta_{eff-opt_x} \tag{3.10}$$

Since the TLD is the DVA used in this study, therefore, the effective damping that must be added by the TLD to achieve the target modal RMS displacement response ($\sigma_{x-target-m1}$) can be calculated by (Love et al. 2011)

$$\zeta_{TLD-eff-opt_x} = \zeta_{tot-x} - 0.8\zeta_s = \zeta_s \frac{\sigma_{x-initial-m1}^2}{\sigma_{x-target-m1}^2} - 0.8\zeta_s \tag{3.11}$$

The initial modal peak hourly acceleration response value of the structure ($\ddot{x}_{initial-m1}$) can be related to the initial modal RMS acceleration response value ($\sigma_{\ddot{x}-initial-m1}$) using the peak factor (PF_{m1}) (Davenport 1964)

$$\sigma_{\ddot{x}-initial-m1} = \frac{\ddot{x}_{initial-m1}}{PF_{m1}}, \text{ where } \ddot{x}_{initial-m1} = \ddot{x}_{initial}. MF \tag{3.12}$$

Thus, the initial modal RMS displacement response value ($\sigma_{x-initial-m}$) can be estimated using

$$\sigma_{x-initial-m1} = \frac{\sigma_{\ddot{x}-initial-m1}}{\omega_{s-m1}^2} \tag{3.13}$$

Therefore, the target modal peak hourly RMS displacement response values ($\sigma_{x-target-m1}$) can be estimated using Equation 3.11 assuming that ζ_s is equal to 2% in this study.

The target modal RMS displacement response ($\sigma_{x-target-m1}$) enables the target modal RMS acceleration response ($\sigma_{\ddot{x}-target-m1}$) and the target RMS fluid response amplitude (TLD response, σ_{r-x}) to be determined by

$$\sigma_{\ddot{x}-target-m1} = \omega_{s-m1}^2 \sigma_{x-target-m1} \tag{3.14}$$

$$\sigma_{r-x} = R_{opt_x} \sigma_{x-target-m1} \tag{3.15}$$

Knowledge of the optimal TLD natural frequency in the x-direction corresponding to mode 1 ($f_{TLD-opt_x}$) using the calculated optimal tuning ratio (Ω_{opt_x}) allows the dimensions of the TLD to be estimated by

$$f_{TLD-opt_x} = \frac{1}{2\pi} \sqrt{\frac{\pi g}{L_x} \tanh\left(\frac{\pi h}{L_x}\right)} \tag{3.16}$$

where g is the gravitational acceleration.

The TLD damping ratio (ζ_{TLD-x}) is a function of the fluid viscosity, the target RMS fluid response amplitude (σ_{r-x}), the screen loss coefficient (C_{l-x}) and the location of the damping screen(s) (x_j) (Tait 2008)

$$\zeta_{TLD-x} = C_{l-x}\sqrt{\frac{32}{\pi^3}}\,tanh^2\left(\frac{\pi h}{L_x}\right)\Delta_x \Xi_x \frac{\sigma_{r-x}}{L_x} \tag{3.17}$$

where

$$\Delta_x = \left(\frac{1}{3} + \frac{1}{sinh^2\left(\frac{\pi h}{L_x}\right)}\right) \tag{3.18}$$

$$\Xi_x = \sum_{j=1}^{ns_x}\left|sin^3\left(\frac{\pi x_j}{L_x}\right)\right| \tag{3.19}$$

where ns_x is the number of damping screen(s) inside the tank in the x-direction.

Bi-directional TLDs, which act as two independent TLDs, can be used to control the first two sway modes of the structure in the x- and y-directions, simultaneously (Tait 2004; Tait et al. 2005a; Tait et al. 2008). To design a bi-directional TLD, the previous procedure is repeated considering the same fluid height obtained previously (h) and the assumed mass ratio for the second mode of vibration in the y-direction (μ_y). The calculation steps and the equations used in the TLD design to suppress the second mode of vibration the y-direction are shown in Table A1 (Appendix-A). The above design calculations in the x- and y-directions may have to be repeated in an iterative manner to achieve the selected mass ratio in both directions (μ_x; μ_y) as L_x represents the width of the tank in the y-direction and L_y represents the width of the tank in the x-direction. This is necessary when the water mass calculations, mentioned in detail in the next section, result in a different numbers of tanks in the x- and y-directions based on the chosen lengths of L_x and L_y to satisfy the selected mass ratios in both directions (μ_x; μ_y). It should be noted that an increased number of multiple tanks can be used to satisfy space restrictions. Section 3.6.5 presents a TLD design example to suppress the first two vibration modes of the Indianapolis building.

3.6.4 TLD Water Mass Calculations

The mass of water in a bi-directional TLD, $m_{w(1tank)}$ can be calculated using

$$m_{w(1tank)} = \rho_w.L.b.h \tag{3.20}$$

where ρ_w is the density of water, L is tank length, b is the tank width and h is the water depth.

By placing the TLD at the top of the building and for a pure translational mode shapes, the TLD mass ratio values for the first two mode shapes in the x- and y-directions, respectively (μ_x; μ_y) are defined as

$$\mu_x = \frac{m_{TLD-x}}{M_x^*}\phi_{TLD-x}^2 \tag{3.21}$$

$$\mu_y = \frac{m_{TLD-y}}{M_y^*}\phi_{TLD-y}^2 \tag{3.22}$$

where ϕ_{TLD-x} and ϕ_{TLD-y} are the mode shape values at the TLDs locations in both x- and y-directions, respectively.

In general, the mode shapes have both translational and torsional components. Thus, the resulting mass coupling terms introduced by the TLD must be considered. The generalized mass of the TLD(s) corresponding to the nth structural mode can be obtained using the following relationship

$$m_{TLD_n} = \{\phi_n\}^T[M_{TLD}]\{\phi_n\} \tag{3.23}$$

where $[M_{TLD}]$ is the TLD mass matrix and can be determined by transferring the mass of the TLDs back to the centre of mass of the structure (CM).

The TLD mass matrix can be determined by direct force equilibrium method. Thus, a unit acceleration is imposed on each degree-of-freedom (DOF) and the resulting mass influence coefficients can be determined. The derivation of the tuned mass damper (TMD) mass matrix, $[M_{TMD}]$, for a 3-dimensional mode shape was introduced by Yat (2009) (see Figure 3.12) and expressed as

$$[M_{TMD}] = \begin{bmatrix} m_1 + m_2 & 0 & m_2 e_{y2} - m_1 e_{y1} \\ 0 & m_1 + m_2 & m_2 e_{x2} - m_1 e_{x1} \\ m_2 e_{y2} - m_1 e_{y1} & m_2 e_{x2} - m_1 e_{x1} & m_1\left(e_{x1}^2 + e_{y1}^2\right) + m_2\left(e_{x2}^2 + e_{y2}^2\right) \end{bmatrix} \tag{3.24}$$

Due to the analogy between the TLD and the TMD, Equation 3.24 (Yat 2009) can be used to estimate the tuned liquid damper (TLD) mass matrix, $[M_{TLD}]$, for a 3-dimensional mode shape. The TLD tanks to suppress the first two modes of the Indianapolis building are placed at the centre of mass (CM), thus $e_{x1} = e_{x2} = e_{y1} = e_{y2} = 0$ leading to m_{TLD_n} equal to the summation of the participating water mass in these tanks (i.e. m_{TLD-x}; m_{TLD-y}), where

the participating water mass can be estimated using Equations 3.29 and 3.30 in the x- and y-directions, respectively. Consequently, Equations 3.21 and 3.22 can be used to determine the TLD mass ratio values for the first and second mode shapes in the x- and y-directions, respectively.

Thus, the required TLD mass in the x- and y-directions can be evaluated where M_x^* and M_y^* are the generalized mass of the structure in the x- and y-directions, respectively, corresponding to the structure's modes of vibration to be suppressed. The generalized mass values of the structure can be determined by

$$M_x^* = \sum_{i=1}^{i=N_f} (m_f)_i \, (\phi_{TLD-x}^2)_i \tag{3.25}$$

$$M_y^* = \sum_{i=1}^{i=N_f} (m_f)_i \, (\phi_{TLD-y}^2)_i \tag{3.26}$$

where N_f is the total floor numbers, m_f is the mass of each floor.

The number of TLDs required in both directions (N_{TLD-x}; N_{TLD-y}) is calculated using the following equations

$$N_{TLD-x} = \frac{m_{TLD-x}}{m_{TLD-x(1tank)}} \tag{3.27}$$

$$N_{TLD-y} = \frac{m_{TLD-y}}{m_{TLD-y(1tank)}} \tag{3.28}$$

where $m_{TLD-x(1tank)}$ and $m_{TLD-y(1tank)}$ are the participating mass of the sloshing fluid corresponding to the fundamental sloshing mode (Graham and Rodriguez 1952) and can be estimated in both directions by

$$m_{TLD-x(1tank)} \approx m_{1-x} = \frac{8 \, tanh\left(\pi \frac{h}{L_x}\right)}{\pi^3 \left(\frac{h}{L_x}\right)} m_{w(1tank)} \tag{3.29}$$

$$m_{TLD-y(1tank)} \approx m_{1-y} = \frac{8 \, tanh\left(\pi \frac{h}{L_y}\right)}{\pi^3 \left(\frac{h}{L_y}\right)} m_{w(1tank)} \tag{3.30}$$

The actual mass ratio values ($\mu_{x-actual}$; $\mu_{y-actual}$) as well as the total mass ratio of contained water (μ_w) can be calculated after the same numbers of tanks (N_{TLD-xy}) are determined for both directions of the bi-directional TLD tanks

$$\mu_{x-actual} = \frac{N_{TLD-xy} m_{TLD-x(1tank)}}{M_x^*} \tag{3.31}$$

$$\mu_{y-actual} = \frac{N_{TLD-xy} m_{TLD-y(1tank)}}{M_y^*} \tag{3.32}$$

$$\mu_w = \frac{N_{TLD-xy}m_{w(1tank)}}{M_s}$$ (3.33)

where M_s is the total structure mass given by

$$M_s = \sum_{i=1}^{i=N_f}(m_f)_i$$ (3.34)

3.7. Modelling and Response of the Indianapolis Building Equipped with Bi-Directional TLDs to Suppress the First Two Modes of Vibration

This section considers designing and adding bi-directional TLDs to reduce structural response levels to acceptable wind-induced motion criteria (Isyumov 1994) in two directions, simultaneously. For a bi-directional TLD (2D-TLD), a one-directional (1D) nonlinear TLD fluid model capable of simulating a TLD equipped with damping screens is employed to model a 2D-TLD. Application of this particular model requires the assumption that the response is decoupled and can be treated as the summation of two independent 1D-TLDs. Tait et al. (2005b) compared results from the nonlinear fluid model with 2D experimental shake table test values leading to a validation of the decoupled response assumption. Moreover, a structure-2D-TLD behaviour was experimentally examined over a range of excitation amplitude values covering the practical range of serviceability accelerations for buildings subjected to wind loads (Tait et al. 2007). Therefore, 2D-TLDs to suppress the first two modes of vibration are designed and installed in the Indianapolis building. Also, an evaluation of the two nonlinear TLD models, introduced in Chapter 2, and model selection are conducted.

3.7.1 TLD Models

This section presents briefly the two nonlinear TLD models, the nonlinear fluid model and the equivalent amplitude dependent tuned mass damper (EADTMD) model, which are used to simulate the TLD sloshing force in Section 3.7.2. Consequently, a TLD design example for a bi-directional TLD to suppress the first two modes of the Indianapolis building is presented using both nonlinear TLD models

3.7.1.1 Fluid Model (TLD Model 1)

A nonlinear numerical model of a TLD equipped with damping screens, developed by Kaneko and Ishikawa (1999) and assessed by Tait et al. (2005b). The nonlinear numerical model is briefly described below. Considering the tank, shown in Figure 3.11c, is excited in a

uni-directional motion, the nonlinear sloshing response can be expressed using shallow water theory as (Lepelletier and Raichlen 1988)

$$\frac{\partial \eta}{\partial t} + \frac{\partial}{\partial x}[(h + \eta)u] = 0 \tag{3.35}$$

$$\frac{\partial u}{\partial t} + u\frac{\partial u}{\partial x} + g\frac{\partial \eta}{\partial x} - \frac{1}{3}(h + \eta)^2 \frac{\partial^3 u}{\partial t \partial x^2} + \zeta_w u + \ddot{X} = 0 \tag{3.36}$$

where $\eta(x, t)$ is the free surface elevation, $u\,(x, t)$ is the horizontal velocity averaged through the liquid depth, L is the tank length, h is still liquid depth, g is the gravitational acceleration, $\ddot{X}$ is the horizontal base excitation acceleration of the tank, which is equal to that of the nodal acceleration at the TLD location and in the direction of the tank placement ($\ddot{x}_s$), and ζ_w is a damping coefficient, introduced by Miles (1967) to account for the viscous dissipation.

The above set of nonlinear shallow water equations can be solved numerically once the initial state of the liquid is prescribed, i.e. the values of η and h are given at time $t = 0$. A one-dimensional finite difference discretization scheme is applied for both η and h. The boundary conditions on the end walls of the tank are given as $u(-L/2, t) = u(L/2, t) = 0$. For a certain excitation amplitude, Equations 3.35 and 3.36 are integrated numerically using the Runge-Kutta-Fehlberg method after assigning the initial conditions for $\eta(x, 0) = 0$ and $u(x, 0) = 0$. The influence of the damping screens is modelled using a screen loss coefficient (C_l).

As described in Chapter 2, momentum theory to calculate the TLD base shear force, the mass of the ith element can be given by the following equation (Kaneko and Ishikawa 1999)

$$m_i = \rho \times \frac{L}{n_e} \times b \times \left(\frac{\eta_{i-1} + \eta_i}{2} + h\right) \tag{3.37}$$

where n_e is the total number of elements, L is the tank length, b is the tank width and ρ is the liquid unit weight.

Consequently, the momentum of the ith element can be described as follows

$$P = \sum_{i=1}^{n_e} m_i u_i = \frac{\rho L b}{n_e} \sum_{i=1}^{n_e} \left(\frac{\eta_{i-1} + \eta_i}{2} + h\right) u_i \tag{3.38}$$

The TLD base shear force ($F_{TLD_x-Model\,1}$) can be determined by the following equation

$$F_{TLD_x-Model\,1} = \frac{1}{\Delta t}(P(t) - P(t + \Delta t))$$

(3.39)

A significant reduction in the dynamic response of a high-rise building can be achieved if the TLD has sufficient inherent damping. The design procedure, outlined in Section 3.6.3, is used to estimate the initial damping screen requirements. Consequently, two different initial modal RMS acceleration response values ($\sigma_{\ddot{x}-initial-m1}$; $\sigma_{\ddot{y}-initial-m2}$) of 6.0 milli-g and 3.4 milli-g lead to two different target modal RMS acceleration values ($\sigma_{\ddot{x}-target-m1}$; $\sigma_{\ddot{y}-target-m2}$) of 3.1 milli-g and 1.8 milli-g in the x- and y-directions, respectively, for a selected mass ratio value of 6% ($\mu_x = \mu_y = 6\%$). It should be noted that the generalized mass ratio is equal to 6% ($\mu_x^* = \mu_y^* = 6\%$), where $e_x = e_y = 0$ for the TLDs placed at the CM. As a result, total target RMS acceleration response values ($\sigma_{\ddot{x}-target-t}$; $\sigma_{\ddot{y}-target-t}$) of 3.2 milli-g and 2.0 milli-g in the x- and y-directions, respectively, can be estimated using (see Tables 3.1 and 3.2)

$$(\sigma_{\ddot{x}-target-t})_i = (\sigma_{\ddot{x}-initial})_i - (\sigma_{\ddot{x}-initial-m})_i + (\sigma_{\ddot{x}-target-m})_i$$

(3.40)

$$(\sigma_{\ddot{y}-target-t})_i = (\sigma_{\ddot{y}-initial})_i - (\sigma_{\ddot{y}-initial-m})_i + (\sigma_{\ddot{y}-target-m})_i$$

(3.41)

where i is the vibration mode number.

The screens are designed to achieve the optimal damping ratio ($\zeta_{TLD-opt_x}$; $\zeta_{TLD-opt_y}$) at the above target modal RMS acceleration response values ($\sigma_{\ddot{x}-target-m1}$; $\sigma_{\ddot{y}-target-m2}$) (Tait 2004; Tait 2008; Cassolato et al. 2011). Table 3.3 shows the calculation steps used in the design procedure of the first mode tanks in the x-direction, while the same steps are repeated in the y-direction and are presented in Table A1 (Appendix-A). The screens are located at 40% and 60% of the tank length in both directions with loss coefficient values of $C_{l-x} = 9.8$ and $C_{l-y} = 20.3$, respectively. TLD tank dimensions are established as $L_x = 16.0$ m, $L_y = 13.4$ m, and $h = 1.9$ m. A total of 2 tanks are required to satisfy the selected mass ratio values following the water mass calculations found in Table 3.4.

3.7.1.2 EADTMD Model (TLD Model 2)

An equivalent amplitude dependent tuned mass damper (EADTMD) representing a partially fluid tank containing screens (TLD) can be determined based on either experimental results or using the nonlinear fluid model as described in Chapter 2. The dynamic characteristics of the equivalent TMD model, in terms of mass, stiffness and damping

parameters can be determined by energy equivalence. The validity of this nonlinear TLD model has been examined (Tait et al. 2004b). The energy dissipated by the equivalent TMD (E_d) shown in Figure 3.11d can be expressed in terms of the excitation amplitude, as

$$E_d = m_{TLD}(2\pi f)^2 A^2 \pi |H_{z/x}(f)| \left(\frac{f}{f_{TLD}}\right)^2 \sin(\theta_{z/x}) \tag{3.42}$$

Normalizing this expression by $1/2\, m_w (A2\pi f)^2$, results in

$$E_d' = \frac{m_{TLD}}{m_w} |H_{z/x}(f)| \left(\frac{f}{f_{TLD}}\right) 2\pi \sin(\theta_{z/x}) \tag{3.43}$$

where $|H_{z/x}(f)|$ is the frequency response function, referred to the modulus of the mechanical admittance function, between the TMD relative response motion and the shake table input motion

$$|H_{z/x}(f)| = \frac{1}{\sqrt{\left(1 - \left(\frac{f}{f_{TLD}}\right)^2\right)^2 + \left(2\zeta_{TLD}\left(\frac{f}{f_{TLD}}\right)\right)^2}} \tag{3.44}$$

and ($\theta_{z/x}$) is the corresponding phase angle given by

$$\theta_{z/x} = tan^{-1}\left(\frac{2\zeta_{TLD}\left(\frac{f}{f_{TLD}}\right)}{1 - \left(\frac{f}{f_{TLD}}\right)^2}\right) \tag{3.45}$$

A curve fitting procedure with constraints forcing the theoretical expression E_d' to match both the maximum value of the energy dissipated and the total energy dissipated over the range of frequencies tested is employed. This procedure is used to estimate the EADTMD parameters m_{TLD}, f_{TLD} and ζ_{TLD} (Tait et al. 2004a; Tait et al. 2004b).

The equation of motion of the equivalent TMD system can be written as

$$M_{TLD}.\ddot{x}_{TLD} + C_{TLD}.\dot{x}_{TLD} + K_{TLD}.x_{TLD} = -M_{TLD}.\ddot{x}_s \tag{3.46}$$

Hence, the TLD force $F_{TLD_x-Model\,2}$ can be expressed as

$$F_{TLD_x-Model\,2} = -M_{TLD}(\ddot{x}_s + \ddot{x}_{TLD}) \tag{3.47}$$

where x_s and x_{TLD} are the structure displacement and the relative displacement between the TLD and the structure, respectively.

The nonlinear TLD fluid model, using the tank properties obtained in Section 3.7.1.1, is employed to design the first mode (i.e. L_x; h; C_{l-x}) and the second mode (i.e. L_y; h; C_{l-y})

tanks, respectively, by sinusoidal discrete frequency sweep analysis on the TLD at selected amplitudes of excitation (A). Consequently, an equivalent TMD mass (m_{TLD}), frequency (f_{TLD}) and damping ratio (ζ_{TLD}) can be produced. A least squares fit is carried out to determine the amplitude dependent properties of the TLDs for mode 1 as shown in Figure 3.12. The same steps are repeated for mode two tanks in the y-direction and are presented in Figure A3 (Appendix-A). A unique set of these properties are determined for each mode to be suppressed and are used in the response evaluation of the Indianapolis building using the 3D-Structure-MTLD system model.

3.7.2   Modelling of Structure-TLD Systems

The high-rise building (i.e. primary system) is modelled as a discrete lumped mass system consisting of n lumped masses (see Figure 3.6b). The tuned liquid dampers (i.e. secondary system) can be attached to any level of the primary system and at any location on the floor plate.

The equation of motion of the combined system can be written as

$$[M]\{\ddot{x}\} + [C]\{\dot{x}\} + [K]\{x\} = \{F_{ext}(t)\} + [H]\{F_{TLD}(t)\} \tag{3.48}$$

where $[M]$, $[C]$ and $[K]$ are the mass, damping and stiffness matrices of the building (i.e. primary structure), $\{x\}$, $\{\dot{x}\}$ and $\{\ddot{x}\}$ represent the structural displacement, velocity and acceleration vectors, $\{F_{ext}(t)\}$ is the external load acting on the structure, $\{F_{TLD}(t)\}$ is control force vector of the TLD (i.e. base shear forces), and $[H]$ is the position matrix of the TLD in which its ith column vector $\{H\}_i = [0 \ldots 0 \; 1 \; 0 \ldots 0]_{1 \times n}^T$ (1 is in the jth column) indicates the ith group TLDs that are installed on the jth story.

Consideration of the non-participating mass component for both TLD Model 1 and Model 2 is described, in detail, in Chapter 2 for uni- and bi-directional tanks. The resulting mass matrix of the combined system, $[M]$, for TLD Model 1 is expressed as

$$[M] = [M_S] + [H]\left[M_{fluid}^{TLD-Model\,1}\right] = \begin{bmatrix} m_{1x} & & & & & & \\ & m_{1y} & & \cdots & & 0 & \\ & & m_{1z} & & & & \\ & \vdots & & \ddots & & \vdots & \\ & & & & m_{nx} & & \\ & 0 & & \cdots & & m_{ny} & \\ & & & & & & m_{nz} \end{bmatrix} +$$

$$[H] \begin{bmatrix} m_{1x-slosh.}^{TLD-Model\ 1} & & & & & \\ & m_{1y-orth.}^{TLD-Model\ 1} & & \cdots & & 0 \\ & & m_{1z}^{TLD-Model\ 1} & & & \\ & \vdots & & \ddots & & \vdots \\ & & & & m_{nx-slosh.}^{TLD-Model\ 1} & \\ & 0 & & \cdots & & m_{ny-orth.}^{TLD-Model\ 1} \\ & & & & & & m_{nz}^{TLD-Model\ 1} \end{bmatrix}$$

$$(3.49)$$

where $[M_S]$ is the stiffness matrix of the primary system and $\left[\mathrm{M_{fluid}^{TLD-Model\ 1}}\right]$ is the added mass to the primary structure at the TLD locations in the x, y and z directions considering the fluid model (TLD Model 1).

The following equation represents the mass matrix of the combined systems using the EADTMD model

$$[M] = [M_S] + [H]\left[M_{fluid}^{TLD-Model\ 2}\right] = \begin{bmatrix} m_{1x} & & & & & \\ & m_{1y} & & \cdots & & 0 \\ & & m_{1z} & & & \\ & \vdots & & \ddots & & \vdots \\ & & & & m_{nx} & \\ & 0 & & \cdots & & m_{ny} \\ & & & & & & m_{nz} \end{bmatrix} +$$

$$[H] \begin{bmatrix} m_{1x-slosh.}^{TLD-Model\ 2} & & & & & \\ & m_{1y-orth.}^{TLD-Model\ 2} & & \cdots & & 0 \\ & & m_{1z}^{TLD-Model\ 2} & & & \\ & \vdots & & \ddots & & \vdots \\ & & & & m_{nx-slosh.}^{TLD-Model\ 2} & \\ & 0 & & \cdots & & m_{ny-orth.}^{TLD-Model\ 2} \\ & & & & & & m_{nz}^{TLD-Model\ 2} \end{bmatrix}$$

$$(3.50)$$

where $\left[M_{fluid}^{TLD-Model\ 2}\right]$ is the added mass to the primary structure at the TLD locations in the x, y and z directions considering the amplitude dependent TMD model (TLD Model 2).

In cases where the secondary system has a considerable mass ratio value, the updated mode shapes of the primary structure can be determined and utilized in the design process. For example, Roffel et al. (2011) used the updated mode shapes to re-tune the DVA and better control the structural response to achieve improved performance. In this study, it was determined that the added mass had a negligible effect and as a result the original mode shapes and the natural frequencies were used in the TLD design.

3.7.3   Evaluation of Improved Performance Using TLDs (2 Modes)

The Indianapolis building is analyzed using measured wind loads from wind tunnel tests at 14 different heights to produce a time history of four hours duration. The computational time required for the nonlinear TLD fluid model is approximately 20 times greater than the time required for the EADTMD model. As previously mentioned in Chapter 2, the time step (Δt_1) used in TLD fluid model is less than $1/180$ of the structure's time period as recommended by Kaneko and Ishikawa (1999) in order to solve for the one-dimensional finite difference scheme. The time step (Δt_2) used for the EADTMD model is about $1/10$ of the structure's period to which the damper is tuned too in order to achieve suitable accuracy (Chopra 2001). In addition, a total of 4902 three dimensional beam elements are used to model the Indianapolis building, which must be updated and solved every time step during the entire numerical simulation process. Each simulation requires approximately 1.5 million time steps to complete and takes more than 75 hours of run time/hour time history using an Intel® Core™2 Quad processor 2.4 GHz.

Powerful computational machines with high capacity storage capabilities are essential to carrying out the dynamic analysis using the nonlinear TLD fluid model. SHARCNET™ (Shared Hierarchical Academic Research Computing Network) has been used to perform the analysis, as the building must be solved according to the time step dictated by the nonlinear TLD fluid model. SHARCNET™ is one of seven "HPC" (High Performance Computing) consortia in Canada that operates under the umbrella of Compute Canada. SHARCNET™ is a consortium of Canadian academic institutions who share a network of high performance computers. ["HPC" is the use of high-end computing resources (computers, storage, networking and visualization) to help solve highly complex problems, perform business critical analyses, or to run computationally intensive workloads that are in scale far beyond the tasks that could be achieved on today's leading desktop systems (www.sharcnet.ca)].

Figures 3.14a and 3.14b show a 300-second duration time history of the structural displacement response of the centre of mass (CM) of the building at the uppermost floor ($z = 154.6$ m) at the critical wind loading angle (θ_w) of 210° in the x- and y-directions, respectively. The nonlinear fluid model is denoted as TLD Model 1, while the EADTMD model is denoted as TLD Model 2. Structural velocity and acceleration responses, in the x- and y-directions, are shown in Figures A4 and A5 (Appendix-A), respectively.

As can be observed from Figures 3.14a and 3.14b, excellent agreement is found between the results obtained from the two models with a maximum percentage difference of 2% found between the RMS response values of the displacement, velocity and acceleration in both x- and y-directions. As a result, the TLD Model 2 is selected to be used for the rest of the study reported on in this chapter as it is found to achieve sufficient accuracy.

The effect of adding TLDs to suppress the first two modes of the building is shown in Figures 3.15 and 3.16 by comparing the response histories of displacement, velocity and acceleration with and without TLDs installed in the x- and y-directions, respectively. The response time histories are taken at the centre of mass (CM) of the uppermost floor for the first 300 seconds of the applied wind excitation. As can be seen from Figures 3.15 and 3.16, all response values are reduced.

3.7.4   Response Evaluation of the Indianapolis Building

In this section, a total of 36-time history analyses, corresponding to wind loading angles (θ_w) between 0° and 360°, are carried out utilizing the 3D-Structure-MTLD system model implemented with bi-directional TLDs to suppress the first two modes of vibration of the Indianapolis building.

It can be observed from Figure 3.8 that all corners have nearly the same RMS structural acceleration response values ($\sigma_{\ddot{x}}$) as that of the centre of mass (CM) in the x-direction for the No-TLD case. This can be attributed to the fact that centre of twist (CT) is located close to the x-axis (see Figure 3.6a). Due to the location of CT in $(+)y$-direction, a small increase in the RMS acceleration response values for corners $C1$ and $C2$ occurs. Figure 3.17 shows an RMS structural acceleration response value of 3.1 milli-g at the critical wind loading angle (θ_w) of 210° at the centre of mass (CM) in the x-direction, which is approximately 3% less than the calculated total target response value ($\sigma_{\ddot{x}-target-t}$) of 3.2 milli-g. The initial modal RMS acceleration ($\sigma_{\ddot{x}-initial-m1}$) has been reduced from an original value of 6.0 milli-g to 2.8 milli-g.

Figure 3.18 shows that the resulting RMS structural acceleration response value of 2.2 milli-g in the y-direction at the centre of mass (CM) exceeded the total target RMS structural acceleration response value ($\sigma_{\ddot{y}-target-t}$) of 2.0 milli-g by less than 10%. However, the

initial modal RMS acceleration ($\sigma_{\ddot{y}-initial-m2}$) has been reduced from an original value of 3.4 milli-g to 1.4 milli-g, which is 0.4 milli-g less than the target value.

Changes have also occurred in the percentage contribution to the total structural response from the uncontrolled structural modes. For example, the modal factor value (MF) of the third mode has increased from 0.4% to 2.4%, while the modal factor value (MF) for the remaining higher modes has increased from a value of 0.5% to 3.2% at the CM location in the x-direction. In the y-direction at the CM location, the modal factor value (MF) of the third mode has increased from 1.2% to 9.2%, while the modal factor value (MF) for the remaining higher modes has increased from a value of 0.9% to 7.4%. The first modal RMS response component values at the four corners of the building in the x-direction are reduced by 59.1% to 62.3% compared to a percentage reduction value of 54.0% at the centre of mass (CM) (see Table 3.5). In the y-direction, percentage reduction values of the second modal RMS response component at the corners of the building are found to range between 75.3% and 76.0% compared to 60% reduction at the centre of mass (CM) (see Table 3.6).

In contrast, an amplification of the third mode x- and y-structural acceleration response values has occurred. In the x-direction, the modal factor values (MF) of the third mode ranged between 0.4%, at the CM, and 2.3%, at $C3$ and $C4$, for the uncontrolled structure, while the range has been amplified from 2.4% (at CM) to 37.3% (at $C3$ and $C4$) after installation of the TLDs. Therefore, the third mode structural response component values are increased from 0.1 milli-g to 1.5 milli-g. Although, an amplification of the third modal response components has occurred, a percentage reduction value of the total structural acceleration response of 49.8% is achieved at the CM, while values of 40.4% and 31.9% are achieved at $C1$, $C2$ and $C3$, $C4$, respectively (see Table 3.5).

The third modal factor values (MF) of the structural response components, in the y-direction, are nearly doubled compared to the amplification values found in the x-direction. The modal factor values, which ranged between 1.2% (at CM) and 17.9% (at $C2$ and $C3$) for the uncontrolled structural responses, are increased by 9.2% at the CM and 74.0% at $C2$ and $C3$. As a result, the third mode structural response component values are increased from 0.6 milli-g to 3.8 milli-g. Furthermore, an increase in the total structural response in the y-direction at the corners of the building has occurred. However, at the CM, a response

reduction of 39.3% is achieved as mode 3 only contributes 9.2% to the total structural acceleration response in the y-direction at this location (see Table 3.6).

Overall, positive percentage reduction values of the average peak hourly resultant acceleration ($R_{peak-hr}$) are achieved at the centre of mass and the corners at the critical wind loading angle (θ_w) of 210° (see Table 3.9 and Figure 3.20). Table 3.9 shows that percentage response reduction values range between 6.4% and 24.7% at the four corners, while a reduction response value of 47.1% is achieved at the centre of mass (see Figure 3.18). The resultant acceleration is the acceleration felt by the occupants in the building and is related to human perception thresholds (Isyumov 1994). Hence, the average peak hourly resultant acceleration response values ($R_{peak-hr}$) presented in Figure 3.17 are used to compare with the acceptable wind-induced motions in Section 3.7.5.

3.7.5   Serviceability Check of the Indianapolis Building

Figure 3.10 shows that the maximum average peak hourly resultant acceleration response values ($R_{peak-hr}$) occurred at the corner and at the centre of mass (CM) of the uppermost floor of the Indianapolis building at the critical wind loading angle (θ_w) of 210°. For the No-TLDs case, the maximum corner and CM accelerations are 28.2 milli-g and 26.4 milli-g compared to values of 24.6 milli-g and 13.9 milli-g for the case of TLDs installed, respectively, as shown in Figure 3.19. Therefore, the TLD system installed to suppress the first two modes of vibration of the Indianapolis building is found to reduce the maximum average peak resultant acceleration to the acceptable level for office buildings, i.e. 20 milli-g $\leq R_{peak-hr} \leq 25$ milli-g (Isyumov 1994).

Figure 3.20 shows the percentage response reduction values ($\Psi_{peak-hr}$) of the average peak hourly resultant accelerations ($R_{peak-hr}$) for the centre of mass (CM) and the four corners of the Indianapolis building. $\Psi_{peak-hr}$ is expressed as

$$\Psi_{peak-hr} = \left(\frac{R_{peak-hr\,(No-\,TLD)} - R_{peak-hr\,(with\,TLD)}}{R_{peak-hr\,(No-TLD)}} \right) . 100 \tag{3.51}$$

where $R_{peak-hr\,(with\,TLD)}$ and $R_{peak-hr\,(No-TLD)}$ are the structural acceleration responses with and without TLDs installed, respectively.

Figure 3.20 shows that the reduction values at the CM are significantly greater than at the corners and show less variation with wind angle. The reduction values are found to vary in

the range of 10% and a maximum percentage reduction value ($\Psi_{peak-hr}$) of 50% is achieved at the CM. The response reduction values at the corners ($\Psi_{peak-hr}$) range between -2% and 36% and are found to vary in the range of 20%.

At the critical wind loading angle (θ_w) of 210°, $R_{peak-hr}$ value at the centre of mass (CM) is reduced by 47.1%, while the acceleration response values of the corners are reduced by 6.4% to 24.7% (see Table 3.9). The reduction in RMS acceleration response values ($\sigma_{\ddot{x}}$) in the x-direction at building's corners (see Figure 3.17) exceeds the amplified RMS values ($\sigma_{\ddot{y}}$) in the y-direction. It can be observed that the resultant acceleration response value ($R_{peak-hr}$) at $C3$ increased with the addition of TLDs by only 2% at two wind loading angles (220°; 340°) as shown in Figure 3.20. However, the maximum $R_{peak-hr}$ value is found to remain at the critical wind loading angle (θ_w) of 210°.

3.8. Response of the Indianapolis Building Equipped with Uni/Bi-Directional TLDs to Suppress the First Three Modes of Vibration

By inspecting Figures 3.10 and 3.19, it can be noticed that after the installation of the TLDs, the differences in peak resultant acceleration response values between the centre of mass and the four corners are found to increase significantly (see Figure 3.19). While the first two modes of the building are primarily translation modes in the x- and y-directions, the TLDs, which are designed to suppress these translation modes, are not capable of reducing the structural response resulting from the excitation of higher modes of vibration.

To further reduce structural peak acceleration response values, this section considers adding an additional set of TLDs to achieve acceptable response level for hotels, i.e. 15 milli-g $\leq R_{peak-hr} \leq$ 20 milli-g (Isyumov 1994). Therefore, TLDs to suppress the third mode of vibration are designed and installed in the Indianapolis building, in addition to the TLDs previously provided to suppress the first two translational modes of vibration. This step is important, as adding TLDs to suppress the first two modes of vibration has influenced the total response of the building by increasing the contribution of the torsional vibration mode of the structure under certain wind loading angles.

3.8.1 TLD Design Procedure for the Third Mode of Vibration

In this section, a mass ratio value (μ) of 5.0% is selected for TLDs to be installed to suppress the torsional mode (mode 3) of vibration of the building. As all third mode tanks are

placed at the corners of the building, the distance from the CM and the TLDs in the x- and y-directions is the same. This leads to a generalized mass ratio value ($\mu^* \approx \mu$) (see Equation 3.24). The target modal RMS acceleration response values in both x- and y-directions ($\sigma_{\ddot{x}-target-m3}$; $\sigma_{\ddot{y}-target-m3}$), used in the TLD design process, are determined based on the initial modal RMS acceleration response values ($\sigma_{\ddot{x}-initial-m3}$; $\sigma_{\ddot{y}-initial-m3}$) at the corners in both x- and y-directions, respectively (see Tables 3.5 and 3.6).

Initial third mode RMS acceleration response values in the x-direction ($\sigma_{\ddot{x}-initial-m3}$) of 0.9 milli-g and 1.5 milli-g are obtained from spectral analysis of the time history series at each corner (see Table 3.5). Therefore, tanks are selected to be placed at $C3$ and $C4$ to maximize the TLD resulting shear force due to the amplitude dependent properties of the device (Tait et al. 2004a; Tait et al. 2004b). Consequently, third mode tanks in the y-direction are selected to be placed at $C2$ and $C3$, where the initial RMS acceleration response value of the third mode ($\sigma_{\ddot{y}-initial-m3}$) is 3.8 milli-g compared to 2.5 milli-g at $C1$ and $C4$ (see Table 3.6). Thus, the initial RMS acceleration response values of the third mode ($\sigma_{\ddot{x}-initial-m3}$; $\sigma_{\ddot{y}-initial-m3}$) of 1.5 milli-g and 3.9 milli-g lead to target modal values ($\sigma_{\ddot{x}-target-m3}$; $\sigma_{\ddot{y}-target-m3}$) of 0.8 milli-g and 2.0 milli-g in the x- and y-directions, respectively. Total target RMS acceleration response values ($\sigma_{\ddot{x}-target-t}$; $\sigma_{\ddot{y}-target-t}$) of 3.4 milli-g and 3.4 milli-g are estimated using Equations 3.35 and 3.36 in the x- and y-directions, respectively (see Tables 3.5 and 3.6).

The target modal RMS acceleration response values of the third mode ($\sigma_{\ddot{x}-target-m3}$; $\sigma_{\ddot{y}-target-m3}$) are used to determine the required damping ratio of the screens (ζ_{TLD}), which are designed to achieve an optimal inherent damping ratio ($\zeta_{TLD-opt}$) for a particular amplitude of excitation at the critical wind loading angle (θ_w) of 210° (Tait 2008). The calculation steps used to design the TLDs to suppress the first two modes of vibration are presented in Tables A2 and A3 (Appendix-A) and TLD water mass calculations are presented in Table A4 (Appendix-A). The screens are located at 40% and 60% of the tank length in both directions with calculated loss coefficient values of $C_{l-x} = 35.3$ and $C_{l-y} = 14.1$ in the x- and y-directions, respectively. Figures A6 and A7 (Appendix-A) show the amplitude dependent properties for the tanks used to suppress the third mode of vibration of the building.

Square tanks, which act as two independent 1D-TLDs, are selected to be placed at $C3$ employing the design procedure described in Section 3.6. The tank dimensions are established as $L_x = L_y = 3.0$ m and $h = 0.4$ m. A total of 111 bi-directional tanks are used to achieve half of the specified mass ratio values in both the x- and y-directions. In contrast, 25 uni-directional TLDs are placed at the $C4$ and $C2$ to suppress the third mode of vibration. The tank length and water depth value match those for the bi-directional TLDs, however, a different width is selected in order to satisfy the remaining required mass ratio in both x- and y-directions (see Table A4 Appendix-A). It is common to utilize dozens or even hundreds of small TLD tanks to satisfy the required mass ratio (Tamura et al. 1995; Love et al. 2011). The tanks can be placed and arranged to keep space requirements to a minimum.

3.8.2 Response Evaluation of the Indianapolis Building

In this section, a total number of 36-time history analyses, corresponding to wind loading angles from 0° and 360°, are carried out utilizing wind tunnel data provided by the BLWTL and employing the 3D-Structure-MTLD system model implemented with TLDs designed to suppress the first three modes of vibration.

In the x-direction, Figure 3.21 shows that a RMS acceleration response value of 3.4 milli-g at the critical wind loading angle (θ_w) of 210° at $C3$ and $C4$ ($z = 154.6$ m), matches the predicted total target response value ($\sigma_{\ddot{x}-target-t}$). The initial modal component of the third mode ($\sigma_{\ddot{x}-initial-m}$) is reduced from 1.5 milli-g to 0.8 milli-g resulting in a percentage reduction of 46.3%, while a percentage reduction value of 36.2% is obtained at $C1$ and $C2$ (see Tables 3.5 and 3.7).

In the y-direction, Figure 3.22 shows that the total RMS acceleration response of 3.8 milli-g at $C2$ and $C3$ ($z = 154.6$ m) exceeded the total target RMS acceleration response value ($\sigma_{\ddot{y}-target-t}$) of 3.4 milli-g. However, the modal RMS acceleration of 2.1 milli-g is only 3% greater than the target modal value ($\sigma_{\ddot{y}-target-m}$) of 2.0 milli-g (see Tables 3.6 and 3.8). The larger discrepancy in the total RMS values to modal RMS values is attributed to changes in the percentage contribution of higher uncontrolled modes. The modal factor value (MF) for the higher modes has increased from 9.0% to 13.2% as a result of the contribution from uncontrolled modes in the y-direction, which are not suppressed by the TLDs. It can be observed that the third modal RMS response is reduced from an initial modal value

($\sigma_{\ddot{y}-initial-m}$) of 3.8 milli-g to 2.1 milli-g resulting in a percentage reduction value of 45.9% at $C2$ and $C3$, while a percentage reduction value of 35.5% is achieved at $C1$ and $C4$ (see Table 3.8). Additionally, due to the installation of the third mode tanks, the first two modal RMS acceleration response values at the centre of mass (CM) are further reduced with percentage reduction values of 5.1% and 14.0% in the x- and y-directions, respectively.

Therefore, the percentage reduction values ($\Psi_{peak-hr}$) of the average peak hourly resultant acceleration response ($R_{peak-hr}$) at the critical wind loading angle of (θ_w) 210° are considerably improved compared to the case where TLDs were installed to suppress the first two modes of vibration. It can be observed that $\Psi_{peak-hr}$ increases from 24.7% and 12.2% to 40.4% and 32.3% at $C1$ and $C2$, respectively, and from 6.4% and 19.2% to 27.9% and 36.4% at $C3$ and $C4$, respectively. Also, the percentage reduction ($\Psi_{peak-hr}$) at the centre of mass (CM) increases from 47.1% milli-g to 53.7% (see Figures 3.20, 3.24 and Table 3.9).

3.8.3 Serviceability Check of the Indianapolis Building

The calculated average peak hourly resultant acceleration response values ($R_{peak-hr}$) are compared with acceptable wind-induced motion values set by the wind tunnel (BLWTL). Figure 3.23 shows that the maximum average peak hourly resultant acceleration response value ($R_{peak-hr}$), which occurs at the critical wind loading angle (θ_w) of 210°, is reduced from an uncontrolled value of 28.2 milli-g to 18.9 milli-g (see Table 3.9) that satisfies the criteria of the acceptable acceleration response level for hotels, i.e. 15 milli-g $\leq R_{peak-hr} \leq$ 20 milli-g (Isyumov 1994).

Figure 3.24 shows that the centre of mass (CM) has greater percentage response reduction values ($\Psi_{peak-hr}$) than at the corners with less variation (in the range of 8.0%) and achieves a maximum response reduction value ($\Psi_{peak-hr}$) of 56.0%. In contrast, the corners experience lower $\Psi_{peak-hr}$ values (maximum 48%) with higher variations (in the range of 12.0%). It can be observed from Figure 3.24 that maximum percentage response reduction values ($\Psi_{peak-hr}$) at the corners of the building, which range between 40.0% and 48.0%, are achieved at wind loading angles of 230° and 270°, while minimum values of $\Psi_{peak-hr}$, ranging from 22.0% to 35.0% are found to occur at wind loading angles of 30° and 340°, where the $R_{peak-hr}$ values are less than the maximum values at the critical wind loading

angle of 210° (see Figure 3.23). However, serviceability requirements, which satisfy hotel level requirements, are satisfied at all wind angles.

3.9. Conclusions

A 3D-Structure-TLD system model, developed and validated in Chapter 2, has been expanded to multiple TLDs (3D-Structure-MTLD) and employed to study the response of the 38-story Indianapolis building equipped with TLDs. Two nonlinear TLD models; a nonlinear fluid model (TLD Model 1) and an EADTMD model (TLD Model 2) were investigated. Results of the 3D-Structure-MTLD system model have shown good agreement between both TLD models. Therefore, TLD Model 2 has been selected to carry out the analysis resulting in a significant reduction in computational effort.

TLDs to suppress the first three modes of vibration of the building have been designed, utilizing a preliminary TLD design procedure (Tait 2008). The modal contribution response components have been used to determine the TLD parameters at the critical wind loading angle. A step-by-step TLD design technique has been employed, permitting the influence of the first and second mode tanks and the third mode tanks to be studied.

It was found that the centre of mass (CM) of the Indianapolis building was a suitable location for the first two mode tanks to be placed, where modal factor values in both x- and y-directions are larger than at the corners for uncontrolled structure case. Also, the centre of mass (CM) maintained modal factor values above 91% for modes 1 and 2 in the x- and y-directions, respectively, compared to the corner modal factor values, which reduced due to amplification of higher modal component values. Moreover, the step-by-step TLD design procedure has been used to assess the decision of adding an extra set of tanks, to suppress mode of vibration, and the selection of TLD locations and placement directions. Accordingly, $C3$ and $C4$ have been found suitable for third mode tanks to be placed in the x-direction, while $C2$ and $C3$ have been found suitable for third mode tanks to be placed in the y-direction, due to the amplitude dependent properties of the TLD device.

The ability to capture the contribution of higher modes of vibration on the structure-TLD system using this model has been demonstrated. The wind-induced serviceability levels of accelerations of the Indianapolis building have been evaluated using TLDs to suppress the first two and the first three modes of vibration satisfying the office building and the hotel

level requirements, respectively. As a result of using this particular scheme, the maximum average peak hourly resultant acceleration response value ($R_{peak-hr}$) of the Indianapolis building of 28.2 milli-g at the critical wind loading angle of (θ_w) 210° has been reduced to a value of 18.9 milli-g.

3.10. References

ASCE (American Society of Civil Engineers), (2005). "*Minimum Design Loads for Buildings and Other Structures*", ASCE 7–05, New York, NY, USA.

The Boundary Layer Wind Tunnel Laboratory (BLWTL), (1999). "*Wind Tunnel Testing: A General Outline*", BLWTL, The University of Western Ontario, London, ON, Canada.

Cassolato, M.R., Love, J.S. and Tait, M.J. (2011). "Modelling of Tuned Liquid Damper with Inclined Damping Screens", *Structural Control and Health Monitoring*, 18(6): 674-681.

Chopra, A.K. (2001). "*Dynamics of Structures: Theory and Applications to Earthquake Engineering*", 2nd Ed., Prentice-Hall, Toronto, ON, Canada.

CSI (Computers and Structures Inc.), (2004). "*SAP2000 version 10 Integrated Finite Element Analysis and Design of Structures*", CSI, Berkeley, CA, USA.

Davenport, A.G. (1964). "Note on the Distribution of the Largest Value of a Random Function with Application to Wind Loading", *Proceeding - Institution of Civil Engineer*, 28: 187-196.

Fediw, A.A. (1992). "*Performance of a One Dimensional Tuned Sloshing Water Damper*", M.E.Sc. Thesis. The University of Western Ontario, London, ON, Canada.

Fediw, A.A., Isyumov, N. and Vickery, B.J. (1995). "Performance of a Tuned Sloshing Water Damper", *Journal of Wind Engineering and Industerial Aerodynamics*, 56: 237-247.

Gerges, R.R. and Vickery, B.J. (2003). "Wind Tunnel Study of the Across-Wind Response of a Slender Tower with a Nonlinear Tuned Mass Damper", *Journal of Wind Engineering and Industrial Aerodynamics*, 91: 1069-1092.

Graham, E.W. and Rodriguez, A.M. (1952). "The Characteristics of Fuel Motion Which Affect Airplane Dynamics", *Journal of Applied Mechanics*, 19(3): 381-388.

Institute for Research in Construction (2005). "*National Building Code of Canada (NBC)*", National Research Council of Canada, Ottawa, ON, Canada.

Isyumov, N. (1994). "Criteria for Acceptable Wind-Induced Motions", *Proceedings, 12th ASCE Structures Congress*, 642-653. Atlanta, GA, USA.

Ju, Y.K., Yoon, S.W., and Kim, S.D. (2004). "Experimental Evaluation of a Tuned Liquid Damper System", *Proceeding of Institution of Civil Engineering-Structures and Building*, 157(4): 251–262.

Kaneko, S. and Ishikawa, M. (1999). "Modeling of Tuned Liquid Damper with Submerged Nets", *Journal of Pressure and Vessel Technology*, 121(3): 334–343.

Kareem, A., Kijewski, T. and Tamura, Y. (1999). "Mitigation of Motions of Tall Buildings with Specific Examples of Recent Application", *Wind and Structures*, 2(3): 201-251.

Koh, C.G., Mahatma, S. and Wang, C.M. (1994). "Theoretical and Experimental Studies on Rectangular Liquid Dampers under Arbitrary Excitations", *Journal of Earthquake Engineering and Structural Dynamics*, 23(1): 17–31.

Lamb, H. (1932). "*Hydrodynamics*", the University Press, Cambridge, England.

Love, J.S., Tait, M.J. and Toopchi-Nezhad, H. (2011). "A Hybrid Structural Control System Using a Tuned Liquid Damper to Reduce the Wind Induced Motion of a Base Isolated Structure", *Engineering Structures*, 33: 738–746.

Luft, R.W. (1979). "Optimal Tuned Mass Dampers for Buildings", *Journal of Structural Division*, 105: 2766-2772.

The MathWorks Inc., (2004). "*MATLAB version 7.0.0.19920 (R14)*", The MathWorks Inc., Natick, MA, USA.

McNamara, R.J. (1977). "Tuned Mass Dampers for Building", *Journal of Structural Division*, American Society of Civil Engineer, 103: 1785-1798.

Modi, V.J., Welt, F. and Irani, M.B. (1990). "On the Suppression of Vibrations Using Nutation Dampers", *Journal of Wind Engineering and Industerial Aerodynamics*, 33(1–2): 273–282.

Roffel, A., Lourenco, R., Narasimhan, S. and Yarusevych, S. (2011). "Adaptive Compensation for Detuning in Pendulum Tuned Mass Dampers" *ASCE Journal of Structural Engineering*, 137(2): 242-251.

SHARCNET: is one of seven HPC consortia in Canada that operates under the umbrella of Compute/Calcul Canada, (https://www.sharcnet.ca).

Soong, T.T. and Dargush, G.F. (1997). "*Passive Energy Dissipation Systems in Structural Engineering*", Wiley, New York, NY, USA.

Sun, L.M., Fujino, Y., Pacheco, B.M. and Isobe, M. (1989). "Nonlinear Waves and Dynamic Pressures in Rectangular Tuned Liquid Dampers: Simulation and Experimental Verification", *Structural Engineering/Earthquake Engineering*, 6(2): 251–262.

Sun, L.M., Fujino, Y. and Chaiseri, P. (1992). "Modeling of Tuned Liquid Damper (TLD)", *Journal of Wind Engineering and Industrial Aerodynamics*, 43(1–3): 1883–1894.

Tait, M.J. (2004). "*The Performance of 1D and 2D Tuned Liquid Dampers*", Ph.D. Thesis, The University of Western Ontario, London, ON, Canada.

Tait, M.J., E1 Damatty, A.A. and Isyumov, N. (2004a). "Testing of Tuned Liquid Damper with Screens and Development of Equivalent TMD Model", *Wind and Structures*, 7(4): 215–234.

Tait, M.J., Isyumov, N. and E1 Damatty, A.A. (2004b). "The Efficiency and Robustness of a Unidirectional Tuned Liquid Damper and Modelling with an Equivalent TMD", *Wind and Structures*, 7(4): 235–250.

Tait, M.J., El Damatty, A.A. and Isyumov, N. (2005a). "An Investigation of Tuned Liquid Dampers Equipped with Damping Screens Subjected to 2D Excitation", *Earthquake Engineering and Structural Dynamics*, 34(7): 719–735.

Tait, M.J., El Damatty, A.A., Isyumov, N. and Siddique, M.R. (2005b). "Numerical Flow Models to Simulate Tuned Liquid Dampers (TLD) with Slat Screens", *Journal of Fluid and Structures*, 20: 1007–1023.

Tait, M.J., Isyumov, N. and E1 Damatty, A.A. (2007). "Effectiveness of a 2D TLD and Its Numerical Modeling", *Journal of Structural Engineering*, 133(2): 251–263.

Tait, M.J. (2008). "Modelling and Preliminary Design of a Structure–TLD System", *Engineering Structures*, 30: 2644–2655.

Tamura, Y., Fujii K., Ohtsuki, T., Wakahara, T. and Kohaska, R. (1995). "Effectiveness of Tuned Liquid Dampers under Wind Excitation", *Engineering Structures*, 17: 609-621.

Vickery, B.J. and Davenport, A.G. (1970). "An Investigation of the Behaviour in Wind of the Proposed Centre Point Tower in Sydney, Australia", *Research Report BLWT-1-70*, The Boundary Layer Wind Tunnel Laboratory, The University of Western Ontario, London, ON, Canada.

Warburton, G.B. (1982). "Optimum Absorber Parameters for Various Combinations of Response and Excitation Parameters", *Earthquake Engineering and Structural Dynamics*, 10(3): 381–401.

Warnitchai, P. and Pinkaew, T. (1998). "Modeling of Liquid Sloshing in Rectangular Tanks with Flow-Dampening Devices", *Engineering Structures*, 20(7): 593–600.

Xu, Z. and Ho, T.C.E. (2007). "A Study of Wind Effects for One Indiana Square, Indianapolis, Indiana. *Research Report BLWT-SS3-2007*, The Boundary Layer Wind Tunnel Laboratory (BLWTL), The University of Western Ontario, London, ON, Canada.

Yat, F.H. (2009). "*Performance of Dynamic Vibration Absorbers on Buildings with Coupled Modes*", Master Thesis, McMaster University, Hamilton, ON, Canada.

Table 3.1. Modal Acceleration Response Components in the x-direction for the Indianapolis Building with No-TLDs

| | Results of the Indianapolis Building with No-TLDs | | | | | | | | Design of TLDs | |
| | $\sigma_{\ddot{x}-initial}$ (milli-g) | Modal Factor, MF (%) | | | | $\sigma_{\ddot{x}-initial-m}$ (milli-g) | | | $\sigma_{\ddot{x}-target-m}$ (milli-g) | $\sigma_{\ddot{x}-target-t}$ (milli-g) |
Node	Total	Mode 1	Mode 2	Mode 3	Higher Modes	Mode 1	Mode 2	Mode 3	Mode 1	Total
Corner 1	6.3	96.9	0.8	1.5	0.8	6.1	0.1	0.1	-	-
Corner 2	6.3	96.9	0.8	1.5	0.8	6.1	0.1	0.1	-	-
Corner 3	6.1	96.3	1.0	2.3	0.4	5.8	0.1	0.1	-	-
Corner 4	6.1	96.3	1.0	2.3	0.4	5.8	0.1	0.1	-	-
Centre	6.1	98.3	0.9	0.4	0.5	6.0	0.1	0.0	3.1	3.2

Table 3.2. Modal Acceleration Response Components in the y-direction for the Indianapolis Building with No-TLDs

| | Results of the Indianapolis Building with No-TLDs | | | | | | | | Design of TLDs | |
| | $\sigma_{\ddot{y}-initial}$ (milli-g) | Modal Factor, MF (%) | | | | $\sigma_{\ddot{y}-initial-m}$ (milli-g) | | | $\sigma_{\ddot{y}-target-m}$ (milli-g) | $\sigma_{\ddot{y}-target-t}$ (milli-g) |
Node	Total	Mode 1	Mode 2	Mode 3	Higher Modes	Mode 1	Mode 2	Mode 3	Mode 2	Total
Corner 1	4.2	3.5	85.3	8.4	2.7	0.2	3.6	0.4	-	-
Corner 2	3.7	3.4	77.7	17.9	1.0	0.1	2.8	0.7	-	-
Corner 3	3.7	3.4	77.7	17.9	1.0	0.1	2.8	0.7	-	-
Corner 4	4.2	3.5	85.3	8.4	2.7	0.2	3.6	0.4	-	-
Centre	3.6	3.8	94.1	1.2	0.9	0.1	3.4	0.0	1.8	2.0

Table 3.3. TLD Design for Mode 1 (x-direction) for the Indianapolis Building

Quantity	Equation(s)	Value	
Initial peak hourly acceleration, $\ddot{x}_{initial}$		**22.52**	**milli-g**
Modal Factor, MF		**98.30**	**%**
Initial modal peak hourly acceleration, $\ddot{x}_{initial-m}$	$\ddot{x}_{initial-m} = \ddot{x}_{initial}.MF$	**22.37**	**milli-g**
Structure cyclic frequency, f_{s-x}		0.14	Hz
Structure time period, T_{s-x}	$T_{s-x} = 1/f_{s-x}$	7.31	sec
Structure natural frequency, ω_{s-x}	$\omega_{s-x} = 2\pi/T_{s-x}$	0.86	rad/sec
Peak factor, PF_x	$PF_x = \sqrt{2\ln(573\omega_{s-x})} + \frac{0.577}{\sqrt{2\ln(573\omega_{s-x})}}$	3.69	
Initial RMS acceleration, $\sigma_{\ddot{x}-initial-m}$	$\sigma_{\ddot{x}-initial-m} = \frac{\ddot{x}_{initial-m}}{PF_x}$	**6.01**	**milli-g**
Initial RMS displacement, $\sigma_{x-initial-m}$	$\sigma_{x-initial-m} = \frac{\sigma_{\ddot{x}-initial-m}}{\omega_{s-x}^2}\frac{g}{1000}$	0.08	m
Assumed mass ratio, μ		0.06	(6.0%)
Effective damping provided by TLD, $\zeta_{TLD-eff-opt_x}$	$\zeta_{TLD-eff-opt_x} = \frac{1}{4}\sqrt{\frac{\mu_x+\mu_x^2}{1+\frac{3}{4}\mu_x}}$	0.06	(6.2%)
Optimal damping ratio, $\zeta_{TLD-opt_x}$	$\zeta_{TLD-opt_x} = \sqrt{\frac{\mu_x+\frac{3}{4}\mu_x^2}{4+6\mu_x+2\mu_x^2}}$	0.12	(12.0%)
Optimal tuning ratio, Ω_{opt_x}	$\Omega_{opt_x} = \frac{\sqrt{1+\frac{1}{2}\mu_x}}{1+\mu_x}$	0.96	(95.7%)
Optimal TLD cyclic frequency, $f_{TLD-opt_x}$	$\Omega_{opt_x} = \frac{f_{TLD-opt_x}}{f_{s-x}}$	0.13	Hz
Optimal response ratio, R_{opt_x}	$R_{opt_x} = \frac{\sigma_{r-x}}{\sigma_x} = \frac{1+\mu_x}{\sqrt{2\mu_x+\frac{3}{2}\mu_x^2}}$	2.99	
Structure damping ratio, ζ_s		0.02	(2.0%)
Total structure damping, ζ_{tot-x}	$\zeta_{tot-x} = 0.8\zeta_s + \zeta_{TLD-eff-opt_x}$	0.08	(7.8%)
Target RMS displacement, $\sigma_{x-target-m}$	$\zeta_{tot-x} = \zeta_s\frac{\sigma_{x-initial-m}^2}{\sigma_{x-target-m}^2}$	0.04	m
Target RMS acceleration, $\sigma_{\ddot{x}-target-m}$	$\sigma_{\ddot{x}-target-m} = \omega_s^2\,\sigma_{x-target-m}$	**3.08**	**milli-g**
Target peak hourly acceleration, $\ddot{x}_{target-m}$	$\sigma_{\ddot{x}-target-m} = \frac{\ddot{x}_{target-m}}{PF_x}$	**11.35**	**milli-g**
TLD response, σ_{r-x}	$\sigma_{r-x} = R_{opt_x}\,\sigma_{x-target-m}$	0.12	m
Select tank dimensions, L_x, h	$f_{TLD-opt_x} = \frac{1}{2\pi}\sqrt{\frac{\pi g}{L_x}\tanh\left(\frac{\pi h}{L_x}\right)}$	**L_x= 16.0**	**m** **h = 1.87 m**
Shallow water theory check, h/L_x		0.12	
Select screen properties, x_1, x_2, C_{l-x}	$\zeta_{TLD-x} = C_{l-x}\sqrt{\frac{32}{\pi^3}}\tanh^2\left(\frac{\pi h}{L_x}\right)\Delta_x\Xi_x\frac{\sigma_{r-x}}{L_x}$ $\Delta_x = \left(\frac{1}{3}+\frac{1}{\sinh^2\left(\frac{\pi h}{L_x}\right)}\right)$ $\Xi_x = \sum_{j=1}^{ns_x}\left\|\sin^3\left(\frac{\pi x_j}{L_x}\right)\right\|$	**$x_1 = 0.4\,L_x$** **$x_2 = 0.6\,L_x$** **$C_{l-x} = 9.76$**	

Table 3.4. Water Mass Calculations for TLDs to Suppress Modes 1 and 2 for the Indianapolis Building

Quantity	Equation(s)	Value
Selected tank dimensions, L_x, L_y, h		$L_x = 16.00$ m $L_y = 13.41$ m $h = 1.87$ m
Water height to tanks length ratio in x-dir	h/L_x	0.12
Water height to tanks length ratio in y-dir	h/L_y	0.14
Water mass of 1 tank, $m_{w(1tank)}$	$m_{w(1tank)} = L_x L_y h$	401255 kg
TLD mass of 1 tank in x-dir, $m_{TLD-x(1tank)}$	$m_{TLD-x(1tank)} \approx m_{1-x} =$ $\dfrac{8\,tanh\left(\pi\frac{h}{L_x}\right)}{\pi^3\left(\frac{h}{L_x}\right)} m_{w(1tank)}$	$0.77\, m_{w(1tank)} =$ 311370 kg
TLD mass of 1 tank in y-dir, $m_{TLD-y(1tank)}$	$m_{TLD-y(1tank)} \approx m_{1-y} =$ $\dfrac{8\,tanh\left(\pi\frac{h}{L_y}\right)}{\pi^3\left(\frac{h}{L_y}\right)} m_{w(1tank)}$	$0.76\, m_{w(1tank)} =$ 305904 kg
Total building mass, M_s	$M_s = \sum_{i=1}^{i=N_f} m_f$	36412955 kg
Generalized building mass in x-dir, M_x^*	$M_x^* = \sum_{i=1}^{i=N_f} (m_f)_i (\phi_x^2)_i$	10523344 kg
Generalized building mass in y-dir, M_y^*	$M_y^* = \sum_{i=1}^{i=N_f} (m_f)_i (\phi_y^2)_i$	10013563 kg
Required TLD mass in x-dir, m_{TLD-x}	$m_{TLD-x} = \mu_x M_x^*$	631401 kg
Required TLD mass in y-dir, m_{TLD-y}	$m_{TLD-y} = \mu_y M_y^*$	600814 kg
No. of Tanks required in x-dir, N_{TLD-x}	$N_{TLD-x} = m_{TLD-x}/m_{TLD-x(1tank)}$	2.03
No. of Tanks required in y-dir, N_{TLD-y}	$N_{TLD-y} = m_{TLD-y}/m_{TLD-y(1tank)}$	1.96
Chosen No. of tanks for modes 1 and 2, N_{TLD-xy}	(Bi-directional tanks)	**2**
Actual mass ratio in x-dir, $\mu_{x-actual}$	$\mu_{x-actual} = N_{TLD-xy} m_{TLD-x(1tank)}/M_x^*$	**5.92 %**
Actual mass ratio in y-dir, $\mu_{y-actual}$	$\mu_{y-actual} = N_{TLD-xy} m_{TLD-y(1tank)}/M_y^*$	**6.11 %**
Mass ratio of contained water, μ_w	$\mu_w = N_{TLD-xy} m_{w(1tank)}/M_s$	**2.20 %**

Table 3.5. Modal Acceleration Response Components in the x-direction for the Indianapolis Building with TLDs to Suppress the First Two Modes of Vibration

| | Results of the Indianapolis Building Equipped with 2 Modes TLDs (1 & 2) | | | | | | | | | | | Design of TLDs | |
| | $\sigma_{\ddot{x}-initial}$ (milli-g) | Modal Factor, MF (%) | | | | $\sigma_{\ddot{x}-initial-m}$ (milli-g) | | | % Reduction w.r.t. No-TLD Case | | | $\sigma_{\ddot{x}-target-m}$ (milli-g) | $\sigma_{\ddot{x}-target-t}$ (milli-g) |
Node	Total	Mode 1	Mode 2	Mode 3	Higher Modes	Mode 1	Mode 2	Mode 3	Mode 1	Mode 3	Total	Mode 3	Total
Corner 1	3.8	67.2	2.0	22.6	8.3	2.5	0.1	0.9	59.1	-870	40.4	-	-
Corner 2	3.8	67.2	2.0	22.6	8.3	2.5	0.1	0.9	59.1	-870	40.4	-	-
Corner 3	4.1	54.0	4.0	37.3	4.7	2.2	0.2	1.5	62.3	-1170	31.9	0.8	3.4
Corner 4	4.1	54.0	4.0	37.3	4.7	2.2	0.2	1.5	62.3	-1170	31.9	0.8	3.4
Centre	3.1	91.0	3.5	2.4	3.2	2.8	0.1	0.1	54.0	-413	49.8	-	-

Table 3.6. Modal Acceleration Response Components in the y-direction for the Indianapolis Building with TLDs to Suppress the First Two Modes of Vibration

| | Results of the Indianapolis Building Equipped with 2 Modes TLDs (1 & 2) | | | | | | | | | | | Design of TLDs | |
| | $\sigma_{\ddot{y}-initial}$ (milli-g) | Modal Factor, MF (%) | | | | $\sigma_{\ddot{y}-initial-m}$ (milli-g) | | | % Reduction w.r.t. No-TLD case | | | $\sigma_{\ddot{y}-target-m}$ (milli-g) | $\sigma_{\ddot{y}-target-t}$ (milli-g) |
Node	Total	Mode 1	Mode 2	Mode 3	Higher Modes	Mode 1	Mode 2	Mode 3	Mode 2	Mode 3	Total	Mode 3	Total
Corner 1	4.3	6.8	21.5	57.3	14.5	0.3	0.9	2.5	75.3	-616	-2.6	-	-
Corner 2	5.2	2.9	14.0	74.0	9.0	0.2	0.7	3.8	76.0	-554	-42.2	2.0	3.4
Corner 3	5.2	2.9	14.0	74.0	9.0	0.2	0.7	3.8	76.0	-554	-42.2	2.0	3.4
Corner 4	4.3	6.8	21.5	57.3	14.5	0.3	0.9	2.5	75.3	-616	-2.6	-	-
Centre	2.2	18.8	64.6	9.2	7.4	0.4	1.4	0.2	60.1	-589	39.3	-	-

Table 3.7. Modal Acceleration Response Components in the x-direction for the Indianapolis Building with TLDs to Suppress the First Three Modes of Vibration

	Results of the Indianapolis Building Equipped with 3 Modes TLDs (1, 2 & 3)											
	$\sigma_{\ddot{x}-initial}$ (milli-g)	Modal Factor, *MF* (%)				$\sigma_{\ddot{x}-initial-m}$ (milli-g)			% Reduction w.r.t. 2 Modes TLDs Case	% Reduction w.r.t. No-TLD Case		
Node	Total	Mode 1	Mode 2	Mode 3	Higher Modes	Mode 1	Mode 2	Mode 3	Mode 3	Mode 1	Mode 3	Total
Corner 1	3.1	70.6	1.4	17.3	10.8	2.2	0.0	0.5	36.2	63.7	-489.0	50.2
Corner 2	3.1	70.6	1.4	17.3	10.8	2.2	0.0	0.5	36.2	63.7	-489.0	50.2
Corner 3	3.4	57.2	12.4	24.4	6.1	1.9	0.4	0.8	46.3	66.8	-485.1	44.0
Corner 4	3.4	57.2	12.4	24.4	6.1	1.9	0.4	0.8	46.3	66.8	-485.1	44.0
Centre	2.8	89.6	3.5	2.7	4.2	2.5	0.1	0.1	-2.0	59.0	-244.1	55.1

Table 3.8. Modal Acceleration Response Components in the y-direction for the Indianapolis Building with TLDs to Suppress the First Three Modes of Vibration

	Results of the Indianapolis Building Equipped with 3 Modes TLDs (1, 2 & 3)											
	$\sigma_{\ddot{y}-initial}$ (milli-g)	Modal Factor, *MF* (%)				$\sigma_{\ddot{y}-initial-m}$ (milli-g)			% Reduction w.r.t. 2 Modes TLDs	% Reduction w.r.t. No-TLD case		
Node	Total	Mode 1	Mode 2	Mode 3	Higher Modes	Mode 1	Mode 2	Mode 3	Mode 3	Mode 2	Mode 3	Total
Corner 1	3.3	13.1	18.1	48.9	20.0	0.4	0.6	1.6	35.5	83.6	-349.2	22.4
Corner 2	3.8	6.2	26.2	54.5	13.2	0.2	1.0	2.1	45.9	64.7	-217.7	-4.7
Corner 3	3.8	6.2	26.2	54.5	13.2	0.2	1.0	2.1	45.9	64.7	-217.7	-4.7
Corner 4	3.3	13.1	18.1	48.9	20.0	0.4	0.6	1.6	35.5	83.6	-349.2	22.4
Centre	1.8	33.3	47.7	9.2	9.8	0.6	0.9	0.2	16.4	74.1	-282.3	49.0

Table 3.9. Percentage Reductions of the Average Peak Hourly Resultant Acceleration Responses for the Indianapolis Building Utilizing 2 and 3 Mode TLDs

Node	$R_{peak-hr}$ (milli-g)			$\Psi_{peak-hr}$ (%)	
	No-TLD	2 Mode-TLDs	3 Mode-TLDs	2 Mode-TLDs	3 Mode-TLDs
Corner 1	28.2	21.2	16.8	24.7	40.4
Corner 2	27.1	23.8	18.4	12.2	32.3
Corner 3	26.3	24.6	18.9	6.4	27.9
Corner 4	27.3	22.1	17.4	19.2	36.4
Centre	26.4	14.0	12.2	47.1	53.7
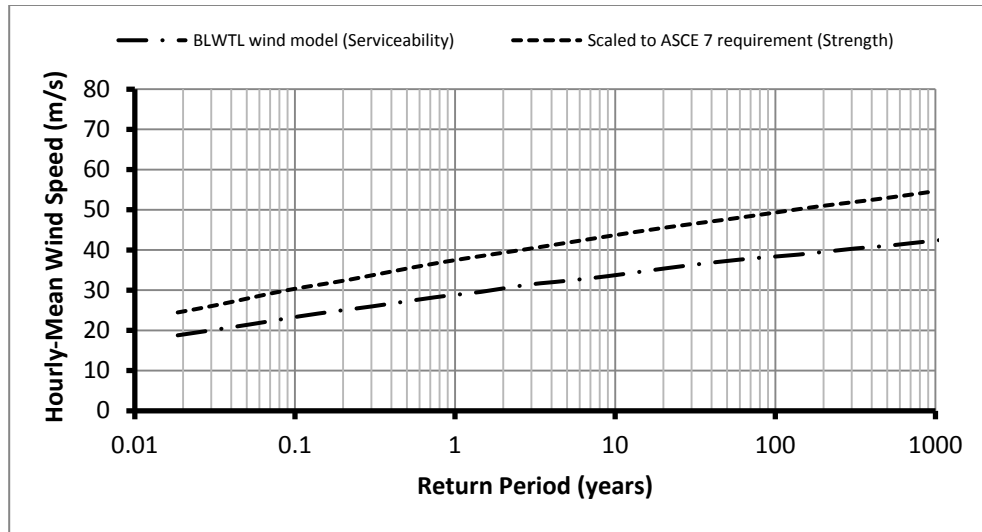
Fig. 3.1. Predicted Annual Extreme Upper Level (500 m) Wind Speed for Various Return Periods (from BLWT-SS3-2007)
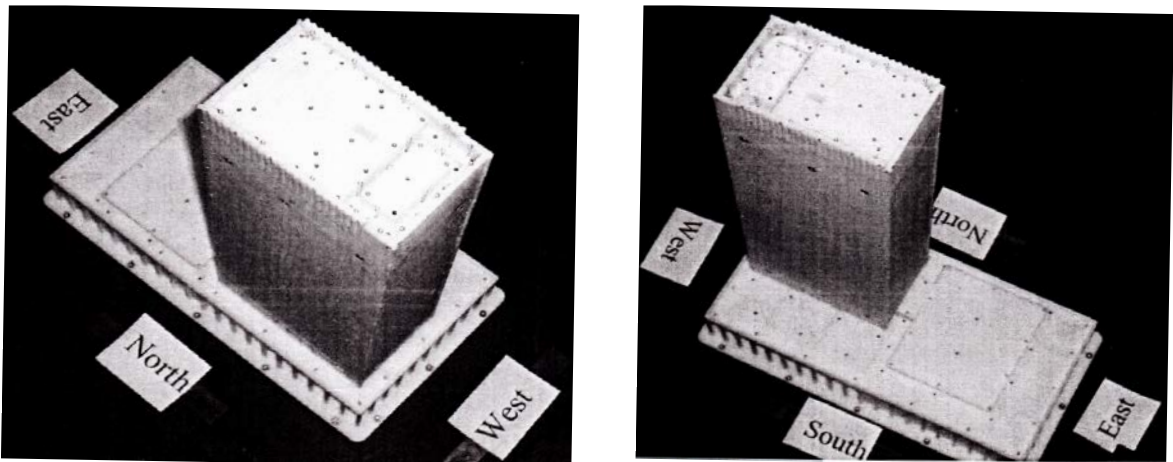
Fig. 3.2. Close up Views of the Pressure Model (from BLWT-SS3-2007)
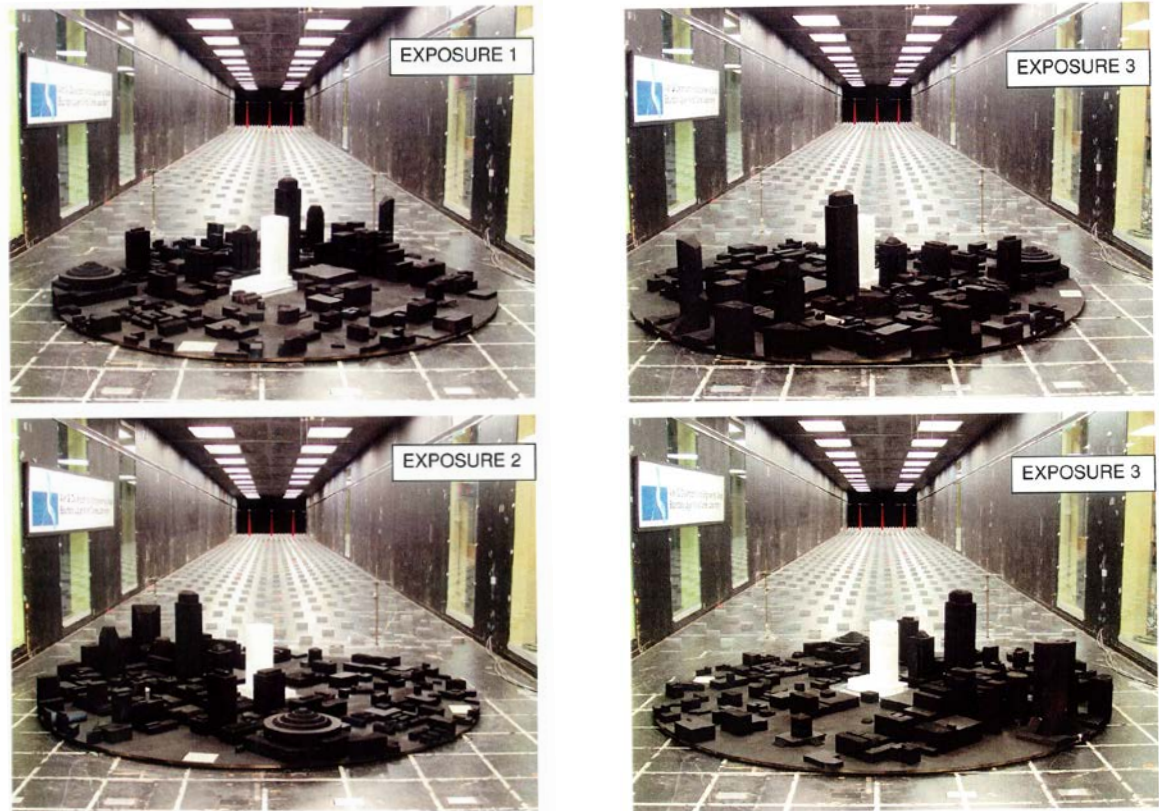
Fig. 3.3. Photographs of the High-Rise Building Model in the Wind Tunnel Showing the Upstream Terrain Models for Different Exposures (from BLWT-SS3-2007)
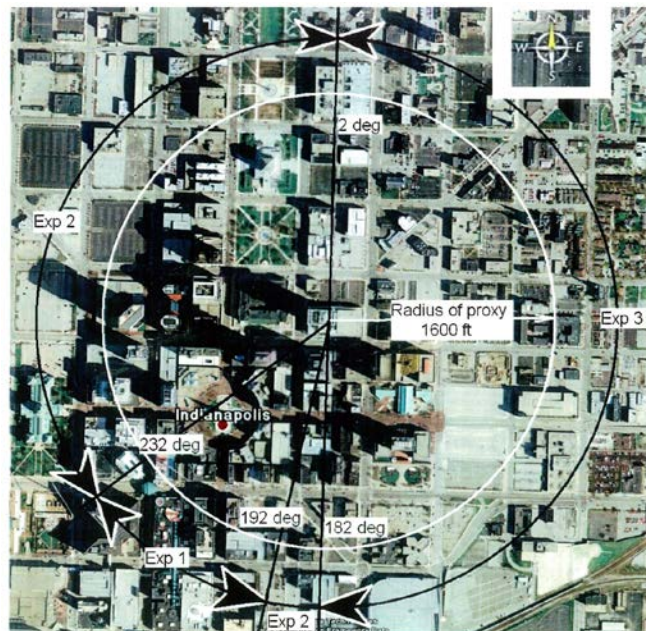
Fig. 3.4. Azimuth Ranges Over Which the Upstream Terrain Models were Used (from BLWT-SS3-2007)

(a) $T = 7.31$ s   (b) $T = 6.18$ s   (c) $T = 3.01$ s
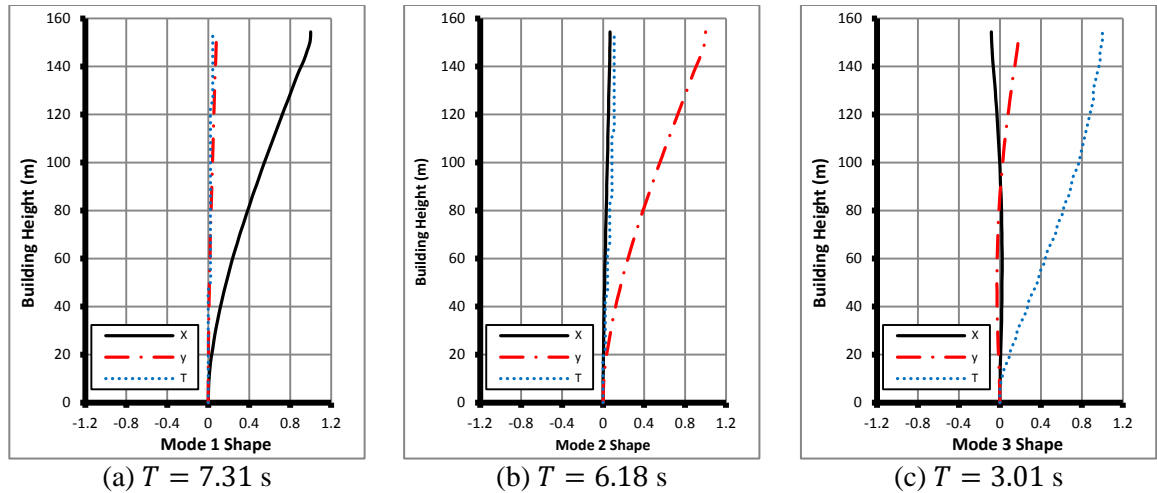
Fig. 3.5. Mode Shapes of the Indianapolis Building for (a) Mode 1, (b) Mode 2, and (c) Mode 3
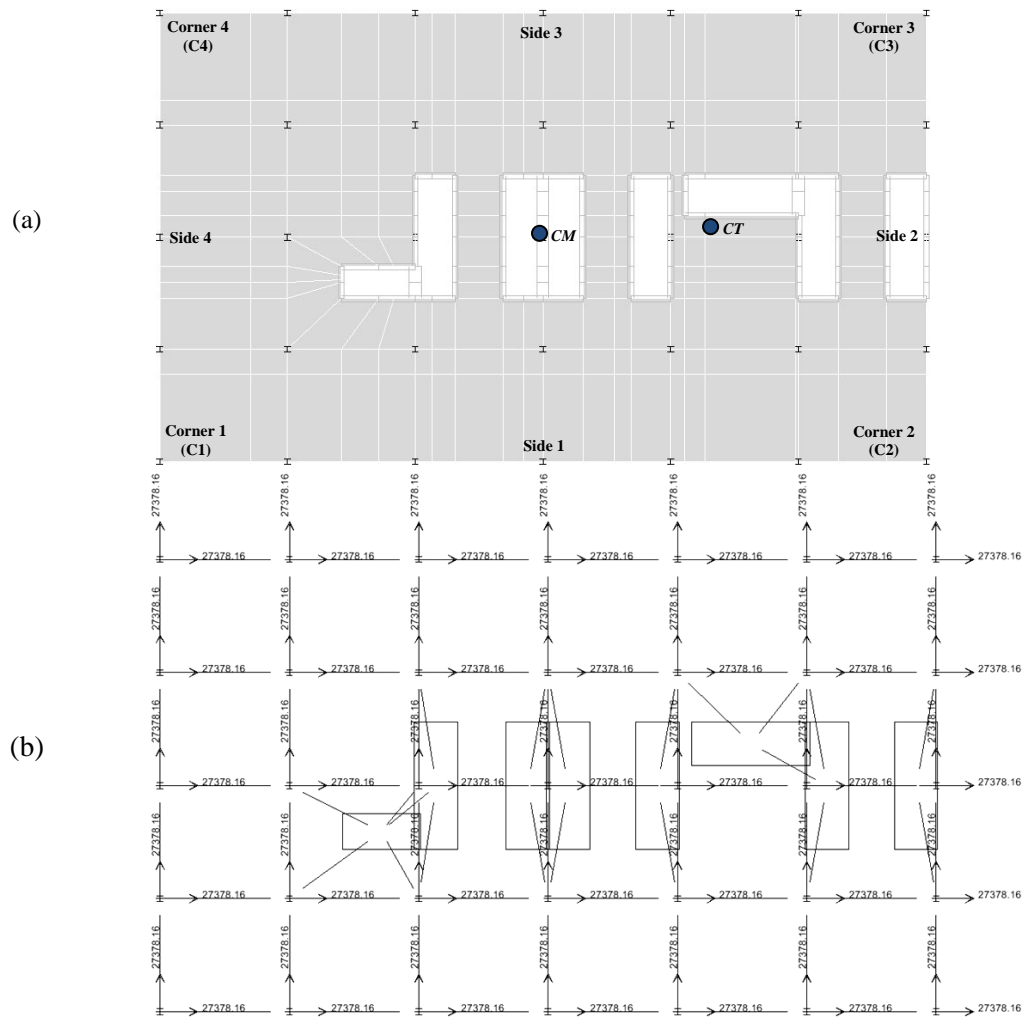
Fig. 3.6. Floor Plan of the Indianapolis Building Showing the Statical System Consists of (a) Real Slabs and Shear Walls, and (b) Frame Elements and Slab Beams Installed with Lumped Masses (kg)
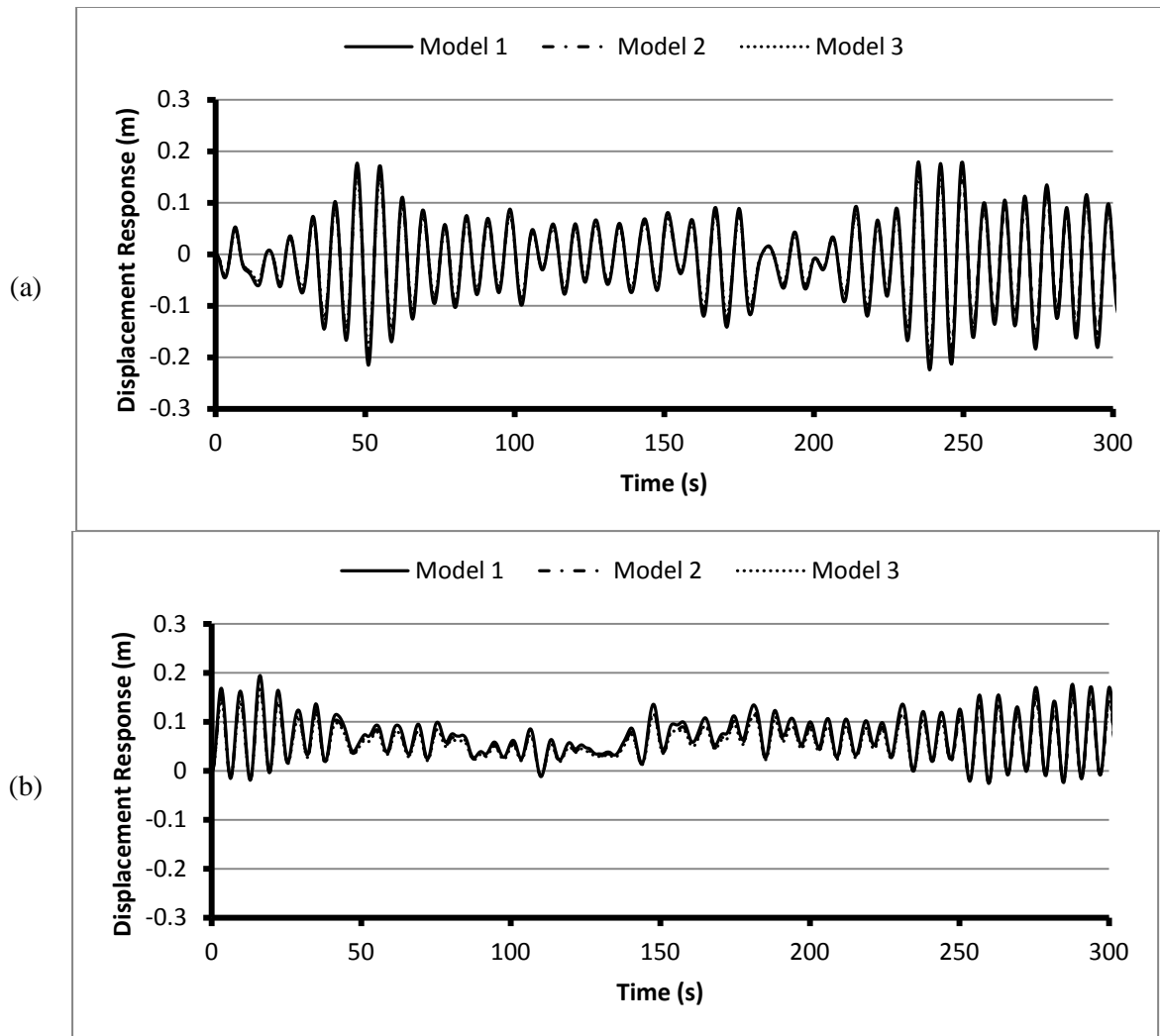
Fig. 3.7. Displacement Time History of the Indianapolis Building at the CM with No-TLD Installed in the (a) x-direction, (b) y-direction ($z = 154.6$ m; $\theta_w = 210°$)
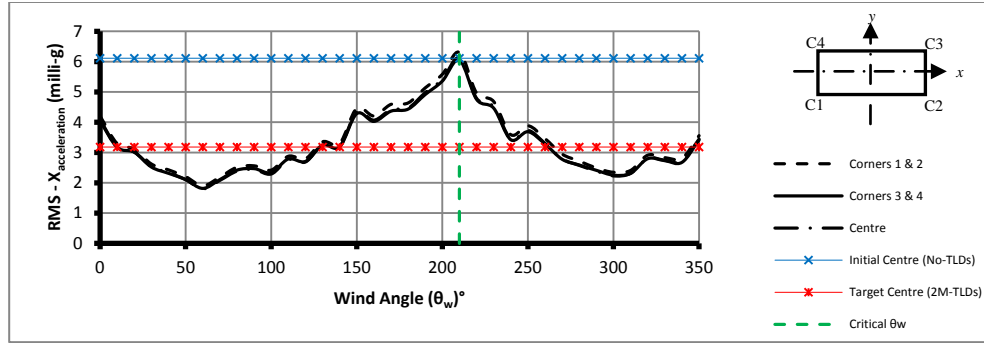
Fig. 3.8. RMS Acceleration Responses of the Indianapolis Building in the x-direction with No-TLDs Installed
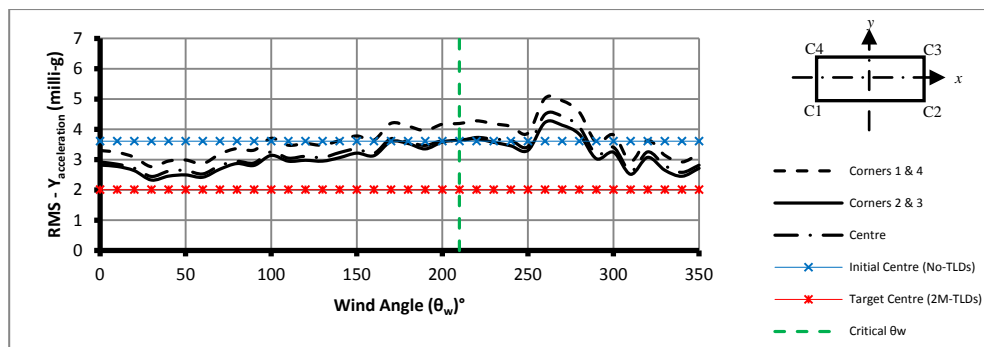
Fig. 3.9. RMS Acceleration Responses of the Indianapolis Building in the y-direction with No-TLDs Installed
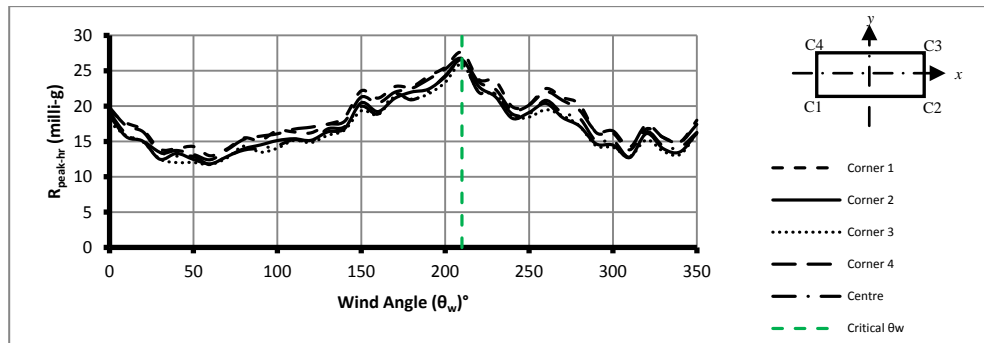
Fig. 3.10. Average Peak Hourly Resultant Acceleration Responses of the Indianapolis Building with No-TLDs Installed

(a)

(b)

(c)

(d)
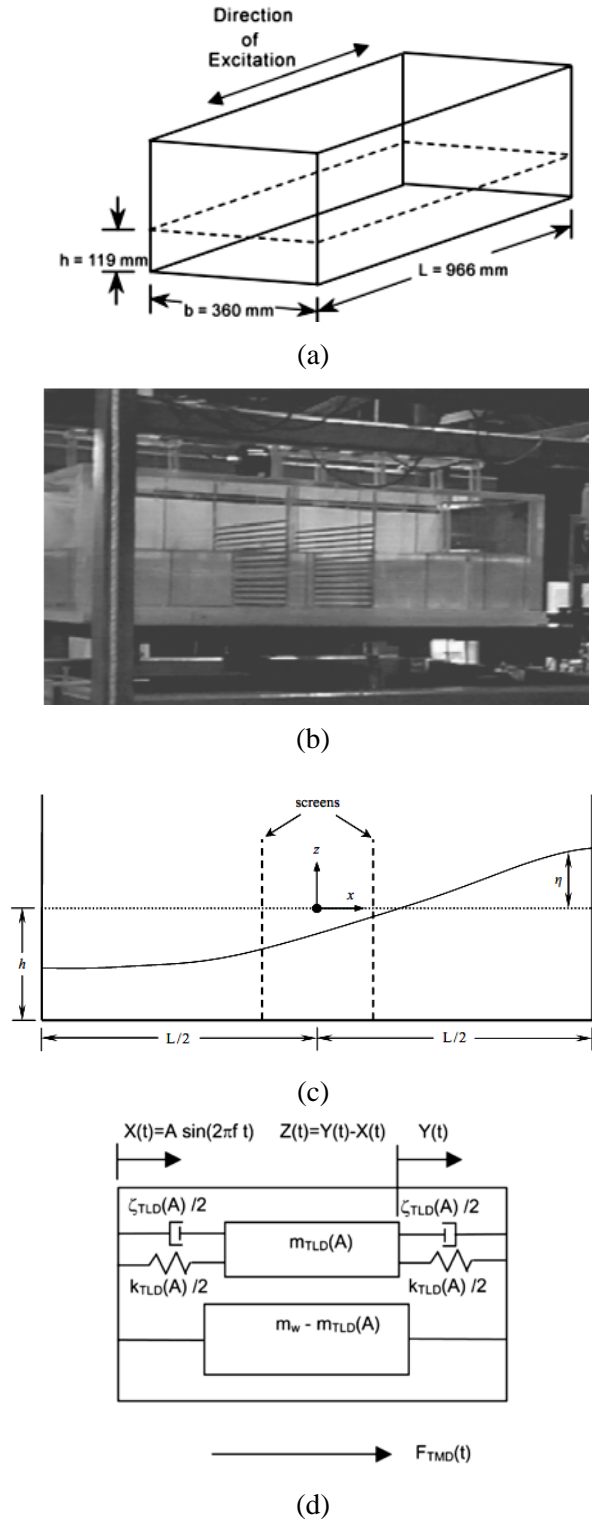
Fig. 3.11. (a) Schematic of a TLD and Its Dimensions; (b) Photo of a TLD Equipped with Internal Damping Screens; (c) Coordinate System for Nonlinear Shallow Water System; and (d) EADTMD Model (from Tait 2004)
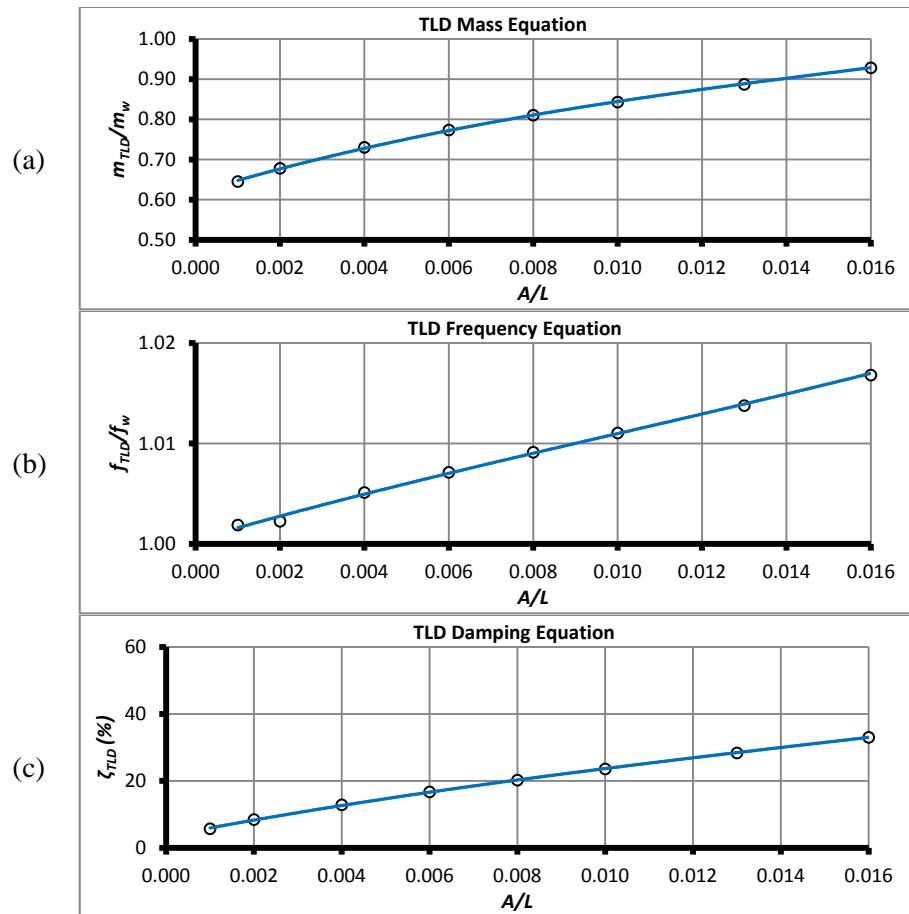
Fig. 3.12. TLD (a) Mass Ratio, (b) Frequency Ratio, and (c) Damping Ratio with respect to the Normalized Amplitude of Excitation for Mode 1 tanks in the x-direction of the Indianapolis Building
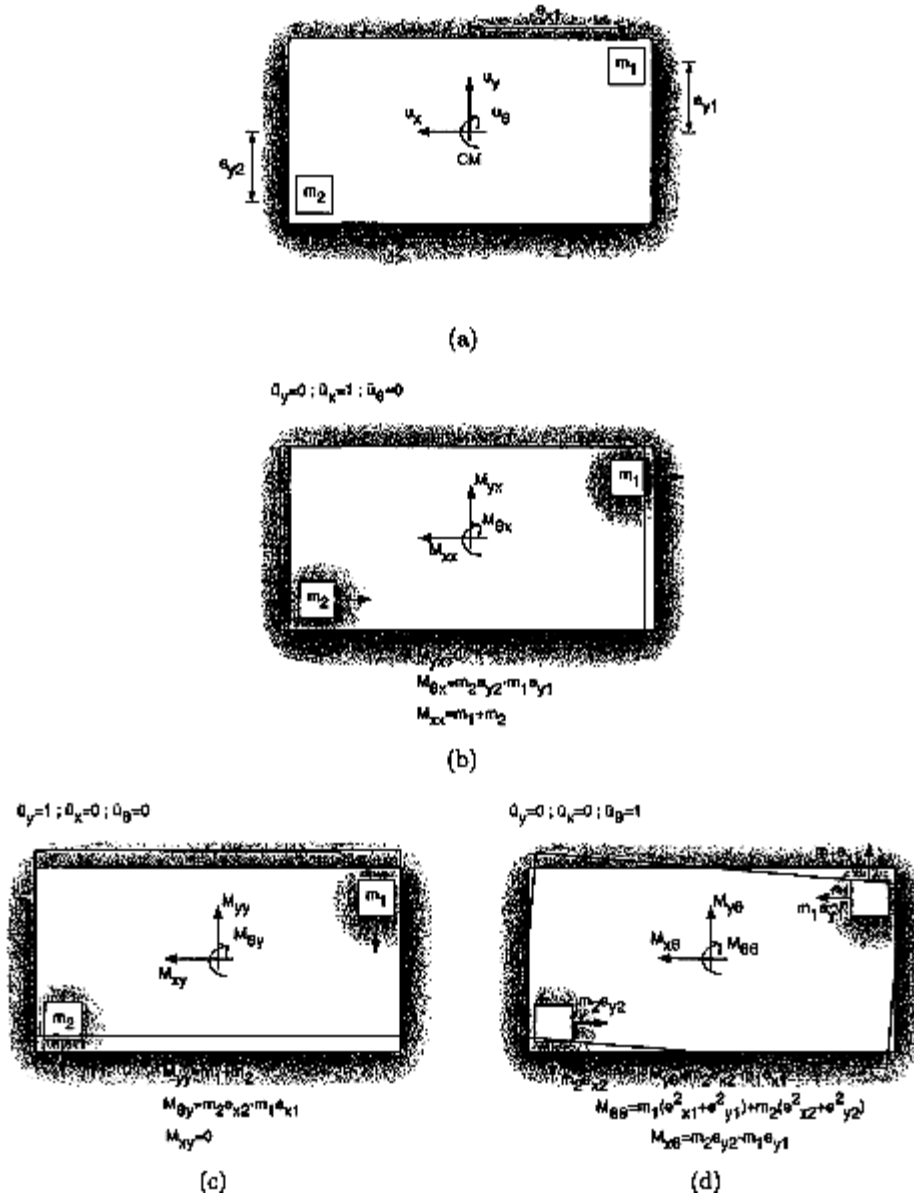
Fig. 3.13. Development of TMD Mass Matrix (from Yat 2009)
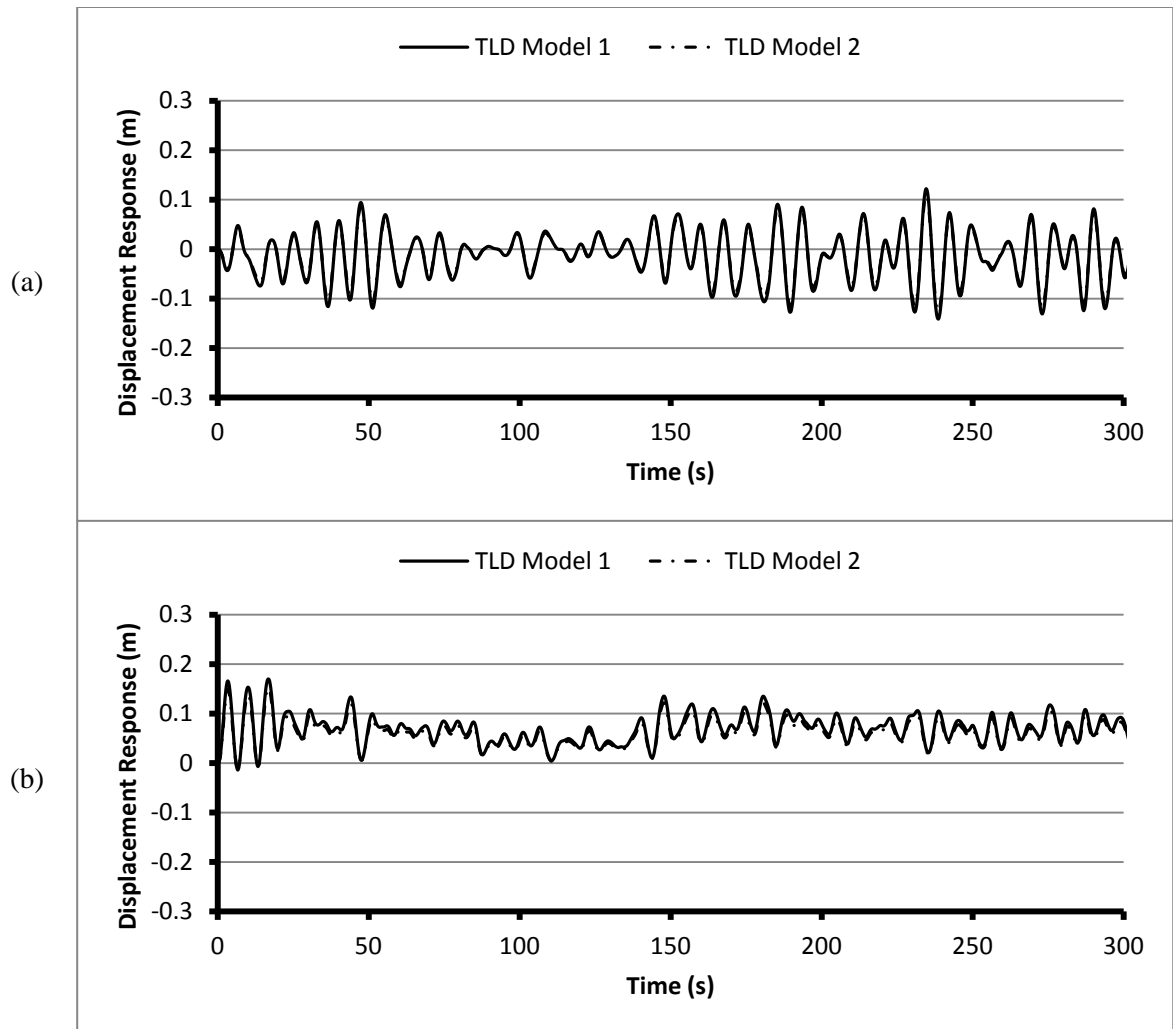
Fig. 3.14. Displacement Time History of the Indianapolis Building with TLDs Installed to Suppress the First two Modes at the CM in the (a) x-direction, (b) y-direction ($z = 154.6$ m; $\theta_w = 210°$)
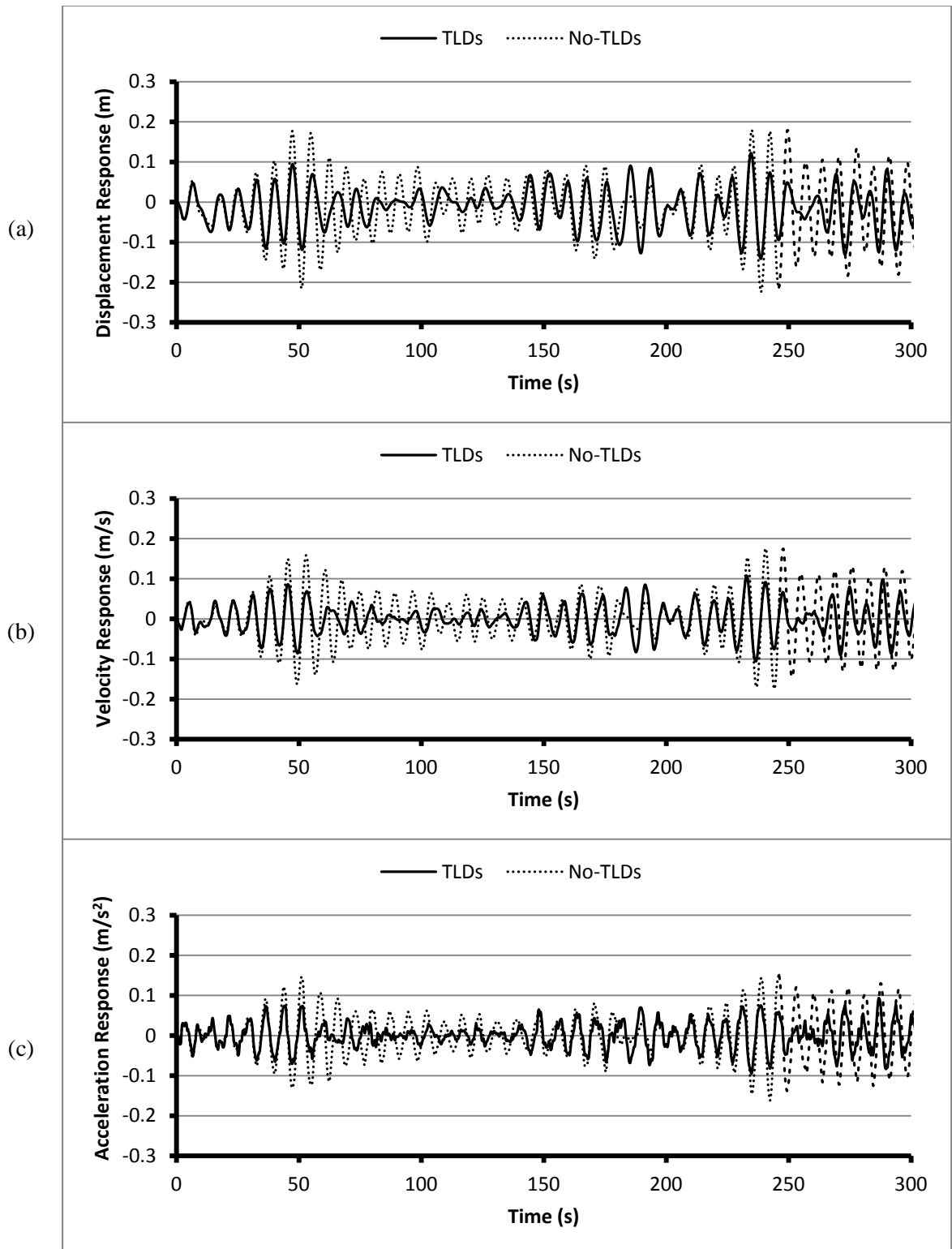
Fig. 3.15. A Comparison Time History of the Indianapolis Building at CM with/without TLDs Installed to Suppress the First two Modes for the (a) Displacement, (b) Velocity, and (c) Acceleration in the x-direction ($z = 154.6$ m, $\theta_w = 210°$)
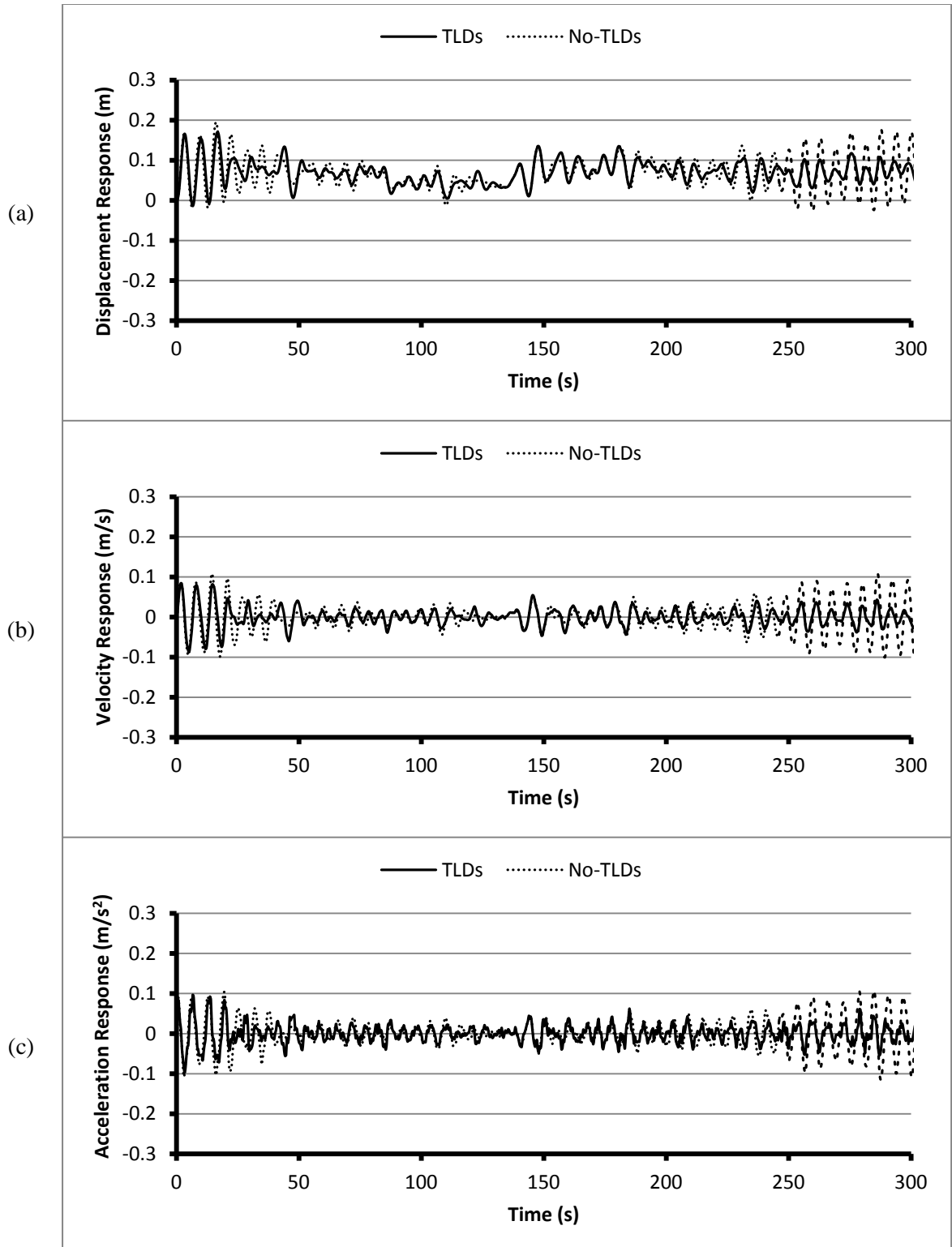
Fig. 3.16. A Comparison Time History of the Indianapolis Building at CM with/without TLDs Installed to Suppress the First two Modes for the (a) Displacement, (b) Velocity, and (c) Acceleration in the y-direction ($z = 154.6$ m, $\theta_w = 210°$)
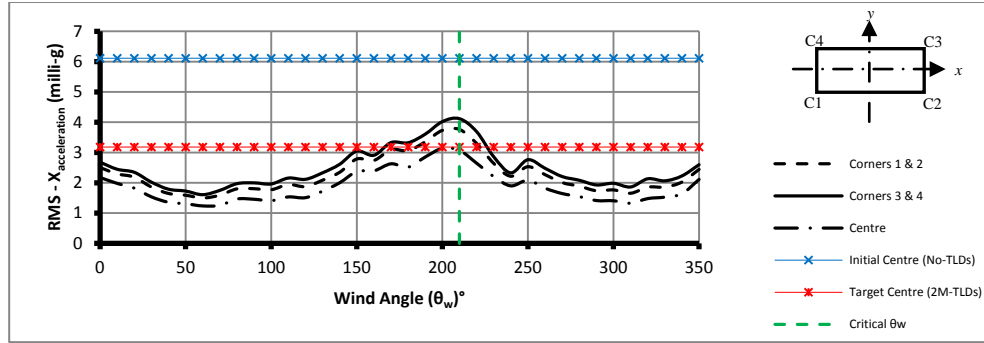
Fig. 3.17. RMS Acceleration Responses of the Indianapolis Building in the x-direction with TLDs Installed to Suppress the First Two Modes
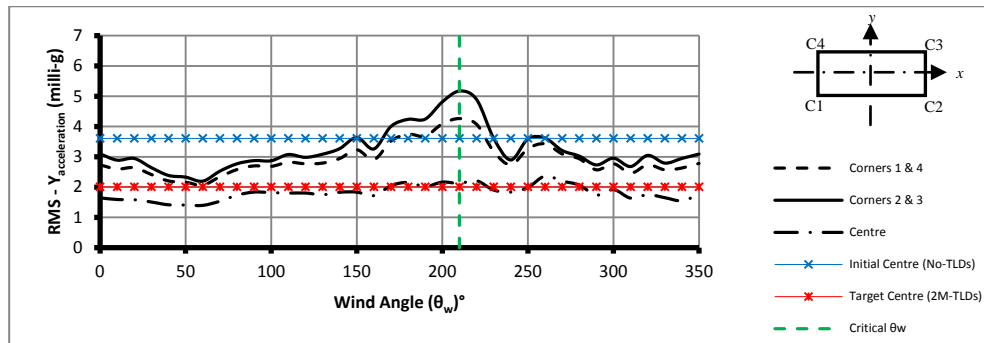
Fig. 3.18. RMS Acceleration Responses of the Indianapolis Building in the y-direction with TLDs Installed to Suppress the First Two Modes
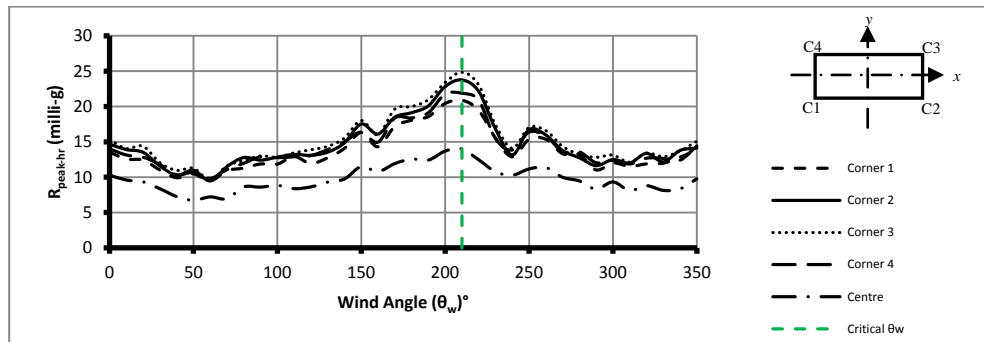
Fig. 3.19. Average Peak Hourly Resultant Acceleration Responses of the Indianapolis Building with TLDs Installed to Suppress the First Two Modes
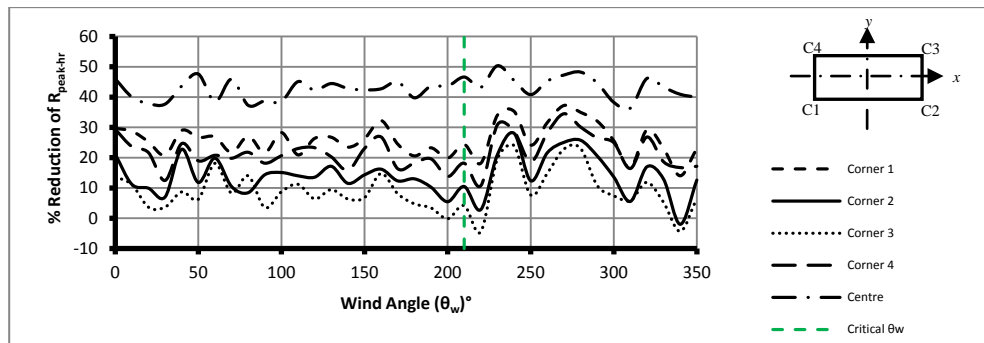
Fig. 3.20. Percentage Response Reductions of the Average Peak Hourly Resultant Accelerations of the Indianapolis Building with TLDs Installed to Suppress the First Two Modes
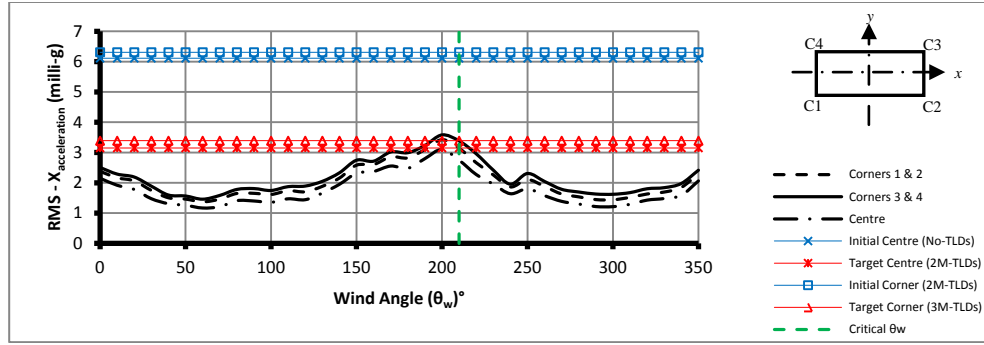
Fig. 3.21. RMS Acceleration Responses of the Indianapolis Building in the x-direction with TLDs Installed to Suppress the First Three Modes
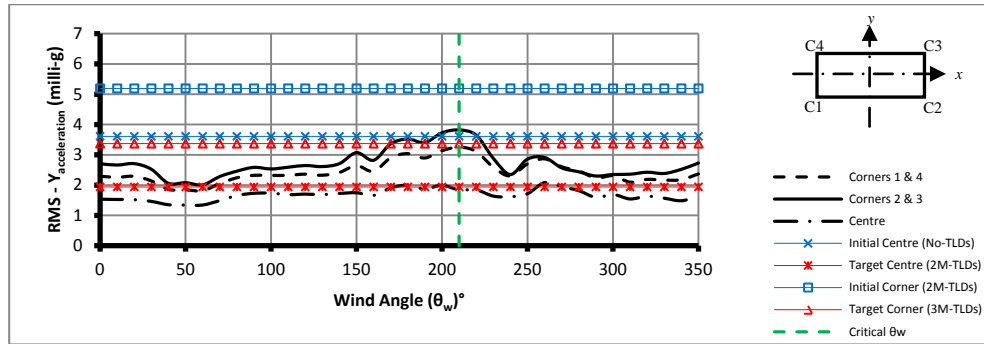
Fig. 3.22. RMS Acceleration Responses of the Indianapolis Building in the y-direction with TLDs Installed to Suppress the First Three Modes
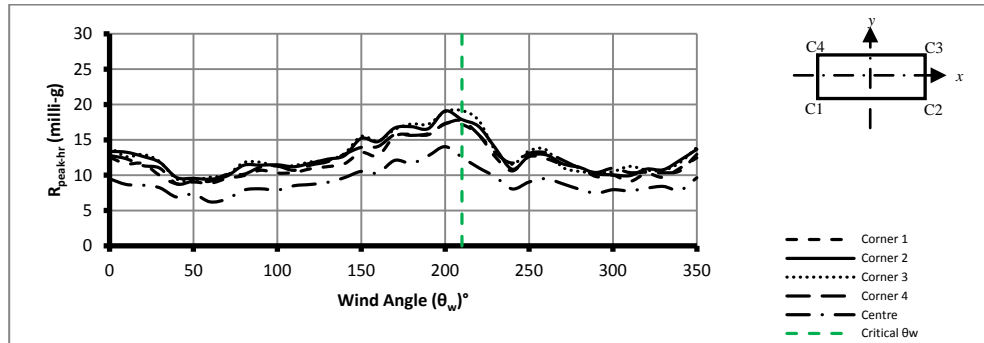
Fig. 3.23. Average Peak Hourly Resultant Acceleration Responses of the Indianapolis Building with TLDs Installed to Suppress the First Three Modes
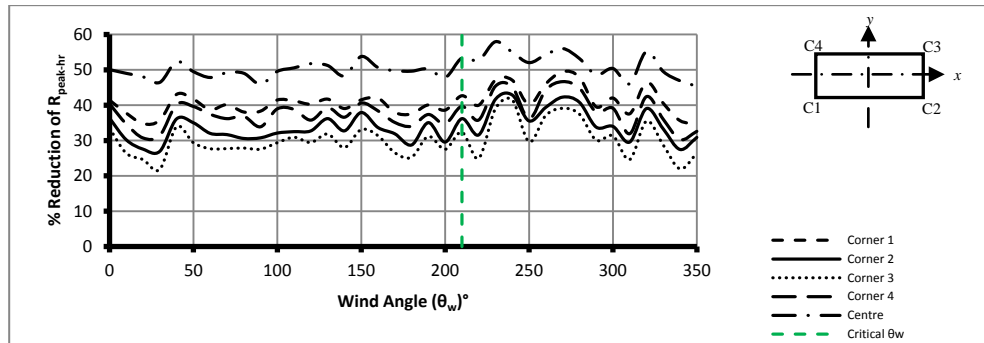
Fig. 3.24. Percentage Response Reductions of the Average Peak Hourly Resultant Accelerations of the Indianapolis Building with TLDs Installed to Suppress the First Three Modes

Chapter 4: Finite Element Modelling of Structure-MTLD Systems with Inclined Damping Screens

4.1. Introduction

Current trends in high-rise structures include increased heights and the use of lightweight and high-strength materials, which has led to very flexible and lightly damped structures. As a result, structures of this type can display increased sensitivity to external dynamic excitation (i.e. wind and earthquake). Among the different solutions considered to control their response, dynamic vibration absorbers (DVA) have been introduced and found to be very effective. A tuned liquid damper (TLD) is one of the more commonly employed dynamic vibration absorbers. It is a special type of dynamic vibration absorber (DVA) that consists of a rigid tank which is partially filled with a liquid, usually water. The sloshing liquid inside the tank creates inertia forces, which counteract the forces acting on the structure, thus reducing the building motion (Soong and Dargush 1997; Kareem et al. 1999; Yalla and Kareem 2003; Tait et al. 2004a; Tait et al. 2005a).

The performance of a TLD for a given mass ratio (μ) is a function of the tuning ratio (Ω) and the inherent TLD damping ratio (ζ_{TLD}) (Tait et al. 2004b). The damping ratio of a TLD equipped with fixed vertical damping screens is related to the screen pressure loss coefficient (C_l) and the square of the fluid velocity at the screen location (Tait 2004). Therefore, the inherent damping ratio that develops due to the screen is amplitude dependent. As a result, a TLD equipped with damping screens may only operate optimally at a single excitation amplitude, unless the screen angle is adjusted (Cassolato 2007). The ability to control the inherent damping ratio in a tuned liquid damper (ζ_{TLD}) over a range of excitation amplitudes was first introduced theoretically by Cassolato and Tait (2005). Cassolato et al. (2011) experimentally investigated the modification of ζ_{TLD} by adjusting the screen angle (θ), which alters the screen loss coefficient (C_l). Results from this work indicated that rotating the damping screens inside the TLD to adjust their loss coefficient values (C_θ) is a plausible method to maintain a constant level of ζ_{TLD} over a range of excitation amplitudes.

Cassolato (2007) experimentally studied thin sharp-edged-horizontal slat screens held at various fixed angles in a tuned liquid damper. Also, Cassolato (2007) employed two existing formulations of the pressure loss coefficient for inclined screens (C_θ) and developed a new one, using results from the study, to theoretically investigate the effect of fixed inclined

damping screens using two linear fluid models. The linear flow models were based on shallow water wave theory and potential flow theory, respectively. The linear model results were found to deviate from the experimental test results at higher screen inclination values (i.e. $\theta > 45.0°$), and could not simulate the actual response of the nonlinear free-surface elevation (Fediw 1992; Tait 2004; Tait et al. 2004a; Tait et al. 2004b; Fediw et al. 1995). In addition, the shift in resonant frequency values (amplitude dependent hardening), which was observed to occur at high response amplitudes and high screen inclination angles was not captured by the two linear models as no amplitude dependent hardening characteristic were considered.

In order to include the hardening behaviour and accurately predict the free surface response, a nonlinear TLD fluid model capable of simulating the inclined damping screens is required. Accordingly, the robustness of a structure-TLD system model due to mistuning can be addressed as the nonlinear TLD fluid model captures the shift in the tuning ratio (Ω) from its original value at high response amplitudes and high screen inclination angles. Furthermore, an increase in the efficiency of a TLD equipped with screens over a range of amplitudes can be achieved if the screens can provide constant damping to control the response.

As a result, a nonlinear TLD fluid model, developed by Kaneko and Ishikawa (1999), is updated and validated with experimental results (Cassolato 2007; Cassolato et al. 2011) to simulate the effect of inclined damping screens. A single pressure loss coefficient (C_θ) is utilized for the damping effect of the angled screens based on the inclination angle (θ). Consequently, the updated nonlinear TLD fluid model is implemented in a three dimensional finite element system model (3D-Structure-TLD), developed and validated in Chapter 2 and expanded for multiple TLDs system model (3D-Structure-MTLD) in Chapter 3. Both structure-TLD system models (i.e. 3D-Structure-TLD and 3D-Structure-MTLD) are employed in this chapter, utilizing the updated nonlinear TLD fluid model, to investigate TLD performance over a range of structural response amplitudes.

4.2.   Damping Screens (Background)

4.2.1   Slat Screens

Often, poles, screens, and other objects are submerged in the water to provide additional energy dissipating mechanisms as the damping provided by the water alone is often

insufficient (Warnitchai and Pinkaew 1998). Warnitchai and Pinkaew (1998) developed a mathematical model based on potential flow theory and determined the damping characteristics of poles and wire-mesh screens. Ju (2004) performed experiments and created an equivalent mechanical model for a WSDE (water sloshing damper with embossments).

Fediw (1992) and Tait (2004) successfully tested and modelled screens in a TLD showing that their drag characteristics can often be considered independent of the sloshing fluid inside a TLD with mesh and thin-sharp-edged-horizontal-slat screens, respectively. Both studies utilized a linearized velocity loss coefficient.

The fundamental damping characteristics of screens are related to the square of the velocity given by the well-known relationship

$$C_l = \frac{\Delta p}{\frac{1}{2} \rho U_\circ^2}$$

(4.1)

where Δp is the pressure drop across the screen and C_l is the resulting pressure loss coefficient of the screen. A loss coefficient independent of the sloshing fluid simplifies the design process of TLDs equipped with damping screens. Ultimately, screens (or any motion control device) can be optimally designed to achieve the optimum damping ratio (ζ_{opt}) for a particular amplitude of excitation. The efficiency of TLDs equipped with damping screens reduces, if the amplitude of excitation increases or decreases from the optimized target amplitude (Tait 2004; Tait et al. 2004b; Tait 2008).

An important parameter that determines the primary influence of the screens in fluid flow is the solidity ratio (S), which is a characteristic of the screen and defined as the ratio of the slat width to the slat spacing

$$S = \frac{d}{b_s}$$

(4.2)

where d is the slat width and b_s is the slat spacing as shown in Figure 4.1b. Figures 4.1a and 4.1c show a schematic of a TLD and a photograph of a TLD equipped with internal inclined damping screens, respectively. The solidity ratio can be used to estimate the vertical loss coefficient of sharp-edged slat screens (C_l) as suggested by Tait (2004) and described later in Section 4.3.1.

4.2.2   Smart Screens

Smart screens was the name given to the concept of a self-adjusting set of screens with important characteristics. First, they change angle to vary the loss coefficient (C_l) to control the inherent damping ratio (ζ_{TLD}). Second, they change their orientation in the flow automatically amidst the sloshing liquid motion if the excitation amplitude increases or decreases (Cassolato 2007).

Many studies have reported on the pressure drop characteristics of angled screens in open channel steady flow (Schubauer et al. 1950; Baines and Peterson 1951; Cornell 1957; Hoerner 1964; Carrothers and Baines 1965; Laws and Livesey 1978; Blevins 1984; Garrison 1985; Idelehik 1986; Yeh and Shrestha's 1989; Brundrett 1993; Richards and Robinson 1999; Reuter et al. 2001). For oscillatory flow, little work exists on the nature of inclined screens. Badr 1994 studied the fluid losses of inclined elliptic cylinders with flat plates as a special case. Badr's drag coefficient formulation (1994) for an inclined flat plate was reduced from an elliptic cylinder as a function of the angle inclination and Strouhal number. No experimental support was given in Badr (1994) and no applicable ranges of Reynolds or Strouhal numbers were given. Okajima et al. (1998) examined the drag coefficients (pressure loss) versus the Keulegan-Carpenter number for oscillatory flow. Although their experimental study was insightful, no clear theoretical formulation was created.

To the best of the author's knowledge, the only extensive experimental and linear numerical studies on the orientation of the damping screens submerged in a TLD at various angles have been reported in Cassolato and Tait (2005), Cassolato (2007), and Cassolato et al. (2011) in order to change the pressure loss coefficient (C_l), which altered the absorber damping, intending to optimize the TLD at different excitation amplitudes.

4.3.   Loss Coefficient for Damping Screens in a TLD

The pressure loss coefficient (C_l) is important to be evaluated in order to correctly describe the influence of damping screens in oscillating fluid flow. In this section, a brief description of existing methods used to determine the pressure loss coefficient for vertical and inclined damping screens (C_l and C_θ), is presented.

4.3.1 Pressure Loss Coefficient for Vertical Damping Screen (C_l)

Baines and Peterson (1951) suggest using the following equation to estimate C_l in steady flow

$$C_l = \left(\frac{1}{C_c(1-S)} - 1\right)^2 \tag{4.3}$$

where S is the solidity ratio and C_c is the contraction coefficient for the screen type. A contraction coefficient suggested by Tait (2004) as a function of S can be used for sharp-edged slat-screens based on the experimental work by Weisbach (1855)

$$C_c = 0.405e^{-\pi S} + 0.595 \tag{4.4}$$

The drag coefficient (C_D) is related to the loss coefficient (C_l) by the following equation

$$C_D = \frac{C_l}{S} \tag{4.5}$$

For solidity ratio (S) higher than 0.30, Equations 4.3 and 4.5 can be used to estimate the coefficients C_l and C_D without using the modified curves presented in Baines and Peterson (1951). Consequently, the drag force (F_D) being exerted on the screen, normal to the screen plane can be evaluated by

$$F_D = \frac{1}{2}\rho C_D u^2 A_s \tag{4.6}$$

where ρ is the density of water and u is the fluid velocity at the screen location inside the tank.

4.3.2 Pressure Loss Coefficient for Inclined Damping Screen (C_θ)

The pressure loss coefficient for inclined slat-screens depends on the normal component of fluid flow through the screen; even though the flow approaches with an angle of incidence assumed to be equivalent to the screen angle (θ) and leaves with the deflection angle (Ψ) on the leeward side of the screen (Schubauer et al. 1950). Cassolato (2007) presented and evaluated three different C_θ values. The values of C_θ were determined based on the following:

● First, a common description of the oblique fluid flow on any object or structure. Schubauer et al. (1950) reported the pressure drop to be proportional to the square of component of the average fluid velocity throughout the depth ($U_\circ$) normal to the screen for

screens whose normal direction vector (i.e. perpendicular to the plane of the screen) is at an angle ($0° \leq \theta \leq 45°$) to the incident flow using the relation

$$\Delta P = \frac{1}{2}\rho C_\theta (U_\circ cos\theta)^2 \tag{4.7}$$

Equation 4.7 combined with the well-known Equation 4.1 for the pressure drop coefficient yields

$$C_{\theta 1} = C_l \, cos^2\theta \tag{4.8}$$

Therefore, C_l equals C_θ at a vertical screen position ($\theta = 0°$). Laws and Livesey (1978) and Richards and Robinson (1999) found the pressure loss through a screen to be proportional to the square of the cosines of the angle of incidence. However, at angles greater than 45°, it has been found that this relationship underpredicts fluid losses as examined by Cassolato (2007)

● Second, an empirical method based on experimental findings attempting to capture the overall losses found at low and very high screen angles. Cassolato (2007) provided a 3rd order polynomial using the regression analysis for the results provided in Table 4.1 by Blevins (1984) to correct for the under prediction of losses at angles greater than 45°. Blevins provided a table of reduction in losses (γ_θ) as a fraction of the losses for a vertical screen at 0° and his values selected from experimental results by Carrothers and Baines (1965). The values in Table 4.1 from 0° to 40° are exactly $cos^2\theta$, whereas values from 50° to 85° are from the experimental results and deviate from the $cos^2\theta$ trend. Therefore, the second estimated angled screen loss coefficient is

$$C_{\theta 2} = C_l \, \gamma_\theta \tag{4.9}$$

where

$$\gamma_\theta = 0.46\theta^3 - 1.05\theta^2 - 0.06\theta + 1 \tag{4.10}$$

and θ is expressed in radians.

● Third, an estimate of the loss coefficient developed by Cassolato (2007), based on the well established use of C_l by Baines and Peterson (1951) with modifications based on the analytical and experimental work of Yeh and Shrestha (1989), can be determined using

$$C_{\theta 3} = \left(\frac{cos\theta}{C.cos\psi} - 1\right)^2 \tag{4.11}$$

where

$$C = C_c(1 - S) \tag{4.12}$$

Equations 4.8, 4.9 and 4.11 were plotted by Cassolato (2007) as shown in Figure 4.2. As can be seen in the figure, $C_{\theta 2}$ reflects the curve of $C_{\theta 1}$ except for $\theta > 45°$. $C_{\theta 3}$ plotted for various Ψ/θ values, with 0.6 selected as the lowest bound essentially limited by the $cos\theta^2$ losses and 0.9 selected as the upper bound since theoretically, $\Psi \neq \theta$ or $\Psi/\theta \neq 1$. $C_{\theta 2}$ and $C_{\theta 3}$ appeared to estimate the pressure loss coefficient more accurately as $C_{\theta 1}$ underestimates the pressure loss at high screen angles ($45° \leq \theta \leq 70°$). From experimental observations, Cassolato (2007) selected a value of $\Psi/\theta = 0.8$ for $\theta \leq 45°$, $\Psi/\theta = 0.9$ at $\theta = 60°$ for $S = 42\%$, and $\Psi/\theta = 0.85$ at $\theta = 60°$ for $S = 52\%$.

$C_{\theta 2}$ and $C_{\theta 3}$ were used to estimate the pressure loss coefficients of angled screens in two linear TLD models, one based on shallow water wave theory (Cassolato and Tait 2005), and the other based on potential flow theory (Cassolato 2007; Cassolato et al. 2011). Results from both linear models were compared to experimental values. The primary difference between the two linear models was that the potential flow model more accurately captures the influence of the screen losses over the height and length of the screen.

4.4. Nonlinear Simulation and Validation of a TLD Equipped with Inclined Damping Screens

The nonlinear simulation of inclined damping screens in a TLD using a nonlinear fluid model was beyond the scope of previous studies (Cassolato and Tait 2005; Cassolato 2007; Cassolato et al. 2011). Thus in this section, the nonlinear simulation of inclined damping screens submerged in a TLD is addressed to overcome linear fluid model limitations.

4.4.1 Nonlinear Fluid Model of a TLD Equipped with Inclined Damping Screens

The nonlinear numerical model of a TLD equipped with damping screens, described in detail in Chapter 2, is utilized in this study. The liquid is assumed to be inviscid, irrotational and incompressible. Considering the tank, shown in Figure 4.3, is excited in a unidirectional motion, the nonlinear sloshing response can be expressed using shallow water theory as (Lepelletier and Raichlen 1988)

$$\frac{\partial \eta}{\partial t} + \frac{\partial}{\partial x}[(h + \eta)u] = 0 \tag{4.13}$$

$$\frac{\partial u}{\partial t} + u\frac{\partial u}{\partial x} + g\frac{\partial \eta}{\partial x} - \frac{1}{3}(h+\eta)^2\frac{\partial^3 u}{\partial t \partial x^2} + \zeta_w u + \ddot{X} = 0 \tag{4.14}$$

where $\eta(x,t)$ is the free-surface elevation, $u\,(x,t)$ is the horizontal velocity averaged through the liquid depth, L is the tank length, h is still liquid depth, g is the gravitational acceleration, $\ddot{X}$ is the horizontal base excitation acceleration of the tank and ζ_w is a damping coefficient (Miles 1967) to account for viscous dissipation. The set of nonlinear shallow water equations can be solved numerically once the initial state of the liquid is prescribed, i.e. the values of η and h are given at time $t = 0$. A one-dimensional finite difference discretization scheme is applied for both η and h as shown in Figure 4.4.

Using the method outlined by Kaneko and Ishikawa (1999) at locations where a damping screens is inserted as shown in Figure 4.5, the velocity at a particular screen (U_{DSi}) can be expressed as

$$U_{Dsi} = \frac{u_i + u_{i+1}}{2} \tag{4.15}$$

The pressure drop (Δp) caused by the screen can be expressed as

$$\Delta p = C_l \frac{\rho U_{DSi}^2}{2} \tag{4.16}$$

where C_l is the pressure loss coefficient for vertical screens ($\theta = 0°$).

The relationship between the pressure loss coefficient and the free-surface height difference across the screen is given by

$$|\eta_L - \eta_R| = \Delta \eta = C_l \frac{U_{DSi}^2}{2g} \tag{4.17}$$

To incorporate the influence of screen angle on fluid response, C_l in Equations 4.16 and 4.17 is replaced by C_θ. Consequently, Equations 4.16 and 4.17 can be written as

$$\Delta p = C_\theta \frac{\rho U_{DSi}^2}{2} \tag{4.18}$$

$$|\eta_L - \eta_R| = \Delta \eta = C_\theta \frac{U_{DSi}^2}{2g} \tag{4.19}$$

Upon integrating the discretized continuity and momentum equations with respect to time, the values of free-surface on the left (η_L) and right (η_R) sides of the screen can be determined by

$$\eta_L = \eta_i + \text{sign}[U_{DSi}]\frac{\Delta\eta}{2} \tag{4.20}$$

$$\eta_R = \eta_i - \text{sign}[U_{DSi}]\frac{\Delta\eta}{2} \tag{4.21}$$

Subsequently, the velocity, the base shear force and the wave height can be determined. Cassolato (2007) presented and evaluated three different C_θ values, which are summarized as follows (see Section 4.2.4.2):

$$C_{\theta 1} = C_l \cos^2\theta \tag{a}$$

$$C_{\theta 2} = C_l \left(0.46\theta^3 - 1.05\theta^2 - 0.06\theta + 1\right) \tag{b} \quad (4.22)$$

$$C_{\theta 3} = \left(\left(\sqrt{C_l} + 1\right)\frac{\cos\theta}{\cos\psi} - 1\right)^2 \tag{c}$$

Due to the similarity between pressure loss coefficients $C_{\theta 1}$ and $C_{\theta 2}$ and the knowledge that $C_{\theta 1}$ underestimates fluid losses at practical high screen angles ($45° \le \theta \le 70°$), $C_{\theta 1}$ is not considered. In the current study, $C_{\theta 2}$ is found to better simulate the loss coefficient of inclined damping screens compared to $C_{\theta 3}$. Thus, $C_{\theta 2}$ is used in the nonlinear simulation of a TLD equipped with inclined damping screens and results are compared with experimental values (Cassolato 2007; Cassolato et al. 2011) in the next section.

The base shear force that develops when the TLD is forced to move can be separated into the following three components: first, the inertial force due to the container (f_1); second, the inertial force due to the dead weight of the contained liquid (f_2); and third, fluid force generated by sloshing (f_3). Therefore, the TLD base shear force caused by the liquid motion is denoted by $F_{TLD_x-Model\,1} = f_2 + f_3$. Applying momentum theory to calculate the TLD base shear force, the mass of the ith element can be expressed as follows (Kaneko and Ishikawa 1999)

$$m_i = \rho \times \frac{L}{n_e} \times b \times \left(\frac{\eta_{i-1} + \eta_i}{2} + h\right) \tag{4.23}$$

where n_e is the total number of elements, L is the tank length, b is the tank width and ρ is the liquid unit weight.

Consequently, the momentum of the ith element can be described as follows

$$P = \sum_{i=1}^{n_e} m_i u_i = \frac{\rho L b}{n_e} \sum_{i=1}^{n_e} \left(\frac{\eta_{i-1} + \eta_i}{2} + h \right) u_i \tag{4.24}$$

The TLD base shear force ($F_{TLD_x-Model\,1}$) can be determined by the following equation

$$F_{TLD_x-Model\,1} = \frac{1}{\Delta t} (P(t) - P(t + \Delta t)) \tag{4.25}$$

4.4.2 Nonlinear Simulation of a TLD Equipped with Inclined Damping Screens

Comparisons between the updated nonlinear fluid model and experimental results found in the literature are presented in this section for damping screens, with different inclination angles (θ). Three key TLD response parameters are compared: the free-surface response, the base shear force and the overall average energy dissipated per cycle of excitation. The following definitions are used in the verification study presented in this section.

i. Non-dimensional free-surface amplitude (η') determined as

$$\eta' = \frac{\eta}{h} \tag{4.26}$$

where η is the free-surface response amplitude and h is the quiescent water depth.

ii. Non-dimensional excitation amplitude (Λ) determined as

$$\Lambda = \frac{A}{L} \tag{4.27}$$

where A is the applied excitation amplitude

iii. Excitation frequency ratio (β) determined as

$$\beta = \frac{f}{f_n} \tag{4.28}$$

where f_n is the natural sloshing frequency (f) is the forcing frequency

iv. Non-dimensional base shear force [$F_w'(t)$] determined as

$$F_w'(t) = \frac{F_w(t)}{m_w A \omega^2} \tag{4.29}$$

where $F_w(t)$ is the base shear force produced by the nonlinear TLD fluid model and the denominator is the maximum inertial force of the entire water mass (m_w) treated as a solid mass.

v. The non-dimensional energy dissipation per cycle (E_w') determined as

$$E_w' = \frac{E_w}{\frac{1}{2}m_w(A\omega)^2} \tag{4.30}$$

where the denominator is the maximum kinetic energy of the entire water mass (m_w) treated as a solid mass and the numerator represents the energy dissipated per cycle

$$E_w = \oint_T F_w(t)dx \tag{4.31}$$

where T is the applied excitation period.

4.4.2.1 Frequency Response Comparison

Figures 4.6 and 4.7 show the non-dimensional energy dissipation (E_w') frequency response curves produced using the nonlinear fluid model for one of two sets of slat screens (used in experimental tests Cassolato 2007 and Cassolato et al. 2011) at normalized excitation amplitude values (Λ) of 0.005 and 0.021, respectively, for angles of 0°, 30° and 60°. Figures B1 and B2 (Appendix-B) show E_w' frequency response curves for the second set of slat screens. Cassolato (2007) conducted a series of shake table tests on a tank of length (L) equal to 0.966 m, width (b) equal to 0.360 m and mean water depth (h) equal to 0.019 m with damping screens inserted at distances of 0.4L and 0.6L from the tank end wall as shown in Figures 4.1a and 4.1c. The vertical loss coefficients (C_l) for the damping screens used in the tests were 3.53 and 5.69. For both amplitudes, a discrete frequency sweep test was experimentally conducted to obtain frequency response curves. The updated nonlinear fluid model is found to be in good agreement with the experimental test values for both sets of screens at all inclination angles (θ), with a maximum percentage difference of 2.5% over the entire excitation frequency ratio values (β). The presence of higher harmonics and the hardening behaviour are captured by the nonlinear fluid model, which are clearly shown at an excitation frequency ratio (β) equal to 0.93 and the increased frequency peak values for cases of high screen inclination angles, respectively.

Figure 4.8 shows that increasing the screen inclination angle (θ) has resulted in a decreased in damping ratio (ζ_{TLD}) for a given excitation amplitude ($\Lambda = 0.010$). The maximum difference between the updated nonlinear fluid model results and the experimental test results is found to be less than 2.3% over the entire range of excitation frequency ratio values (β). Figure 4.8 clearly shows that screen angle values directly affect the normalized

energy dissipated by the TLD, which is demonstrated by the change in the frequency response curves. The level of non-dimensional energy dissipation (E_w') is found to increase with increasing screen angle (θ).

Furthermore, the nonlinear fluid model is used to simulate experimental results (Cassolato 2007; Cassolato et al. 2011) demonstrating a level of peak response that was nearly constant over a range of excitation amplitude ratio values from $\Lambda = 0.005$ to 0.016 at different screen angle values from $\theta = 0°$ to 60° as shown in Figure 4.9. The near constant peak response values indicates that a near constant damping value is being maintained. The maximum difference between the updated nonlinear fluid model results and the experimental test results is found to be less than 2.7%. Therefore, the concept of altering the screen inclination angle to provide constant damping (ζ_{TLD}) if the correct screen angle (θ) is selected can be applied utilizing the updated nonlinear fluid model.

4.4.2.2 Time History Comparison

Time history simulations of the normalized free-surface motion (η') and the normalized base shear forces $[F_w'(t)]$ are presented in Figures 4.10 and 4.11, respectively. The screens have a vertical pressure loss coefficient (C_l) equal to 3.53 and are subjected to a normalized excitation amplitude (Λ) of 0.021 at screen angles of $0°, 30°$ and 60°. Figures B3 and B4 (Appendix-B) present η' and $F_w'(t)$, respectively, for the second set of screens having $C_l = 5.69$ and subjected to $\Lambda = 0.005$. Excellent agreement is found between the experimental test results and the nonlinear simulations for both sets of screens at all angles for both wave height and base shear force time histories with maximum percentage differences of 1.8% and 2.0%, respectively. Therefore, the updated model is able to accurately estimate the resultant base shear force for practical inclination angles of screens (θ) at low and high excitation amplitude ratio values (Λ). This is in contrast with linear simulation results that deviated from experimental test values at $\theta = 60°$ and $\Lambda = 0.021$ (Cassolato 2007).

4.5. Performance of a 3D-Structure-TLD System Model Equipped with Inclined Damping Screens

The updated nonlinear TLD fluid model is implemented into both the 3D-Structure-TLD and 3D-Structure-MTLD system models to investigate the performance of a 3D single-story structure (see Section 4.6) and a high-rise building (see Sections 4.7 and 4.8) with TLDs

equipped with inclined damping screens over a range of structural response amplitudes. First, the main parameters, which affect the response and efficiency of a structure-TLD system, are briefly described in this section. Second, the ability of the updated nonlinear fluid model to simulate near constant damping if a correct screen angle is selected is examined.

4.5.1 Response/Efficiency of a 3D-Structure-TLD System Model

The response of a structure equipped with a TLD is a function of three main parameters (Tait 2004; Tait et al. 2004a; Tait et al. 2007).

i. The tuning ratio, which influences the performance of the TLD, is defined by

$$\Omega = \frac{f_{TLD}}{f_s} \tag{4.32}$$

where f_{TLD} is the natural frequency of the TLD; and f_s is the natural frequency of the 3D structure. An estimate of the natural frequency of the TLD, f_{TLD} for small sloshing fluid response amplitude is approximately equal to f_w (Warnitchai and Pinkaew 1998; Ju et al. 2004; Tait et al. 2004a). The fundamental sloshing frequency (f_w) for the water inside a TLD using the linear wave theory (Lamb 1932) can be estimated as

$$f_w = \frac{1}{2\pi} \sqrt{\frac{\pi g}{L} tanh\left(\frac{\pi h}{L}\right)} \tag{4.33}$$

where g is the gravitational acceleration and L is the tank length in the direction of the fundamental sloshing mode of interest.

ii. The mass ratio (μ) which is given by

$$\mu = \frac{\phi^2 m_{TLD}}{M^*} \tag{4.34}$$

where M^* is the generalized mass of the primary structure corresponding to the vibration mode being suppressed; and ϕ is the normalized modal deflection value of the structure at the TLD location. The absorber mass (m_{TLD}) for a TLD with damping screens can be approximated using potential flow theory (i.e. $m_{TLD} \approx m_1$). The value m_1 is calculated using the following equation (Graham and Rodriguez 1952)

$$m_1 = \frac{8 \, tanh\left(\frac{\pi h}{L}\right)}{\frac{\pi^3 h}{L}} m_w \tag{4.35}$$

where m_w is the total mass of the contained water.

iii. The inherent damping ratio (ζ_{TLD}) of the sloshing fluid inside the tank. The damping related to the sloshing liquid inside the tank without the presence of additional energy dissipating devices can be estimated by Sun (1991) using the following equation

$$\zeta_{TLD} = \frac{1}{2\pi}\sqrt{\frac{v_w}{\pi f_w}}\left(1 + \frac{h}{b}\right) \tag{4.36}$$

where v_w is the kinematic viscosity of water.

Optimum inherent damping ($\zeta_{TLD-opt}$) and optimum tunning ratio (Ω_{opt}) values for a linear structure-tuned mass damper (TMD) as a function of the mass ratio (μ) can be obtained for the special case of zero structural damping ($\zeta_s = 0$) based on the derivation presented by Warburton (1982). Due to the analogy between the TMD and TLD devices, Warburton's solutions based on H_2 optimization, are used to calculate the target values of $\zeta_{TLD-opt}$ and Ω_{opt}

$$\zeta_{TLD-opt} = \sqrt{\frac{\mu(1 + 3\mu/4)}{4(1 + \mu)(1 + \mu/2)}} \tag{4.37}$$

And

$$\Omega_{opt} = \frac{\sqrt{1 + \mu/2}}{1 + \mu} \tag{4.38}$$

On the other hand, three important parameters, commonly used to evaluate the performance of a structure-TLD system, are the efficiency, effectiveness and robustness (Tait 2004; Tait et al. 2004a; Tait et al. 2007). These parameters are briefly discussed in this section to study the performance of a 3D-Structure-TLD system model equipped with inclined damping screens

i. The effectiveness of a TMD can be expressed in terms of the amount of additional effective viscous damping that it adds to the primary structure (Vickery and Davenport 1970), denoted by the effective viscous damping ratio (ζ_{eff}). This can be accomplished by equating the area under the frequency response of the combined system to that of a single degree of freedom system (SDOF) with the same frequency and solving for the effective damping (ζ_{eff}) (McNamara 1977).

For a special case of zero structural damping (i.e. $\zeta_s = 0$), ζ_{eff} can be obtained using Gerges and Vickery (2003) formula as

$$\zeta_{eff} = \frac{\Omega\mu\zeta_{TLD}}{(1+\mu)^2\Omega^4 + (1+\mu)2\Omega^2(2\zeta_{TLD}^2 - 1) + \Omega^2\mu + 1} \tag{4.39}$$

The optimal parameter for the effective damping ($\zeta_{eff-opt}$) can be obtained by substituting Equations 4.37 and 4.38 into Equation 4.39, leading to

$$\zeta_{eff-opt} = \frac{1}{4}\sqrt{\frac{\mu(1+\mu)}{1+3\mu/4}} \tag{4.40}$$

ii. The efficiency (ψ) of a TLD is defined as the amount of effective damping that a TLD provides, compared to an optimal equivalent TMD with equivalent TMD mass, and expressed as a percentage using

$$\psi = \frac{\zeta_{eff}}{\zeta_{eff-opt}}.100 \tag{4.41}$$

iii. Robustness is defined as the change in effectiveness with changes in the tuning ratio (Ω), TLD damping ratio (ζ_{TLD}) and the structural response amplitude. The TLD is modelled using the nonlinear fluid model, based on shallow water theory. Thus, in addition to the amplitude dependent damping ratio, the amplitude dependent hardening characteristics are also considered.

4.6. Investigation of a Single-Story Structure with TLD Equipped with Vertical/Inclined Damping Screens under Random Excitation

Previous sections focused on the impact of inclined damping screens on the dynamic response behaviour of a TLD under sinusoidal excitation. Wind excitation is often modelled as a random (white noise) excitation since a typical wind spectrum is nearly constant over the resonant domain of the frequency response of the structure. This section demonstrates the ability of an idealized TLD equipped with angled screens to operate optimally over a range of structural response amplitudes. Consequently, the updated 3D-Structure-TLD system model is employed to conduct a parametric study on a single-story structure utilizing practical mass ratio values (μ).

4.6.1 Efficiency of a Structure-TLD System Model Equipped with Vertical Damping Screens

A 3D single-story structure shown in Figure 4.12, whose generalized properties match those used in experimental work reported on by Tait (2004) and subjected to random excitation, are listed in Table 4.2. The 3D-Structure-TLD system model is excited by a number of 3.7-hour duration random force excitation time histories having increasing

excitation amplitude values (F_{max}). A one-minute duration portion of the random excitation selected at the 1ˢᵗ minute of the time history is shown in Figure 4.13. A tank length (L) equal to 0.966 m is selected to match that used in the experimental work reported by Tait (2004). The water depth (h) is selected to achieve the optimal tuning ratio (Ω) according to the selected mass ratio (μ). The tank width (b) is then selected to achieve the selected mass ratio (μ). The mass ratio values (μ) for the parametric study are 1.0%, 2.5%, 3.5% and 5.0%. Table 4.3 shows the properties of the TLDs used in the parametric study. Equations 4.37 and 4.38 are used to calculate the optimum TLD damping ratio ($\zeta_{TLD-opt}$) and the optimal tunning ratio (Ω_{opt}) values for each selected mass ratio (μ).

A set of damping screens, which have a solidity ratio value (S) equal to 60% and corresponding vertical loss coefficient value (C_l) of 8.17, are placed at 0.4L and 0.6L. In the case of normal vertical damping screens ($\theta = 0°$) and in an iterative manner, the 3D single-story structure is analyzed under the random excitation force time history with increasing values of excitation amplitude (F_{max}) during each iteration. This leads to increasing values of the root-mean-square (RMS) structural response acceleration ($\sigma_{\ddot{x}}$), which are determined from the dynamic analysis. Consequently, the average peak hourly structural acceleration response ($\ddot{x}_{peak-hr}$) is calculated using the RMS structural acceleration response ($\sigma_{\ddot{x}}$) and the peak factor (PF) (Davenport 1964). The following equation is used to determine the average peak hourly structural acceleration responses ($\ddot{x}_{peak-hr}$)

$$\ddot{x}_{peak-hr} = \sigma_{\ddot{x}} PF_x \tag{4.42}$$

A peak factor value (PF) of 3.75 is determined for the single-story structure using (Davenport 1964)

$$PF_x = \sqrt{2\ln\left(\frac{T_d}{2\pi}\omega_{s-x}\right)} + \frac{0.577}{\sqrt{2\ln\left(\frac{T_d}{2\pi}\omega_{s-x}\right)}} \tag{4.43}$$

where ω_{s-x} is the structure's natural frequency in the x-directions, which is the direction of the applied external random excitation, and T_d is the duration time in seconds used to calculate the average peak factor value, which is an hour in this study. The model tested by Tait (2004) was a 1/10 scaled model, therefore, $T_d = \frac{3600}{\sqrt{SF}} = \frac{3600}{\sqrt{10}} = 1138$ seconds is used in the peak factor calculation, where SF is the scale factor.

The selected vertical damping screens ($\theta = 0°$) are found to provide 100% TLD efficiency (ψ) for the mass ratio values (μ) of 1.0%, 2.5%, 3.5% and 5.0% at peak hourly structural acceleration response values of 2.7 milli-g, 6.5 milli-g, 9.0 milli-g and 12.5 milli-g, respectively (see Figure 4.14). These structural response values represent the target response of the structure-TLD system ($\ddot{x}_{target}$) at different mass ratio values (μ) for the case of vertical screens.

4.6.2 Procedure to Estimate Damping Screen Angle for Improved TLD Efficiency

A preliminary TLD design procedure (Tait 2008), which is discussed in detail in Chapter 3, is employed in this section to determine the inclined damping screen properties [i.e. the inclined screen loss coefficient values (C_θ) required to achieve 100% TLD efficiency (ψ) at different selected target peak hourly acceleration response values ($\ddot{x}_{target}$) and mass ratio values (μ)]. Consequently, the required inclination angles for the damping screens (θ) can be determined using Equation 4.22-b.

First, the accuracy of the TLD design procedure is checked by determining the required vertical screen loss coefficient values (C_l), which achieve various target peak hourly acceleration response values ($\ddot{x}_{target}$) at 100% TLD efficiency (ψ), obtained previously from Figure 4.14 for different selected mass ratio values (μ). Excellent agreement is obtained between the calculated vertical loss coefficient values (C_l) and the value of 8.17 utilized in the numerical analysis (i.e. 3D-Structure-TLD) with a maximum percentage difference value of 2.4% (see Section 4.6.1). Table 4.4 shows the calculation steps followed utilizing the preliminary TLD design procedure at mass ratio value (μ) of 1.0%, while Tables B1-B3 (Appendix-B) show the calculation steps at mass ratio values (μ) equal to 2.5%, 3.5% and 5.0%, respectively (see also Table 4.5 at $\theta = 0°$).

Subsequently, the preliminary TLD design procedure is employed to determine the required inclined damping screen properties (C_θ), to achieve different target structural acceleration response values ($\ddot{x}_{target}$) at 100% TLD efficiency (ψ) for practical limits of screen rotation (see Table 4.5). In the following section, the resulting C_θ values, listed in Table 4.5 are used to analyze the single-story structure-TLD system, shown in Figure 4.12, under increasing excitation amplitudes (F_{max}) to determine TLD efficiency (ψ).

4.6.3 Improved Efficiency of a Structure-TLD System Model Equipped with Inclined Damping Screens

The dynamic analysis proceeds in an iterative manner resulting in incremental values of the peak hourly structural acceleration response ($\ddot{x}_{peak-hr}$) of the single-story structure-TLD system utilizing inclined screen loss coefficient values (C_θ) from Table 4.5. Results from the structure-TLD system model are shown in Figures 4.14a-4.14d for mass ratio values (μ) of 1.0%, 2.5%, 3.5% and 5.0%, respectively. As the maximum allowable acceleration set by the wind tunnel for criteria of wind-induced motion is 30.0 milli-g for office buildings (Isyumov 1994), the incremental iterations for different dynamic analysis of the 3D-Structure-TLD system model are stopped when the peak hourly structural acceleration value ($\ddot{x}_{peak-hr}$) reaches 40.0 milli-g.

As can be observed from Figure 4.14, vertical screens (i.e. $\theta = 0.0°$) can be designed to operate optimally for only one particular structural acceleration response value (i.e. $\ddot{x}_{peak-hr} = \ddot{x}_{target}$). Throughout different screen angles (θ), an envelope is drawn capturing 100% TLD efficiency (ψ) over a range of structural response accelerations as shown in each figure. The general trends of the results are found to be in good agreement with those obtained by Cassolato (2007) from his study on a theoretical single degree of freedom system model (SDOF) employing a linear TLD numerical model. The envelope curves show that angled screens are able to maintain 100% TLD efficiency (ψ) over a range of structural response accelerations ($\ddot{x}_{peak-hr}$) in contrast with the vertical screens.

To investigate the general trends obtained using different mass ratio values (μ) in Figure 4.14, the mass ratio value (μ) of 2.5% is first selected. Figure 4.14b shows that for μ=2.5%, the vertical screens operate optimally [i.e. achieving 100% TLD efficiency (ψ)] at 6.50 milli-g, while an efficiency value (ψ) of 75% is achieved at a structural response acceleration value ($\ddot{x}_{peak-hr}$) of 30.0 milli-g. The angled screens, which are tilted according to results from Table 4.5, cover a range of $\ddot{x}_{peak-hr}$ values between 6.5 milli-g at $\theta = 0.0°$ and 20.0 milli-g at $\theta = 59.0°$ at ψ=100%. The use of angled screens is shown to maintain an efficiency value (ψ) of 95% at a large structural response value of 30.0 milli-g compared to an efficiency value (ψ) of 75% utilizing vertical damping screens.

For a mass ratio value (μ) of 1.0%, Figure 4.14a shows that an extension over the peak hourly structural response acceleration ($\ddot{x}_{peak-hr}$) is achieved using a three-position range of

the angled screens. For 100% TLD efficiency (ψ), target structural response acceleration values ($\ddot{x}_{target}$) are found to be 4.5 milli-g, 6.5 milli-g and 9.0 milli-g, corresponding to screen angle values (θ) equal to $41.0°, 53.5°,$ and $61.5°$, respectively. For 100% TLD efficiency (ψ) and at a mass ratio value (μ) of 3.5%, the structural response acceleration is extended from a value of 9.0 milli-g at a vertical screen angle to values of $\ddot{x}_{target}$ equal to 15.0 milli-g, 20.0 milli-g, 25.0 milli-g and 30.0 milli-g corresponding to screen angle values (θ) of $40.0°, 50.5°, 56.5°$ and $61.0°$, respectively, as shown in Figure 4.14c. Finally, for a mass ratio value (μ) of 5.0%, 100% TLD efficiency (ψ) is maintained over a range of structural response values ($\ddot{x}_{target}$) between 12.5 milli-g and 30.0 milli-g using a four-position range of the angled screens as shown in Figure 4.14d. Therefore, the suitability of using C_θ values from the preliminary TLD design procedure to achieve 100% TLD efficiency (ψ) over a range of structural amplitudes ($\ddot{x}_{peak-hr}$) and for different mass ratios (μ) is confirmed.

4.7. Response of a High-Rise Building-MTLD-System with Inclined Damping Screens at Various Serviceability Return Periods

In this section, a study on an actual high-rise building equipped with TLDs utilizing inclined damping screens is conducted employing the 3D-Structure-MTLD system model. The building is subjected to recorded wind tunnel loads and analyzed without and with TLDs at the critical wind loading angle ($\theta_w = 210°$) over a range of return periods. The TLD design procedure, utilized above in Section 4.6.2, which has shown excellent accuracy to predict the required inclination angle (θ) of the inclined damping screens to achieve 100% TLD efficiency (ψ), is updated in this section to be used in a multi-modal high-rise building. Also, TLDs with inclined damping screens are designed to cover a wide range of serviceability return from 1 month to 50 years. Wind speed values between 23 and 34 m/s, listed in Table 4.6, are selected from the lower curve in Figure 4.15, which represents recommended serviceability wind speeds (BLWT-SS3-2007). Finally, a comparison of percentage response reduction values ($\psi_{peak-hr}$) of the average peak hourly resultant accelerations ($R_{peak-hr}$) is presented utilizing TLDs equipped with inclined and vertical damping screens.

4.7.1 Brief Description of the Indianapolis Building and Its Dynamic Characteristics

A 38-story reinforced concrete building with a height of 154.6 m and plan dimensions of 32.0 m by 54.0 m, which is discussed in detail elsewhere (Chapter 3), is considered in this study (see Figure 4.16). Figure 4.17 displays the first three mode shapes, which correspond to natural periods of 7.31, 6.18 and 3.01 seconds. The torsional component of the mode shapes is multiplied by the overall radius of gyration 18.8 m of the building to maintain dimensional consistency. It can be observed from Figure 4.17 that the structure has a dominate translational mode in the x-direction, a dominate translational mode in the y-direction and dominate torsional mode in the θ-direction with a small coupling action between the x- and y-directions.

4.7.2 Response of the Indianapolis Building with No-TLDs

A dynamic analysis of the 38-story high-rise building is carried out using wind tunnel loads recorded at the critical wind loading angle (θ_w) of 210°. Consequently, a time history analysis utilizing a number of 4-hour recorded wind tunnel loads is conducted at the selected return periods employing the 3D finite element model (developed and validated in Chapter 2). Result includes average peak hourly resultant acceleration response values ($R_{peak-hr}$) and RMS structural acceleration response values ($\sigma_{\ddot{x}}$; $\sigma_{\ddot{y}}$) at the centre of mass (CM) and the four corners ($C1$; $C2$; $C3$; $C4$) of the building in the x- and y- directions, respectively, at the uppermost floor ($z = 154.6$ m). These results are utilized to investigate the building's serviceability conditions. Figure 4.18 shows the uncontrolled average peak hourly resultant acceleration response ($R_{peak-hr}$) values resulting from different serviceability return periods. A range of $R_{peak-hr}$ values between 8.0 and 34.0 milli-g is found from the dynamic analysis corresponding to return period wind speeds between 23 m/s (1 month) and 37 m/s (50 years), respectively.

4.7.3 Placement Selection and Design of TLDs

TLDs to suppress the first three modes of vibration of the Indianapolis building are designed and their locations selected utilizing the modal contribution response components [modal factors (MF)] discussed in Chapter 3. The preliminary TLD design procedure (Tait 2008), which has been expanded in Chapter 3 to determine the parameters of multiple TLDs

equipped in a multi-modal high-rise building utilizing the structural modal response components (MF), is employed in this section.

Following the procedure used in Chapter 3, the first two mode tanks are designed according to the target modal structural acceleration response values $(\sigma_{\ddot{x}-target-m1};$ $\sigma_{\ddot{y}-target-m2})$ of the first two modes determined from the uncontrolled modal response values $(\sigma_{\ddot{x}-initial-m1}; \sigma_{\ddot{y}-initial-m2})$ at the TLD locations and in their placement directions. Subsequently, TLDs to suppress the third mode of vibration are designed according to the target modal structural response acceleration values of the third mode.

To achieve the optimal inherent damping in a multiple TLD system located in a multi-modal high-rise building, the loss coefficients are selected based on the target modal acceleration response values $(\sigma_{\ddot{x}-target-m1}; \sigma_{\ddot{y}-target-m2})$ at the TLD locations. Therefore, the modal contribution factor values (MF) corresponding to each structural mode of vibration to be suppressed must be determined. Table 4.7 shows the initial RMS acceleration response values $(\sigma_{\ddot{x}-initial}; \sigma_{\ddot{y}-initial})$ of the Indianapolis building and their corresponding modal response values $(\sigma_{\ddot{x}-initial-m1}; \sigma_{\ddot{y}-initial-m2})$ in the x- and y-directions, respectively. The target modal RMS acceleration response values $(\sigma_{\ddot{x}-target-m1}; \sigma_{\ddot{y}-target-m2})$ are evaluated at different serviceability return periods (see Table 4.7) for a selected mass ratio value of 2%. A detailed TLD design example is presented in the following section considering a serviceability return period of 50 years.

4.7.3.1   TLD Design Procedure (50-Year Serviceability Return Period)

The TLD design procedure, outlined in Chapter 3, is used to design uni-directional tanks to suppress the first and second modes of vibration in the x- and y-directions, respectively, at the 50-year serviceability return period.

Employing the TLD design procedure, tank dimensions are established as $L_x = 16.0$ m, $b_x = 4.3$ m and $h_x = 2.0$ m, while $L_y = 12.0$ m, $b_y = 3.4$ m and $h_y = 1.9$ m. The initial modal RMS acceleration response values $(\sigma_{\ddot{x}-initial-m1}; \sigma_{\ddot{y}-initial-m2})$ at the centre of mass (CM) of 6.9 milli-g and 4.7 milli-g lead to modal target RMS response values of 4.3 milli-g for $\sigma_{\ddot{x}-target-m1}$ and 2.9 milli-g for $\sigma_{\ddot{y}-target-m2}$. The modal target RMS acceleration response values $(\sigma_{\ddot{x}-target-m1}; \sigma_{\ddot{y}-target-m2})$ are used to determine the screen loss coefficients (Tait 2004; Cassolato et al. 2011). Table 4.9 shows the steps employed to

complete the expanded TLD design procedure (Chapter 3; Tait 2008) for the first mode tanks in the x-direction, while Table 4.10 presents TLD water mass calculations. Tables B4 and B5 (Appendix-B) show the calculation steps to design the second mode tanks in the y-direction and TLD water mass calculations, respectively.

The modal RMS acceleration values for the third mode at the four corners show high modal factor values (MF) in the y-direction compared to the x-direction (see Table 4.8). Moreover, corners $C2$ and $C3$ have modal factor values (MF), in the y-direction, between 40.6% and 57.1%, while corners $C1$ and $C4$ have modal factor values (MF) between 24.1% and 34.0%. Therefore, TLDs are installed at $C2$ and $C3$ and oriented in the y-direction. In contrast, the four corners have modal factor values (MF) in the range between 7.4% and 18.1%, in the x-direction, for all return periods. Consequently, the TLD design procedure is employed and the modal target RMS acceleration response values ($\sigma_{\ddot{y}-target-m2}$), presented in Table 4.8, are used to determine the optimal TLD design parameters to suppress the third vibration mode of the structure.

With location and orientation determined, the TLDs are designed to suppress the first three modes of vibration of the Indianapolis building, at four selected values of serviceability return periods. The TLD design procedure described in Section 4.6.2 is utilized (12 times) to determine the required inclination angle values (θ) at a selected mass ratio value (μ) equal to 2.0% as listed in Table 4.11. The table represents a design summary sheet for different return period wind speeds and vibration modes to be suppressed. It also contains the optimal tunning ratio and tank frequency values, tank dimensions and water heights, optimal damping screen properties and corresponding inclination angles.

The maximum optimal loss coefficient values, for different mode tanks determined at the minimum return period wind speed of 1 month, are utilized as the vertical loss coefficient values (C_l) for each mode tank. Therefore, with increasing wind speed values, the damping screens are tilted at an angle (θ) to reduce their loss coefficients to values that match the optimal C_θ values listed in Table 4.11. Consequently, Equation 4.22-b is used to determine the required inclination angle values (θ) of the damping screens shown in Table 4.11.

4.7.4 Response of the Indianapolis Building with TLDs to Suppress the First Three Modes

A dynamic analysis of the 38-story Indianapolis building is carried out at the critical wind loading angle (θ_w) of 210° with TLDs equipped with inclined damping screens (i.e. rotatable damping screens). The TLD damping screens are set to the desired inclination angle values (θ), shown in Table 4.11, corresponding to the serviceability return periods.

Figures 4.18 and 4.19 show the average peak resultant accelerations ($R_{peak-hr}$) at the centre of mass (CM) and the four corners ($C1; C2; C3; C4$) at $z = 154.6$ m for different serviceability return periods with no-TLDs and with TLDs equipped with inclined damping screens, respectively. Results from the dynamic analysis show that average peak resultant acceleration response values of the Indianapolis building ($R_{peak-hr}$) range between 8.0 to 34.5 milli-g for the uncontrolled case compared with 6.0 to 22.5 milli-g for the controlled cases, respectively. Figure 4.18 shows that the maximum uncontrolled response ($R_{peak-hr}$) of 28.2 milli-g, at a serviceability return period of a 10-year exceeds the criteria recommended by the wind tunnel (BLWTL). Acceptable wind-induced motions for a 10-year return period, recommended by the BLWTL, range between 10 and 15 milli-g for residential buildings, 15 and 20 milli-g for hotels, 20 to 25 milli-g for office buildings (Isyumov 1994).

To evaluate the performance and robustness of the TLD systems (i.e. TLDs with screens fixed at a single angle and TLDs with screens set at different angles), the dynamic analysis of the Indianapolis building is repeated at lower return periods of 1 month, 1 year and 10 years utilizing the same TLD properties (i.e. fixed angle of the damping screens) obtained at a 50-year return period. Consequently, the percentage response reduction values ($\Psi_{peak-hr}$) of the average peak hourly resultant accelerations ($R_{peak-hr}$) of the Indianapolis building with TLDs to suppress the first three modes equipped with inclined and fixed (single angle) damping screens are evaluated using Equation 4.44 and presented in Figures 4.20a and 4.20b, respectively.

The percentage response reduction values ($\Psi_{peak-hr}$) of the average peak hourly resultant accelerations ($R_{peak-hr}$) can be calculated by

$$\Psi_{peak-hr} = \left(\frac{R_{peak-hr(No-TLD)} - R_{peak-hr(with\,TLD)}}{R_{peak-hr(No-TLD)}} \right) . 100 \qquad (4.44)$$

where $R_{peak-hr(with\,TLD)}$ and $R_{peak-hr(No-TLD)}$ are the resultant acceleration responses with and without TLDs installed, respectively.

Utilizing the inclined damping screen approach, percentage response reduction values ($\Psi_{peak-hr}$) between 32% and 37% are achieved at a 50-year return period, while values ($\Psi_{peak-hr}$) in the range between 29% and 34% are achieved at a 1-month return period (see Figure 4.20a). Employing the inclined damping screens leads to approximately constant percentage response reduction values ($\Psi_{peak-hr}$), i.e. nearly constant TLD efficiency, over the considered range of serviceability return periods with a maximum difference of 5%. It can be noticed that the controlled structural responses achieve the wind-induced motion criteria for hotels (i.e. $R_{peak-hr_{10-years}} < 20$ milli-g).

These results demonstrate the ability of inclined damping screens, installed in the TLDs, to control the response of an actual structure subjected to a range of return periods that produce wind loads with variable speeds. Thus, overall performance of a structure-TLD system, under simulated natural events, is improved at no additional cost utilizing inclined damping screens (i.e. TLDs could be designed to cover a range of return periods utilizing the same sets of damping screens).

4.8. Response of a High-Rise Building-MTLD-System over a Range of Mixed Return Periods (Dual Design Approach)

A novel dual design approach for TLDs be installed in structures is introduced in this section. TLDs are primarily used for serviceability related issues. Results from the above section show structural response improvements over a wide range of serviceability return periods with TLDs equipped with inclined damping screens. In this section, TLDs equipped with inclined damping screens are designed and installed in the Indianapolis building to check their efficiency under design level wind loads.

For strength related issues such as loads and building cladding pressure, the BLWTL wind climate model (BLWT-SS3-2007) is scaled to match wind speed requirements in ASCE-7-05 (see the upper curve in Figure 4.15) considering a 50-year strength return period (see Chapter 3). The TLDs are subsequently designed for a 50-year strength return period. Furthermore, the inclined damping screens are employed to extend the ability of TLD installation to cover serviceability return periods. As a result, criteria set by the wind tunnel

for wind-induced motions at a 10-year serviceability return period (Isyumov 1994) can also be achieved.

4.8.1 Response of the Indianapolis Building with No-TLDs

A wind speed value of 47.5 m/s is selected for a 50-year strength return period using the upper curve plotted in Figure 4.15. This curve represents the design wind speeds in the Indianapolis area as recommended by the wind tunnel study (BLWT-SS3-2007) and ASCE 7-05. Figure 4.21 shows the uncontrolled $R_{peak-hr}$ values of the centre of mass (CM) and the four corners at the uppermost floor ($z = 154.6$ m), at the critical wind loading angle (θ_w) of 210° utilizing mixed return period wind speeds, listed in Table 4.12. It can be noticed from the figure that uncontrolled $R_{peak-hr}$ values, ranging between 16.0 to 70.0 milli-g are obtained from the dynamic analysis.

4.8.2 Placement Selection and Design of TLDs

A mass ratio (μ) of 2.0% is selected for TLDs installed to suppress the first three modes of the Indianapolis building over the selected range of mixed return periods. Tables 4.13 and 4.14 show the target modal acceleration response values ($\sigma_{\ddot{x}-target-m1}$; $\sigma_{\ddot{y}-target-m2}$), in the x- and y-directions, at the selected range of mixed return periods for TLDs to suppress the first two and the first three modes of vibration. TLDs are selected to be installed at the centre of mass (CM) to suppress the first two vibration modes, in the x- and y-directions, respectively, while at corners $C2$ and $C3$ in the y-direction to suppress the third mode of vibration. The TLD design procedure is repeated (12 times) and results are listed in Table 4.15.

4.8.3 Response of the Indianapolis Building with TLDs to Suppress the First Three Modes Including the Design Level Wind Speed

Results from the dynamic analysis utilizing the inclination angles, listed in Table 4.15 over the selected range of mixed return periods, are shown in Figure 4.22. The figure shows that average peak hourly resultant acceleration response values ($R_{peak-hr}$) of the centre of mass (CM) and the four corners are found to range between 10.0 and 41.0 milli-g. Figure 4.23a shows percentage response reduction values ($\Psi_{peak-hr}$) at the centre of mass (CM) and the four corners range between 38% and 41% at a 50-year strength return period, while $\Psi_{peak-hr}$ values are found in the range between 32% and 37% at a 1-year serviceability

return period. In other words, using TLDs equipped with inclined damping screens leads to approximately constant percentage response reduction values ($\Psi_{peak-hr}$), i.e. nearly constant TLD efficiency (ψ), over the range of mixed return periods considered in this study.

The dynamic analysis of the Indianapolis building is repeated at lower serviceability return periods of 1 and 10 years utilizing the TLD designed for the 50-year strength return period. Figure 4.23b shows the percentage response reduction values ($\Psi_{peak-hr}$) of the average peak hourly resultant acceleration responses ($R_{peak-hr}$) of the centre of mass (CM) and the four corners. It can be observed that lower response reduction values ($\Psi_{peak-hr}$) are obtained compared to their counterpart values, shown in Figure 4.23a, utilizing TLDs equipped with inclined damping screens.

4.9. Conclusions

A nonlinear TLD fluid model of a TLD equipped with inclined damping screens has been extended and validated. The updated TLD fluid model has been found to be in excellent agreement with experimental test values obtained from a previously reported shake table testing program. Also, unlike linear fluid models, the updated nonlinear TLD fluid model can capture the effect of higher harmonics and the amplitude dependent hardening behaviour.

The ability to passively control the inherent damping ratio in a tuned liquid damper (ζ_{TLD}) over a range of excitation amplitudes has been demonstrated utilizing a 3D finite element structure-tuned liquid damper system model in the following two cases:

i. A dynamic analysis of a 3D single-story structure has been carried out employing the 3D-Structure-TLD system model, under random excitation for different mass ratios (μ). The vertical screens have been found to operate optimally at only one particular structural response acceleration. For different screen angles (θ), an envelope has been drawn capturing 100% TLD efficiency (ψ) over a range of structural response accelerations. The envelope curves have shown that angled screens are able to maintain 100% TLD efficiency (ψ) over a range of structural response accelerations, in contrast with conventional vertical screens.

ii. A dynamic analysis of a 38-story high-rise building has been carried out utilizing recorded wind tunnel loads at the critical wind loading angle ($\theta_w = 210°$) employing the 3D-Structure-MTLD system model. The response of the building has been determined over a

range of serviceability and strength-serviceability (mixed) return period wind speeds without and with TLDs equipped with inclined and fixed (single angle) damping screens. Results have shown that employing inclined damping screens in the TLDs has led to approximately constant TLD performance over the selected serviceability and mixed return periods.

The Indianapolis building response values obtained for a 50-year return period wind speed, which is used in the design requirements as suggested by ASCE 7-05, have shown percentage response reduction values ($\Psi_{peak-hr}$) ranging between 38% and 41%. Therefore, the study indicates the potential of using TLDs to reduce the force effects in members (i.e. normal force, shear force, bending moment and torque). Consequently, cost savings could be achieved if the reduced loads are used in the design process.

Finally, the ability to adjust the inherent damping ratios (ζ_{TLD}) of the TLDs has been demonstrated utilizing inclined damping screens. Thus, by monitoring the structural responses, inherent damping ratio values of the TLDs could be adjusted if required.

4.10.   References

ASCE (American Society of Civil Engineers), (2005). "*Minimum Design Loads for Buildings and Other Structures*", ASCE 7-05, New York, NY, USA.

Badr, H.M. (1994). "Oscillating Inviscid Flow over Elliptic Cylinders with Flat Plates and Circular Cylinders as Special Cases", *Ocean Engineering*, 21(1): 105-113.

Baines, W.D. and Peterson, E.G. (1951). "An Investigation of Flow through Screens", *Transactions of the ASME*, 73: 467-480.

Bathe, K. J. and Bolourchi, S. (1979). "Large Displacement Analysis of Three-Dimensional Beam Structures", *International Journal for Mechanical Methods of Engineering*, 14: 961-986.

Blevins, R.D. (1984). "*Applied Fluid Dynamics Handbook*", Macmillan: Agincourt, ON, Canada.

Brundrett, E. (1993). "Prediction of Pressure Drop for Incompressible Flow through Screens", *Journal of Fluid Engineering*, 115: 239-242.

Carrothers, P.J. and Baines, W.D. (1965). "Forces on Screens Inclined to a Fluid Flow", *Journal of Fluids Engineering*, 97: 116-117.

Cassolato, M. and Tait, M. (2005). "A Preliminary Study of a Tuned Liquid Damper with Smart Screens", *Proceeding of the 1ˢᵗ Canadian Conference on Effective Design of Structures*, 960-971, McMaster University, Hamilton, ON, Canada.

Cassolato, M.R. (2007). "*The Performance of a Tuned Liquid Damper Equipped with Inclined and Oscillating Damping Screens*", M.E.Sc. Thesis, McMaster University, Hamilton, ON, Canada.

Cassolato, M.R., Love, J.S. and Tait, M.J. (2011). "Modelling of Tuned Liquid Damper with Inclined Damping Screens", *Structural Control and Health Monitoring*, 18(6): 674-681.

Cornell, W.G. (1957). "Losses in Flow Normal to Plane Screens", *Meeting of the American Society of Mechanical Engineers*, Hartford, CT, 791-799.

Davenport, A.G. (1964). "Note on the Distribution of the Largest Value of a Random Function with Application to Wind Loading", *Proceeding - Institution of Civil Engineer*, 28: 187-196.

Fediw, A.A. (1992). "*Performance of a One Dimensional Tuned Sloshing Water Damper*", M.E.Sc. Thesis. The University of Western Ontario, London, ON, Canada.

Fediw, A.A., Isyumov, N. and Vickery, B.J. (1995). "Performance of a Tuned Sloshing Water Damper", *Journal of Wind Engineering and Industrial Aerodynamics*, 56: 237-247.

Garrison, C.J. (1985). "Comments on Cross-Flow Principle and Morrison's Equation", *Journal of Waterway, Port, Coastal, and Ocean Engineering*, 111(6): 1075-1079.

Gerges, R. R. and Vickery, B. J. (2003). "Wind Tunnel Study of the Across-Wind Response of a Slender Tower with a Nonlinear Tuned Mass Damper", *Journal of Wind Engineering and Industrial Aerodynamics*, 91: 1069-1092.

Graham, E.W. and Rodriguez, A.M. (1952) "The Characteristics of Fuel Motion which Affect Airplane Dynamics", *Journal of Applied Mechanics*, 19(3): 381-388.

Hoerner, S.F. (1964). "*Fluid Dynamics Drag*", Horner Fluid Dynamics, Brick Town, NJ, USA.

Idelchik, I.E. (1986), "*Handbook of Hydraulic Resistance*", 2nd Edition, Hemisphere Publishing Corporation: NY, USA.

Isyumov, N. (1994). "Criteria for Acceptable Wind-Induced Motions", *Proceedings, 12th ASCE Structures Congress*, 642-653. Atlanta, GA, USA.

Ju, Y.K. (2004). "Structural Behaviour of Water Sloshing Damper with Embossments Subject to Random Excitation", *Canadian Journal of Civil Engineering*, 31: 120-132.

Ju, Y.K., Yoon, S.W. and Kim, S.D. (2004). "Experimental Evaluation of a Tuned Liquid Damper System", *Proceeding of Institution of Civil Engineering-Structures and Building*, 157(4): 251-262.

Kaneko, S. and Ishikawa, M. (1999). "Modeling of Tuned Liquid Damper with Submerged Nets", *Journal of Pressure and Vessel Technology*, 121(3): 334-343.

Kareem, A., Kijewski, T. and Tamura, Y. (1999). "Mitigation of Motions of Tall Buildings with Specific Examples of Recent Application", *Wind and Structures: An International Journal*, 2(3): 201-251.

Lamb, H. (1932). "*Hydrodynamics*", the University Press, Cambridge, England.

Laws, E.M. and Livesey, J.L. (1978). "Flow through Screens", *Annual Review of Fluid Mechanics*, 10: 247-266.

Lepelletier, T.G. and Raichlen, F. (1988). "Nonlinear Oscillations in Rectangular Tanks", *Journal of Engineering Mechanics*, 114(1): 1-23.

The MathWorks Inc., (2004). "*MATLAB version 7.0.0.19920 (R14)*", The MathWorks Inc., Natick, MA, USA.

McNamara, R., Kareem, A. and Kijewski, T. (2002). "Ask the Experts ... Perception of the Motion Criteria for Tall Buildings Subjected to Wind: A Panel Discussion", *Conference Abstract for Reflections from ASCE Structures Congress*, Denver, CO, USA.

Miles, J.W. (1967). "Surface Wave Damping in Closed Basins", *In: Proceedings of the Royal Society of London*, 297: 459-475.

Okajima, A., Matsumuto, T. and Kimura, S. (1998). "Aerodynamic Characteristics of Flat Plates with Various Angles of Attack in Oscillatory Flow", *Ocean Engineering*, 41(1): 214-220.

Reed, D., Yu, J., Yeh, H. and Gardarsson, S. (1998a). "Investigation of Tuned Liquid Damper under Large Amplitude Excitation", *Journal of Engineering Mechanics*, 124(4): 405-413.

Reed, D., Yeh, H., Yu, J. and Gardarsson, S. (1998b). "Tuned Liquid Damper under Large Amplitude Excitation", *Journal of Wind Engineering and Industrial Aerodynamics*, 74-76: 923-930.

Richards, P.J. and Robinson, M. (1999). "Wind Loads on Porous Structures", *Journal of Wind Engineering and Industrial Aerodynamics*, 83, 455-465.

Reuter, C., Rettemeier, K. and Köngeter, J. (2001). "Experimental Head Loss Determination at Inclined Wedge Wire Fish Protection Screen", *29th IAHR Congress Proceeding*, Beijing, China.

Schubauer, G.B., Spangenberg, W.G. and Klenanoff, P.S. (1950). "Aerodynamic Characteristics of Damping Screens", *National Advisory Committee for Aeronautics (NACA)*, Technical Note (2001).

Soong, T.T. and Dargush, G.F. (1997). "*Passive Energy Dissipation Systems in Structural Engineering*", Wiley, New York, USA.

Sun, L.M. (1991). "*Semi-Analytical Modelling of Tuned Liquid Damper (TLD) with Emphasis on Damping of Liquid Sloshing*", Ph.D. Thesis, University of Tokyo, Tokyo, Japan.

Sun, L.M., Fujino, Y. and Koga, K. (1995). "A Model of Tuned Liquid Damper for Suppressing Pitching Motion of Structures", *Earthquake of Engineering and Structure Dynamics*, 24: 625-636.

Tait, M.J. (2004). "*The Performance of 1D and 2D Tuned Liquid Dampers*" Ph.D. Thesis, The University of Western Ontario, London, ON, Canada.

Tait, M.J., E1 Damatty, A.A. and Isyumov, N. (2004a). "Testing of Tuned Liquid Damper with Screens and Development of Equivalent TMD Model", *Wind and Structures*, 7(4): 215-234.

Tait, M.J., Isyumov, N. and E1 Damatty, A.A. (2004b). "The Efficiency and Robustness of a Unidirectional Tuned Liquid Damper and Modelling with an Equivalent TMD", *Wind and Structures*, 7(4): 235-250.

Tait, M.J., El Damatty, A.A. and Isyumov, N. (2005a). "An Investigation of Tuned Liquid Dampers Equipped with Damping Screens Subjected to 2D Excitation", *Earthquake Engineering and Structural Dynamics*, 34(7): 719-735.

Tait, M.J., El Damatty, A.A., Isyumov, N. and Siddique, M.R. (2005b). "Numerical Flow Models to Simulate Tuned Liquid Dampers (TLD) with Slat Screens", *Journal of Fluid and Structures*, 20: 1007-1023.

Tait, M.J., Isyumov, N. and E1 Damatty, A.A. (2007). "Effectiveness of a 2D TLD and Its Numerical Modeling", *Journal of Structural Engineering*, 133(2): 251-263.

Tait, M.J. (2008). "Modelling and Preliminary Design of a Structure-TLD System", *Engineering Structures*, 30: 2644-2655.

Vickery, B J. and Davenport, A.G. (1970). "An Investigation of the Behaviour in Wind of the Proposed Centre Point Tower in Sydney, Australia", *Research Report BLWT-1-70*, The Boundary Layer Wind Tunnel Laboratory, The University of Western Ontario, London, ON, Canada.

Warburton, G.B. (1982). "Optimum Absorber Parameters for Various Combinations of Response and Excitation Parameters", *Earthquake Engineering and Structural Dynamics*, 10(3): 381-401.

Warnitchai, P. and Pinkaew, T. (1998). "Modeling of Liquid Sloshing in Rectangular Tanks with Flow-Dampening Devices", *Engineering Structures*, 20(7): 593-600.

Xu, Z. and Ho, T.C.E. (2007). "A Study of Wind Effects for One Indiana Square, Indianapolis, Indiana. *Research Report BLWT-SS3-2007*, The Boundary Layer Wind Tunnel Laboratory (BLWTL), The University of Western Ontario, London, ON, Canada.

Weisbach, J. (1855). "*Die Experimental-Hydraulic*", p: 133, Engelhard, Freiburg.

Yalla, S. and Kareem, A. (2003). "Semiactive Tuned Liquid Column Dampers: Experimental Study", *Journal of Structural Engineering*, 129(7): 960-971.

Yeh, H.H. and Shrestha, M. (1989). "Free-Surface Flow through Screens", *Journal of Hydraulic Engineering*, 115(10): 1371-1385.

Table 4.1. Fraction of C_l with Angle (from Cassolato 2007)

θ (degrees)	0	10	20	30	40	50	60	70	80	80
γ_θ	1.00	0.97	0.88	0.75	0.59	0.45	0.3	0.23	0.15	0.09

Table 4.2. Building Properties

Excitation Type	f_s (Hz)	Generalized Model			Frame Element Model		
		M^* (kg)	K^* (N/m)	C^* (kg/s)	ζ_s (%)	L_c (m)	EI_{c_2} (N.m²)
Random	0.558	4040	49,656	17.00	0. 06	3.0	446,904

Table 4.3. TLD Properties

Excitation Type	μ (%)	Ω_{opt} (%)	$f_{TLD-opt}$ (Hz)	h (m)	L (m)	b (m)	m_{TLD} (kg)	m_w (kg)	S (%)	C_l
Random	1.0	99.26	0.554	0.123	0.966	0.442	040.4	052.5	60	8.17
	2.5	98.17	0.547	0.120	0.966	1.129	101.0	130.9		
	3.5	97.46	0.543	0.118	0.966	1.605	141.4	182.9		
	5.0	96.42	0.538	0.115	0.966	2.342	260.8	202.0		

Table 4.4. TLD Design for Vertical Damping Screens ($\mu = 1.0\%$)

Quantity	Equation(s)	Value	
Initial peak hourly acceleration, $\ddot{x}_{initial}$		**13.57**	**milli-g**
Structure cyclic frequency, f_{s-x}		0.558	Hz
Structure time period, T_{s-x}	$T_{s-x} = 1/f_{s-x}$	1.792	s
Structure natural frequency, ω_{s-x}	$\omega_{s-x} = 2\pi/T_{s-x}$	3.507	rad/s
Peak factor, PF_x	$PF_x = \sqrt{2\ln(181\omega_{s-x})} + \frac{0.577}{\sqrt{2\ln(181\omega_{s-x})}}$	3.753	
Initial RMS acceleration, $\sigma_{\ddot{x}-initial}$	$\sigma_{\ddot{x}-initial} = \frac{\ddot{x}_{initial}}{PF_x}$	**3.620**	**milli-g**
Initial RMS displacement, $\sigma_{x-initial}$	$\sigma_{x-initial} = \frac{\sigma_{\ddot{x}-initial}}{\omega_{s-x}^2}\frac{g}{1000}$	2.890	mm
Assumed water mass ratio, μ_w		0.010	(1.00%)
Assumed mass ratio, μ		0.077	(0.77%)
Effective damping provided by TLD, $\zeta_{TLD-eff-opt_x}$	$\zeta_{TLD-eff-opt_x} = \frac{1}{4}\sqrt{\frac{\mu_x+\mu_x^2}{1+\frac{3}{4}\mu_x}}$	0.025	(2.50%)
Optimal damping ratio, $\zeta_{TLD-opt_x}$	$\zeta_{TLD-opt_x} = \sqrt{\frac{\mu_x+\frac{3}{4}\mu_x^2}{4+6\mu_x+2\mu_x^2}}$	0.049	(4.98%)
Optimal tuning ratio, Ω_{opt_x}	$\Omega_{opt_x} = \frac{\sqrt{1+\frac{1}{2}\mu_x}}{1+\mu_x}$	0.992	(99.2%)
Optimal TLD cyclic frequency, $f_{TLD-opt_x}$	$\Omega_{opt_x} = \frac{f_{TLD-opt_x}}{f_{s-x}}$	0.554	Hz
Optimal response ratio, R_{opt_x}	$R_{opt_x} = \frac{\sigma_{r-x}}{\sigma_x} = \frac{1+\mu_x}{\sqrt{2\mu_x+\frac{3}{2}\mu_x^2}}$	7.115	
Structure damping ratio, ζ_s		0.0006	(0.06%)
Total structure damping, ζ_{tot-x}	$\zeta_{tot-x} = 0.8\zeta_s + \zeta_{TLD-eff-opt_x}$	0.0255	(2.55%)
Target RMS displacement, $\sigma_{x-target}$	$\zeta_{tot-x} = \zeta_s\frac{\sigma_{x-initial}^2}{\sigma_{x-target}^2}$	0.440	mm
Target RMS acceleration, $\sigma_{\ddot{x}-target}$	$\sigma_{\ddot{x}-target} = \omega_s^2\,\sigma_{x-target}$	**0.71**	**milli-g**
Target peak hourly acceleration, $\ddot{x}_{target}$	$\sigma_{\ddot{x}-target} = \frac{\ddot{x}_{target}}{PF_x}$	**2.65**	**milli-g**
TLD response, σ_{r-x}	$\sigma_{r-x} = R_{opt_x}\,\sigma_{x-target}$	3.150	mm
Select tank dimensions, L_x, h	$f_{TLD-opt_x} = \frac{1}{2\pi}\sqrt{\frac{\pi g}{L_x}\tanh\left(\frac{\pi h}{L_x}\right)}$	**L_x= 0.966**	**m** **h = 0.123 m**
Shallow water theory check, h/L_x		0.127	
Select screen properties, x_1, x_2, C_{l-x}	$\zeta_{TLD-x} = C_{l-x}\sqrt{\frac{32}{\pi^3}}\tanh^2(\frac{\pi h}{L_x})\Delta_x\Xi_x\frac{\sigma_{r-x}}{L_x}$ $\Delta_x = \left(\frac{1}{3}+\frac{1}{\sinh^2(\frac{\pi h}{L_x})}\right)$ $\Xi_x = \sum_{j=1}^{ns_x}\left|\sin^3\left(\frac{\pi x_j}{L_x}\right)\right|$	**$x_1 = 0.4\,L_x$** **$x_2 = 0.6\,L_x$** **$C_{l-x} = 8.21$**	

Table 4.5. Inclined Damping Screen Loss Coefficient values (C_θ) Used in the Parametric Study for the Single-Story Structure-TLD System

Excitation Type	S (%)	μ (%)	θ (Degree)	C_θ (Inclined)	$\ddot{x}_{target}$ (milli-g)
Random	60	1	0	8.2	2.7
			41.0	4.8	4.5
			53.5	3.3	6.5
			61.5	2.4	9.0
		2.5	0.0	8.3	6.5
			37.0	5.3	10.0
			51.5	3.5	15.0
			59.0	2.7	20.0
		3.5	0	8.3	9.0
			40.0	4.9	15.0
			50.5	3.7	20.0
			56.5	2.9	25.0
			61.0	2.5	30.0
		5.0	0	8.4	12.5
			22.5	6.9	15.0
			38.0	5.2	20.0
			46.5	4.1	25.0
			52.5	3.4	30.0

Table 4.6. Serviceability Return Periods and Wind Speeds

	Return Period (year)	Wind Speed (m/s)
Serviceability	50	37
	10	34
	1	29
	1/12	23

Table 4.7. Modal Acceleration Response Components in the x- and y-directions at the Centre of Mass with No-TLDs over a Range of Serviceability Return Period Wind Speeds ($\theta_w = 210°$, $z = 154.6$ m)

Node	Return Period (years)	Wind Speed (m/s)	$\sigma_{\ddot{x}-initial}$ (milli-g)	**Mode 1** MF (%)	$\sigma_{\ddot{x}-initial-m1}$ (milli-g)	$\sigma_{\ddot{x}-target-m2}$ (milli-g)	$\sigma_{\ddot{y}-initial}$	**Mode 2** MF (%)	$\sigma_{\ddot{y}-initial-m}$ (milli-g)	$\sigma_{\ddot{y}-target-m}$ (milli-g)
CM	50	37	7.1	97.4	6.9	4.3	5.0	94.7	4.7	2.9
	10	34	6.1	98.3	6.0	3.8	3.6	94.1	3.4	2.3
	1	29	3.5	98.7	3.4	2.2	2.5	95.5	2.4	1.5
	1/12	23	1.6	98.3	1.6	1.0	1.5	96.4	1.5	0.9

Table 4.8. Modal Acceleration Response Components in the x- and y-directions at the Four Corners Equipped with TLDs to Suppress the First Two Modes over a Range of Serviceability Return Period Wind Speeds ($\mu = 2\%$, $\theta_w = 210°$, $z = 154.6$ m)

Node	Return Period (years)	Wind Speed (m/s)	$\sigma_{\ddot{x}-initial}$ (milli-g)	**Mode 3** MF (%)	$\sigma_{\ddot{x}-initial-m}$ (milli-g)	$\sigma_{\ddot{x}-target-m}$ (milli-g)	$\sigma_{\ddot{y}-initial}$	**Mode 3** MF (%)	$\sigma_{\ddot{y}-initial-m}$ (milli-g)	$\sigma_{\ddot{y}-target-m}$ (milli-g)
C1	50	37	4.0	9.3	0.4	-	5.5	30.7	1.7	-
C2			4.0	9.3	0.4	-	4.6	53.8	2.5	1.6
C3			4.4	18.1	0.8	-	4.6	53.8	2.5	1.6
C4			4.4	18.1	0.8	-	5.5	30.7	1.7	-
C1	10	34	3.8	7.4	0.3	-	4.2	34.0	1.4	-
C2			3.8	7.4	0.3	-	3.7	57.1	2.1	1.3
C3			4.1	14.9	0.6	-	3.7	57.1	2.1	1.3
C4			4.1	14.9	0.6	-	4.2	34.0	1.4	-
C1	1	29	2.3	7.8	0.2	-	2.8	30.4	0.9	-
C2			2.3	7.8	0.2	-	2.4	50.5	1.2	0.8
C3			2.5	14.3	0.4	-	2.4	50.5	1.2	0.8
C4			2.5	14.3	0.4	-	2.8	30.4	0.9	-
C1	1/12	23	1.1	9.4	0.1	-	1.6	24.1	0.4	-
C2			1.1	9.4	0.1	-	1.4	44.6	0.6	0.4
C3			1.2	16.4	0.2	-	1.4	44.6	0.6	0.4
C4			1.2	16.4	0.2	-	1.6	24.1	0.4	-

Table 4.9. TLD Design for Mode 1 in the x-direction ($\mu = 2.0\%$, Serviceability Return Period $= 50$ years)

Quantity	Equation(s)	Value	
Initial peak hourly acceleration, $\ddot{x}_{initial}$		**25.979**	**milli-g**
Modal Factor, MF		**97.380**	**%**
Initial modal peak hourly acceleration, $\ddot{x}_{initial-m}$	$\ddot{x}_{initial-m} = \ddot{x}_{initial} \cdot MF$	**25.298**	**milli-g**
Structure cyclic frequency, f_{s-x}		0.136	Hz
Structure time period, T_{s-x}	$T_{s-x} = 1/f_{s-x}$	7.310	s
Structure natural frequency, ω_{s-x}	$\omega_{s-x} = 2\pi/T_{s-x}$	0.853	rad/s
Peak factor, PF_x	$PF_x = \sqrt{2\ln(573\omega_{s-x})} + \frac{0.577}{\sqrt{2\ln(573\omega_{s-x})}}$	3.685	
Initial RMS acceleration, $\sigma_{\ddot{x}-initial-m}$	$\sigma_{\ddot{x}-initial-m} = \frac{\ddot{x}_{initial-m}}{PF_x}$	**6.870**	**milli-g**
Initial RMS displacement, $\sigma_{x-initial-m}$	$\sigma_{x-initial-m} = \frac{\sigma_{\ddot{x}-initial-m}}{\omega_{s-x}^2}\frac{g}{1000}$	0.091	m
Assumed mass ratio, μ		0.020	(2.0%)
Effective damping provided by TLD, $\zeta_{TLD-eff-opt_x}$	$\zeta_{TLD-eff-opt_x} = \frac{1}{4}\sqrt{\frac{\mu_x+\mu_x^2}{1+\frac{3}{4}\mu_x}}$	0.035	(3.5%)
Optimal damping ratio, $\zeta_{TLD-opt_x}$	$\zeta_{TLD-opt_x} = \sqrt{\frac{\mu_x+\frac{3}{4}\mu_x^2}{4+6\mu_x+2\mu_x^2}}$	0.072	(7.2%)
Optimal tuning ratio, Ω_{opt_x}	$\Omega_{opt_x} = \frac{\sqrt{1+\frac{1}{2}\mu_x}}{1+\mu_x}$	0.985	(98.5%)
Optimal TLD cyclic frequency, $f_{TLD-opt_x}$	$\Omega_{opt_x} = \frac{f_{TLD-opt_x}}{f_{s-x}}$	0.135	Hz
Optimal response ratio, R_{opt_x}	$R_{opt_x} = \frac{\sigma_{r-x}}{\sigma_x} = \frac{1+\mu_x}{\sqrt{2\mu_x+\frac{3}{2}\mu_x^2}}$	5.062	
Structure damping ratio, ζ_s		0.020	(2.0%)
Total structure damping, ζ_{tot-x}	$\zeta_{tot-x} = 0.8\zeta_s + \zeta_{TLD-eff-opt_x}$	0.051	(5.1%)
Target RMS displacement, $\sigma_{x-target-m}$	$\zeta_{tot-x} = \zeta_s\frac{\sigma_{x-initial-m}^2}{\sigma_{x-target-m}^2}$	0.057	M
Target RMS acceleration, $\sigma_{\ddot{x}-target-m}$	$\sigma_{\ddot{x}-target-m} = \omega_s^2\,\sigma_{x-target-m}$	**4.284**	**milli-g**
Target peak hourly acceleration, $\ddot{x}_{target-m}$	$\sigma_{\ddot{x}-target-m} = \frac{\ddot{x}_{target-m}}{PF_x}$	**15.786**	**milli-g**
TLD response, σ_{r-x}	$\sigma_{r-x} = R_{opt_x}\,\sigma_{x-target-m}$	0.288	M
Select tank dimensions, L_x, h	$f_{TLD-opt_x} = \frac{1}{2\pi}\sqrt{\frac{\pi g}{L_x}\tanh\left(\frac{\pi h}{L_x}\right)}$	**$L_x= 16.00$ m** $h = 1.99$ m	
Shallow water theory check, h/L_x		0.125	
Select screen properties, x_1, x_2, C_{l-x}	$\zeta_{TLD-x} = C_{l-x}\sqrt{\frac{32}{\pi^3}}\tanh^2(\frac{\pi h}{L_x})\Delta_x\Xi_x\frac{\sigma_{r-x}}{L_x}$ $\Delta_x = \left(\frac{1}{3}+\frac{1}{\sinh^2(\frac{\pi h}{L_x})}\right)$ $\Xi_x = \sum_{j=1}^{ns_x}\left|\sin^3\left(\frac{\pi x_j}{L_x}\right)\right|$	$x_1 = 0.4\,L_x$ $x_2 = 0.6\,L_x$ $C_{l-x} = 2.46$	

Table 4.10. Water Mass Calculations for TLDs to Suppress Mode 1 ($\mu = 2.0\%$)

Quantity	Equation(s)	Value
Selected tank dimensions, L_x, B_x, h_x		$L_x = 16.00$ m $B_x = 4.30$ m $h_x = 1.99$ m
Water height to tanks length ratio in x-dir	h_x/L_x	0.125
Water mass of 1 tank, $m_{w(1tank)}$	$m_{w(1tank)} = L_x B_x h_x$	137055.4 kg
TLD mass of 1 tank in x-dir, $m_{TLD-x(1tank)}$	$m_{TLD-x(1tank)} \approx m_{1-x} =$ $\dfrac{8\,tanh\left(\pi\frac{h}{L_x}\right)}{\pi^3\left(\frac{h}{L_x}\right)} m_{w(1tank)}$	$0.77\,m_{w(1tank)} =$ 105753.9 kg
Total building mass, M_s	$M_s = \sum_{i=1}^{i=N_f} m_f$	36412955 kg
Generalized building mass in x-dir, M_x^*	$M_x^* = \sum_{i=1}^{i=N_f}(m_f)_i(\phi_t^2)_i$	10523344 kg
Required TLD mass in x-dir, m_{TLD-x}	$m_{TLD-x} = \mu_{TLD-x} M_x^*$	210467 kg
No. of Tanks required in x-dir, N_{TLD-x}	$N_{TLD-x} = m_{TLD-x}/m_{TLD-x(1tank)}$	1.99
Chosen No. of tanks for mode 1, N_{TLD-x}		**2**
Actual mass ratio in x-dir, $\mu_{x-actual}$	$\mu_{x-actual} = N_{TLD-x}m_{TLD-x(1tank)}/M_x^*$	**2.01 %**
Mass ratio of contained water, μ_w	$\mu_w = N_{TLD-x}m_{w(1tank)}/M_s$	**0.75 %**

Table 4.11. Properties of TLDs Equipped with Inclined Damping Screens to Suppress the First Three Modes of Vibration over a Range of Serviceability Return Period Wind Speeds ($\mu = 2.0\%$, $\theta_w = 210°$)

											Return Period					
									1 month serviceability		1 year serviceability		10 years serviceability		50 years serviceability	
Ω_{opt}	Mode Number	f_s	f_{TLD}	L	b	h	Number of Tanks	S	C_l	$\theta°$	C_θ	$\theta°$	C_θ	$\theta°$	C_θ	$\theta°$
	1	0.137	0.135	16.00	4.30	1.99	2	0.64	10.62	0	4.91	49.41	2.98	62.63	2.46	66.83
0.985	2	6.180	0.159	12.00	3.40	1.58	4	0.66	12.35	0	7.62	39.05	4.92	53.83	3.81	60.40
	3	3.013	0.327	2.75	2.75	0.34	120	0.71	19.92	0	9.85	47.26	5.83	61.67	3.20	65.68

Table 4.12. Mixed Return Periods and Wind Speeds

	Return Period (year)	Wind Speed (m/s)
Strength	50	47.5
Serviceability	10	34.0
	1	29.0

Table 4.13. Modal Factors in the x- and y-directions at the Centre of Mass with No-TLDs at Mixed Return Period Wind Speeds ($\theta_w = 210°$, $z = 154.6$ m)

| Node | Return Period (years) | Wind Speed (m/s) | $\sigma_{\ddot{x}-initial}$ (milli-g) | Mode 1 | | | $\sigma_{\ddot{y}-initial}$ | Mode 2 | | |
				MF (%)	$\sigma_{\ddot{x}-initial-m}$ (milli-g)	$\sigma_{\ddot{x}-target-m}$ (milli-g)		MF (%)	$\sigma_{\ddot{y}-initial-m}$ (milli-g)	$\sigma_{\ddot{y}-target-m}$ (milli-g)
CM	50 (Str.)	47.5	12.4	97.6	12.1	7.5	11.0	96.5	10.6	6.6
	10 (Ser.)	34.0	6.1	98.3	6.0	3.8	3.6	94.1	3.4	2.3
	1 (Ser.)	29.0	3.5	98.7	3.4	2.2	2.5	95.5	2.4	1.5

Table 4.14. Modal Factors in the x- and y-directions at the Four Corners with TLDs to Suppress the First Two Modes of Vibration over a Range of Mixed Return Period Wind Speeds ($\mu = 2.0\%$, $\theta_w = 210°$, $z = 154.6$ m)

| Node | Return Period (years) | Wind Speed (m/sec) | $\sigma_{\ddot{x}-initial}$ (milli-g) | Mode 3 | | | $\sigma_{\ddot{y}-initial}$ | Mode 3 | | |
				MF (%)	$\sigma_{\ddot{x}-initial-m}$ (milli-g)	$\sigma_{\ddot{x}-target-m}$ (milli-g)		MF (%)	$\sigma_{\ddot{y}-initial-m}$ (milli-g)	$\sigma_{\ddot{y}-target-m}$ (milli-g)
C1			8.1	6.8	0.6	-	11.6	19.5	2.3	-
C2	50 (Str.)	47.5	8.1	6.8	0.6	-	9.3	40.9	3.8	2.4
C3			8.9	15.6	1.4	-	9.3	40.9	3.8	2.4
C4			8.9	15.6	1.4	-	11.6	19.5	2.3	-
C1			3.8	7.4	0.3	-	4.2	34.0	1.4	-
C2	10 (Ser.)	34.0	3.8	7.4	0.3	-	3.7	57.1	2.1	1.3
C3			4.1	14.9	0.6	-	3.7	57.1	2.1	1.3
C4			4.1	14.9	0.6	-	4.2	34.0	1.4	-
C1			2.3	7.8	0.2	-	2.8	30.4	0.9	-
C2	1 (Ser.)	29.0	2.3	7.8	0.2	-	2.4	50.5	1.2	0.8
C3			2.5	14.3	0.4	-	2.4	50.5	1.2	0.8
C4			2.5	14.3	0.4	-	2.8	30.4	0.9	-

Table 4.15. Optimal Properties of TLDs Equipped with Inclined Damping Screens to Suppress the First Three Modes of Vibration over a Range of Mixed Return Period Wind Speeds ($\mu = 2.0\%$, $\theta_w = 210°$)

| Ω_{opt} | Mode Number | f_s | f_{TLD} | L | b | h | Number of Tanks | S | Return Period | | | | | |
| | | | | | | | | | 1 year serviceability | | 10 years serviceability | | 50 years strength | |
									C_l	$\theta°$	C_θ	$\theta°$	C_θ	$\theta°$
0.985	1	0.137	0.135	16.00	4.30	1.99	2	0.54	4.91	0	2.98	39.67	1.40	62.24
	2	6.180	0.159	12.00	3.40	1.58	4	0.60	7.62	0	4.92	37.11	1.69	67.67
	3	3.013	0.327	2.75	2.75	0.34	120	0.63	9.85	0	5.83	40.74	3.20	59.12
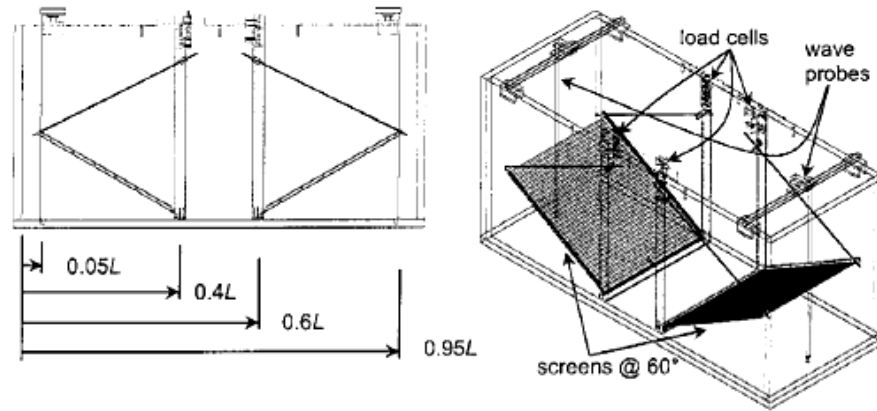
(a)
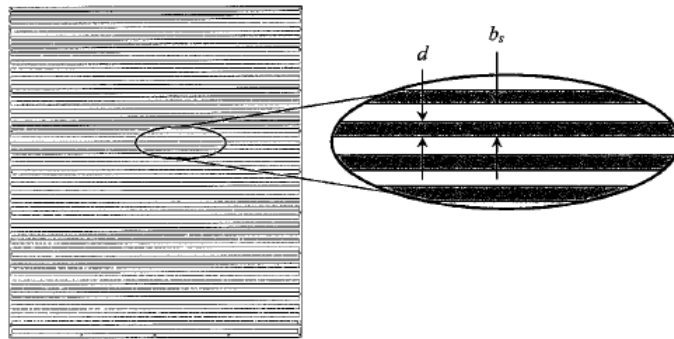
(b)
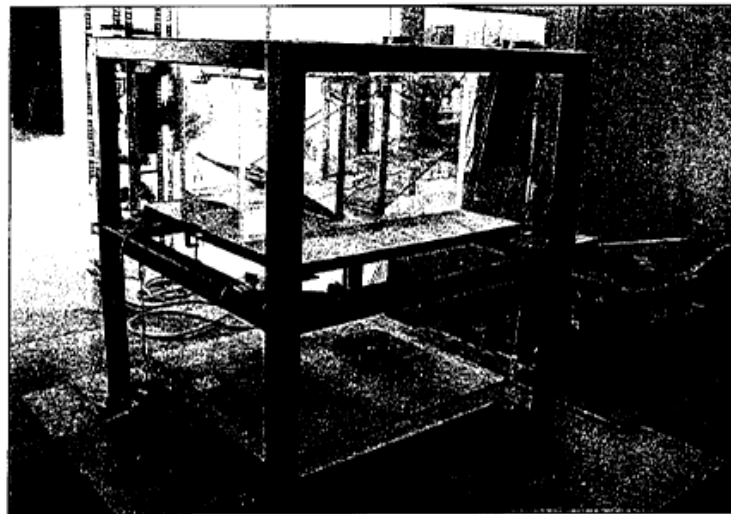
(c)

Fig. 4.1. TLD Equipped with Inclined Screens: (a) Schematic of a TLD Showing the Location of Screens and Wave Probes; (b) Enlarged View of the Screen; and (c) Photo of TLD Equipped with Internal Inclined Damping Screens (from Cassolato 2007)
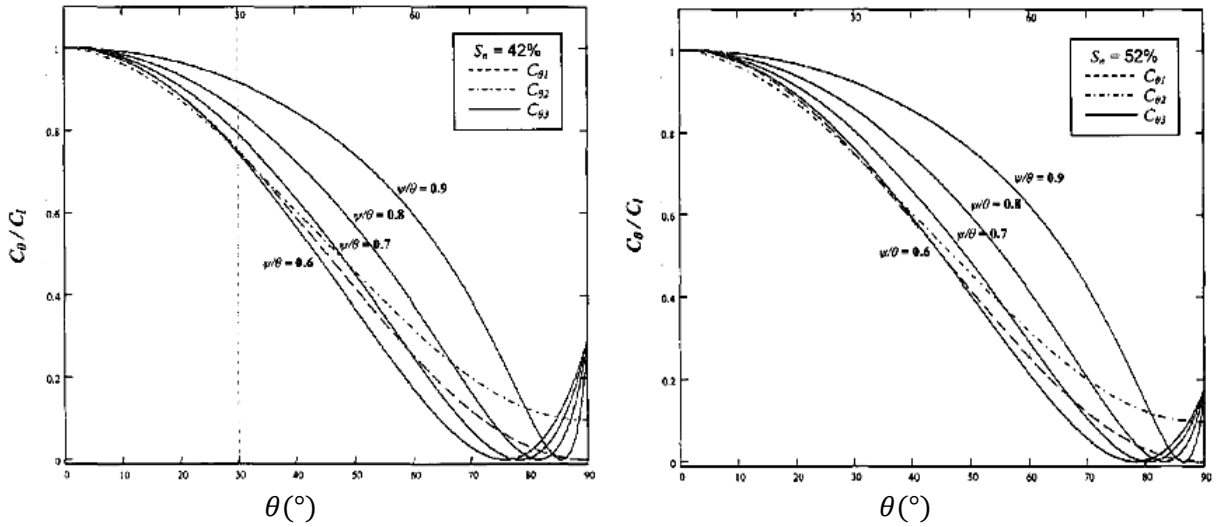
Fig. 4.2. Normalized Various C_θ from Equation 4.22 for Two Different Screens (from Cassolato 2007)
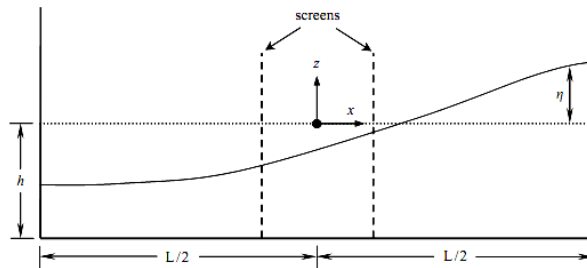
Fig. 4.3. Coordinate System for Nonlinear Shallow Water System (from Tait et al. 2005b)
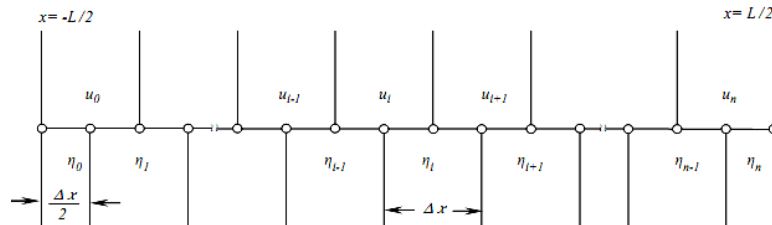
Fig. 4.4. Discretization of the Tank Length with Respect to x (from Tait et al. 2005b)
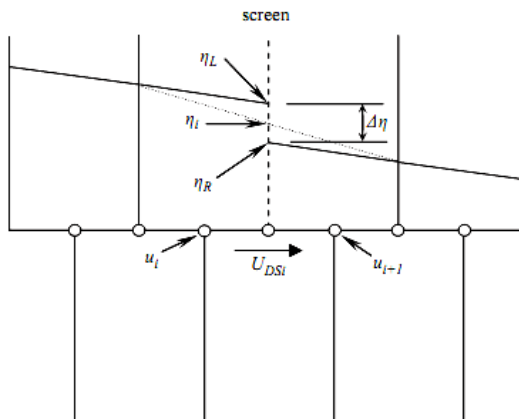
Fig. 4.5. Discretization and Modelling of the Screen (from Tait et al. 2005b)
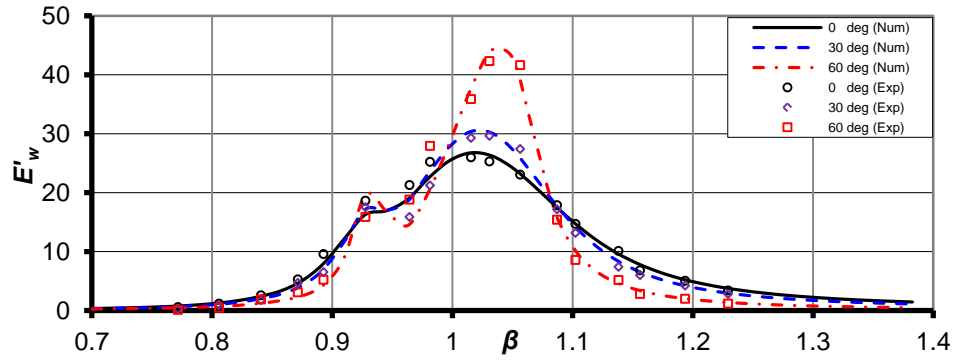
Fig. 4.6. Energy Dissipation Frequency Response Curves for $C_l = 3.53$ and $\Lambda = 0.005$
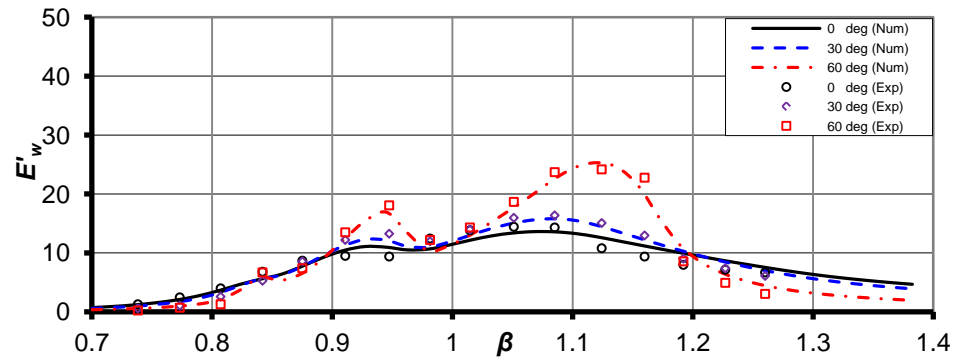
Fig. 4.7. Energy Dissipation Frequency Response Curves for $C_l = 3.53$ and $\Lambda = 0.021$
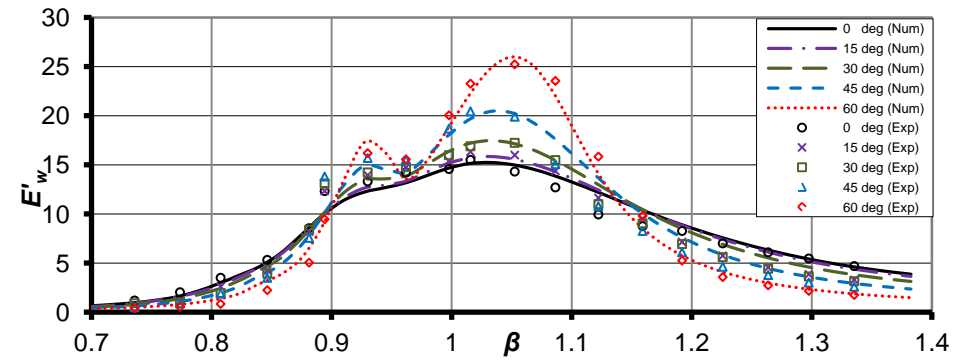
Fig. 4.8. Non-Dimensional Energy Dissipation for Various Screen Angles ($\Lambda = 0.010$, $C_l = 5.69$)
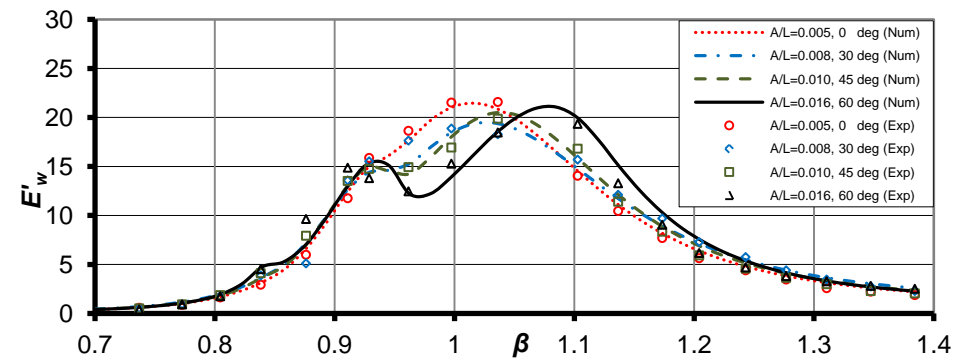
Fig. 4.9. Constant Normalized Energy Dissipation through Inclined Screens ($C_l = 5.69$)
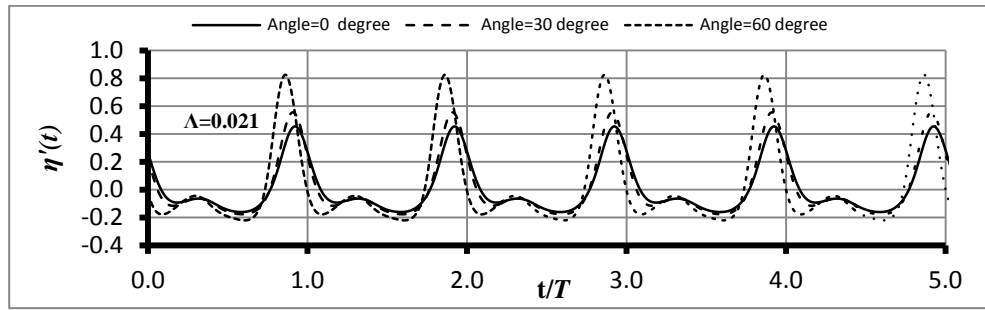
Fig. 4.10. Time Histories of η' for $\theta = 0°, 30°$ and $60°$ at $\beta = 1.01$ for $C_l = 3.53$
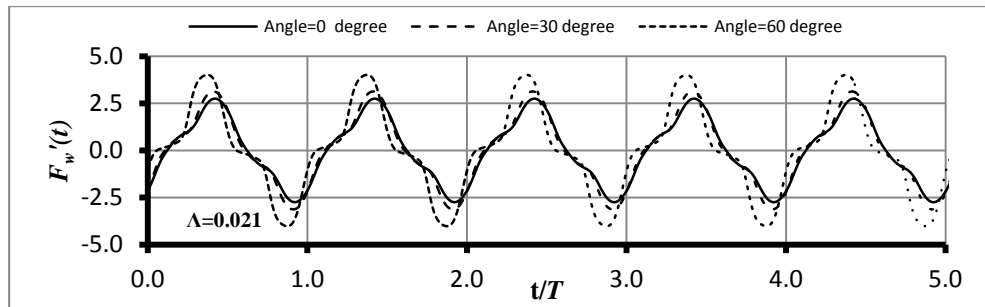
Fig. 4.11. Time Histories of F_w' for $\theta = 0°, 30°$ and $60°$ at $\beta = 1.01$ for $C_l = 3.53$

(a) (b)
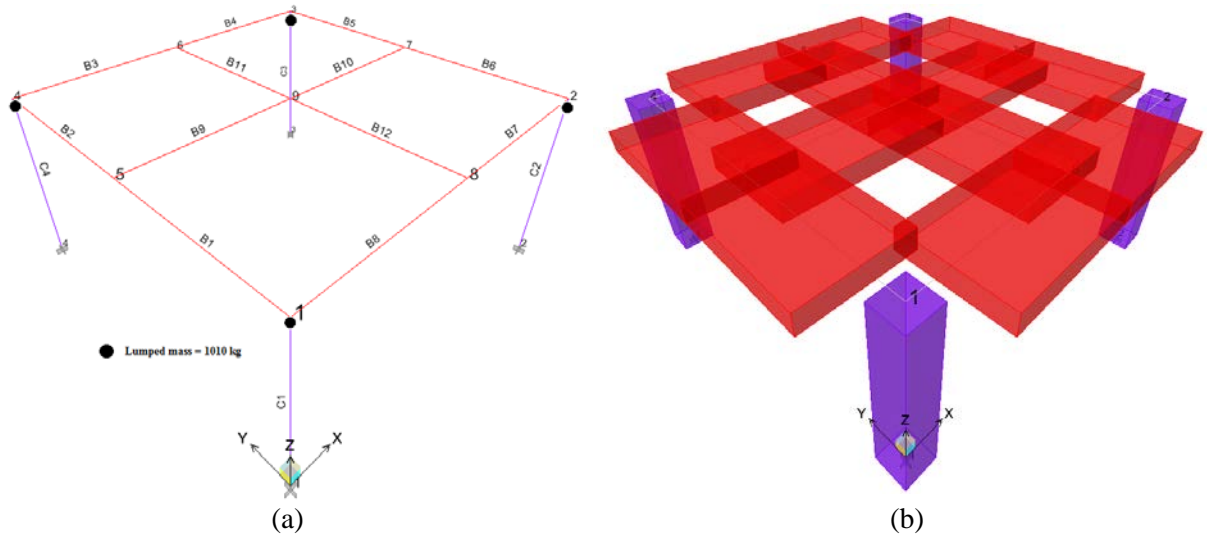
Fig. 4.12. 3D Single-Story Structure Used in the Parametric Analysis (a) A Schematic Diagram, and (b) 3D View
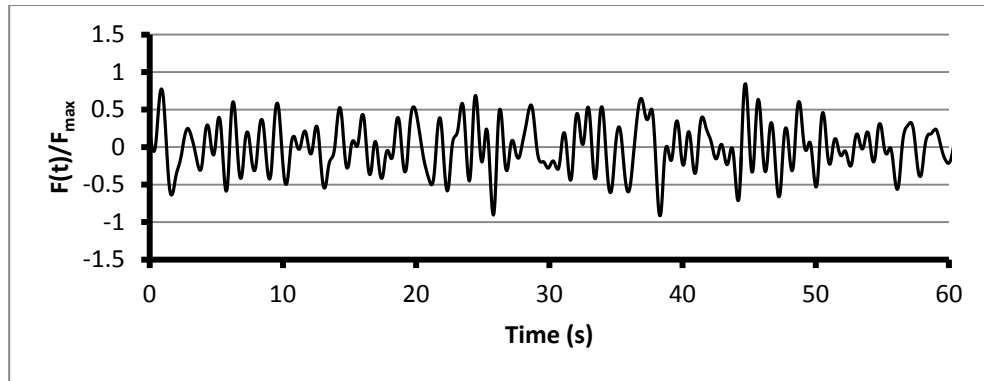
Fig. 4.13. One Minute Portion of a 3.7-Hour Time History of Random Excitation Force
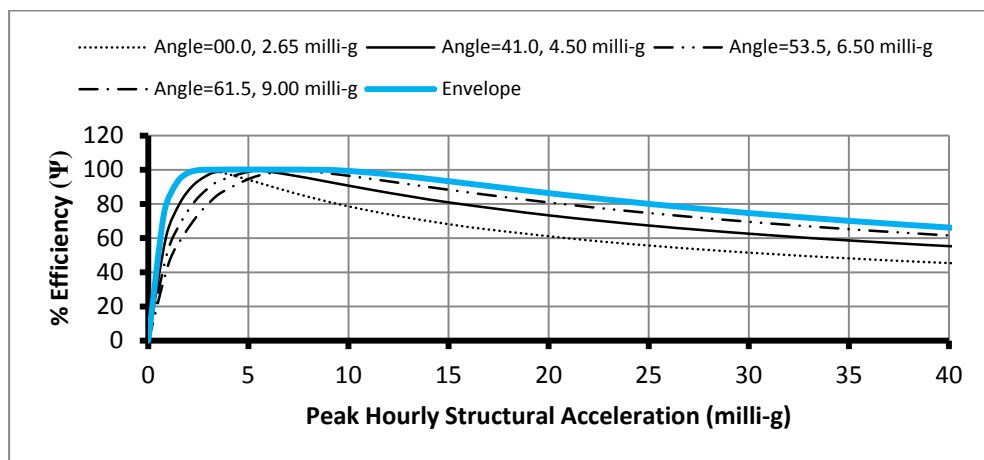
(a)
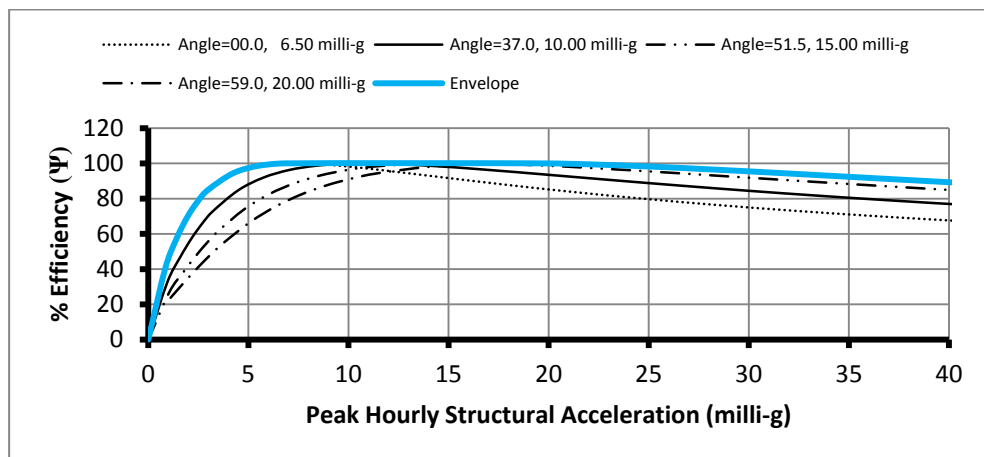
(b)
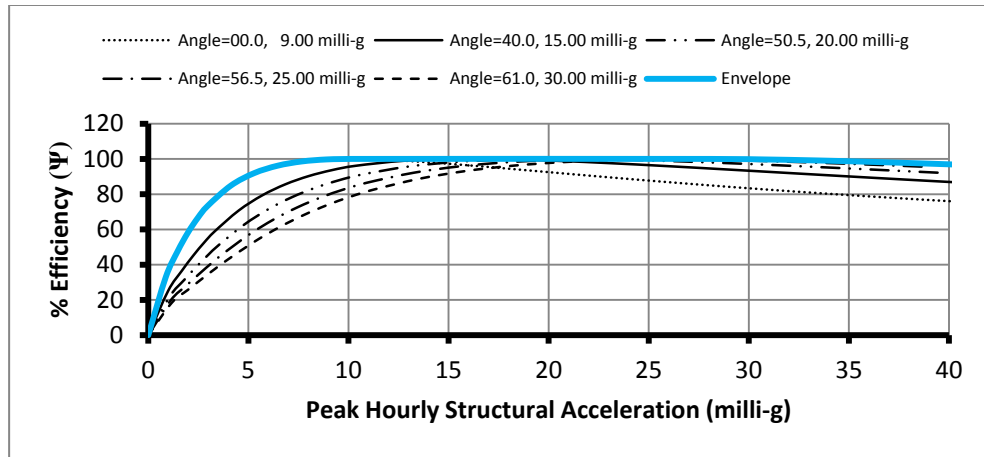
(c)
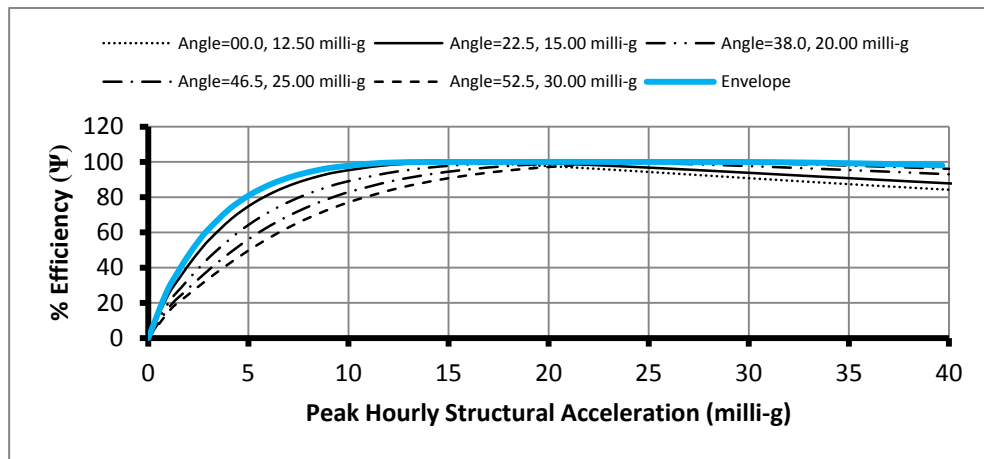
(d)

Fig. 4.14. Efficiency over Range of Structural Responses (a) $\mu = 1.0\%$, (b) $\mu = 2.5\%$, (c) $\mu = 3.5\%$, and (d) $\mu = 5.0\%$ ($S = 60\%$)
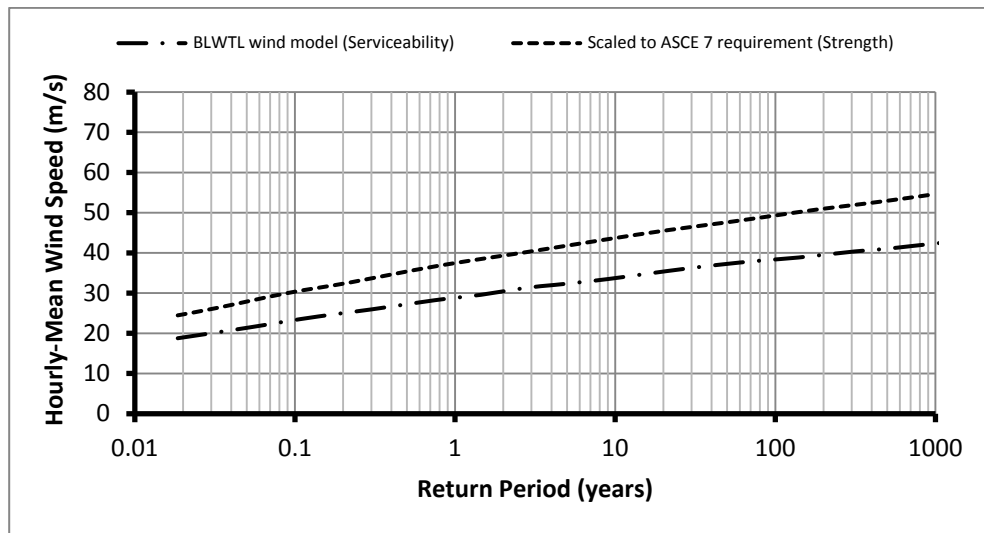
Fig. 4.15. Predicted Annual Extreme Upper Level (500 m) Wind Speed for Various Return Periods (BLWT-SS3-2007)
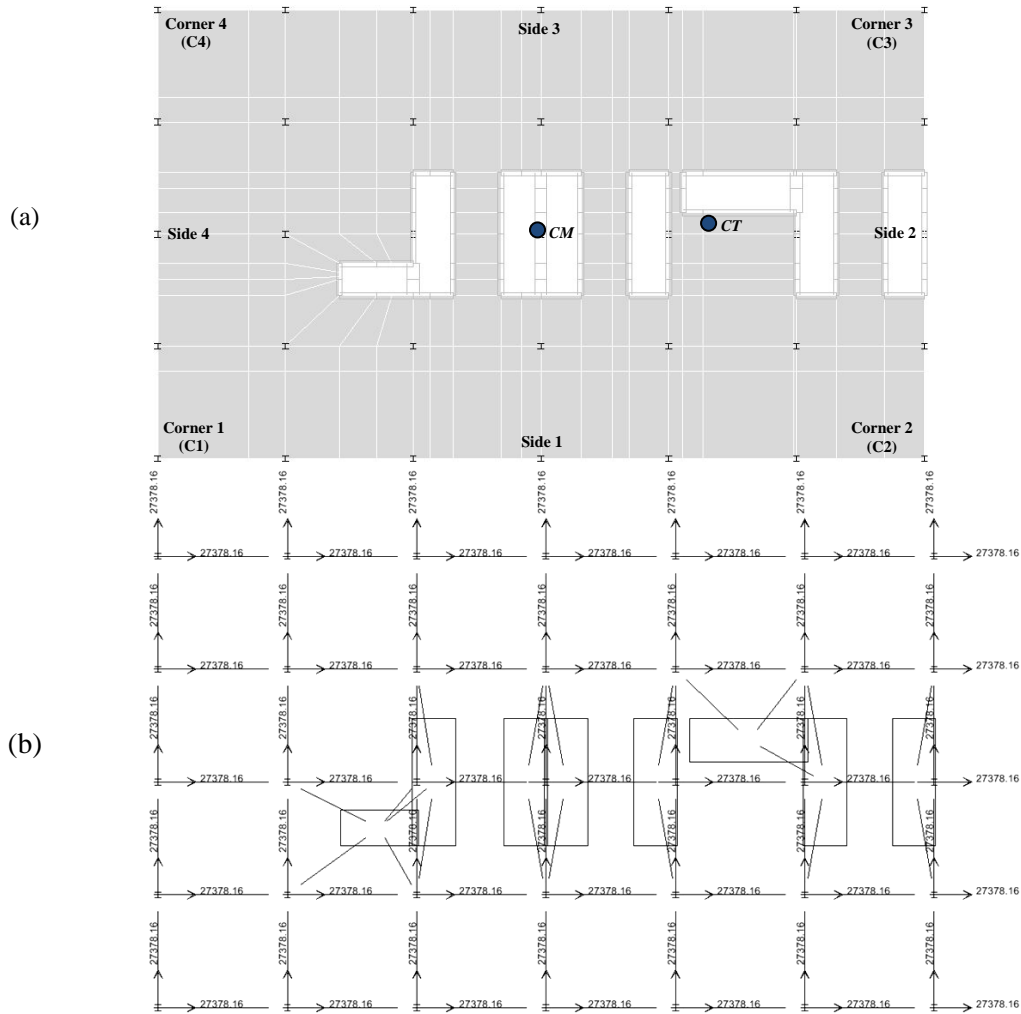
Fig. 4.16. Floor Plan of the Indianapolis Building Showing the Statical System Consists of (a) Real Slabs and Shear Walls, and (b) Frame Elements and Slab Beams Installed with Lumped Masses (kg)

(a) $T = 7.31$ s   (b) $T = 6.18$ s   (c) $T = 3.01$ s
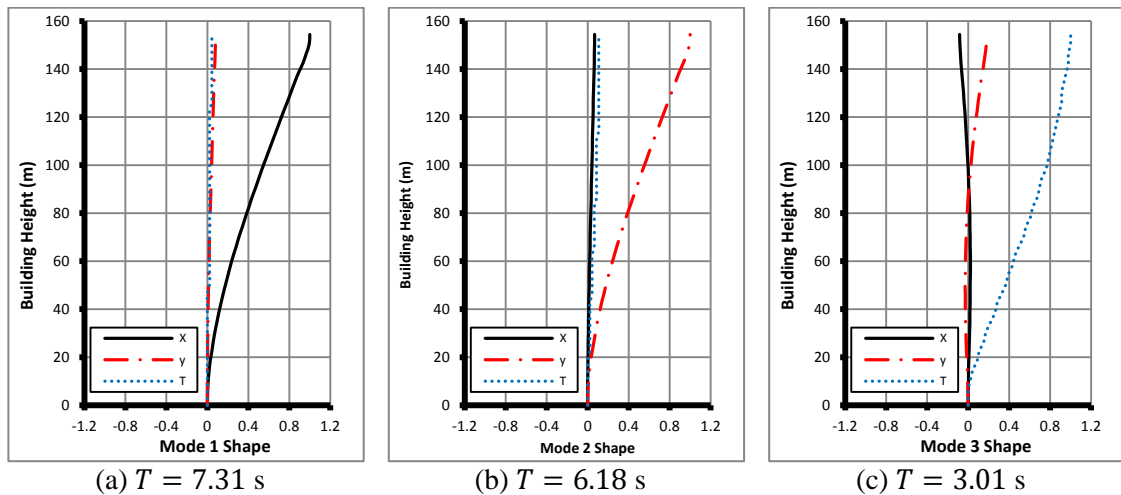
Fig. 4.17. Mode Shapes of the Indianapolis Building for (a) Mode 1, (b) Mode 2, and (c) Mode 3
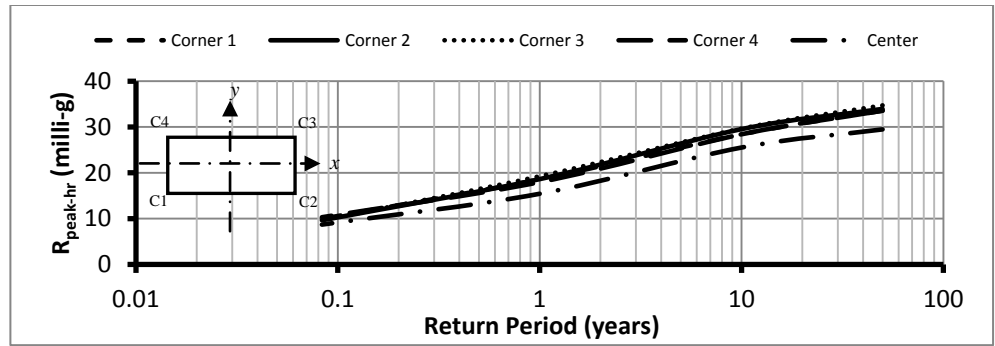
Fig. 4.18. Average Peak Hourly Resultant Accelerations with No-TLDs Installed ($\theta_w = 210°$, $z = 154.6$ m)
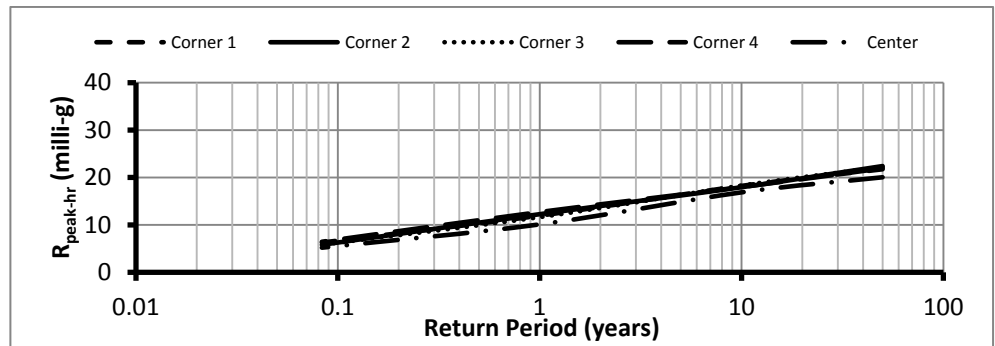
Fig. 4.19. Average Peak Hourly Resultant Accelerations with TLDs to Suppress the First 3 Modes Equipped with Inclined Damping Screens ($\mu = 2.0\%$, $\theta_w = 210°$, $z = 154.6$ m)

(a)

(b)
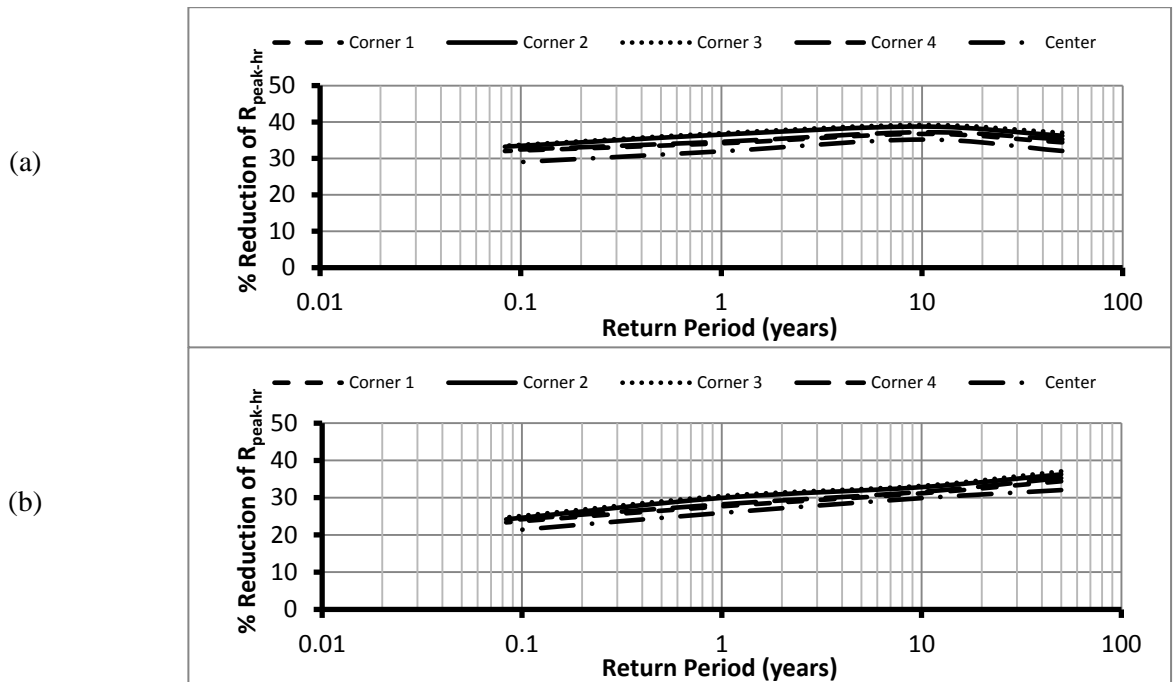
Fig. 4.20. Percentage Response Reductions of the Average Peak Hourly Resultant Accelerations with TLDs to Suppress the First 3 Modes Equipped with (a) Inclined Damping Screens; and (b) Fixed (Single Angle) Damping Screens ($\mu = 2.0\%$, $\theta_w = 210°$, $z = 154.6$ m)
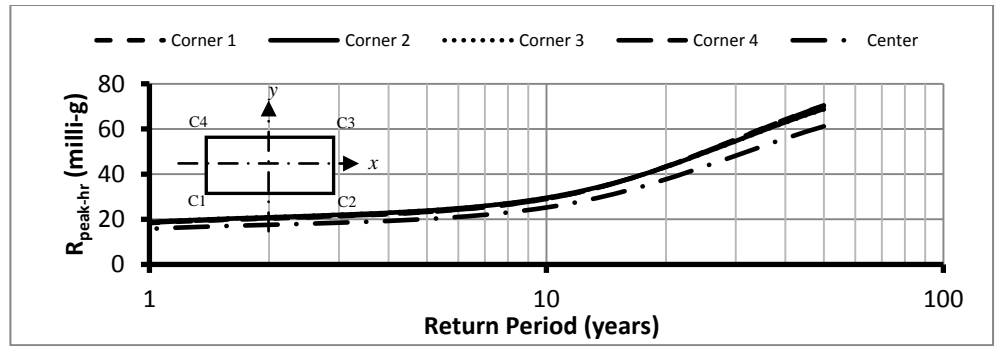
Fig. 4.21. Average Peak Hourly Resultant Accelerations for Mixed Return Periods with No-TLDs Installed ($\theta_w = 210°$, $z = 154.6$ m)
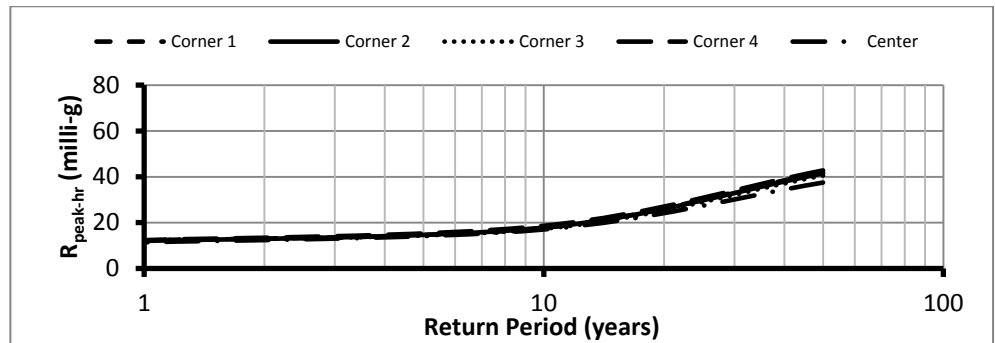
Fig. 4.22. Average Peak Hourly Resultant Accelerations for Mixed Return Periods with TLDs to Suppress the First 3 Modes Equipped with Inclined Damping Screens ($\mu = 2.0\%$, $\theta_w = 210°$, $z = 154.6$ m)

(a)

(b)
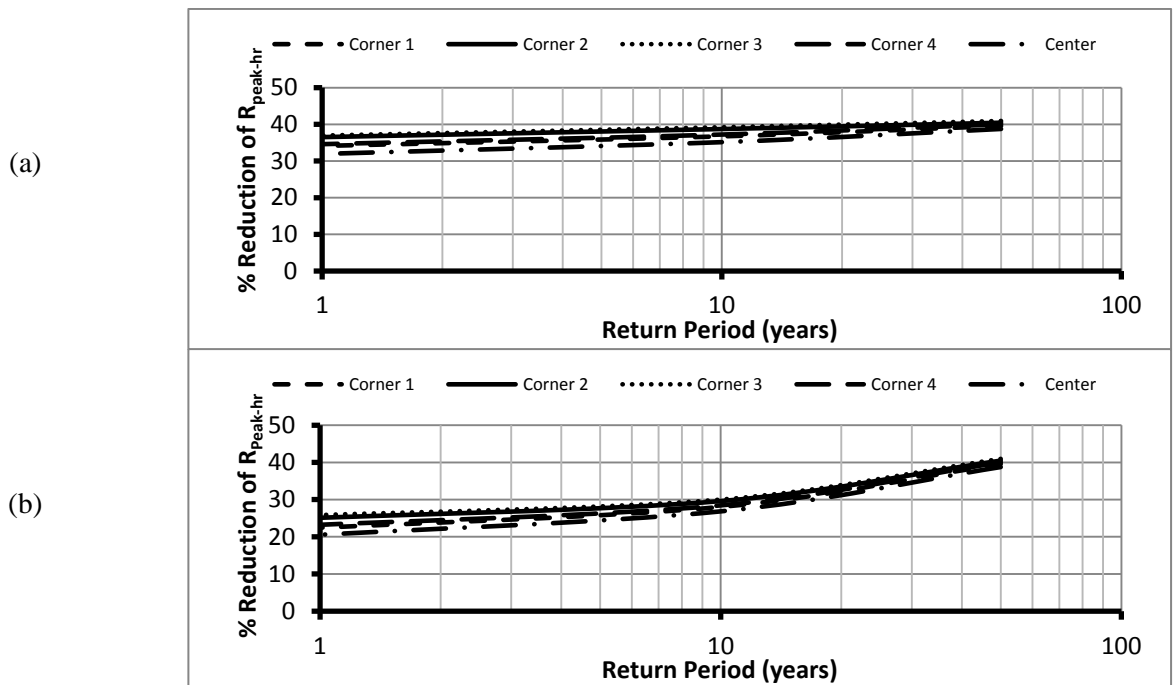
Fig. 4.23. Percentage Response Reductions of the Average Peak Hourly Resultant Accelerations for Mixed Return Periods with TLDs to Suppress the First 3 Modes Equipped with (a) Inclined Damping Screens; and (b) Fixed (Single Angle) Damping Screens ($\mu = 2.0\%$, $\theta_w = 210°$, $z = 154.6$ m)

Chapter 5: Development and Validation of a Finite Element Structure Semi-Active Tuned Liquid Damper System Model

5.1.   Introduction

Similar to a tuned mass damper (TMD) device, tuned liquid damper (TLD) and tuned liquid column damper (TLCD) devices can reduce resonant vibrations of a structure by modifying its frequency response function. In both systems (i.e. structure-TLD and structure-TLCD), the secondary mass is liquid and the damping forces primarily result from the motion of liquid through energy dissipating device such as damping screens in a TLD (Kaneko and Ishikawa 1999; Tait et al. 2004a; Tait et al. 2004b; Tait et al. 2005a; Tait et al. 2005b), or through an orifice in a TLCD (Kareem et al. 1999; Yalla et al. 2001). If the effective mass of liquid in a TLD or TLCD is equal to the mass of a TMD, then the same level of performance can be achieved if the system properties are properly selected. However, the primary difference from a TMD is the amplitude dependent (nonlinear) nature of a TLD/TLCD (Sun et al. 1995; Tait 2004). In particular, the damping introduced by energy dissipating mechanisms can be highly amplitude dependent (Tait 2008). Additionally, not all the fluid in a TLD/TLCD tank participates in the sloshing motion of the water. The non-participating portion of the water is essentially added to the primary mass of the structure, while only the participating mass in the TLD/TLCD only contributes to the dynamic vibration absorber (DVA) inertial forces (Yu et al. 1999; Tait 2004).

Studies on passive tuned liquid column damper (TLCD) include a full scale installation of a bidirectional TLCD on a 67 m steel communications tower by Hitchcock et al. (1999). The device did not include an orifice and hence, it was not possible to control the damping in the TLCD. It was acknowledged that due to the absence of an orifice, the damping ratio of the TLCD was not expected to be optimal. It was also observed that TLCD did not perform optimally at all wind speeds. Similar observations were made concerning tuned liquid dampers (TLD), both involving scaled experiments and full-scale studies (Tamura et al.1996).

Studies have also focused on improving the performance of the fully conventional passive TLCD. Haroun et al. (1994 and 1995) introduced the concept of a hybrid liquid column damper by actively controlling the orifice opening ratio. Yalla et al. (2001) introduced a semi-active (SA) TLCD that achieves variable damping by using a controllable

valve to adjust the orifice opening. The effectiveness of different control algorithms for the TLCD for structural control applications was also investigated. Yalla and Kareem (2003) examined the performance of a prototype semi-active TLCD. In addition, they verified a control strategy based on gain scheduling with experimental results. Kim and Adeli (2005a; 2005b) proposed wind-induced motion control of 76-story benchmark building using hybrid damper-TLCD system. Wang et al. (2005) introduced a semi-active TLCD using magneto-rheological fluid (MR-TLCD) for wind induced vibration mitigation of tall building structures.

To the best of the author's knowledge, no previous study has considered structural control of tall buildings using multiple semi-active TLDs. It would be beneficial to provide TLDs with variable damping that can be adjusted through a certain mechanism to achieve an optimal control performance over a wide range of loading conditions in a semi-active mode of control (i.e. different wind loading angles and return period wind speeds). The ability to control the inherent damping ratio of a TLD (ζ_{TLD}) was first introduced, theoretically, by Cassolato and Tait (2005). The modification of ζ_{TLD} by adjusting the screen angle, which alters the screen loss coefficient (C_θ), has also been experimentally investigated (Cassolato 2007; Cassolato et al. 2011). Results from that work indicated that rotating the damping screen(s) inside the TLD to adjust the screen loss coefficient (C_θ) is a plausible method to maintain a constant ζ_{TLD} value over a range of excitation amplitudes.

Therefore, the semi-active TLD operational principle can be achieved by adjusting the damping screen(s) inclination angle (θ). The semi-active TLD is a consequence of the fact that the control of the damping screen inclination angle requires a small amount of input energy, as opposed to a fully-conventional passive TLD. However, the required amount of energy to change the damping screen inclination angle is expected to be small in comparison with the total energy dissipated by the damping screen(s). In contrast with the fully-active TMD control system, the semi-active TLD system has low power requirements, hardware simplicity, low construction cost, robustness and reliability. Therefore, the semi-active TLD is considered to be a promising alternative to both fully-passive TLD and fully-active TMD.

The aim of this study is to develop a three dimensional finite element structure semi-active TLD system model (3D-Structure-SA-TLD). Installing a TLD permits the suppression of a particular vibration mode of the structure, while the semi-active control strategy

maintains the inherent damping ratio (ζ_{TLD}) of the TLD at its optimal value ($\zeta_{TLD-opt}$). The nonlinear TLD fluid model, updated and validated in Chapter 4, is used to simulate the damping screen(s) at different inclination angles (θ), while the three dimensional finite element structure-TLD system model, developed and validated in Chapter 2, is used to conduct the structural response analysis for a single-story structure equipped with a semi-active TLD.

Most semi-active (SA) devices (for e.g., MR and ER dampers, semi-active TLCDs, etc.) are intrinsically non-linear, which makes it challenging to develop control strategies to optimally exploit their unique features (Yalla et al. 2001). Some of the common examples of such algorithms are sliding mode control and non-linear H_∞ strategies (Yoshida et al. 1998). Another innovative algorithm, which focuses on the shaping of the force-deformation loop in a variable damper, is reported by Kurino and Kobori (1998). Other researchers have used fuzzy control schemes to effectively implement semi-active control (Sun and Goto 1994; Symans and Kelly 1999). Kim and Adeli (2005a; 2005b) calculated TLCD head loss coefficients for the semi-active control system using the wavelet-based optimal control algorithm to control wind-induced motion of a 76-story benchmark building. Also, Djajakesukma et al. (2002) reported semi-active stiffness damper systems with various control laws, such as resetting control, switching control, linear-quadratic regulator (LQR) and modified LQR systems, while Chase et al. (2003; 2004) proposed a series of SA control laws based on optimal control design. Chey et al. (2010) used SA resetable devices to mitigate structural response due to seismic loads, where the reset criteria were determined to be the point of zero velocity at displacement peaks.

From the above, it can be seen that different complex semi-active algorithms can be used to optimize the screen(s) inclination angle values and thus minimize an objective function such as structural displacement response, velocity response, or acceleration response values, which is not the goal of this study. The objective of this study is to employ a simple technique to achieve the same optimal passive TLD performance at different wind loading directions and return period wind speeds, which is not possible using conventional passive TLDs, due to the amplitude properties of the device (Tait 2004).

In this chapter, a control strategy based on a gain scheduling scheme (see Figure 5.1c), which was introduced and verified experimentally by Yalla and Kareem (2003) (see Figures

5.1a and 5.1b), is utilized by controlling the inclination angle (θ) of the damping screen(s) and consequently the screen loss coefficient value(s) (C_θ). The gain scheduling control strategy is employed on a three dimensional single-story structure equipped with a semi-active TLD in order to maintain the optimal damping value ($\zeta_{TLD-opt}$) based on a prescribed look-up table. Results are assessed with scaled experimental values for conventional passive TLDs. Finally, a performance comparison between the semi-active TLD control system and the conventional passive TLD control system is performed.

5.2. Response/Efficiency of a Structure-TLD System Model

The response of a structure equipped with a TLD is a function of three main parameters (Tait 2004; Tait et al. 2004a; Tait et al. 2007):

i. The tuning ratio (Ω), which influences the performance of the TLD, is defined by

$$\Omega = \frac{f_{TLD}}{f_s} \tag{5.1}$$

where f_{TLD} is the natural frequency of the TLD; and f_s is the natural frequency of the 3D-structure. For small response amplitudes, the natural frequency of the TLD (f_{TLD}) is approximately equal to f_w (Warnitchai and Pinkaew 1998; Ju et al. 2004; Tait et al. 2004a). The fundamental sloshing frequency (f_w) for the water inside a TLD can be estimated using the linear wave theory (Lamb 1932)

$$f_w = \frac{1}{2\pi}\sqrt{\frac{\pi g}{L}\tanh\left(\frac{\pi h}{L}\right)} \tag{5.2}$$

where g is the gravitational acceleration and L is the tank length in the direction of the fundamental sloshing mode of interest.

ii. The mass ratio (μ), which is given by

$$\mu = \frac{\phi^2 m_{TLD}}{M^*} \tag{5.3}$$

where M^* is the generalized mass of the primary structure corresponding to the vibration mode being suppressed; and ϕ is the normalized modal deflection value of the structure at the TLD location. The absorber mass (m_{TLD}) for a TLD with damping screen(s) can be approximated using potential flow theory (i.e. $m_{TLD} \approx m_1$). The value m_1 is calculated using the following equation (Graham and Rodriguez 1952)

$$m_1 = \frac{8\,tanh\left(\frac{\pi h}{L}\right)}{\frac{\pi^3 h}{L}} m_w \tag{5.4}$$

where m_w is the total mass of the contained water.

iii. The inherent damping ratio (ζ_{TLD}) of the sloshing fluid inside the tank. The damping related to the sloshing liquid inside the tank without the presence of additional energy dissipating devices, which can be estimated by Sun (1991) using the following equation

$$\zeta_{TLD} = \frac{1}{2\pi}\sqrt{\frac{v_w}{\pi f_w}}\left(1 + \frac{h}{b}\right) \tag{5.5}$$

where v_w is the kinematic viscosity of water.

An optimum inherent damping ratio (ζ_{opt}) and optimum tuning ratio (Ω_{opt}) for a linear structure-tuned mass damper (TMD) as a function of the mass ratio (μ) can be obtained for the special case of zero structural damping ($\zeta_s = 0$) (Warburton 1982). Due to the analogy between TMD and TLD devices, the H_2 optimized value are used to calculate $\zeta_{TLD-opt}$ and Ω_{opt}

$$\zeta_{TLD-opt} = \sqrt{\frac{\mu(1 + 3\mu/4)}{4(1 + \mu)(1 + \mu/2)}} \tag{5.6}$$

and

$$\Omega_{opt} = \frac{\sqrt{1 + \mu/2}}{1 + \mu} \tag{5.7}$$

Furthermore, three important parameters, commonly used to evaluate the performance of a structure-TLD system, are the efficiency, effectiveness and robustness (Tait 2004; Tait et al. 2004a; Tait et al. 2007). These parameters are utilized in this section to study the performance of a 3D-Structure-TLD system model equipped with inclined damping screen(s)

i. The effectiveness of a TMD can be expressed in terms of the amount of additional effective viscous damping, which is added to the primary structure (Vickery and Davenport 1970), denoted by the effective viscous damping ratio (ζ_{eff}). This can be accomplished by equating the area under the frequency response curve of the combined system to that of a single degree of freedom system (SDOF) with the same frequency and solving for the effective damping (ζ_{eff}) (McNamara 1977).

For a special case of zero structural damping (i.e. $\zeta_s = 0$), ζ_{eff} can be obtained using Gerges and Vickery (2003) formula as

$$\zeta_{eff} = \frac{\Omega \mu \zeta_{TLD}}{(1+\mu)^2 \Omega^4 + (1+\mu)2\Omega^2(2\zeta_{TLD}^2 - 1) + \Omega^2 \mu + 1} \tag{5.8}$$

The optimal parameter for the effective damping ($\zeta_{eff-opt}$) can be obtained by substituting Equations 5.6 and 5.7 into Equation 5.8, leading to

$$\zeta_{eff-opt} = \frac{1}{4}\sqrt{\frac{\mu(1+\mu)}{1+3\mu/4}} \tag{5.9}$$

ii.   The efficiency (ψ) of a TLD is defined as the amount of effective damping the TLD provides, compared to an optimal TMD with the same equivalent mass, expressed as a percentage using

$$\psi = \frac{\zeta_{eff}}{\zeta_{eff-opt}} \cdot 100 \tag{5.10}$$

iii. The robustness is defined as the changes in the effectiveness with changes in the tuning ratio (Ω), TLD damping ratio (ζ_{TLD}), and the structural response amplitude. The robustness of a TLD is dependent on tuning ratio (Ω) and the structural response amplitude as the TLD inherent damping ratio is found amplitude dependent (Sun et al. 1995; Reed et al. 1998a; Reed et al. 1998b; Tait 2004; Tait et al. 2004a; Tait et al. 2007).

The TLD is modelled using a nonlinear fluid model; therefore, the amplitude dependent hardening characteristics are also considered, in contrast with the two linear models proposed by Cassolato (2007). In other words, the nonlinear simulation considers the tuning ratio (Ω). Therefore, the robustness due to TLD mistuning is also considered.

5.3.   Modelling of a Three Dimensional Finite Element Structure Semi-Active Tuned Liquid Damper System (3D-Structure-SA-TLD)

5.3.1   Gain Scheduling Method for Semi-Active TLD Mode of Control

Yalla and Kareem (2003) describe the procedure of using a look-up table for a semi-active mode of control. The look-up table permits the range of the inclination angles (θ) of the damping screens, resulting in 100% TLD efficiency (ψ), to be identified at a selected mass ratio (μ). Gain scheduling is an open-loop control scheme with a nonlinear regulator whose parameters are modified as a function of the operating conditions in a pre-

programmed way (Astrom and Wittenmark 1989). This kind of gain scheduled control is commonly used in aerospace and process control applications.

In this chapter, a modified gain scheduling procedure is employed in a semi-active control scheme (see Figure 5.1c), described by Yalla and Kareem (2003) and shown in Figures 5.1a and 5.1b. In gain scheduling, the regulator parameters can be changed rapidly in response to process dynamics, the process dynamics is the combined 3D-Structure-SA-TLD system model employed to evaluate the acceleration of the building at the semi-active TLD location. The look-up table, which is constructed in the next section, is the gain scheduler, the regulator is the controllable inclination angle of the damping screens, the external environment is the applied external load on the building (i.e. wind or earthquake) and the pressure loss coefficient (C_θ) is the parameter being changed. Gain scheduling is an efficient control scheme for maintaining the TLD inherent damping ratio (ζ_{TLD}) at its optimum value ($\zeta_{TLD-opt}$). As shown in Figure 5.1c, for a given structural acceleration response, the pressure loss coefficient (C_θ) is modified in accordance with the look-up table. The study assumes that a mechanism exists to adjust the damping screens to the desired symmetric screen inclination (θ).

5.3.2   Look-Up Tables for Semi-Active TLD Mode of Control

To feedback the semi-active TLD control algorithm (i.e. gain scheduling control scheme) with the optimal inclination angles (θ) that achieve the optimal TLD inherent damping ratios ($\zeta_{TLD-opt}$) corresponding to structural response values in real time, construction of the look-up table is required. Therefore, the section describes, in detail, the necessary steps required to the construct a look-up table.

A 3D single-story structure (see Figure 5.2) whose generalized properties match that used in an experimental study by Tait (2004) and are listed in Table 5.1, is modelled and analyzed utilizing the 3D-Structure-TLD system model that simulates inclined damping screens, which was developed and validated in Chapter 4. As a result, the 3D single-story structure is excited by a number of random excitation force time history records, where the values of the excitation amplitude (F_{max}) are varied to achieve different structural response values. A TLD length (L) equal to 0.966 m is selected to match that used in the experimental work. The TLD water depth (h) is selected to achieve the optimal tuning ratio (Ω) according to the chosen mass ratio (μ). The TLD width (b) is then selected to achieve the assumed mass ratio (μ).

The mass ratio values (μ) selected for the construction of the look-up tables are 1.0%, 2.5%, 3.5% and 5.0%. Table 5.2 shows the properties of TLDs used in the construction of the look-up tables. Subsequently, Equations 5.6 and 5.7 are used to calculate different values of the optimum TLD damping ratios ($\zeta_{TLD-opt}$) and the optimum tuning ratios (Ω_{opt}), respectively, according to the selected mass ratio (μ).

Damping screens, having a solidity ratio (S) equal to 60% and corresponding vertical loss coefficient (C_l) equal to 8.17, are placed inside the tank at $0.4L$ and $0.6L$. For vertical damping screens (i.e. $\theta = 0.0°$) and in an iterative manner, the 3D single-story, structure shown in Figure 5.2, is analyzed employing the 3D-Structure-TLD system model under random excitation with incremental values of amplitude (F_{max}) during each iteration. As a result, RMS structural acceleration response values ($\sigma_{\ddot{x}}$) are obtained from the dynamic analysis for each F_{max} value. Consequently, average peak hourly structural acceleration response values ($\ddot{x}_{peak-hr}$) are calculated utilizing the resulting RMS structural acceleration response values ($\sigma_{\ddot{x}}$) and the modal peak factor value (PF) (Davenport 1964). The following equation is used to determine the average peak hourly structural acceleration response values ($\ddot{x}_{peak-hr}$)

$$\ddot{x}_{peak-hr} = \sigma_{\ddot{x}}\, PF \tag{5.11}$$

A full-scale peak factor value (PF) of 3.75 is determined for the 3D single-story structure utilized in the 3D-Structure-TLD system model by (Davenport 1964)

$$PF = \sqrt{2\ln\left(\frac{T_d}{2\pi}\omega_{s-x}\right)} + \frac{0.577}{\sqrt{2\ln\left(\frac{T_d}{2\pi}\omega_{s-x}\right)}} \tag{5.12}$$

where ω_{s-x} is the structure's natural frequency in the x-direction, which is the direction of the applied external random excitation, and T_d is the duration time in seconds used to calculate the average peak factor value over the desired time, which is an hour in this study.

The selected damping screen characteristics are found to provide 100% TLD efficiency (ψ) according to the mass ratio values (μ) selected for the construction of the look-up tables of 1.0%, 2.5%, 3.5% and 5.0% with corresponding optimum average peak hourly structural acceleration response values of 2.65 milli-g, 6.50 milli-g, 9.00 milli-g and 12.50 milli-g, respectively, at vertical inclination angle (i.e. $\theta = 0.0°$). These structural response values

represent the target response values of the 3D-Structure-TLD system model ($\ddot{x}_{target}$) at different mass ratio values (μ) and can be obtained from Figures 5.3 to 5.6, respectively.

5.3.2.1 Preliminary TLD Design Procedure to Estimate the Required Inclination Angle of the Damping Screens for 100% TLD Efficiency

The preliminary TLD design procedure (Tait 2008), which was discussed in detail and expanded for multiple TLDs in Chapter 3, is employed in this section to determine the inclined damping screen properties, i.e. the inclined screen loss coefficient values (C_θ) required to achieve 100% TLD efficiency (ψ) at different selected target peak hourly structural acceleration response values ($\ddot{x}_{target}$) and mass ratio values (μ). Consequently, the required inclination angles for the damping screens (θ) can be determined using Equation 5.13 (Cassolato 2007), which was validated in Chapter 4 with experimental values from Cassolato et al. (2011)

$$C_\theta = C_l \left(0.46\theta^3 - 1.05\theta^2 - 0.06\theta + 1\right) \tag{5.13}$$

First, the accuracy of the preliminary TLD design procedure is checked by determining the required vertical screen loss coefficient values (C_l) that achieve the target acceleration response values ($\ddot{x}_{target}$) at 100% TLD efficiency (ψ) obtained previously from Figures 5.3 to 5.6 for different mass ratios (μ). Excellent agreement is obtained for the predicted vertical loss coefficient values (C_l) and the actual value utilized in the numerical analysis (i.e. 3D-Structure-TLD) that equal to 8.17. By utilizing the preliminary TLD design procedure (Tait 2008), the calculated vertical C_l value of 8.21 is determined in Table 5.3 at a mass ratio value (μ) equal to 1.0%. The TLD design procedure is repeated in Tables C1-C3 (Appendix-C) to determine vertical C_l values of 8.27, 8.31 and 8.35 at mass ratio values (μ) of 2.5%, 3.5% and 5.0%, respectively.

As a result, the preliminary TLD design procedure is used to determine the required inclined damping screen properties (C_θ) that achieve different target structural acceleration response values ($\ddot{x}_{target}$) at 100% TLD efficiency (ψ) according to selected mass ratio values (μ) and considering the practical limit of screen rotation (i.e. $\theta \leq 65.0°$). Table 5.4 shows different inclined damping screen loss coefficient values (C_θ) and their corresponding inclination angle values (θ), resulting from the preliminary TLD design procedure according to selected target peak hourly structural acceleration response values ($\ddot{x}_{target}$).

Therefore, in the next section, the resulting C_θ values are utilized in the 3D-Structure-TLD system model to analyze the scaled 3D single-story structure shown in Figure 5.2. The single-story structure is subjected to a random excitation time history with incremental amplitude values (F_{max}) to confirm the predicted values of the inclined damping screens (θ) and to produce the envelope of the improved TLD efficiency (ψ) with their corresponding target structural acceleration response values ($\ddot{x}_{target}$) in the practical range of damping screen inclination angles.

5.3.2.2   Construction of 100% TLD Efficiency Envelope Curves

The dynamic analysis proceeds in an iterative manner resulting in increasing values of the average peak hourly structural acceleration response ($\ddot{x}_{peak-hr}$) utilizing the inclined screen loss coefficient values (C_θ) obtained from Table 5.4 for the selected mass ratio values (μ). Results are shown in Figures 5.3 to 5.6 for mass ratio values (μ) of 1.0%, 2.5%, 3.5% and 5.0%, respectively. As the maximum allowable acceleration set by the wind tunnel criteria (Isyumov 1994) for wind-induced acceleration is 30.0 milli-g for the office buildings, the incremental iterations are stopped when the average peak hourly structural acceleration response values ($\ddot{x}_{peak-hr}$) exceeded 40.0 milli-g.

As can be observed from Figures 5.3 to 5.6, normal vertical screens (i.e. $\theta = 0.0°$) can be designed to operate optimally for only one particular structural acceleration response value, $\ddot{x}_{peak-hr}$ (i.e. $\ddot{x}_{peak-hr} = \ddot{x}_{target}$). Throughout different screen inclination angles (θ), an envelope is drawn capturing 100% TLD efficiency (ψ) over a range of structural acceleration responses as shown in each figure. The general trends of the results are found to be in good agreement with those obtained by Cassolato (2007) from his study on a theoretical single degree of freedom system model (SDOF) using a linear TLD numerical model. The envelope curves show that adjustable screens are able to maintain 100% TLD efficiency (ψ) over a range of structural acceleration responses ($\ddot{x}_{peak-hr}$), in contrast with the normal vertical screens.

For a mass ratio value (μ) of 1.0%, Figure 5.3 shows that an extension of 100% efficiency over the average peak hourly structural acceleration response ($\ddot{x}_{peak-hr}$) is achieved utilizing three different values of the angled screens (θ). Therefore, for 100% TLD efficiency (ψ), target structural response values ($\ddot{x}_{target}$) are found to be 4.5 milli-g, 6.5

milli-g and 9.0 milli-g corresponding to screen angle values (θ) equal to 41.0°, 53.5°, and 61.5°, respectively. Figure 5.4 shows that for $\mu = 2.5\%$, the angled screens, which are optimally set to different inclination angles utilizing results from the preliminary TLD design procedure mentioned previously, can cover a range of peak structural acceleration response values ($\ddot{x}_{peak-hr}$) in the range between 6.5 milli-g at $\theta = 0.0°$ and 20.0 milli-g at $\theta = 59.0°$ for 100% TLD efficiency (ψ). Similar trends can be observed in Figures 5.5 and 5.6 for mass ratio values (μ) of 3.5 and 5.0%, respectively.

5.3.2.3   Construction and Discussion of the Look-Up Tables

Figure 5.7 shows a summary for the data presented in Figures 5.3 to 5.6 and represents the look-up table for various mass ratio values (μ) of 1.0%, 2.5%, 3.5% and 5.0%. The figure shows the extent of screen rotation (θ) at various mass ratio values (μ) of 1.0%, 2.5%, 3.5% and 5.0% that maintains 100% TLD efficiency (ψ). As the mass ratio value (μ) increases, a greater level of the TLD inherent damping ratio (ζ_{TLD}) is required. Therefore, the start values of the structural response acceleration ($\ddot{x}_{peak-hr}$), which provide 100% TLD efficiency (ψ) are found higher than their counterpart values for lower mass ratio values (μ). For example, at the highest mass ratio value (μ) of 5.0% and at target structural acceleration response value ($\ddot{x}_{target}$) equal to 8.0 milli-g, the damping screens can not provide sufficient TLD inherent damping ratio (ζ_{TLD}), even in their upright position (i.e. $\theta = 0.0°$). Figure 5.7 shows that a mass ratio value (μ) of 3.5% at a vertical screen position or at a mass ratio value (μ) of 2.5% at an inclination angle of screens equal to $\theta = 30.0°$ can provide the required TLD inherent damping ratio (ζ_{TLD}) to operate at 100% efficiency (ψ). This emphasizes the importance of constructing the look-up table, which permits the ability of a selected mass ratio value (μ) to achieve 100% TLD efficiency (ψ) at lower structural response values. Figure 5.7 also shows the largest angle (θ) needed to maintain the TLD inherent damping ratio (ζ_{TLD}) at its optimum value ($\zeta_{TLD-opt}$) throughout different structural acceleration response values ($\ddot{x}_{peak-hr}$) for the selected mass ratios (μ).

Reduced TLD efficiency (ψ) as a function of structural response acceleration is found to be less noticeable for high mass ratio values (μ). For a mass ratio value (μ) of 2.5%, 100% TLD efficiency (ψ) is achieved in the range of acceleration response values between 6.5 milli-g and 20.0 milli-g that corresponds to a range of screen angles between 0° and 59.0°,

respectively (see Figure 5.4). Also, it can be observed that at high structural response values ranging between 20.0 milli-g to 40.0 milli-g, the TLD inherent damping ratio (ζ_{TLD}) exceeds its optimal ($\zeta_{TLD-opt}$), since ζ_{TLD} is amplitude dependent due to the velocity squared losses introduced by the damping screens, resulting in a reduction in the effectiveness of the TLD (Tait et al. 2008). Similarly, if the response acceleration is less than the target level, ζ_{TLD} is found to be less than the optimal value $\zeta_{TLD-opt}$ and the effectiveness of the TLD decreases. This is observed for the envelope curve for peak structural acceleration response values ($\ddot{x}_{peak-hr}$) less than 6.5 milli-g (i.e. $\ddot{x}_{peak-hr} < \ddot{x}_{target-min}$).

The above findings are found to be in agreement with results obtained from the performance charts developed by Tait et al. (2008) for a linear structure-TMD system (see Figure 5.8). The effectiveness of a linear TMD can be expressed in terms of the amount of effective viscous damping ζ_{eff} (see Equation 5.8) that it adds to the primary structure (Vickery and Davenport 1970). The value of ζ_{eff} is determined by equating the variance of the response of a structure-TLD or structure-TMD system (see Figures 5.9a and 5.9b) to that of a single degree of freedom (SDOF) structure with an equivalent viscous damper (see Figure 5.9c). A performance diagram for a linear TMD provides a measure of ζ_{eff} (see Figure 5.8a) and the corresponding displacement ratio of RMS relative motion between the absorber and the primary structure (x_r) (see Figure 5.8b) as a function of the tuning ratio (Ω) and the absorber damping ratio (ζ_A) for a specified value of the mass ratio (μ). In case of a TLD, the relative motion corresponds to the free surface motion. For the above optimal parameters, the resulting optimal effective damping ($\zeta_{eff-opt}$) and the corresponding displacement ratio (x_{r-opt}) between the absorber and the primary structure (assuming $\zeta_s = 0$) are given by Equations 5.9 and 5.14, respectively

$$x_{r-opt} = \frac{1 + \mu}{\sqrt{2\mu + \dfrac{3\mu^2}{2}}} \tag{5.14}$$

It can be observed from Figure 5.8a that at the optimal tuning ratio (Ω_{opt}), the reduction in system efficiency is significantly less for an over-damped TLD (i.e. $\zeta_{TLD} > \zeta_{TLD-opt}$) compared to an under-damped TLD (i.e. $\zeta_{TLD} < \zeta_{TLD-opt}$), which agrees with results obtained in Figure 5.4. Fortunately, the performance of a TLD is less critical at accelerations that are below serviceability limit requirements. In addition, the over-damped system is

found to better control the fluid response height as smaller x_r values are obtained at $\zeta_{TLD} >$ $\zeta_{TLD-opt}$ compared to an under-damped system (see Figure 5.8b).

5.3.3 Averaging Time (AT), Updating Time (UT) and Initial Time (IT) Parameters for a 3D-Structure-SA-TLD System Model and Sensitivity Analysis of AT and UT

To implement the gain scheduling scheme in a 3D-Structure-TLD system model, two parameters must be defined and added to the semi-active TLD system model (3D-Structure-SA-TLD), in addition to the fitted equation of the look-up table. These two parameters are the averaging time (AT) and the updating time (UT). The averaging time (AT) is the time used to calculate the acceleration root-mean-square (RMS) response value at the TLD location and placement direction ($\sigma_{\ddot{x}_{AT\,(i)}}$) over a time history prior to the time step (i), selected to update the screen loss coefficient value ($C_{\theta_{AT\,(i)}}$). As a result, the average peak hourly structural acceleration response value ($\ddot{x}_{peak-hr_{AT\,(i)}}$) is evaluated using Equation 5.11. The optimal inclination angle value of the damping screen ($\theta_{AT\,(i)}$) is then evaluated using $\ddot{x}_{peak-hr_{AT\,(i)}}$ value and the look-up table. Consequently, the loss coefficient value ($C_{\theta_{AT\,(i)}}$) is evaluated using Equation 5.13. The numerical simulation proceeds with the updated $C_{\theta_{AT\,(i)}}$ value over a period of time equal to the updating time (UT). Therefore, at the end of the updating time (UT), a new $C_{\theta_{AT\,(i+UT)}}$ value is determined and used as the feedback value in the semi-active simulation process over the next UT period utilizing the updated value of $\ddot{x}_{peak-hr_{AT\,(i+UT)}}$.

The initial time (IT) is an extra time parameter that controls the start time of the semi-active control mode. The numerical analysis initially operates under the passive control mode (i.e. conventional passive TLDs with vertical damping screens) during the selected initial time period value (IT). An initial time value (IT) of 15 minutes (full-scale) is selected as it is considered a sufficient period of time for the activation of the semi-active control system. In fact, semi-active control systems are usually designed to act as fully passive systems below a predetermined structural response threshold. Therefore, the IT value allows the simulation of the transition from a passive mode of control to a semi-active mode of control. Hence, all time history figures in this chapter show the simulation results for a scaled time ≥ 15 minutes.

With the aim of selecting the first two parameter values, AT and UT, a sensitivity study is performed utilizing the 3D single-story structure shown in Figure 5.2 equipped with a TLD with a mass ratio value (μ) equal to 3.5%. An updating time value (UT) is selected to be $1.0\ T$, where T is the natural period of the structure. Different values of the averaging time period values (AT) ranging between 5 and 60 minutes (full-scale) are selected for the sensitivity analysis. The 3D single-story structure is subjected to a random excitation S7, listed in Table 5.5 (Section 5.4 provides additional details on the applied forces), and analyzed employing the 3D-Structure-SA-TLD system model. The random excitation force S7 produces an uncontrolled RMS structural response value ($\sigma_{\ddot{x}-initial}$) equal to 40.0 milli-g. Figure 5.10 shows the time history of RMS acceleration response values ($\sigma_{\ddot{x}}$) of the 3D single-story structure calculated every updating time (UT) equal $1.0\ T$ for various averaging time values (AT) during the entire time history. For a given averaging time value (AT), the resulting $\sigma_{\ddot{x}_{AT}\ (i)}$ value is used to evaluate the screen loss coefficient value ($C_{\theta_{AT}\ (i)}$) to feedback to the semi-active control strategy over the time history $i + UT$ (see Figure 5.11).

It can be observed from Figure 5.10 that for small AT values (i.e. $AT \leq 10$ minutes), higher fluctuations in RMS structural acceleration values ($\sigma_{\ddot{x}}$) occur compared to $\sigma_{\ddot{x}}$ values that converge rapidly to a near constant value utilizing high AT values. It can also be observed that all selected AT values have achieved lower RMS structural response values than the target RMS response value ($\sigma_{\ddot{x}-target}$) of 4.5 milli-g predicted for a passive TLD control system with the same tank properties and mass ratio value used in the semi-active control system.

Figure 5.11 shows that averaging time values, $AT \geq 15$ minutes result in reduced fluctuation of C_{θ} values that lead to a suitable rotation of the damping screens. It can be observed that the best performance of the semi-active TLD system model is achieved for an averaging time value (AT) of 5 minutes (see Figure 5.10), however this requires higher fluctuating damping screen(s) motions (see Figure 5.11).

By selecting an averaging time value (AT) equal to 60 minutes, good performance is achieved with minor adjustments to the damping screen inclination angle (see Figure 5.11). By selecting a 60-minute averaging time value (AT), the rotational motion of the damping screens will not alter the overall flow pattern inside the tank. Also, a long damping screen system life cycle is expected as the damping screens are subjected to reduced wear and tear

resulting in low maintenance costs over its operating life. Moreover, a small actuator capacity and power supply are needed to achieve the required rotational motion of the damping screens in real time. Finally, only basic monitoring and control system components are required compared to more expensive and highly sophisticated control components needed in a fully-active control system.

A second sensitivity study is performed to investigate the updating time value (UT). Different UT values ranging between $0.25\ T$ and $32.00\ T$ (i.e. $0.5 < UT < 60.0$ seconds) are selected to conduct the sensitivity analysis with the averaging time value (AT) held constant at 60 minutes. Figures 5.12 and 5.13 show that constant acceleration ($\sigma_{\ddot{x}}$) and damping screen loss coefficient (C_θ) values are obtained. This can be attributed to the nature of the wind excitation and the selected value of AT. In an earthquake excitation scenario, where the time scale of the applied load is in a scale of seconds compared to a scale of hours, a small UT value would be required to capture the instantaneous structural response variation allowing the TLDs to counteract the applied load more efficiently. Therefore, the updating time value (UT) is considered less sensitive for the wind loading case and the selected AT value. As such, a UT value equal to $1.0\ T$ is selected.

5.4. Influence of Excitation Amplitude on the Response of a 3D-Structure-SA-TLD System Model

The 3D-Structure-SA-TLD system model is employed to analyze a 3D single-story structure equipped with a SA-TLD with a mass ratio value (μ) of 3.5% (see Table 5.2). The system is subjected to random excitation forces scaled from S1 to S13 (see Table 5.5) utilizing an averaging time value (AT) equal to 60 minutes and an updating time (UT) equal to $1.0\ T$.

The look-up table presented in Figure 5.7 shows that for a mass ratio value (μ) of 3.5%, the minimum average peak hourly structural acceleration response value ($\ddot{x}_{target-min}$) that achieves 100% TLD efficiency is 9.0 milli-g (i.e. $\sigma_{\ddot{x}} \approx 2.4$ milli-g), which corresponds to a vertical screen position (i.e. $\theta = 0.0°$). Applying random forces S1 to S3, listed in Table 5.5, results in controlled RMS structural acceleration response values ($\sigma_{\ddot{x}}$) lower than 2.4 milli-g, as shown in Figure 5.14. Consequently, the semi-active TLD algorithm sets the screen loss coefficient value (C_θ) to the maximum value of 8.17 (C_{l-max}) as shown in Figure 5.15.

Applying the scaled random excitations S4-S10 results in different screen angles and corresponding damping screen loss coefficient values (C_θ) in order to achieve the optimal TLD damping ratio ($\zeta_{TLD-opt}$). In addition, a slight change of the screen loss coefficient value (C_θ) is found to occur every updating time (UT). The change of C_θ, in real time, is a direct results of changing the screen inclination angle value (θ) (see Equation 5.13). In contrast, applying random excitation forces S11-S13 results in maximum allowable rotation of the damping screens ($C_{\theta-max}$) and corresponding minimum damping screen loss coefficient value (C_{l-min}) being selected by the semi-active TLD control algorithm.

It must be recognized that a trade off exists between the maximum damping screen loss coefficient value (C_{l-max}), which is related to the damping screen solidity ratio (S) at the vertical position, and the maximum structural response value ($\ddot{x}_{target-max}$) that achieves 100% TLD efficiency (ψ). Therefore, it is recommended that the vertical damping screen loss coefficient value (C_{l-max}) be able to achieve 100% TLD efficiency (ψ) for an average peak hourly structural acceleration response value, $\ddot{x}_{target-min} \leq 10.0$ milli-g, for example, for residential buildings (Isyumov 1994). As a result, an over-damped system at response amplitudes higher than $\ddot{x}_{target-max}$, utilizing the maximum allowable inclination angle (θ_{max}) of the damping screens will occur. As mentioned above in Section 5.3.2.3, an over-damped system is more robust than an under-damped system (see Figure 5.8a). In addition, the over-damped system is found to better control the fluid response height at large excitation amplitudes (see Figure 5.8b).

5.5. Performance Semi-Active TLD Control System versus the Passive TLD Control System

In this a section, a comparison between the semi-active TLD control system and the passive TLD control system is made, when both systems are subjected to a particular scaled random excitation force (S7 listed in Table 5.5). The comparison investigates the additional reduction achieved, in terms of RMS ($\sigma_{\ddot{x}}$) and average peak hourly ($\ddot{x}_{peak-hr}$) structural acceleration response values, utilizing the semi-active TLD control system.

Figure 5.16 shows that for a particular applied random force (S7), the semi-active TLD control system provides lower RMS structural acceleration response values ranging between 12.7% at $AT = 5$ minutes to 5.9% at $AT = 60$ minutes compared to the passive TLD control system. In contrast, negligible difference in the hourly peak structural acceleration response

values is observed in Figure 5.17 between the passive and semi-active TLD control systems. In addition, the calculated average hourly peak factor values (PF)

$$PF = \frac{1}{n}\sum_{i=1}^{n} \frac{\ddot{x}_{peak-hr_i}}{\sigma_{\ddot{x}_i}} \tag{5.15}$$

where n is the number of hours are found to be in good agreement with that obtained using Equation 5.12 (see Figure 5.18)

The negligible reduction in the peak hourly structural acceleration response values is attributed to the selected values of the semi-active control technique parameters, which are utilized in the numerical simulations. The selected parameter values used in the semi-active control technique, which consider suitable motions of the damping screen, monitoring and computational system requirements, prevent the SA-TLD from responding efficiently to instantaneous changes in structural accelerations. In order to provide an instantaneous feedback at every time step (Δt), AT and UT are set equal to Δt, where $\Delta t = 0.019$ seconds (full-scale) in order to calculate optimal angle values (θ) in response to instantaneous changes in structural accelerations. It can be observed from Figure 5.19 that extremely high fluctuating screen motions occur compared to moderate and low fluctuating motions at $AT = 5$ minutes and $AT = 60$ minutes, respectively.

RMS and peak hourly structural acceleration response values are presented in Figures 5.20 and 5.21 for the instantaneous ($AT = \Delta t$), $AT = 5$ minutes, $AT = 60$ minutes and the passive systems, respectively. While percentage reduction values of 5.9% and 12.7% in the RMS structural acceleration response are achieved employing the semi-active TLD control system utilizing AT values of 60 and 5 minutes, respectively, compared to the passive TLD control system, a 17.6% percentage response reduction is achieved utilizing the instantaneous semi-active TLD control strategy (see Figure 5.20).

An average peak hourly structural acceleration response value ($\ddot{x}_{peak-hr}$) of 13.2 milli-g is obtained using the instantaneous semi-active TLD control strategy compared to values of 15.7 milli-g and 15.9 milli-g obtained utilizing the semi-active ($AT = 60$ minutes; $UT = 1.0\,T$) and the passive TLD control systems, respectively (see Figure 5.21). Finally, the evaluated average peak factor values (PF), using Equation 5.15, for the instantaneous semi-active TLD control strategy ($AT = UT = \Delta T$), semi-active TLD control strategy ($AT = 60$

minutes; $UT = 1.0\,T$), and the passive TLD control system are found to be in good agreement with the value predicted by Davenport (1964), using Equation 5.12, with a minimum accuracy of 97% (see Figure 5.22).

5.6.   Influence of Semi-Active Control on Fluid Response

Figure 5.23 shows that the normalized peak hourly fluid response ratio values (η/h where η is the free surface height and h is the water height inside the TLD) at the TLD end wall are higher for the semi-active control strategy. It can be observed that utilizing the averaging time values (AT) of 5 minutes and 60 minutes lead to similar peak hourly fluid response ratio values, while utilizing the instantaneous averaging time value ($AT = \Delta T$) leads to values that are nearly double the passive values.

Figures 5.24 and 5.25 show the peak hourly fluid response ratio values using random forces S4, S7 and S10 excitation amplitudes utilizing the passive and semi-active control strategies, respectively. An averaging time (AT) and updating time (UT) values of 60 minutes and $1.0\,T$, respectively, are used for the semi-active control strategy. By comparing Figures 5.24 and 5.25, it can be observed that using the semi-active control strategy leads to higher peak hourly fluid response ratio values with a maximum ratio value of 0.57 compared to the passive control counterpart value of 0.26 for all excitation amplitudes. Although higher peak hourly fluid response ratio values are obtained using the semi-active control strategy, they remain within the recommended free board allowance value in the range of $1.5\,h$ to $2.0\,h$ (Tait 2004).

5.7.   Conclusions

In this study, a control strategy based on gain scheduling, which was previously employed and verified experimentally by Yalla and Kareem (2003), has been utilized by actively controlling the damping screen inclination angle (θ) and consequently the corresponding loss coefficient (C_θ). Gain scheduling is an efficient control scheme to maintain the inherent damping ratios of the TLDs (ζ_{TLD}) at their optimal values ($\zeta_{TLD-opt}$). For a given structural response acceleration, the pressure loss coefficient (C_θ) has been modified in accordance with the look-up table.

The nonlinear fluid model of a TLD equipped with damping screens, which was updated and validated with experimental results to simulate inclined damping screens in Chapter 4,

has been used in this chapter to determine the resulting TLD base shear force and fluid response amplitude in real time. The robustness of a structure-TLD system model due to mistuning has been addressed in all simulations conducted in this chapter due to the ability of the updated nonlinear TLD fluid model to capture the resulting shift in the tuning ratio (hardening) from its optimal value at high response amplitudes and high screen inclination values.

A 3D single-story structure has been modelled and analyzed utilizing the 3D-Structure-SA-TLD system model. As a result, the TLD inherent damping ratio (ζ_{TLD}) maintained its optimal damping value ($\zeta_{TLD-opt}$) based on a prescribed look-up table and results have been assessed under scaled random excitation force time histories.

The necessary steps toward the construction of the look-up table have been described, in detail, and practical mass ratio values (μ) have been selected to construct look-up tables, which fall within a typical range μ used in most TMD/TLD applications for tall structures. Therefore, the feedback process of the semi-active TLD control strategy with the optimal inclination values of the damping screens (θ), which result in the optimal TLD inherent damping ratio ($\zeta_{TLD-opt}$) corresponding to structural response values, has been achieved in real time.

Three parameters have been defined and were added in the semi-active TLD system model (3D-Structure-SA-TLD), in addition to the fitted equation of the look-up table in order to implement the gain scheduling scheme in a 3D-Structure-TLD system model. These parameters are, the averaging time (AT), the updating time (UT) and the initial time (IT).

A sensitivity study has been performed utilizing the 3D single-story structure equipped with a TLD with the aim of selecting the first two parameter values (AT; UT). The following important findings have been drawn:

1. The semi-active TLD control system with practical control parameters (AT; UT) exceeds the efficiency (ψ) of the passive TLD control system for additional reduction of the RMS structural acceleration response value ($\sigma_{\ddot{x}}$) of up to 12.7%.

2. The semi-active TLD control system with practical control parameters (AT; UT) matches the efficiency (ψ) of the passive TLD control system in reducing the average peak hourly structural acceleration response values ($\ddot{x}_{peak-hr}$).

3. The semi-active TLD control system with instantaneous control parameters ($AT = UT = \Delta t$) exceeds the efficiency (ψ) of the passive TLD control system for additional reduction of the RMS ($\sigma_{\ddot{x}}$) and the average peak hourly ($\ddot{x}_{peak-hr}$) structural acceleration response values of 17.6% and 16.9%, respectively.

4. As for overall performance, the semi-active TLD control system provides the aforementioned three findings over a wide range of applied excitations (i.e. wide range of structural response amplitudes) compared to the passive TLD control system.

5. Although the fluid response amplitude for a SA-TLD was found to exceed that of a passive TLD, it did not exceed free board limits recommended for passive TLDs.

As a result, AT equal to 60 minutes, which is quite achievable with a simple controller, has been selected for the rest of the study to provide the lowest variation in the loss coefficient values (C_θ) and consequently, the damping screen inclination angle values (θ). This choice has led to practical and economical benefits such as:

i. Reasonable rotation of the damping screens inside the TLD during excitation events.

ii. A long life cycle of the damping screen system is expected as the damping screens are subjected to reduced wear and tear, which should lower the maintenance costs over the SA-TLD operating life.

iii. A small actuator capacity and low power requirements are needed to rotate the damping screens in real time.

iv. Only basic monitoring and control components are required for the SA-TLD compared to expensive and sophisticated control components needed in a fully-active control system.

5.8.   References

Astrom, K. J. and Wittenmark, B. (1989). "*Adaptive Control*", Addison-Wesley, 2nd Ed, 1994, Reading, MA, USA.

Cassolato, M. and Tait, M. (2005). "A Preliminary Study of a Tuned Liquid Damper with Smart Screens", *Proceeding of the 1st Canadian Conference on Effective Design of Structures*, McMaster University, Hamilton, ON, Canada: 960-971.

Cassolato, M.R. (2007). "*The Performance of a Tuned Liquid Damper Equipped with Inclined and Oscillating Damping Screens*", M.E.Sc. Thesis. McMaster University, Hamilton, ON, Canada.

Cassolato, M.R., Love, J.S. and Tait, M.J. (2011). "Modelling of Tuned Liquid Damper with Inclined Damping Screens", *Structural Control and Health Monitoring*, 18(6): 674-681.

Chey, M, Chase, J.G., Mander, J.B. and Carr, A. (2010). "Semi-Active Tuned Mass Damper Building Systems: Design", *Earthquake Engineering and Structural Dynamics*, 39, 119-139.

Chase, J.G., Barroso, L.R. and Hunt, S. (2003). "Quadratic Jerk Regulation and the Seismic Control of Civil Structures", *Earthquake Engineering and Structural Dynamics*, 32(13), 2047-2062.

Chase, J.G., Barroso, L.R. and Hunt, S. (2004). "The Impact of Total Acceleration Control for Semi-Active Earthquake Hazard Mitigation", *Engineering Structures*, 26(2), 201-209.

Davenport, A.G. (1964). "Note on the Distribution of the Largest Value of a Random Function with Application to Wind Loading", *Proceeding - Institution of Civil Engineer*, 28: 187-196.

Djajakesukma, S.L., Samali, B. and Nguyen, H. (2002). "Study of a Semi-Active Stiffness Damper under Various Earthquake Inputs", *Earthquake Engineering and Structural Dynamics*, 31(10), 1757-1776.

Gerges, R.R. and Vickery, B.J. (2003). "Wind Tunnel Study of the Across-Wind Response of a Slender Tower with a Nonlinear Tuned Mass Damper", *Journal of Wind Engineering and Industrial Aerodynamics*, 91: 1069-1092.

Graham, E.W. and Rodriguez, A.M. (1952). "The characteristics of fuel motion which affect airplane dynamics", *Journal of Applied Mechanics*, 19(3): 381-388.

Haroun, M. A., Pires, J. A. and Won, A. (l994). "Active Orifice Control in Hybrid Liquid Column Dampers", *Proceeding of the First World Conference on Structural Control*, Los Angeles, CA, USA, FA1, 69-78.

Haroun, M. A., Pires J. A. and Won, A. Y. J. (1995). "Effectiveness of Hybrid Liquid Column Dampers for Suppressing Structural Vibrations", *Proceedings of the 13th International Modal Analysis Conference*, Nashville, Tennessee, 1, 525–531.

Hitchcock, P. A, Glanville, M. J, Kwok, K. C. S, Watkins, R. D. and Samali, B. (1999). "Damping Properties and Wind-Induced Response of a Steel Frame Tower Fitted with Liquid Column Vibration Absorbers", *Journal of Wind Engineering and Industrial Aerodynamics*, 83(1-3), 183-196.

Isyumov, N. (1994). "Criteria for Acceptable Wind-Induced Motions", *Proceedings, 12th ASCE Structures Congress*, 642-653. Atlanta, GA, USA.

Ju, Y.K., Yoon, S.W. and Kim, S.D. (2004). "Experimental Evaluation of a Tuned Liquid Damper System", *Proceeding of Institution of Civil Engineering-Structures and Building*, 157(4): 251-262.

Kaneko, S. and Ishikawa, M. (1999). "Modeling of Tuned Liquid Damper with Submerged Nets", *Journal of Pressure and Vessel Technology*, 121(3): 334–343.

Kareem, A., Kijewski, T. and Tamura, Y. (1999). "Mitigation of Motions of Tall Buildings with Specific Examples of Recent Application", *Wind Structures: An International Journal*, 2(3): 201-251.

Kim, H. and Adeli, H. (2005a). "Hybrid Control of Smart Structures using a Novel Wavelet-Based Algorithm", *Computer Aided Civil and Infrastructure Engineering*, 20(1): 7-22.

Kim, H. and Adeli, H. (2005b). "Wind-Induced Motion Control of 76-Story Benchmark Building using the Hybrid Damper-TLCD System", *Journal of Structural Engineering*, 131(12): 1794-1802.

Kurino, H. and Kobori, T. (1998). "Semi-Active Structural Response Control by Optimizing the Force–Deformation Loop of Variable Damper" *Proceedings of Second World Conference on Structural Control*, Kyoto, Japan, UK: John Wiley, 407–417.

Lamb, H. (1932). "*Hydrodynamics*", the University Press, Cambridge, England.

The MathWorks Inc., (2004). "*MATLAB version 7.0.0.19920 (R14)*", The MathWorks Inc., Natick, MA, USA.

McNamara, R.J. (1977). "Tuned Mass Dampers for Building", Journal of Structural Division, American Society of Civil Engineer, 103, 1785-1798.

Reed, D., Yu, J., Yeh, H. and Gardarsson, S. (1998a). "Investigation of Tuned Liquid Damper under Large Amplitude Excitation", *Journal of Engineering Mechanics*, 124(4): 405-413.

Reed, D., Yeh, H., Yu, J., and Gardarsson, S. (1998b). "Tuned Liquid Damper under Large Amplitude Excitation", *Journal of Wind Engineering and Industrial Aerodynamics*, 74-76: 923-930.

Samail, B., Kwok, K. and Gao, H. (1998). "Wind Induced Motion Control of a 76 Storey Building By Liquid Dampers", *Proceeding of the 2nd World Conference on Structural Control*, Volume 2, Wiley, NY, USA, p: 1473-1480.

Symans, M.D. and Kelly, S.W. (1999). "Fuzzy Logic Control of Bridge Structures Using Intelligent Semi-Active Seismic Isolation Systems". Earthquake Engineering and Strucutral Dynamics, 28, 37–60.

Sun, L.M. (1991). "*Semi-Analytical Modelling of Tuned Liquid Damper (TLD) with Emphasis on Damping of Liquid Sloshing*", Ph.D.Thesis, University of Tokyo, Tokyo, Japan.

Sun, L.M., Fujino, Y. and Koga, K. (1995). "A Model of Tuned Liquid Damper for Suppressing Pitching Motion of Structures", *Earthquake of Engineering and Structure Dynamics*, 24: 625-636.

Sun, L. and Goto, Y. (1994). "Application of Fuzzy Theory to Variable Dampers for Bridge Vibration Control" *Proceedings of the First World Conference on Structural Control*, Los Angeles, CA, USA, 31–40.

Tait, M.J. (2004). "*The Performance of 1D and 2D Tuned Liquid Dampers*", Ph.D. Thesis, The University of Western Ontario, London, ON, Canada.

Tait, M.J., E1 Damatty, A.A. and Isyumov, N. (2004a). "Testing of Tuned Liquid Damper with Screens and Development of Equivalent TMD Model", *Wind and Structures*, 7(4): 215–234.

Tait, M.J., Isyumov, N. and E1 Damatty, A.A. (2004b). "The Efficiency and Robustness of a Unidirectional Tuned Liquid Damper and Modelling with an Equivalent TMD", *Wind and Structures*, 7(4): 235–250.

Tait, M.J., El Damatty, A.A. and Isyumov, N. (2005a). "An Investigation of Tuned Liquid Dampers Equipped with Damping Screens Subjected to 2D Excitation", *Earthquake Engineering and Structural Dynamics*, 34(7): 719–735.

Tait, M.J., El Damatty, A.A., Isyumov, N. and Siddique, M.R. (2005b). "Numerical Flow Models to Simulate Tuned Liquid Dampers (TLD) with Slat Screens", *Journal of Fluid and Structures*, 20: 1007–1023.

Tait, M.J., Isyumov, N. and E1 Damatty, A. A. (2007). "Effectiveness of a 2D TLD and Its Numerical Modeling", *Journal of Structural Engineering*, 133(2): 251-263.

Tait, M.J. (2008). "Modelling and Preliminary Design of a Structure-TLD System", *Engineering Structures*, 30: 2644-2655.

Tait, M.J., Isyumov, N. and El Damatty, A.A. (2008). "Performance of Tuned Liquid Dampers", *Journal of Engineering Mechanics*, 134(5): 417-427.

Tamura Y., Kohsaka R., Nakamura O., Miyashita K-i. and Modi V.J. (1996). "Wind Induced Responses of an Airport Tower-Efficiency of Tuned Liquid Damper", *Journal of Wind Engineering and Industrial Aerodynamics*, 65(1): 121-131.

Vickery, B.J. and Davenport, A.G. (1970). "An Investigation of the Behaviour in Wind of the Proposed Centre Point Tower in Sydney, Australia", *Research Report BLWT-1-70*, The Boundary Layer Wind Tunnel Laboratory, The University of Western Ontario, London, ON, Canada.

Wang, J. Y., Ni, Y. Q., Ko, J. M. and Spencer, B. F. Jr. (2005). "Magneto-Rheological Tuned Liquid Column Dampers (MR-TLCDs) for Vibration Mitigation of Tall Buildings: Modelling and Analysis of Open-Loop Control", *Computer and Structures*, 83, 2023-2034.

Warburton, G.B. (1982). "Optimum Absorber Parameters for Various Combinations of Response and Excitation Parameters", *Earthquake Engineering and Structural Dynamics*, 10(3): 381-401.

Warnitchai, P. and Pinkaew, T. (1998). "Modeling of Liquid Sloshing in Rectangular Tanks with Flow-Dampening Devices", *Engineering Structures*, 20(7): 593-600.

Yalla, S. K., Kareem, A. and Kantor, J. C. (2001). "Semi-Active Tuned Liquid Column Dampers for Vibration Control of Structures", *Engineering Structures*, 23, 1496-1479.

Yalla, S. and Kareem, A. (2003). "Semiactive Tuned Liquid Column Dampers: Experimental Study", *Journal of Structural Engineering*, 129(7): 960-971.

Yoshida, K., Yoshida S. and Takeda Y. (1998). "Semi-Active Control of Base Isolation using Feedforward Information of Disturbance", *Proceeding of Second World Conference on Structural Control*, Kyoto, Japan, UK: John Wiley, 377-386.

Yu, J. K, Wakahara, T. and Reed, D. A. (1999). "A Non-Linear Numerical Model of the Tuned Liquid Damper", *Earthquake Engineering and Structural Dynamics*, 28, 671-686.

Table 5.1. Building Properties

Excitation Type	f_s (Hz)	Generalized Model			Frame Element Model		
		M^* (kg)	K^* (N/m)	C^* (kg/s)	ζ_s (%)	L_c (m)	EI_c (N.m^2)
Random	0.558	4040	49,656	17.00	0.06	3.0	446,904

Table 5.2. TLD Properties

Excitation Type	μ (%)	Ω_{opt} (%)	$f_{TLD-opt}$ (Hz)	h (m)	L (m)	b (m)	m_{TLD} (kg)	m_w (kg)	S (%)	C_l
Random	1.0	99.3	0.554	0.123	0.966	0.442	40.4	52.5	60	8.17
	2.5	98.2	0.547	0.120	0.966	1.129	101.0	130.9		
	3.5	97.5	0.543	0.118	0.966	1.605	141.4	182.9		
	5.0	96.4	0.538	0.115	0.966	2.342	260.8	202.0		

Table 5.3. Preliminary TLD Design for Vertical Damping Screens ($\mu = 1.0\%$)

Quantity	Equation(s)	Value	
Initial peak hourly acceleration, $\ddot{x}_{initial}$		**13.57**	**milli-g**
Structure cyclic frequency, f_{s-x}		0.56	Hz
Structure time period, T_{s-x}	$T_{s-x} = 1/f_{s-x}$	1.79	s
Structure natural frequency, ω_{s-x}	$\omega_{s-x} = 2\pi/T_{s-x}$	3.51	rad/s
Peak factor, PF_x	$PF_x = \sqrt{2\ln(181\omega_{s-x})} + \dfrac{0.577}{\sqrt{2\ln(181\omega_{s-x})}}$	3.75	
Initial RMS acceleration, $\sigma_{\ddot{x}-initial}$	$\sigma_{\ddot{x}-initial} = \dfrac{\ddot{x}_{initial}}{PF_x}$	**3.62**	**milli-g**
Initial RMS displacement, $\sigma_{x-initial}$	$\sigma_{x-initial} = \dfrac{\sigma_{\ddot{x}-initial}}{\omega_{s-x}^2}\dfrac{g}{1000}$	2.89	mm
Assumed mass ratio, μ		0.010	(1.00%)
Effective damping provided by TLD, $\zeta_{TLD-eff-opt_x}$	$\zeta_{TLD-eff-opt_x} = \dfrac{1}{4}\sqrt{\dfrac{\mu_x+\mu_x^2}{1+\frac{3}{4}\mu_x}}$	0.025	(2.50%)
Optimal damping ratio, $\zeta_{TLD-opt_x}$	$\zeta_{TLD-opt_x} = \sqrt{\dfrac{\mu_x+\frac{3}{4}\mu_x^2}{4+6\mu_x+2\mu_x^2}}$	0.049	(4.98%)
Optimal tuning ratio, Ω_{opt_x}	$\Omega_{opt_x} = \dfrac{\sqrt{1+\frac{1}{2}\mu_x}}{1+\mu_x}$	0.992	(99.2%)
Optimal TLD cyclic frequency, $f_{TLD-opt_x}$	$\Omega_{opt_x} = \dfrac{f_{TLD-opt_x}}{f_{s-x}}$	0.554	Hz
Optimal response ratio, R_{opt_x}	$R_{opt_x} = \dfrac{\sigma_{r-x}}{\sigma_x} = \dfrac{1+\mu_x}{\sqrt{2\mu_x+\frac{3}{2}\mu_x^2}}$	7.115	
Structure damping ratio, ζ_s		0.0006	(0.06%)
Total structure damping, ζ_{tot-x}	$\zeta_{tot-x} = 0.8\zeta_s + \zeta_{TLD-eff-opt_x}$	0.0255	(2.55%)
Target RMS displacement, $\sigma_{x-target}$	$\zeta_{tot-x} = \zeta_s \dfrac{\sigma_{x-initial}^2}{\sigma_{x-target}^2}$	0.440	mm
Target RMS acceleration, $\sigma_{\ddot{x}-target}$	$\sigma_{\ddot{x}-target} = \omega_s^2\,\sigma_{x-target}$	**0.71**	**milli-g**
Target peak hourly acceleration, $\ddot{x}_{target}$	$\sigma_{\ddot{x}-target} = \dfrac{\ddot{x}_{target}}{PF_x}$	**2.65**	**milli-g**
TLD response, σ_{r-x}	$\sigma_{r-x} = R_{opt_x}\,\sigma_{x-target}$	3.15	mm
Select tank dimensions, L_x, h	$f_{TLD-opt_x} = \dfrac{1}{2\pi}\sqrt{\dfrac{\pi g}{L_x}\tanh\left(\dfrac{\pi h}{L_x}\right)}$	**$L_x = 0.966$ m** **$h = 0.123$ m**	
Shallow water theory check, h/L_x		0.127	
Select screen properties, x_1, x_2, C_{l-x}	$\zeta_{TLD-x} = C_{l-x}\sqrt{\dfrac{32}{\pi^3}}\tanh^2\left(\dfrac{\pi h}{L_x}\right)\Delta_x\Xi_x\dfrac{\sigma_{r-x}}{L_x}$ $\Delta_x = \left(\dfrac{1}{3}+\dfrac{1}{\sinh^2(\frac{\pi h}{L_x})}\right)$ $\Xi_x = \sum_{j=1}^{ns_x}\left|\sin^3\left(\dfrac{\pi x_j}{L_x}\right)\right|$	**$x_1 = 0.4\,L_x$** **$x_2 = 0.6\,L_x$** **$C_{l-x} = 8.21$**	

Table 5.4. Inclined Damping Screens Loss Coefficient values (C_θ) Used in the Validation Study

Excitation Type	S (%)	μ (%)	θ (Degree)	C_θ (Inclined)	$\ddot{x}_{target}$ (milli-g)
Random	60	1	0	8.2	2.7
			41.0	4.8	4.5
			53.5	3.3	6.5
			61.5	2.4	9.0
		2.5	0	8.3	6.5
			37.0	5.3	10.0
			51.5	3.5	15.0
			59.0	2.7	20.0
		3.5	0	8.3	9.0
			40.0	4.9	15.0
			50.5	3.7	20.0
			56.5	2.9	25.0
			61.0	2.5	30.0
		5.0	0	8.4	12.5
			22.5	6.9	15.0
			38.0	5.2	20.0
			46.5	4.1	25.0
			52.5	3.4	30.0

Table 5.5. Scaled Random Forces Used in the Validation Study

Excitation Type	S (%)	μ (%)	Scaled Force	$\sigma_{\ddot{x}(No-TLD)}$ (milli-g)
Random	60	3.5	S1	10
			S2	15
			S3	20
			S4	25
			S5	30
			S6	35
			S7	40
			S8	45
			S9	50
			S10	55
			S11	60
			S12	65
			S13	70
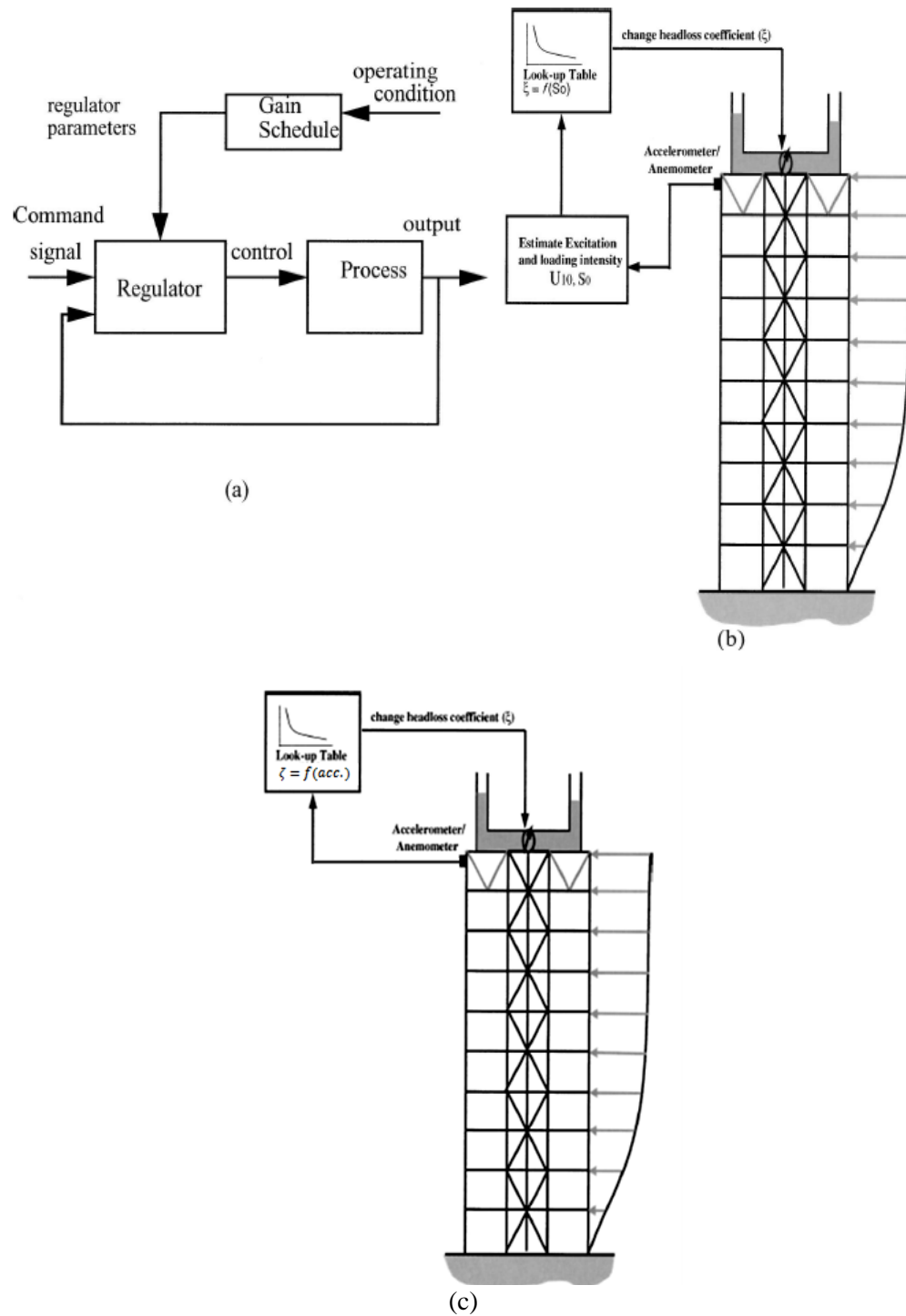
Fig. 5.1. (a) Gain Scheduling Concept; (b) Semi-Active Control Strategy in Tall Buildings (Yalla and Kareem 2003); and (c) Semi-Active Control Strategy Used in This Study

(a) (b)
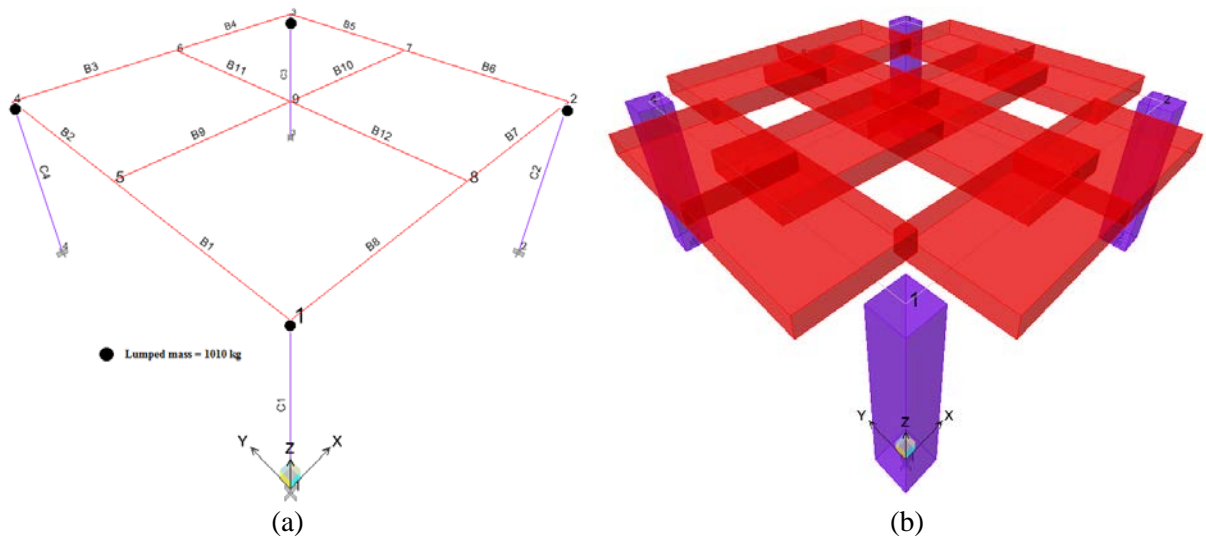
Fig. 5.2. 3D Single-Story Structure Used in the Semi-Active Control Strategy Validation (a) A Schematic Diagram; and (b) 3D View
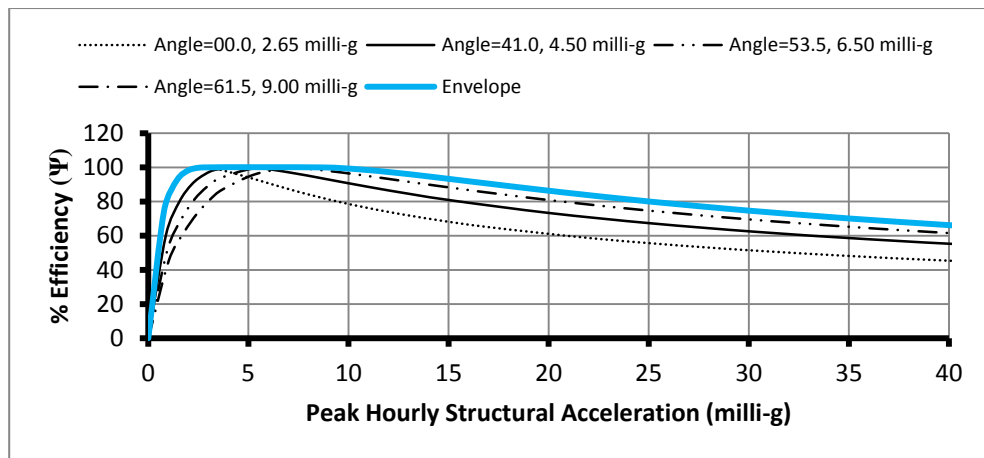
Fig. 5.3. Efficiency over Range of Structural Responses for $\mu = 1.0\%$ ($S = 60\%$)
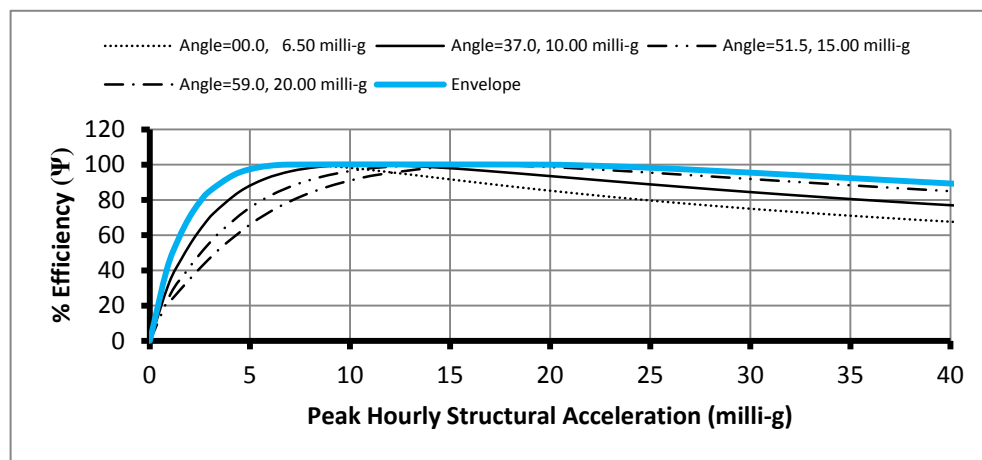
Fig. 5.4. Efficiency over Range of Structural Responses for $\mu = 2.5\%$ ($S = 60\%$)
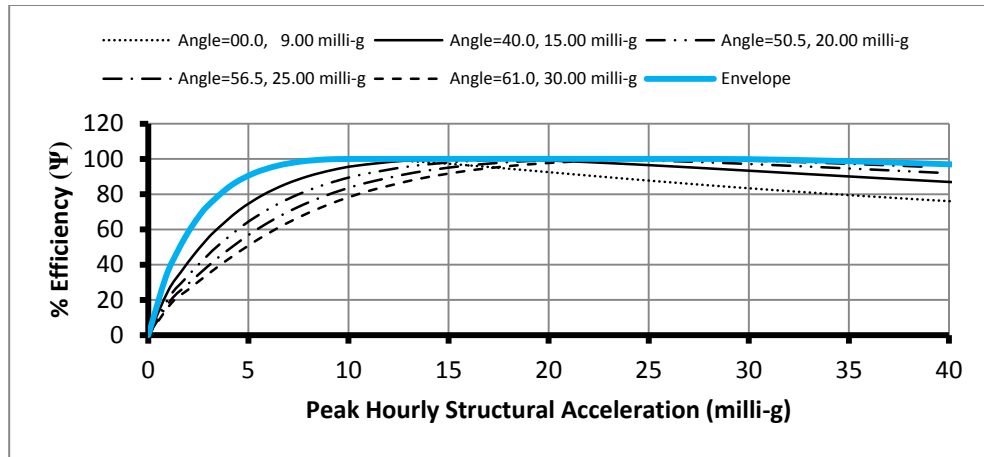
Fig. 5.5. Efficiency over Range of Structural Responses for $\mu = 3.5\%$ ($S = 60\%$)
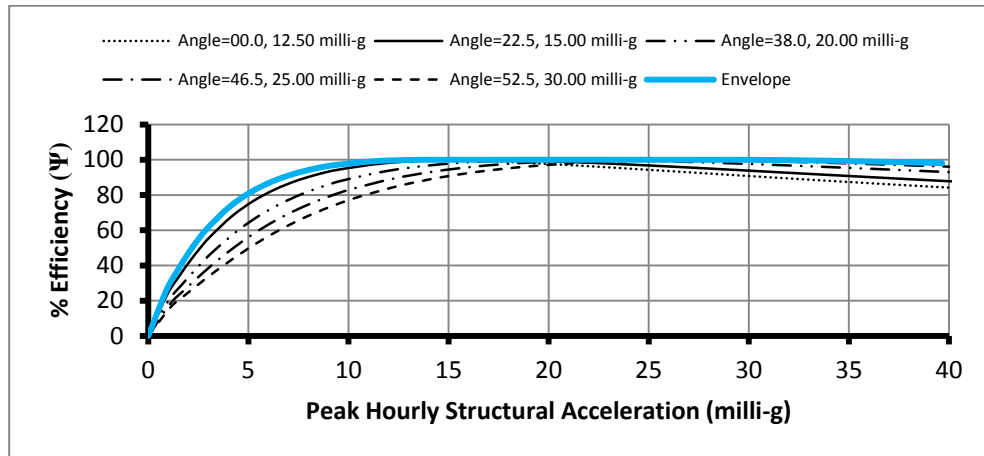
Fig. 5.6. Efficiency over Range of Structural Responses for $\mu = 5.0\%$ ($S = 60\%$)
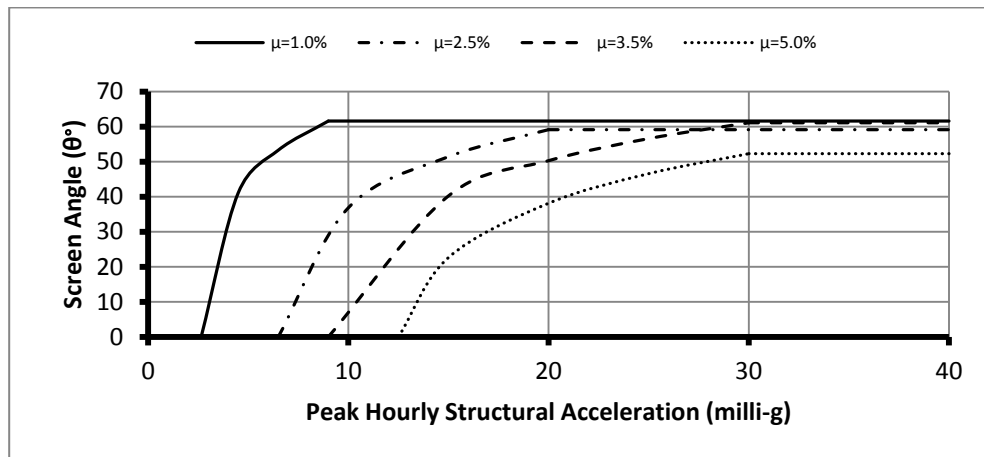
Fig. 5.7. Look-Up Table for Semi-Active Control Strategy at Various Mass Ratios
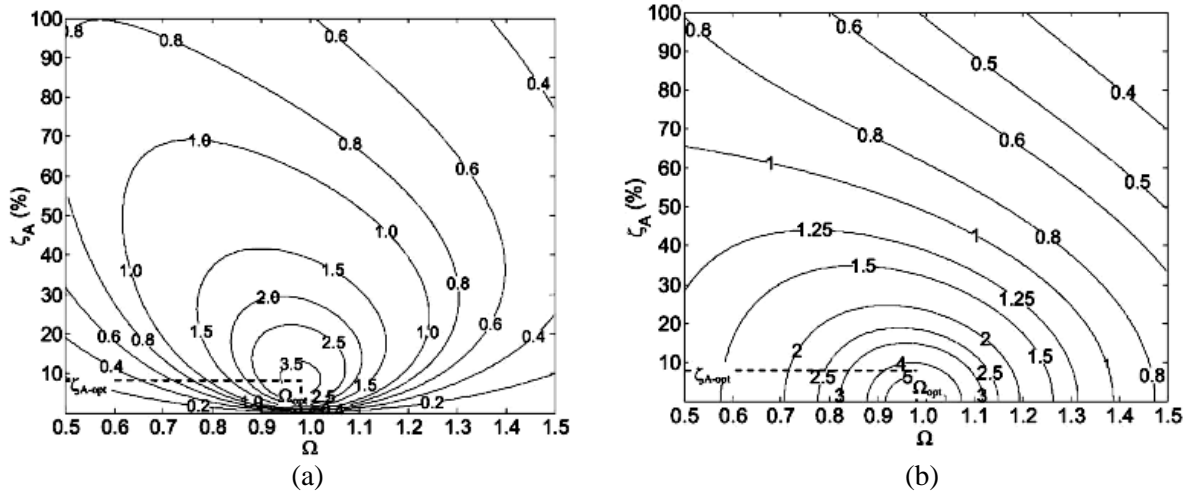
Fig. 5.8. Performance Charts Showing Values of (a) ζ_{eff} (%); (b) x_r for $\mu = 2.5\%$, $0.5 < \Omega < 1.5$, and $0 < \zeta_A(\%) < 100$ (from Tait et al. 2008)

(a) Structure-TLD System   (b) Structure-TMD System   (c) Equivalent SDOF System
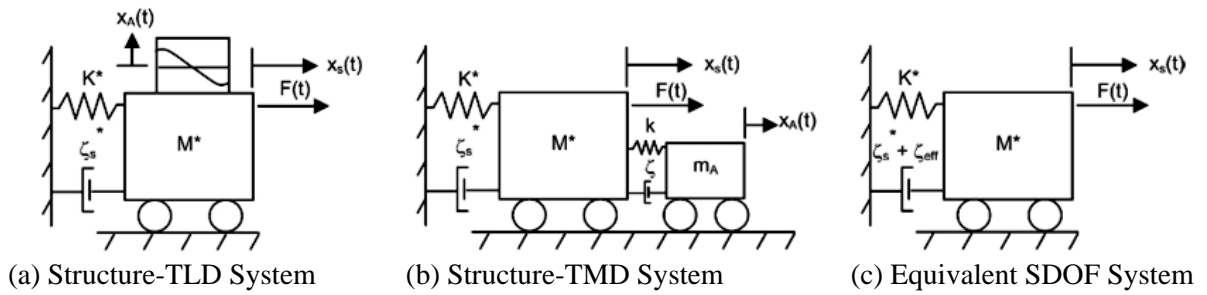
Fig. 5.9. Modeling of Structure with TLD/TMD Vibration Absorber and Equivalent SDOF System (from Tait et al. 2008)
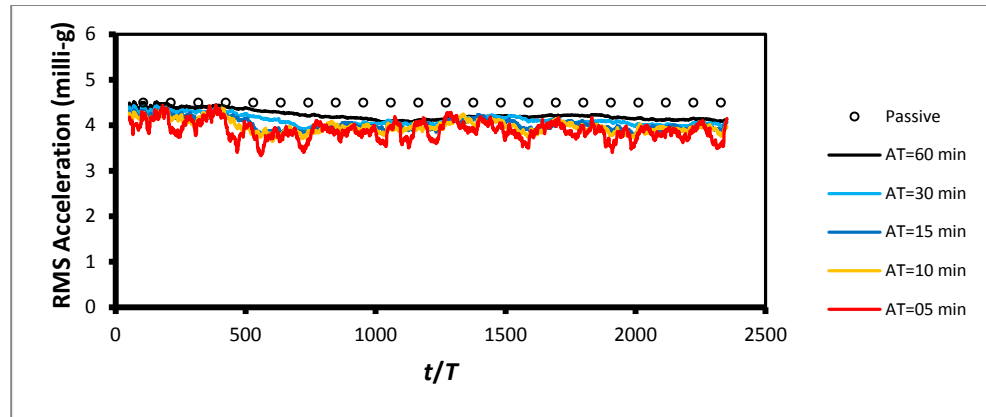
Fig. 5.10. RMS Structural Acceleration Response Values Resulting from the Semi-Active Control Strategy Utilizing Various Averaging Time Values, AT (S7-Random Force, $\mu = 3.5\%$, $UT = 1.0\,T$)
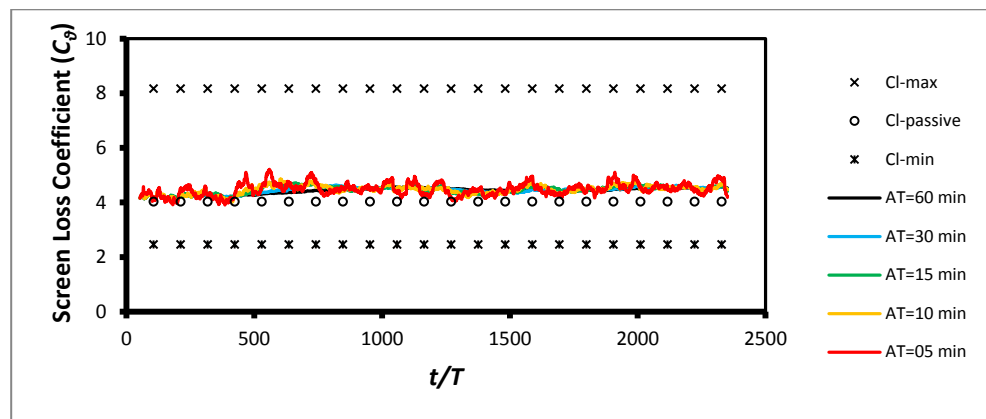
Fig. 5.11. Screen Loss Coefficient Values Resulting from the Semi-Active Control Strategy Utilizing Various Averaging Time Values, AT (S7-Random Force, $\mu = 3.5\%$, $UT = 1.0\,T$)
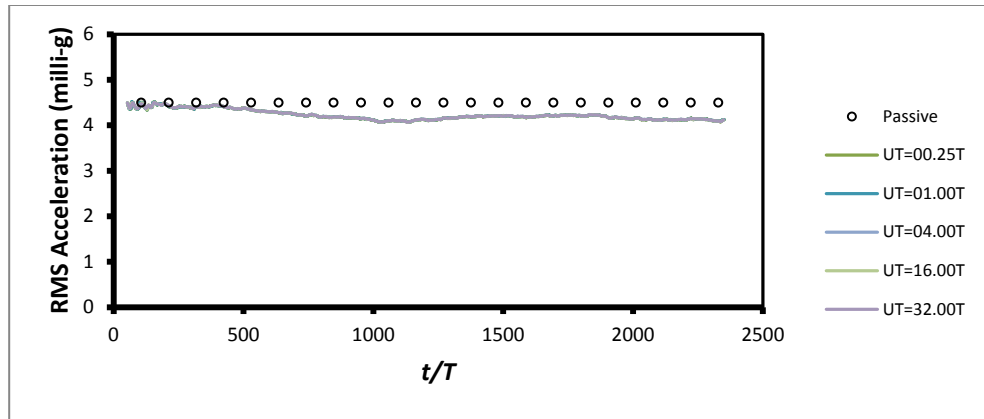
Fig. 5.12. Average Peak Hourly Structural Acceleration Response Values Resulting from the Semi-Active Control Strategy for Various Updating Time Values, UT (S7-Random Force, $\mu = 3.5\%$, $AT = 60$ min)
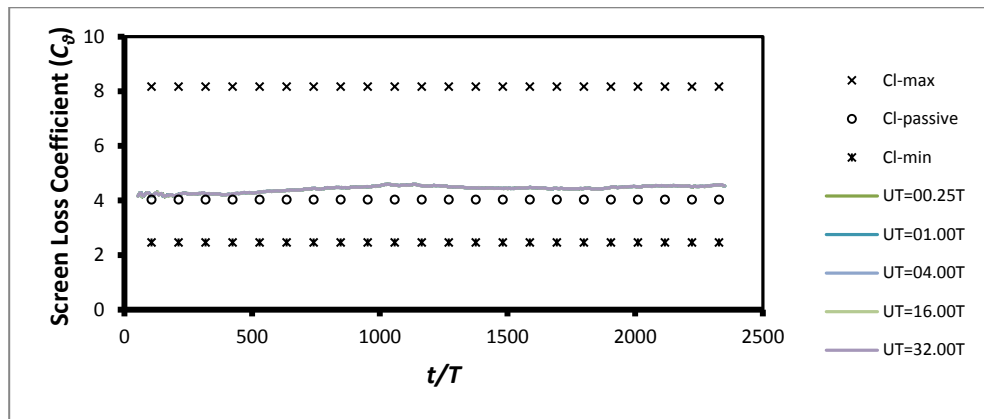
Fig. 5.13. Screen Loss Coefficient Values Resulting from the Semi-Active Control Strategy for Various Updating Time Values, UT (S7-Random Force, $\mu = 3.5\%$, $AT = 60$ min)
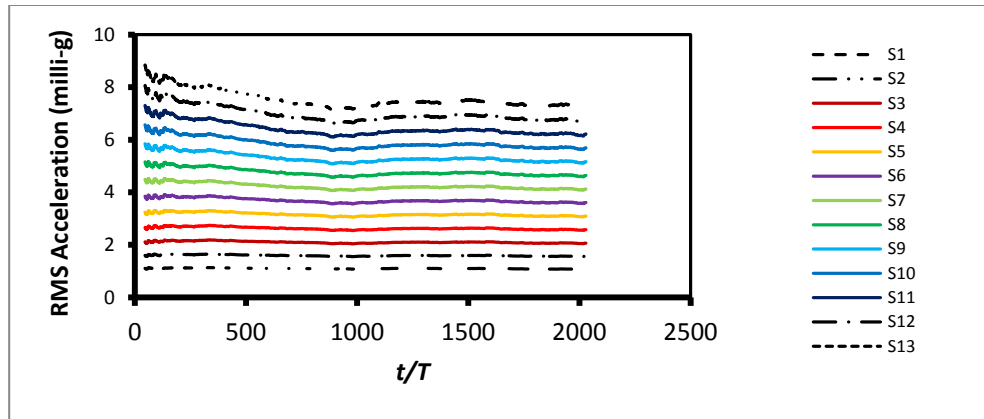
Fig. 5.14. RMS Structural Acceleration Response Values Resulting from the Semi-Active Control Strategy Subjected to Various Random Forces S1-S13 ($\mu = 3.5\%$, $AT = 60$ min, $UT = 1.0\,T$)
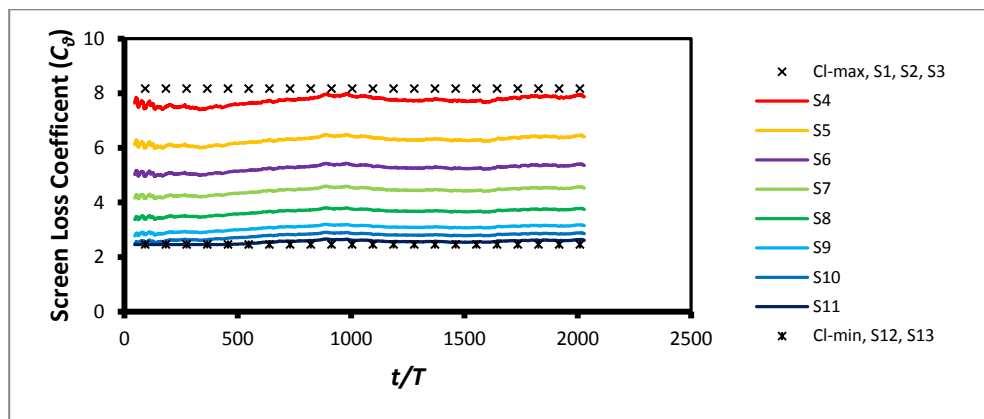
Fig. 5.15. Screen Loss Coefficient Values Resulting from the Semi-Active Control Strategy Subjected to Various Random Forces S1-S13 ($\mu = 3.5\%$, $AT = 60$ min, $UT = 1.0\,T$)
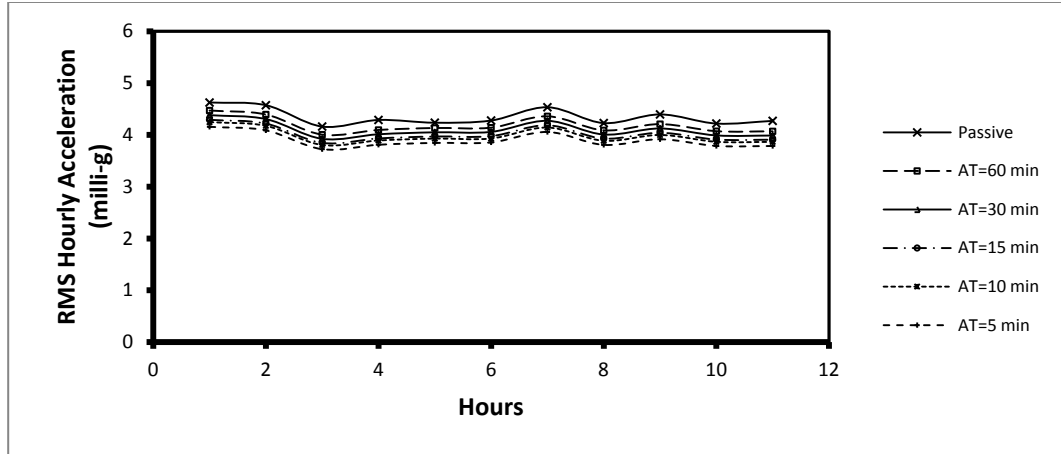
Fig. 5.16. RMS Hourly Structural Acceleration Response Values Resulting from the Passive and the Semi-Active Control Strategy for Various Averaging Time Values (AT) (S7-Random Force, $\mu = 3.5\%$, $UT = 1.0\ T$)
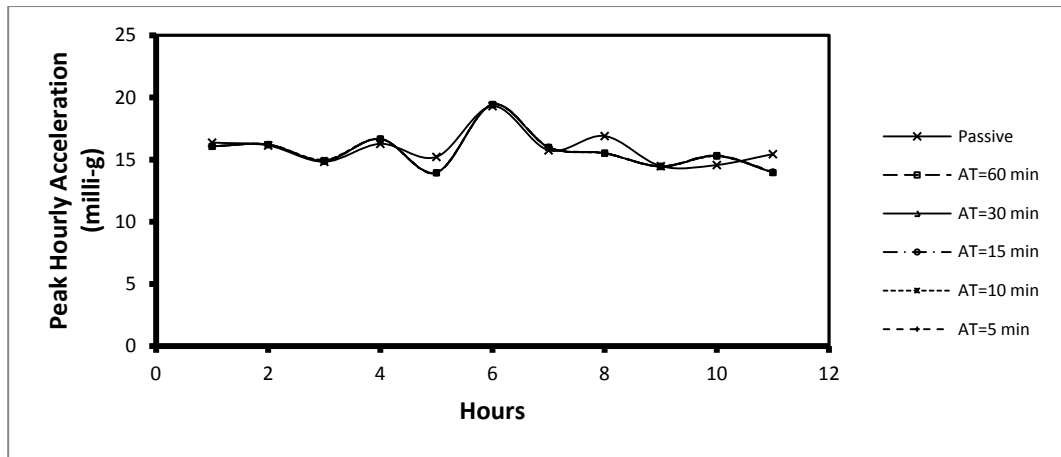
Fig. 5.17. Peak Hourly Structural Acceleration Response Values Resulting from the Passive and the Semi-Active Control Strategy for Various Averaging Time Values (AT) (S7-Random Force, $\mu = 3.5\%$, $UT = 1.0\ T$)
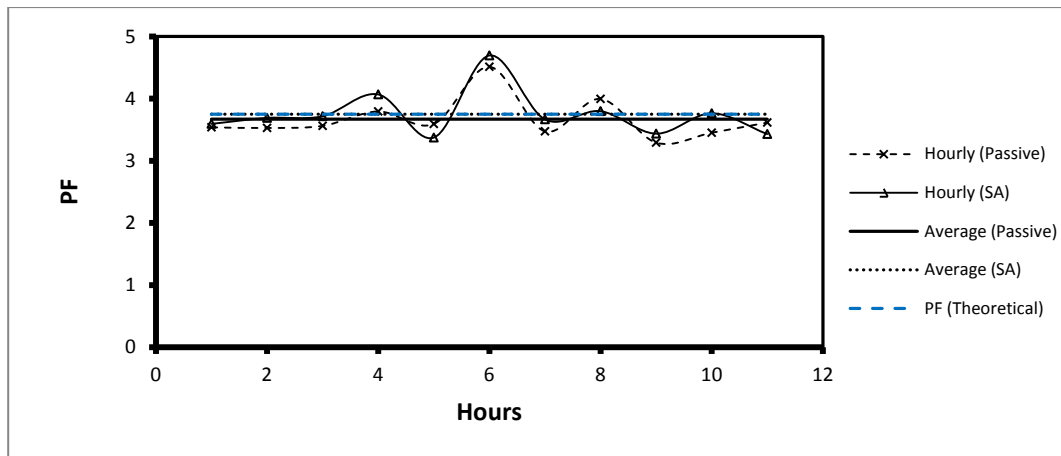
Fig. 5.18. Hourly and Average Peak Factor Values Resulting from the Passive and the Semi-Active Control Strategy ($AT = 60$ min, $UT = 1.0\ T$)
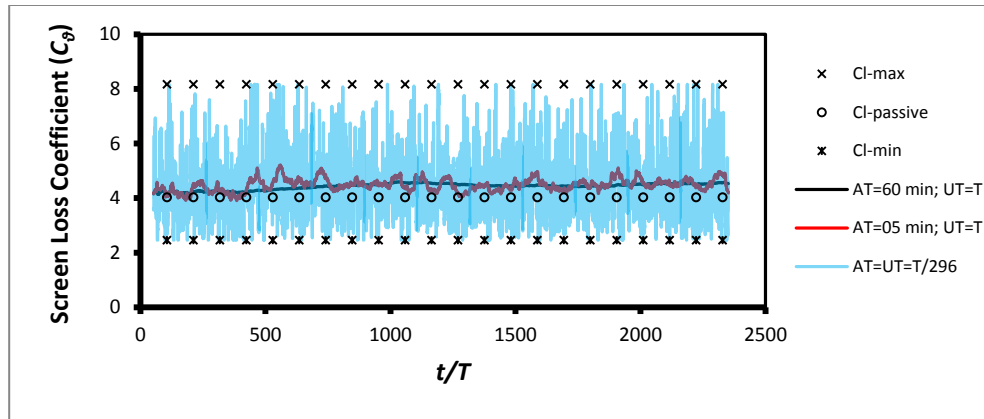
Fig. 5.19. Screen Loss Coefficient Values Resulting from the Passive and Semi-Active Control Strategy for Minimum and Maximum Studied Averaging Time Values (AT) Compared to the Instantaneous Control Case (S7-Random Force, $\mu = 3.5\%$)
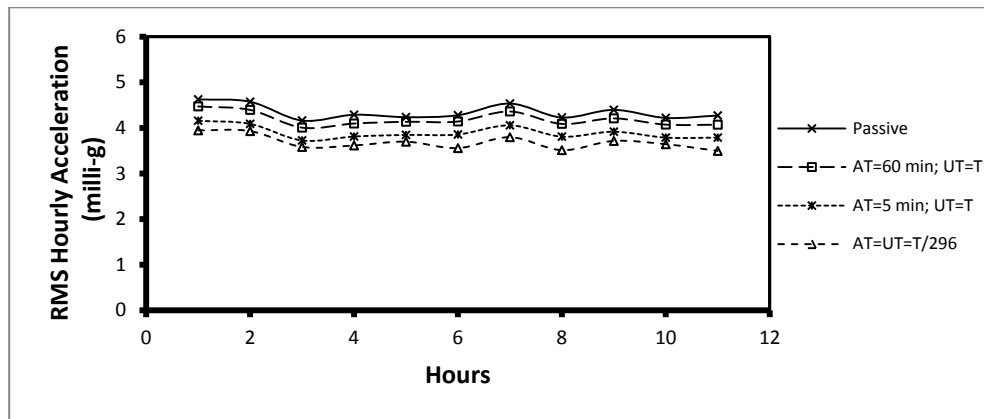
Fig. 5.20. RMS Hourly Structural Acceleration Response Values Using Passive and Semi-Active Control Strategies (S7-Random Force, $\mu = 3.5\%$)
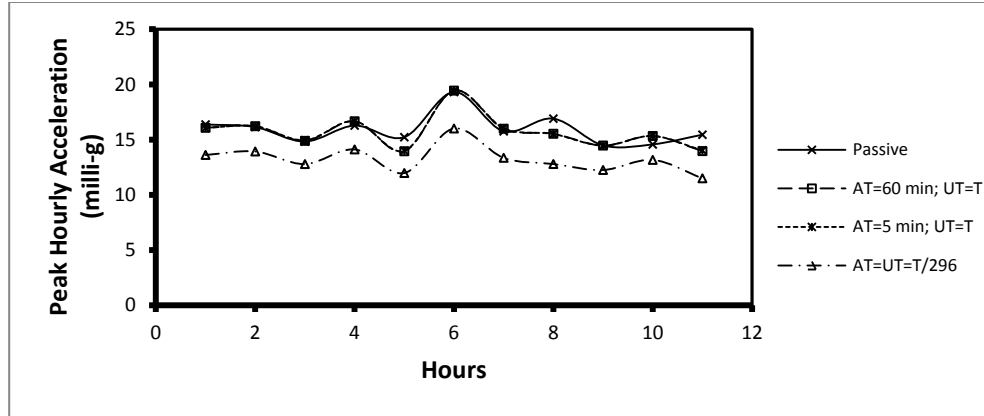
Fig. 5.21. Peak Hourly Structural Acceleration Response Values Using Passive and Semi-Active Control Strategies (S7-Random Force, $\mu = 3.5\%$)
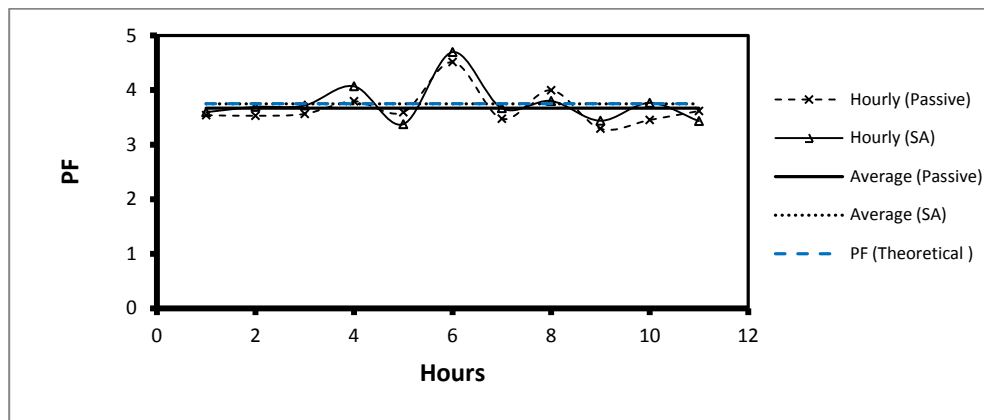
Fig. 5.22. Average Hourly and Peak Factor Values from the Passive and Semi-Active Control Strategy [$(AT = 60$ min, $UT = 1.0\,T)$ & $(AT = UT = T/296)$] (S7-Random Force, $\mu = 3.5\%$)
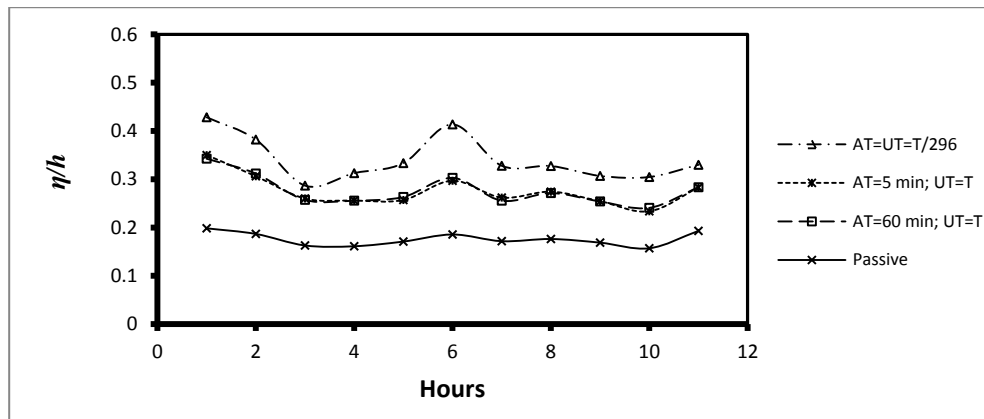
Fig. 5.23. Peak Hourly Fluid Response Ratio at the TLD End Wall Resulting Using Passive and Semi-Active Control Strategies (S7-Random Force, $\mu = 3.5\%$)
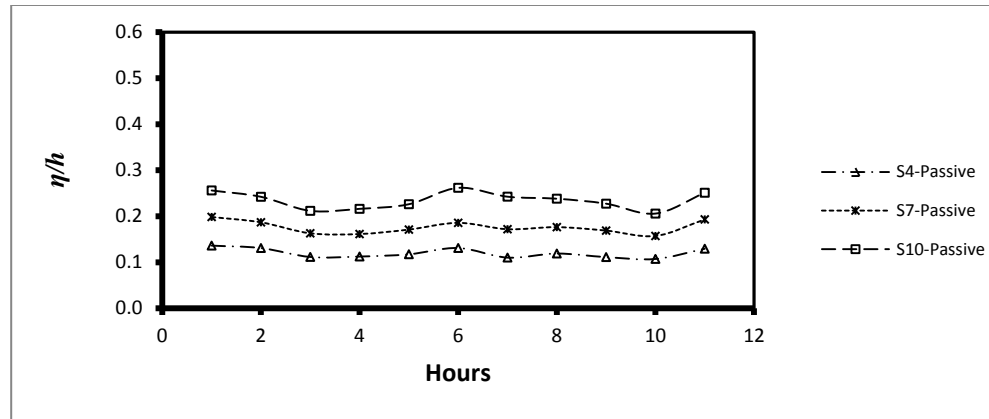
Fig. 5.24. Peak Hourly Fluid Response Ratio at the TLD End Wall Resulting from the Passive Control Strategy for Various Random Forces ($\mu = 3.5\%$)
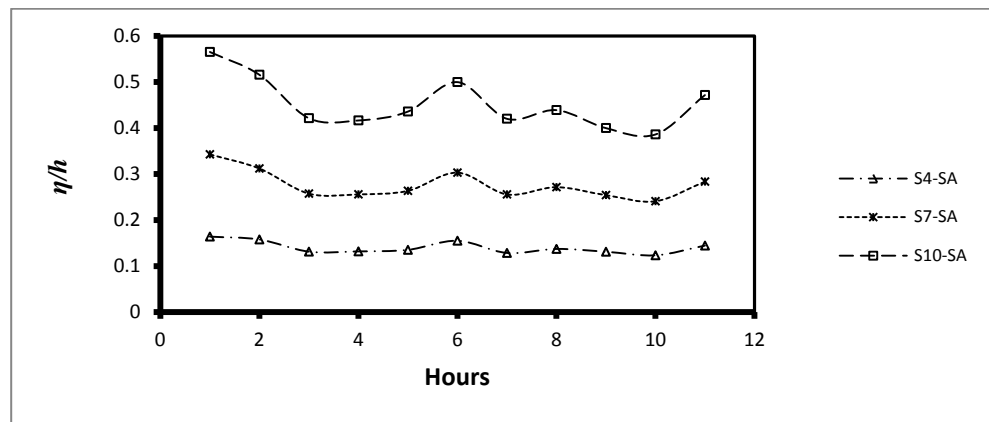
Fig. 5.25. Peak Hourly Fluid Response Ratio at the TLD End Wall Resulting from the Semi-Active Control Strategy for Various Random Forces ($\mu = 3.5\%,\ AT = 60$ min, $UT = 1.0\ T$)

Chapter 6: Applications of Multiple Semi-Active TLDs for Structural Control of Three Dimensional High-Rise Buildings Using Wind Tunnel Loads

6.1.   Introduction

Wind induced resonant vibration motions in tall buildings can be reduced using dynamic vibration absorbers (DVAs). The inertial forces, which develop from the DVA motion, modify the frequency response of the primary structure's mode to which the DVA is tuned to (Kareem et al. 1999; Tait et al. 2008). Housner et al. (1997) described different DVA systems utilized for structural control including active, semi-active, passive and hybrid systems.

Full-scale active control systems have been installed in several structures, mainly in Japan; however, cost effectiveness and reliability considerations have limited their wide spread acceptance (Spencer and Nagarajaiah 2003). Thus, there is a growing need for innovative and effective techniques to reduce the resonant vibration response of increasingly taller, lighter, and more flexible buildings. Due to their mechanical simplicity, low power requirements, and large controllable force capacity, semi-active control systems provide an attractive alternative to active and hybrid control systems. The use of tuned liquid dampers (TLDs) is still a relatively new concept compared to tuned mass dampers (TMD); however, they are a promising device for controlling the dynamic response of high-rise buildings (Kareem et al. 1999; Tait 2004). The implementation of passive TLDs in buildings has confirmed the benefits and effectiveness of this cost effective type of absorber. Therefore, expanding the novel semi-active TLD control system, developed and assessed in Chapter 5, to multiple semi-active TLDs for multi-modal high-rise building applications is of significant interest.

The aim of this study is to develop a three dimensional finite element structure semi-active multiple tuned liquid damper system model (3D-Structure-SA-MTLD) equipped with adjustable damping screen(s). Multiple TLDs provide the ability to suppress different critical vibration modes of the structure, while the semi-active control strategy keeps the inherent damping ratios (ζ_{TLD}) of all TLDs at a near optimal value ($\zeta_{TLD-opt}$).

The nonlinear fluid model, updated in Chapter 4, is used to simulate the damping screen(s) at different inclination angles (θ). Subsequently, the three dimensional finite element structure-TLD system model is used to conduct analyses on a high-rise building equipped with multiple semi-active TLDs.

The updated 3D-Structure-SA-MTLD system model is employed to investigate the response improvement of a high-rise building compared to a conventional passive TLD control system, studied in detail elsewhere (Chapter 3), over (1) a wide range of wind loading directions (θ_w) between 0° and 360° (see Section 6.5); (2) a wide range of serviceability and strength return period wind speeds between 1 month and 50 years (see Section 6.6).

To the best of the author's knowledge, no previous study has considered the simulation of a 3D-Structure-SA-MTLD system model accounting for the coupling of higher structural modes, utilizing wind tunnel loads, equipped with multiple TLDs operating efficiently over abroad range of wind loading angles and return period wind speeds.

In order to expand the use of the gain scheduling control strategy in a three dimensional high-rise building equipped with multiple semi-active TLDs (3D-Structure-SA-MTLD), the development of an alternative to the standard look-up table is desirable (see Figure 6.1). A TLD design procedure introduced by Tait (2008) allows a direct relationship between structural response acceleration and optimal screen angle value to be determined. This relationship, based on an H_2 optimized passive TLD, is employed to evaluate the required damping screen loss coefficient values (C_θ) for a multiple SA TLD system.

6.2.   A Brief Description of the High-Rise Building and Its Dynamic Characteristics

The Indianapolis building is a 38-story (154.6 m tall) reinforced concrete building with outer plan dimensions of 32 m by 54 m. This building was modelled and studied in Chapter 3 utilizing conventional passive TLDs. The lateral load resisting elements of the building are concrete shear walls. The stiffness disparity and non-coinciding centre of mass (CM) and centre of twist (CT) (see Figure 6.2) lead to a coupled lateral and torsional response. In addition, the applied wind loads from different directions cause high torsional action at certain wind angles (θ_w).

Figure 6.3 displays the first three mode shapes, which correspond to natural periods of 7.31, 6.18 and 3.01 seconds. The torsional component of the mode shapes is multiplied by the overall radius of gyration 18.8 m of the building to maintain dimensional consistency. It can be observed from Figure 6.3 that the structure has a dominate translational mode in the x-direction, a dominate translational mode in the y-direction and dominate torsional mode in the θ-direction with a small coupling action between the x- and y-directions.

6.3.   Response Evaluation High-Rise Building with No-TLDs

A dynamic analysis of the 38-story Indianapolis building was carried out employing the 3D-Structure-MTLD system model in Chapter 3 using recorded wind tunnel loads corresponding to a 10-year serviceability return period (see Figure 6.4 and Table 6.1). A total of 36 numerical simulation were conducted in order to cover different wind loading angles (θ_w) ranging from 0° to 360°. The root-mean-square (RMS) structural acceleration at the centre of mass (CM) and the four corners ($C1; C2; C3; C4$) of the building in the x- and y-directions ($\sigma_{\ddot{x}}; \sigma_{\ddot{y}}$) at the uppermost floor ($z = 154.6$ m) are determined. In addition, the RMS and average peak hourly resultant acceleration values ($R_{peak-hr}$) are calculated and compared to the acceptable serviceability limits. Both the RMS and $R_{peak-hr}$ values are expressed in terms of gravitational acceleration (milli-g).

Figures 6.5a and 6.5b show the RMS structural acceleration response values of the Indianapolis building in the x- and y-directions ($\sigma_{\ddot{x}}; \sigma_{\ddot{y}}$), respectively, for all wind loading angles (θ_w). In the x-direction, $\sigma_{\ddot{x}}$ values at the four corners and the centre of mass (CM) of the uppermost occupied floor of the building ($z = 154.6$ m) have both similar values and trends. A maximum $\sigma_{\ddot{x}}$ value of 6.31 milli-g is found to occur at a wind loading angle (θ_w) equal to 210°. In the y-direction, a maximum $\sigma_{\ddot{y}}$ value of 5.19 milli-g occurs at a 260° wind loading angle at corners 1 and 4 ($C1; C4$). These results are in agreement with the BLWTL report (BLWT-SS3-2007), which states that for strong winds, southwest directions are the most critical, i.e. $180° \leq \theta_w \leq 270°$ as θ_w equals 0° facing the north direction and increases in the clock-wise direction. The maximum calculated average peak hourly resultant acceleration response value ($R_{peak-hr}$) of 28.15 milli-g is found to occur at 210°, which is displayed in Figure 6.14a for comparative purposes with results of the controlled structural responses in Figure 6.14b. The calculated $R_{peak-hr}$ value is found to exceed the acceptable limits for wind-induced motion for a 10-year serviceability return period for residential buildings, hotels and office buildings. Acceptable limits corresponding to a 10-year serviceability return period are 10 to 15 milli-g for residential buildings, 15 to 20 milli-g for hotels and 20 to 25 milli-g for office buildings (Isyumov 1994).

6.4. Implementation of an Alternative to Look-Up Tables for Semi-Active Control Strategy

Yalla and Kareem (2003) described using a look-up table for a semi-active mode of control. The look-up table permits the range of the inclination angles (θ) of the damping screens, resulting in 100% TLD efficiency (ψ), to be identified for a selected mass ratio (μ). Gain scheduling is an open-loop control scheme with a nonlinear regulator whose parameters are modified as a function of the operating conditions in a pre-programmed way (Astrom and Wittenmark 1989). This type of control is commonly used in aerospace and process control applications. In Chapter 5, a modified gain scheduling technique, described by Yalla and Kareem (2003) and shown in Figure 6.1, was employed in a semi-active control scheme. In gain scheduling, the regulator parameters can be varied quickly in response to process dynamics. The process dynamics is the combined 3D-Structure-SA-TLD system model employed to evaluate the acceleration of the building at the semi-active TLD locations, the look-up table is the gain scheduler, the regulator is the controllable inclination of the inclined damping screen angles (θ) and the pressure loss coefficient (C_θ) is the parameter being changed.

In order to expand the use of the gain scheduling control strategy in a three dimensional high-rise building equipped with semi-active multiple TLDs (3D-Structure-SA-MTLD), an alternative to construction of look-up tables is investigated. The relationship between structural response acceleration and optimal screen loss coefficient for a TLD (Tait 2008) is employed in the semi-active control strategy in this section.

Using H_2 optimization, the optimal absorber damping ratio (for undamped primary structure) is expressed as

$$\zeta_{a-opt} = \sqrt{\frac{\mu+\frac{3}{4}\mu^2}{4+6\mu+2\mu^2}} \tag{6.1}$$

where μ is the mass ratio.

The ratio of the relative motion between the absorber (σ_r) and the structure (σ_x) is defined as

$$R = \frac{\sigma_r}{\sigma_x} \tag{6.2}$$

For an optimally designed absorber, the relative motion ratio is given as

$$R_{opt} = \frac{1+\mu}{\sqrt{2\mu+\frac{3}{2}\mu^2}}$$

(6.3)

For a TLD equipped with screens, the generalized damping ratio (ζ_{TLD}) is given by (Tait 2008)

$$\zeta_{TLD} = C_{l-x}\sqrt{\frac{32}{\pi^3}}\tanh^2\left(\frac{\pi h}{L_x}\right)\Delta\Xi\frac{\sigma_r}{L}$$

(6.4)

Relating the modal acceleration to displacement

$$\sigma_x = \frac{\sigma_{\ddot{x}}}{\omega_x^2}$$

(6.5)

and substituting Equation 6.5 into Equation 6.2, the following relationship is obtained

$$\sigma_r = R_{opt}\frac{\sigma_{\ddot{x}}}{\omega_x^2}$$

(6.6)

Thus, the optimal screen loss coefficient (C_{l-opt}) can be determined setting Equation 6.4 equal to Equation 6.1.

Finally, once C_{l-opt} has been determined, the corresponding screen angle (C_{l-opt}) can be calculated using the following relationship

$$C_\theta = C_l\left(0.46\theta^3 - 1.05\theta^2 - 0.06\theta + 1\right)$$

(6.7)

where C_l is the loss coefficient corresponding to the screen in its vertical position and C_θ is set equal to C_{l-opt}.

As a result, gain scheduling becomes an efficient control scheme for maintaining the TLD inherent damping ratios (ζ_{TLD}) at near optimum values ($\zeta_{TLD-opt}$) for multiple semi-active TLDs. As a result, for given structural acceleration responses at the semi-active TLD locations, the pressure loss coefficients (C_θ) are changed in accordance with the expanded TLD design procedure. The study assumes that mechanisms exist to adjust the damping screens to the desired screen inclination values (θ).

Modal factor values (MF) presented in Chapter 3 are used to evaluate the target modal RMS acceleration response values ($\sigma_{\ddot{x}-target-m1}$; $\sigma_{\ddot{y}-target-m2}$) utilizing the initial modal RMS acceleration response values ($\sigma_{\ddot{x}-initial-m1}$; $\sigma_{\ddot{y}-initial-m2}$), which are calculated during the numerical simulation in real time. This procedure was selected in order to maintain consistency with the process employed in Chapter 3. It is recognized that filtering techniques

could be employed to extract the modal response contributions (MF); however, this is beyond the scope of this study.

Consequently, at every updating time step (UT) during the entire time history, $\sigma_{\ddot{x}-initial-m1}$ and $\sigma_{\ddot{y}-initial-m2}$ are calculated simultaneously for all installed TLDs utilizing the 3D-Structure-SA-MTLD system model over a selected averaging time period (AT) at all TLD locations (see Table 6.3) and used as feedback in the numerical simulation over a selected updating time period (UT). Subsequently, the optimal inclination angle values (θ) of the damping screens are updated using Equation 6.7. These steps are repeated, and updated screen loss coefficient values (C_θ) are evaluated during the entire time history keeping the TLD inherent damping ratios (ζ_{TLD}) for all TLDs at their optimal values ($\zeta_{TLD-opt}$). A detailed example for designing semi-active TLDs to suppress the first three modes of the Indianapolis building is presented in the next section utilizing the modal contribution response components (MF) and the expanded TLD design procedure (Chapter 3).

6.4.1 Design Procedure and Damping Screen Loss Coefficient Range Selection for a Semi-Active TLD Control Strategy

In this section, TLDs are initially designed according to structural response values occurring at the critical wind loading direction (θ_w) of 210° for a 10-year serviceability return period wind speed. A mass ratio value (μ) of 6% is selected for the first and second modes of vibration, while a mass ratio value (μ) of 5% is selected for the third mode of vibration in this study. This permits direct comparisons between the semi-active TLD control system, utilized in this chapter, and the conventional passive TLD control system, utilized in Chapter 3, to be made.

It is recommended that for semi-active TLDs to suppress different building vibration modes, TLD damping screens be designed and constructed [i.e. the selection of screen solidity ratio (S)] to achieve their initially evaluated C_θ values (see Sections 6.4.1.1 and 6.4.1.2) at the mid-range between the minimum and maximum damping screen loss coefficient values (C_{l-min}; C_{l-max}). Therefore, for reduced structural response amplitudes either produced at different wind loading angles (θ_w) or at lower return period wind speeds, the damping screens are rotated to lower inclination angle values (θ) to increase their loss coefficient values (C_θ) until the damping screens reach a vertical position, where $\theta = 0°$ and $C_\theta = C_{l-max}$. In contrast, for increased structural response amplitudes due to higher return

period wind speeds, the damping screens are rotated to higher inclination angle values (θ) to decrease their loss coefficient values (C_θ) until the damping screens reach their maximum inclination position, where $\theta_{max} \approx 65°$ and $C_\theta = C_{l-min}$. Accordingly, TLD inherent damping ratio values (ζ_{TLD}) can be kept at their optimal values ($\zeta_{TLD-opt}$) over a wide range of structural response amplitudes.

6.4.1.1   Semi-Active TLD Design Procedure for the First Two Modes of Vibration

The TLDs placed at the centre of mass (CM) of the uppermost occupied floor of the Indianapolis building ($z = 154.6$ m) are designed to suppress the first two vibration modes that are translational in the x- and y-directions. This is consistent with the TLD design layout used in Chapter 3. However, uni-directional tanks are employed to allow straight forward implementation of the adjustable screens.

Initial modal RMS structural accelerations response values ($\sigma_{\ddot{x}-initial-m1}$; $\sigma_{\ddot{y}-initial-m2}$) of 6.0 milli-g and 3.4 milli-g at CM at the critical wind loading angle (θ_w) of 210° lead to target RMS structural acceleration response values ($\sigma_{\ddot{x}-target-m1}$; $\sigma_{\ddot{y}-target-m2}$) of 3.1 milli-g and 1.8 milli-g for a selected mass ratio value (μ_x; μ_y) of 6% in the x- and y-directions, respectively. Since the target modal response values are based on an optimal passive TLD design procedure, TLDs target values match the target values presented in Chapter 3. The total target RMS acceleration response values are estimated to be $\sigma_{\ddot{x}-target-t} = 3.2$ milli-g and $\sigma_{\ddot{y}-target-t} = 2.0$ milli-g in the x- and y-directions and are presented in Figures 6.5a and 6.5b, respectively.

The screens loss coefficient values (C_{l-x}; C_{l-y}) are evaluated to achieve the optimal damping ratio values ($\zeta_{TLD-opt_x}$; $\zeta_{TLD-opt_y}$). Table 6.4 shows the calculation steps utilized in the preliminary TLD design procedure (Tait 2008) of the uni-directional tanks aligned in the x-direction, while the same procedure is repeated for the TLDs in the y-direction and is listed in Table D1 (Appendix-D). The screens are located at 40% and 60% of the tank length with loss coefficient values of $C_{l-x} = 9.8$ and $C_{l-y} = 20.3$. The uni-directional tank length dimensions are established as $L_x = 16.0$ m, $L_y = 13.4$ m with a water depth $h = 1.9$ m.

Equation 6.7 is used to evaluate the screen loss coefficient range and subsequently the solidity ratio, by setting the calculated C_{l-x} and C_{l-y} values near to the average value of

C_{l-min} and C_{l-max}. As a result, screen loss coefficient values of $C_{lx-min_1} = 5.0$ and $C_{lx-max_1} = 15.0$ are calculated for the x-direction, which correspond to damping screen inclination angle values (θ_{x_1}) of $\theta_{x-max_1} = 58.5°$ and $\theta_{x-min_1} = 0°$. Also, screen loss coefficient values of $C_{ly-min_2} = 10.0$ and $C_{ly-max_2} = 30.0$ are determined in the y-direction, which correspond to inclination angle values (θ_{y_2}) of $\theta_{y-max_2} = 58.5°$ and $\theta_{y-min_2} = 0°$. As a result, the screen loss coefficient values $(C_{\theta x_1}; C_{\theta y_2})$ of 9.8 and 20.3 occur at screen inclination angle values $(\theta_{x_1}; \theta_{y_2})$ of 36.7° and 35.1°, respectively.

6.4.1.2   Semi-Active TLD Design Procedure for the Third Mode of Vibration

In this section, TLDs to suppress the third mode of vibration of the Indianapolis building are designed and installed in the building utilizing a mass ratio value (μ) of 5%. As improved performance is the focus of this study, design parameters consistent with those in Chapter 3 resulting from adjustable damping screens, such as TLD placement and initial and target response values, are used.

Hence, TLDs to suppress the third mode of the Indianapolis building are installed at corners $C3$ and $C4$ in the x-direction and corners $C2$ and $C3$ in the y-direction. The procedure followed to design the uni-directional tanks to suppress the third vibration mode in the x- and y-directions is presented in Tables D2 and D3 (Appendix-D), respectively. A total of 4 sets of 11 uni-directional tanks with dimensions of $L_x = L_y = 3$ m and $h = 0.4$ m are required to satisfy the mass ratio value (μ) using the water mass calculations presented in Table D4 (Appendix-D). It is common to utilize dozens or even hundreds of small TLD tanks to satisfy the required mass ratio (Tamura et al. 1995; Love et al. 2011). The tanks can be placed and arranged to keep space requirements to a minimum.

Based on the modal target RMS acceleration values $\sigma_{\ddot{x}-target-m3} = 0.8$ milli-g and $\sigma_{\ddot{y}-target-m3} = 2.0$ milli-g, screen loss coefficient values of $C_{\theta x_3} = 35.3$ and $C_{\theta y_3} = 14.1$ are required. The screens are located at 40% and 60% of the tank length. Equation 6.7 is used to evaluate the screen loss coefficient range for the semi-active TLD control strategy. This results in screen loss coefficient values $(C_{\theta x_3})$ ranging between $C_{lx-min_3} = 15.0$ and $C_{lx-max_3} = 55.0$ for the third mode tanks placed in the x-direction and corresponding to damping screen inclination angle values (θ_{x_3}) between $\theta_{x-max_3} = 63.3°$ and $\theta_{x-min_3} = 0°$, respectively. Consequently, $C_{\theta y_3}$ values between $C_{ly-min_3} = 7.0$ and $C_{ly-max_3} = 22.0$ are

established for the third mode tanks placed in the y-direction, which correspond to θ_{y_3} values between $\theta_{y-max_3} = 59.6°$ and $\theta_{y-min_3} = 0°$, respectively. Therefore, screen loss coefficient values ($C_{\theta x_3}$; $C_{\theta y_3}$) of 35.3 and 14.1, obtained above from the initial TLD design, occur at screen inclination angle values (θ_{x_3}; θ_{y_3}) of 37.4° and 37.3°, respectively.

6.4.2 Sensitivity Analysis for Averaging Time (AT) and Updating Time (UT) and Damping Screen Loss Coefficient Range Selection Checks

With the aim of selecting the two parameter values, the averaging time (AT) and the updating time (UT), a sensitivity analysis is performed in this section. The Indianapolis building is equipped with semi-active TLDs to suppress the first three modes of vibration, designed in Section 6.4.1, and subjected to the wind tunnel loading history recorded at the critical wind loading angle (θ_w) of 210° utilizing a 10-year serviceability return period wind speed. Consequently, the 3D-Structure-SA-MTLD is employed to conduct the dynamic analysis of the Indianapolis building considering an updating time value, $UT = 1.0\ T$ (i.e. $UT = 7.31$ seconds) and utilizing different averaging time values (AT) equal to 15, 30 and 60 minutes.

Figure 6.6 shows the variation of the modal RMS structural acceleration response calculated every updating time period (UT) and over different selected averaging time values (AT) at the TLD location to suppress mode 1 in the x-direction. Employing the preliminary TLD design procedure at every updating time period (UT), C_θ values for TLDs installed to suppress first structural vibration mode are evaluated based on the modal RMS acceleration values and used in the numerical simulation, in real time, as shown in Figure 6.7.

It can be observed from Figure 6.6 that for all selected averaging time values (AT), lower modal RMS structural acceleration response values, utilizing the semi-active TLD control system, are achieved compared to that predicated for the passive TLD control system employed in Chapter 3. This can be attributed to the differences found between the constant and updated damping screen loss coefficient values utilized to feedback the numerical simulation of the conventional passive and semi-active TLD control systems, respectively, during the entire time history as shown in Figure 6.7.

Also, Figure 6.6 shows that utilizing small AT values lead to low total and modal RMS structural acceleration response values with maximum percentage difference found equal to

10% at minutes 22 and 25 of the time history for TLDs installed in the x- and y-directions, respectively, while small percentage differences in the range between 1% and 5% are found for the remaining of the time history. These results are in agreement with those obtained in Section 5.3.3 utilizing a 3D single-story structure. In contrast, utilizing high AT values result in a reduction in the modal structural response values and the damping screen loss coefficient values (see Figure 6.7). In addition, Figure 6.7 shows that the selected range of C_θ values for the first TLD mode tanks are valid as all C_θ values are found in the range between C_{l-min} and C_{l-max} at the critical wind loading direction (θ_w) of 210°. The same trend and behaviour are obtained for the tanks installed to suppress mode 2 in the y-direction and mode 3 in the x- and y-directions (see Figures D1-D6 Appendix-D). Therefore, a 60-minute AT value is selected for use in the remainder of this study.

A second sensitivity analysis is performed utilizing the 3D-Structure-SA-MTLD system model to study the effect of various updating time value (UT) on the RMS structural response results. Different UT values of $0.25\,T$, $1.00\,T$ and $8.00\,T$ (i.e. $1.8 < UT < 58.5$ seconds) are selected to conduct the sensitivity analysis setting the averaging time value (AT) equal to 60 minutes. Figure 6.8 shows the modal RMS structural acceleration response values remain constant for different selected UT values at the location of TLDs to suppress mode 1 in the x-direction. The same trend and behaviour are obtained for mode 2 in the y-direction and mode 3 in the x- and y-directions (see Figures D7-D12 Appendix-D). Results for the high-rise building are found to be in agreement with that obtained for the single-story structure studied in Chapter 5 (see Section 5.3.3). Therefore a UT value equal to $1.00\,T$ is selected to be used for the remainder of this study.

6.5. Improved Responses of an Actual High-Rise Building Utilizing Multiple SA-TLDs Over a Range of Wind Loading Directions

This section investigates the potential of improved efficiency by employing the semi-active TLD control system to control the high-rise building responses subjected to a wide range of wind loading directions (θ_w) compared to the conventional passive TLD control system in Chapter 3.

A total of 36 two-hour numerical simulations are conducted in this section by employing the 3D-Structure-SA-MTLD system model with selected AT and UT values equal to 60 minutes and $1.0\,T$, respectively, utilizing the recorded wind loading directions in the range

between 0° and 360°. The semi-active TLD tank geometries for the first three modes of vibration to be suppressed, which have been presented in Section 6.4.1, match those of the conventional passive TLD tanks utilized in Chapter 3 (i.e. L, b, h, damping screens properties (S), TLD locations, and the mass ratios (μ) for all mode tanks). The damping screen loss coefficient values $C_{\theta x_1}$, $C_{\theta y_2}$, $C_{\theta x_3}$ and $C_{\theta x_3}$ for mode 1 in the x-direction, mode 2 in the y-direction, mode 3 in the x-direction and mode 3 in the y-direction, respectively, are set by the semi-active TLD control strategy to be within the ranges selected in Section 6.4.1 as follows

$$C_{lx-min_1} \leq C_{\theta x_1} \leq C_{lx-max_1}; \text{i.e. } 5 \leq C_{\theta x_1} \leq 15 \tag{6.8}$$

$$C_{ly-min_2} \leq C_{\theta y_2} \leq C_{ly-max_2}; \text{i.e. } 10 \leq C_{\theta y_2} \leq 30 \tag{6.9}$$

$$C_{lx-min_3} \leq C_{\theta x_3} \leq C_{lx-max_3}; \text{i.e. } 15 \leq C_{\theta x_3} \leq 55 \tag{6.10}$$

$$C_{ly-min_3} \leq C_{\theta y_3} \leq C_{ly-max_3}; \text{i.e. } 7 \leq C_{\theta y_3} \leq 22 \tag{6.11}$$

Results from the numerical simulations show that the maximum uncontrolled RMS structural acceleration response values ($\sigma_{\ddot{x}-initial}$; $\sigma_{\ddot{y}-initial}$) of 6.3 milli-g and 4.2 milli-g (see Figures 6.5a and 6.5b) at the critical wind loading direction (θ_w) of 210° are reduced to values of 3.4 milli-g and 3.8 milli-g, utilizing the conventional passive TLD control system (see Figures 6.10a and 6.11a), compared to values of 2.9 milli-g and 2.6 milli-g, utilizing the semi-active TLD control system, respectively (see Figures 6.10b and 6.11b).

In addition, at different wind loading angles (θ_w), it can be observed that further reductions in the structural accelerations are achieved utilizing the semi-active TLD control system compared to the conventional passive TLD control system in the x- and y-directions as shown in Figures 6.10 and 6.11, respectively (note that all conventional passive TLDs were designed to achieve their optimal design parameters according to the critical wind loading angle of 210°). As a result, RMS resultant acceleration response values (R_{RMS}), calculated using Equation 6.12 and presented in Figure 6.12, are reduced by a nearly constant percentage range between 40-50% $\mp 5\%$, calculated using Equation 6.13 and presented in Figure 6.13

$$R_{RMS} = \sqrt{(\sigma_{\ddot{x}})^2 + (\sigma_{\ddot{y}})^2} \tag{6.12}$$

$$\% \ \Psi_{RMS} = \left(\frac{R_{RMS(No-TLD)} - R_{RMS(with\ TLD)}}{R_{RMS(No-TLD)}}\right).100 \tag{6.13}$$

where $R_{RMS(with\ TLD)}$ and $R_{RMS(No-TLD)}$ are the RMS resultant acceleration response values with and without TLDs installed, respectively.

Criteria for acceptable wind-induced motions are related to human perception thresholds, which are calculated using a probabilistic approach and experimental evaluation. Based on this concept, the Boundary Layer Wind Tunnel Laboratory (BLWTL) has recommended the following criteria for acceptable accelerations in a 10-year serviceability return period: 10 to 15 milli-g for residential buildings, 15 to 20 milli-g for hotels and 20 to 25 milli-g for office buildings (Isyumov 1994). The serviceability criteria in the National Building Code of Canada (NBC) only address inter-story drift; therefore, serviceability criteria dictated by the BLWTL are taken as the acceptable limits. Hence, for all wind loading angles (θ_w), the controlled average peak hourly resultant acceleration response values ($R_{peak-hr}$) are presented compared to the uncontrolled responses in Figures 6.14c and 6.14a, respectively. It can be noticed that the maximum uncontrolled $R_{peak-hr}$ value is reduced from a value of 28.2 milli-g to a value of 13.6 milli-g at the critical wind loading angle (θ_w) of 210° achieving a percentage response reduction value (Ψ_{RMS}) of 51%. This is also a significant improvement over the passive system peak response acceleration of 18.9 milli-g as shown in Figure 6.14b. As a result, utilizing the semi-active TLD control system is found to satisfy wind-induced serviceability levels for residential buildings compared to the hotel serviceability requirements achieved utilizing conventional passive TLDs (Chapter 3).

6.5.1 Investigation of SA-TLDs Response History Over a Range of Wind Loading Directions

In this section, the semi-active TLD response histories at selected wind loading directions (θ_w), which produce various average peak hourly resultant acceleration response levels ($R_{peak-hr}$) of the Indianapolis building, are studied. This allows a detailed picture of the semi-active TLD response behaviour over a wide range of wind loading directions (θ_w) to be examined. As the SA-TLDs are placed either in the x- or y-direction, therefore, their responses are controlled by the modal structural response component in these directions. As a result, criteria for selecting wind loading directions to be studied in this section are set as the wind loading angles (θ_w) that produce the minimum, maximum and approximately mid-range RMS structural acceleration response values in the x- and y-directions ($\sigma_{\ddot{x}}$; $\sigma_{\ddot{y}}$). Consequently, wind loading angle values (θ_w) of 60°, 150° and 210° are selected from

Figure 6.5a, while wind loading angle values (θ_w) of 60°, 180° and 260° are selected from Figure 6.5b. These selected wind loading angles produce different peak levels of $R_{peak-hr}$ in the range between the upper and lower $R_{peak-hr}$ values.

6.5.1.1 Response History of SA-TLDs for Mode 1 in the x-Direction

Figure 6.15 shows the first modal RMS acceleration response component values used to evaluate the damping screen loss coefficient values ($C_{\theta x_1}$). Figure 6.16 shows the evaluated screen loss coefficient values ($C_{\theta x_1}$) utilized in the numerical simulation during the entire time history. It can be noticed from Figure 6.16 that at critical wind loading angle (θ_w) of 210°, the semi-active TLDs are fully-efficient [i.e. the damping screen loss coefficient value ($C_{\theta x_1}$) remains within the C_{lx-min_1} to C_{lx-max_1} range].

The constant damping screen loss coefficient value ($C_{lx-passive_1}$) of 9.8 is near the $C_{\theta x_1}$ values obtained for the first 10 minutes of the response history, while a difference if approximately 20% is found throughout the rest of the time history. This is attributed to the reduced modal RMS structural response at the TLD location due to higher efficiency (ψ) of the installed semi-active TLDs compared to the conventional passive TLDs. This is found to be in agreement with the study utilizing a single-story structure studied in Chapter 5 (see Section 5.5). Therefore, good agreement was found between both $C_{\theta x_1}$ and $C_{lx-passive_1}$ during the first 10 minutes of the response history before further structural response reduction is achieved leading to higher $C_{\theta x_1}$ values.

For the wind loading angle (θ) of 180°, the semi-active TLDs are found to remain fully-efficient except a during few time periods (between 5-10 minutes, 25-30 minutes and 95-100 minutes) as shown in Figure 6.16, where the structural response values are found to be small. Although, all screen loss coefficient values ($C_{\theta x_1}$) are set by the semi-active control strategy to their maximum values (C_{lx-max_1}) of 15.0 at wind loading angles (θ) of 60°, 150° and 260°, the semi-active TLDs efficiency (ψ) is found higher than its counterpart value of the conventional passive TLDs due to a significant difference between damping screen loss coefficient value ($C_{lx-passive_1}$) of 9.8 of the conventional passive TLD and its semi-active counterpart value ($C_{\theta x_1} = C_{lx-max_1}$) of 15.0.

By shifting the selected damping screen loss coefficient range higher in order to include the $C_{\theta x_1}$ values at wind loading angles of 60°, 150° and 260°, higher TLD efficiency (ψ) could be obtained. However, there are two important reasons to maintain the selected range of $C_{\theta x_1}$ values. First, the structural acceleration response values at these wind loading angles are small and, therefore, do not require the semi-active TLDs to be fully-efficient (i.e. achieving an efficiency value (ψ) of 100%). Secondly, in order for the semi-active TLDs to be fully-efficient at higher structural acceleration response values considering higher return period wind speeds, low $C_{\theta x_1}$ values are required (see Section 6.6).

6.5.1.2   Response History of SA-TLDs for Mode 2 in the y-Direction

The semi-active TLDs to suppress the second mode of vibration are found to be fully-efficient during the entire 2-hour time history at all wind loading angles (θ_w) considered, except at wind loading angle (θ_w) equal to 60°. Fluctuations in the screen loss coefficient values for mode 2 tanks ($C_{\theta y_2}$) in Figure 6.17 is found to be higher than for mode 1 tanks ($C_{\theta x_1}$) in Figure 6.16. This is attributed to the higher fluctuations in modal RMS structural acceleration response values in the y-direction (see Figure D13 Appendix-D) compared to the x-direction (see Figure 6.15).

6.5.1.3   Response History of SA-TLDs for Mode 3 in the x- and y-Directions

The semi-active TLDs placed at corners $C3$ and $C4$ in the x-direction are fully-efficient at wind loading angels of 150°, 180°, 210° and 260° as shown Figure 6.18. In contrast, upright position of the damping screens is set by the semi-active TLD control strategy for the TLDs at wind loading angle of 60° (i.e. $C_{\theta x_3} = C_{lx-max_3}$). Also, it can be observed that $C_{\theta x_3}$ values resulting from the semi-active TLD control strategy (see Figure 6.18) are higher than their counterpart values resulting in the y-direction ($C_{\theta y_3}$) (see Figure 6.19). In the y-direction, the semi-active TLDs placed at corners $C2$ and $C3$ are fully-efficient during the entire time history at wind loading angles of 180°, 210° and 260°, while damping screens are set to their vertical position at wind loading angles of 60° and 150°. As a result, a maximum damping screen loss coefficient value of 22.0 (i.e. $C_{\theta y_3} = C_{ly-max_3}$) is utilized at these wind angles compared to its counterpart value of 14.1 utilized in the conventional passive TLD control system, which was designed for a different wind loading angle (θ_w) equal to 210° (see Figure 6.19).

6.6. Improved Responses of an Actual High-Rise Building Utilizing Multiple SA-TLDs Over a Range of Mixed Return Periods

In this section, a study on an actual high-rise building (Indianapolis building) both without and with TLDs utilizing the semi-active TLD control strategy is conducted over a wide range of serviceability and strength (mixed) return period wind speeds at the critical wind loading direction (θ_w) of 210° employing the 3D-Structure-SA-MTLD system model. This allows the semi-active TLD efficiency to be examined for both strength and serviceability wind speeds. Also, a performance comparison between the conventional passive and semi-active TLD control systems is conducted over the considered range of return periods.

For strength related issues, such as design loads and cladding pressure zones, the boundary layer wind tunnel laboratory (BLWTL) wind climate model is scaled (see Figure 6.4) to match the wind speed requirement in ASCE-7-05 (see Chapter 3 for additional details). Therefore, a 50-year strength return period is found equal to 47.5 m/s using the upper curve plotted in Figure 6.4. This curve represents the design wind speeds in the Indianapolis area as recommended by the wind tunnel study (BLWT-SS3-2007) and ASCE 7-05. Table 6.1 shows different wind speed values corresponding to different return period wind speeds utilized in this study.

For serviceability related issues, the semi-active TLDs, which were originally designed for a serviceability return period of 10 years (see Section 6.4.1), are employed in this section to examine their efficiency at serviceability return periods ranging from 1 month to 50 years, in addition to an extreme wind speed value that is equivalent to a strength related return period wind speed of 50 years, which exceeds a 1000-year serviceability return period (see Figure 6.4).

In addition, a dynamic analysis of the Indianapolis building is conducted over the same selected range of mixed return periods utilizing the conventional passive TLD control system, which was designed at the critical wind loading angle (θ_w) of 210° at the 10-year serviceability return period with tanks of the same geometries (i.e. L, b, h), damping screens properties (S) and mass ratio values (μ) for the first three modes as of the semi-active TLD control system. Consequently, percentage response reduction values of the resultant RMS and average peak hourly structural acceleration response values (R_{RMS}; $R_{peak-hr}$) are

determined to permit a direct comparison between both TLD control systems. Finally, the response behaviour of the semi-active TLDs over the studied range of return period wind speeds is investigated for each mode tank during the entire time history.

6.6.1 Response Evaluation with No-TLDs

The 3D finite element model is employed in this section to conduct a dynamic analysis of the Indianapolis building utilizing mixed return period wind speeds (see Table 6.1) recorded at the BLWTL (BLWT-SS3-2007) at the critical wind loading angle (θ_w) of 210°. The result is RMS and average peak hourly resultant acceleration response values (R_{RMS}; $R_{peak-hr}$) of the centre of mass (CM) and the four corners ($C1$; $C2$; $C3$; $C4$) at the uppermost floor ($z = 154.6$ m) of the Indianapolis building. Consequently, ranges of uncontrolled R_{RMS} and $R_{peak-hr}$ values between 2.5-17.0 milli-g and 9.5-62.0 milli-g are determined from the dynamic analysis and presented in Figures 6.20a and 6.22a, respectively. It can be noticed that a nonlinear increase of the building responses is found to occur and is related to the increase in wind speed, especially when a linear elastic 3D structure model is considered in all simulations as recommended in wind-type analyses. This can be attributed to the change of the frequency content of the wind, which is accompanied by the change of the wind speeds. In fact, the fluctuations in the wind can be thought of as resulting from a composite of sinusoidally varying winds superimposed on the mean steady wind, which varies along the building's height (see Figure 6.23). Theses sinusoidal variations have a variety of frequencies, amplitudes and phases that change with the wind speed (van der Tempel 2006; Manwell et al. 2010). The resulting structural acceleration response values are found to increase by nearly an order of magnitude at the 50-year strength return period compared to the 50-year serviceability return period achieving R_{RMS} values of 17.0 and 8.0 milli-g, and $R_{peak-hr}$ values of 62.0 milli-g and 32.5 milli-g, which correspond to wind speed values of 47.5 m/s and 34.0 m/s, respectively.

6.6.2 Response Evaluation Utilizing Semi-Active and Conventional Passive TLD Control Systems

In this section, two sets of analyses are conducted on the Indianapolis building over a range of mixed return period wind speeds, listed in Table 6.1, at the critical wind loading angle (θ_w) of 210° utilizing the conventional passive and semi-active TLD control systems. Subsequently, the 3D-Structure-MTLD and 3D-Structure-SA-MTLD system models are used

to conduct this analysis, where the first 3 modes of vibration are suppressed. The result is resultant RMS structural acceleration response values (R_{RMS}) for the centre of mass (CM) and the four corners ($C1$; $C2$; $C3$; $C4$) at the uppermost floor ($z = 154.6$ m) of the Indianapolis building, using Equation 6.11, equipped with both TLD control systems separately. Consequently, percentage response reduction values (Ψ_{RMS}) of R_{RMS} are determined, using Equation 6.12. Therefore, a direct comparison between both TLD control systems is conducted in the next section.

It can be seen that uncontrolled resultant RMS acceleration response values in the range of 2.5 milli-g to 17.0 milli-g (see Figure 6.20a) are reduced to values between 1.2 milli-g and 8.0 milli-g (see Figure 6.20b) utilizing the semi-active TLD control system. As a result, minimum percentage response reduction values (Ψ_{RMS}) of R_{RMS} ranging between 46% and 50% are achieved at the 1-month serviceability return period, while maximum percentage response reduction values (Ψ_{RMS}) ranging between 50% and 53% are observed at the 10-year serviceability return period. This leads to nearly constant percentage response reduction values (Ψ_{RMS}) of R_{RMS} over the considered mixed return periods utilizing the semi-active TLD control system (i.e. variation range $\approx$ 3-4%, see Figure 6.21b) compared to considerable differences of Ψ_{RMS} values (i.e. variation range $\approx$ 18-19%, see Figure 6.21a) utilizing the conventional passive TLD control system. Also, the calculated uncontrolled average peak hourly resultant acceleration response values ($R_{peak-hr}$), calculated using Equation 6.1, which are found to range between 9.5 milli-g to 62.0 milli-g (see Figure 6.22a) are reduced to values in the range between 5.0 milli-g and 30.5 milli-g utilizing the semi-active TLD control system (see Figure 6.22b). It can be noticed that the maximum uncontrolled $R_{peak-hr}$ value is reduced from a value of 28.2 milli-g to a value of 13.6 milli-g at the 10-year return period wind speed.

6.6.3 Investigation of SA-TLDs Response History and Performance Comparison with Passive TLDs

In this section, the behaviour of semi-active TLDs, installed to suppress the first three modes of vibration, is investigated in detail at selected values of serviceability and strength return period wind speeds. Performance comparisons in terms of response reduction of R_{RMS} and $R_{peak-hr}$ values are also made.

6.6.3.1 Response History of SA-TLDs for Different Return Periods

At the 1-month return period wind speed, Figure 6.24 shows that low first modal RMS structural acceleration response values are achieved for TLDs to suppress mode 1 in the x-direction. Similar observations are found for mode 2 in the y-direction and mode 3 in the x- and y-directions (see Figures D16-D18 Appendix-D). As a result, all damping screens are set by the semi-active TLD control strategy to the upright position to achieve their maximum screen loss coefficient values (i.e. $C_{\theta x_1} = C_{lx-max_1} = 15.0$, $C_{\theta y_2} = C_{ly-max_2} = 30.0$, $C_{\theta x_3} = C_{lx-max_3} = 55.0$ and $C_{\theta y_3} = C_{ly-max_3} = 22.0$ compared to $C_{\theta x_1} = 9.8$, $C_{\theta y_2} = 20.3$, $C_{\theta x_3} = 35.3$ and $C_{\theta y_3} = 14.1$ for the conventional passive TLDs, designed at the 10-year serviceability return period, as shown Figures 6.25-6.28, respectively. Therefore, higher percentage response reduction values (Ψ_{RMS}) of R_{RMS} in the range between 45% and 49% are achieved utilizing the semi-active TLDs, while percentage response reduction values (Ψ_{RMS}) in the range between 28% and 31% are achieved utilizing the conventional passive TLDs (see Figure 6.21). This can be attributed to the fact that the conventional passive TLDs are highly under-damped compared to the semi-active TLDs, which leads to a significant decrease in the TLD efficiency (ψ_{TLD}) of the passive system (Tait et al. 2008) compared to the semi-active system (see Chapter 5 - Figure 9a). Therefore, a percentage response reduction improvement (Ψ_{RMS}) equal to 19% is achieved at the 1-month serviceability return period utilizing the semi-active TLD control system. Similar results are found for the 1-year serviceability return period. However, a lower percentage response reduction value of 11% is achieved.

At the 10-year serviceability return period wind speed, maximum percentage response reduction values (Ψ_{RMS}) are found to range between 50% and 53% and between 45% and 48% utilizing the semi-active TLDs and the conventional passive TLDs as shown in Figure 6.21, respectively. The maximum Ψ_{RMS} values achieved at this particular return period can be attributed to the fact that the passive TLDs are designed to 10-year serviceability return period. However, the percentage response reduction values (Ψ_{RMS}) achieved utilizing the semi-active TLDs are found 5% higher than their counterpart values utilizing the conventional passive TLD control system as all semi-active TLDs are found to be fully-efficient during the entire time history (see Figures 6.25-6.28). These results are in agreement

with those obtained from a single-story structure, discussed in detail in Chapter 5 (Section 3.5).

At the 50-year serviceability return period wind speed, Figure 6.21 shows that percentage response reduction values (Ψ_{RMS}) range between 50% and 52% utilizing semi-active TLDs compared to Ψ_{RMS} values between 42% to 44% utilizing conventional passive TLDs, respectively. It can be noticed that the percentage response reduction values (Ψ_{RMS}) utilizing the conventional passive TLDs are only 8% less than their counterpart values for the semi-active TLDs, although all semi-active TLDs are found to remain found fully-efficient during the entire time history (see Figures 6.25-6.28).

Due to the amplitude dependent properties of the TLDs (Tait et al. 2004a; Tait et al. 2004b), the conventional passive TLDs experience high response amplitudes and as a result, the inherent damping ratio values of the conventional passive TLDs exceed their design values (i.e. $\zeta_{TLD} > \zeta_{TLD-opt}$). Consequently, the conventional passive TLD control system is over-damped compared to the under-damped cases at the 1 month and 1year return periods. As a result, the increased system efficiency (ψ) using the semi-active control is lower. This is in agreement with that observed in the efficiency chart for an over-damped TLD system (see Chapter 5 - Figure 9a).

It is also observed that damping screen loss coefficient values of the conventional passive TLDs are found to be similar to the average values of their counterparts utilizing the semi-active TLDs to suppress mode 1 in the x-direction (i.e. $C_{lx-passive_1} \approx C_{\theta x_1-average}$), mode 2 in the y-direction (i.e. $C_{ly-passive_2} \approx C_{\theta y_2-average}$) and mode 3 in the y-direction (i.e. $C_{ly-passive_3} \approx C_{\theta y_3-average}$) as shown in Figures 6.25, 6.26 and 6.28, respectively. Although, significant discrepancy is found between $C_{lx-passive_3}$ and $C_{\theta x_3-average}$ for mode 3 tanks in the x-direction, it has insignificant effect on the percentage response reduction values (Ψ_{RMS}) of R_{RMS} due to the small contribution of the third modal RMS acceleration response component in the x-direction at corners $C3$ and $C4$ (see Table 6.3, Figure D17 Appendix-D).

Figure 6.21 shows that percentage response reduction values (Ψ_{RMS}) range between 48% and 50% utilizing semi-active TLDs compared to 37% to 38% utilizing conventional passive TLDs. The percentage response reduction values (Ψ_{RMS}) achieved utilizing the conventional

passive TLDs are 11% less than their counterpart values achieved utilizing the semi-active TLDs. This can be attributed to the fact that all passive TLDs are over-damped due to the high response amplitude values at the 50-year strength return period. It can be observed that only the semi-active TLDs to suppress mode 1 in the x-direction are found fully-efficient during the entire time history (see Figure 6.25), while semi-active TLDs to suppress mode 3 in the y-direction are found to be partially-efficient (see Figure 6.28) as the semi-active TLDs to suppress mode 3 in the y-direction are found to be fully-efficient starting at minute 25 of the time history (see Figure D18 Appendix-D). The damping screen loss coefficient values for semi-active TLDs to suppress mode 2 in the y-direction and mode 3 in the x-direction are set by the semi-active TLD control strategy to their minimum values (i.e. $C_{\theta y_2} = C_{ly-min_2} = 10.0$; $C_{\theta x_3} = C_{lx-min_3} = 15.0$) compared to higher damping screen loss coefficient values utilized for the conventional passive TLDs (i.e. $C_{ly-passive_2} = 20.3$; $C_{lx-passive_3} = 35.3$) as shown in Figures 6.26 and 6.27, respectively. Consequently, the semi-active TLDs to suppress mode 2 in the y-direction and mode 3 in the x-direction are over-damped resulting in a reduction in TLD efficiency.

6.7.   Conclusions

In this chapter, a control strategy based on gain scheduling, which was introduced and verified experimentally by Yalla and Kareem (2003), has been incorporated into a multi semi-active TLD model. The developed 3D-Structure-SA-MTLD system model has been employed to analyze a multi-modal high-rise building subjected to recorded wind tunnel loads. A preliminary TLD design procedure has been expanded for use on a multi-modal high-rise building utilizing modal structural response components. It has been implemented in a programmable way in the 3D-Structure-SA-MTLD system model as an alternative to look-up tables. A detailed example of designing multiple semi-active TLDs to suppress the first three modes of vibration of an actual multi-modal high-rise building (Indianapolis building) has been described. Also, a suggested procedure for the damping screen loss coefficient range selection has been presented and evaluated.

Gain scheduling has been found to be an efficient control scheme to maintain the inherent damping ratios of the TLDs (ζ_{TLD}) at their selected values ($\zeta_{TLD-opt}$). For given structural response accelerations at the multiple SA-TLD locations, the pressure loss coefficients (C_θ) for the multiple SA-TLDs to suppress different structural vibration modes have been changed

in accordance with the expanded preliminary TLD design procedure. The use of practical parameter values of averaging time ($AT = 60$ minutes) and updating time ($UT = 1.0T$) has also been confirmed utilizing the sensitivity analysis conducted in this chapter.

Employing the preliminary TLD design procedure for multiple TLDs to suppress the first three modes of vibration of the Indianapolis building, subjected to recorded wind tunnel loads, has led to the evaluation of the required damping screen loss coefficient values (C_θ) that maintain the TLD inherent damping ratios (ζ_{TLD}) during the entire time history as feedback to the numerical simulation. Consequently, two significant improvements have been gained:

i. Employing the semi-active TLD control strategy has improved the response of an actual high-rise building over a wide range of wind loading directions ($0° - 360°$), where nearly constant percentage response reduction values (Ψ_{RMS}) ranging between 40% and 50% have been achieved. In additions, a performance comparison between the semi-active and the conventional passive TLD control systems has been conducted at the critical wind loading angle, and at the return period wind speed utilized to design the conventional passive TLD control system.

ii. Employing the semi-active TLD control strategy has shown the efficiency of multiple SA-TLDs to provide control at both serviceability and strength wind speed levels. In other words, results over a wide range of serviceability and strength return period wind speeds at the critical wind loading angle (θ_w) of $210°$ have indicated nearly constant percentage response reduction values (Ψ_{RMS}) with a maximum percentage difference value of 4% found utilizing the semi-active TLD control system compared to 19% utilizing the conventional passive TLD control system.

Therefore, improved performance of the semi-active TLD control system compared to the conventional passive TLD control system has been demonstrated.

6.8.   References

Astrom, K. J. and Wittenmark, B. (1989). "*Adaptive Control*", Addison-Wesley, 2nd Ed, 1994, Reading, MA, USA.

ASCE (American Society of Civil Engineers), (2005). "*Minimum Design Loads for Buildings and Other Structures*", ASCE 7-05, New York, NY, USA.

Cassolato, M.R. (2007). "*The Performance of a Tuned Liquid Damper Equipped with Inclined and Oscillating Damping Screens*", M.E.Sc. Thesis. McMaster University, Hamilton, ON, Canada.

Cassolato, M.R., Love, J.S. and Tait, M.J. (2011). "Modelling of Tuned Liquid Damper with Inclined Damping Screens", *Structural Control and Health Monitoring*, 18(6): 674-681

Davenport, A.G. (1964). "Note on the Distribution of the Largest Value of a Random Function with Application to Wind Loading", *Proceeding - Institution of Civil Engineer*, 28: 187-196.

Housner, G. W., Bergman, L. A., Caughey, T. K., Chassiakos, A. G., Claus, R. O., Masri, S. F., Skelton, R. E., Soong, T. T., Spencer, B. F. and Yao, J. T. P. (1997) "Structural Control: Past, Present, and Future", *Journal of Engineering Mechanics*, 123 (9), 897-971.

Isyumov, N. (1994). "Criteria for Acceptable Wind-Induced Motions", *Proceedings, 12th ASCE Structures Congress*, 642-653. Atlanta, GA, USA.

Institute for Research in Construction (2005). "*National Building Code of Canada (NBCC)*", National Research Council of Canada, Ottawa, ON, Canada.

Kaneko, S. and Ishikawa, M. (1999). "Modeling of Tuned Liquid Damper with Submerged Nets", *Journal of Pressure and Vessel Technology*, 121(3): 334–343.

Kareem, A., Kijewski, T. and Tamura, Y. (1999). "Mitigation of Motions of Tall Buildings with Specific Examples of Recent Application", *Wind Structures: An International Journal*, 2(3): 201-251.

Love, J. S., Tait, M. J. and Toopchi-Nezhad, H. (2011). "A Hybrid Structural Control System using a Tuned Liquid Damper to Reduce the Wind Induced Motion of a Base Isolated Structure", *Engineering Structures*, 33: 738–746.

The MathWorks Inc., (2004). "*MATLAB version 7.0.0.19920 (R14)*", The MathWorks Inc., Natick, MA, USA.

Manwell, J.F., McGowan, J.G. and Rogers, A.L. (2010). "*Wind Energy Explained: Theory, Design and Application*", Wiley, Chichester, England.

Tait, M.J., E1 Damatty, A.A. and Isyumov, N. (2004a). "Testing of Tuned Liquid Damper with Screens and Development of Equivalent TMD Model", *Wind and Structures*, 7(4): 215–234.

Tait, M.J., Isyumov, N. and E1 Damatty, A.A. (2004b). "The Efficiency and Robustness of a Unidirectional Tuned Liquid Damper and Modelling with an Equivalent TMD", *Wind and Structures*, 7(4): 235–250.

Tait, M.J., El Damatty, A.A. and Isyumov, N. (2005a). "An Investigation of Tuned Liquid Dampers Equipped with Damping Screens Subjected to 2D Excitation", *Earthquake Engineering and Structural Dynamics*, 34(7): 719–735.

Tait, M.J., El Damatty, A.A., Isyumov, N. and Siddique, M.R. (2005b). "Numerical Flow Models to Simulate Tuned Liquid Dampers (TLD) with Slat Screens", *Journal of Fluid and Structures*, 20: 1007–1023.

Tait, M.J. (2008). "Modelling and Preliminary Design of a Structure-TLD System", *Engineering Structures*, 30: 2644-2655.

Tait, M.J., Isyumov, N. and El Damatty, A.A. (2008). "Performance of Tuned Liquid Dampers", *Journal of Engineering Mechanics*, 134(5): 417-427.

Tamura, Y., Fujii K., Ohtsuki, T., Wakahara, T. and Kohaska, R. (1995). "Effectivness of Tuned Liquid Dampers under Wind Excitation", Engineering Structures. 17, 609-621.

van der Tempel, J. (2006). "*Design of Support Structures for Offshore Wind Turbines*", Ph.D. Thesis, Delft University of Technology, Delft, Netherland.

Xu, Z. and Ho, T. C. E. (2007). "A Study of Wind Effects for One Indiana Square, Indianapolis, Indiana. *Research Report BLWT-SS3-2007*, The Boundary Layer Wind Tunnel Laboratory (BLWTL), The University of Western Ontario, London, ON, Canada

Yalla, S. and Kareem, A. (2003). "Semiactive Tuned Liquid Column Dampers: Experimental Study", *Journal of Structural Engineering*, 129(7): 960-971.

Table 6.1. Serviceability and Strength (Mixed) Return Periods and Wind Speeds

	Return Period (year)	Wind Speed (m/s)
Serviceability	50	37.0
	10	34.0
	1	29.0
	1/12	23.0
Strength	50	47.5

Table 6.2. Modal Acceleration Response Components in the x- and y-directions at the Centre of Mass with No-TLDs ($\theta_w = 210°$, $z = 154.6$ m)

Node	Return Period (years)	Wind Speed (m/s)	$\sigma_{\ddot{x}-initial}$ (milli-g)	MF (%)	$\sigma_{\ddot{x}-initial-m}$ (milli-g)	$\sigma_{\ddot{x}-target-m}$ (milli-g)	$\sigma_{\ddot{x}-target-t}$ (milli-g)
				Mode 1			
Centre	10	34	6.1	98.3	6.0	3.1	3.2

Node	Return Period (years)	Wind Speed (m/s)	$\sigma_{\ddot{y}-initial}$	MF (%)	$\sigma_{\ddot{y}-initial-m}$ (milli-g)	$\sigma_{\ddot{y}-target-m}$ (milli-g)	$\sigma_{\ddot{y}-target-t}$ (milli-g)
				Mode 2			
Centre	10	34	3.6	94.1	3.4	1.8	2.0

Table 6.3. Modal Acceleration Response Components in the x- and y-directions at the Four Corners with TLDs to Suppress the First Two Modes ($\mu = 6\%$, $\theta_w = 210°$, $z = 154.6$ m)

Node	Return Period (years)	Wind Speed (m/s)	$\sigma_{\ddot{x}-initial}$ (milli-g)	MF (%)	$\sigma_{\ddot{x}-initial-m}$ (milli-g)	$\sigma_{\ddot{x}-target-m}$ (milli-g)	$\sigma_{\ddot{x}-target-t}$ (milli-g)
				Mode 3			
Corner 1	10	34	3.8	22.6	0.9	-	-
Corner 2			3.8	22.6	0.9	-	-
Corner 3			4.1	37.3	1.5	0.8	3.4
Corner 4			4.1	37.3	1.5	0.8	3.4

Node	Return Period (years)	Wind Speed (m/s)	$\sigma_{\ddot{y}-initial}$ (milli-g)	MF (%)	$\sigma_{\ddot{y}-initial-m}$ (milli-g)	$\sigma_{\ddot{y}-target-m}$ (milli-g)	$\sigma_{\ddot{y}-target-t}$ (milli-g)
				Mode 3			
Corner 1	10	34	4.3	57.3	2.5	-	-
Corner 2			5.2	74.0	3.8	2.0	3.4
Corner 3			5.2	74.0	3.8	2.0	3.4
Corner 4			4.3	57.3	2.5	-	-

Table 6.4. Preliminary TLD Design for Mode 1 in the x-direction ($\mu = 6.0\%$, Serviceability Return Period = 10 years)

Quantity	Equation(s)	Value	
Initial peak hourly acceleration, $\ddot{x}_{initial}$		**22.516**	**milli-g**
Modal Factor, MF		**98.300**	**%**
Initial modal peak hourly acceleration, $\ddot{x}_{initial-m}$	$\ddot{x}_{initial-m} = \ddot{x}_{initial}.MF$	**22.368**	**milli-g**
Structure cyclic frequency, f_{s-x}		0.137	Hz
Structure time period, T_{s-x}	$T_{s-x} = 1/f_{s-x}$	7.310	s
Structure natural frequency, ω_{s-x}	$\omega_{s-x} = 2\pi/T_{s-x}$	0.860	rad/s
Peak factor, PF_x	$PF_x = \sqrt{2\ln(573\omega_{s-x})} + \frac{0.577}{\sqrt{2\ln(573\omega_{s-x})}}$	3.685	
Initial RMS acceleration, $\sigma_{\ddot{x}-initial-m}$	$\sigma_{\ddot{x}-initial-m} = \frac{\ddot{x}_{initial-m}}{PF_x}$	**6.010**	**milli-g**
Initial RMS displacement, $\sigma_{x-initial-m}$	$\sigma_{x-initial-m} = \frac{\sigma_{\ddot{x}-initial-m}}{\omega_{s-x}^2}\frac{g}{1000}$	0.081	m
Assumed mass ratio, μ		0.060	(6.00%)
Effective damping provided by TLD, $\zeta_{TLD-eff-opt_x}$	$\zeta_{TLD-eff-opt_x} = \frac{1}{4}\sqrt{\frac{\mu_x+\mu_x^2}{1+\frac{3}{4}\mu_x}}$	0.062	(6.20%)
Optimal damping ratio, $\zeta_{TLD-opt_x}$	$\zeta_{TLD-opt_x} = \sqrt{\frac{\mu_x+\frac{3}{4}\mu_x^2}{4+6\mu_x+2\mu_x^2}}$	0.120	(12.0%)
Optimal tuning ratio, Ω_{opt_x}	$\Omega_{opt_x} = \frac{\sqrt{1+\frac{1}{2}\mu_x}}{1+\mu_x}$	0.957	(95.7%)
Optimal TLD cyclic frequency, $f_{TLD-opt_x}$	$\Omega_{opt_x} = \frac{f_{TLD-opt_x}}{f_{s-x}}$	0.131	Hz
Optimal response ratio, R_{opt_x}	$R_{opt_x} = \frac{\sigma_{r-x}}{\sigma_x} = \frac{1+\mu_x}{\sqrt{2\mu_x+\frac{3}{2}\mu_x^2}}$	2.993	
Structure damping ratio, ζ_s		0.020	(2.00%)
Total structure damping, ζ_{tot-x}	$\zeta_{tot-x} = 0.8\zeta_s + \zeta_{TLD-eff-opt_x}$	0.078	(7.80%)
Target RMS displacement, $\sigma_{x-target-m}$	$\zeta_{tot-x} = \zeta_s\frac{\sigma_{x-initial-m}^2}{\sigma_{x-target-m}^2}$	0.043	m
Target RMS acceleration, $\sigma_{\ddot{x}-target-m}$	$\sigma_{\ddot{x}-target-m} = \omega_s^2\,\sigma_{x-target-m}$	**3.080**	**milli-g**
Target peak hourly acceleration, $\ddot{x}_{target-m}$	$\sigma_{\ddot{x}-target-m} = \frac{\ddot{x}_{target-m}}{PF_x}$	**11.350**	**milli-g**
TLD response, σ_{r-x}	$\sigma_{r-x} = R_{opt_x}\,\sigma_{x-target-m}$	0.122	m
Select tank dimensions, L_x, h	$f_{TLD-opt_x} = \frac{1}{2\pi}\sqrt{\frac{\pi g}{L_x}\tanh\left(\frac{\pi h}{L_x}\right)}$	**$L_x = 16.0$** $\quad$ **$h = 1.87$**	**m** **m**
Shallow water theory check, h/L_x		0.12	
Select screen properties, x_1, x_2, C_{l-x}	$\zeta_{TLD-x} = C_{l-x}\sqrt{\frac{32}{\pi^3}}\tanh^2\left(\frac{\pi h}{L_x}\right)\Delta_x\Xi_x\frac{\sigma_{r-x}}{L_x}$ $\Delta_x = \left(\frac{1}{3} + \frac{1}{\sinh^2\left(\frac{\pi h}{L_x}\right)}\right)$ $\Xi_x = \sum_{j=1}^{ns_x}\left|\sin^3\left(\frac{\pi x_j}{L_x}\right)\right|$	**$x_1 = 0.4\,L_x$** **$x_2 = 0.6\,L_x$** **$C_{l-x} = 9.76$**	

Table 6.5. Water Mass Calculations for TLDs to Suppress Modes 1 and 2 ($\mu = 6.0\%$)

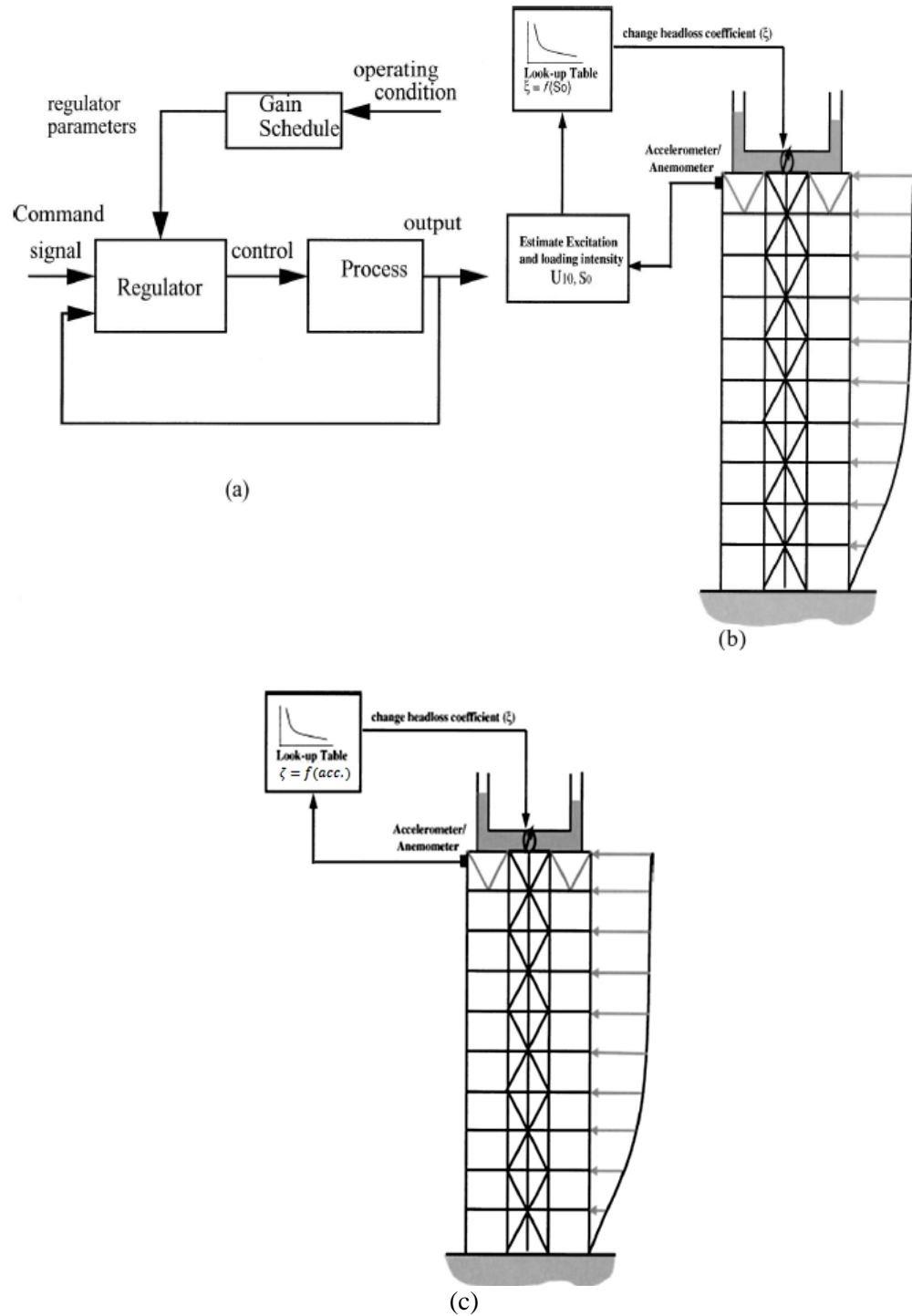| Quantity	Equation(s)	Value
Selected tank dimensions, L_x, B_x, L_y, B_y, h		$L_x = 16.00$ m $B_x = 13.41$ m $L_y = 13.41$ m $B_y = 16.00$ m $h = 1.87$ m
Water height to tanks length ratio in x-dir	h/L_x	0.12
Water height to tanks length ratio in y-dir	h/L_y	0.14
Water mass of 1 tank, $m_{w(1tank)}$	$m_{w(1tank)} = L_x B_x h = L_y B_y h$	401255 kg
TLD mass of 1 tank in x-dir, $m_{TLD-x(1tank)}$	$m_{TLD-x(1tank)} \approx m_{1-x} = \dfrac{8\,tanh\left(\pi\frac{h}{L_x}\right)}{\pi^3\left(\frac{h}{L_x}\right)} m_{w(1tank)}$	$0.776\, m_{w(1tank)} =$ 311370 kg
TLD mass of 1 tank in y-dir, $m_{TLD-y(1tank)}$	$m_{TLD-y(1tank)} \approx m_{1-y} = \dfrac{8\,tanh\left(\pi\frac{h}{L_y}\right)}{\pi^3\left(\frac{h}{L_y}\right)} m_{w(1tank)}$	$0.762\, m_{w(1tank)} =$ 305904 kg
Total building mass, M_s	$M_s = \sum_{i=1}^{i=N_f} m_f$	36412955 kg
Generalized building mass in x-dir, M_x^*	$M_x^* = \sum_{i=1}^{i=N_f} (m_f)_i (\phi_x^2)_i$	10523344 kg
Generalized building mass in y-dir, M_y^*	$M_y^* = \sum_{i=1}^{i=N_f} (m_f)_i (\phi_y^2)_i$	10013563 kg
Required TLD mass in x-dir, m_{TLD-x}	$m_{TLD-x} = \mu_x M_x^*$	631401 kg
Required TLD mass in y-dir, m_{TLD-y}	$m_{TLD-y} = \mu_y M_y^*$	600814 kg
No. of Tanks required in x-dir, N_{TLD-x}	$N_{TLD-x} = m_{TLD-x}/m_{TLD-x(1tank)}$	2.03
No. of Tanks required in y-dir, N_{TLD-y}	$N_{TLD-y} = m_{TLD-y}/m_{TLD-y(1tank)}$	1.96
Chosen No. of tanks for modes 1 and 2, N_{TLD-xy}	(Uni-directional tanks)	**2 sets of 2 tanks**
Actual mass ratio in x-dir, $\mu_{x-actual}$	$\mu_{x-actual} = N_{TLD-xy} m_{TLD-x(1tank)}/M_x^*$	**5.92 %**
Actual mass ratio in y-dir, $\mu_{y-actual}$	$\mu_{y-actual} = N_{TLD-xy} m_{TLD-y(1tank)}/M_y^*$	**6.11 %**
Mass ratio of contained water, μ_w	$\mu_w = N_{TLD-xy} m_{w(1tank)}/M_s$	**4.40 %**

Fig. 6.1. (a) Gain Scheduling Concept; (b) Semi-Active Control Strategy in Tall Buildings (from Yalla and Kareem 2003); and (c) Semi-Active Control Strategy Updated in This Study
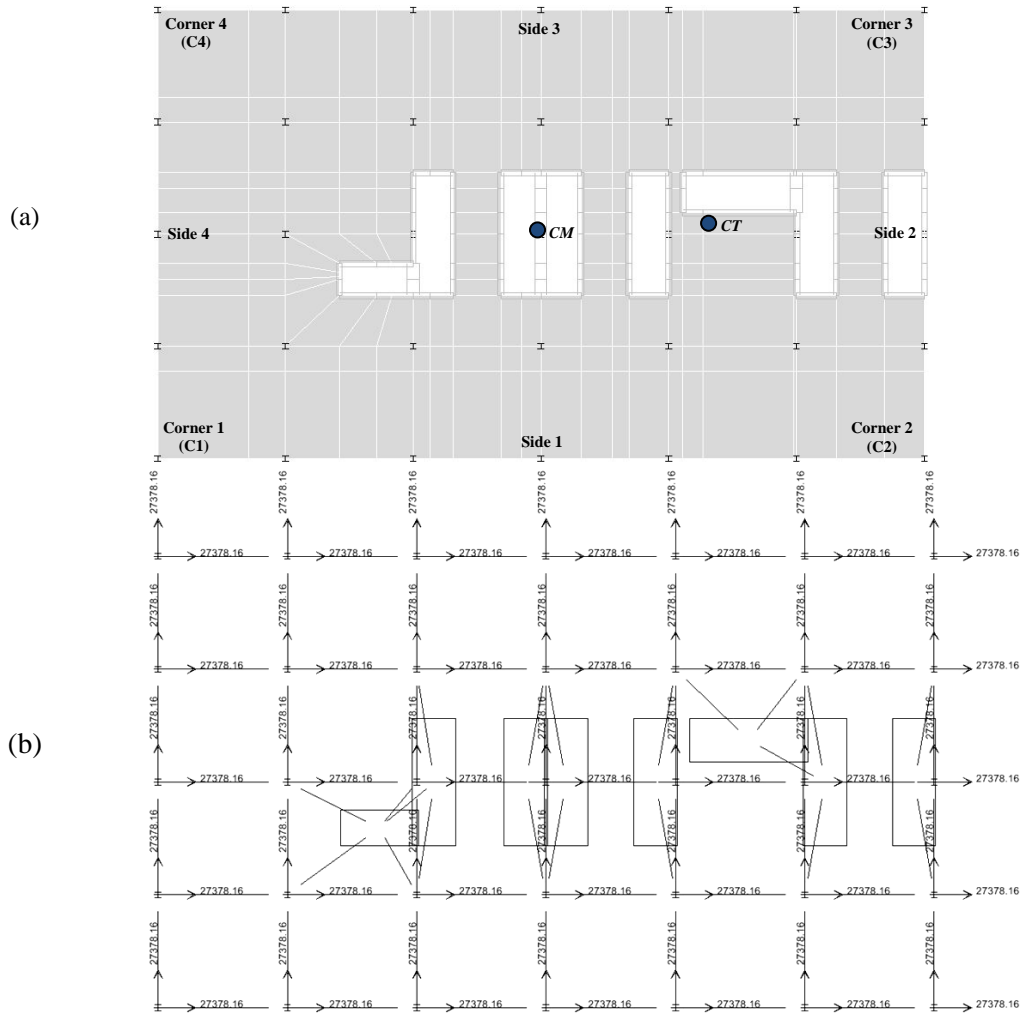
Fig. 6.2. Floor Plan of the Indianapolis Building Showing the Statical System Consists of (a) Real Slabs and Shear Walls; and (b) Frame Elements and Slab Beams Installed with Lumped Masses (kg)

(a) $T = 7.31$ s   (b) $T = 6.18$ s   (c) $T = 3.01$ s
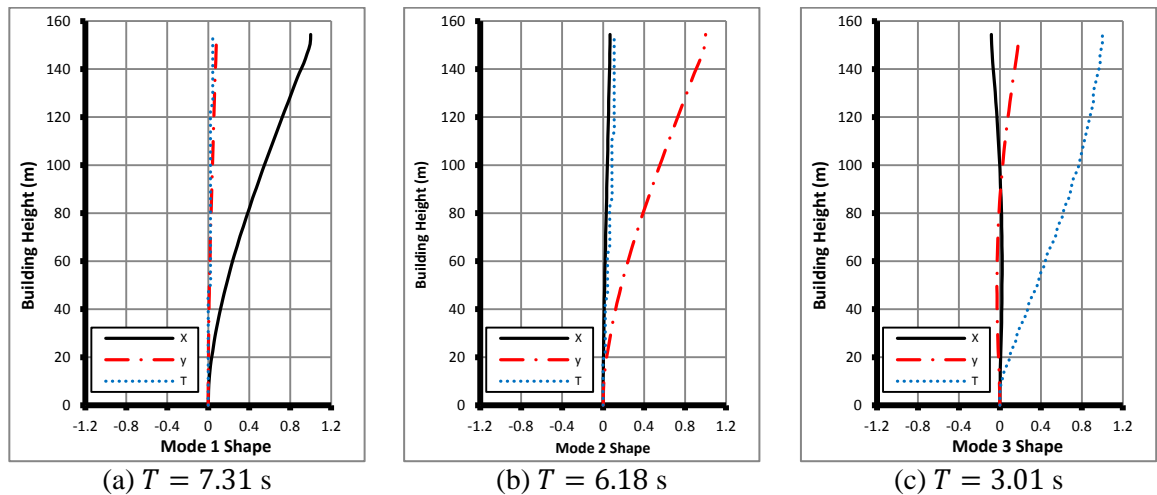
Fig. 6.3. Mode Shapes of the Indianapolis Building for (a) Mode 1; (b) Mode 2; and (c) Mode 3

Fig. 6.4. Predicted Annual Extreme Upper Level (500 m) Wind Speed for Various Return Periods (from BLWT-SS3-2007)

(a)

(b)

Fig. 6.5. RMS Structural Accelerations of the Indianapolis Building with No-TLDs Installed in (a) the x-direction; and (b) in the y-direction (Return Period=10 Years)

[Note: 2M-TLDs indicates TLDs to Suppress the First 2 Modes]

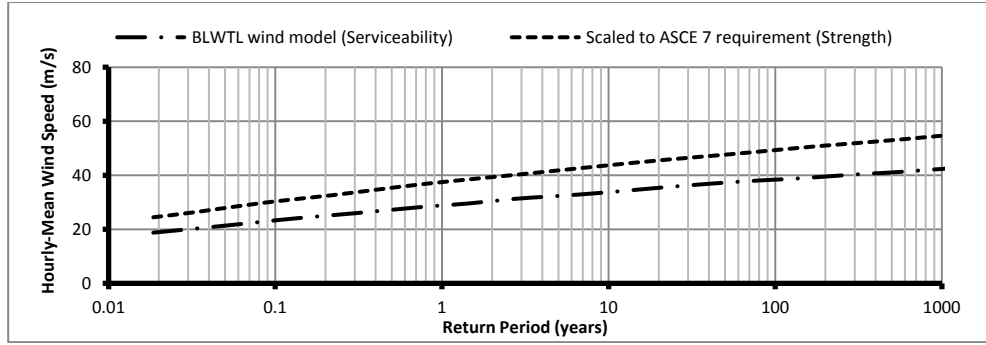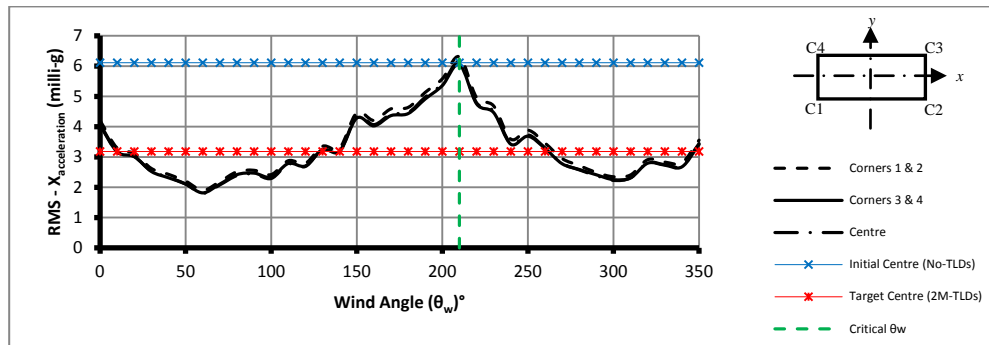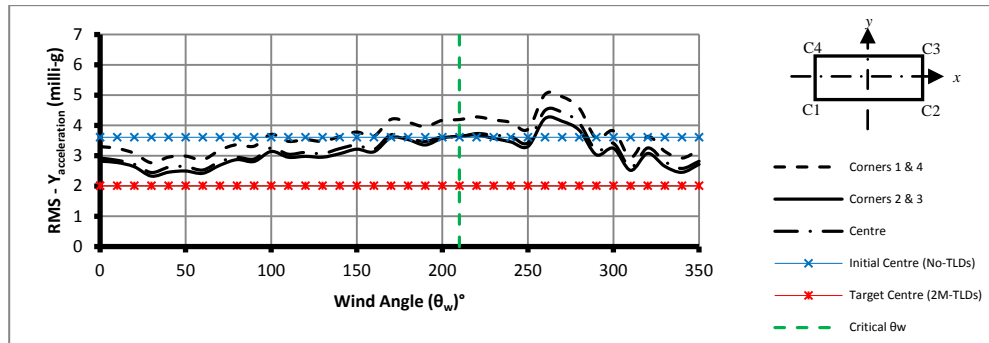**Fig. 6.6.** Influence of Averaging Time (AT) on RMS Structural Accelerations at the CM in the x-direction ($UT = 1.0\ T$, $\theta_w = 210°$, Return Period=10 Years)
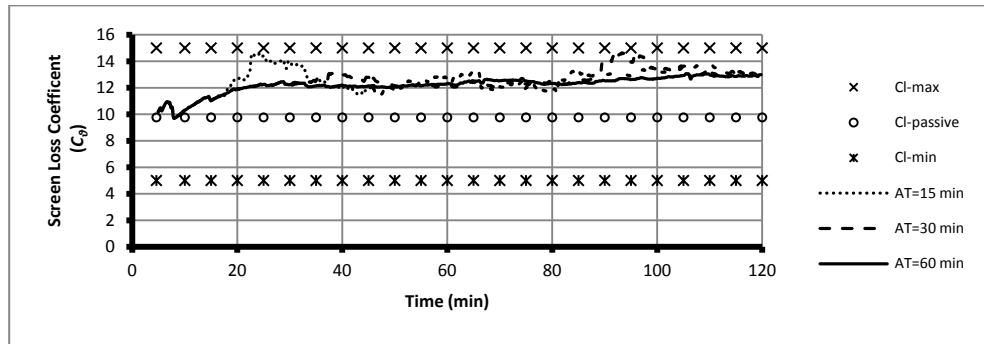
Fig. 6.7. Influence of Averaging Time (AT) on Screen Loss Coefficient Values of Mode 1 Tanks Placed at the CM in the x-direction ($UT = 1.0\ T$, $\theta_w = 210°$, Return Period=10 Years)
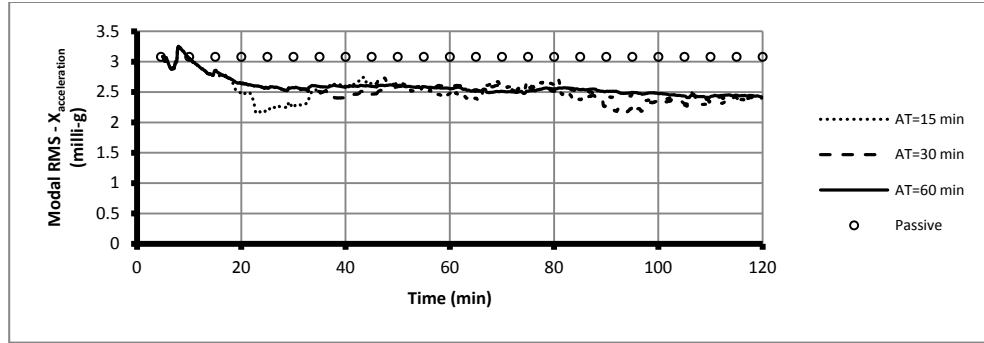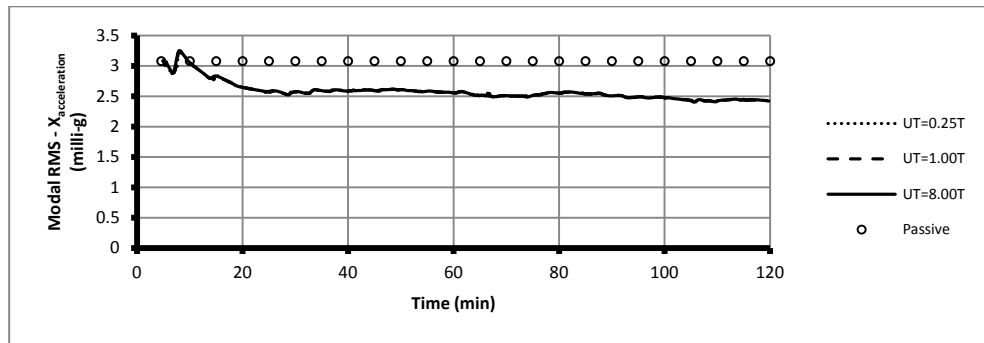

Fig. 6.8. Influence of Updating Time (UT) on RMS Structural Accelerations at the CM in the x-direction ($AT = 60$ min, $\theta_w = 210°$, Return Period=10 Years)
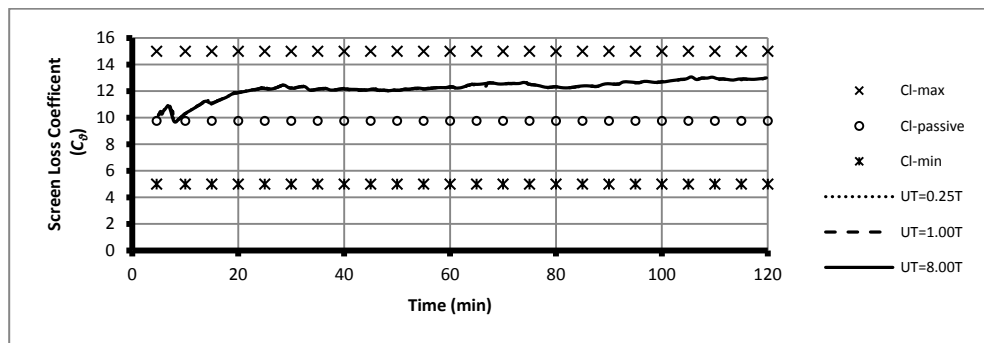
Fig. 6.9. Influence of Updating Time (UT) on Screen Loss Coefficient Values of Mode 1 Tanks Placed at the CM in the x-direction ($AT = 60$ min, $\theta_w = 210°$, Return Period=10 Years)
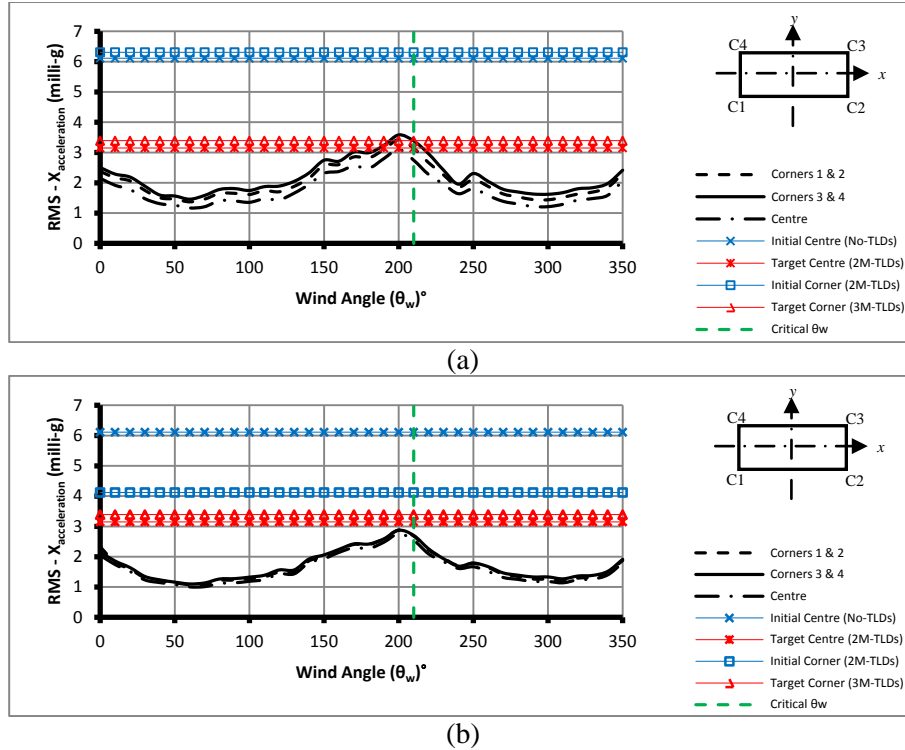
Fig. 6.10. RMS Structural Accelerations in the x-direction of the Indianapolis Building Using (a) Passive TLD System; and (b) Semi-Active TLD System ($AT = 60$ min, $UT = 1.0\ T$, Return Period=10 Years)
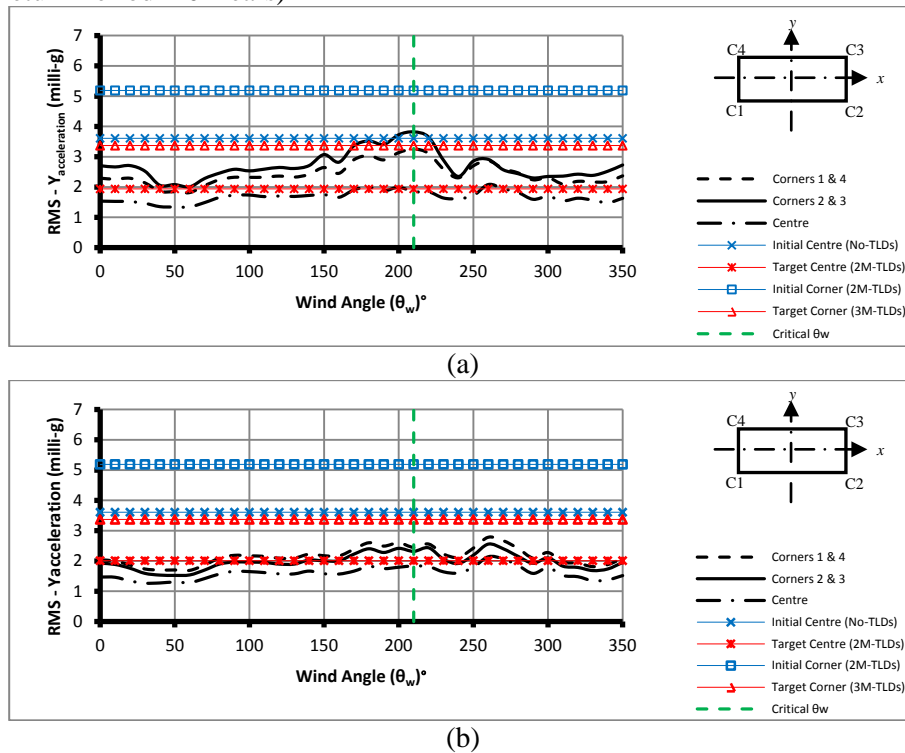
Fig. 6.11. RMS Structural Accelerations in the y-direction of the Indianapolis Building Using (a) Passive TLD System; and (b) Semi-Active TLD System ($AT = 60$ min, $UT = 1.0\ T$; Return Period=10 Years)

[Note: 2M-TLDs and 3M-TLDs indicate TLDs to Suppress the First 2 and 3 Modes, respectively]
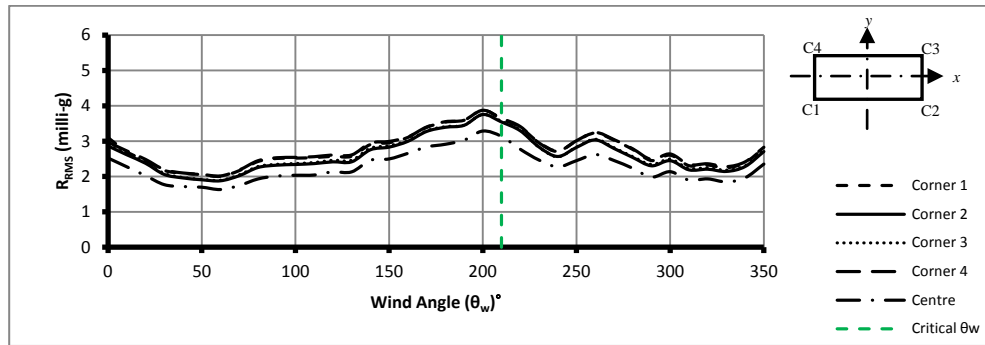
Fig. 6.12. RMS Resultant Accelerations of the Indianapolis Building Using Semi-Active TLD System to Suppress the First 3 Modes ($AT = 60$ min, $UT = 1.0\,T$, Return Period=10 Years)
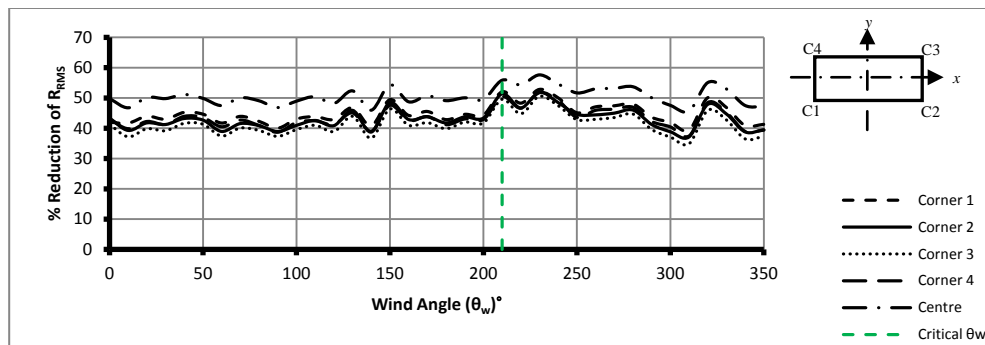
Fig. 6.13. Percentage Reduction of RMS Resultant Accelerations of the Indianapolis Building Using Semi-Active TLD System to Suppress the First 3 Modes ($AT = 60$ min, $UT = 1.0\,T$, Return Period=10 Years)
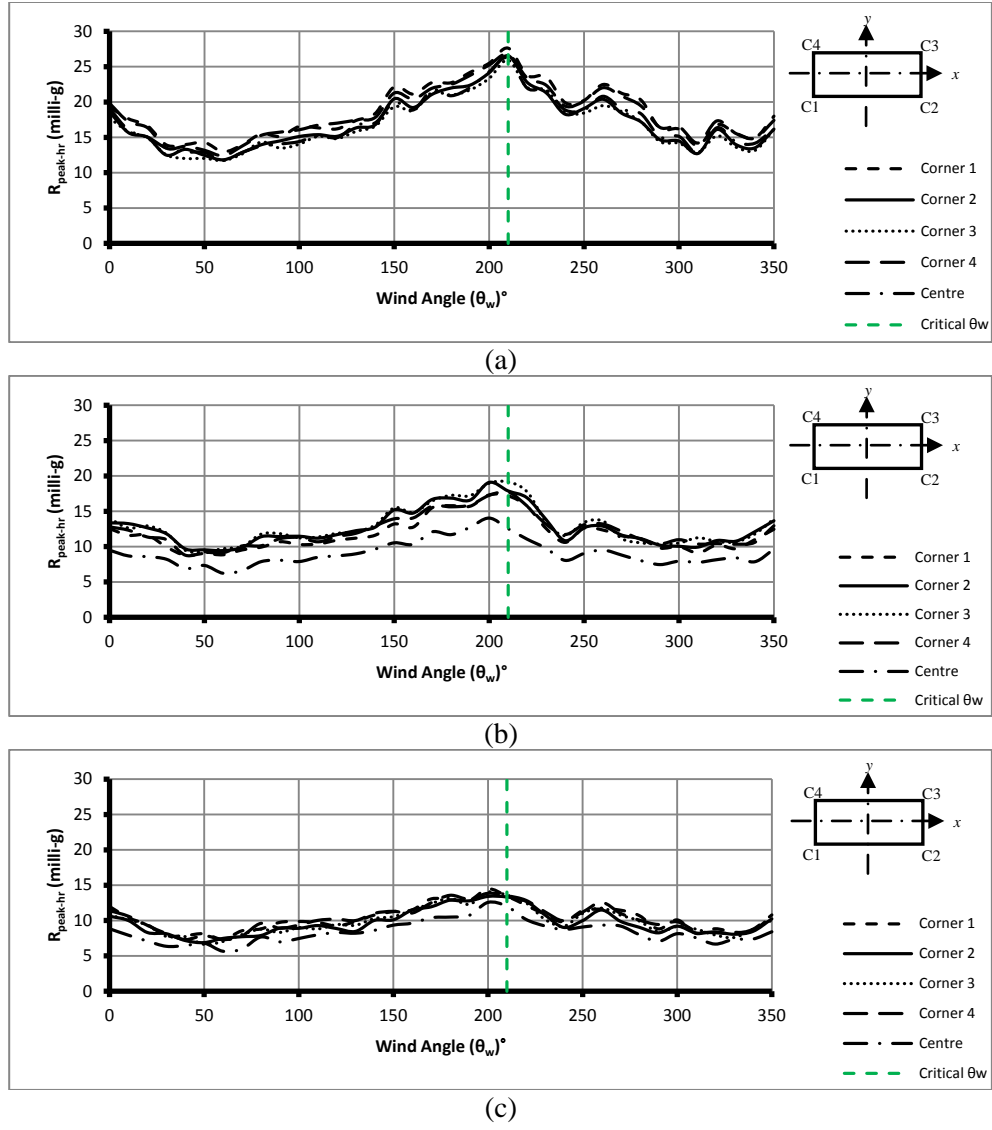
Fig. 6.14. Average Peak Hourly Resultant Accelerations Using (a) No-TLDs; (b) Passive TLD System; and (c) Semi-Active TLD System ($AT = 60$ min, $UT = 1.0\,T$, Return Period=10 Years)
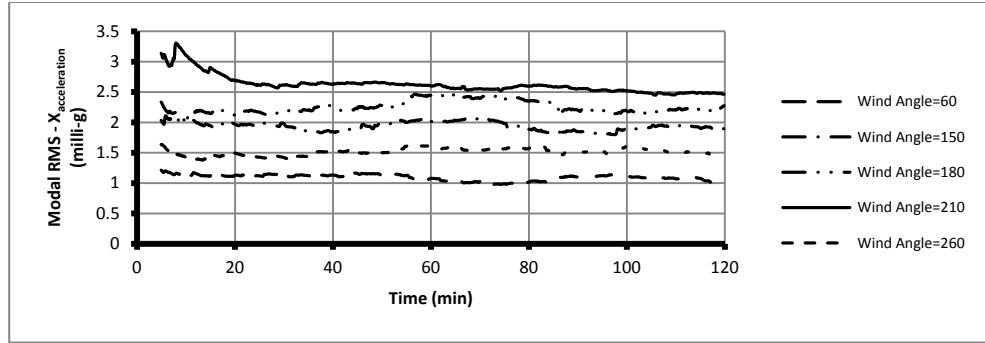
Fig. 6.15. Influence of Wind Loading Direction on RMS Structural Acceleration at the CM in the x-direction Using Semi-Active TLD System ($AT = 60$ min, $UT = 1.0\ T$, Return Period=10 Years)
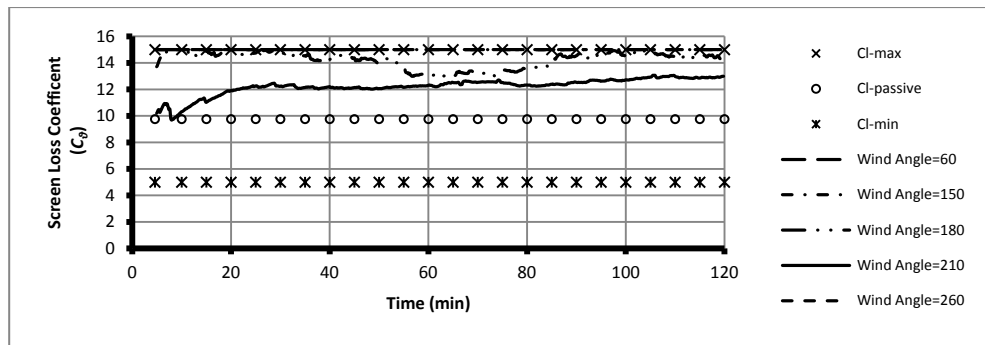
Fig. 6.16. Influence of Wind Loading Direction on Screen Loss Coefficient of Mode 1 Tanks Placed at the CM in the x-direction Using Semi-Active TLD System ($AT = 60$ min, $UT = 1.0\ T$, Return Period=10 Years)
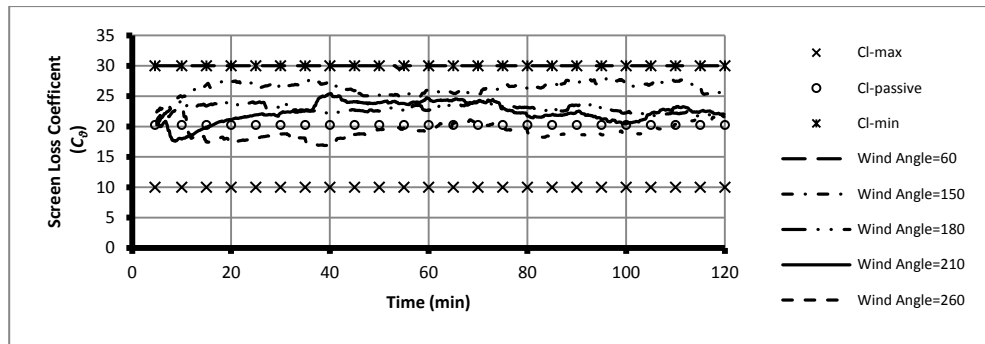
Fig. 6.17. Influence of Wind Loading Direction on Screen Loss Coefficient of Mode 2 Tanks Placed at the CM in the y-direction Using Semi-Active TLD System ($AT = 60$ min, $UT = 1.0\ T$, Return Period=10 Years)
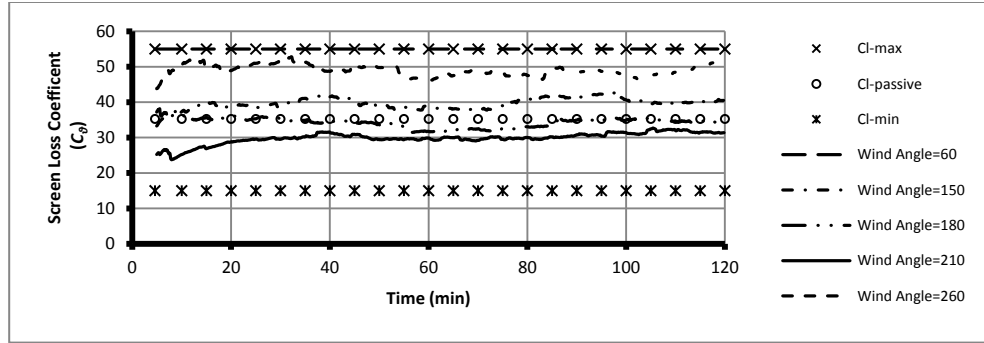
Fig. 6.18. Influence of Wind Loading Direction on Screen Loss Coefficient of Mode 3 Tanks Placed at $C3$ and $C4$ in the x-direction Using Semi-Active TLD System ($AT = 60$ min, $UT = 1.0\ T$, Return Period=10 Years)
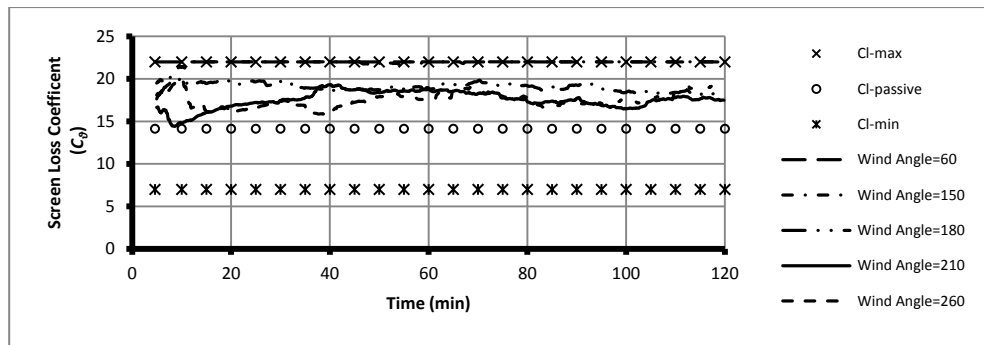
Fig. 6.19. Influence of Wind Loading Direction on Screen Loss Coefficient of Mode 3 Tanks Placed at $C3$ and $C4$ in the y-direction Using Semi-Active TLD Ssytem ($AT = 60$ min, $UT = 1.0\ T$, Return Period=10 Years)
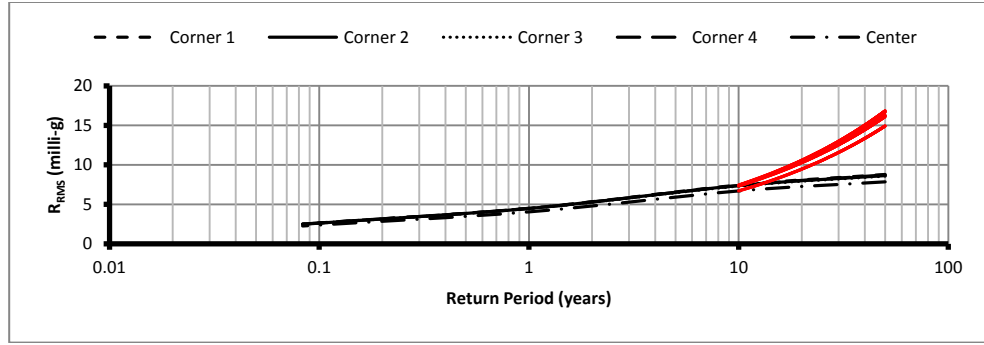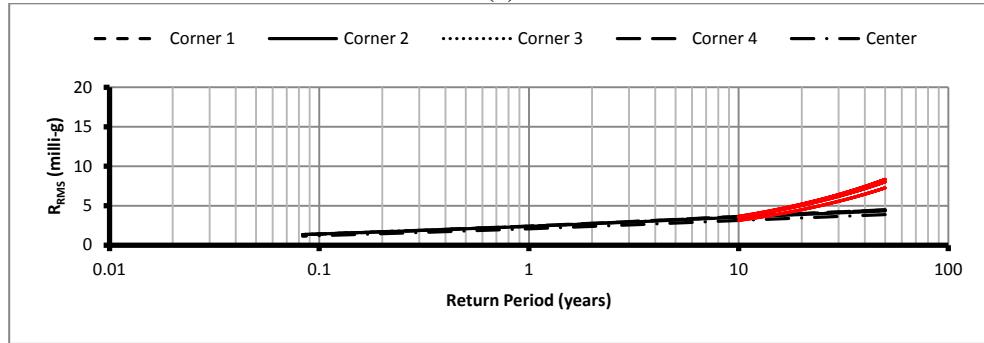
Fig. 6.20. RMS Resultant Accelerations ($\theta_w = 210°$) over a Range of Serviceability (black) and Strength (red) Return Periods Using (a) No-TLDs; and (b) Semi-Active TLD System ($AT = 60$ min, $UT = 1.0\,T$)
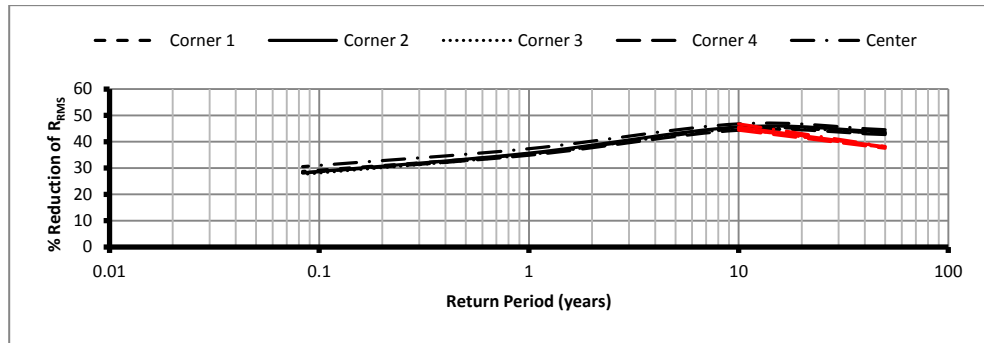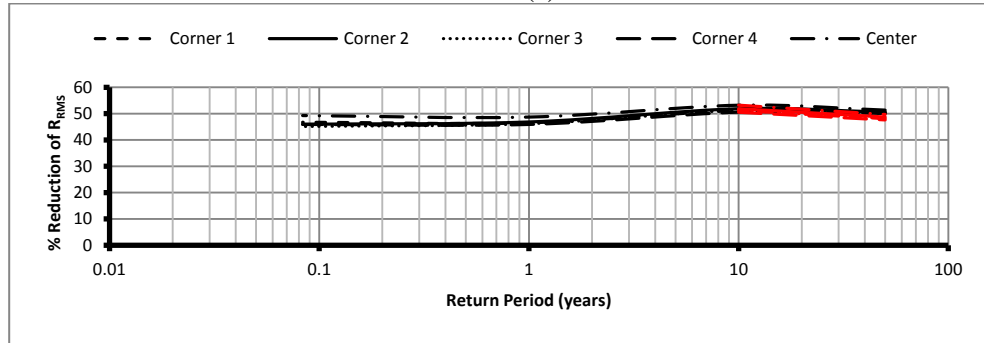
Fig. 6.21. Percentage Reduction of RMS Resultant Accelerations ($\theta_w = 210°$) over a Range of Serviceability (black) and Strength (red) Return Periods Using (a) Passive TLD System; and (b) Semi-Active TLD System ($AT = 60$ min, $UT = 1.0\,T$)
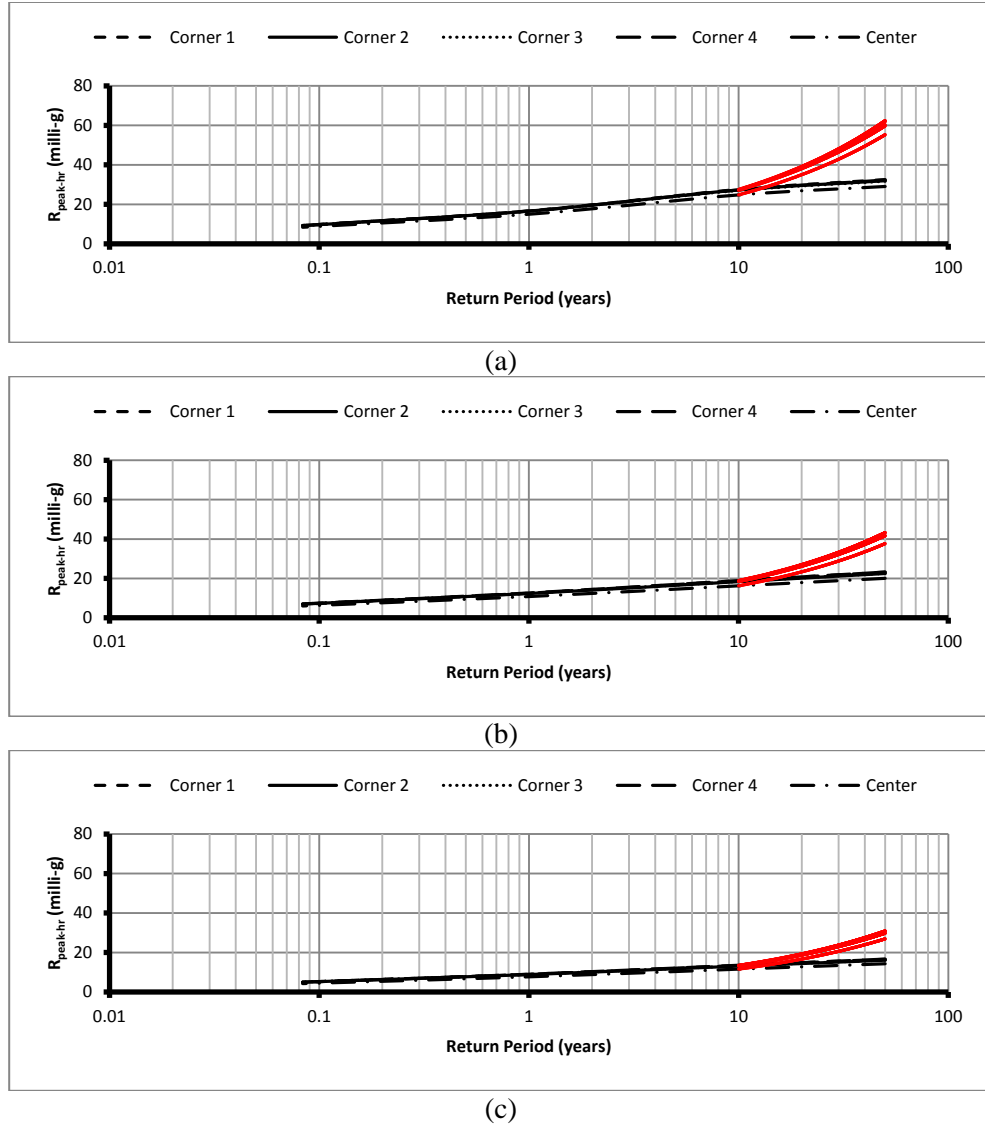
Fig. 6.22. Average Peak Hourly Resultant Accelerations ($\theta_w = 210°$) over a Range of Serviceability (black) and Strength (red) Return Periods Using (a) No-TLDs; (b) Passive TLD System; and (c) Semi-Active TLD System ($AT = 60$ min, $UT = 1.0\,T$)
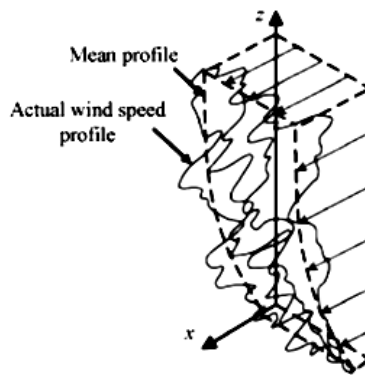
Fig. 6.23. Experimental Speed Profile (from van der Tempel 2006)
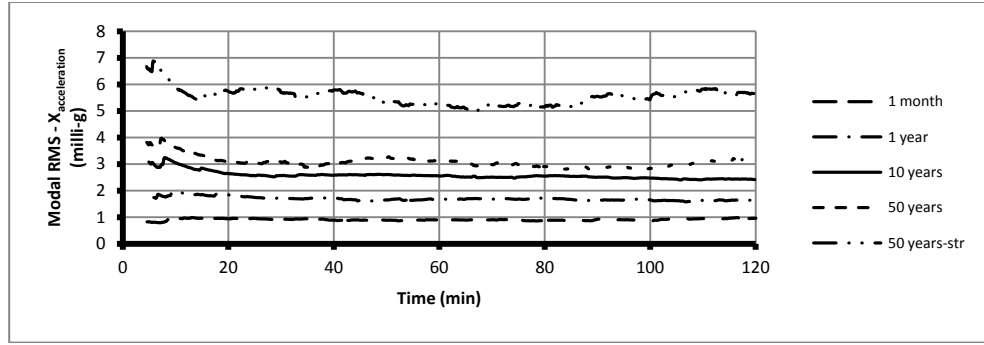
Fig. 6.24. Influence of Return Period on RMS Structural Acceleration at the CM of the Indianapolis Building in the x-direction Using Semi-Active TLD System ($AT = 60$ min, $UT = 1.0\ T$, $\theta_w = 210°$)
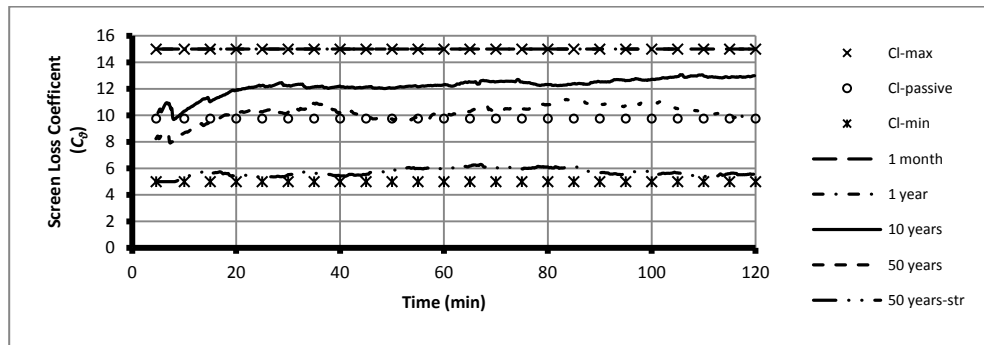
Fig. 6.25. Influence of Return Period on Screen Loss Coefficient of Mode 1 Tanks Placed at the CM in the x-direction Using Semi-Active TLD System ($AT = 60$ min, $UT = 1.0\ T$, $\theta_w = 210°$)
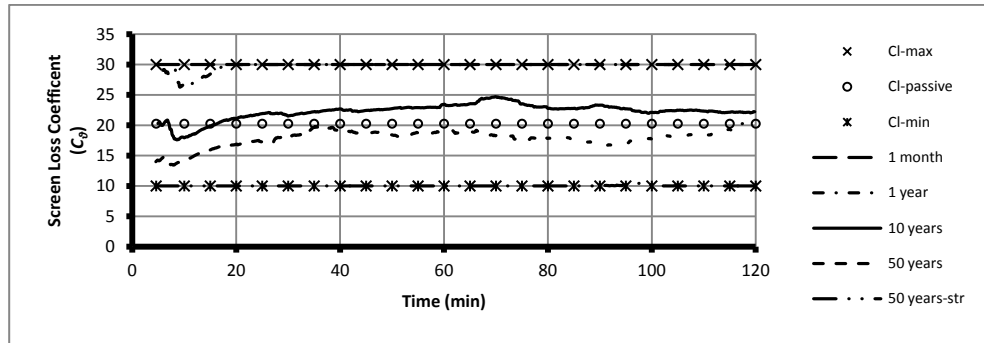
Fig. 6.26. Influence of Return Period on Screen Loss Coefficient of Mode 2 Tanks Placed at the CM in the y-direction Using Semi-Active TLD System ($AT = 60$ min, $UT = 1.0\ T$, $\theta_w = 210°$)
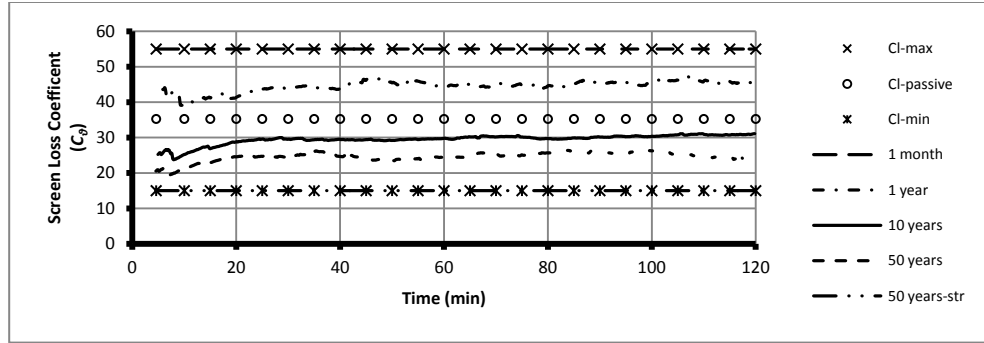
Fig. 6.27. Influence of Return Period on Screen Loss Coefficient of Mode 3 Tanks Placed at $C3$ and $C4$ in the x-direction Using Semi-Active TLD System ($AT = 60$ min, $UT = 1.0\ T$, $\theta_w = 210°$)
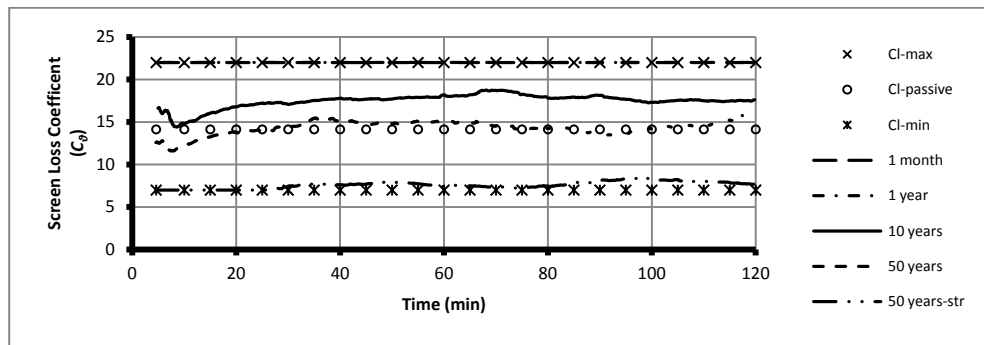
Fig. 6.28. Influence of Return Period on Screen Loss Coefficient of Mode 3 Tanks Placed at $C2$ and $C3$ in the y-direction Using Semi-Active TLD System ($AT = 60$ min, $UT = 1.0\ T$, $\theta_w = 210°$)

Chapter 7: Conclusions and Recommendations

7.1.   Summary and Conclusions

The research presented in this thesis has focussed on two major areas. First, on the ability to evaluate the dynamic response behaviour of single and 3D multi-degree-of-freedom structures equipped with single and multiple passive tuned liquid dampers. Research work completed includes developing and validating a 3D finite element model coupled with two different nonlinear TLD models to evaluate the resulting TLD base shear forces. TLD systems were designed to suppress two and subsequently three modes of vibration, respectively. In this study, the structural response behaviour at different wind loading directions (between 0° and 360°) and at different return period wind speeds (1 month to 50 years) was evaluated. The second area of focus was on the development and validation of a novel semi-active TLD system based on a gain scheduling technique (3D-Structure-SA-TLD). This included updating and validating the nonlinear TLD fluid model to simulate the TLD equipped with fixed inclined and adjustable damping screens, constructing required look-up tables and implementing the novel control technique in the proposed 3D finite element model. This novel technique was expanded to semi-active multiple TLDs (3D-Structure-SA-MTLD) for multi-modal high-rise building applications. Different wind loading directions and different return period wind speeds were considered. Conclusions pertaining to the research presented in the five main chapters conducted in this thesis (Chapters 2-6) are presented below.

7.1.1   Development and Validation of Finite Element Structure-Tuned Liquid Damper System Models

A finite element model capable of simulating the behaviour of a 3D-Structure, using 3D-beam elements, is developed and validated under dynamic loading. The validated finite element model is used to estimate the response of a 3D-Structure outfitted with TLDs (3D-Structure-TLD). The interaction base shear force resulting from the TLD is estimated using two nonlinear TLD models; a nonlinear fluid model that simulates the TLD sloshing force (TLD Model 1) and an equivalent amplitude dependent TMD model (TLD Model 2). Numerical simulations are carried out using both nonlinear TLD models and both models are subsequently coupled with the finite element model.

The following points summarize the main findings in this chapter:

- A significant reduction in the computational effort to a conduct dynamic analysis of a 3D-Structure-TLD system model is achieved utilizing the equivalent amplitude dependent tuned mass damper (EADTMD) model (TLD Model 2). The computational time required for the EADTMD model is approximately 18 times less than that required for the nonlinear fluid model. In order to use this particular model, two important steps are introduced.

  o First, the nonlinear fluid model is used to generate TLD energy dissipation curves (instead of using shake table test data). Theses curves are required to evaluate equivalent TMD parameters ($m_{TLD}, f_{TLD}, \zeta_{TLD}$) for the EADTMD model.

  o Second, a modified implementation method of the EADTMD model in the finite element model using the velocity tracking technique is presented. This method, which is applicable for any type of loading (i.e. wind or earthquake), is introduced to allow for mean structural displacements.

- The developed finite element model is validated under harmonic and random excitation forces with experimental values utilizing both nonlinear TLD models.

7.1.2 Three Dimensional Analysis of a High-Rise Building Equipped with Multiple Tuned Liquid Dampers Using Wind Tunnel Loads

In this chapter, a 38-story high-rise building (Indianapolis building) is modelled using the 3D finite element model, developed and validated in Chapter 2. The 3D-Strucutre-TLD system model is expanded to consider multiple TLDs (3D-Strucutre-MTLD) and used to conduct time history analyses on a high-rise building equipped with multiple TLDs to suppress either the first two or the first three structural modes of vibration, respectively. Recorded wind tunnel data is used as the excitation input over a range of wind loading directions ($0°$ and $360°$). An existing TLD design procedure (Tait 2008) is expanded, using modal factors (MF), to design multiple TLDs utilized to suppress selected structural modes of vibration. A spectral analysis is employed using MATLAB$^®$ and the modal factors are evaluated (MF) for the uncontrolled and controlled structural time history responses.

The major findings from this study are:

- Excellent agreement is observed between both nonlinear TLD models, the TLD fluid model and the EADTMD model. Therefore, the second TLD model (i.e. EADTMD

model) has been used to carry out the remaining analyses resulting in a significant reduction in computational time.

- A two-step TLD design procedure provides the ability to assess the decision of installing extra sets of TLD tanks to suppress higher modes of the building. This design procedure also allows the selected TLD tank locations and placement directions to be evaluated. By employing the two-step TLD design procedure, the following findings are observed:

  o The floor centre of the Indianapolis building is found to be an ideal location for the first two mode tanks to be installed, where the modal factor values at the floor centre in both x- and y-directions have higher values than the corners for the uncontrolled structural responses.

  o The maximum average peak hourly resultant acceleration response value ($R_{peak-hr}$) of the Indianapolis building at the critical wind loading angle of $210°$ is reduced by minimum values of 32% and 53% at the centre of mass and the four corners, respectively. As a result, the Indianapolis building is found to satisfy acceptable acceleration response level criteria for office buildings using TLDs to suppress the first two modes of vibration compared to acceptable criteria for hotels with TLDs installed to suppress the first three modes of vibration.

7.1.3 Finite Element Modelling of Structure-MTLD Systems with Inclined Damping Screens

In the first part of this chapter, the nonlinear TLD fluid model is updated and validated with experimental values found in the literature to simulate inclined damping screens in a TLD by reproducing the non-dimensional energy (E'_w) and the frequency response curves for two sets of slat screens, at different normalized excitation amplitudes

The main findings from this part of the study include:

- The updated fluid model is found to be in excellent agreement with the experimental test values obtained from a shake table testing program found in the literature.

- The updated TLD fluid model is found to overcome the limitations of existing linear models as following:

  o The robustness of a structure-TLD system model due to mistuning is addressed utilizing the updated nonlinear TLD fluid model as it captures the hardening behaviour.

o The updated TLD fluid model provides an accurate estimation for the resultant base shear forces at higher screen inclination angles (θ) compared to existed linear models. In addition, the nonlinear response of free-surface is also simulated.

In the second part of this chapter, the updated nonlinear TLD fluid model is implemented into a 3D finite element model (3D-Structure-TLD) and expanded to model multiple TLDs (3D-Structure-MTLD). The ability to passively control the inherent damping ratio in a tuned liquid damper (ζ_{TLD}) over a range of excitation amplitudes is demonstrated.

The main findings from the second part of this study include:

- The vertical screens are found to operate optimally for only one particular structural response acceleration. Throughout different screen angles (θ) an envelope is drawn capturing 100% TLD efficiency (ψ) over a range of structural response accelerations. The envelope curves show that angled screens are able to maintain 100% TLD efficiency (ψ) over a range of structural response accelerations.

- The use of the preliminary TLD design procedure (Tait 2008) to estimate the damping screen properties to achieve 100% TLD efficiency (ψ) at different selected target peak hourly acceleration responses and mass ratios is investigated. Results are found to be in agreement with nonlinear numerical results. Thus, the preliminary TLD design procedure is employed to estimate the required inclination angle values (θ) for the damping screens.

- Dynamic analysis of a 38-story high-rise building is carried out utilizing a 4-hour duration recorded wind tunnel loading time history at the critical wind loading direction of 210° at different return period wind speeds ranging between 1 month and 50 years. The results show that employing inclined damping screens in the TLDs leads to approximately constant TLD inherent damping ratio values (ζ_{TLD}) over the selected return periods.

7.1.4 Development and Validation of a Finite Element Structure Semi-Active Tuned Liquid Damper System Model

A control strategy based on the gain scheduling scheme is developed, by actively controlling the damping screen inclination angles (θ) and their resulting loss coefficient values (C_θ). Results from the semi-active TLD numerical simulation for a 3D single-story structure subjected to random excitation are compared with values from manually adjusted damping screen inclination angles. An updated nonlinear fluid model of a TLD equipped

with inclined damping screens, developed and validated in Chapter 4, is used to determine the resulting TLD base shear force in real time. The necessary steps for constructing the look-up table are described in detail. To implement the gain scheduling scheme in the numerical simulation, three parameters are added in the semi-active TLD control technique (3D-Structure-SA-TLD), in addition to the fitted equation of the look-up table. These parameter are, the averaging time (AT), the updating time (UT) and the initial time (IT). A sensitivity study is performed utilizing a 3D single-story structure equipped with a TLD with the aim of selecting the first two parameter values (AT and UT).

Important findings that can be drawn from this chapter include:

- The semi-active TLD control system with practical control parameters (i.e. $5 \leq AT \leq 60$ min, $UT = T$) exceeds the efficiency (ψ) of the passive TLD control system in further reduction of the RMS structural acceleration response value ($\sigma_{\ddot{x}}$) up to 11.7% and matches the efficiency of the passive TLD control system in reducing the peak hourly structural response values ($\ddot{x}_{peak-hr}$).

- The semi-active TLD control system with instantaneous control parameters (i.e. $AT = UT = \Delta t$) exceeds the efficiency (ψ) of the passive TLD control system; both in a reduction of the average peak hourly ($\ddot{x}_{peak-hr}$) and RMS ($\sigma_{\ddot{x}}$) structural acceleration response values.

- The semi-active TLD control system provides the ability to achieve the above three results over a wide range of applied excitations compared to the passive TLD control system.

7.1.5   Applications of Multiple Semi-Active TLDs for Structural Control of Three Dimensional High-Rise Buildings Using Wind Tunnel Loads

In this chapter, the semi-active TLD control technique is expanded to semi-active multiple TLDs (3D-Structre-SA-MTLD) and employed to analyze a multi-modal high-rise building subjected to recorded wind tunnel data ($0° - 360°$) at a 10 year serviceability return period; and at the critical wind loading angle of $210°$ for return periods from 1 month to 50 years. A proposed procedure for selecting the damping screen loss coefficient range is presented and evaluated. An alternative procedure to the look-up table is developed and implemented in the numerical simulation based on the preliminary TLD design procedure, which was introduced by Tait (2008) and expanded for a multi-modal high-rise building in

Chapter 3. As a result, TLD inherent damping ratios (ζ_{TLD}) are maintained in real time by evaluating the required damping screen loss coefficient values (C_θ).

The main findings from this chapter are:

- A nearly constant percentage response reduction values of the resultant RMS structural acceleration responses (R_{RMS}) between 40% and 50% at the centre of mass (CM) and the four corners ($C1$; $C2$; $C3$; $C4$) is achieved over a wide range of wind loading directions ($0° - 360°$) employing the semi-active control technique.

- At the critical wind loading angle of $210°$ and at a 10-year serviceability return period, used for the design of the conventional passive TLD system, the semi-active TLD control system attains a 5% greater RMS acceleration percentage response reduction value.

- At the critical wind loading angle of $210°$ and at return periods ranging from 1 month to 50 years, the semi-active control system provides nearly constant percentage response reduction with maximum percentage difference of 4% compared to 19% for the conventional passive TLD control system. As a result, improved overall performance of the semi-active TLD control system, over a wide range of wind loading angles and return periods, is demonstrated compared to the conventional passive TLD control system.

7.2.   Recommendations for Future Study

This section presents recommendations for future work

[1] Model scale testing of a structure-SA-TLD system subjected to random and earthquake excitation is highly recommended, allowing the numerical simulation results to be compared with experimental values. A particularly interesting case to experimentally investigate is the SA-TLD control technique with instantaneous control parameters (i.e. $AT = UT = \Delta t$), which responds instantaneously to highly fluctuated structural response values of a structure under random forces.

[2] Full-scale implementation and monitoring of structures equipped with semi-active multiple TLDs (SA-MTLD) should be conducted and compared with numerical simulations of the 3D-Structure-SA-MTLD system model.

[3] The three dimensional finite element model in conjunction with single/multiple conventional passive/SA-TLD system models provides the ability to accurately predict the reduced straining actions in the lateral load resisting elements of full-scale structures (i.e. normal force, shear force and bending moment). The following question arises. Can

the SA-TLD control technique be relied upon for strength consideration and wind related serviceability issues at the same time?

Table 1.   TLD Design for Mode 2 (y-direction) for the Indianapolis Building

Quantity	Equation(s)	Value	
Initial peak hourly acceleration, $\ddot{y}_{initial}$		**14.14**	**milli-g**
Modal Factor, MF		**94.08**	**%**
Initial modal peak hourly acceleration, $\ddot{y}_{initial-m}$	$\ddot{y}_{initial-m} = \ddot{y}_{initial}.MF$	**13.24**	**milli-g**
Structure cyclic frequency, f_{s-y}		0.16	Hz
Structure time period, T_{s-y}	$T_{s-y} = 1/f_{s-y}$	6.18	sec
Structure natural frequency, ω_{s-y}	$\omega_{s-y} = 2\pi/T_{s-y}$	1.02	rad/sec
Peak factor, PF_y	$PF_y = \sqrt{2\ln(573\omega_{s-y})} + \dfrac{0.577}{\sqrt{2\ln(573\omega_{s-y})}}$	3.73	
Initial RMS acceleration, $\sigma_{\ddot{y}-initial-m}$	$\sigma_{\ddot{y}-initial-m} = \dfrac{\ddot{y}_{initial-m}}{PF_y}$	**3.40**	**milli-g**
Initial RMS displacement, $\sigma_{y-initial-m}$	$\sigma_{y-initial-m} = \dfrac{\sigma_{\ddot{y}-initial-m}}{\omega_{s-y}^2}\dfrac{g}{1000}$	0.03	m
Assumed mass ratio, μ		0.06	(6.0%)
Effective damping provided by TLD, $\zeta_{TLD-eff-opt_y}$	$\zeta_{TLD-eff-opt_y} = \dfrac{1}{4}\sqrt{\dfrac{\mu_y+\mu_y^2}{1+\frac{3}{4}\mu_y}}$	0.06	(6.2%)
Optimal damping ratio, $\zeta_{TLD-opt_y}$	$\zeta_{TLD-opt_x} = \sqrt{\dfrac{\mu_x+\frac{3}{4}\mu_x^2}{4+6\mu_x+2\mu_x^2}}$	0.12	(12.0%)
Optimal tuning ratio, Ω_{opt_y}	$\Omega_{opt_y} = \dfrac{\sqrt{1+\frac{1}{2}\mu_y}}{1+\mu_y}$	0.96	(95.7%)
Optimal TLD cyclic frequency, $f_{TLD-opt_y}$	$\Omega_{opt_y} = \dfrac{f_{TLD-opt_y}}{f_{s-y}}$	0.16	Hz
Optimal response ratio, R_{opt_y}	$R_{opt_y} = \dfrac{\sigma_{r-y}}{\sigma_y} = \dfrac{1+\mu_y}{\sqrt{2\mu_y+\frac{3}{2}\mu_y^2}}$	2.99	
Structure damping ratio, ζ_s		0.02	(2.0%)
Total structure damping, ζ_{tot-y}	$\zeta_{tot-y} = 0.8\zeta_s + \zeta_{TLD-eff-opt_y}$	0.08	(7.8%)
Target RMS displacement, $\sigma_{y-target-m}$	$\zeta_{tot-y} = \zeta_s\dfrac{\sigma_{y-initial-m}^2}{\sigma_{y-target-m}^2}$	0.02	m
Target RMS acceleration, $\sigma_{\ddot{y}-target-m}$	$\sigma_{\ddot{y}-target-m} = \omega_s^2\,\sigma_{y-target-m}$	**1.80**	**milli-g**
Target peak hourly acceleration, $\ddot{y}_{target-m}$	$\sigma_{\ddot{y}-target-m} = \dfrac{\ddot{y}_{target-m}}{PF_y}$	**6.72**	**milli-g**
TLD response, σ_{r-y}	$\sigma_{r-y} = R_{opt_y}\,\sigma_{y-target-m}$	0.05	m
Select tank dimensions, L_y, h	$f_{TLD-opt_y} = \dfrac{1}{2\pi}\sqrt{\dfrac{\pi g}{L_y}\tanh\left(\dfrac{\pi h}{L_y}\right)}$	**L_y = 13.41 m** **h = 1.87 m**	
Shallow water theory check, h/L_y		0.14	
Select screen properties, y_1, y_2, C_{l-y}	$\zeta_{TLD-y} = C_{l-y}\sqrt{\dfrac{32}{\pi^3}}\tanh^2\left(\dfrac{\pi h}{L_y}\right)\varDelta_y\varXi_y\dfrac{\sigma_{r-y}}{L_y}$ $\varDelta_y = \left(\dfrac{1}{3}+\dfrac{1}{\sinh^2(\frac{\pi h}{L_y})}\right)$ $\varXi_y = \sum_{j=1}^{ns_y}\left|\sin^3\left(\dfrac{\pi y_j}{L_y}\right)\right|$	**$y_1 = 0.4\,L_y$** **$y_2 = 0.6\,L_y$** **$C_{l-y} = 20.26$**	

Table 2.   Preliminary TLD Design for Mode 3 (x-direction) for the Indianapolis Building

Quantity	Equation(s)	Value	
Initial peak hourly acceleration, $\ddot{x}_{initial}$		**16.14**	**milli-g**
Modal Factor, MF		**37.31**	**%**
Initial modal peak hourly acceleration, $\ddot{x}_{initial-m}$	$\ddot{x}_{initial-m} = \ddot{x}_{initial} \cdot MF$	**6.03**	**milli-g**
Structure cyclic frequency, f_{s-x}		0.33	Hz
Structure time period, T_{s-x}	$T_{s-x} = 1/f_{s-x}$	3.01	sec
Structure natural frequency, ω_{s-x}	$\omega_{s-x} = 2\pi/T_{s-x}$	2.09	rad/sec
Peak factor, PF_x	$PF_x = \sqrt{2\ln(573\omega_{s-x})} + \frac{0.577}{\sqrt{2\ln(573\omega_{s-x})}}$	3.92	
Initial RMS acceleration, $\sigma_{\ddot{x}-initial-m}$	$\sigma_{\ddot{x}-initial-m} = \frac{\ddot{x}_{initial-m}}{PF_x}$	**1.54**	**milli-g**
Initial RMS displacement, $\sigma_{x-initial-m}$	$\sigma_{x-initial-m} = \frac{\sigma_{\ddot{x}-initial-m}}{\omega_{s-x}^2} \frac{g}{1000}$	0.00	m
Assumed mass ratio, μ		0.05	(5.0%)
Effective damping provided by TLD, $\zeta_{TLD-eff-opt_x}$	$\zeta_{TLD-eff-opt_x} = \frac{1}{4}\sqrt{\frac{\mu_x + \mu_x^2}{1+\frac{3}{4}\mu_x}}$	0.06	(5.6%)
Optimal damping ratio, $\zeta_{TLD-opt_x}$	$\zeta_{TLD-opt_x} = \sqrt{\frac{\mu_x + \frac{3}{4}\mu_x^2}{4+6\mu_x+2\mu_x^2}}$	0.11	(11.0%)
Optimal tuning ratio, Ω_{opt_x}	$\Omega_{opt_x} = \frac{\sqrt{1+\frac{1}{2}\mu_x}}{1+\mu_x}$	0.96	(96.4%)
Optimal TLD cyclic frequency, $f_{TLD-opt_x}$	$\Omega_{opt_x} = \frac{f_{TLD-opt_x}}{f_{s-x}}$	0.32	Hz
Optimal response ratio, R_{opt_x}	$R_{opt_x} = \frac{\sigma_{r-x}}{\sigma_x} = \frac{1+\mu_x}{\sqrt{2\mu_x+\frac{3}{2}\mu_x^2}}$	3.26	
Structure damping ratio, ζ_s		0.02	(2.0%)
Total structure damping, ζ_{tot-x}	$\zeta_{tot-x} = 0.8\zeta_s + \zeta_{TLD-eff-opt_x}$	0.07	(7.2%)
Target RMS displacement, $\sigma_{x-target-m}$	$\zeta_{tot-x} = \zeta_s \frac{\sigma_{x-initial-m}^2}{\sigma_{x-target-m}^2}$	0.01	m
Target RMS acceleration, $\sigma_{\ddot{x}-target-m}$	$\sigma_{\ddot{x}-target-m} = \omega_s^2 \sigma_{x-target-m}$	**0.81**	**milli-g**
Target peak hourly acceleration, $\ddot{x}_{target-m}$	$\sigma_{\ddot{x}-target-m} = \frac{\ddot{x}_{target-m}}{PF_x}$	**3.18**	**milli-g**
TLD response, σ_{r-x}	$\sigma_{r-x} = R_{opt_x} \sigma_{x-target-m}$	0.01	m
Select tank dimensions, L_x, h	$f_{TLD-opt_x} = \frac{1}{2\pi}\sqrt{\frac{\pi g}{L_x}\tanh\left(\frac{\pi h}{L_x}\right)}$	**L_x =3.00 m** **$h = 0.40$ m**	
Shallow water theory check, h/L_x		0.13	
Select screen properties, x_1, x_2, C_{l-x}	$\zeta_{TLD-x} = C_{l-x}\sqrt{\frac{32}{\pi^3}}\tanh^2\left(\frac{\pi h}{L_x}\right)\Delta_x \Xi_x \frac{\sigma_{r-x}}{L_x}$ $\Delta_x = \left(\frac{1}{3} + \frac{1}{\sinh^2\left(\frac{\pi h}{L_x}\right)}\right)$ $\Xi_x = \sum_{j=1}^{ns_x}\left|\sin^3\left(\frac{\pi x_j}{L_x}\right)\right|$	**$x_1 = 0.4\, L_x$** **$x_2 = 0.6\, L_x$** **$C_{l-x} = 35.26$**	

Table 3.   Preliminary TLD Design for Mode 3 (y-direction) for the Indianapolis Building

Quantity	Equation(s)	Value	
Initial peak hourly acceleration, $\ddot{y}_{initial}$		**20.33**	**milli-g**
Modal Factor, MF		**74.01**	**%**
Initial modal peak hourly acceleration, $\ddot{y}_{initial-m}$	$\ddot{y}_{initial-m} = \ddot{y}_{initial}.MF$	**15.04**	**milli-g**
Structure cyclic frequency, f_{s-y}		0.33	Hz
Structure time period, T_{s-y}	$T_{s-y} = 1/f_{s-y}$	3.01	sec
Structure natural frequency, ω_{s-y}	$\omega_{s-y} = 2\pi/T_{s-y}$	2.09	rad/sec
Peak factor, PF_y	$PF_y = \sqrt{2\ln(573\omega_{s-y})} + \dfrac{0.577}{\sqrt{2\ln(573\omega_{s-y})}}$	3.92	
Initial RMS acceleration, $\sigma_{\ddot{y}-initial-m}$	$\sigma_{\ddot{y}-initial-m} = \dfrac{\ddot{y}_{initial-m}}{PF_y}$	**3.84**	**milli-g**
Initial RMS displacement, $\sigma_{y-initial-m}$	$\sigma_{y-initial-m} = \dfrac{\sigma_{\ddot{y}-initial-m}}{\omega_{s-y}^2}\dfrac{g}{1000}$	0.01	m
Assumed mass ratio, μ		0.05	(5.0%)
Effective damping provided by TLD, $\zeta_{TLD-eff-opt_y}$	$\zeta_{TLD-eff-opt_y} = \dfrac{1}{4}\sqrt{\dfrac{\mu_y+\mu_y^2}{1+\frac{3}{4}\mu_y}}$	0.06	(5.6%)
Optimal damping ratio, $\zeta_{TLD-opt_y}$	$\zeta_{TLD-opt_x} = \sqrt{\dfrac{\mu_x+\frac{3}{4}\mu_x^2}{4+6\mu_x+2\mu_x^2}}$	0.11	(11.0%)
Optimal tuning ratio, Ω_{opt_y}	$\Omega_{opt_y} = \dfrac{\sqrt{1+\frac{1}{2}\mu_y}}{1+\mu_y}$	0.96	(96.4%)
Optimal TLD cyclic frequency, $f_{TLD-opt_y}$	$\Omega_{opt_y} = \dfrac{f_{TLD-opt_y}}{f_{s-y}}$	0.32	Hz
Optimal response ratio, R_{opt_y}	$R_{opt_y} = \dfrac{\sigma_{r-y}}{\sigma_y} = \dfrac{1+\mu_y}{\sqrt{2\mu_y+\frac{3}{2}\mu_y^2}}$	3.26	
Structure damping ratio, ζ_s		0.02	(2.0%)
Total structure damping, ζ_{tot-y}	$\zeta_{tot-y} = 0.8\zeta_s + \zeta_{TLD-eff-opt_y}$	0.07	(7.2%)
Target RMS displacement, $\sigma_{y-target-m}$	$\zeta_{tot-y} = \zeta_s\dfrac{\sigma_{y-initial-m}^2}{\sigma_{y-target-m}^2}$	0.01	m
Target RMS acceleration, $\sigma_{\ddot{y}-target-m}$	$\sigma_{\ddot{y}-target-m} = \omega_s^2\,\sigma_{y-target-m}$	**2.02**	**milli-g**
Target peak hourly acceleration, $\ddot{y}_{target-m}$	$\sigma_{\ddot{y}-target-m} = \dfrac{\ddot{y}_{target-m}}{PF_y}$	**7.92**	**milli-g**
TLD response, σ_{r-y}	$\sigma_{r-y} = R_{opt_y}\,\sigma_{y-target}$	0.02	m
Select tank dimensions, L_y, h	$f_{TLD-opt_y} = \dfrac{1}{2\pi}\sqrt{\dfrac{\pi g}{L_y}\tanh\left(\dfrac{\pi h}{L_y}\right)}$	**L_y =3.00** **$h = 0.40$**	**m** **m**
Shallow water theory check, h/L_y		0.13	
Select screen properties, y_1, y_2, C_{l-y}	$\zeta_{TLD-y} = C_{l-y}\sqrt{\dfrac{32}{\pi^3}}\tanh^2(\dfrac{\pi h}{L_y})\Delta_y\Xi_y\dfrac{\sigma_{r-y}}{L_y}$ $\Delta_y = \left(\dfrac{1}{3}+\dfrac{1}{\sinh^2(\frac{\pi h}{L_y})}\right)$ $\Xi_y = \sum_{j=1}^{ns_y}\left\lvert\sin^3\left(\dfrac{\pi y_j}{L_y}\right)\right\rvert$	$y_1 = 0.4\,L_y$ $y_2 = 0.6\,L_y$ $C_{l-y} = 14.14$	

Table 4.   Water Mass Calculations for TLDs to Suppress Mode 3 for the Indianapolis Building

	Quantity	Equation(s)	Value
Corner 3	Selected tank dimensions, L_x, L_y, h		$L_x = 3.00$ m $L_y = 3.00$ m $h = 0.40$ m
	Water height to tanks length ratio in x-dir	h/L_x	0.13
	Water height to tanks length ratio in y-dir	h/L_y	0.13
	Water mass of 1 tank, $m_{w(1tank)}$	$m_{w(1tank)} = L_x L_y h$	3575.4 kg
	TLD mass of 1 tank in θ-dir, $m_{TLD-\theta(1tank)}$	$m_{TLD-\theta(1tank)} \approx m_{1-\theta} = \dfrac{8\,tanh\left(\pi\frac{h}{L_x}\right)}{\pi^3\left(\frac{h}{L_x}\right)} m_{w(1tank)}$	$0.77\,m_{w(1tank)} = $ 2741.7 kg
	Total building mass, M_s	$M_s = \sum_{i=1}^{i=N_f} m_f$	36412955 kg
	Generalized building mass in θ-dir, M_θ^*	$M_\theta^* = \sum_{i=1}^{i=N_f} (m_f)_i\,(\phi_t^2)_i$	12198340 kg
	Required TLD mass in θ-dir, $m_{TLD-\theta}$	$m_{TLD-\theta} = \mu_{TLD-\theta} M_\theta^*$	609917 kg
	No. of Tanks required in θ-dir, $N_{TLD-\theta}$	$N_{TLD-\theta} = m_{TLD-\theta}/m_{TLD-\theta(1tank)}$	222.46
	Chosen No. of tanks for mode 3, $N_{TLD-\theta}$	(Bi-directional tanks)	**111**
	Actual mass ratio in θ-dir, $\mu_{\theta-actual}$	$\mu_{\theta-actual} = N_{TLD-\theta} m_{TLD-\theta(1tank)}/M_\theta^*$	**2.49 %**
	Mass ratio of contained water, μ_w (Bi-directional)	$\mu_w = N_{TLD-\theta} m_{w(1tank)}/M_s$	**1.09 %**
Corners 2 and 4	Selected tank dimensions, L_x, B_x, L_y, B_y, h		$L_x = 3.00$ m $B_x = 13.32$ m $L_y = 3.00$ m $B_y = 13.32$ m $h = 0.40$ m
	Chosen No. of tanks for mode 3, $N_{TLD-\theta}$	(Uni-directional tanks)	**25*2**
	Actual mass ratio in θ-dir, $\mu_{\theta-actual}$	$\mu_{\theta-actual} = N_{TLD-\theta} m_{TLD-\theta(1tank)}/M_\theta^*$	**2.49 %**
	Mass ratio of contained water, μ_w (Uni-directional)	$\mu_w = N_{TLD-\theta} m_{w(1tank)}/M_s$	**1.09 %**
	Mass ratio of contained water, μ_w (Bi/Uni-directional)		**2.18 %**
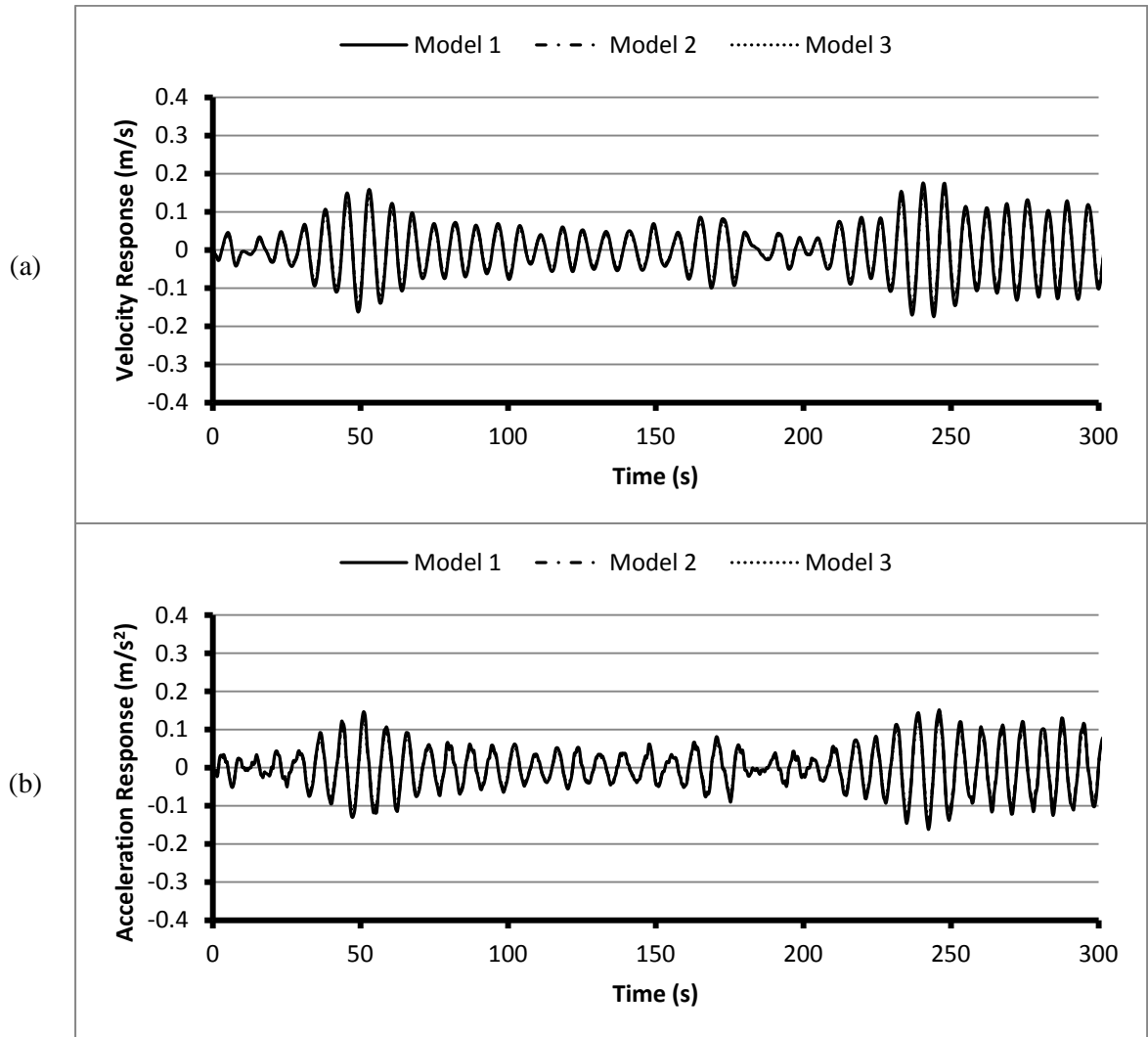
Fig. 1. Time History of the Indianapolis Building at CM with No-TLD Installed for the (a) Velocity and (b) Acceleration in the x-direction ($z = 154.6$ m; $\theta_w = 210°$)
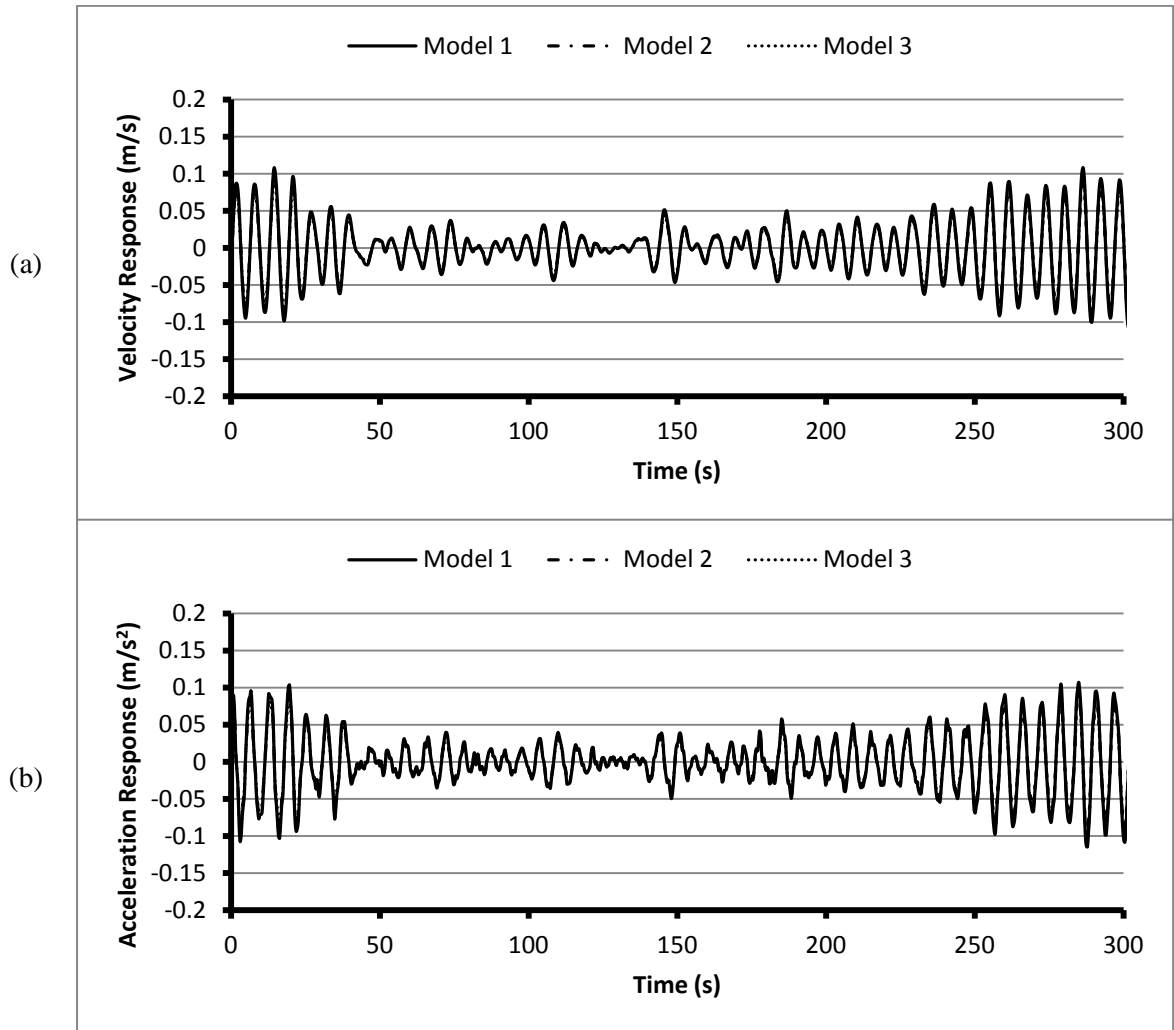
Fig. 2. Time History of the Indianapolis Building at CM with No-TLD Installed for the (a) Velocity and (b) Acceleration in the y-direction ($z = 154.6$ m; $\theta_w = 210°$)
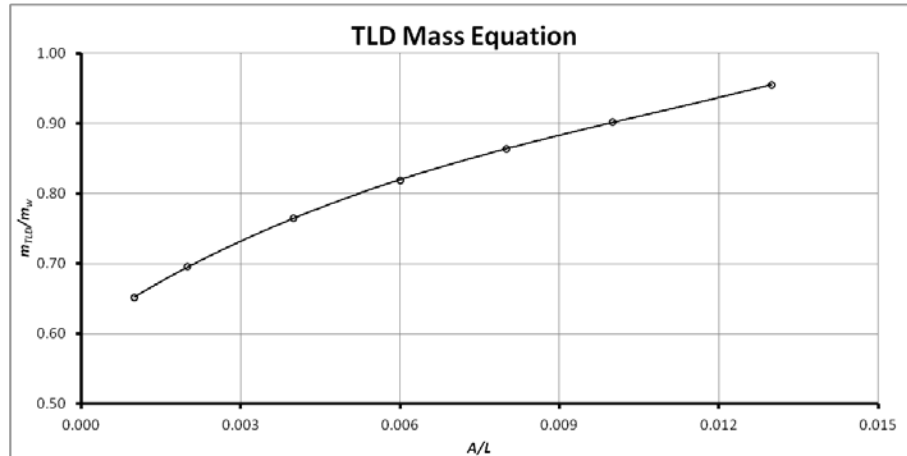
(a)
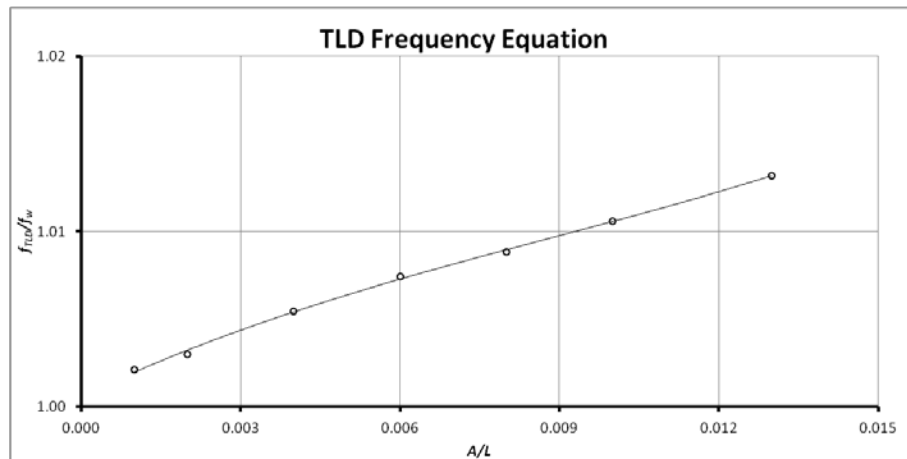
(b)
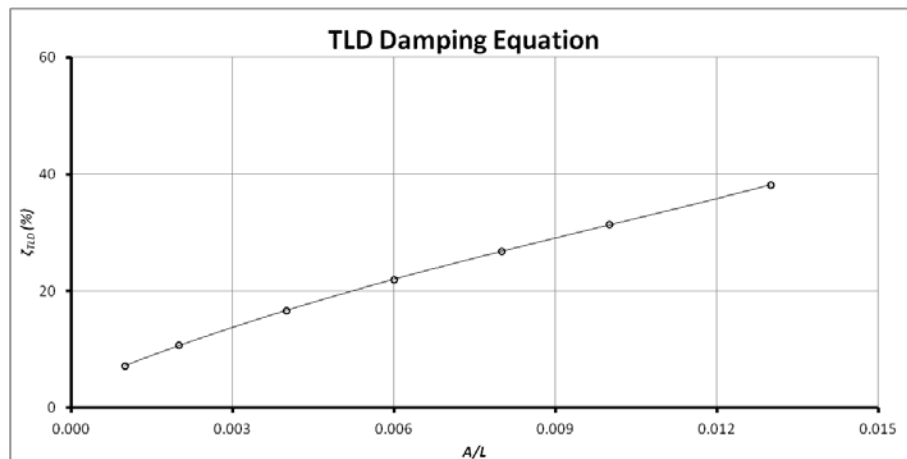
(c)

Fig. 3.   TLD (a) Mass Ratio, (b) Frequency Ratio, and (c) Damping Ratio with respect to the Normalized Amplitude of Excitation for Mode 2 tanks in the y-direction of the Indianapolis Building
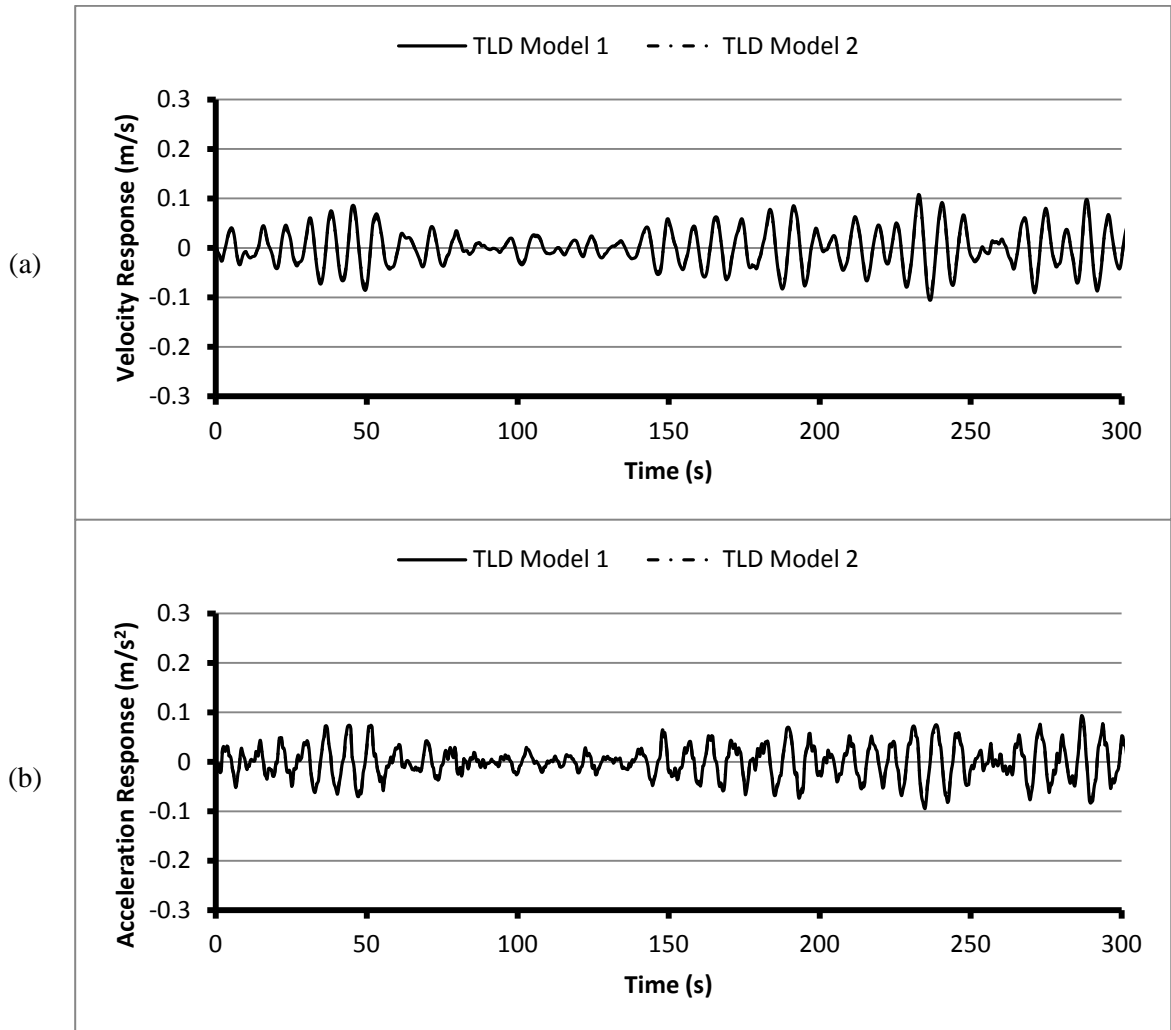
Fig. 4. Time Histories of the Indianapolis Building at the CM with TLDs Installed to Suppress the First two Modes for the (a) Velocity, and (c) Acceleration in the x-direction ($z = 154.6$ m; $\theta_w = 210°$)
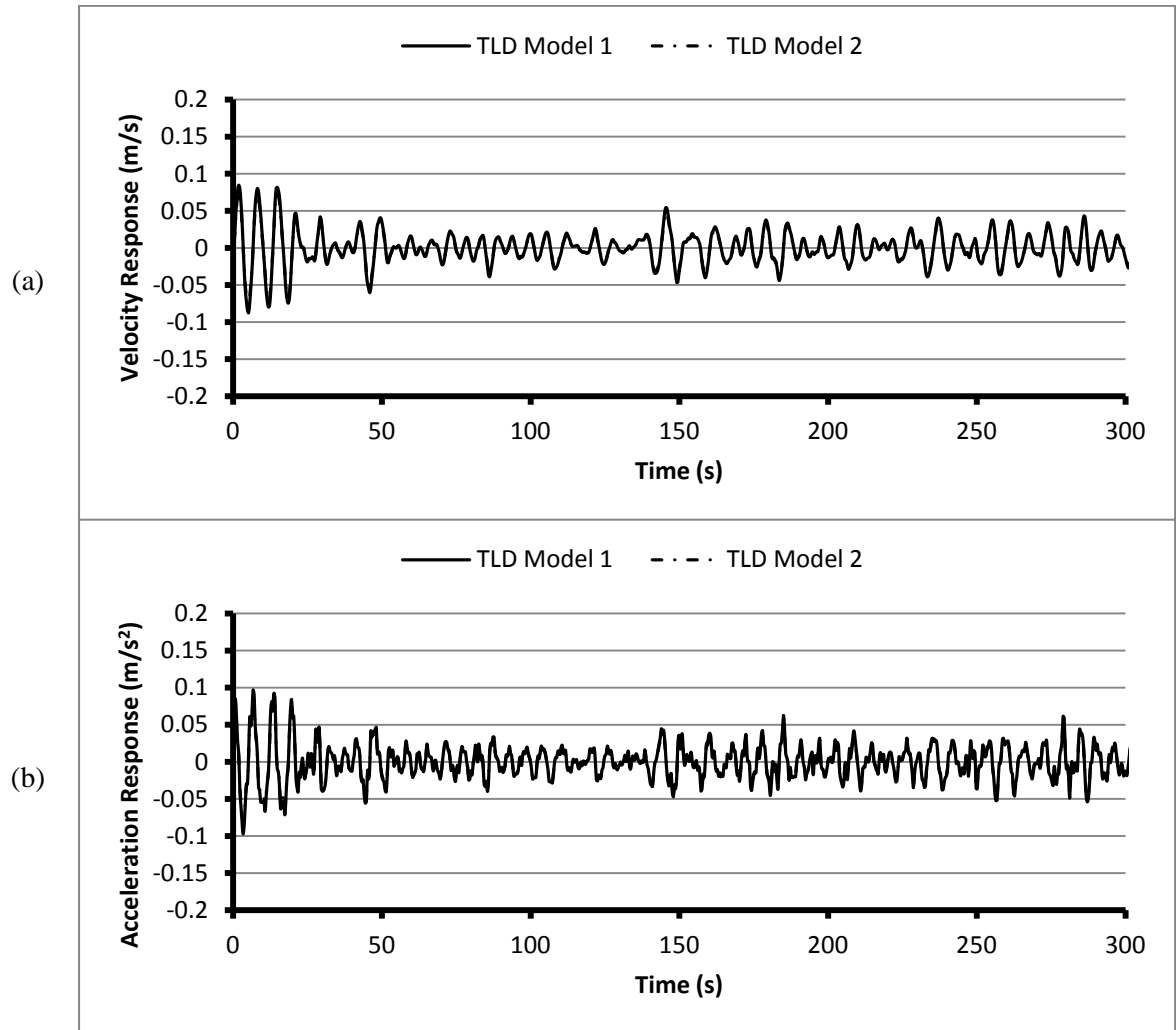
Fig. 5.   Time Histories of the Indianapolis Building at the CM with TLDs Installed to Suppress the First two Modes for the (a) Velocity, and (b) Acceleration in the y-direction ($z = 154.6$ m; $\theta_w = 210°$)
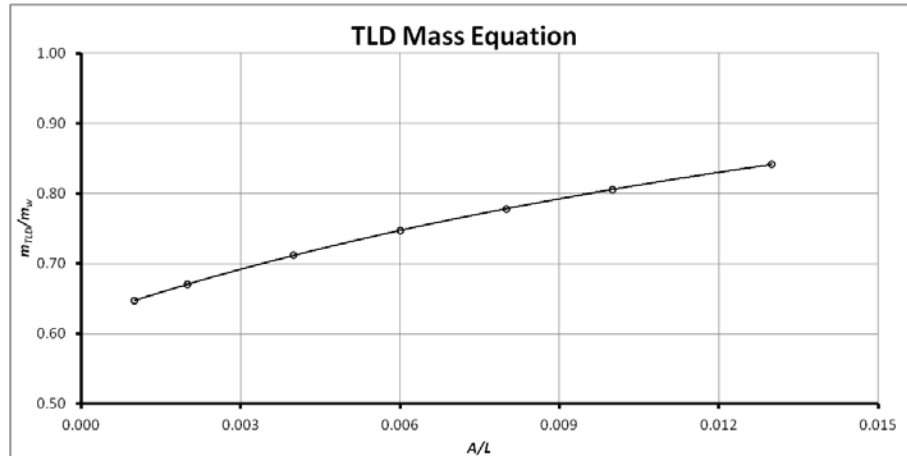
(a)
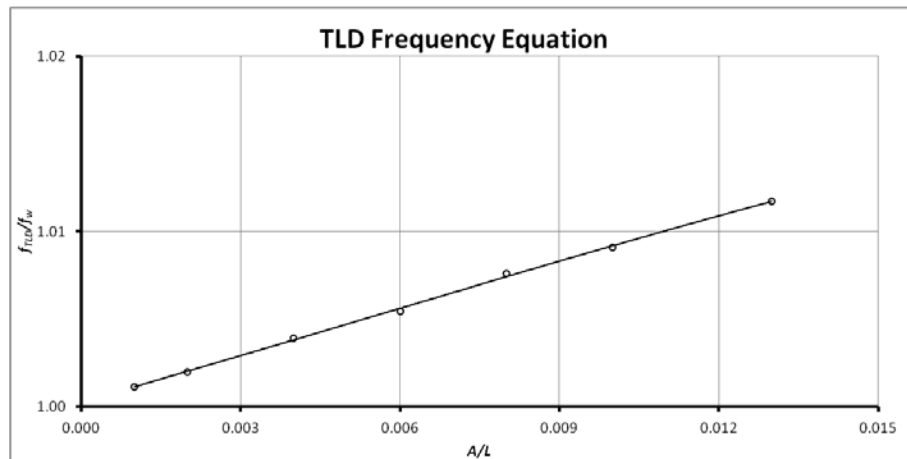
(b)
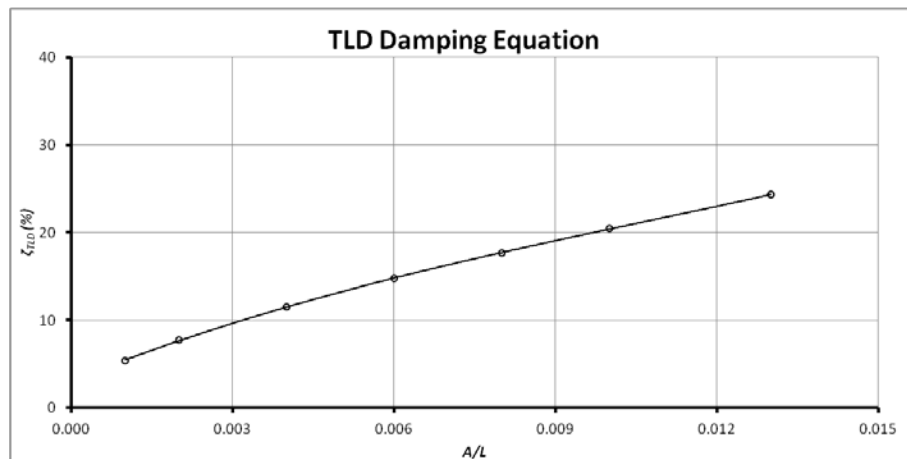
(c)

Fig. 6.   TLD (a) Mass Ratio, (b) Frequency Ratio, and (c) Damping Ratio with respect to the Normalized Amplitude of Excitation for Mode 3 tanks in the x-direction of the Indianapolis Building

(a)

(b)

(c)

Fig. 7.   TLD (a) Mass Ratio, (b) Frequency Ratio, and (c) Damping Ratio with respect to the Normalized Amplitude of Excitation for Mode 3 tanks in y-direction of the Indianapolis Building

Table 1. TLD Design for Vertical Damping Screens ($\mu = 2.5\%$)

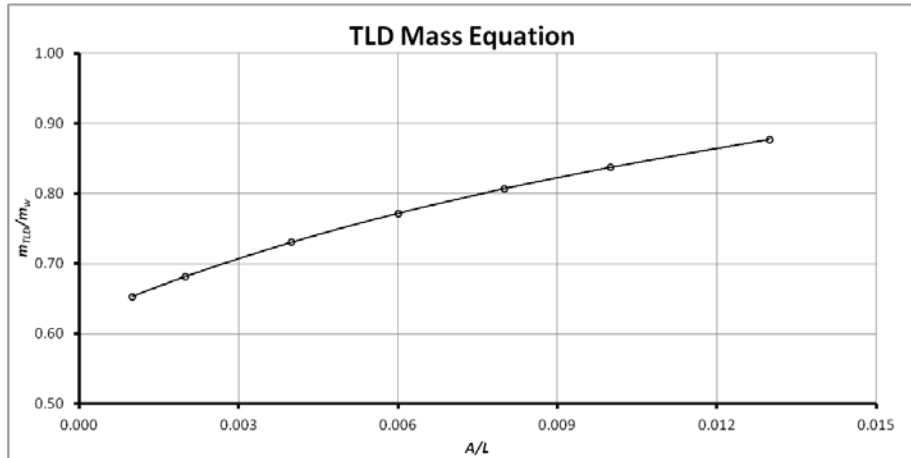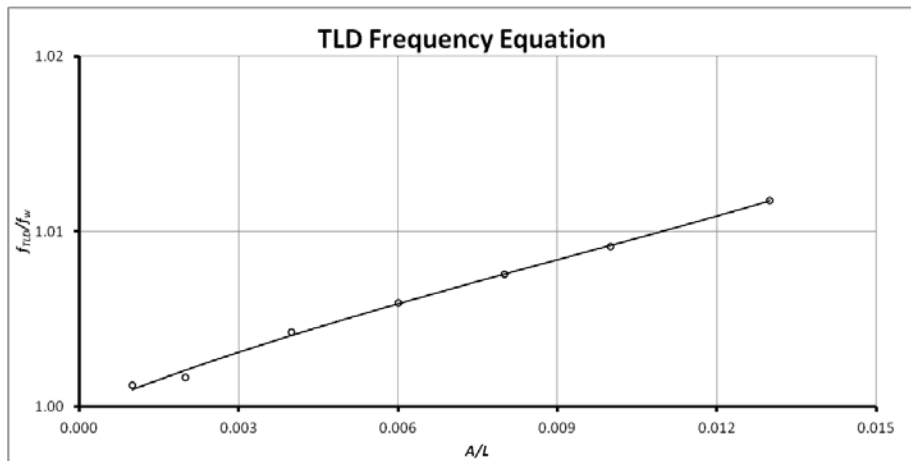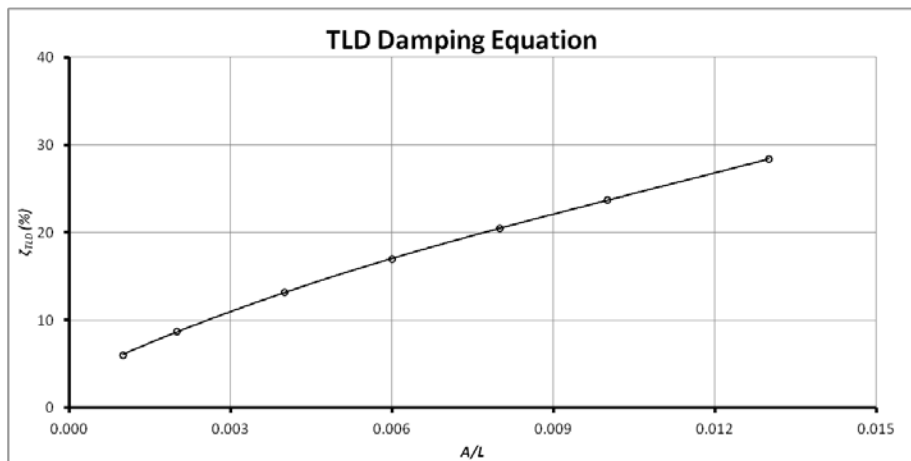| Quantity	Equation(s)	Value	
Initial peak hourly acceleration, $\ddot{x}_{initial}$		**45.56**	**milli-g**
Structure cyclic frequency, f_{s-x}		0.558	Hz
Structure time period, T_{s-x}	$T_{s-x} = 1/f_{s-x}$	1.792	s
Structure natural frequency, ω_{s-x}	$\omega_{s-x} = 2\pi/T_{s-x}$	3.507	rad/s
Peak factor, PF_x	$PF_x = \sqrt{2\ln(181\omega_{s-x})} + \frac{0.577}{\sqrt{2\ln(181\omega_{s-x})}}$	3.753	
Initial RMS acceleration, $\sigma_{\ddot{x}-initial}$	$\sigma_{\ddot{x}-initial} = \frac{\ddot{x}_{initial}}{PF_x}$	**12.15**	**milli-g**
Initial RMS displacement, $\sigma_{x-initial}$	$\sigma_{x-initial} = \frac{\sigma_{\ddot{x}-initial}}{\omega_{s-x}^2}\frac{g}{1000}$	9.700	mm
Assumed water mass ratio, μ_w		0.035	(3.50%)
Assumed mass ratio, μ		0.027	(2.69%)
Effective damping provided by TLD, $\zeta_{TLD-eff-opt_x}$	$\zeta_{TLD-eff-opt_x} = \frac{1}{4}\sqrt{\frac{\mu_x+\mu_x^2}{1+\frac{3}{4}\mu_x}}$	0.039	(3.96%)
Optimal damping ratio, $\zeta_{TLD-opt_x}$	$\zeta_{TLD-opt_x} = \sqrt{\frac{\mu_x+\frac{3}{4}\mu_x^2}{4+6\mu_x+2\mu_x^2}}$	0.078	(7.83%)
Optimal tuning ratio, Ω_{opt_x}	$\Omega_{opt_x} = \frac{\sqrt{1+\frac{1}{2}\mu_x}}{1+\mu_x}$	0.981	(98.1%)
Optimal TLD cyclic frequency, $f_{TLD-opt_x}$	$\Omega_{opt_x} = \frac{f_{TLD-opt_x}}{f_{s-x}}$	0.547	Hz
Optimal response ratio, R_{opt_x}	$R_{opt_x} = \frac{\sigma_{r-x}}{\sigma_x} = \frac{1+\mu_x}{\sqrt{2\mu_x+\frac{3}{2}\mu_x^2}}$	4.541	
Structure damping ratio, ζ_s		0.0006	(0.06%)
Total structure damping, ζ_{tot-x}	$\zeta_{tot-x} = 0.8\zeta_s + \zeta_{TLD-eff-opt_x}$	0.0401	(4.01%)
Target RMS displacement, $\sigma_{x-target}$	$\zeta_{tot-x} = \zeta_s \frac{\sigma_{x-initial}^2}{\sigma_{x-target}^2}$	1.190	mm
Target RMS acceleration, $\sigma_{\ddot{x}-target}$	$\sigma_{\ddot{x}-target} = \omega_s^2\,\sigma_{x-target}$	**01.73**	**milli-g**
Target peak hourly acceleration, $\ddot{x}_{target}$	$\sigma_{\ddot{x}-target} = \frac{\ddot{x}_{target}}{PF_x}$	**06.50**	**milli-g**
TLD response, σ_{r-x}	$\sigma_{r-x} = R_{opt_x}\,\sigma_{x-target}$	5.380	mm
Select tank dimensions, L_x, h	$f_{TLD-opt_x} = \frac{1}{2\pi}\sqrt{\frac{\pi g}{L_x}\tanh\left(\frac{\pi h}{L_x}\right)}$	**$L_x= 0.966$ m** **$h = 0.120$ m**	
Shallow water theory check, h/L_x		0.124	
Select screen properties, x_1, x_2, C_{l-x}	$\zeta_{TLD-x} = C_{l-x}\sqrt{\frac{32}{\pi^3}}\tanh^2\left(\frac{\pi h}{L_x}\right)\Delta_x\Xi_x\frac{\sigma_{r-x}}{L_x}$ $\Delta_x = \left(\frac{1}{3}+\frac{1}{\sinh^2\left(\frac{\pi h}{L_x}\right)}\right)$ $\Xi_x = \sum_{j=1}^{ns_x}\left|\sin^3\left(\frac{\pi x_j}{L_x}\right)\right|$	**$x_1 = 0.4\,L_x$** **$x_2 = 0.6\,L_x$** **$C_{l-x} = 8.27$**	

Table 2. TLD Design for Vertical Damping Screens (μ =3.5%)

Quantity	Equation(s)	Value	
Initial peak hourly acceleration, $\ddot{x}_{initial}$		**65.81**	**milli-g**
Structure cyclic frequency, f_{s-x}		0.558	Hz
Structure time period, T_{s-x}	$T_{s-x} = 1/f_{s-x}$	1.792	s
Structure natural frequency, ω_{s-x}	$\omega_{s-x} = 2\pi/T_{s-x}$	3.507	rad/s
Peak factor, PF_x	$PF_x = \sqrt{2\ln(181\omega_{s-x})} + \dfrac{0.577}{\sqrt{2\ln(181\omega_{s-x})}}$	3.753	
Initial RMS acceleration, $\sigma_{\ddot{x}-initial}$	$\sigma_{\ddot{x}-initial} = \dfrac{\ddot{x}_{initial}}{PF_x}$	**17.55**	**milli-g**
Initial RMS displacement, $\sigma_{x-initial}$	$\sigma_{x-initial} = \dfrac{\sigma_{\ddot{x}-initial}}{\omega_{s-x}^2}\dfrac{g}{1000}$	14.01	mm
Assumed water mass ratio, μ_w		0.035	(3.50%)
Assumed mass ratio, μ		0.027	(2.69%)
Effective damping provided by TLD, $\zeta_{TLD-eff-opt_x}$	$\zeta_{TLD-eff-opt_x} = \dfrac{1}{4}\sqrt{\dfrac{\mu_x+\mu_x^2}{1+\frac{3}{4}\mu_x}}$	0.046	(4.69%)
Optimal damping ratio, $\zeta_{TLD-opt_x}$	$\zeta_{TLD-opt_x} = \sqrt{\dfrac{\mu_x+\frac{3}{4}\mu_x^2}{4+6\mu_x+2\mu_x^2}}$	0.092	(9.23%)
Optimal tuning ratio, Ω_{opt_x}	$\Omega_{opt_x} = \dfrac{\sqrt{1+\frac{1}{2}\mu_x}}{1+\mu_x}$	0.974	(97.4%)
Optimal TLD cyclic frequency, $f_{TLD-opt_x}$	$\Omega_{opt_x} = \dfrac{f_{TLD-opt_x}}{f_{s-x}}$	0.543	Hz
Optimal response ratio, R_{opt_x}	$R_{opt_x} = \dfrac{\sigma_{r-x}}{\sigma_x} = \dfrac{1+\mu_x}{\sqrt{2\mu_x+\frac{3}{2}\mu_x^2}}$	3.861	
Structure damping ratio, ζ_s		0.0006	(0.06%)
Total structure damping, ζ_{tot-x}	$\zeta_{tot-x} = 0.8\zeta_s + \zeta_{TLD-eff-opt_x}$	0.0047	(4.74%)
Target RMS displacement, $\sigma_{x-target}$	$\zeta_{tot-x} = \zeta_s\dfrac{\sigma_{x-initial}^2}{\sigma_{x-target}^2}$	1.570	mm
Target RMS acceleration, $\sigma_{\ddot{x}-target}$	$\sigma_{\ddot{x}-target} = \omega_s^2\,\sigma_{x-target}$	**02.40**	**milli-g**
Target peak hourly acceleration, $\ddot{x}_{target}$	$\sigma_{\ddot{x}-target} = \dfrac{\ddot{x}_{target}}{PF_x}$	**09.00**	**milli-g**
TLD response, σ_{r-x}	$\sigma_{r-x} = R_{opt_x}\,\sigma_{x-target}$	6.080	mm
Select tank dimensions, L_x, h	$f_{TLD-opt_x} = \dfrac{1}{2\pi}\sqrt{\dfrac{\pi g}{L_x}\tanh\left(\dfrac{\pi h}{L_x}\right)}$	**L_x= 0.966**	**m**
		h = 0.118	**m**
Shallow water theory check, h/L_x		0.122	
Select screen properties, x_1, x_2, C_{l-x}	$\zeta_{TLD-x} = C_{l-x}\sqrt{\dfrac{32}{\pi^3}}tanh^2(\dfrac{\pi h}{L_x})\Delta_x\varXi_x\dfrac{\sigma_{r-x}}{L_x}$ $\Delta_x = \left(\dfrac{1}{3}+\dfrac{1}{sinh^2(\frac{\pi h}{L_x})}\right)$ $\varXi_x = \sum_{j=1}^{ns_x}\left|sin^3\left(\dfrac{\pi x_j}{L_x}\right)\right|$	**$x_1 = 0.4\,L_x$** **$x_2 = 0.6\,L_x$** **$C_{l-x} = 8.31$**	

Table 3. TLD Design for Vertical Damping Screens ($\mu = 5.0\%$)

Quantity	Equation(s)	Value	
Initial peak hourly acceleration, $\ddot{x}_{initial}$		**90.00**	**milli-g**
Structure cyclic frequency, f_{s-x}		0.558	Hz
Structure time period, T_{s-x}	$T_{s-x} = 1/f_{s-x}$	1.792	s
Structure natural frequency, ω_{s-x}	$\omega_{s-x} = 2\pi/T_{s-x}$	3.507	rad/s
Peak factor, PF_x	$PF_x = \sqrt{2\ln(181\omega_{s-x})} + \frac{0.577}{\sqrt{2\ln(181\omega_{s-x})}}$	3.753	
Initial RMS acceleration, $\sigma_{\ddot{x}-initial}$	$\sigma_{\ddot{x}-initial} = \frac{\ddot{x}_{initial}}{PF_x}$	**24.00**	**milli-g**
Initial RMS displacement, $\sigma_{x-initial}$	$\sigma_{x-initial} = \frac{\sigma_{\ddot{x}-initial}}{\omega_{s-x}^2}\frac{g}{1000}$	19.15	mm
Assumed water mass ratio, μ_w		0.050	(3.50%)
Assumed mass ratio, μ		0.039	(3.85%)
Effective damping provided by TLD, $\zeta_{TLD-eff-opt_x}$	$\zeta_{TLD-eff-opt_x} = \frac{1}{4}\sqrt{\frac{\mu_x+\mu_x^2}{1+\frac{3}{4}\mu_x}}$	0.056	(5.62%)
Optimal damping ratio, $\zeta_{TLD-opt_x}$	$\zeta_{TLD-opt_x} = \sqrt{\frac{\mu_x+\frac{3}{4}\mu_x^2}{4+6\mu_x+2\mu_x^2}}$	0.011	(10.98%)
Optimal tuning ratio, Ω_{opt_x}	$\Omega_{opt_x} = \frac{\sqrt{1+\frac{1}{2}\mu_x}}{1+\mu_x}$	0.964	(96.42%)
Optimal TLD cyclic frequency, $f_{TLD-opt_x}$	$\Omega_{opt_x} = \frac{f_{TLD-opt_x}}{f_{s-x}}$	0.538	Hz
Optimal response ratio, R_{opt_x}	$R_{opt_x} = \frac{\sigma_{r-x}}{\sigma_x} = \frac{1+\mu_x}{\sqrt{2\mu_x+\frac{3}{2}\mu_x^2}}$	3.259	
Structure damping ratio, ζ_s		0.0006	(0.06%)
Total structure damping, ζ_{tot-x}	$\zeta_{tot-x} = 0.8\zeta_s + \zeta_{TLD-eff-opt_x}$	0.0057	(5.67%)
Target RMS displacement, $\sigma_{x-target}$	$\zeta_{tot-x} = \zeta_s \frac{\sigma_{x-initial}^2}{\sigma_{x-target}^2}$	1.970	mm
Target RMS acceleration, $\sigma_{\ddot{x}-target}$	$\sigma_{\ddot{x}-target} = \omega_s^2 \sigma_{x-target}$	**03.33**	**milli-g**
Target peak hourly acceleration, $\ddot{x}_{target}$	$\sigma_{\ddot{x}-target} = \frac{\ddot{x}_{target}}{PF_x}$	**12.50**	**milli-g**
TLD response, σ_{r-x}	$\sigma_{r-x} = R_{opt_x}\sigma_{x-target}$	6.420	mm
Select tank dimensions, L_x, h	$f_{TLD-opt_x} = \frac{1}{2\pi}\sqrt{\frac{\pi g}{L_x}\tanh\left(\frac{\pi h}{L_x}\right)}$	**$L_x = 0.966$ m** **$h = 0.115$ m**	
Shallow water theory check, h/L_x		0.119	
Select screen properties, x_1, x_2, C_{l-x}	$\zeta_{TLD-x} = C_{l-x}\sqrt{\frac{32}{\pi^3}}\tanh^2\left(\frac{\pi h}{L_x}\right)\Delta_x \Xi_x \frac{\sigma_{r-x}}{L_x}$ $\Delta_x = \left(\frac{1}{3}+\frac{1}{\sinh^2\left(\frac{\pi h}{L_x}\right)}\right)$ $\Xi_x = \sum_{j=1}^{ns_x}\left|\sin^3\left(\frac{\pi x_j}{L_x}\right)\right|$	**$x_1 = 0.4\,L_x$** **$x_2 = 0.6\,L_x$** **$C_{l-x} = 8.35$**	

Table 4. TLD Design for Mode 2 of the Indianapolis Building in the y-direction (μ = 2.0%, Serviceability Return Period = 50 years)

Quantity	Equation(s)	Value	
Initial peak hourly acceleration, $\ddot{y}_{initial}$		**18.501**	**milli-g**
Modal Factor, MF		**94.670**	**%**
Initial modal peak hourly acceleration, $\ddot{y}_{initial-m}$	$\ddot{y}_{initial-m} = \ddot{y}_{initial}.MF$	**17.515**	**milli-g**
Structure cyclic frequency, f_{s-y}		0.162	Hz
Structure time period, T_{s-y}	$T_{s-y} = 1/f_{s-y}$	6.180	s
Structure natural frequency, ω_{s-y}	$\omega_{s-y} = 2\pi/T_{s-y}$	1.017	rad/s
Peak factor, PF_y	$PF_y = \sqrt{2\ln(573\omega_{s-y}) + \frac{0.577}{\sqrt{2\ln(573\omega_{s-y})}}}$	3.730	
Initial RMS acceleration, $\sigma_{\ddot{y}-initial-m}$	$\sigma_{\ddot{y}-initial-m} = \frac{\ddot{y}_{initial-m}}{PF_y}$	**4.700**	**milli-g**
Initial RMS displacement, $\sigma_{y-initial-m}$	$\sigma_{y-initial-m} = \frac{\sigma_{\ddot{y}-initial-m}}{\omega_{s-y}^2} \frac{g}{1000}$	0.045	m
Assumed mass ratio, μ		0.020	(2.00%)
Effective damping provided by TLD, $\zeta_{TLD-eff-opt_y}$	$\zeta_{TLD-eff-opt_y} = \frac{1}{4}\sqrt{\frac{\mu_y + \mu_y^2}{1 + \frac{3}{4}\mu_y}}$	0.035	(3.50%)
Optimal damping ratio, $\zeta_{TLD-opt_y}$	$\zeta_{TLD-opt_x} = \sqrt{\frac{\mu_x + \frac{3}{4}\mu_x^2}{4 + 6\mu_x + 2\mu_x^2}}$	0.070	(7.02%)
Optimal tuning ratio, Ω_{opt_y}	$\Omega_{opt_y} = \frac{\sqrt{1 + \frac{1}{2}\mu_y}}{1 + \mu_y}$	0.985	(98.53%)
Optimal TLD cyclic frequency, $f_{TLD-opt_y}$	$\Omega_{opt_y} = \frac{f_{TLD-opt_y}}{f_{s-y}}$	0.159	Hz
Optimal response ratio, R_{opt_y}	$R_{opt_y} = \frac{\sigma_{r-y}}{\sigma_y} = \frac{1 + \mu_y}{\sqrt{2\mu_y + \frac{3}{2}\mu_y^2}}$	5.062	
Structure damping ratio, ζ_s		0.020	(2.00%)
Total structure damping, ζ_{tot-y}	$\zeta_{tot-y} = 0.8\zeta_s + \zeta_{TLD-eff-opt_y}$	0.051	(5.14%)
Target RMS displacement, $\sigma_{y-target-m}$	$\zeta_{tot-y} = \zeta_s \frac{\sigma_{y-initial-m}^2}{\sigma_{y-target-m}^2}$	0.028	m
Target RMS acceleration, $\sigma_{\ddot{y}-target-m}$	$\sigma_{\ddot{y}-target-m} = \omega_s^2\,\sigma_{y-target-m}$	**2.930**	**milli-g**
Target peak hourly acceleration, $\ddot{y}_{target-m}$	$\sigma_{\ddot{y}-target-m} = \frac{\ddot{y}_{target-m}}{PF_y}$	**10.921**	**milli-g**
TLD response, σ_{r-y}	$\sigma_{r-y} = R_{opt_y}\,\sigma_{y-target-m}$	0.141	m
Select tank dimensions, L_y, h	$f_{TLD-opt_y} = \frac{1}{2\pi}\sqrt{\frac{\pi g}{L_y}\tanh\left(\frac{\pi h}{L_y}\right)}$	**L_y= 12.00** **h = 1.58**	**m** **m**
Shallow water theory check, h/L_y		0.131	
Select screen properties, y_1, y_2, C_{l-y}	$\zeta_{TLD-y} = C_{l-y}\sqrt{\frac{32}{\pi^3}}\tanh^2\left(\frac{\pi h}{L_y}\right)\Delta_y \Xi_y \frac{\sigma_{r-y}}{L_y}$ $\Delta_y = \left(\frac{1}{3} + \frac{1}{\sinh^2\left(\frac{\pi h}{L_y}\right)}\right)$ $\Xi_y = \sum_{j=1}^{ns_y}\left|\sin^3\left(\frac{\pi y_j}{L_y}\right)\right|$	**$y_1 = 0.4\,L_y$** **$y_2 = 0.6\,L_y$** **$C_{l-y} = 3.81$**	

Table 5. Water Mass Calculations for TLDs to Suppress Mode 2 for the Indianapolis Building $(\mu = 2.0\%)$

Quantity	Equation(s)	Value
Selected tank dimensions, L_y, B_y, h_y		$L_y = 12.00$ m $B_y = 3.40$ m $h_y = 1.58$ m
Water height to tanks length ratio in y-dir	h_y/L_y	0.13
Water mass of 1 tank, $m_{w(1tank)}$	$m_{w(1tank)} = L_y B_y h_y$	64309.3 kg
TLD mass of 1 tank in y-dir, $m_{TLD-y(1tank)}$	$m_{TLD-y(1tank)} \approx m_{1-y} =$ $\dfrac{8\,tanh\left(\pi\frac{h}{L_y}\right)}{\pi^3\left(\frac{h}{L_y}\right)} m_{w(1tank)}$	$0.77\,m_{w(1tank)} =$ 49357.0 kg
Total building mass, M_s	$M_s = \sum_{i=1}^{i=N_f} m_f$	36412955 kg
Generalized building mass in y-dir, M_y^*	$M_y^* = \sum_{i=1}^{i=N_f}(m_f)_i\,(\phi_t^2)_i$	10013563 kg
Required TLD mass in y-dir, m_{TLD-y}	$m_{TLD-y} = \mu_{TLD-y}M_y^*$	100136 kg
No. of Tanks required in y-dir, N_{TLD-y}	$N_{TLD-y} = m_{TLD-y}/m_{TLD-y(1tank)}$	4.058
Chosen No. of tanks for mode 2, N_{TLD-y}		**4**
Actual mass ratio in y-dir, $\mu_{y-actual}$	$\mu_{y-actual} = N_{TLD-y}m_{TLD-y(1tank)}/M_y^*$	**1.97 %**
Mass ratio of contained water, μ_w	$\mu_w = N_{TLD-y}m_{w(1tank)}/M_s$	**0.71 %**

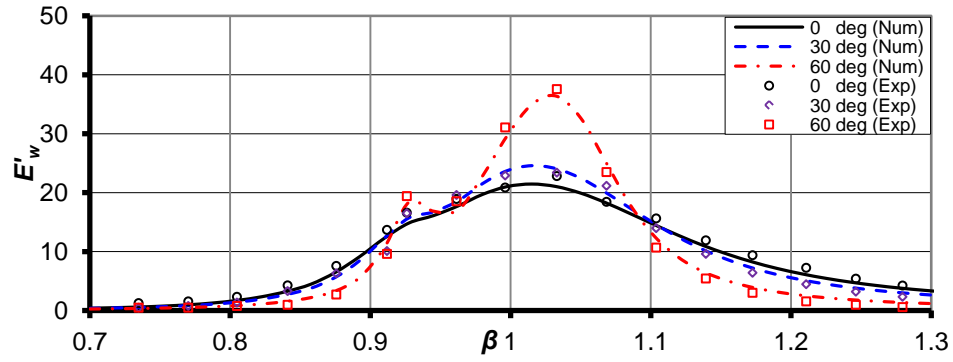**Fig. 1.**   Energy Dissipation Frequency Response Curves for $C_l = 5.69$ and $\Lambda = 0.005$
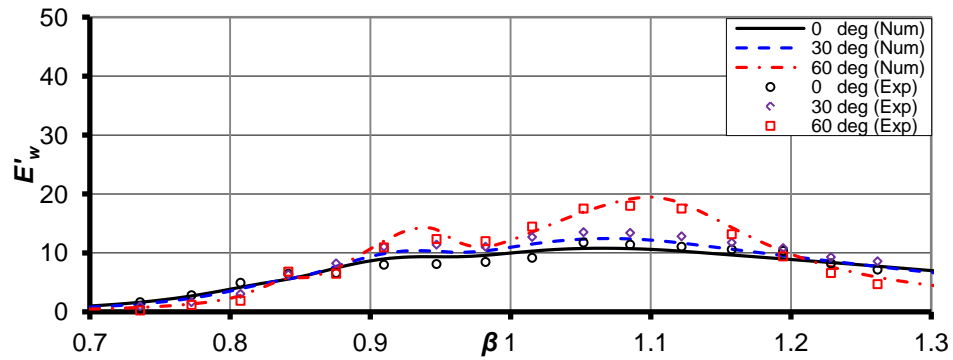

Fig. 2.   Energy Dissipation Frequency Response Curves for $C_l = 5.69$ and $\Lambda = 0.021$
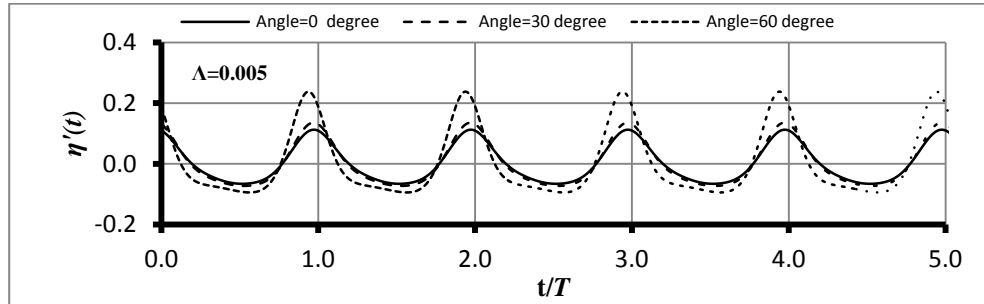

Fig. 3.   Time Histories of η' for $\theta = 0°, 30°$ and $60°$ at $\beta = 1.01$ for $C_l = 5.69$
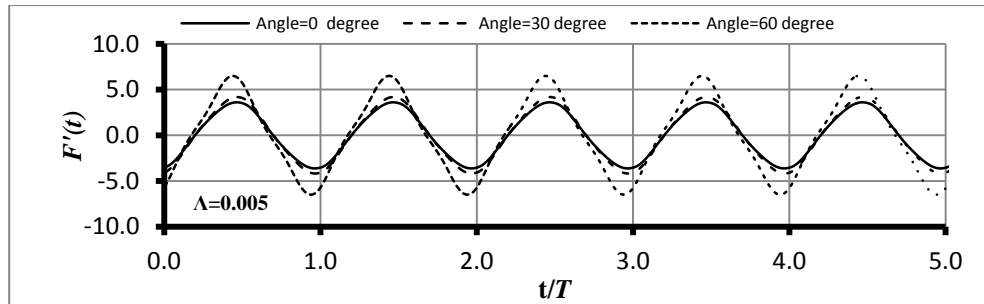

Fig. 4.   Time Histories of F_w' for $\theta = 0°, 30°$ and $60°$ at $\beta = 1.01$ for $C_l = 5.69$

Table 1. Preliminary TLD Design for Vertical Damping Screens ($\mu = 2.5\%$)

Quantity	Equation(s)	Value	
Initial peak hourly acceleration, $\ddot{x}_{initial}$		**45.56**	**milli-g**
Structure cyclic frequency, f_{s-x}		0.59	Hz
Structure time period, T_{s-x}	$T_{s-x} = 1/f_{s-x}$	1.79	s
Structure natural frequency, ω_{s-x}	$\omega_{s-x} = 2\pi/T_{s-x}$	3.51	rad/s
Peak factor, PF_x	$PF_x = \sqrt{2\ln(181\omega_{s-x})} + \dfrac{0.577}{\sqrt{2\ln(181\omega_{s-x})}}$	3.75	
Initial RMS acceleration, $\sigma_{\ddot{x}-initial}$	$\sigma_{\ddot{x}-initial} = \dfrac{\ddot{x}_{initial}}{PF_x}$	**12.15**	**milli-g**
Initial RMS displacement, $\sigma_{x-initial}$	$\sigma_{x-initial} = \dfrac{\sigma_{\ddot{x}-initial}}{\omega_{s-x}^2}\dfrac{g}{1000}$	9.70	mm
Assumed mass ratio, μ		0.025	(2.50%)
Effective damping provided by TLD, $\zeta_{TLD-eff-opt_x}$	$\zeta_{TLD-eff-opt_x} = \dfrac{1}{4}\sqrt{\dfrac{\mu_x+\mu_x^2}{1+\frac{3}{4}\mu_x}}$	0.039	(3.96%)
Optimal damping ratio, $\zeta_{TLD-opt_x}$	$\zeta_{TLD-opt_x} = \sqrt{\dfrac{\mu_x+\frac{3}{4}\mu_x^2}{4+6\mu_x+2\mu_x^2}}$	0.078	(7.83%)
Optimal tuning ratio, Ω_{opt_x}	$\Omega_{opt_x} = \dfrac{\sqrt{1+\frac{1}{2}\mu_x}}{1+\mu_x}$	0.981	(98.1%)
Optimal TLD cyclic frequency, $f_{TLD-opt_x}$	$\Omega_{opt_x} = \dfrac{f_{TLD-opt_x}}{f_{s-x}}$	0.547	Hz
Optimal response ratio, R_{opt_x}	$R_{opt_x} = \dfrac{\sigma_{r-x}}{\sigma_x} = \dfrac{1+\mu_x}{\sqrt{2\mu_x+\frac{3}{2}\mu_x^2}}$	4.541	
Structure damping ratio, ζ_s		0.0006	(0.06%)
Total structure damping, ζ_{tot-x}	$\zeta_{tot-x} = 0.8\zeta_s + \zeta_{TLD-eff-opt_x}$	0.0401	(4.01%)
Target RMS displacement, $\sigma_{x-target}$	$\zeta_{tot-x} = \zeta_s\dfrac{\sigma_{x-initial}^2}{\sigma_{x-target}^2}$	1.190	mm
Target RMS acceleration, $\sigma_{\ddot{x}-target}$	$\sigma_{\ddot{x}-target} = \omega_s^2\,\sigma_{x-target}$	**01.73**	**milli-g**
Target peak hourly acceleration, $\ddot{x}_{target}$	$\sigma_{\ddot{x}-target} = \dfrac{\ddot{x}_{target}}{PF_x}$	**06.50**	**milli-g**
TLD response, σ_{r-x}	$\sigma_{r-x} = R_{opt_x}\,\sigma_{x-target}$	5.380	mm
Select tank dimensions, L_x, h	$f_{TLD-opt_x} = \dfrac{1}{2\pi}\sqrt{\dfrac{\pi g}{L_x}\tanh\left(\dfrac{\pi h}{L_x}\right)}$	**$L_x = 0.966$ m** **$h = 0.120$ m**	
Shallow water theory check, h/L_x		0.124	
Select screen properties, x_1, x_2, C_{l-x}	$\zeta_{TLD-x} = C_{l-x}\sqrt{\dfrac{32}{\pi^3}}\tanh^2\left(\dfrac{\pi h}{L_x}\right)\Delta_x\Xi_x\dfrac{\sigma_{r-x}}{L_x}$ $\Delta_x = \left(\dfrac{1}{3}+\dfrac{1}{\sinh^2\left(\frac{\pi h}{L_x}\right)}\right)$ $\Xi_x = \sum_{j=1}^{ns_x}\left|\sin^3\left(\dfrac{\pi x_j}{L_x}\right)\right|$	**$x_1 = 0.4\,L_x$** **$x_2 = 0.6\,L_x$** **$C_{l-x} = 8.27$**	

Table 2. Preliminary TLD Design for Vertical Damping Screens ($\mu = 3.5\%$)

Quantity	Equation(s)	Value	
Initial peak hourly acceleration, $\ddot{x}_{initial}$		**65.81**	**milli-g**
Structure cyclic frequency, f_{s-x}		0.558	Hz
Structure time period, T_{s-x}	$T_{s-x} = 1/f_{s-x}$	1.792	s
Structure natural frequency, ω_{s-x}	$\omega_{s-x} = 2\pi/T_{s-x}$	3.507	rad/s
Peak factor, PF_x	$PF_x = \sqrt{2\ln(181\omega_{s-x})} + \dfrac{0.577}{\sqrt{2\ln(181\omega_{s-x})}}$	3.753	
Initial RMS acceleration, $\sigma_{\ddot{x}-initial}$	$\sigma_{\ddot{x}-initial} = \dfrac{\ddot{x}_{initial}}{PF_x}$	**17.55**	**milli-g**
Initial RMS displacement, $\sigma_{x-initial}$	$\sigma_{x-initial} = \dfrac{\sigma_{\ddot{x}-initial}}{\omega_{s-x}^2}\dfrac{g}{1000}$	14.01	mm
Assumed mass ratio, μ		0.035	(3.50%)
Effective damping provided by TLD, $\zeta_{TLD-eff-opt_x}$	$\zeta_{TLD-eff-opt_x} = \dfrac{1}{4}\sqrt{\dfrac{\mu_x+\mu_x^2}{1+\frac{3}{4}\mu_x}}$	0.046	(4.69%)
Optimal damping ratio, $\zeta_{TLD-opt_x}$	$\zeta_{TLD-opt_x} = \sqrt{\dfrac{\mu_x+\frac{3}{4}\mu_x^2}{4+6\mu_x+2\mu_x^2}}$	0.092	(9.23%)
Optimal tuning ratio, Ω_{opt_x}	$\Omega_{opt_x} = \dfrac{\sqrt{1+\frac{1}{2}\mu_x}}{1+\mu_x}$	0.974	(97.4%)
Optimal TLD cyclic frequency, $f_{TLD-opt_x}$	$\Omega_{opt_x} = \dfrac{f_{TLD-opt_x}}{f_{s-x}}$	0.543	Hz
Optimal response ratio, R_{opt_x}	$R_{opt_x} = \dfrac{\sigma_{r-x}}{\sigma_x} = \dfrac{1+\mu_x}{\sqrt{2\mu_x+\frac{3}{2}\mu_x^2}}$	3.861	
Structure damping ratio, ζ_s		0.0006	(0.06%)
Total structure damping, ζ_{tot-x}	$\zeta_{tot-x} = 0.8\zeta_s + \zeta_{TLD-eff-opt_x}$	0.0047	(4.74%)
Target RMS displacement, $\sigma_{x-target}$	$\zeta_{tot-x} = \zeta_s \dfrac{\sigma_{x-initial}^2}{\sigma_{x-target}^2}$	1.570	mm
Target RMS acceleration, $\sigma_{\ddot{x}-target}$	$\sigma_{\ddot{x}-target} = \omega_s^2\,\sigma_{x-target}$	**02.40**	**milli-g**
Target peak hourly acceleration, $\ddot{x}_{target}$	$\sigma_{\ddot{x}-target} = \dfrac{\ddot{x}_{target}}{PF_x}$	**09.00**	**milli-g**
TLD response, σ_{r-x}	$\sigma_{r-x} = R_{opt_x}\,\sigma_{x-target}$	6.080	mm
Select tank dimensions, L_x, h	$f_{TLD-opt_x} = \dfrac{1}{2\pi}\sqrt{\dfrac{\pi g}{L_x}\tanh\left(\dfrac{\pi h}{L_x}\right)}$	**$L_x = 0.966$** **$h = 0.118$**	**m** **m**
Shallow water theory check, h/L_x		0.122	
Select screen properties, x_1, x_2, C_{l-x}	$\zeta_{TLD-x} = C_{l-x}\sqrt{\dfrac{32}{\pi^3}}\tanh^2\left(\dfrac{\pi h}{L_x}\right)\Delta_x\Xi_x\dfrac{\sigma_{r-x}}{L_x}$ $\Delta_x = \left(\dfrac{1}{3} + \dfrac{1}{\sinh^2(\frac{\pi h}{L_x})}\right)$ $\Xi_x = \sum_{j=1}^{ns_x}\left|\sin^3\left(\dfrac{\pi x_j}{L_x}\right)\right|$	**$x_1 = 0.4\,L_x$** **$x_2 = 0.6\,L_x$** **$C_{l-x} = 8.31$**	

Table 3. Preliminary TLD Design for Vertical Damping Screens ($\mu = 5.0\%$)

Quantity	Equation(s)	Value	
Initial peak hourly acceleration, $\ddot{x}_{initial}$		**90.00**	**milli-g**
Structure cyclic frequency, f_{s-x}		0.59	Hz
Structure time period, T_{s-x}	$T_{s-x} = 1/f_{s-x}$	1.79	s
Structure natural frequency, ω_{s-x}	$\omega_{s-x} = 2\pi/T_{s-x}$	3.51	rad/s
Peak factor, PF_x	$PF_x = \sqrt{2\ln(181\omega_{s-x})} + \dfrac{0.577}{\sqrt{2\ln(181\omega_{s-x})}}$	3.75	
Initial RMS acceleration, $\sigma_{\ddot{x}-initial}$	$\sigma_{\ddot{x}-initial} = \dfrac{\ddot{x}_{initial}}{PF_x}$	**24.00**	**milli-g**
Initial RMS displacement, $\sigma_{x-initial}$	$\sigma_{x-initial} = \dfrac{\sigma_{\ddot{x}-initial}}{\omega_{s-x}^2}\dfrac{g}{1000}$	19.15	mm
Assumed mass ratio, μ		0.050	(5.00%)
Effective damping provided by TLD, $\zeta_{TLD-eff-opt_x}$	$\zeta_{TLD-eff-opt_x} = \dfrac{1}{4}\sqrt{\dfrac{\mu_x+\mu_x^2}{1+\frac{3}{4}\mu_x}}$	0.056	(5.62%)
Optimal damping ratio, $\zeta_{TLD-opt_x}$	$\zeta_{TLD-opt_x} = \sqrt{\dfrac{\mu_x+\frac{3}{4}\mu_x^2}{4+6\mu_x+2\mu_x^2}}$	0.011	(10.98%)
Optimal tuning ratio, Ω_{opt_x}	$\Omega_{opt_x} = \dfrac{\sqrt{1+\frac{1}{2}\mu_x}}{1+\mu_x}$	0.964	(96.42%)
Optimal TLD cyclic frequency, $f_{TLD-opt_x}$	$\Omega_{opt_x} = \dfrac{f_{TLD-opt_x}}{f_{s-x}}$	0.538	Hz
Optimal response ratio, R_{opt_x}	$R_{opt_x} = \dfrac{\sigma_{r-x}}{\sigma_x} = \dfrac{1+\mu_x}{\sqrt{2\mu_x+\frac{3}{2}\mu_x^2}}$	3.259	
Structure damping ratio, ζ_s		0.0006	(0.06%)
Total structure damping, ζ_{tot-x}	$\zeta_{tot-x} = 0.8\zeta_s + \zeta_{TLD-eff-opt_x}$	0.0057	(5.67%)
Target RMS displacement, $\sigma_{x-target}$	$\zeta_{tot-x} = \zeta_s \dfrac{\sigma_{x-initial}^2}{\sigma_{x-target}^2}$	1.970	mm
Target RMS acceleration, $\sigma_{\ddot{x}-target}$	$\sigma_{\ddot{x}-target} = \omega_s^2\,\sigma_{x-target}$	**03.33**	**milli-g**
Target peak hourly acceleration, $\ddot{x}_{target}$	$\sigma_{\ddot{x}-target} = \dfrac{\ddot{x}_{target}}{PF_x}$	**12.50**	**milli-g**
TLD response, σ_{r-x}	$\sigma_{r-x} = R_{opt_x}\,\sigma_{x-target}$	6.420	mm
Select tank dimensions, L_x, h	$f_{TLD-opt_x} = \dfrac{1}{2\pi}\sqrt{\dfrac{\pi g}{L_x}\tanh\left(\dfrac{\pi h}{L_x}\right)}$	**$L_x = 0.966$ m** **$h = 0.115$ m**	
Shallow water theory check, h/L_x		0.119	
Select screen properties, x_1, x_2, C_{l-x}	$\zeta_{TLD-x} = C_{l-x}\sqrt{\dfrac{32}{\pi^3}}\tanh^2\left(\dfrac{\pi h}{L_x}\right)\Delta_x \Xi_x \dfrac{\sigma_{r-x}}{L_x}$ $\Delta_x = \left(\dfrac{1}{3}+\dfrac{1}{\sinh^2\left(\frac{\pi h}{L_x}\right)}\right)$ $\Xi_x = \sum_{j=1}^{ns_x}\left|\sin^3\left(\dfrac{\pi x_j}{L_x}\right)\right|$	**$x_1 = 0.4\,L_x$** **$x_2 = 0.6\,L_x$** **$C_{l-x} = 8.35$**	

Table 1. Preliminary TLD Design for Mode 2 of the Indianapolis Building in the y-direction ($\mu = 6.0\%$, Serviceability Return Period $= 10$ years)

Quantity	Equation(s)	Value	
Initial peak hourly acceleration, $\ddot{y}_{initial}$		**14.138**	**milli-g**
Modal Factor, MF		**94.080**	**%**
Initial modal peak hourly acceleration, $\ddot{y}_{initial-m}$	$\ddot{y}_{initial-m} = \ddot{y}_{initial}.MF$	**13.243**	**milli-g**
Structure cyclic frequency, f_{s-y}		0.162	Hz
Structure time period, T_{s-y}	$T_{s-y} = 1/f_{s-y}$	6.180	s
Structure natural frequency, ω_{s-y}	$\omega_{s-y} = 2\pi/T_{s-y}$	1.017	rad/s
Peak factor, PF_y	$PF_y = \sqrt{2\ln(573\omega_{s-y})} + \dfrac{0.577}{\sqrt{2\ln(573\omega_{s-y})}}$	3.730	
Initial RMS acceleration, $\sigma_{\ddot{y}-initial-m}$	$\sigma_{\ddot{y}-initial-m} = \dfrac{\ddot{y}_{initial-m}}{PF_y}$	**3.400**	**milli-g**
Initial RMS displacement, $\sigma_{y-initial-m}$	$\sigma_{y-initial-m} = \dfrac{\sigma_{\ddot{y}-initial-m}}{\omega_{s-y}^2}\dfrac{g}{1000}$	0.034	M
Assumed mass ratio, μ		0.060	(6.00%)
Effective damping provided by TLD, $\zeta_{TLD-eff-opt_y}$	$\zeta_{TLD-eff-opt_y} = \dfrac{1}{4}\sqrt{\dfrac{\mu_y+\mu_y^2}{1+\frac{3}{4}\mu_y}}$	0.062	(6.20%)
Optimal damping ratio, $\zeta_{TLD-opt_y}$	$\zeta_{TLD-opt_x} = \sqrt{\dfrac{\mu_x+\frac{3}{4}\mu_x^2}{4+6\mu_x+2\mu_x^2}}$	0.120	(12.0%)
Optimal tuning ratio, Ω_{opt_y}	$\Omega_{opt_y} = \dfrac{\sqrt{1+\frac{1}{2}\mu_y}}{1+\mu_y}$	0.957	(95.7%)
Optimal TLD cyclic frequency, $f_{TLD-opt_y}$	$\Omega_{opt_y} = \dfrac{f_{TLD-opt_y}}{f_{s-y}}$	0.155	Hz
Optimal response ratio, R_{opt_y}	$R_{opt_y} = \dfrac{\sigma_{r-y}}{\sigma_y} = \dfrac{1+\mu_y}{\sqrt{2\mu_y+\frac{3}{2}\mu_y^2}}$	2.993	
Structure damping ratio, ζ_s		0.020	(2.00%)
Total structure damping, ζ_{tot-y}	$\zeta_{tot-y} = 0.8\zeta_s + \zeta_{TLD-eff-opt_y}$	0.078	(7.80%)
Target RMS displacement, $\sigma_{y-target-m}$	$\zeta_{tot-y} = \zeta_s\dfrac{\sigma_{y-initial-m}^2}{\sigma_{y-target-m}^2}$	0.017	m
Target RMS acceleration, $\sigma_{\ddot{y}-target-m}$	$\sigma_{\ddot{y}-target-m} = \omega_s^2\,\sigma_{y-target-m}$	**1.801**	**milli-g**
Target peak hourly acceleration, $\ddot{y}_{target-m}$	$\sigma_{\ddot{y}-target-m} = \dfrac{\ddot{y}_{target-m}}{PF_y}$	**6.720**	**milli-g**
TLD response, σ_{r-y}	$\sigma_{r-y} = R_{opt_y}\,\sigma_{y-target-m}$	0.051	m
Select tank dimensions, L_y, h	$f_{TLD-opt_y} = \dfrac{1}{2\pi}\sqrt{\dfrac{\pi g}{L_y}\tanh\left(\dfrac{\pi h}{L_y}\right)}$	$L_y = 13.41$ m $h = 1.87$ m	
Shallow water theory check, h/L_y		0.14	
Select screen properties, y_1, y_2, C_{l-y}	$\zeta_{TLD-y} = C_{l-y}\sqrt{\dfrac{32}{\pi^3}}\tanh^2\left(\dfrac{\pi h}{L_y}\right)\Delta_y\Xi_y\dfrac{\sigma_{r-y}}{L_y}$ $\Delta_y = \left(\dfrac{1}{3}+\dfrac{1}{\sinh^2\left(\frac{\pi h}{L_y}\right)}\right)$ $\Xi_y = \sum_{j=1}^{ns_y}\left\lvert\sin^3\left(\dfrac{\pi y_j}{L_y}\right)\right\rvert$	$y_1 = 0.4\,L_y$ $y_2 = 0.6\,L_y$ $C_{l-y} = 20.26$	

Table 2. Preliminary TLD Design for Mode 3 (x-direction) for the Indianapolis Building ($\mu = 5.0\%$, Serviceability Return Period = 10 years)

Quantity	Equation(s)	Value	
Initial peak hourly acceleration, $\ddot{x}_{initial}$		**16.141**	**milli-g**
Modal Factor, MF		**37.310**	**%**
Initial modal peak hourly acceleration, $\ddot{x}_{initial-m}$	$\ddot{x}_{initial-m} = \ddot{x}_{initial}.MF$	**6.033**	**milli-g**
Structure cyclic frequency, f_{s-x}		0.332	Hz
Structure time period, T_{s-x}	$T_{s-x} = 1/f_{s-x}$	3.013	s
Structure natural frequency, ω_{s-x}	$\omega_{s-x} = 2\pi/T_{s-x}$	2.085	rad/s
Peak factor, PF_x	$PF_x = \sqrt{2\ln(573\omega_{s-x})} + \frac{0.577}{\sqrt{2\ln(573\omega_{s-x})}}$	3.918	
Initial RMS acceleration, $\sigma_{\ddot{x}-initial-m}$	$\sigma_{\ddot{x}-initial-m} = \frac{\ddot{x}_{initial-m}}{PF_x}$	**1.540**	**milli-g**
Initial RMS displacement, $\sigma_{x-initial-m}$	$\sigma_{x-initial-m} = \frac{\sigma_{\ddot{x}-initial-m}}{\omega_{s-x}^2}\frac{g}{1000}$	0.003	m
Assumed mass ratio, μ		0.050	(5.00%)
Effective damping provided by TLD, $\zeta_{TLD-eff-opt_x}$	$\zeta_{TLD-eff-opt_x} = \frac{1}{4}\sqrt{\frac{\mu_x+\mu_x^2}{1+\frac{3}{4}\mu_x}}$	0.056	(5.60%)
Optimal damping ratio, $\zeta_{TLD-opt_x}$	$\zeta_{TLD-opt_x} = \sqrt{\frac{\mu_x+\frac{3}{4}\mu_x^2}{4+6\mu_x+2\mu_x^2}}$	0.110	(11.0%)
Optimal tuning ratio, Ω_{opt_x}	$\Omega_{opt_x} = \frac{\sqrt{1+\frac{1}{2}\mu_x}}{1+\mu_x}$	0.964	(96.4%)
Optimal TLD cyclic frequency, $f_{TLD-opt_x}$	$\Omega_{opt_x} = \frac{f_{TLD-opt_x}}{f_{s-x}}$	0.320	Hz
Optimal response ratio, R_{opt_x}	$R_{opt_x} = \frac{\sigma_{r-x}}{\sigma_x} = \frac{1+\mu_x}{\sqrt{2\mu_x+\frac{3}{2}\mu_x^2}}$	3.260	
Structure damping ratio, ζ_s		0.020	(2.00%)
Total structure damping, ζ_{tot-x}	$\zeta_{tot-x} = 0.8\zeta_s + \zeta_{TLD-eff-opt_x}$	0.072	(7.20%)
Target RMS displacement, $\sigma_{x-target-m}$	$\zeta_{tot-x} = \zeta_s\frac{\sigma_{x-initial-m}^2}{\sigma_{x-target-m}^2}$	0.007	m
Target RMS acceleration, $\sigma_{\ddot{x}-target-m}$	$\sigma_{\ddot{x}-target-m} = \omega_s^2\,\sigma_{x-target-m}$	**0.810**	**milli-g**
Target peak hourly acceleration, $\ddot{x}_{target-m}$	$\sigma_{\ddot{x}-target-m} = \frac{\ddot{x}_{target-m}}{PF_x}$	**3.175**	**milli-g**
TLD response, σ_{r-x}	$\sigma_{r-x} = R_{opt_x}\,\sigma_{x-target-m}$	0.006	m
Select tank dimensions, L_x, h	$f_{TLD-opt_x} = \frac{1}{2\pi}\sqrt{\frac{\pi g}{L_x}\tanh\left(\frac{\pi h}{L_x}\right)}$	**L_x =3.00** **m** $h = 0.40$ **m**	
Shallow water theory check, h/L_x		0.13	
Select screen properties, x_1, x_2, C_{l-x}	$\zeta_{TLD-x} = C_{l-x}\sqrt{\frac{32}{\pi^3}}\tanh^2\left(\frac{\pi h}{L_x}\right)\Delta_x\Xi_x\frac{\sigma_{r-x}}{L_x}$ $\Delta_x = \left(\frac{1}{3} + \frac{1}{\sinh^2\left(\frac{\pi h}{L_x}\right)}\right)$ $\Xi_x = \sum_{j=1}^{ns_x}\left|\sin^3\left(\frac{\pi x_j}{L_x}\right)\right|$	**$x_1 = 0.4\,L_x$** **$x_2 = 0.6\,L_x$** **$C_{l-x} = 35.26$**	

Table 3. Preliminary TLD Design for Mode 3 (y-direction) for the Indianapolis Building ($\mu =$ 5.0%, Serviceability Return Period = 10 years)

Quantity	Equation(s)	Value	
Initial peak hourly acceleration, $\ddot{y}_{initial}$		**20.333**	**milli-g**
Modal Factor, MF		**74.010**	**%**
Initial modal peak hourly acceleration, $\ddot{y}_{initial-m}$	$\ddot{y}_{initial-m} = \ddot{y}_{initial}.MF$	**15.044**	**milli-g**
Structure cyclic frequency, f_{s-y}		0.332	Hz
Structure time period, T_{s-y}	$T_{s-y} = 1/f_{s-y}$	3.013	s
Structure natural frequency, ω_{s-y}	$\omega_{s-y} = 2\pi/T_{s-y}$	2.085	rad/s
Peak factor, PF_y	$PF_y = \sqrt{2\ln(573\omega_{s-y})} + \frac{0.577}{\sqrt{2\ln(573\omega_{s-y})}}$	3.918	
Initial RMS acceleration, $\sigma_{\ddot{y}-initial-m}$	$\sigma_{\ddot{y}-initial-m} = \frac{\ddot{y}_{initial-m}}{PF_y}$	**3.840**	**milli-g**
Initial RMS displacement, $\sigma_{y-initial-m}$	$\sigma_{y-initial-m} = \frac{\sigma_{\ddot{y}-initial-m}}{\omega_{s-y}^2}\frac{g}{1000}$	0.009	m
Assumed mass ratio, μ		0.050	(5.00%)
Effective damping provided by TLD, $\zeta_{TLD-eff-opt_y}$	$\zeta_{TLD-eff-opt_y} = \frac{1}{4}\sqrt{\frac{\mu_y+\mu_y^2}{1+\frac{3}{4}\mu_y}}$	0.056	(5.60%)
Optimal damping ratio, $\zeta_{TLD-opt_y}$	$\zeta_{TLD-opt_x} = \sqrt{\frac{\mu_x+\frac{3}{4}\mu_x^2}{4+6\mu_x+2\mu_x^2}}$	0.110	(11.0%)
Optimal tuning ratio, Ω_{opt_y}	$\Omega_{opt_y} = \frac{\sqrt{1+\frac{1}{2}\mu_y}}{1+\mu_y}$	0.964	(96.4%)
Optimal TLD cyclic frequency, $f_{TLD-opt_y}$	$\Omega_{opt_y} = \frac{f_{TLD-opt_y}}{f_{s-y}}$	0.320	Hz
Optimal response ratio, R_{opt_y}	$R_{opt_y} = \frac{\sigma_{r-y}}{\sigma_y} = \frac{1+\mu_y}{\sqrt{2\mu_y+\frac{3}{2}\mu_y^2}}$	3.260	
Structure damping ratio, ζ_s		0.020	(2.00%)
Total structure damping, ζ_{tot-y}	$\zeta_{tot-y} = 0.8\zeta_s + \zeta_{TLD-eff-opt_y}$	0.072	(7.20%)
Target RMS displacement, $\sigma_{y-target-m}$	$\zeta_{tot-y} = \zeta_s \frac{\sigma_{y-initial-m}^2}{\sigma_{y-target-m}^2}$	0.006	m
Target RMS acceleration, $\sigma_{\ddot{y}-target-m}$	$\sigma_{\ddot{y}-target-m} = \omega_s^2\, \sigma_{y-target-m}$	**2.020**	**milli-g**
Target peak hourly acceleration, $\ddot{y}_{target-m}$	$\sigma_{\ddot{y}-target-m} = \frac{\ddot{y}_{target-m}}{PF_y}$	**7.916**	**milli-g**
TLD response, σ_{r-y}	$\sigma_{r-y} = R_{opt_y}\,\sigma_{y-target}$	0.015	m
Select tank dimensions, L_y, h	$f_{TLD-opt_y} = \frac{1}{2\pi}\sqrt{\frac{\pi g}{L_y}\tanh\left(\frac{\pi h}{L_y}\right)}$	**L_y =3.00** $h = 0.40$	**m** m
Shallow water theory check, h/L_y		0.13	
Select screen properties, y_1, y_2, C_{l-y}	$\zeta_{TLD-y} = C_{l-y}\sqrt{\frac{32}{\pi^3}}\tanh^2(\frac{\pi h}{L_y})\Delta_y \Xi_y \frac{\sigma_{r-y}}{L_y}$ $\Delta_y = \left(\frac{1}{3}+\frac{1}{\sinh^2(\frac{\pi h}{L_y})}\right)$ $\Xi_y = \sum_{j=1}^{n_{S_y}}\left|\sin^3\left(\frac{\pi y_j}{L_y}\right)\right|$	**$y_1 = 0.4\,L_y$** **$y_2 = 0.6\,L_y$** **$C_{l-y} = 14.14$**	

Table 4.   Water Mass Calculations for TLDs to Suppress Mode 3 for the Indianapolis Building ($\mu = 5.0\%$)

| Quantity	Equation(s)	Value
Selected tank dimensions, $L_x, B_x\ L_y, B_y, h_x, h_y$		$L_x = L_y = 3.00$ m $B_x = B_y = 15.00$ m $h_x = h_y = 0.40$ m
Water height to tanks length ratio in x-dir	h_x/L_x	0.13
Water height to tanks length ratio in y-dir	h_y/L_y	0.13
Water mass of 1 tank, $m_{w(1tank)}$	$m_{w(1tank)} = L_x B_x h_x = L_y B_y h_y$	18000 kg
TLD mass of 1 tank in θ-dir, $m_{TLD-\theta(1tank)}$	$m_{TLD-\theta(1tank)} \approx m_{1-\theta} =$ $\dfrac{8\tanh\left(\pi\frac{h}{L_x}\right)}{\pi^3\left(\frac{h}{L_x}\right)} m_{w(1tank)}$	$0.767\, m_{w(1tank)} =$ 13806 kg
Total building mass, M_s	$M_s = \sum_{i=1}^{i=N_f} m_f$	36412955 kg
Generalized building mass in θ-dir, M_θ^*	$M_\theta^* = \sum_{i=1}^{i=N_f} (m_f)_i\,(\phi_t^2)_i$	12198340 kg
Required TLD mass in θ-dir, $m_{TLD-\theta}$	$m_{TLD-\theta} = \mu_{TLD-\theta} M_\theta^*$	609917 kg
No. of Tanks required in θ-dir, $N_{TLD-\theta}$	$N_{TLD-\theta} = m_{TLD-\theta}/m_{TLD-\theta(1tank)}$	44.17
Chosen No. of tanks for mode 3, $N_{TLD-\theta}$	(Uni-directional tanks)	**4 sets of 11 tanks**
Actual mass ratio in θ-dir, $\mu_{\theta-actual}$	$\mu_{\theta-actual} = N_{TLD-\theta}m_{TLD-\theta(1tank)}/M_\theta^*$	**4.98 %**
Mass ratio of contained water, μ_w	$\mu_w = N_{TLD-\theta}m_{w(1tank)}/M_s$	**4.35 %**
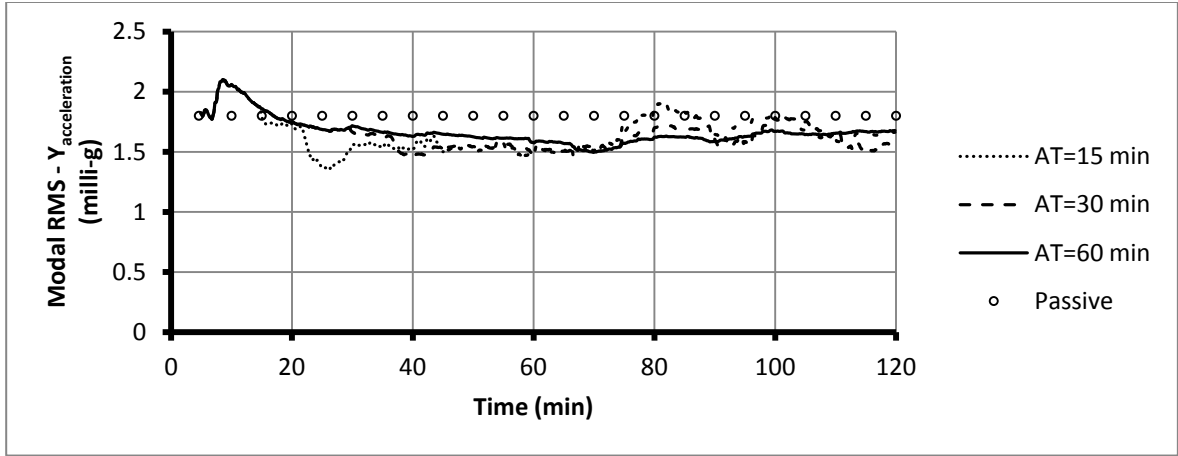
Fig. 1.   Second Modal RMS Structural Accelerations at the CM of the Indianapolis Building in the y-direction (z =154.6 m) Employing Semi-Active TLDs Utilizing Various Averaging Time ($UT = 1.0\ T$, $\theta_w = 210°$, Return Period=10 Years)
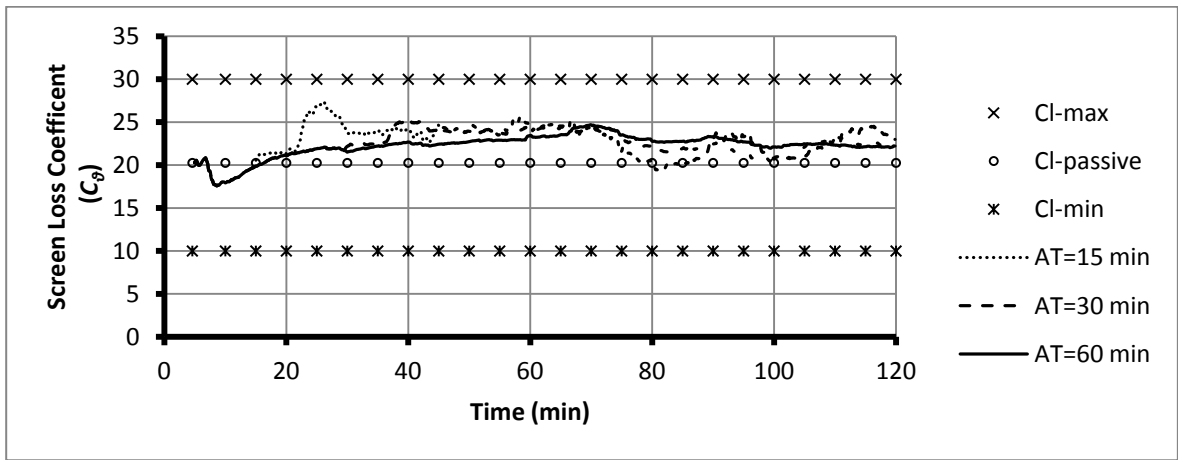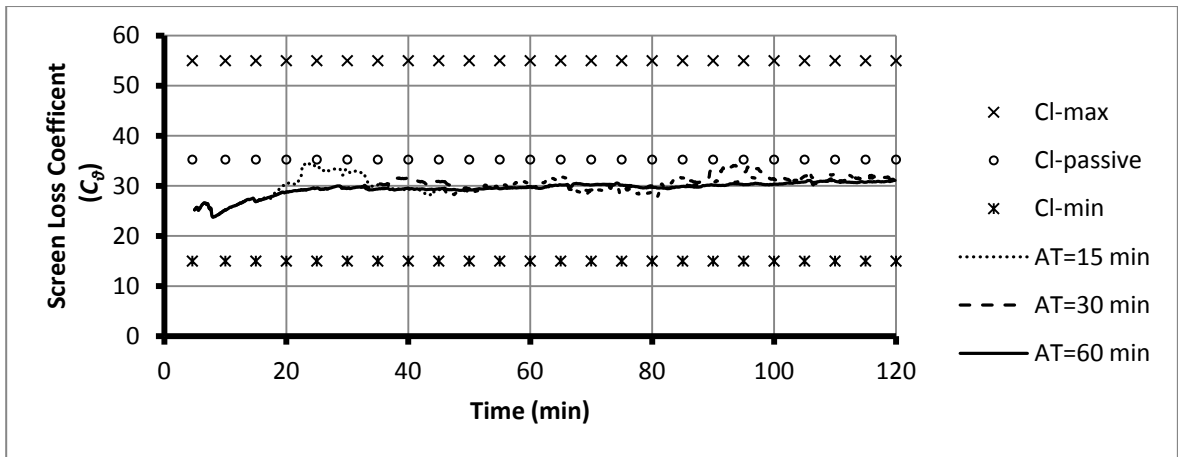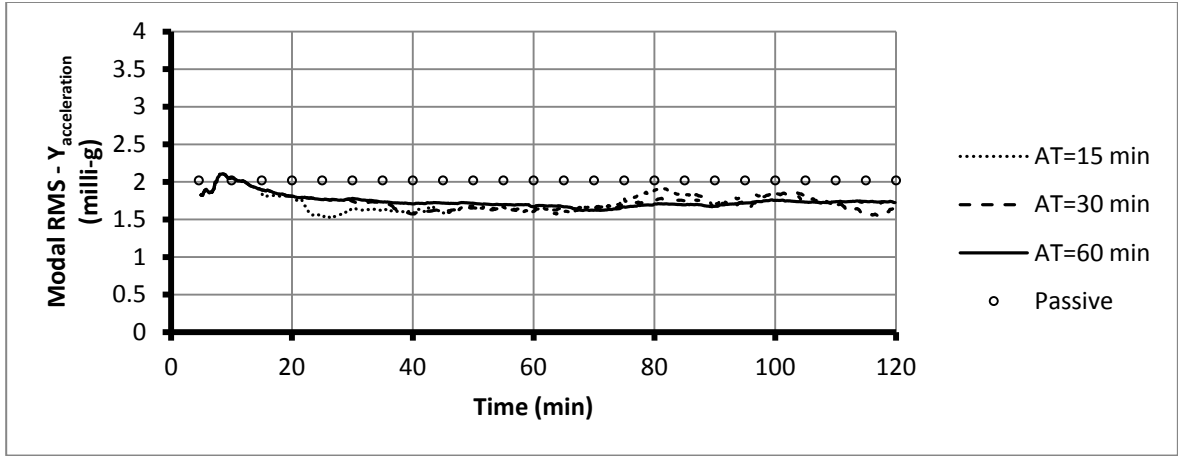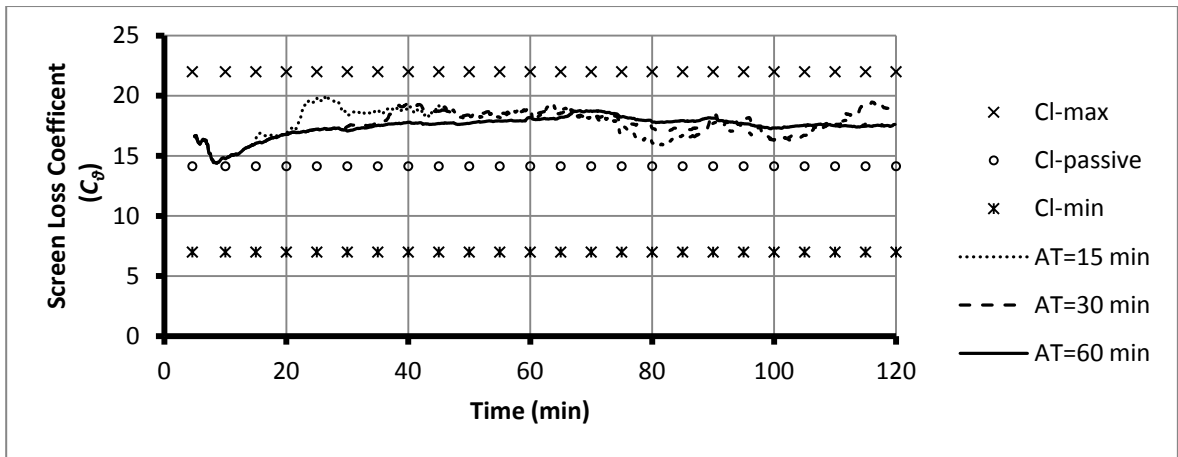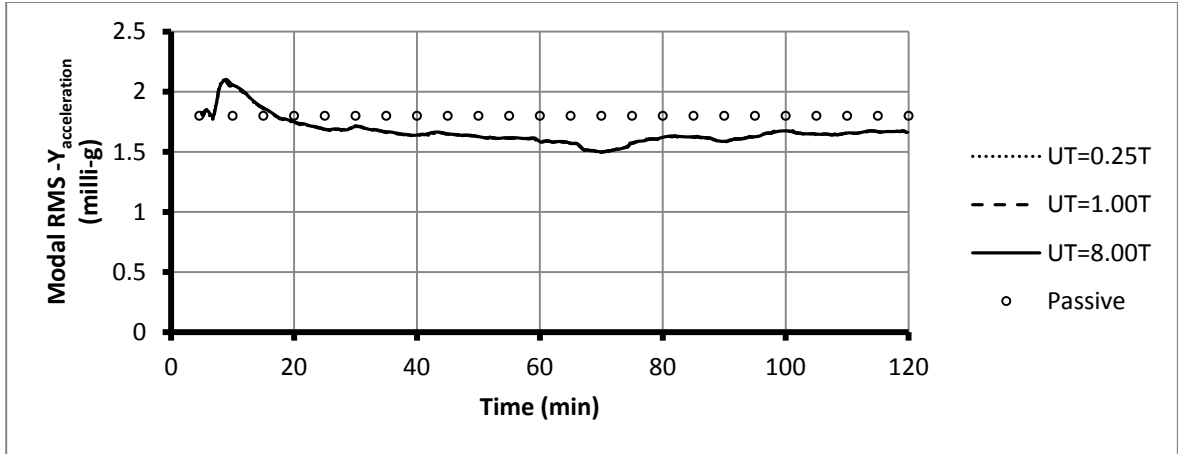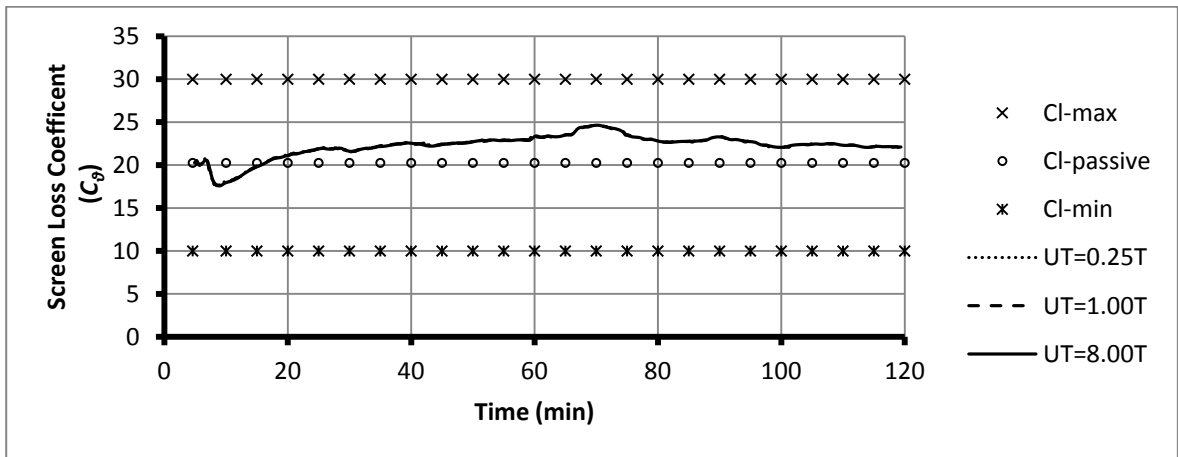

Fig. 2.   Screen Loss Coefficient Values of Semi-Active TLDs Installed to Suppress Mode 2 of the Indianapolis Building Placed at the CM in the y-direction (z =154.6 m) Utilizing Various Averaging Time ($UT = 1.0\ T$, $\theta_w = 210°$, Return Period=10 Years)
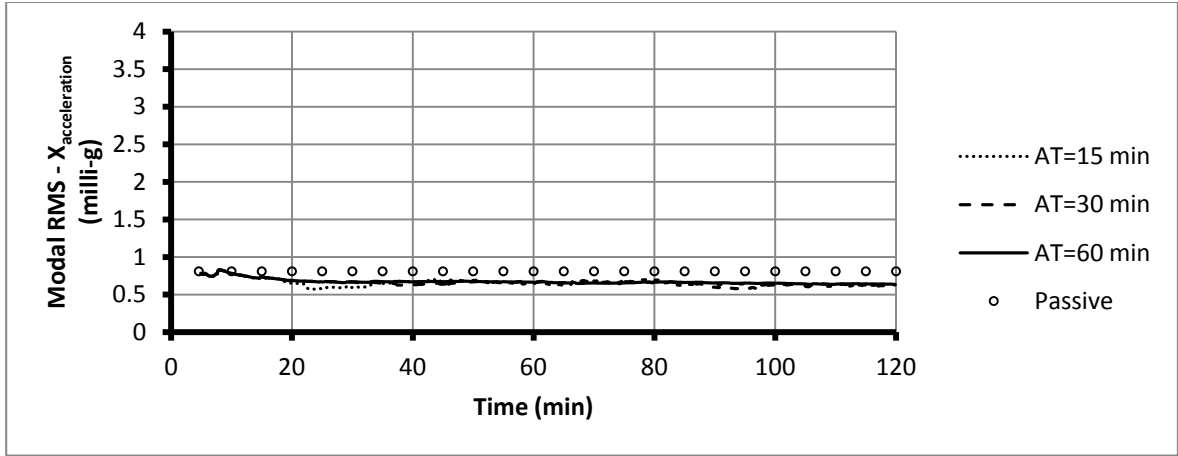
Fig. 3. Third Modal RMS Structural Accelerations at Corners 3 and 4 of the Indianapolis Building in the x-direction (z =154.6 m) Employing Semi-Active TLDs Utilizing Various Averaging Time ($UT = 1.0\,T$, $\theta_w = 210°$, Return Period=10 Years)

Fig. 4. Screen Loss Coefficient Values of Semi-Active TLDs Installed to Suppress Mode 3 of the Indianapolis Building Placed at Corners 3 and 4 in the x-direction (z =154.6 m) Utilizing Various Averaging Time ($UT = 1.0\,T$, $\theta_w = 210°$, Return Period=10 Years)
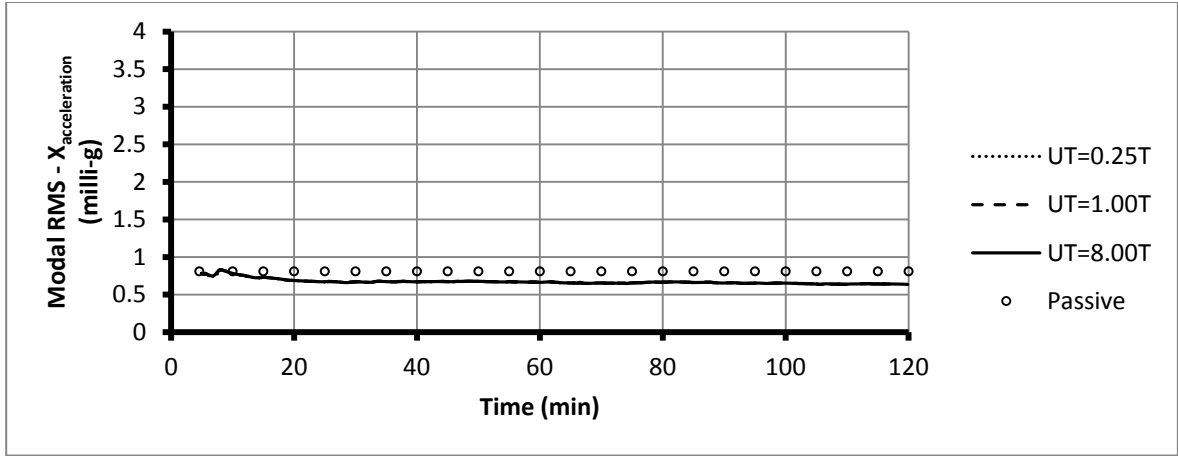
Fig. 5.   Third Modal RMS Structural Accelerations at Corners 2 and 3 of the Indianapolis Building in the y-direction ($z =154.6$ m) Employing Semi-Active TLDs Utilizing Various Averaging Time ($UT = 1.0\,T$, $\theta_w = 210°$, Return Period=10 Years)
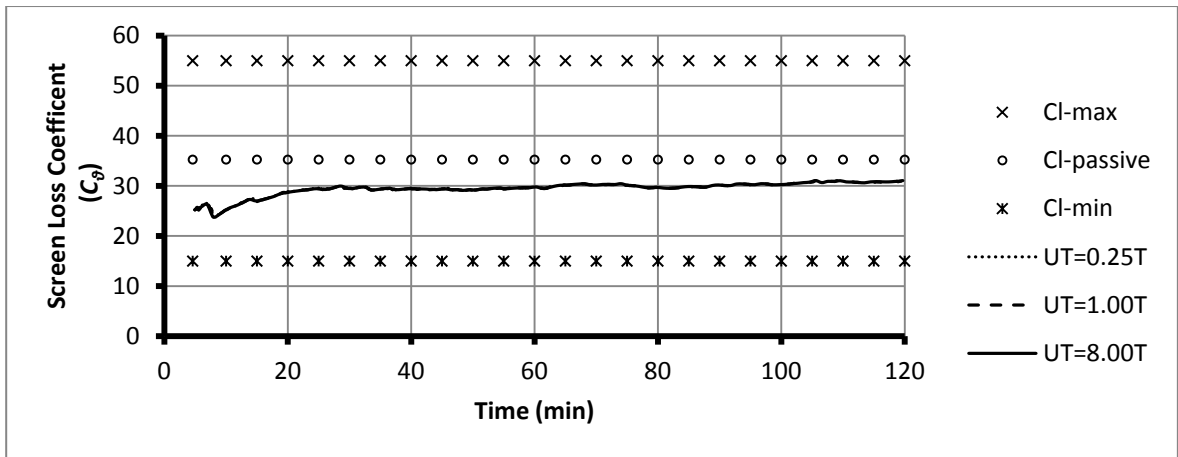

Fig. 6.   Screen Loss Coefficient Values of Semi-Active TLDs Installed to Suppress Mode 3 of the Indianapolis Building Placed at Corners 2 and 3 in the y-direction ($z =154.6$ m) Utilizing Various Averaging Time ($UT = 1.0\,T$, $\theta_w = 210°$, Return Period=10 Years)

Fig. 7.   Second Modal RMS Structural Accelerations at the CM of the Indianapolis Building in the y-direction (z =154.6 m) Employing Semi-Active TLDs Utilizing Various Updating Time ($AT = 60$ min, $\theta_w = 210°$, Return Period=10 Years)

Fig. 8.   Screen Loss Coefficient Values of Semi-Active TLDs Installed to Suppress Mode 2 of the Indianapolis Building Placed at the CM in the y-direction (z =154.6 m) Utilizing Various Updating Time ($AT = 60$ min, $\theta_w = 210°$, Return Period=10 Years)
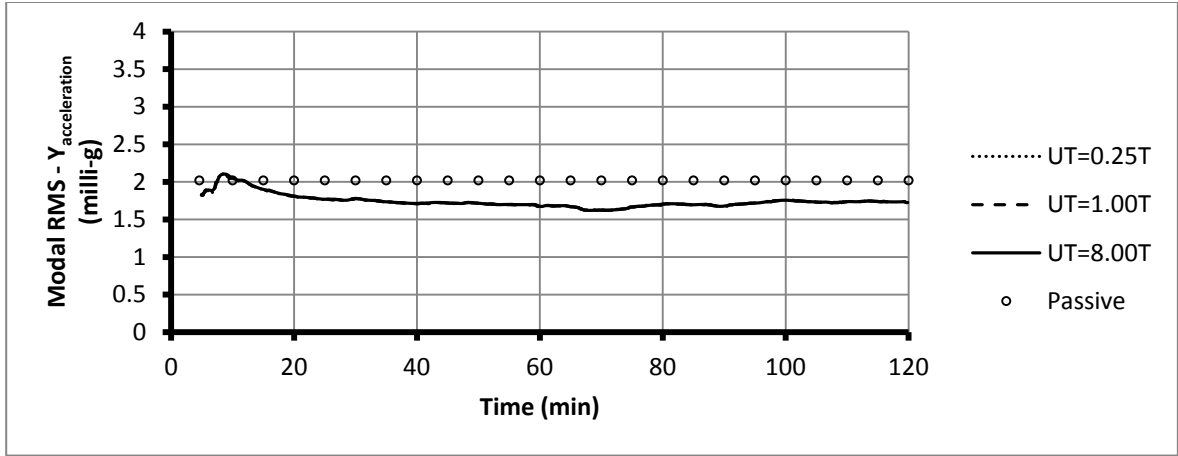
Fig. 9.   Third Modal RMS Structural Accelerations at Corners 3 and 4 of the Indianapolis Building in the x-direction ($z =$ 154.6 m) Employing Semi-Active TLDs Utilizing Various Updating Time ($AT = 60$ min, $\theta_w = 210°$, Return Period=10 Years)
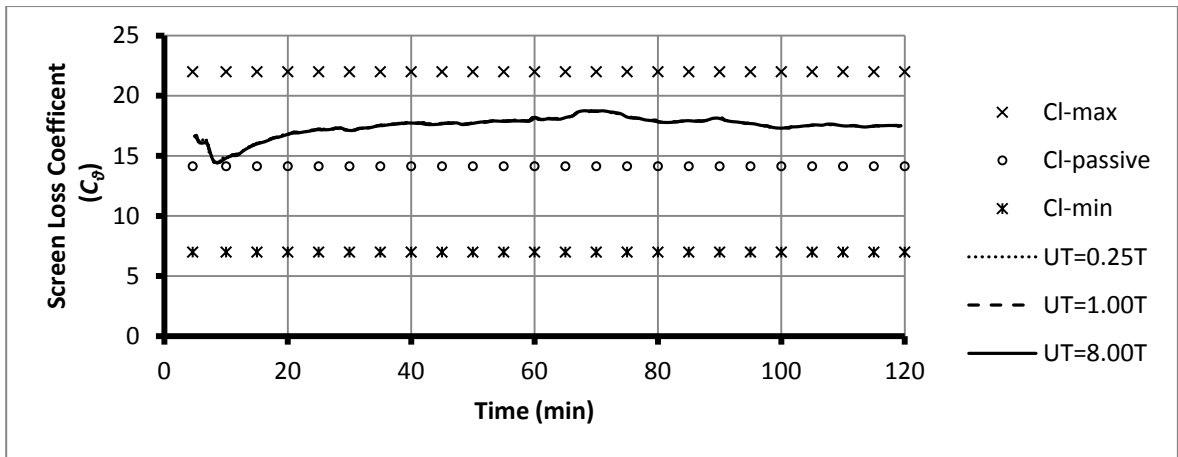

Fig. 10.   Screen Loss Coefficient Values of Semi-Active TLDs Installed to Suppress Mode 3 of the Indianapolis Building Placed at Corners 3 and 4 in the x-direction ($z =$ 154.6 m) Utilizing Various Updating Time ($AT = 60$ min, $\theta_w = 210°$, Return Period=10 Years)
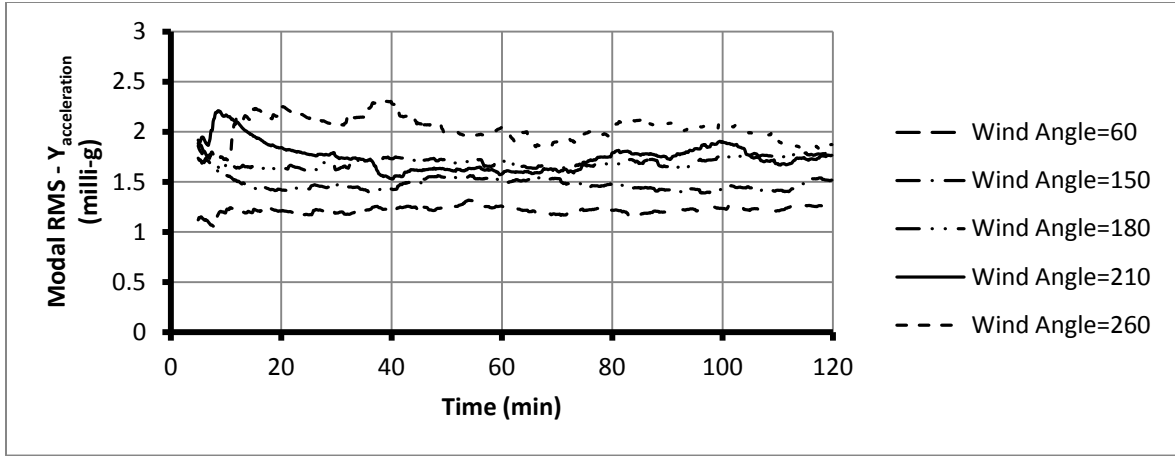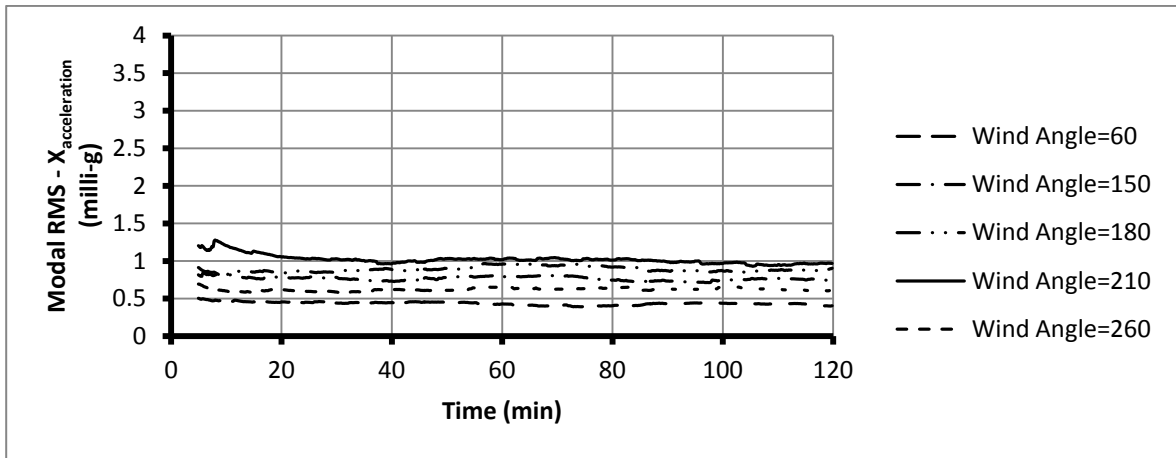
Fig. 11. Third Modal RMS Structural Accelerations at Corners 2 and 3 of the Indianapolis Building in the y-direction ($z =154.6$ m) Employing Semi-Active TLDs Utilizing Various Updating Time ($AT = 60$ min, $\theta_w = 210°$, Return Period=10 Years)

Fig. 12. Screen Loss Coefficient Values of Semi-Active TLDs Installed to Suppress Mode 3 of the Indianapolis Building Placed at Corners 2 and 3 in the y-direction ($z =154.6$ m) Utilizing Various Updating Time ($AT = 60$ min, $\theta_w = 210°$, Return Period=10 Years)

Fig. 13. Second Modal RMS Structural Accelerations at the *CM* of the Indianapolis Building in the *y*-direction (*z* =154.6 m) Employing the Semi-Active TLDs Utilizing Various Wind Loading Directions (*AT* = 60 min, *UT* = 1.0 *T*, Return Period=10 Years)
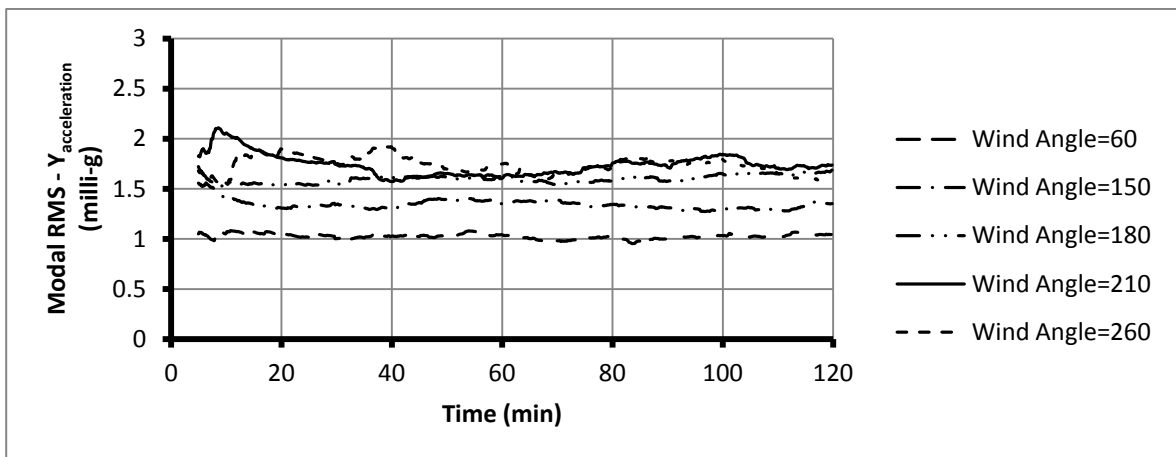

Fig. 14. Third Modal RMS Structural Accelerations at Corners 3 and 4 of the Indianapolis Building in the *x*-direction (*z* =154.6 m) Employing Semi-Active TLDs Utilizing Various Wind Loading Directions (*AT* = 60 min, *UT* = 1.0 *T*, Return Period=10 Years)

Fig. 15. Third Modal RMS Structural Accelerations at Corners 2 and 3 of the Indianapolis Building in the *y*-direction (*z* =154.6 m) Employing Semi-Active TLDs Utilizing Various Wind Loading Directions (*AT* = 60 min, *UT* = 1.0 *T*, Return Period=10 Years)
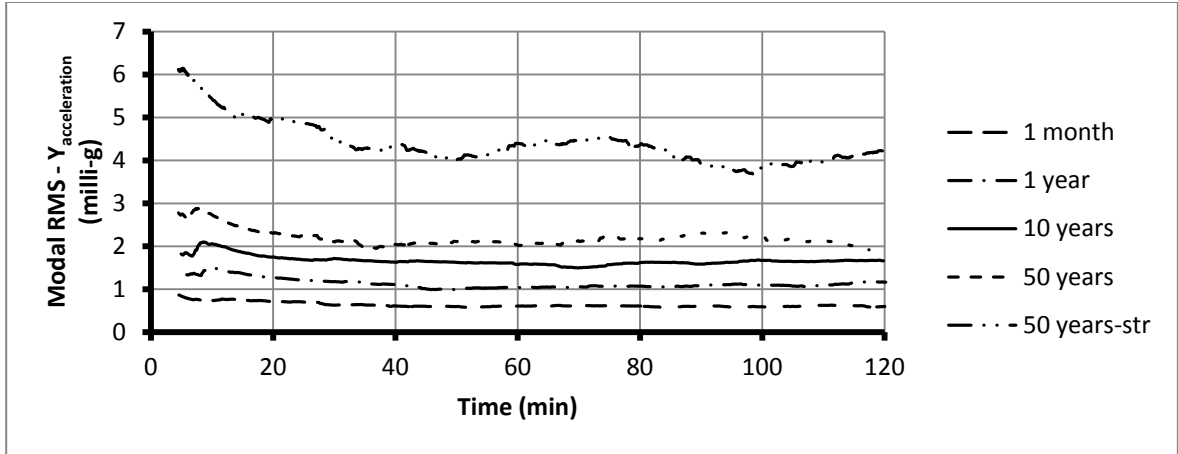
Fig. 16. Second Modal RMS Structural Accelerations at the CM of the Indianapolis Building in the y-direction (z =154.6 m) Employing the Semi-Active Control Strategy Utilizing Various Return Periods ($AT = 60$ min, $UT = 1.0\ T, \theta_w = 210°$)
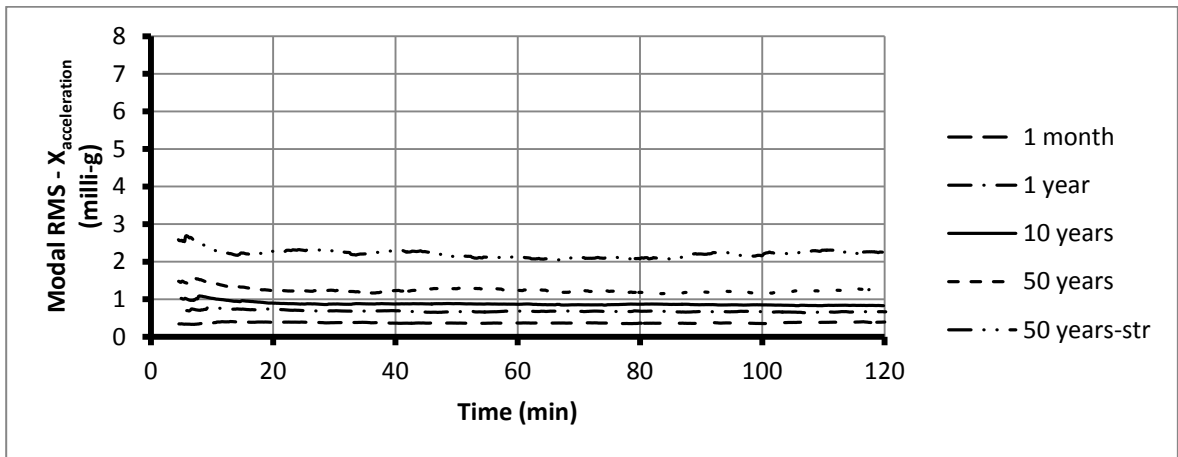

Fig. 17. Third Modal RMS Structural Accelerations at Corners 3 and 4 of the Indianapolis Building in the x-direction (z =154.6 m) Employing the Semi-Active Control Strategy Utilizing Various Return Periods ($AT = 60$ min, $UT = 1.0\ T, \theta_w = 210°$)
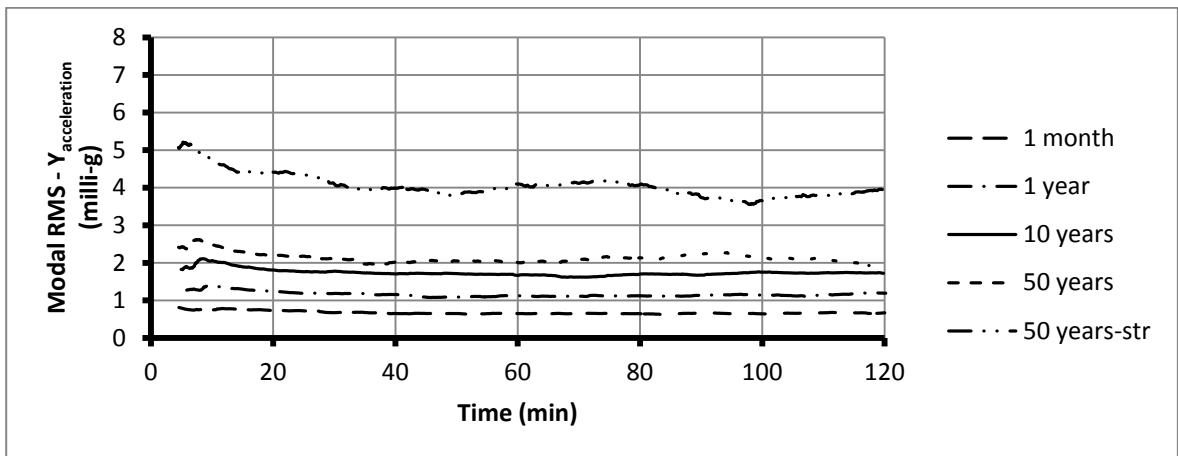

Fig. 18. Third Modal RMS Structural Accelerations at Corners 2 and 3 of the Indianapolis Building in the y-direction (z =154.6 m) Employing Semi-Active Control Strategy Utilizing Various Return Periods ($AT = 60$ min, $UT = 1.0\ T, \theta_w = 210°$)

Curriculum Vitae

Name:	Islam M. Soliman
Place of Birth:	Zagazig, Egypt
Year of Birth:	October 26, 1976
Post Secondary Education and Degree	B.Sc., 1999 Zagazig University, Egypt
	M.Sc., 2004 Zagazig University, Egypt
Honours and Awards	Western Graduate Research Scholarship (WGRS) The University of Western Ontario, Canada (2007-2012)
	Egyptian Post-Graduate Research Scholarship The Ministry of Higher Education and Scientific Research of Egypt (2007-2009)
	Graduate Honor Scholarship Zagazig University, Egypt (2000-2004)
	Outstanding Undergraduate Scholarship Zagazig University, Egypt (1994-1999)